842

1970 LIGHTNING AND STATIC ELECTRICITY CONFERENCE, 9-11 DECEMBER

Sponsored Jointly By

AIR FORCE AVIONICS LABORATORY

and

SOCIETY OF AUTOMOTIVE ENGINEERS

19960207 146

DECEMBER 1970

PLASTEC 22132-22140

This document has been approved for public release and sale; its distribution is unlimited.

DTIC QUALITY INSPECTED 1

1970 LIGHTNING AND STATIC ELECTRICITY CONFERENCE, 9-11 DECEMBER

This document has been approved for public release
and sale; its distribution is unlimited.

PERMISSION TO REPRODUCE
Information Transmission Branch
AFRL/IAI X 55855

FOREWORD

The Air Force Avionics Laboratory (AFSC) and the Society of Automotive Engineers jointly sponsored the "1970 Lightning and Static Electricity Conference" on 9-11 December 1970 in San Diego, California. This report presents the proceedings of the conference. Mr. C. R. Austin, Air Force Avionics Laboratory was the Conference Organizer and compiled the information for this conference report.

Research described herein represents the efforts of many persons in many organizations. The Air Force Avionics Laboratory and Society of Automotive Engineers wish to express their gratitude and appreciation to the following for their contributions in the conduct of this conference and preparation of the proceedings:

Members of the General Committee, the Program Planning Committee, AE-4 Electromagnetic Compatibility Committee of SAE, the San Diego Chapter of SAE and Mr. J. E. Chamberlain, Chief, Experimental Evaluation Group of AFAL.

Messrs Tom Wolff, Larry E. Cummings, H. M. Bartman and Mrs. Linda Dill who spent many hours in assisting in organizing the conference and preparing material.

Publication of this proceeding does not constitute Air Force or Society of Automotive Engineers approval of the findings or conclusions. The proceedings are published only for the exchange and stimulation of ideas.

R. W. STIMMEL
W. D. McKERCHAR
Conference CoChairman

ABSTRACT

Information is presented on lightning and static electricity phenomena from the standpoint of their relation to, and interaction with, aerospace vehicles and ground complexes. Interactions and the effects of lightning and static electricity on electrical, electronic, structural, static discharger systems and fly-by-wire systems of aerospace systems are described. The information presented is considered to be of interest to scientists and engineers in the fields of electronics, advanced composite materials and structures, and atmospheric electrical phenomena.

CONFERENCE TECHNICAL SPONSOR

Air Force Avionics Laboratory (AFSC)
Electronic Warfare Division
Wright-Patterson AFB, Ohio 45433

Col John E. Kulpa, Jr., Laboratory Director
Lt Col John B. Sturges, Jr., Division Chief

CONFERENCE ADMINISTRATIVE SPONSOR

Society of Automotive Engineers, Inc.
Two Pennsylvania Plaza, New York NY 10001

H. F. Barr, President
M. J. Kittler, Treasurer
Joseph Gilbert, Secretary and General Manager

EXECUTIVE COMMITTEE

C. R. Austin, Conference Organizer, AF Avionics Laboratory
T. Wolff, Exec Manager, AF Avionics Laboratory
J. M. Kelly, Registration & Security, Aeron Sys Div
A. J. Favata, Administrator, Society of Automotive Engrs

GENERAL COMMITTEE

W. D. McKerchar, General CoChairman, Breeze-Illinois, Inc
R. G. Stimmel, General CoChairman, AF Avionics Laboratory
C. R. Austin, Technical Program Chr, AF Avionics Laboratory
B. Weinbaum, Local Support Activities Chr, GD/San Diego
C. F. Gotschalk, Jr., San Diego Sect Chr, Solar Electronics
T. K. Pembleton, Plant Tour & Trip Chr, Solar Electronics

PROGRAM PLANNING COMMITTEE

Col J. E. Kulpa, AFAL
C. R. Austin, AFAL
L. R. Avery, GD/Ft Worth
L. E. Cummings, AFAL
D. M. Hish, Hish Associates
H. M. Hoffart, General Electric
J. L. Moe, GD/Fort Worth
K. A. Moore, Continental Airlines
J. E. Nanevicz, SRI
J. D. Robb, LTRI
H. Schultz, Hughes Acft
H. Schwartz, AFML
C. E. Seth, ASD
A. G. Zimbalatti, Grumman Acft

PROGRAM

INTRODUCTION Wednesday Morning

Welcome
G. F. Gotschalk, Jr., Chairman, SAE San Diego Section

Opening Remarks
W. D. McKerchar, Breeze-Illinois, Inc
R. G. Stimmel, Air Force Avionics Lab, AF Systems Command

Keynote Address
G. P. Bate, Jr., Director, Aircraft Division, Systems Research & Development, Federal Aviation Administration

SESSION 1A GENERAL LIGHTNING Wednesday Morning

Chairman: M. P. Amason, Tech Staff, Electrical & Electronic Engineering, Douglas Aircraft Co;, McDonnell Douglas Corp.

SESSION 1B STATIC ELECTRICITY Wednesday Afternoon

Chairman: J. E. Nanevicz, Program Mgr., Electromagnetic Sciences Lab, Stanford Research Institute

SOCIAL HOUR Wednesday Evening

SESSION 2A COMMERCIAL AIRCRAFT Thursday Morning

Chairman: K. A. Moore, Mgr., Electronics Engrg., Continental Airlines

SESSION 2B CLASSIFIED SESSION Thursday Morning

Chairman: L. E. Cummings, Electronics Engr., Avionics Laboratory, US Air Force Systems Command

SESSION 2C MILITARY AIRCRAFT Thursday Afternoon

Chairman: C. E. Seth, Compatibility Engineer, Aeronautical Systems Division, US Air Force Systems Command

BUFFET Thursday Evening

SESSION 3A ADVANCED MATERIALS Friday Morning

Chairman: H. S. Schwartz, Asst to the Chief, Nonmetallic Materials Division, Materials Laboratory, US Air Force Systems Command

SESSION 3B GROUND COMPLEXES Friday Morning

Chairman: H. M. Hoffart, EMC Consulting Engr, General Electric Company

SESSION 3C SPACE BOURNE VEHICLES Friday Afternoon

Chairman: H. M. Hoffart, EMC Consulting Engr, General Electric Company

INDEX OF AUTHORS

	Page
Amason, M. P.	99
Amman, E. A.	321
Arabian, D. D.	319
Blalock, T. J.	309
Breland, J. G. Capt	233
Brick, R. O.	139
Cummings, L. E.	47
Fisher, F. A.	299, 309
Fitzgerald, Dr. D. R.	3
Hackenburger, G.	189
Hacker, P. T.	111
Huber, R. F.	39
Kawiecki, C. J.	39, 207
Kung, J. T.	99
Kuo, C. J.	233
Lloyd, K. J.	253
Nanevicz, J. E.	73
Newman, M. M.	11, 25
Oh, L. L.	139
Penton, A. P.	253
Perry, B. L.	17
Perry, J. L.	253
Pierce, E. T.	89
Plummer, J. A.	111
Quinlivan, Dr. J. T.	233
Rivera, E. R.	177
Robb, J. D.	11, 25, 39, 215
Rogers, M. E.	57
Schneider, S. D.	139
Solak, B. J.	179
Stahmann, J. R.	13, 25, 189
Truax, R. L.	157
Vance, E. F.	73
Weinstock, G.	195
Woodrum, G. T. Lt	223

TABLE OF CONTENTS

SESSION 1A	GENERAL LIGHTNING	PAGE
	Aircraft and Rocket Triggered Natural Lightning Discharges Dr. D. R. Fitzgerald, Air Force Cambridge Research Laboratories	3
	Rocket and Supersonic Aircraft Influence In Triggering Lightning and Intentional Cloud Discharge Triggering for Launch Protection M. M. Newman and J. D. Robb, Lightning & Transients Research Institute	11
	Model Studies of Stroke Probability to Selected Points on Aerospace Vehicles J. R. Stahmann, Lightning & Transients Research Institute	13
	Lightning and Static Hazards Relative to Airworthiness B. L. Perry, Air Registration Board Brabazon House, England	17
	Recent Developments in Lightning Protection For Aircraft and Helicopters J. D. Robb and J. R. Stahmann, Lightning & Transients Research Institute	25
SESSION 1B	STATIC ELECTRICITY	
	Lightning Test Facilities Measurement Techniques R. F. Huber, Joslyn Mfg & Supply; J. D. Robb Lightning and Transients Research Institute; C. J. Kawiecki, Joslyn Electronic Systems Div	39
	Microwave Noise Produced by Triboelectric Charging L. E. Cummings, Air Force Avionics Laboratory	47
	A Study of Some Fundamental Helicopter Charging Mechanisms M. E. Rogers, Avionics Dept, Royal Aircraft Establishment, England	57
	Studies of Supersonic Vehicle Electrification E. F. Vance and J. E. Nanevicz, Stanford Research Institute	73

22133

SESSION 1B (CONTD) PAGE

Waterfalls, Bathrooms & Perhaps Super-tanker Explosions 89
E. T. Pierce, Stanford Research Institute

SESSION 2A COMMERCIAL AIRCRAFT

Lightning Current Transfer Characteristics of the P-Static Discharger Installations 99 ✓ 22134
M. P. Amason & J. T. Kung, Electrical & Electronics Engineering Staff, Douglas Aircraft Company

Measurements and Analysis of Lightning Induced Voltages in Aircraft Electrical Circuits 111
P. T. Hacker, NASA Lewis Research Center; J. A. Plummer, General Electric High Voltage Laboratory

The Effects of Lightning Attachment Phenomena on Aircraft Design 139
S. D. Schneider, L. L. Oh, & R. O. Brick Electronics Technology Staff, Boeing Company

Electrostatic Charging and Noise Quieting 157 ✓ 22135
R. L. Truax, Dayton Aircraft Products

SESSION 2B CLASSIFIED SESSION (Not included)

SESSION 2C MILITARY AIRCRAFT

Importance of Lightning Protection and Static Electricity Design for Military Aircraft 177
E. R. Rivera, Naval Air Systems Command

Influence of Lightning and Static Electricity as Applied to Helicopter Design 179 ✓ 22136
B. J. Solak, Vertol Div, Boeing Company

SESSION 2C (CONTD) PAGE

Lightning Protection for Nonmetallic Rotor Blades 189
G. Hackenburger, Kaman Aircraft Corp.

Lightning Protection on Advanced Fighter Aircraft 195
G. Weinstock, McDonnell Douglas Corporation

Lightning and Surge Protective Devices For Surviviability of Electrical Systems 207
C. J. Kawiecki & Associates, Joslyn Electronic Systems Division

SESSION 3A ADVANCED MATERIALS

Lightning Protection for Dielectric Composites 215
J. D. Robb, Lightning & Transients Research Institute

Lightning Protection for Advanced Composite Aircraft Structures 223
Lt G. T. Woodrum, Air Force Materials Laboratory

Lightning Protective Coatings for Boron And Graphite Fiber Reinforced Plastics 233
Dr. J. T. Quinlivan and C. J. Kuo, The Boeing Company; Capt J. G. Breland, Air Force Materials Laboratory

Fundamental Investigations of High Intensity Electric Current Flow Processes and Resultant Damage in Advanced Composites 253
A. P. Penton & J. L. Perry, Philco-Ford Corp; and K. J. Lloyd, General Electric Co

Electromagnetic Shielding Characteristics of Advanced Structural Composites
Panel Discussion (Not included)

SESSION 3B GROUND COMPLEXES PAGE

Voltages Produced by Transient Currents Flowing into Shields of Cables 299
F. A. Fisher, High Voltage Laboratory, General Electric Company

Protection of Aerospace Ground Facilities From the Effects of Lightning 309
F. A. Fisher & T. J. Blalock, High Voltage Laboratory, General Electric Company

Film- Static Electrification in Fuel Tanks
B. L. Perry, Air Registration Board, England (Not included)

SESSION 3C SPACE BOURNE VEHICLES

The Aspects of the Apollo 12 Lightning Incident 319
D. D. Arabian, National Aeronautics & Space Administration, Manned Spacecraft Center

The Problem of Lightning and Static Electricity at the Kennedy Space Center 321
E. A. Amman, US Department of Commerce Environmental Science Services Admin Weather Bureau, Kennedy Space Center

Lightning and Electrostatic Effects on Spacecraft - Panel
Dr. J. C. Bryner & C. H. Child, North American Rockwell Corp
(Not included)

SESSION 1A

GENERAL LIGHTNING PROTECTION

Organizer - J. D. Robb

Lightning & Transients Research Institute

Chairman, M. P. Amason

Douglas Aircraft Co.

700913

Aircraft and Rocket Triggered Natural Lightning Discharges

Donald R. Fitzgerald
Air Force Cambridge Research Laboratories

ABSTRACT

Electrostatic field measurements in thunderstorms were obtained from the "Roughrider" F-100F aircraft, and from above storms with a U-2 aircraft. Analysis of data associated with lightning strikes to or near the aircraft indicates that most of the strikes occurred in a transition zone from positive over negative charge to the reverse as indicated by the vertical electric field component and that they occurred in or on the edge of an intense negative space charge concentration at flight level. These transition zones and charge centers are closely linked to the precipitation and draft structure in the cloud. Data taken at cloud base and on the surface has also been used to indicate conditions for rocket-triggered lightning. Small wire-pulling rockets fired by LTRI were successful in triggering strokes at an altitude of several hundred feet when the over-water storm field was about 200 v/cm. The Apollo 12 vehicle triggered strokes at 6400 ft when the surface field was about 35 v/cm. Post-flight analysis of data obtained at Cape Kennedy and Patrick AFB indicates two or three natural intra-or inter-cloud lightning events had occurred within 30 km of the Cape in the 25 minute period prior to launch.

RECOGNITION and increased familiarity with cloud factors that are conducive to an imminent lightning stroke may aid a pilot in making a proper response to damage and may lead to development of new electrical sensors that could be employed for warning and course correction purposes. In this paper electric field measurements obtained during the 1965 "Roughrider" flights in Florida thunderstorms and electrical data associated with the launch of Apollo 12 have been examined for significant patterns and magnitudes associated with lightning strikes to the vehicles. Earlier information from the "Roughrider" lightning current study was reported by Petterson and Wood (1)*. General results of the flight program were described by Fitzgerald (2).

LOW ALTITUDE TRIGGERED LIGHTNING

One objective of the flights conducted near Cape Kennedy was to induce cloud-to-water lightning through the instrumented F-100F aircraft and to surge instrumentation on the LTRI ship. Small wire-pulling rockets were fired from the ship to about 350 meters altitude as the aircraft came overhead at 550 to 600 meters. Lightning strikes were triggered to the ship on the first two of three trials, however the aircraft was not struck. The field components measured at cloud base just prior to rocket launch, and the estimated fields at the ship location are shown in Table 1.

The time history of the field at cloud base indicates a fairly localized low altitude negative charge center near the ship which generally decreased in intensity during the experiment. The region was about 2 km in diameter. Excess negative charge was drained in each of the triggered strokes, but only a portion of the negative charge was removed in the strokes. The storm was part of a large weakly organized group of showers showing radar echoes over the water in a 55 by 90 km area. The peak field values here of about 200 v/cm are about twice as large as those normally measured at

* Numbers in parentheses designate References at end of paper.

Table 1 - Summary 30 July 1965 Triggered Lightning Test

ROCKET LAUNCH TIME - EST	SHIP POINT DISCHARGE	ESTIMATED SURFACE FIELD	CLOUD BASE FIELD - V/CM			AIRCRAFT CHARGE	LIGHTNING PARAMETER	
			E_z	E_y	|E|	μC	I_{MAX}	dI/dt
1550:55.7	30 μA	-190 TO -175	-165	-25	-170	-19	14 KA	9.3 $\frac{KA}{\mu SEC}$
1553:31.6	30	-190 TO -175	-190	-35	-195	-5	NA - STROKE HIT SEVERAL PARTS OF SHIP	
1558:25.1	15	-160 TO -125	-115	-15	-115	-15	NO STROKE	

land points during overhead thunderstorms and may account for the generally much more successful efforts to trigger lightning with low altitude rockets over water than over land.

The Apollo 12 incident represents a most spectacular rocket triggered event. In this case a number of convective cloud showers were developing and moving through the area, presenting complex electrical records on Merritt Island. Our after-the-event analysis of electrostatic field measurements at Cape Kennedy and lightning flash counter data from Cape Kennedy and Patrick AFB indicates two and probably three natural lightning events occurred within a radius of about 30 km of the Cape in the time period from 25 to 2 minutes prior to launch. The first event at 1057 EST was observed by both flash counters and the field meter. The second, three minutes before launch was observed from the vicinity of Patrick AFB as a cloud-cloud stroke in the general direction of the Cape, (comment at Washington, D. C. AGU meeting), and confirmed by the field meter record. The probable third stroke two minutes before launch was indicated only on the field meter.

The static field change associated with the cloud-ground lightning experienced at 36.5 sec after launch has been used to calculate the total charge transfer through or near the spacecraft. Values range from 7.7 coulombs if the charge destroyed was at 3 km height to 4.5 coulombs if the charge was at 6 km. These values are about one-quarter of those associated with an "average" lightning strike but well within the range of normal lightning. In this case the cloud bases overhead at launch time contained excess negative charge, as in the overwater case, with surface field values of about 35 v/cm. The lightning was triggered at the much higher altitude of about 6400 ft with a field change indicating that excess positive charge was removed in the stroke. The weather situation of mixed phase convective cells imbedded in stratiform decks was very similar to that in which the majority of non-thunderstorm strikes occur to aircraft.

HIGH ALTITUDE MEASUREMENTS

A statistical analysis of the ratio of aircraft lightning strikes to the overall number of strikes associated with the storm while the test aircraft was in the cloud was presented by Fitzgerald (3). The data taken at altitudes from 10,000 to 29,000 ft indicated an average probability of 2% hits in a sample of 1554 strikes. In two of the storms this probability increased to 100% and 50% respectively. Subsequent analysis of the cloud electric field components, and of the field due to charge accumulation on the aircraft, indicates that the strikes on these two days occurred when the aircraft had been flying in a general area of positive charge above negative and as it was entering a small area of reversed polarity. If one accepts the hypothesis that the aircraft charge is predominately the same as that of the excess particle space charge impacting on the aircraft, the strikes occurred in or on the boundary of an intense negative space charge cell at flight level which was adjacent to a considerably less intense zone of excess positive space charge. The general nature of these charge areas can be seen from the E_q trace shown in Figure 1 for a traverse at 27,000 ft. An 8-12 micron radiometer profile of the cloud top temperature as measured by U-2 aircraft is superimposed on the trace to indicate approximate storm dimensions. The transition zone from the positive to negative space charge is seen from reference to the accelerometer trace to be in a smooth part of the cloud preceding the region of maximum up and down motion.

In this instance, the peak nose boom current was +5800 amp, indicating electron flow away from the boom. A nose boom photograph indicates a number of luminous points on the top of the boom suggesting the leaders were connecting with positive charge concentrations above the aircraft. Film from the other probes was inadvertently lost in processing. Magnetic tape playback of the electric field records indicates on the E_z vertical field channel that an overall excess positive charge was removed during the transient interval of about 0.3 sec. Three or four partial discharges of each polarity seem to have been involved. The initial E_z field breakdown produced a field change at the aircraft of 1670 v/cm as seen in the top E_z trace of Figure 1. The aircraft charge-E_q-displays a complex pattern. Initial displacement was positive going, followed by three steps in the negative direction, and then by three larger positive going steps.

This case, and another on 3 August in which strikes were obtained on three successive passes, were associated with storms that had been in existence for some time and whose precipitation radar echoes and draft structures were weakening with time. Another strike on 6 August was encountered in a weak downdraft region on the edge of a vigorous updraft in a rapidly developing storm. It also occurred in a small excess negative charge center generally similar in appearance to the case illustrated. The vertical and horizontal field structure was more complex, but again the strike was associated with the field transition from a positive to negative charge overhead as on 12 August.

Another example of the concentrated negative space charge area is shown in the lower portion of Figure 2 for a traverse at 29,000 ft through an oceanic thunderstorm located about 50 miles off Cape Kennedy. The low value of E_z suggests that the aircraft passed through the vertical center of the negative charge zone. In this case no lightning occurred. The draft calculation shows little or no vertical motion at the location of this electrical charge center. Further review of data on other days with lightning strikes to the aircraft indicate a generally similar pattern to that described above. It now seems likely that further detailed analysis of each cloud traverse will lead to a reasonably systematic cloud structure model for aircraft triggering of lightning strikes and will permit a considerable refinement in probability estimates for strike likelihood in specific cloud conditions.

The upper portion of Figure 2 illustrates that the lightning strike problem can not be restricted to low and intermediate flight levels. The flight track of an instrumented U-2 aircraft

around the dome of a large Florida storm is seen in the upper right corner. The dome is located in the area above the letter N. The vertical and horizontal field components measured along the track are shown in the upper left. The E_y trace indicates excess positive charge in this dome with the lightning transients removing portions of the excess charge. The E_z trace shows excess positive charge below the aircraft as it moves from SSE to NNW and a reversal to excess negative charge below after the northernmost point of the flight track. An intense localized positive charge center was found at this point. The insert shows some partial breakdown activity in the center, followed by the lightning. The horizontal component of field change was somewhat larger than the vertical component. In this case, the free air temperature was -68° C and the altitude about 50,000 ft.

SUMMARY

Recognition and possible avoidance of cloud areas of potential lightning activity is a desirable goal for aerospace vehicle operations. This paper has illustrated and discussed several instances of rocket and aircraft-triggered lightning events. Post-flight analysis indicates that the Apollo 12 vehicle was launched into a cloud system from which several natural intra or inter-cloud lightning events had occurred. The resultant transfer of four to eight coulombs of charge is characteristic of lightning. A surface field value of about 35 volts/cm was associated with this launch. The in-cloud breakdown occurred at 6400 ft vehicle altitude. This event may be contrasted with the over-water small rocket launch data which suggests surface fields of about 175 volts/cm were associated with successful lightning initiation when the rocket and trailing wire were only a few hundred feet above the LTRI ship.

The electrical and meteorological data obtained during thunderstorm passes with the "Roughrider" F-100F aircraft indicates a systematic relation between initial peak current polarities measured on the aircraft and the cloud electrostatic field orientation. Nose boom and vertical fin sensors generally indicated electron currents away from the aircraft toward an upper positive charge region. Wing tip currents were the reverse, indicating a flow from a lower negative charge area. If the overall field was inverted, a reversal in aircraft currents was observed.

Most of the lightning strikes to the aircraft occurred in a transition zone from positive over negative charge to negative over positive. These transitions are closely associated with the precipitation and draft structure of the cloud. The very rapid recovery of the field near the aircraft in contrast to the relatively slow recovery as measured by another aircraft outside the cloud indicates that somewhat distant charge centers rather than the space charge near the aircraft were predominately discharged in the stroke.

It is believed that aircraft interception or near approach to high charged precipitation streamers is an important factor in triggering lightning strokes through the aircraft to charge cell concentrations. It has been shown that these concentrations are not restricted to low altitudes, but can also be found very near tops of active convective towers and associated anvils.

ACKNOWLEDGEMENTS

Data acquired for this work was obtained with aircraft and technical support of AFCRL Project 8620 by ASD, AFFTC, and ESD, in cooperation with AFWL, Sandia Laboratories, FAA, and LTRI personnel and programs.

REFERENCES

1. B. J. Petterson and W. R. Wood, "Measurements of Lightning Strikes to Aircraft." Final Report to Federal Aviation Agency under Contracts FA65WA1-94 and FA66NF-AP-12, January 1968.

2. D. R. Fitzgerald, "USAF Flight Lightning Research" Proceedings, Lightning and Static Electricity Conference, 3-5 December 1968. Technical Report AFAL-TR-68-290, Part II, pp 123-134, May 1969.

3. D. R. Fitzgerald, "Probable Aircraft Triggering of Lightning in Certain Thunderstorms." Monthly Weather Review, Vol 95, December 1967, pp 835-842.

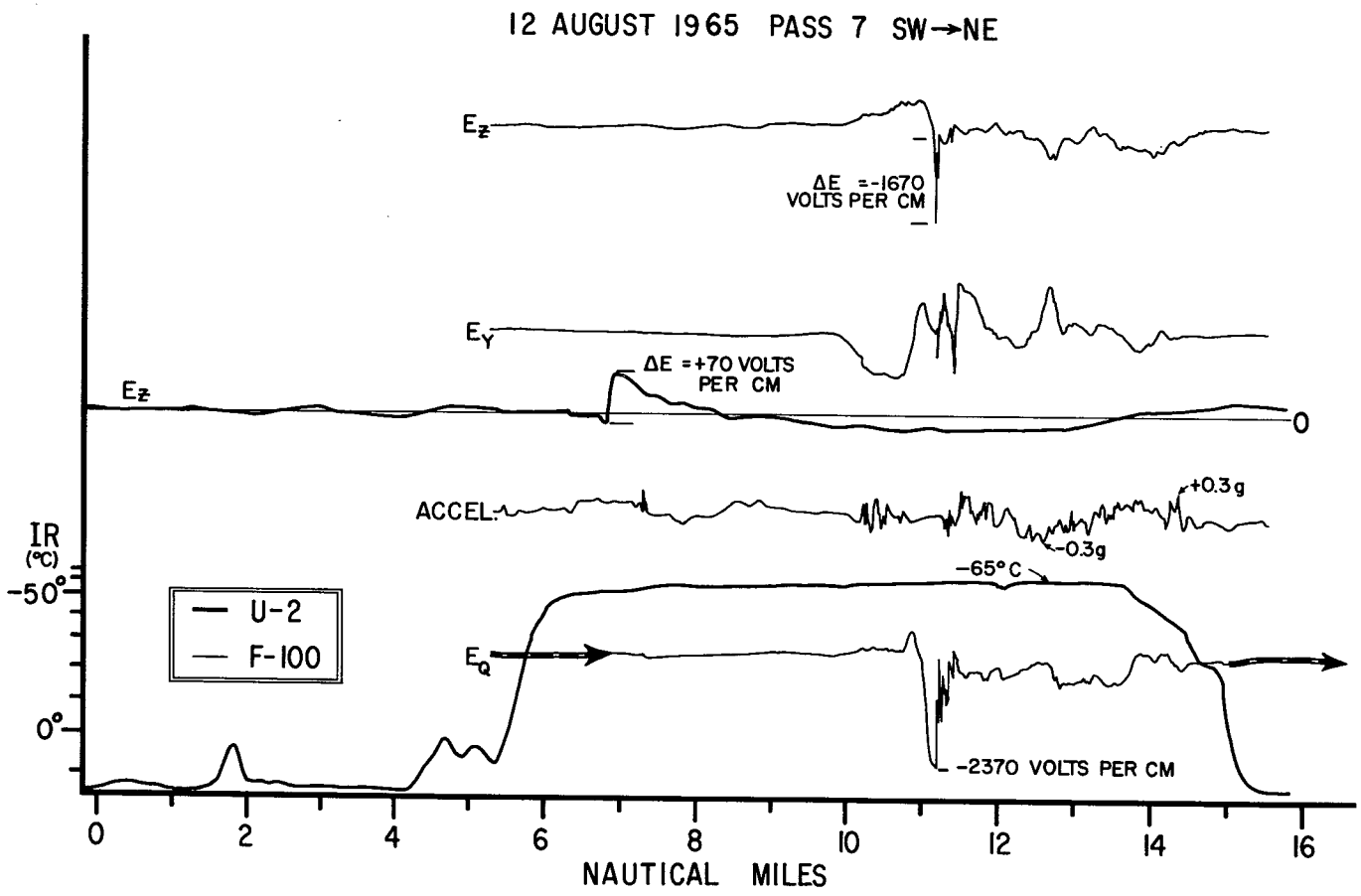

Fig. 1 - Electric field and lightning strike data 27,000 ft aircraft altitude.

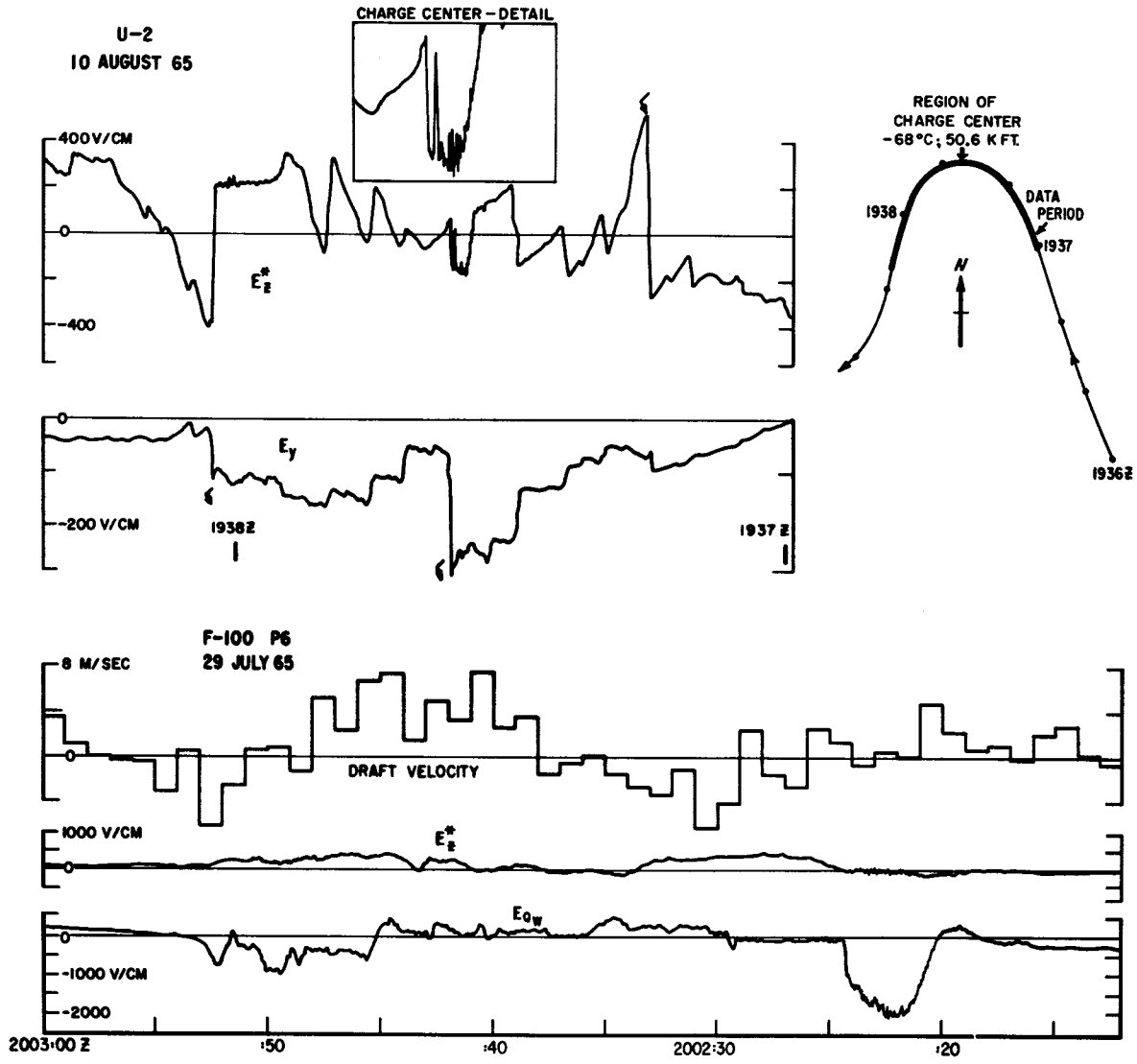

Fig. 2 - Negative charge center at 29,000 ft and positive center at 50,000 ft.

700914

ROCKET AND SUPERSONIC AIRCRAFT INFLUENCE IN TRIGGERING LIGHTNING AND INTENTIONAL CLOUD DISCHARGE TRIGGERING FOR LAUNCH PROTECTION

M. M. Newmann and J. D. Robb

Lightning & Transients Research Institute

(Paper not submitted for publication. For reprints, contact the author or the Society of Automotive Engineers directly.)

700915

MODEL STUDIES OF STROKE PROBABILITY TO SELECTED POINTS ON AEROSPACE VEHICLES

J.R. Stahmann
Lightning & Transients Research Institute

THE GENERAL METHOD OF ESTIMATING the probability of lightning stroke contact to various points on an aerospace vehicle, by the use of simulated lightning discharges to a model of the vehicle, requires the selection of a number of positions for the high voltage probe tip relative to the model. The distance between the probe and the model is usually measured from the center of the model and generally corresponds to the minimum distance at which the probability distribution does not change significantly as the distance is increased. To make the number of probe positions used in a general study manageable, the probe positions are usually uniformly distributed in 15° increments in the yaw, pitch and roll planes, Figure 1. The probability of stroke contact to a particular point on the vehicle, such as a wingtip, is then computed as the number of strokes contacting that point divided by the total number of strokes used, assuming a uniform distribution of approach angles. For a more detailed study, additional probe positions in a plane at 45° to the yaw and pitch planes have been used, Figure 2. With the additional plane, about 66 discharges are typically required for a general study of a model, not including those probe positions that are redundant due to symmetry. The general study provides an estimate of the probabilities of stroke contact to the major extremities of the vehicle, such as its wingtips, nose, fuselage, vertical and horizontal stabilizers, etc.

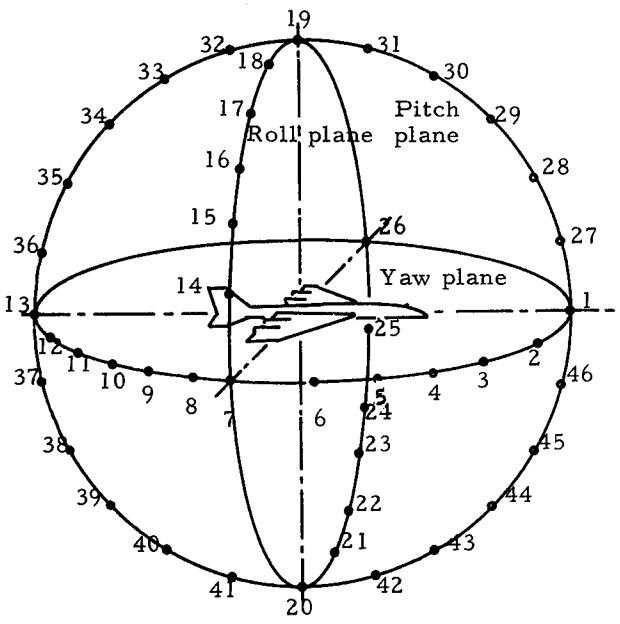

Figure 1. Sketch of yaw, pitch, and roll plane discharge probe positions at 15° increments.

ABSTRACT

About sixty-six uniformly spaced fixed probed positions are usually used for a general study to determine the probability of lightning stroke contact to various points on a complete aerospace vehicle. More detailed studies are usually considered prohibitive because of the large number of discharges required.

For estimating very low probability of contact for detailed studies of critical regions, probe positions can be restricted to the small solid angle from which contact is possible. Then, with a relatively small number of probe positions and enough discharges to measure statistical variations, a very low probability can be estimated with a limited number of discharges, typically about thirty.

Occasionally it may also be important to estimate the probability of stroke contact to points where the probability is very low. Such points may be partially shielded such as the leading edge of a wing at the root, which is shielded by the nose and wingtip in the yaw plane. These regions might be considered for possible location of lightning vulnerable fuel vents, antennas or other equipment, if the probability of stroke contact can be shown to be very low. The standard general probability study may not include any of the probe positions from which a stroke might approach to contact the selected point on the vehicle. Expanding the number of probe positions used in the general study sufficiently to measure low probabilities would be prohibitive. For example, for a measurement sphere radius of one meter, a probe position for every square inch of surface area would be of interest. It is also desirable to repeat discharges from the same probe position, to obtain as much statistical data as possible.

If the probe positions are restricted to only a small region on the surface of the measurement sphere from which direction stroke contact to the selected shielded point is possible, the desired probability can be estimated with a limited number of measurements, typically about 30 strokes. Only a few probe positions are required, allowing enough discharges for a study of statistical variations.

As an example, consider the wing leading edge root of an aircraft having swept-back wings. As a first step, initial streamering studies are carried out, arresting the streamers in time before they can meet to form a stroke. The lengths of the streamers help reveal the regions of low probability of strike contact at a glance, using only a few discharges. As can be seen in Figures 3 and 4, the stroke probability is greatest at nose and wingtip with a lower probability in between. The region just forward of the root of the wing leading edge evidently has a very low probability of initial stroke contact as indicated by the "dark space", Figure 4, in this region. The probability appears so low that only contact by strokes sweeping into the region need be considered. However, strokes to the nearby region on the leading edge of the wing near the root, Figure 5, are close to the shielded region and the probability of stroke contact here can be measured by the technique described in this paper.

As a lightning stroke leader approaches an aerospace vehicle in flight, the field strength near the surface of the vehicle increases until it becomes high enough to cause corona and streamering. The stroke leader then joins one or more of the vehicle streamers and continues on its way to ground or to another charged cloud region with the vehicle as part of its path. The distance from leader to vehicle at which streamering begins is estimated to average about 50 meters, corresponding to an average leader

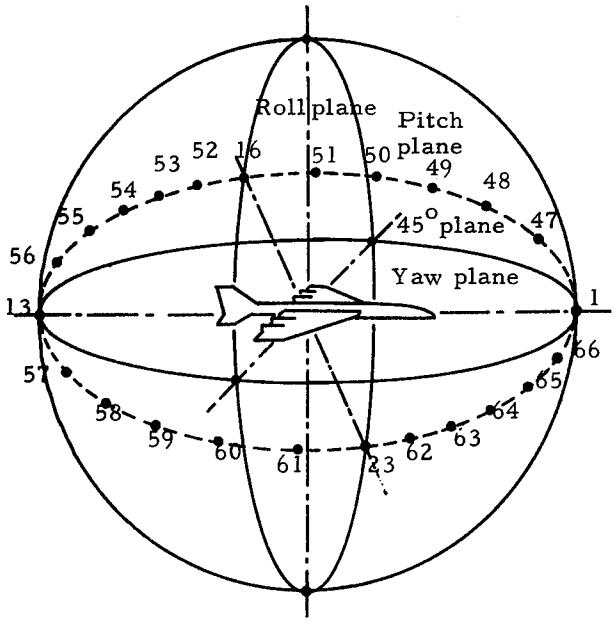

Figure 2. Sketch of 45° plane discharge probe positions at 15° increments.

Figure 3. Arrested streamering between nose and wingtip of model for leader approach in the yaw plane. Points of highest stroke contact probability are nose, wingtip and leading edge of the wing root.

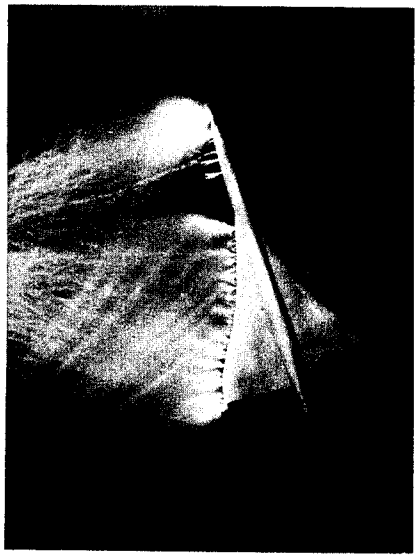

Figure 4. Arrested streamering, similar to that shown in Figure 3 above, but showing a corona free "dark space" on the fuselage, just ahead of the leading edge of the wing root.

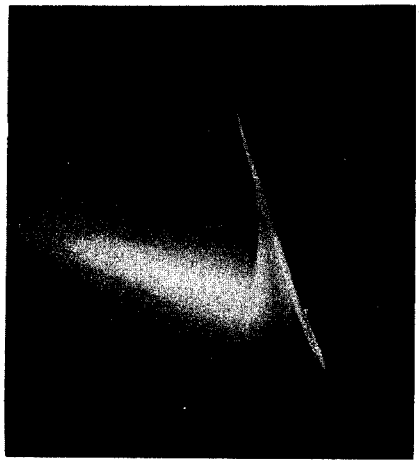

Figure 6. Typical stroke contact to model near wingtip. Competing streamers are also visible.

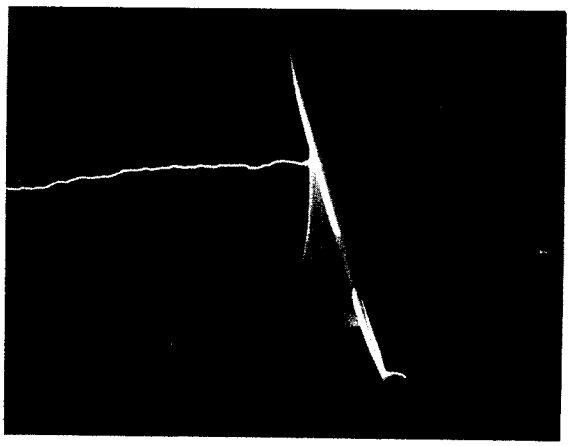

Figure 5. Typical stroke contact to wing root leading edge of model.

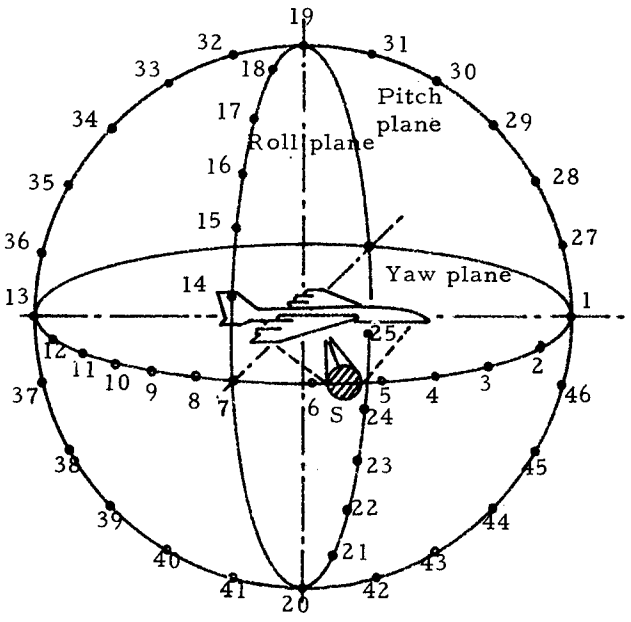

Figure 7. Small surface area, S, on the surface of the measurement sphere from which strokes to the leading edge of the wing root can be directed with a measurable probability of contact.

step length and to the scaled minimum probe distance required in model studies for good correlation with flight data. For a 1/40 scale model, the 50 meter distance would be simulated by a probe spacing of 50 inches. The probe can then be positioned in the small region on the surface of the measurement sphere whose boundary is determined by those probe positions where 100% of the strokes go to nonroot points, such as to a wingtip, Figure 6, or nose. The small surface area of probe positions, S, usually not circular, from which the wing root leading edge might be contacted, is illustrated in Figure 7. This area, divided by the total surface area of the measurement sphere and multiplied by average probability, measured in S for leading edge root contacts, gives an estimate of the total probability of strokes to the selected point. By symmetry, this probability can be doubled to take into account the other wing.

The average probability of wing root leading edge contact by leaders directed from region S, for the model shown in Figures 4-6, was estimated as 10^{-4}, using only about 30 discharges and three probe positions, about an inch apart in region S. For other points of low stroke contact probability on models of aerospace vehicles selected for special study, a region S, corresponding to the worst angles of stroke approach for the selected point, can usually be found and the probability of contact quickly measured.

700916

Lightning and Static Hazards Relative to Airworthiness

B. L. Perry, B.Sc.(Eng.), C.Eng., M.I.E.E., A.F.R.Ae.S.
Air Registration Board

ABSTRACT

The paper updates, and briefly extends, the statistical information on lightning strikes to aircraft given in the author's 1968 paper. The problems and potential dangers of both lightning strikes and static build-up on aircraft are discussed and illustrated with particular reference to airworthiness. Conclusions are drawn regarding problem and potential problem areas where further information is required and towards which research effort should be directed.

In the light of the above, current and future airworthiness requirements are considered.

IT IS THE AIM of airworthiness authorities to lay down requirements which can, by guidance, warning, or, if required, legal force, ensure that during the design of an aircraft, all reasonable steps are taken to prevent hazardous situations occurring in flight. In the lightning and static field this presents problems, since when dealing with these natural phenomena it is difficult to quantify the actual risk, although attempts are made in the relevant requirements to give practical guidance. For example one aircraft may fly for years without being struck by lightning, another of the same type flying in the same airspace, may be struck several times in as many days and still not be damaged, a third may be struck once only and yet be severely damaged. Is it reasonable then to require that on all aircraft design steps be taken to cover such an unpredictable hazard?

It is then this necessity to determine what are reasonable requirements which dictates the need for the airworthiness authorities to keep abreast of and, if possible, ahead of the current and potential problem areas. Some of these problems, in both the lightning and static areas, are discussed later, and in the light of these the current airworthiness codes are reconsidered.

ANALYSIS OF LIGHTNING STRIKE REPORTS

At the December 1968 Lightning and Static Electricity Conference the writer presented summarised data on lightning strikes which had been collected with the co-operation of several British airlines (1)*. Since that time collection of data has continued for the VC10 aircraft and commenced for the BAC 1-11 aircraft. Tables 1, 2 and 3 present this information in the same form as previously, but they now cover Viscount, Vanguard, Comet 4B, Trident, BAC 1-11, Britannia, Boeing 707 and VC10 aircraft. These tables cover varying periods for each aircraft from 1959 to date and the recordings were obtained for over two million flying hours, during which over seven hundred strikes were recorded, a further 120 strikes being added since the last report.

The particularly high incidence of strikes on the BAC 1-11 aircraft as recorded in Table 1 is worthy of note. Of the 72 strikes recorded 52, or 70%, occurred while the aircraft was flying to or from Berlin. Since the Berlin air corridor is only 10,000 feet high it is to be expected that the aircraft would be exposed to a greater risk than aircraft which are free to fly at higher altitude and hence above thunderstorm activity. Reference to Figure 2 shows that 68% of all strikes can be expected below 10,000 feet. During May 1969 thunderstorm activity was recorded for 26 days out of 31 and during this month this particular aircraft type was struck 15 times while flying on the German routes. Thus the particular route, combined with a month of high thunderstorm activity, accounts for the high incidence of strikes on this particular aircraft.

The total incidence of strikes given in Table 1 has been modified to include the new BAC 1-11 and additional VC10 reports. The former has, perhaps unfairly as explained above, loaded the European rate, but in general terms an average of one strike per year still appears as a typical figure.

No significant changes have been made either to the type of damage data given in Table 2, or the position of strikes given in Table 3, as a result of the additional reports now included.

Figures 1 and 2 show the percentage of strikes relative to outside air temperature and altitude respectively and these have been modified to include the recent data. While no significant changes have resulted, the slight

*Numbers in parentheses designate References at end of paper.

Table 1 - Incidence of Lightning Strikes Relative to Aircraft Type, Zone of Operation and Flying Hours

Type of Aircraft	Zone of Operation	Period Covered	No. of Strikes	Total Flying Hours	Incidence of Strikes
Viscount	Europe	March 1959 to June 1964	195	567000	1/2900 hrs
Vanguard	Europe	May 1961 to June 1966	79	194000	1/2500 hrs
Comet 4B	Europe	June 1960 to June 1966	86	162000	1/1900 hrs
Trident	Europe	May 1964 to June 1968	92	140000	1/1400 hrs
BAC 1-11	Europe	January 1969 to April 1970	72	56000	1/780 hrs
Britannia	World-Wide	October 1959 to April 1961	6	115000	1/19000 hrs
Boeing 707	World-Wide	January 1962 to December 1967	103	458000	1/4400 hrs
VC 10	World-Wide	August 1964 to June 1970	75	361000	1/4800 hrs
Total	Europe	-	524	1119000	1/2100 hrs
Total	World-Wide	-	184	934000	1/5100 hrs
Total	Europe and World-Wide	-	708	2053000	1/2900 hrs

Table 2 - Damage Caused to Aircraft by Lightning Strikes Relative to Aircraft Types

Type of Aircraft	Period Covered	No. of Strikes	Damage Caused		
			Hole in Structure or Radome %	Slight Damage %	No Damage %
Viscount	May 1961 to June 1964	92	39	42	19
Vanguard	May 1961 to June 1966	79	30	52	18
Comet 4B	May 1961 to June 1966	72	35	25	40
Trident	May 1964 to June 1968	90	11	57	32
BAC 1-11	January 1969 to April 1970	72	18	67	15
Boeing 707	January 1962 to December 1967	96	17	50	33
VC 10	August 1964 to June 1970	75	20	49	31
Total	-	576	24	49	27

increase in the number of strikes above 18,000 feet does emphasize that thunderstorm activity can and does occur at high altitudes.

The position of the strikes recorded on the BAC 1-11 aircraft is shown pictorially in Figure 3. It is particularly interesting to note the way strikes have, in some cases swept right along the fuselage, confirming the

Table 3 - Positions of Lightning Strikes on Aircraft Relative to Aircraft Type

Type of Aircraft	General Area Struck: Axial - Nose, Fuselage, Tail End, including Fin, Rudder and Elevators % of Total Recorded Damage	General Area Struck: Transverse - Wing Area including Propellers, Nacelles, Flaps and Ailerons % of Total Recorded Damage
Viscount	65	35
Vanguard	77	23
Comet	80	20
Trident	75	25
BAC 1-11	72	28
Britannia	64	34
Boeing 707	75	25
VC 10	76	24
Total 'Straight Wing'	69	31
Total 'Swept Wing'	74	26

contention that the whole of the fuselage should be considered as a Zone 2 or swept stroke area. It is also of note that two strikes have been reported inboard of the wing tips. No previous reports of strikes in this area have been recorded in the data covered by this report.

It is proposed to continue recordings of strikes on aircraft in airline service along the lines detailed above and as in the writer's previous paper. Of particular interest will be the data collected on aircraft of significantly different aerodynamic size or shape, such as the Boeing 747 and the Concorde.

PARTICULAR PROBLEMS DUE TO LIGHTNING STRIKES

It is not proposed in this section to review completely the ways in which strikes can hazard the aircraft. It is however desirable to emphasize the areas where the use of new materials or construction techniques, or particular circuit designs can open up new problems. Some of these are discussed below. It is interesting to see how much the future safety of aircraft in this particular field is dependent on the understanding of the problems by the structural engineer. In the past the lightning problem has been emphasized both in the electrical and fuel systems spheres, it is now essential that the structures and materials engineers are aware of how much they are involved.

STRUCTURES AND MATERIALS - The effect of large currents on the mechanical strength of the composite boron and graphite filament materials was discussed at the December 1968 Lightning and Static Conference (2), (3), (4). Since that time research work has continued both in the USA and in Britain. It is not the object of this paper to discuss the detail of the tests, but there is no doubt that these results will have to be considered in great detail when such materials are used for load bearing members in civil aircraft, or in the construction of components particularly liable to lightning strikes, such as propellers.

The effect of lightning strikes on composite materials involving perhaps metal skins with metal honeycomb, or metal skins with plastic honeycomb or even plastic skin with metal honeycomb, should be tested prior to flight. Such structures, used, for example, in helicopter rotor blades or flying control surfaces, may fail in a disastrous way when subjected to a heavy current flow. With the number of variables involved such as material types and thicknesses, the effect of bonded joints, etc., then it is not adequate to estimate the effects - testing is essential.

The problems of radomes are well known and that of the particularly long radome used on the Concorde was discussed in Reynold's paper (5) in December 1968. Figure 4 shows high voltage tests in progress on the radome of the production aircraft. These, combined with high current testing, are an essential tool to ensure the adequacy of protection on such large non-metallic structures.

With the increasing use of non-metallic materials for the surfaces of portions of the wings and fuselage on aircraft, the inherently safe "Faraday Cage" effect is being reduced, with perhaps, a concentration of current in the limited metallic structure remaining. At what stage such a use of non current carrying materials becomes a safety problem is difficult

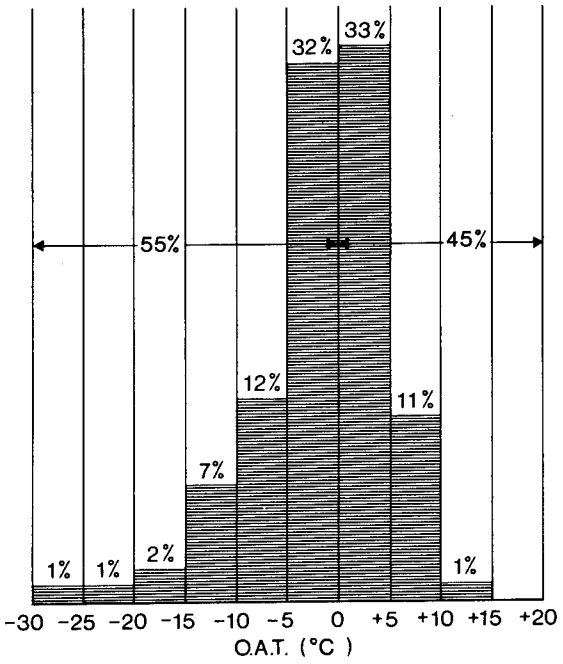

Fig. 1 - Distribution of lightning strikes relative to temperature - Viscount, Vanguard, Comet 4B and BAC 1-11 aircraft.

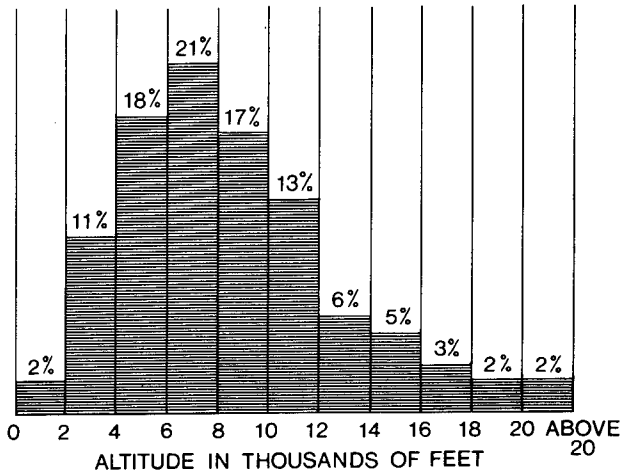

Fig. 2 - Distribution of lightning strikes relative to altitude - Viscount, Vanguard, Comet 4B, Trident, BAC 1-11, VC.10 and Boeing 707 aircraft.

to predict, but it is vital that the designer be aware of the possibilities and that the overall safety situation be watched. In this respect the work being carried out by Plumer (6) on induced voltages is of great interest.

EFFECTS ON ELECTRICAL CIRCUITS - In reference (6) induced voltage effects on electrical circuits are considered. Similar work is in hand in Britain also. With the increasing use of semiconductor devices and low signal level circuits the hazard of such induction coupling effects cannot be ignored. With the use of larger areas of non metallic surfaces the inherent cage effect of the present aircraft, flying in airline service, is reduced, with large currents flowing in perhaps more discrete paths. The effects of such changes on devices with low voltage breakdown levels or in signalling circuits with low current levels must be assessed. It cannot now be assumed that since all was well in the past that it will continue that way in the future.

Perhaps measurements of a similar nature have already been undertaken on the complex circuits used in rocket and satellite engineering. If so, these results would be of great interest to the aircraft engineer.

FUEL SYSTEM HAZARDS - In the past, much emphasis has been placed on the various hazards associated with lightning and fuel ignition. It is to be hoped that the lessons of the past will now be reflected in the future good design of such items as fuel tank access panels, vent pipe location and adequate skin thickness in areas subject to lightning strikes. As mentioned above the effects of induced voltages into the electrical systems associated with fuel systems must also still be considered. It is not proposed here to consider the FAA's decision to require the fitment of fuel inerting systems to the tank and associated fuel, or vapour carrying, pipes of larger aircraft, to prevent ignition from lightning or other sources. This has been discussed in great detail at another conference. It is the opinion of the ARB however that the fitment of such a system should not preclude the continuance of good design practices in the areas of hazard discussed. Such good design will, of course, be particularly vital in the large number of aircraft which will still be flying without inerting systems.

HAZARDS ASSOCIATED WITH STATIC ELECTRIFICATION

The various methods by which an aircraft in flight becomes charged are well known and well documented. It is sufficient to say that the phenomenum is unavoidable on a commercial aircraft and some of the effects, particularly on communications or navigation equipment or aircraft electrical circuits, can be a source of very real danger.

COMMUNICATION AND NAVIGATION EQUIPMENT - The importance of both communication and navigation equipment in the safe operation of aircraft cannot be over emphasized. Such aids need to operate intelligibly and reliably at all times and under all weather conditions. They are of particular importance under bad weather conditions, a time during which static effects may well be at their worst.

Of particular importance therefore is the correct choice of type and location of antenna and since this can well have structural effects on the aircraft, it must be taken into account at an early stage of the aircraft design.

Suppressed antenna in locations remote from direct impingement and located so as to minimise coupling from other corona generating areas can

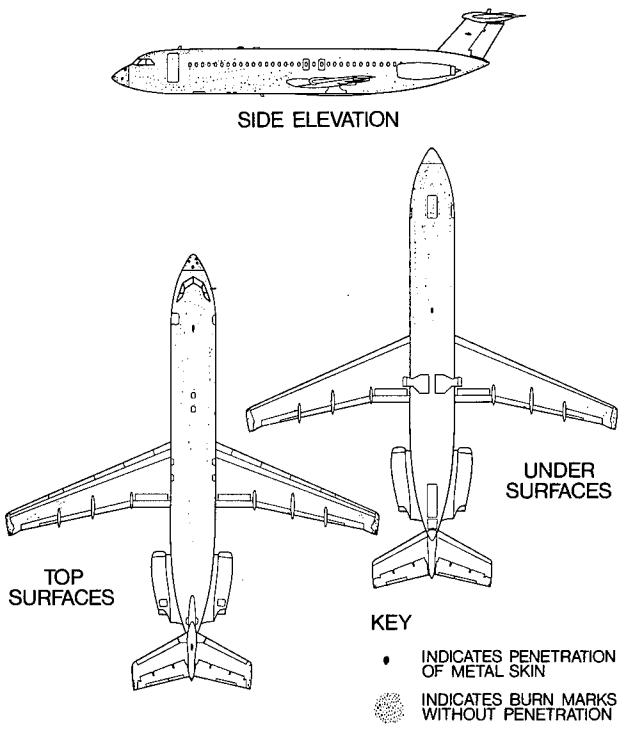

Fig. 3 - Position of lightning strikes on BAC Super One-Eleven aircraft - January 1969 to April 1970.

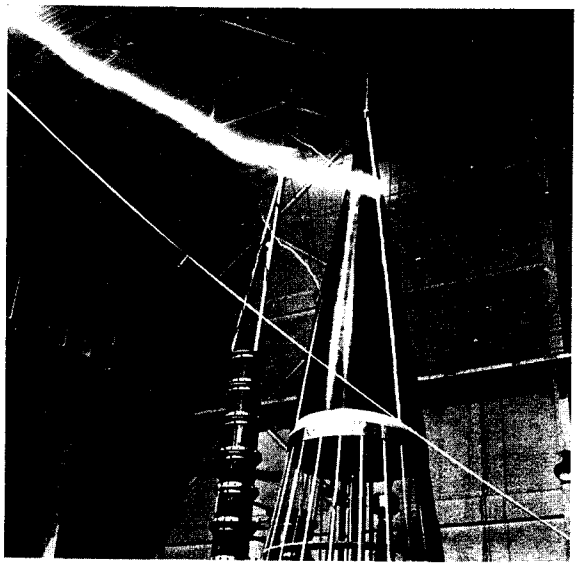

Fig. 4 - High voltage tests on the radome for the Concorde aircraft.

provide a partial cure. The correct location of properly designed static dischargers is also essential on most aircraft, as is the treatment of non-conducting surfaces with semiconducting finishes to reduce build-up of static charge. Research is continuing in the UK into the properties of aircraft paint finishes with respect to their properties under conditions of static electrification.

The implementation of all the above features plus the use of correct equipment bonding techniques has been found essential in some applications and when problems arise after the design and construction of an aircraft is completed this can prove both a long and expensive exercise. Navigation equipment is now available which is designed with static problems in mind and which is capable of dependable operation at low signal to noise ratios.

From the point of view of safety, all these techniques must be considered and implemented at the design stage to ensure an adequate level of performance for equipment vital to safe operation of the aircraft. In the extreme, perhaps active discharges will be necessary in some particularly difficult cases.

EFFECTS ON ELECTRICAL CIRCUITS - as discussed above, the use of semiconductor devices which are susceptable to damage from voltage surges, raises again the potentially dangerous effects on aircraft systems and equipment due to the charging up and surface flash over, of areas connected into the aircraft electrical system, such as windscreens. Figure 5, taken from Sharp's paper (7), illustrates the magnitude and duration of such a surge. Many cases have already been reported of damage to switchgear and transformers, and to semiconductors associated with generator control, due to these voltage surges. Both glass and plastic screens seem to be equally liable to such static surface build-up and until such a time as a suitable transparent, conducting surface can be developed which can stand erosion and the action of the windscreen wipers, then similar problems will occur. Where the increased susceptibility of components and systems to such effects can cause a safety hazard, then it is essential that safety measures be taken in the design of the systems to prevent such damage occurring.

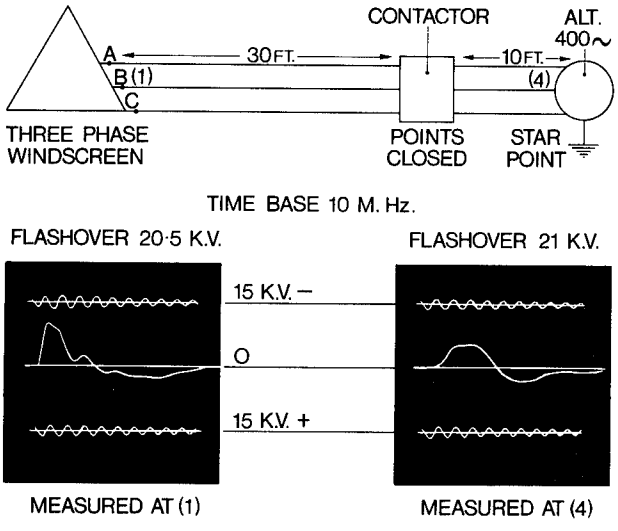

Fig. 5 - Typical power line voltage pulses; approximately 20 kV windscreen external surface flash.

ELECTRO-STATIC EFFECTS ON FUEL - The phenomenum of fuel charging due to its flow through pipes and filters and also spray effects are well known and well detailed in, for example, an NRCC paper (8). While of particular concern during high rate re-fuelling on the ground, the in-flight effects of large quantities of fuel being transferred for centre of gravity control or during fuel jettisoning is not to be ignored. Combined with good design practices, such as grounding of all equipment and the use of conducting pipe lines and hoses, then the world wide use of fuel anti-static additives would provide a worthwhile increase in safety.

THE AIRWORTHINESS REQUIREMENTS

In the face of all these known and potential problems where do the requirements stand? The relevant portions of the Federal Aviation Regulations Parts 25 and 23, and 27 and 29 (9) and British Civil Airworthiness Requirements, Sections D, K and G (10) for aircraft above and below 12,500 lbs and for rotorcraft respectively, are, it is hoped, well known to all concerned. For the Concorde, the Anglo-French Supersonic Aircraft TSS Standard No. 8-0 (11), represented, it was hoped, the latest experience and thinking of all the American, French and British industry. In spite of this it is still found necessary to have Advisory Circulars, Special Conditions for certain aircraft and applications, and Civil Aviation Circulars covering problem areas. The writer is currently involved with rewriting the relevant sections of BCAR (Sections D4-6 and K4-6) and has already found it necessary to modify the requirements given in the recent TSS Standard due to advances in the state of the art, both as regards new materials, and the effects on modern equipment.

A plea has been received from the British Industry, and it is suspected that a similar situation exists in the USA, for guidance on the measures required to protect an aircraft against the effects of static and lightning. While it is not the function of the airworthiness authorities to produce such a document, guidance is often provided in the requirements on methods of design which will provide an acceptable means of compliance with the actual requirements. If such a design guidance document were produced, and it is difficult to envisage who would undertake such a mammoth task, then it too would inevitably suffer from the same problem as the airworthiness requirements, and require continual up-dating. Nevertheless it is suggested that the proceedings of this and the previous conference could provide the basis for such a guidance document. Certainly a vast amount of information is available in these documents and a precis of this would be most useful.

It is suggested that the present situation is in fact acceptable, as far as the airworthiness codes are concerned. Such codes will of course require revisions and at times special conditions and requirements will have to be produced before such amendments can be made. As long as the actual requirements and any special conditions are administered in a technically reasonable fashion, then no major problems should occur. It is the sharing of knowledge, experience and problems at international conferences such as this and the previous conference held in 1968, which provides the airworthiness authorities with the necessary background to make such reasonable decisions as are required to ensure an adequate level of safety. Inevitably particular problems will receive special emphasis from certain authorities at certain times, but this should not seriously upset the overall balanced judgment.

CONCLUSIONS

That there are problems concerning both static and lightning which have major effects on aircraft design is now generally accepted. That these problems can be met at the design stage and adequate safety levels produced at a reasonably economic cost is the aim of all concerned. Such an aim will only be met with continued application of the lessons already learnt and continuing research into new problems as these become apparent.

The airworthiness requirements will require revision as the knowledge concerning new techniques and problems increases but this should not preclude the implementation of increased safety requirements before they become part of the relevant code.

ACKNOWLEDGMENTS

The help and co-operation given by the airlines and their staff in the recording of the data given in this paper is gratefully acknowledged. The author thanks the Air Registration Board for permission to publish this paper and his colleagues within ARB for their help in its compilation. Thanks are also due to the many members of the British aircraft industry for the provision of information and data used in this paper.

REFERENCES

1. Perry B.L. 'British Researches and Protective Recommendations of the British Air Registration Board.' Lightning and Static Electricity Conference, Miami, December 1968.

2. Kelly L.G. and Schwartz H.S. 'Investigation of Lightning Strike Damage to Epoxy Laminates Reinforced with Boron and High Modulus Graphite Fibers.' Lightning and Static Electricity Conference, Miami, December 1968.

3. Robb J.D. 'Mechanisms of Lightning Damage to Composite Materials.' Lightning and Static Electricity Conference, Miami, December 1968.

4. Fassell W.M., Penton A.P. and Plumer J.A. 'The Susceptibility of Advanced Filament Organic Motrix Composites to Damage by Simulated Lightning Strikes.' Lightning and Static Electricity Conference, Miami, December 1968.

5. Reynolds S.T.M. and Newman M.M. 'LTRI - Industry Co-operative Program Research on the Concorde SST.' Lightning and Static Electricity Conference, Miami, December 1968.

6. Plumer J.A. 'Lightning Induced Voltages in Electrical Circuits Associated with Aircraft Fuel Systems.' FAA Fuel System Fire Safety Conference, Washington, May 1970.

7. Sharp P.J. 'Static Electrification of Electrically Heated Aircraft Windscreens.' Aircraft Engineering, July 1969.

8. Bruinzeel C., Luttik C., Vellenga S.J. and Gardner L. 'A Study of Electrostatic Charge Generation during Low Temperature Refuelling on Aircraft.' National Research Council of Canada, October 1963.

9. Federal Aviation Regulations, Parts 23, 25, 27 and 29, Department of Transportation, Federal Aviation Administration.

10. British Civil Airworthiness Requirements, Sections D, K and G published by the Air Registration Board.

11. Supersonic Transport Aircraft, TSS Standard No. 8-0 Issue 2, dated July 1969, Electrical Bonding and Lightning Discharge Protection, published by the Air Registration Board.

700917

RECENT DEVELOPMENTS IN LIGHTNING PROTECTION FOR AIRCRAFT AND HELICOPTERS

J. D. Robb
J. R. Stahmann
M. M. Newman

Lightning & Transients Research Institute

LIGHTNING PROTECTION for aircraft has developed into a new science which although not yet fully organized and established, has made available a wide variety of lightning protection techniques for nearly all types of current aircraft. Although some questions remain to be answered in regard to the characteristics of the natural lightning discharge, the extensive amount of lightning protection in present use has demonstrated that effective protection can be provided without unduly penalizing aircraft designs through excessive weight or cost if adequate testing is carried out. However, the use of new materials and the more critical function of the new electronic systems in future aircraft has suggested a re-evaluation of the basic lightning test criteria, through a more precise definition of effects in light of present knowledge.

Presented in this paper are discussions of the lightning discharge current components and their specific effects including particular consideration of (1) swept stroke effects which have recently become of greater interest because of the trend toward thinner skin materials and new alloys as well as the increasing use of composites and (2) methods of determining the external electromagnetic fields about aircraft as an aid in estimating surge penetration. The above topics are applicable to all types of aircraft; in addition some problems specifically related to helicopters are discussed including consideration of all plastic blades.

LIGHTNING STROKE COMPONENTS - A suggested matrix of the natural lightning discharge components and their effects is presented in Table I. As illsutrated in Table I, the discharge may be arbitrarily separated into six different types of components of the natural lightning discharges in terms of specific damage effects. These include:

a. High voltage effects - puncture of dielectric materials from the extreme potentials of the natural lightning discharge.

b. High voltage (or electric field) rate of change effects - induced streamers capable of producing electrical circuit malfunction and puncture of dielectrics such as radomes accompanying direct or nearby strikes.

c. High current effects - magnetic force, sparking of joints in the lightning current path, resistively coupled voltage into electrical circuits and shock waves from the lightning discharge arc from the initial high current "return stroke".

d. High current rate of change effects - induced voltages in electrical circuits from the steep front of the return stroke.

e. Intermediate current effects (more typical of cloud to cloud discharges) more slowly rising pressures and metal "puncture".

f. Long duration, low current effects - metal erosion. The continuing components of natural lightning discharges of about 100 amperes which may last for nearly one second.

ABSTRACT

The testing of aircraft components for new aircraft has introduced problems in trying to meet the specifications with new materials and construction techniques. Suggested is a more detailed analysis of the lightning characteristics in order that tests may be more precisely defined for specific aircraft components as illustrated in swept stroke studies. Of increasing concern is the performance of more vulnerable electronics systems for new aircraft, and guidelines are developed for simple calculation of approximate electric and magnetic fields to determine pulse penetration into the vehicle electrical and electronic systems. Requirements for testing of all plastic helicopter blades are also suggested.

Table I

Lightning Current Components and Effects

Effects	High Voltage	Fast Field Change	High Current	Fast Current Change	Intermed. Current	Long Duration Current
Dielectric Puncture	X	X				
Electrical Surges	X	X	X	X		
Magnetic Forces			X			
Sparking of Joints			X			
Shock Waves			X	X		
Slow Rising Pressures					X	
Metal Puncture					X	
Metal Erosion						X

g. Multiple components effects - which may include up to 30 restrikes in a single discharge lasting up to 3/4 one second.

h. Effect of stroke sweeping on all of the above.

It should be emphasized that Table I is not necessarily comprehensive and represents an arbitrary division of components and effects. However, there are few observed lightning damage effects which would not be included in the table based on LTRI records of lightning damage to aircraft.

It may be seen that generally only one or two components are significant for any particular type of damage. Thus, if the significant lightning current component can be correctly identified for testing of the particular component or material and correlated with stroke probability and sweeping effects, tests can be made which more truly represent natural lightning.

Thus the important sweeping action of the stroke over fuel tank walls as illustrated in Figure 1 should be considered in the evaluation of lightning hazards and protection. Studies by Boeing and by LTRI (under the LTRI Aircraft Industry Cooperative Program) (1, 2, 3) have shown that probably the key factor, which determines stroke "hang-on" (dwell time) and the amount of charge transfer which may act at any single location on an aircraft (not at a trailing edge) is the specific aircraft skin material and surface coating.

SWEPT STROKE STUDIES

LTRI swept stroke studies have been continued to study the effect of paints which are being used increasingly in wing tank areas to inhibit corrosion.

Records of lightning strikes to aircraft show near midchord holes in a wingtip which require charge transfer of the order of 500 coulombs to duplicate in the laboratory. The present FAA Advisory Circular AC 20-53 which indicates the need for fuel tank components to withstand 500 coulomb discharges is apparently based on this type of strike report. However, it is also apparent in LTRI laboratory tests that many fuel tank component designs proposed for use on future aircraft would not withstand charge transfers of this magnitude without recognition of the more realistic sweeping effects.

In the evaluation of sweeping effects, the time-current waveforms of natural lightning discharges must be considered. As illustrated in Figure 2 and Table I, there are three basic types of current waveforms which could possibly produce punctures. These include (1) the initial high current return stroke characterized by very high currents and very short time durations, (2) the cloud to cloud discharges for which there is less information, but which appear to be of intermediate amplitude and intermediate duration, and (3) the long duration components of relatively low current, of about 100 amperes.

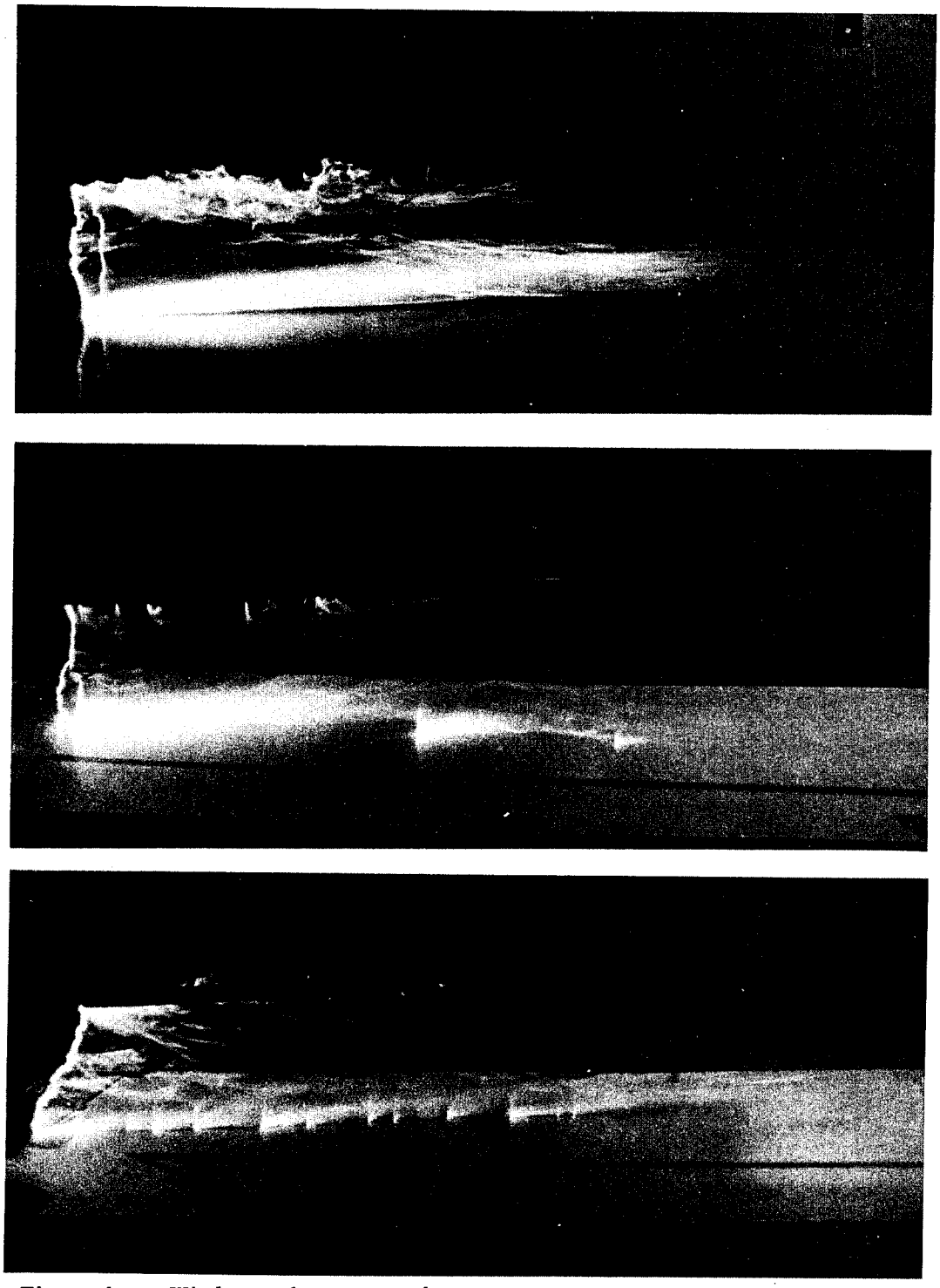

Figure 1. Wind tunnel swept stroke tests with various paint surfaces. Discharge hangs on at one point to transfer total charge - poor (top), re-establishes at two additional points - fair (middle) and re-establishes every few inches - good (bottom).

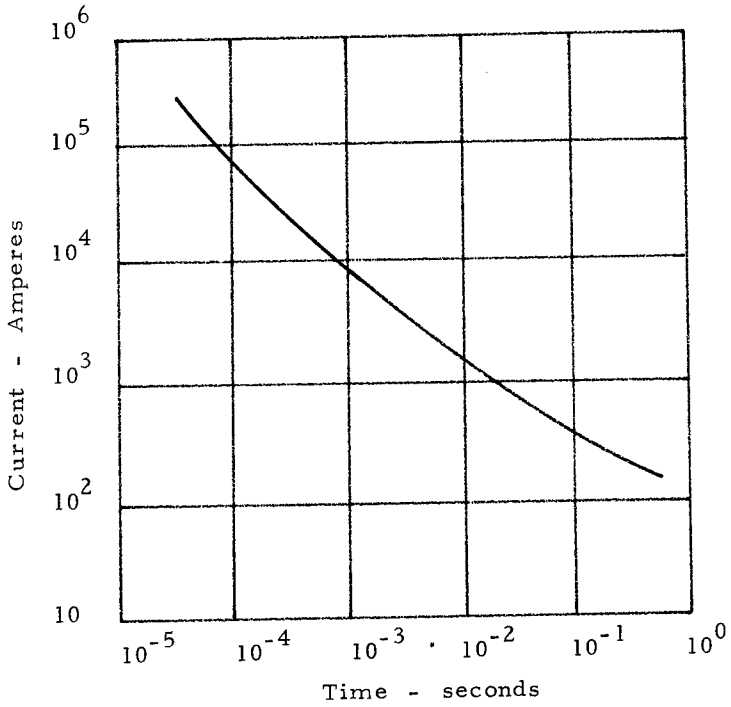

Figure 2. Envelope of probable maximum time-current waveforms for natural lightning components.

Simulated lightning tests of skin materials have indicated that the high current surges in the natural lightning "return stroke" do not produce much penetration of the skin. There appears to be a pseudo skin effect not completely comparable to electromagnetic skin effect which confines most of the energy to the skin surface through melting of the surface layer of metal. Thus, even maximum currents of 200,000 amperes produce little penetration, although they may produce some mechanical damage of the skin in terms of dents from the shock waves and magnetic force effects. The little data available on inter-cloud and intra-cloud lightning strikes from flight research programs and strike reports from the commercial airlines do indicate lower rates of rise, intermediate current magnitudes and intermediate durations, as indicated in area B of Figure 1. The long duration components shown as area C in Figure 2 with currents of only about 100 amperes can produce most of the charge transfer by virtue of the extended time duration. Components A and B because of their short time durations are not severely effected by the sweeping motion of the wind stream over the aircraft surfaces as the arc travel is rather short during this limited time duration. Thus for stroke sweeping effects, the long duration components are of most interest and even here as long as the stroke keeps moving the total amount of charge transfer at any location is relatively small.

What is of primary concern in relation to heating or burning of fuel tank walls is any factor which would stop the stroke movement and cause it to remain at a single location. As has been indicated in earlier LTRI papers, the basic mechanism in establishing and re-establishing the channel at a new location down stream from an earlier strike point is the potential drop along the plasma channel which has to be sufficient to spark over the gap existing between the stroke channel and the skin. Any insulation over the skin such as some high quality paint greatly increases the voltage drop along the channel required to puncture to the skin. Because the voltage is a function of the channel length the distance is increased between contact points along with the time duration of the stroke on any single location. The contact of the down stream portion of the channel with the skin is also affected by the plasma instabilities of the arc which move it around considerably and by the boundary layers which determine how close the channel is spread out over the surface of the skin.

In summary, the short duration high current components do not produce much penetration of fuel tank skin by virtue of a pseudo skin effect, and the intermediate duration discharges are of too short a duration to be spread much by the discharge (this is not to imply that they cannot be a hazard) but the long duration components can be moved considerable distances and the degree to which they fail to re-establish contact along the skin as the discharge is moved determines the amount of charge transfer of any single location and the extent of the metal erosion and pitting.

The results of these initial studies have indicated that stroke concentration effects would be severely altered by aircraft paints. Thus, a study has been undertaken to determine the effects of the typical paints and to determine if special paints could be selected or developed which would enhance stroke movement over the skin to minimize metal erosion and pitting. The initial results have shown stroke concentration effects with typical paints such as polyurethanes, epoxys, and acrylics. For example, a 0.08 inch skin generally accepted throughout the industry (not necessarily by LTRI) as an acceptable skin thickness for withstanding lightning strikes was pitted to a depth of over 50 mils with a discharge of only 16 coulombs in contrast to bare skins which show very light pitting as illustrated in Figure 3. The 50 mil deep pit mark indicates that a slightly greater discharge could have punctured the skin. The results of these tests are shown in Table II and the criteria specified include both the number of pit marks indicating the individual charge concentrations and the hang-on or dwell time. The results of the tests indicate that the alodyne surface was by far the best except for bare aluminum and that the standard aircraft paints such as polyurethanes and acrylics and epoxys do severely inhibit stroke movement and do concentrate the stroke pitting.

One other approach to the problem of protecting thin fuel tank skins in swept stroke areas is the use of insulating materials. By providing bare metal stroke hang-on electrodes at the trailing and leading edges of a fuel tank section and insulation over the tank area, the discharge can be made to sweep over the critical area. This approach requires further

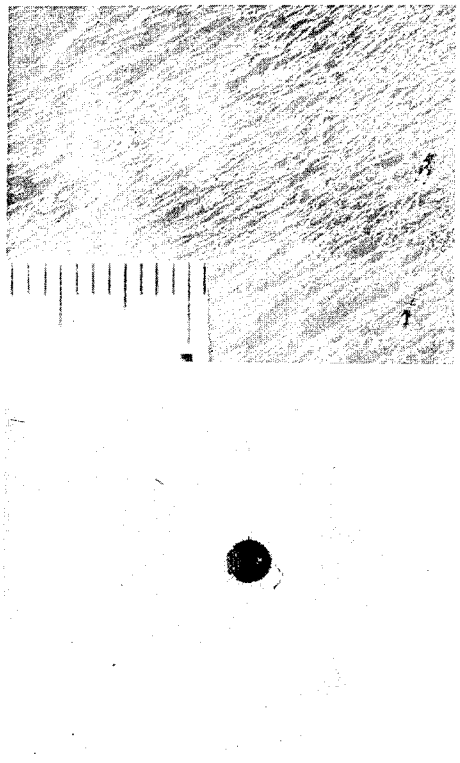

Figure 3. Swept stroke on bare aluminum (above) produces shallow pitting. Pitting on painted surface is 1/8 inch in diameter and 0.050 inches deep.

Table II

Stroke Hang-on (Dwell Time) Distances and Times for Aluminum Test Samples with Various Finishes

(Air Velocity 150 mph)

	No. of Pit Marks on 5' Panel	Maximum Pit Spacing	Time Duration Millisec
1. Alclad	29	3 1/2"	1.5
2. Alclad	41	5 3/4"	2.5
3. Alodyne	325	5 1/2"	2.4
4. Anodize	75	4 3/4"	2.0
5. Iradite	73	4 3/4"	2.0
6. Polyurethane	2	Nearly full panel - 50"	20
7. Acrylic	6	12"	5.1
8. Epoxy #1	2	Nearly full panel - 50"	20
9. Zinc Chromate	14	13"	5.5
10. Acrylic Silver Additive	14	6"	2.6
11. Epoxy Silver Additive	28	5"	2.1
12. Epoxy #2	6	19 1/4"	8.3
13. Epoxy #3 Conductive Additive	8	19" max.	8.1

studies as to the insulation required to withstand possible mid tank area restrikes and streamer puncture from nearby or direct strokes.

The general conclusion drawn from the studies appears that either paint should be deleted in areas of thin fuel tank skins or that specific preparation should be made in the area of thin skins which are painted to provide adequate lightning protection in view of the stroke concentration effects of the paint. The effects of the paint appear to be both 1) the restriction of plasma in stability induced lateral movement as well as 2) the holding of the stroke contact point in spite of a 130 mph windstream tending to move it down stream.

It is clear that unpainted polished aluminum surfaces such as used by some airlines would be far better than a painted surface and would permit a thinner fuel tank skin thickness for the same degree of safety as the present 0.08 inch skin painted.

However, in some cases where present paints are considered unavoidable (because of severe corrosion problems for example) a special stroke guidance strip to keep the discharge on the outside of the paint and keep it moving was found to be fairly effective as long as the strip was aligned with the airflow.

Tests similar to the wind tunnel tests were carried out using rotating discs for simulating the windstream and they essentially confirmed the results of the wind tunnel tests on identically coated samples. The wind tunnel tests appeared to give better information regarding hang-on (dwell time) and the movement of the discharge in the direction of airflow whereas the rotating disc types permitted better evaluation of the lateral motion of the channel and the local plasma instability effects. The paint restricts the movement of the plasma channel in two ways, both in the reestablishment of the channel downstream in a new location and also in restricting the lateral movement of the channel which is normally produced by the plasma instability effects, the snake-like motion of the channel which tends to distribute the energy over the area of several inches width.

In summary the swept stroke studies of the lightning current effects on aircraft skin materials present a good example of how a more detailed study of individual component effects may permit a more effective aircraft design. It should be emphasized that present wave test forms are not considered to be too severe in general as there is ample evidence of aircraft damage pitting of such magnitudes but rather that careful selection of a more realistic test can be made without penalizing the design with over severe current waveforms.

One approach to the problem of specifications has been to throw the burden of proof on the manufacturer to demonstrate that the test being substituted for the standard specification is truly an adequate test. This places a penalty on smaller companies without adequate facilities capable of determining or proving their tests are sufficient. What is apparent however, is that where meeting the present specifications results in unacceptable weight penalties for advance designs, more detailed consideration of the significant effects of the particular lightning components on that particular aircraft part may permit an acceptable lightning protection design.

TECHNIQUES FOR EVALUATION OF ELECTROMAGNETIC FIELD COUPLING INTO AIRCRAFT ELECTRICAL SYSTEMS

It has been verified experimentally and theoretically that the aircraft skin provides an excellent electromagnetic shield for the effects of natural lightning discharges and that little current penetrates the aircraft from natural lightning because of skin effect (4, 5). It should be noted that even though these residual magnitudes are fairly low, with the greatly increased sensitivity of some electronic equipment coming into current use, these residual currents and voltages may still be significant. It was suggested, however, that the principal problem is major entry of voltages and currents through the "electromagnetic windows" such as navigation lights, antennas, etc. This may occur through direct stroke contact to exposed wiring in which case large energies may penetrate the vehicle or may occur through electromagnetic field coupling. Some simple approaches are suggested for evaluating these magnitudes as a function of individual component geometries.

Evaluation of the electromagnetic fields outside the aircraft which are important in relation to induced surges in exposed electrical wiring (such as that exposed by extension of high lift devices), permits intelligent design through selection of optimum wiring geometrical configuration. One of the most readily available techniques and simplest for this purpose is the use of the electrolytic tank. Sections of an aircraft or a small model of an entire aircraft, as illustrated in Figure 4, may be submerged in the conducting electrolyte which is generally tap water, a 400 hertz voltage of perhaps 10 volts is applied to the model and the equipotentials are plotted using a vacuum tube voltmeter or oscilloscope. The use of a 400 cycle voltage source and an oscilloscope permits easy identification of 60 cycle stray fields which can produce obvious large errors.

With this technique and sequences of models of various scales, the detailed structures of the electric field about any external aircraft component can easily be determined. This permits the estimation of cross field and aircraft self-charging potential thresholds which can produce corona or streamer formation on specific components such as fuel vents or antennas. The electrolytic tank may be combined with other techniques such as mathematical analysis for shapes which are mathematically describable, i.e., spherical, cylindrical or ellipsoidal

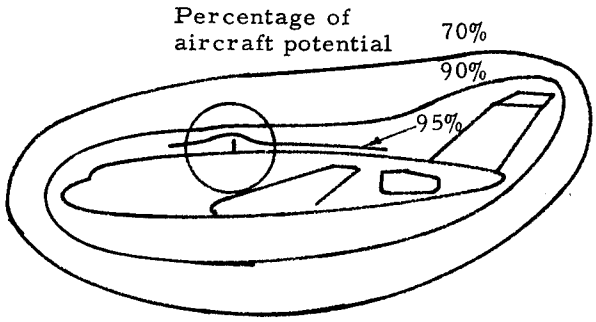

Figure 4. Electrolytic tank plot about model presents free space equipotential structure.

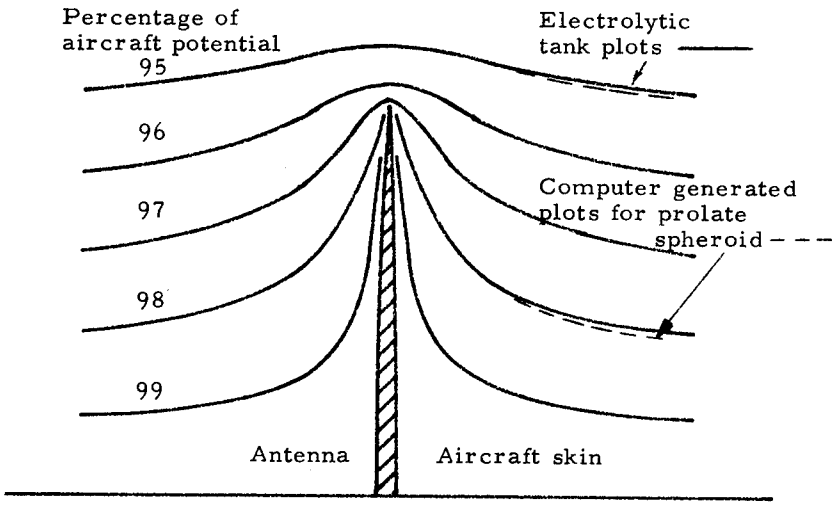

Figure 5. Electrolytic tank plots of small aircraft model and full scale model of antenna permit determination of tip electric field and ionization threshold.

shapes for example, for which the partial differential equations can be explicitly "solved". Generally, the solutions to the partial differential equations are tabulated for these common geometries and it is primarily a matter of selecting the suitable coordinates to fit the particular component geometry. Numerical methods adaptable to computer solutions can also be used for slightly more complex component shapes. It should be noted, however, that in spite of the power of modern digital computers there are still none available which are practical for solution of electric fields existing about a structure as complex as a complete aircraft. For example, with as large a machine as the CDC 6600, an aircraft can be represented only by a series of cylinders for the fuselage wings, engine nacelles, etc. (6). While such approximations are adequate for predicting antenna patterns, they are totally useless for evaluation of electric fields both gross and local. Thus the electrolytic tank represents a fairly effective method for determining quite accurately the electric fields existing on any part of the aircraft. It permits, for example, easy correlation between fields on the aircraft on the ground and in flight for calibration of electric field meters.

As a hypothetical example, consider the evaluation of the ionization threshold of a simple rod type aircraft antenna, as illustrated in Figure 5. An initial electrolytic tank plot of a small model of the aircraft would be used to determine an equipotential surface fairly close to the antenna being studied as shown in Figure 4. A second model would be used with an intermediate scale of perhaps one-quarter full size to permit the selection of a second equipotential surface close to the antenna using the first equipotential surface as the positive electrode. The second and third stages of the plotting can sometimes be eliminated by using numerical techniques or by using the exact solutions of the fields existing about an equivalent geometrical form which is explicitly soluble as suggested above. For example, by selecting a spheroidal coordinate with a suitable fineness ratio corresponding to the antenna tip radius and a second equipotential surface from the previous electrolytic tank plot corresponding to one of the theoretical equipotential surfaces about the prolate spheroid, a good estimate of the electric field can be determined and with this information the actual threshold potential on the aircraft in megavolts which would produce initial ionization on the tip of the antenna can be determined as well as the thunderstorm electric cross fields required for initial ionization.

With this technique, quantitative quality factors can be assigned to specific components. This permits a direct quantitative comparison between two specific installations in terms of the threshold ionization potential in megavolts or the threshold thunderstorm cross field in terms of volts per meter.

Evaluation of magnetic fields outside the aircraft for estimating the coupling into wiring is somewhat more difficult but simplifying assumptions may be made which permit rapid but approximate evaluation of voltage coupling into externally exposed wiring. The externally exposed wiring may not be physically exposed on the outside of the aircraft as it may be covered by plastic doors or aerodynamic fairings.

In this approach the sections of the aircraft are approximated by two geometrical shapes, one a cylinder representing the round surfaces such as fuselages, engine nacelles, etc., and a second section of two parallel planes representing a central area of wings or tail wings and a single number may be obtained which usually gives within less than one order of magnitude a quick estimate of the magnetic field existing external to the aircraft and the associated voltage coupled into wiring for a specific lightning current magnitude, as illustrated in Figure 6. For a cylindrical conductor, the theoretical magnetic field intensity about the conductor is equal to

$$H = I/2\pi r$$

where H = magnetic field, I = total current and r = radius of the cylinder.

The linear current density on the skin assuming a uniform distribution about the periphery is equal to the current divided by the circumference or again

$$J = I/2\pi r$$

where J = surface current density amps/meter thus

$$H = J$$

Thus, the magnetic field intensity is equal to the surface current density. From the Maxwell integral equation, it is known that the voltage induced in a loop is equal to the flux rate of change through the loop. (Lenz law)

$$V = \oint \vec{E} \cdot \hat{dl} = \frac{\partial \varphi}{\partial t}$$

φ = A (Area) x B (flux density)

$B = \mu H$

$\varphi = A \times \mu H$

$$V = A\mu \frac{\partial H}{\partial t} \simeq A\mu \frac{\Delta H}{\Delta t}$$

$A = 1$ meter^2 (assumed)

$\mu = 1.26 \times 10^{-6}$ (permeability of free space)

$t = 10^{-6}$ sec (assumed steep wave)

Therefore

$V = 1.2 \times J$ in amps per linear meter of skin surface.

Assuming a steep rise of one microsecond we may see that the voltage induced per square meter of external loop area is approximately equal to the local current density. Thus for a local current density of 10,000 amperes per linear meter a voltage of 10,000 volts would be induced in a one meter loop or would be in direct proportion to the loop area. For a flat section such as a wing as illustrated in Figure 7 it may be shown that the magnetic field intensity is equal to half the current linear density increasing to somewhat greater than the average at the trailing and leading edge spars.

For a typical example of a 125,000 ampere severe lightning strike along a fuselage with a diameter of four meters, the field would be equal to $I/2\pi r$ or approximately 10,000 ampere turns per meter. For this value an external loop such as a wire running parallel to the fuselage externally with a one meter loop meter area, would have induced 10,000 volts.

With this simple approach the voltage induced in external wiring can be simply calculated. Calculate the peripheral length of the section, divide into the total current and with this value and the loop area, calculate the induced voltage. What is more difficult to calculate is the voltage induced in wiring running more deeply buried inside the leading and trailing edge sections. A calculation of the voltages coupled in such wiring requires either numerical computer techniques or model studies using impulse currents.

LIGHTNING PROTECTION FOR HELICOPTERS

A very limited amount of lightning protection development has been carried out for helicopters. Early helicopters have been relatively simple vehicles which have been intended for visual flight regulations (VFR) operation. However, with the greatly extended use of helicopters the trend is toward more instrument flight regulations (IFR) operations under which lightning strikes become much more probable.

As it appears at the present time that lightning strikes can neither be avoided nor prevented, experience indicates that reliance must be placed on a certain amount of lightning protection.

Helicopter blades represent one of the most probable strike points on a helicopter and as such require careful consideration of lightning protection requirements. Lightning strokes to helicopter blades can produce serious damage from internal arcs whether channeled into the blade interior through blade tip lights, anti-erosion cuffs, trim tabs, control rods, or other metallic components and damage can be produced in either metal or plastic blades. The general approach for either type of blade is, therefore, to keep the lightning currents on the outside where the damage is minimized. If currents do pass through the blade interior it must be assured that they carry maximum currents without serious damage or hazard to the blade. This means that the use of adhesive bonding for adjoining metallic skins through blade sparks or trailing edges must be carefully checked. Also protection must be provided to prevent lightning discharge currents from peeling the metal skin away from the points where the wind stream can possibly amplify the effects. It should also be noted that the worst sources of precipitation static radio interference are caused by electrically floating metallic sections particularly if they are in areas directly contacted by atmospheric particles such as dust and snow. Thus any protection conductors in the form of metal strips or coatings must be tested to assure continuity under all flight conditions.

The use of all plastic blades introduces a serious potential problem which must be carefully considered. It has been demonstrated in the laboratory with early experimental blades that high current discharges can completely break up a blade. The key factor is whether the discharge initiates through the inside of the blade or over the exterior. The quality of fiberglass material is rapidly improving to the extent that all plastic blades appear feasible and it has been demonstrated in limited cases, that the discharges will always take place over the exterior for small sections. What has to be determined with all plastic blades is whether or not high voltage long arcs will pass span-wise through the blade interior. This is determined both by the dielectric strength of the material and also by the joints which are generally of low dielectric strength as well as by the geometrical configuration of the blade hub and tip as illustrated in Figure 6 where streamer initiation will take place under the influence of the approaching natural lightning step leader.

Thus in summary helicopter rotor blades must be designed and tested to insure that either lightning discharge currents will pass harmlessly over the exterior surface or that if they do penetrate the blade interior the currents will carry out any damage to the blade. All plastic blades appear to be feasible from the lightning protection point of view, however, such blades should be tested with chord-wise and span-wise discharges to assure that no discharge will take place through the inside of the blade to produce damage.

CONCLUDING COMMENTS

Performance of tests to governmental specifications on current and new aircraft have indicated that careful analysis of natural lightning discharge components would permit more precise definition of tests with resultant more economical and effective design for lightning protection. This has been demonstrated in lightning swept stroke studies which indicate that some skin materials and coatings are much more vulnerable to lightning damage than others.

Because of the increasing concern with electromagnetic penetration into electronic and

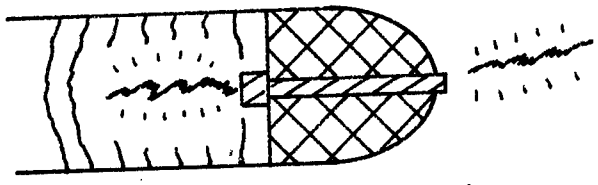

a) Tip with enclosed metal part or air space permits streamer to initiate and produce interior explosion.

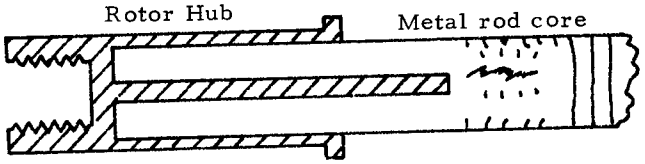

b) Hub design with buried metal permits streamer initiation inside blade.

Figure 6. All-plastic blades with tip or hub design having interior metal or air space permits initiation of interior streamers which can result in severe blade damage or break-up.

electric systems, some guidelines have been developed as an aid in determining surge penetration into aerospace vehicles. Analysis and tests of all plastic helicopter and VTOL blade designs have indicated that such designs are probably feasible from a lightning point of view. Careful testing is required using high voltages and full size blades for span-wise puncture tests.

For such tests plastic blades should have previously been humidity cycled in view of the severe effects of absorbed moisture on high voltage characteristics.

REFERENCES

1. M. M. Newman, J. D. Robb, J. R. Stahmann, and L. A. Boehland, "Test Instrumentation for Studies of Swept Lightning Discharges over Aircraft Fuel Tank Skin Materials," L&T Report 495, Quarterly Report to Air Force Avionics Laboratory, Contract F33615-68-C-1534, Nov. 1968.

2. R. O. Brick, "A Method for Establishing Lightning-Resistance/Skin-Thickness Requirements for Aircraft," Proceedings of the Lightning and Static Electricity Conference, USAF Avionics Laboratory and SAE, Miami, Dec. 1968.

3. M. M. Newman, J. R. Stahmann and J. D. Robb, "Airflow Velocity Effects on Lightning Ignition of Aircraft Fuel Vent Efflux," Final Report to Federal Aviation Agency under Contract FA66WA-1486, July 1967.

4. M. M. Newman, J. R. Stahmann and J. D. Robb "Interference Fields About Aircraft", L&T Report 275. Final Report to USAF Avionics Laboratory under Contract AF-18(600)-183, June 1954.

5. J. D. Robb and J. R. Stahmann, "Lightning Surge Current Hazards to Semi-Conductors and Electroexplosive Systems", Paper presented at the 5th Symposium on Electroexplosive Devices (EED's). The Franklin Institute Research Laboratories, June 13, 14, 1967, Philadelphia, Pa.

6. R. L. Tanner, M. G. Andreasen, "Numerical Solution of Electromagnetic Problems", IEEE Spectrum, pp. 53-61, Sept, 1967.

SESSION 1B

STATIC ELECTRICITY AND INSTRUMENTATION TECHNIQUES

Organizer - J. E. Nanevicz

Stanford Research Institute

Chairman, J. E. Nanevicz

700918

LIGHTNING TEST FACILITIES MEASUREMENT TECHNIQUES

J. D. Robb
Lightning & Transients Research Institute
R. F. Huber
Joslyn Manufacturing & Supply
C. J. Kawiecki
Joslyn Electronic Division

ALTHOUGH HIGH CURRENT MEASUREMENT TECHNIQUES are well documented in the technical literature, there exists little guidance on the practical problems of making current measurements in the strong field environment associated with 200,000 ampere test currents used for the lightning testing of aircraft components. This paper describes the simplified high current generator types used for developmental testing of aircraft components along with the discussion of the measurement devices and the specific techniques required to obtain measurements in the strong electromagnetic field environment without introducing large errors. These techniques permit aircraft company engineers who have set up small artificial lightning generation facilities to make accurate measurements of the current amplitudes and waveforms.

HIGH CURRENT GENERATORS USED FOR AIRCRAFT COMPONENT TESTING

High current generators used for lightning simulation are essentially large moderately low inductance capacitor banks. With linear circuitry (simple combinations of R, L, and C), the maximum current can most easily be obtained by minimizing R and L using undamped oscillatory waveforms.

Some simple relationships may be derived which are useful in evaluating surge current and voltage generator requirements. The current in an R, L, C circuit is:

$$i(t) = \frac{E_o \epsilon^{-\frac{R}{2L}t} \sin 2\pi ft}{\sqrt{LC}} \qquad (1)$$

Where:

E_o = voltage on capacitor
L = inductance
C = capacity
R = resistance
f = resonant frequency
t = time

It should be noted that Marx impulse voltage generators, sometimes used in small facilities (a type of generator in which capacitors are charged in parallel and discharged in series), may also be treated approximately with the following equations even though they should be treated rigorously as multi-stage iterative circuits.

The maximum current in an R, L, C circuit is approximately:

$$I_{max} = E_o / \sqrt{L/C} \times \text{quarter cycle decrement}$$

and the stored energy (W) in the capacitance is equal to

$$W = 1/2CE^2_o \qquad (2)$$

It may be shown that the maximum current is related to the stored energy and inductance by:

$$I_{max} = \sqrt{2W/L} \qquad (3)$$

Also it may be shown for a given configuration the maximum current rate of change, di/dt:

$$di/dt = E_o/L \qquad (4)$$

and the rise time to (1 - (1/e)) or 63%

ABSTRACT

The increasing use of small artificial lightning generation facilities for developmental testing of aircraft components by the manufacturer has required the measurements of the test currents in the presence of the strong electromagnetic fields associated with the high current discharges. Special techniques are presented for the set up of the facility high current paths and for the use of measurement equipment such as the oscilloscopes and high current sensors to assure that reasonably accurate measurements of the current waveforms are obtained.

$$t_r = \frac{2L}{R}$$ for an overdamped wave (5)

$$t_r = \frac{1}{4f_o}$$ quarter cycle time for an oscillatory wave (6)

With these relationships the approximate requirements for impulse current generators may be quickly obtained.

From the above relationships it might be concluded that a given group of capacitors should always be connected in parallel. However, because of specific waveform requirements such as MIL-B-5087B, series-parallel arrangements are often necessary. Multiple connections, preferably widely spaced, should be used to minimize inductance which, as indicated, is generally the limiting parameter in obtaining maximum currents.

A graph of capacity and energy versus inductance for obtaining a 200 kiloampere current is shown in Figure 1. We may see that the energy size of a linear generator required to reach 200,000 amperes, with an optimum capacitor arrangement discharging into a 100 microhenry total load such as a complete aircraft, would be about 2 megajoules. It also may be seen from Figure 1 that it requires only 8 microfarads with an inductance of one-half microhenry to produce 200 K.A. Thus, with careful connections using a few high energy capacitors, an economical bank may be set up to produce the 100,000 to 200,000 ampere currents in small components such as fuel tank filler caps or access doors which are generally of low inductance. This approach is the basis for the artificial lightning generator facilities recommended by LTRI for use by aircraft manufacturers in routine testing of aircraft components to determine their vulnerability to lightning discharge currents. With their small energy and generally non-specification waveforms, the small banks do not generally permit qualification of the components to military of FAA specifications but they do permit inexpensive high energy developmental testing of small components.

For producing steep fronted waves with fairly high energy such as specified in MIL-B-5087B, the required energy is very much greater. The energies required to produce a 1 x 50 microsecond waveform (1 microsecond to crest, 50 microseconds to half value) using linear circuit components, i.e., simple combinations of capacitors, inductors and resistors, are presented in the top curve of Figure 2. Also shown for comparison are the energies required to reach 200 kiloamperes with optimum capacitor arrangement (lower curve) also shown in Fig. 1.

It should be emphasized that this discussion applies only to simple linear circuits and that by using non-linear elements or multiple generators connected to produce combined waves, much less energy would be required as indicated in the middle curve of Figure 2. For example, a high current rate of rise generator can be used to produce the initiating fast rise current and through the use of isolation spark gaps and inductances, the high current generator can be

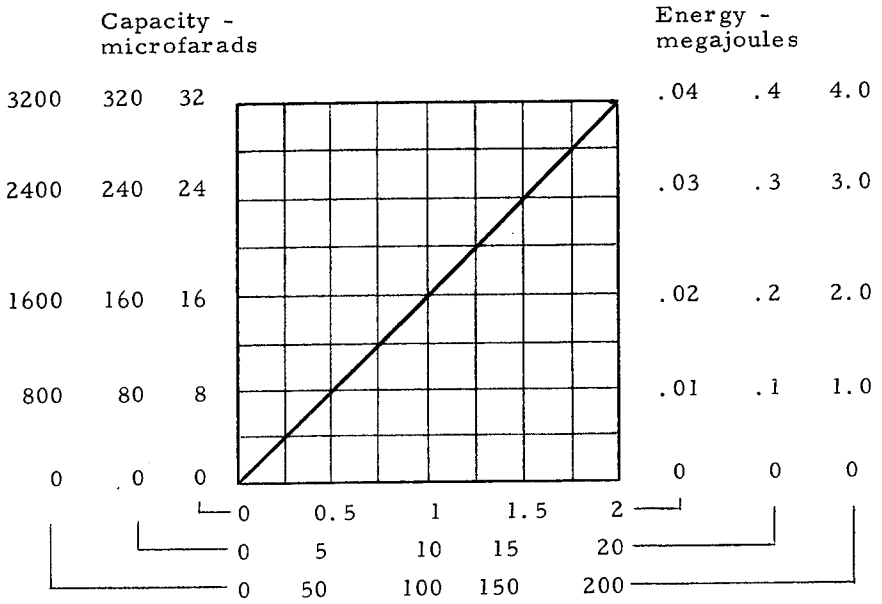

Figure 1. Graph of both capacity required at 50 KV charge and energy required versus inductance for 200 KA crest current with optimum capacitor arrangement.

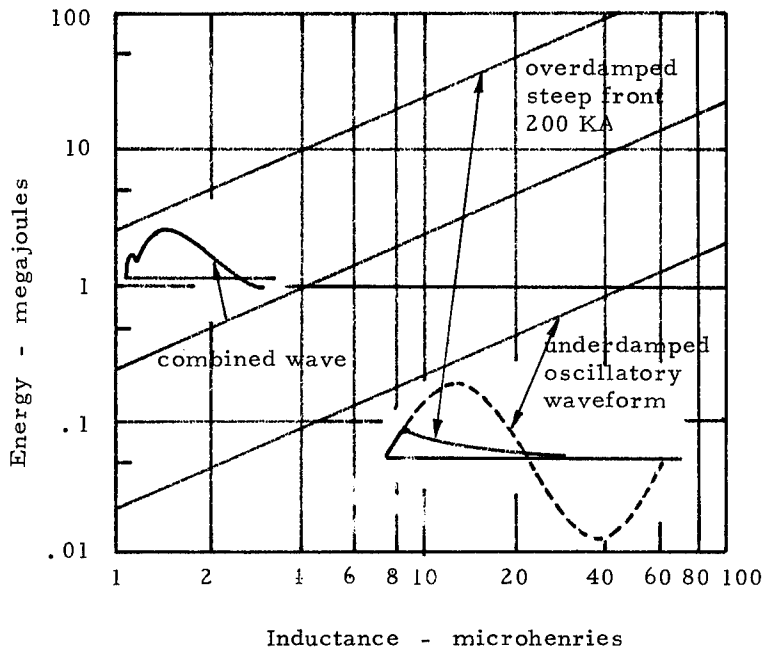

Figure 2. Energy vs. inductance required to produce damped steep front 200 KA waveform with simple linear circuit elements compared with energy required for undamped and combination waves.

discharged through the same test object. This can be done to produce a single combined wave and is routinely done in the testing of aircraft lightning arresters using three separate high current generators each producing a different waveform. However, for a simple test facility, the single discharge underdamped sinusoidal waveform is by far the most efficient in producing maximum currents with a minimum of capacitors.

To produce a more lightning-like unipolarity waveform, all lobes of the damped sinusoid except for the first positive or negative one, can be eliminated by crowbarring (short circuiting) or fusing (open circuiting) after the first half cycle. The unipolarity waveform is not generally recommended for simple test facilities as this further reduces the energy which is generally below most specification requirements.

The unipolarity waveform may be produced by simply using copper wire or aluminum foil as fusing materials. The fuse vaporizes after the first desired half cycle, the current passes through the initially intact fuse and then through the ionized vapor channel of the fuse. For what would be the second half cycle does not occur because the circuit is now open after the current zero. In a sense this method simulates an overdamped wave without paying the penalty of excessive generator capacitance increase, inductance decrease and charging voltage increase.

Using a relatively small generator (for small inductance test loads) various degrees of current oscillation may be achieved with different sizes of fusing materials (see Table A). Figure 3 shows a 200 KA wave with 80% oscillation where no fuses were used. Figure 4 shows a 200 KA wave with oscillations reduced to 35%. Figure 5 shows a 200 KA wave with 0% oscillation produced with a given fuse size and with dead short circuit on the generator terminals. Figure 6 shows the identical conditions as for Figure 5 but with a small test article - the resulting wave became 17% oscillatory. Care therefore must be exercised in setting up tests with "dummy" test articles.

Table A shows the parameters used in deriving waveshapes shown in the figures. In general the individual laboratory must establish its own peculiar parameters as: the size of the capacitor bank in the surge generator; charging voltage; and, the size, length and type of fusing material. By far simplest, the trial and error method is best suited in determining fuse wire size and length. If it can be afforded, the test article type should be placed in the circuit. All

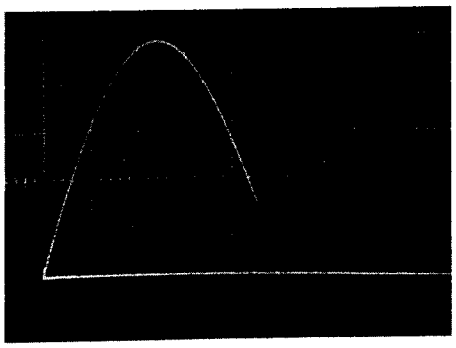

Figure 3.

Oscillograms of 200 KA under damped oscillatory discharge with 80% first negative crest.

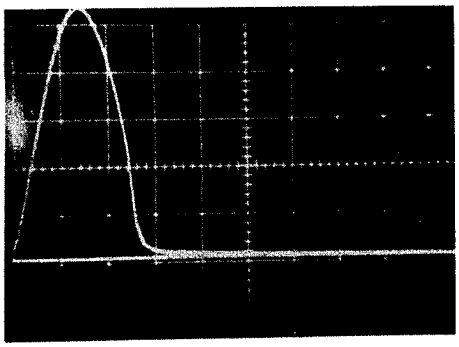

Figure 5.

Oscillogram of 200 KA discharge with first negative crest chopped by fusing.

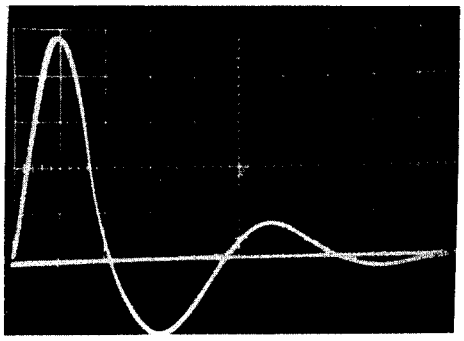

Figure 4.

Oscillogram of 200 KA oscillatory discharge damped to 35% first negative crest.

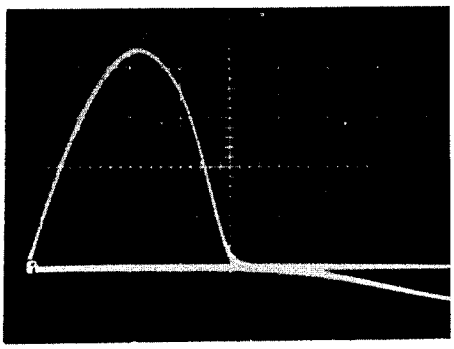

Figure 6.

Oscillogram of 200 KA discharge with identical conditions but with test article resulting in 17% undershoot.

TABLE A

Ref fig	Peak KA	Wave shape μs x μs	% osc.	Surge gen mfd	KV	FUSE WIRE Type	FUSE WIRE Length	Load
3	200	10 x 17	80	3.6	450	None	None	13μh, .28
4	208	12 x 21	80	15	138	None	None	0
5	209	10 x 16	35	18	123	copper wire	2 in parallel, each 34" long, #18 AWG	0
6	191	11 x 17	0	15	138	copper wire	2 in parallel, each 55" long, #18 AWG	0

generator component parts should be fixed and not altered throughout the test sequence otherwise the waveshapes will change. The level of discharge current must also be maintained since the fusing characteristics depend on the energy made available.

Increasing the length of the fuse wire and/or decreasing its cross section causes reductions in the peak current due to the increased impedance. Note that the length of wire must be outstretched between binding posts - coiling or allowing a "droop" produces inconsistent results.

Decreasing the length of the fuse wire and/or increasing the cross section causes oscillations, increases the percentage of oscillations due to lowered impedance, and adds opportunity for the current to use the vaporized trail as a conductor.

Care should be exercised in exhausting the vaporized fuse material away from personnel and equipment. The vapors are highly toxic and equipment suffers metalization, especially insulating structures.

CALIBRATION OF CURRENT MEASUREMENT DEVICES

Although calibration of the test facilities may theoretically be made by using accurate high current measurement devices along with accurately calibrated oscilloscopes, the extreme currents and voltages coupled in complex modes throughout the building power circuits, the building framework and even magnetic field coupling directly into the oscilloscope case can result in large errors in signals which may in some cases be many times the true signal to be measured. Thus, special techniques are required in order to obtain a reasonable assurance that the measured values are accurate. A simple procedure for doing this is to fire an underdamped oscillatory wave train, measure the frequency and from the frequency calculate the inductance. From the inductance voltage and known measured capacity of the generator bank, the theoretical current maximum can be calculated. As shown in earlier sections, this may be obtained from the exact equation for the underdamped sinusoidal waveform current. However, some simple graphs may be used for more quickly attaining the current maximum from this information. The basic charts required are a reactance chart for obtaining the frequency and a damping chart (figure 7) for obtaining the current decrement indicated by the reduction in successive peaks of the underdamped sinusoidal waveform. With this information, the current crests may be quickly determined to a reasonable accuracy of about 5%.

When the theoretical current maximum equals the measured values as indicated by the current measurement device, then reasonable confidence may be had that the current values are accurate within about 5%. Greater accuracy can be obtained with additional care. As noted in the graph in Figure 7, the current corresponds essentially to the logarithmic decrement curve for a quarter cycle and may be obtained explicitly by obtaining the fourth root of the ratio of two successive peaks, for reasonable accuracy with circuits of at least five cycles. The true peak slightly precedes the quarter cycle time.

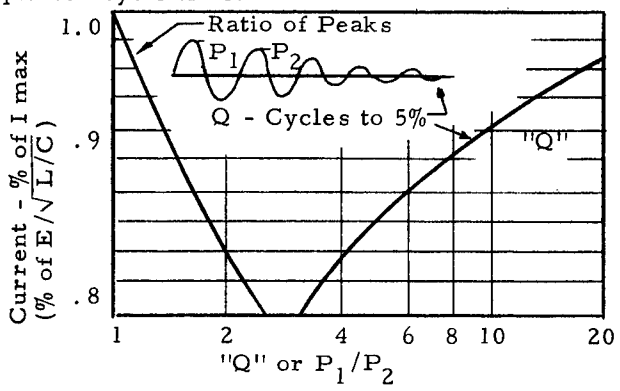

Figure 7.

Quarter cycle decrement from measurement of ratio of two peaks of same polarity and from "Q", number of cycles to 5%.

MEASUREMENT DEVICES

The three generally available types of measurement devices used for measuring the current outputs of the model facility artificial lightning generator banks are: 1) high current shunts, 2) current probes and 3) single turn loops.

The non-inductive coaxial high current shunt was developed by Silsbee of the National Bureau of Standards in 1916 (1)* and further developed by Park and others (2, 3, 4, 5) to a degree which permits the measurement of currents with nanosecond rise times. It has been used by LTRI for many years in a mechanically ruggedized form which can withstand currents of 200,000 amperes crest. The non-inductive coaxial shunts measure the resistive drop across a manganin resistor element without introducing inductive voltages into the measurement circuit. The manganin is used because of its low resistance temperature coefficient. It may be shown that the flux inside a coaxial cylinder carrying current in the outer conductor is essentially zero with the exception of a slight magnetic flux due to the displacement current accompanying the current flow and E field at the interior surface of the outer cylinder. The displacement current component is generally negligible in the working range of lightning current tests. Thus, with almost no flux inside the cylinder, no inductive voltage components are measured and the output voltage is essentially a product of the current passing through the shunt and the resistance of the shunt. The error in this type of shunt is due to the diffusion time required for the current to become uniform throughout the thin outer

cylindrical skin. The rise time of "T" is equal to

$$T = 0.2(d^2/\rho)\ \mu sec$$

where d is the wall thickness and ρ is the specific resistivity.

Current probes are essentially toroidal transformers placed around conductors into which the flux about the conductor couples to produce a voltage proportional to flux and current. The principle problem in the design of these devices is to provide a large enough mutual inductance to give a bandwidth exceeding the bandwidth of the measured waveform. The commercial designs which are available to current maximums of 200,000 amperes have remarkably good bandwidth characteristics, in some cases from a few hertz up to frequencies of 20 to 50 megahertz corresponding to rise times of 20 to 30 nanoseconds (in one single device). One advantage of current probes is that they do not need to be physically connected to the measurement circuit but can be insulated entirely, providing that the discharge circuit passes through the center of the toroidal coil. Caution must be taken, however, to assure that current probes are not used in the high voltage connections of the discharge circuit where flashovers might occur to the probe and which could follow the connecting cable to the measurement oscillograph with possible damage to the oscillograph and possible shock hazard to the operator. Thus, it is always recommended that current probes be installed in the ground leg of the test circuit.

One last simple type device for current measurement is a single turn loop (or, in more sophisticated form, the multi-turn loop in the form of a toroid called a Rogowski coil). This measures the flux rate of change or derivative waveform and may be used with an integration circuit to give the direct current waveform. The single turn loop is convenient for obtaining theoretical calculations of the current value but suffers from the disadvantage that it is sensitive to orientation and position when used for direct current measurement with integration circuitry and must be recalibrated in each new position. The Rogowski coil is generally constructed to have a fixed orientation with respect to the conductor in which the current is being measured and is simpler to use for this reason.

For most of the work, it is preferable to use a current probe or a non-inductive shunt which permits both the theoretical current calculation from the frequency and a direct measure of the current crest. Accurate current probes or non-inductive shunts do not guarantee accurate current measurements, and in fact, error signals far exceeding the measured signal can be obtained if the devices are not properly used. Techniques for avoiding such problems are indicated in the next section.

MEASUREMENT TECHNIQUES

A suggested test arrangement is indicated in Figure 8. A separate raised metal ground plane is provided with a single connection to the building ground. On the ground plane are located all of the components of the system, the test object (or test cabinet for fuel tank components), the power supply and high current bank capacitors, control panel and the measurement oscilloscope and shielded cage. The high current measurement shunt is located at the point on the ground plane where the ground plane is connected to the building ground. This will minimize the potentials existing between the shunt position and the building ground from the high current flow about the test circuit. If this is not done, large potential differences between the shunt and the true building ground may produce some potential on the oscilloscope with possible hazard or at least annoyance to the operator although the operator should not be touching the shielded cage or oscilloscope during the test. This may be visualized more effectively with reference to the equivalent circuit of Figure 9. At some time during the discharge cycle with an undamped sinusoidal waveform, the energy is essentially stored in circuit inductance. The voltage around the circuit is distributed in proportion to the inductance. With such extremely low inductance as is required to obtain the high currents, a section of sheet metal floor can represent a significant proportion of the total circuit inductance and if the shunt is located away from the building ground point, this potential difference will be transmitted up the cable to the oscillograph. Thus, the importance of locating the shunt at the point where the current generator is connected to the building and having the oscillograph and cage isolated from the building power supply and electrically isolated from the building power supply can hardly be over-emphasized. One of the major aircraft companies has suggested that the separate ground plane be located along with the other test facility components on pallets, thus permitting movement of the entire facility to test large components which cannot be easily moved to the test facility area.

For isolation of the oscilloscope from the building power line, several methods can be used including isolation transformers with electrostatic shielding, motor generator sets with insulated drive shafts and battery powered oscillographs. A simple method of isolating the AC power line is indicated in Figure 8. The oscilloscope shield is connected to the shield cage with 0.1 microfarad capacitors for surge isolation.

Other devices such as zener diodes or gas tubes may also be used for surge suppression. If potentials are developed in the shunt area, the oscillograph and shield voltages rise and with this arrangement the failure should occur

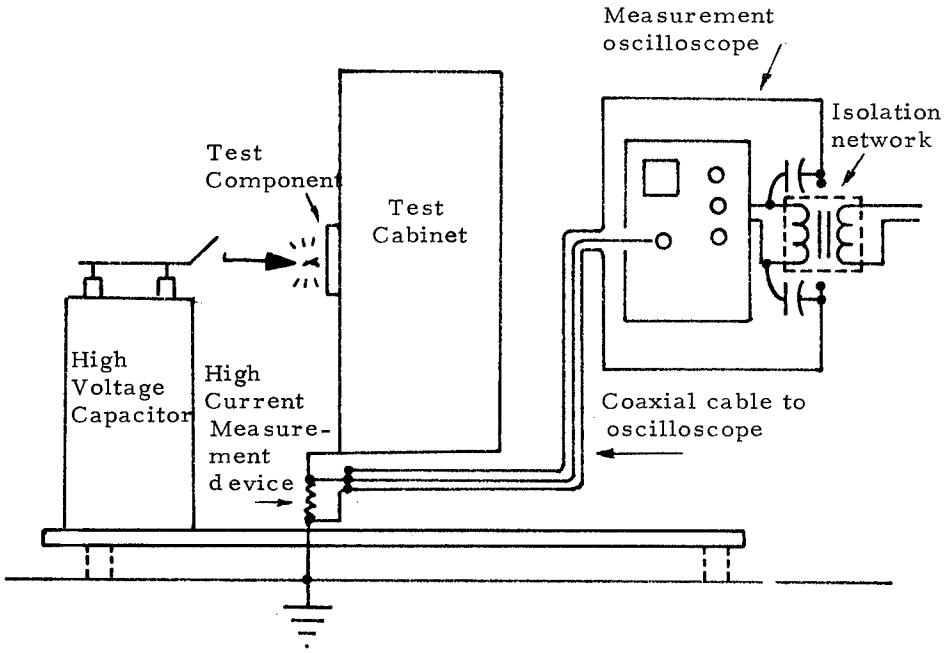

Figure 8. Schematic diagram of small lightning simulation facility.

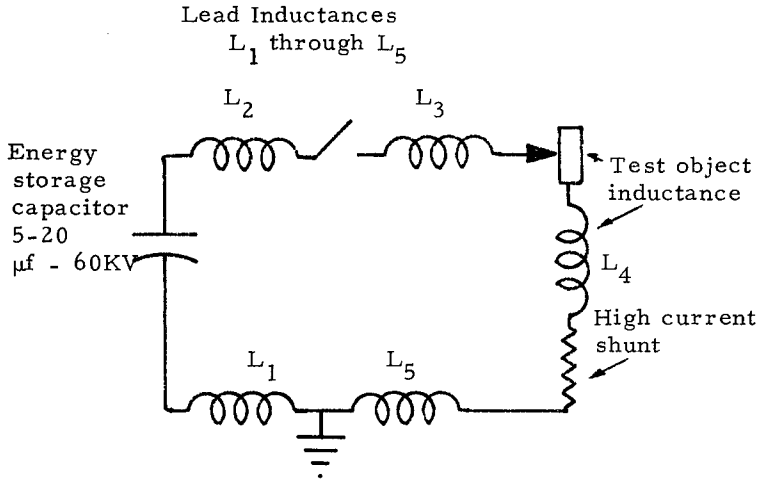

Figure 9. Equivalent circuit diagram of lightning simulation facility.

in the relatively low cost isolation transformer winding rather than in the oscilloscope.

The other methods suggested include the use of a small motor generator set with an insulated drive shaft and a battery powered oscilloscope. Both obviously provide improved isolation for the oscillograph shield cage but suffer from the obvious disadvantages of noise and size for the generator set and the inconvenience of replacing batteries with the battery powered oscilloscope.

One important aspect of surge measurements is being aware when surges penetrate into the oscillograph to give erroneous measurements. An important clue that surges are entering the oscillograph from the power supply may be obtained from observing the waveforms. The vertical portions of the oscillograms sometimes will show negative time. Most oscilloscopes are vulnerable to surge penetration through the power cables and show effects in both the vertical and horizontal amplifier. Thus the surges in the power supply may be seen through negative horizontal deflections of the oscilloscope trace during fast rising portions of the oscillogram. There should be no "negative time" indications on the oscillogram in the form of the trace moving back toward the origin. This is definitely an indication of surge penetration into the oscillograph circuitry and additional isolation is required.

With the current probes, fewer precautions are required. The oscillograph may be grounded to the building at the shielded oscillograph location provided that the current probes are well insulated at the measurement point. Again the current probes should be located as closely as possible in the test circuit to the point of the ground plane which is connected to the building ground in order to minimize possible sparkover and potentials at the oscilloscope.

With simple loop measurements, no particular precautions are required other than to provide good isolation between the probe and the discharge circuits. The loops can be completely floating electrically and can be fairly well isolated from the test circuit because of the large flux densities from the high currents. It should be emphasized, however, that the loop is of primary value in obtaining the self-resonant frequency of the test circuit and should be used with considerable reservations for actually indicating the peak currents even with integration circuitry to provide direct current read out because of the sensitivity of the loop calibration to orientation and test circuit and loop position changes.

CONCLUSION

With the careful application of the above techniques, reasonably accurate surge current measurements can be made in which a high level of confidence can be placed. Test facilities are a major factor in a successful development of aircraft components that are resistant to lightning damage and for this reason the development of the small model facilities with adequate measurement techniques is strongly encouraged.

It should be emphasized that simple simulation techniques have definite limitations and are no substitute for full scale qualification tests and that the suggestions in this paper are not meant to infer that all lightning problems can be solved with relatively trivial efforts.

REFERENCES

1. F. B. Silsbee, "A Study of the Inductance of Four-Terminal Resistance Standards." Bulletin of the Bureau of Standards, Vol. 13, S28, 1916, p. 375.
2. J. H. Park, "Shunts and Inductors for Surge-Current Measurements." Journal of Research of the U.S. Bureau of Standards, Vol. 39, No. 3, Sept. 1947, (RP 1823), p. 191-212.
3. F. D. Bennett and J. W. Marvin, "Current Measurement and Transient Skin Effects in Exploding Wire Circuits." Review of Scientific Instruments, Vol. 33 No. 11, Nov. 1962, p. 1218-1226.
4. R. Malewski, "New Device for Current Measurement in Exploding Wire Circuits." Review of Scientific Instruments, Vol. 39 No. 1, Jan. 1968, p. 90-94.
5. R. J. Thomas, "High-Impulse Current and Voltage Measurement." IEEE Trans. on Instrumentation and Measurements, Vol. IM-19, No. 2, May 1970, p. 102-117.

700919

MICROWAVE NOISE PRODUCED BY TRIBOELECTRIC CHARGING

Larry E. Cummings
Air Force Avionics Laboratory
Wright-Patterson AFB, Ohio

MICROWAVE NOISE PRODUCED BY TRIBOELECTRIC CHARGING

ABSTRACT

The generation of microwave noise (1-4 GHz) by triboelectric charging of dielectric surfaces was produced to determine its magnitude. The noise spectrum is compared with that derived mathematically from collected pulse data. Charging currents are equivalent to those measured on large aircraft. Several different types of dielectrics are examined for generation of triboelectric noise.

THE GENERATION OF RF NOISE by triboelectric charging of dielectric surfaces is well documented, especially below 100 MHz. Recent work by Oh et al (1)* carried the effort to 1 GHz with extrapolated signal strengths to 10 GHz. The effort under discussion was conducted in-house by the Air Force Avionics Laboratory and was particularly interested in the 1-4 GHz region. Materials investigated included ceramics, Fiberglas, acrylics, Teflon, and quartz.

SIMULATION OF THE NATURAL ENVIRONMENT

A relatively air-tight 6' x 4' x 4' chamber was constructed of 1/2" Plexiglas. The bottom consisted of a large tapered funnel of heavy gauge aluminum to collect the charging particles for subsequent reuse. A high pressure spray gun served as the accelerator for the charging particles. Physical construction of the chamber allowed the operator to stand on the outside and have complete control (velocity and area of impact) of the charging medium. The sample could be positioned in any orientation in free space with respect to the spray gun. The test setup also permitted the use of ultraviolet light and high gradient cross fields. An electrooptical targeting system allowed the same area to be charged within a fraction of an inch. This was done for uniformity of results because the amplitude of the RF noise is dependent on the arc breakdown voltage.

SAMPLE POSITIONING AND CALIBRATION

During a portion of the testing program, the samples were placed in open space at an angle of 45° with respect to the charging stream. The coupling factor was obtained by connecting a signal generator to the ring through an isolation resistor. This method will be referred to as Method A.

A ground plane (17"x 17") was constructed with a hole in the center to receive the samples. Isolation was maintained between the ground plane and the sample. The coupling factor was obtained by exciting a short stub (1/4") on the end of a shielded isolation resistor. This resistor assembly was rigidly fixed in place during testing and calibration to eliminate another sticky variable. The 1/4" dimension was chosen so that it would be a small fraction of a wavelength over the frequency range of interest. A distance of 1/8" separated the stub and the radiating device at all times. The radiator was a conductive loop around the sample's perimeter. On the epoxy sample, the coupling factors varied from 54 to 69 db (81% in the low 60s), demonstrating a reasonable amount of frequency independence with respect to the radiating structure. Use of the ground plane will be referred to as Method B. Both methods are illustrated in Figure 1.

Coupling factors were measured for each sample even if the dimensions were the same. This extra measure accounted for slight displacements in the holding assembly, sample curvature, and possible external reflections.

Obtaining coupling factors at 140 kHz required a modification of the former procedure. The isolation resistor had to be connected directly to the radiating structure due to the extreme inefficiency of using a

*Numbers in parentheses designate References at end of paper.

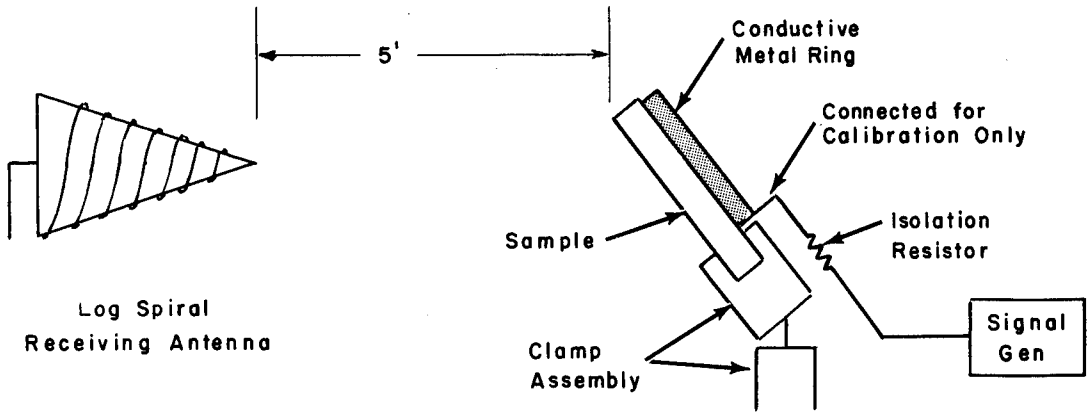

Method A Mounting

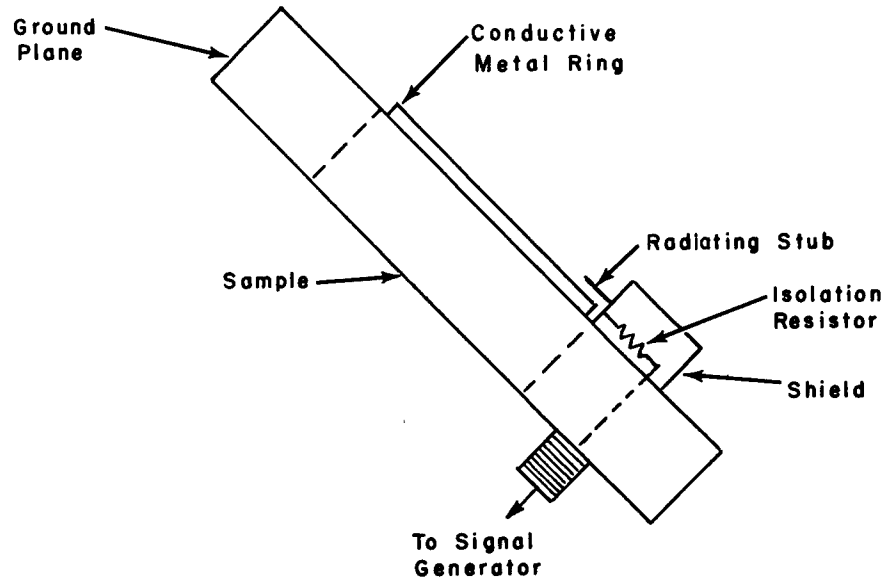

For 140-kHz Calibration, the Stub was Connected Directly to the Metal Ring

Method B Mounting

Fig. 1 - Sample mounting techniques

radiator of 3 x 10^{-5} wavelengths to excite the secondary radiator. No great precision was attempted concerning the results at 140 kHz. These tests were used as a low frequency back-up in an effort to explain the strange results observed at microwave frequencies.

RF reflections were reduced by completely enclosing the Plexiglas chamber in two layers of Eccosorb FL330. External reflections were reduced to 1-2 db at 1000 MHz and were negligible at the higher frequencies.

Source to sample distance was standardized at 5". At this distance, the spray pattern nearly covered the 6" x 3" samples. The velocity of the charging particles (flour) was found to be approximately 465 mph with a standard deviation of 55. The measurement technique consisted of two electrodes and a memoscope. One electrode was placed very close to the spray gun nozzle which intercepted a portion of the spray pattern. The impact noise on this metal plate provided the external trigger for the scope. The other electrode was located successively at larger distances downstream and provided the vertical input to the memoscope. The impact noise on the second metal plate would cause the scope to indicate the elapsed time consumed over the required distance. Such a large deviation is not surprising considering all the variables involved. Particle density at the target is illustrated in Figure 2. The skew is due to the 45° orientation of the sample with respect to the charging stream.

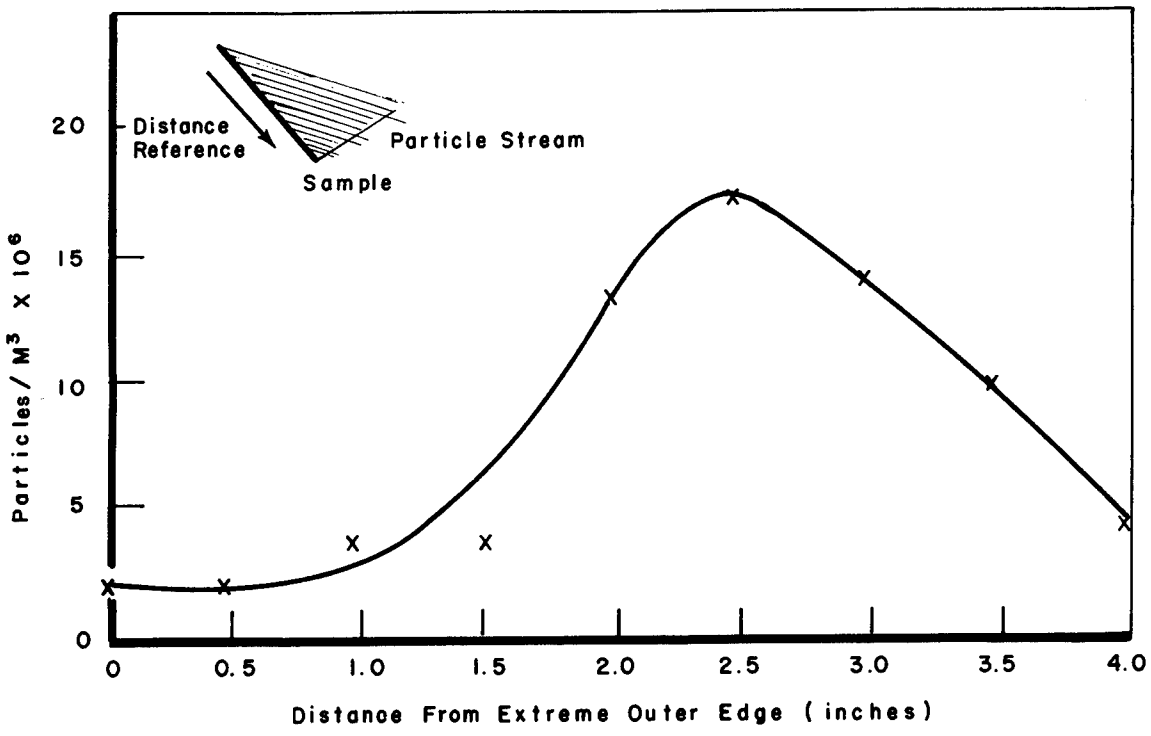

Fig. 2 - Particle density profile

INSTRUMENTATION LIMITS

Measurement of transient nanosecond (ns) risetime pulses is no easy matter. Accordingly, a program was conducted to establish the observational limits of the instrumentation. The minimum observable risetime was determined as follows:

$$t_{r\ min} = \sqrt{(t_{RC})^2 + (t_{RP})^2 + (t_{RO})^2}$$

$$= \sqrt{(0.25 + 2.25 + 15.35) \times 10^{-18}}$$

$$= 4.22 \text{ ns}$$

where

t_{RC} = risetime of cable, 10' of RG-9 = 0.5 ns

t_{RP} = risetime of oscilloscope plug-in = 1.5 ns

t_{RO} = risetime of oscilloscope vertical amplifier = 3.9 ns

This data was confirmed by measuring the systems's impulse response with an Empire Devices IG-118 impulse generator (1-10 GHz). We can use this same method to determine the observed error when attempting to measure risetimes less than 4.2 ns as follows:

$$\text{Step function } t_r = \sqrt{(4.2^2 + 4^2) \times 10^{-18}}$$

$$= 5.8 \text{ ns}$$

where

$t_{r\ min} = 4.2$ ns

Pulse risetime = 4 ns

Therefore, error = 45%

The errors for step functions of various risetimes are tabulated in Table 1.

Table 1 - Observed Risetime Errors

Step Risetime (ns)	Observed Risetime (ns)	Error (%)
2.0	4.65	+ 232
3.0	5.17	+ 72.5
4.0	5.8	+ 45
6.0	7.32	+ 18.9
8.0	9.05	+ 13.1
10.0	10.8	+ 8.0
15.0	15.5	+ 3.3

TEST SAMPLES

The following materials were examined for precipitation static properties:

1. Quartz
2. Teflon
3. Epoxy
4. Epoxy honeycomb section from an operational aircraft
5. Epoxy laminate nose cone from an operational missile
6. Plexiglas
7. Alumina
8. Slotted metallic RF window (SMRFW)- An RF transparent device composed of dielectric-backed perforated metallic sheet (2 slot configurations) referred to as SMRFW (A)
9. Polyester-coated (Selectron 5002 cured with benzol peroxide) slotted metallic RF window referred to as polyester-coated SMRFW (B)
10. Copper (a standard for measuring impact noise).

The slotted metallic RF window is the result of an AFAL sponsored program with Texas Instruments Inc. (Air Force Contract F33615-69-C-1591) (2) to design an antenna

covering to reduce precipitation static and catastrophic damage due to lightning. In effect it is a metallic radome. These windows are pictured in Figure 3.

All signal strength measurements were made in the far field of a conical log spiral antenna (1-10 GHz).

SUMMARY

Figure 4 shows the computed signal strengths at the dielectric surface using Mounting Method A (free space). Note the shallow slope or its complete absence. The high-frequency-noise cutoffs observed with the acrylic and alumina samples were real. A check of receiver sensitivity indicated no system malfunction existed.

Figure 5 shows the average computed generated signal strength provided by mounting the samples on the ground plane, Method B. This series, as well as the previous tests, was conducted on the same day for reasons to be explained later. In this group of tests, the materials were limited to those that would be used to cover antennas.

Signal strengths on any one material showed wide variations. Teflon, for example, had variations of 2-20 db at the same frequency over a period of 15 tests. As a result of the large variations, it is evident that these curves only illustrate approximate signal levels.

Photographs of typical pulses taken across 50 ohms are shown in Figures 6 and 7. The electrical setup is illustrated in Figure 8. Observed risetimes varied from 5-16 ns, corresponding to actual risetimes of 3-16 ns. In many cases what appeared to be a single pulse was actually only one component of an exponentially decaying series of pulses caused by adjacent points of charge attaching themselves to the ionized channel produced by the original discharge. This action lasted for 200-350 μs.

How do these results compare with theory predictions and what actually happens? The theoretical spectrum, derived by Luis Oh (1) under sponsorship of the Air Force Avionics Laboratory, has a negative slope of 24 db over the range of 1-4 GHz. The ground plane method showed a change of 17-22 db.

Left to right: SMRFW (A), Polyester-Coated SMRFW (B) [Note: Pulse collector ring around perimeter], and SMRFW (B).

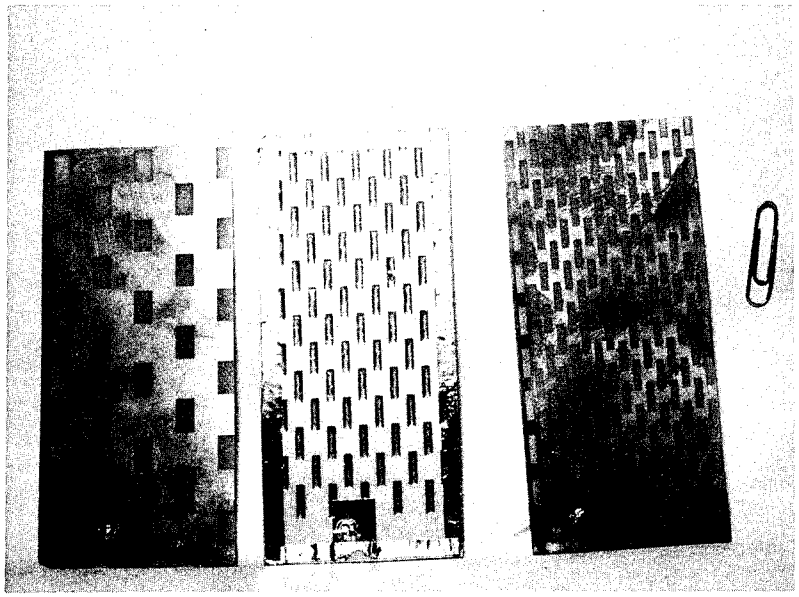

Fig. 3 - Slotted metallic RF windows

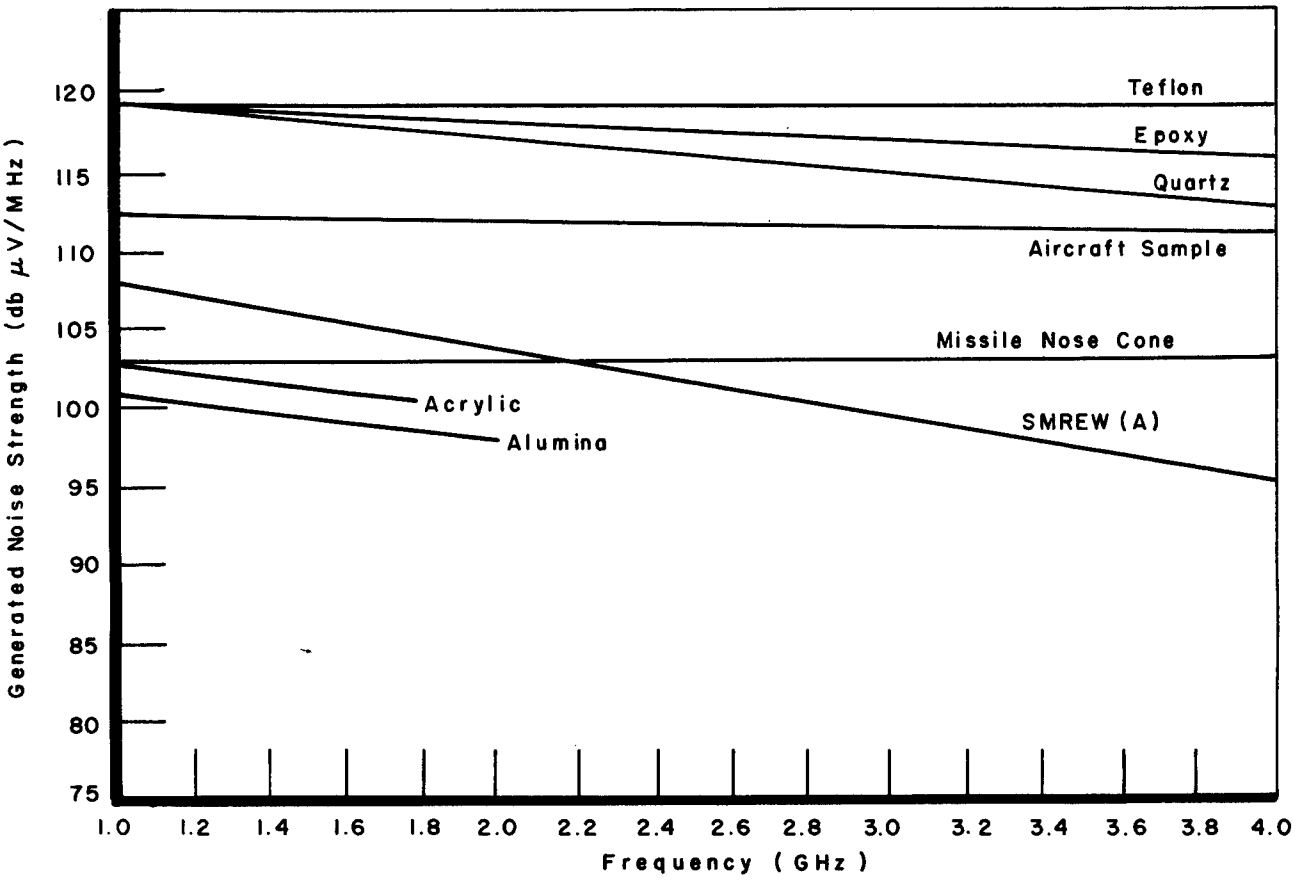

Fig. 4 - Computed generated noise strength vs frequency for Mounting Method A

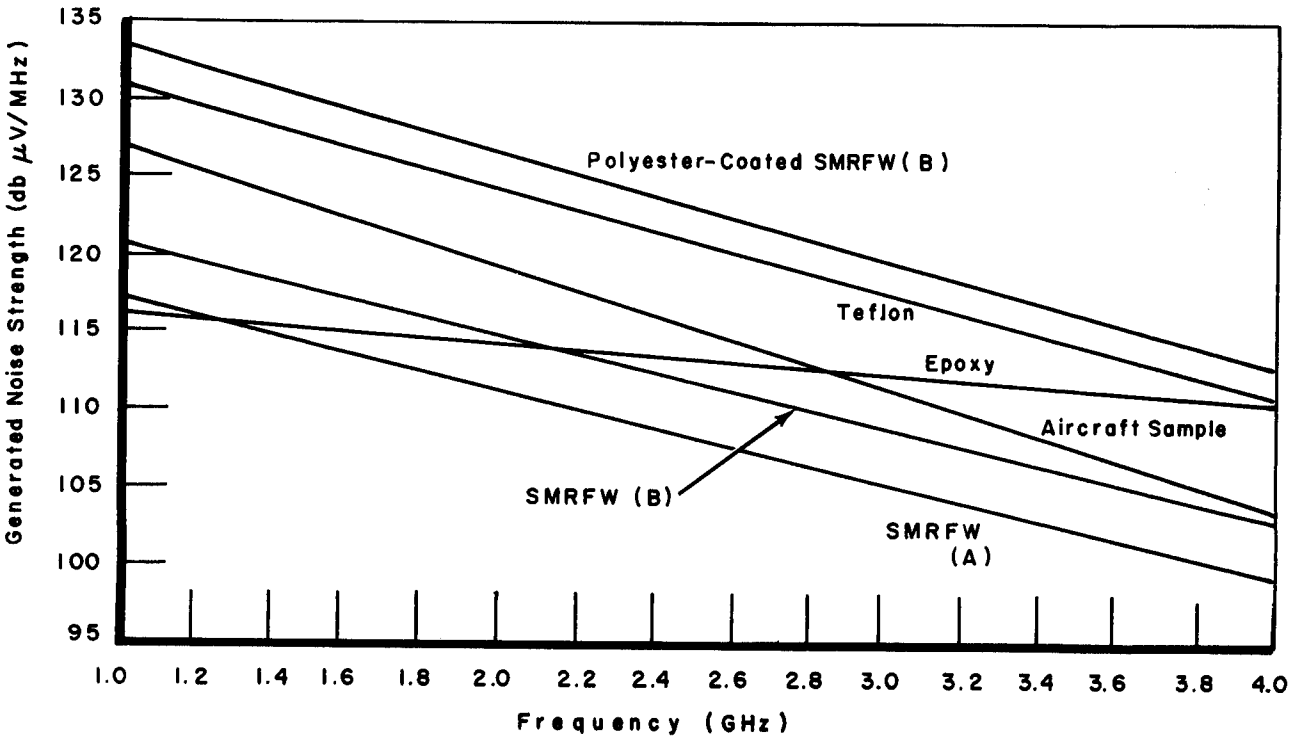

Fig. 5 - Computed generated noise strength vs frequency for Mounting Method B

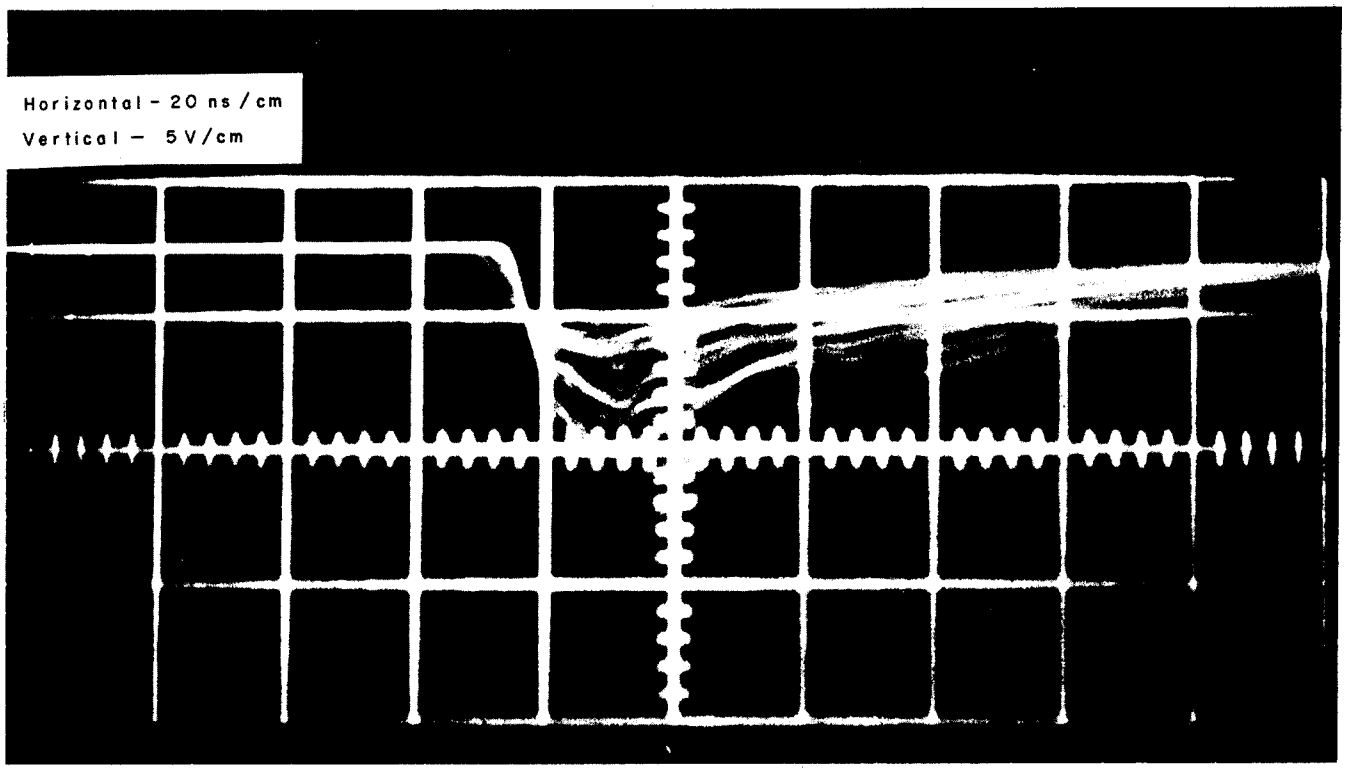

Fig. 6 - Plexiglas pulse

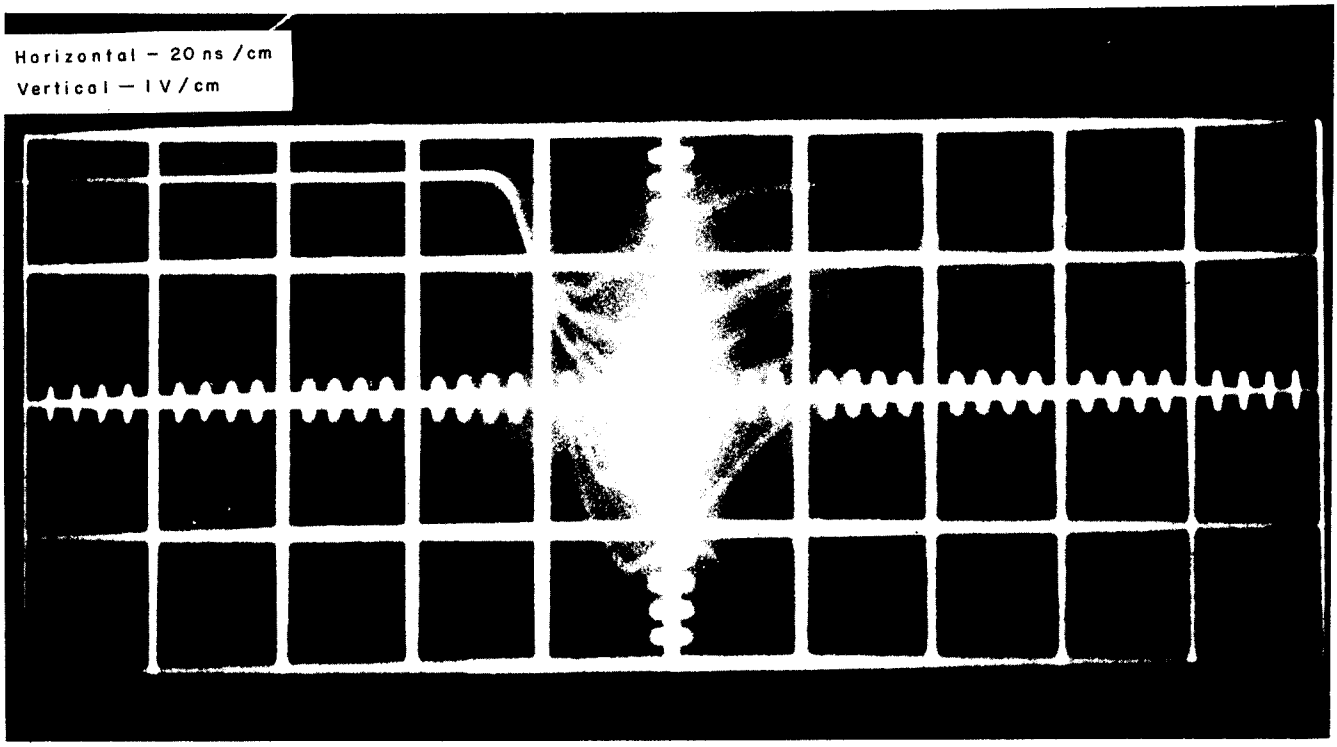

Fig. 7 - Teflon pulse

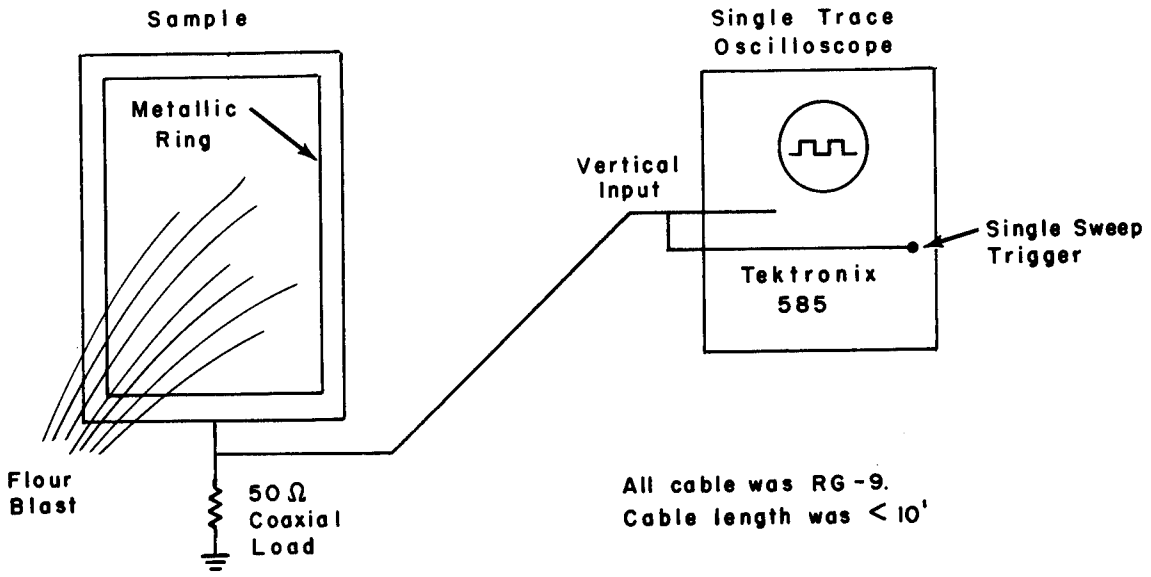

Fig. 8 - Pulse risetime measurement instrumentation

Computation of absolute signal levels is very difficult. The peak pulse voltage varied from 1-60 kV. This voltage was measured by inserting a 103,000-M Ω resistor in series with the oscilloscope. The pulse voltage was observed and the actual value at the sample was calculated. The same sample would show a variation of 3:1 in peak pulse voltage.

Impact noise currents ranged from 5.5-6.6 μ A/ft^2 while the DC charging current contributing to streamer noise was 0-20.8 μA/ft^2; therefore, the total charging rate was 5.5-27.4 μ A/ft^2. The total charging current of a KC-135 is approximately 5-30 μA/ft^2. (3) Thus a good correlation exists under totally different environments.

The generation of reproducible microwave noise by triboelectric charging in the laboratory is no easy matter. Sometimes for no apparent reason, the microwave noise would cease; i. e., it could not be guaranteed. The noise level at 140 kHz was monitored in an attempt to gain further insight to this phenomenon. Each and every blast of the air gun produced noise at 140 kHz. Its noise level was approximately 150-170 db μV/MHz. During the testing program, the 140 kHz would drop 4-10 db for no apparent reason and remain at this level. At both levels (high and low), the received signal strengths varied 1-3 db and could be considered as being constant. This drop in 140-kHz noise was sufficient to eliminate microwave reception. The underlying mechanism is still a mystery.

REFERENCES

1. Luis Oh, et al, "Natural and Induced Electrical Effects On Integrated Antennas and Circuits at Frequencies to 10 GHz." AFAL-TR-69-210. Prepared by The Boeing Company under contract to AF Avionics Laboratory, September 1969.

2. Kent Rogers, et al, "Slotted Metallic RF Window Investigation." AFAL-TR-70-13. Prepared by Texas Instruments Inc. on contract to AF Avionics Laboratory, June 1970.

3. R. L. Tanner and J. E. Nanevicz, "Precipitation Charging and Corona Generated Interference In Aircraft." AFCRL 336. Prepared by Stanford Research Institute under contract to AF Cambridge Research Laboratories, April 1961.

A STUDY OF SOME FUNDAMENTAL HELICOPTER CHARGING MECHANISMS

by

M.E. Rogers

Royal Aircraft Establishment

ABSTRACT

Two fundamental helicopter charging mechanisms are discussed which have received relatively little attention in the past, namely, 'engine' and 'rain precipitation' charging. In each case data collected as part of the Royal Aircraft Establishment's investigation programme are critically examined and working hypotheses are advanced to account for the generation process.

In engines the process is seen as one of preferential trapping of ions previously separated by thermal ionisation. For Whirlwind 10 helicopters where net positive currents are observed it is considered likely that this largely results from positively charged hydrocarbon neuclei colliding with the turbine blades. However because of the relatively small imbalance of ions captured, compared to the total generated by the thermal processes, it is accepted that other engines could exhibit different characteristics.

The rain precipitation process is believed to be an induction effect which occurs when drops are shattered by impact with the rotor leading edge in the presence of an electric field. It is argued that such a process could explain the large variations in charging currents measured in these conditions as well as the frequent changes in polarity. Furthermore this mechanism would predict the observed close relationship between charging current and aircraft all-up=weight (AUW) for different helicopters hovering in identical conditions.

In conclusion it is acknowledged that further work on these mechanisms is required to fully substantiate the theories put forward.

A STUDY OF SOME FUNDAMENTAL HELICOPTER CHARGING MECHANISMS

by

M.E. Rogers

Royal Aircraft Establishment

CONSIDERABLE LITERATURE EXISTS on the problems arising from charging of helicopters in flight (1-4)*and on the difficulties involved in discharging them (5,6), but comparatively little has been said about the fundamental charging mechanisms involved. Of the data which have been published most relates to triboelectrification associated with dust, sand, ice and snow particles being entrained in the rotor downwash. In this paper data on charging currents deriving from the engine power unit and rain precipitation are discussed. Separate mechanisms are suggested which, whilst accounting for the measured data, are not fully proven and are therefore put forward as "working hypotheses".

ENGINE CHARGING

Evidence for Engine Charging on Whirlwind Mk 10 - Since this subject is rather a contentious one it is perhaps worthwhile reviewing some of the data which led us to conclude that the main power unit of the Whirlwind Mk 10 helicopter was producing a small positive component of charging current.

1 Persistent static build-up problems on air sea rescue helicopters in the UK became noticeable with the replacement of the Pratt and Whitney piston engine in the standard Mk 4 Whirlwind by the Gnome 1000 gas turbine and its associated computer control, to give the Mk 10 version. Previous to this only isolated incidents had been reported - all in well defined atmospheric conditions.

2 As shown in Table 1 the comparative measurements made with other types of helicopter under identical conditions clearly indicated a charging mechanism which was unique to this aircraft.

Table 1 - Aircraft Potentials Measured on Different Helicopters at RAE Farnborough in Clear Air Conditions

Type of Helicopter	Number of Readings	Voltage Reading - kV		
		Maximum	Minimum	Mean
Whirlwind 10	5	30.7	23.3	28.8
Wessex 2	5	1.1	< 1.0	-
Wessex 1	5	< 1.0	< 1.0	< 1.0
Whirlwind 1	5	< 1.0	< 1.0	< 1.0

3 Not only was the mechanism common to all Whirlwind 10s, but it was reasonably consistent as shown by the data in Table 2.

Table 2 - Aircraft Potentials Measured on Different Whirlwind Mk 10's in Clear Air Conditions

(Data Obtained at Different Times and Locations)

Helicopter Number	Number of Readings	Voltage Readings		
		Maximum kV	Minimum kV	Mean kV
XP 429	6	30.0	25.7	27.5
XJ 412	6	32.7	25.0	28.4
XP 352	7	20.0	16.6	18.5
XJ 412	6	31.7	22.3	27.2
XP 349	3	40.4	36.4	37.9
XJ 412	3	29.2	23.4	27.0
XP 353	3	35.1	28.9	32.2
XJ 412	3	32.6	25.5	28.8
XP 346	5	27.0	22.4	24.2
XJ 412	5	35.7	28.6	31.1
XJ 396	3	32.2	31.4	31.7
XJ 412	3	30.3	25.4	27.5

4 Similar tests made at a later date in Singapore confirmed the earlier UK measurements - as shown in Table 3. Charging currents and voltages were actually somewhat higher than previous results, due to the higher fuel consumption rates in the hotter climate.

*Numbers in parentheses designate References at end of paper.

Table 3 - Charging Data Measured on Different Helicopters in Singapore in Clear Air Conditions

Aircraft Type	Aircraft No.	Height Above Ground ft	Time Since Last Earthed sec	Charging Current μA	Voltage kV
Wessex 5	XS-517	20	90	+0.05	◀ 6
Belvedere	XG-457	20	60	+0.4	+2.0
Belvedere	XT-468	20	120	< 0.05	+◀ 3
Whirlwind 10	XR-458	20	90	+0.65	+42
Whirlwind 10	XR-458	22	90	+0.65	+48
Whirlwind 10	XR-458	20	90	+0.70	+51
Whirlwind 10	XK-988	22	120	+0.6	+52
Whirlwind 10	XK-988	20	120	+0.6	+55
Whirlwind 10	XR-479	20	120	+0.6	+46
Whirlwind 10	XR-479	20	180	+0.6	+46
Whirlwind 10	XR-479	20	300	+0.6	+40
Whirlwind 10	XR-485	20	90	-	+43
Whirlwind 10	XR-485	20	90	-	+48

5 A net negative charge was observed to be carried away by the exhaust gases.

6 Charging current increased with fuel flow rate. A significant change in slope occurred at the 250 lb/hr rate as shown in Fig 1. (The absence of data in the critical 250-400 lb/hr region is because the free turbine could not be controlled over this range.)

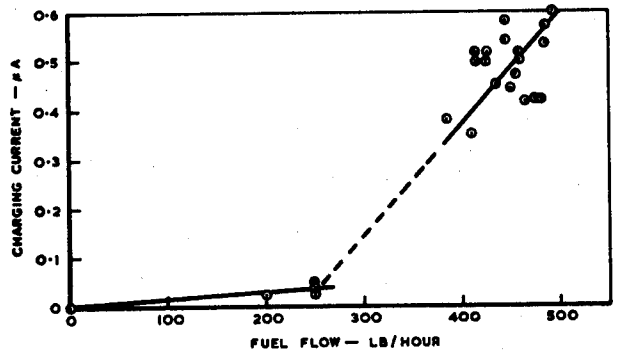

Fig 1 - Variation of Charging Current with Fuel Flow Measured in Clear Air Conditions

7 Voltage built up on the aircraft exponentially with the maximum value being dependent upon the initial charging current. The charging time constant for the aircraft was approximately 90 sec - see Fig 2.

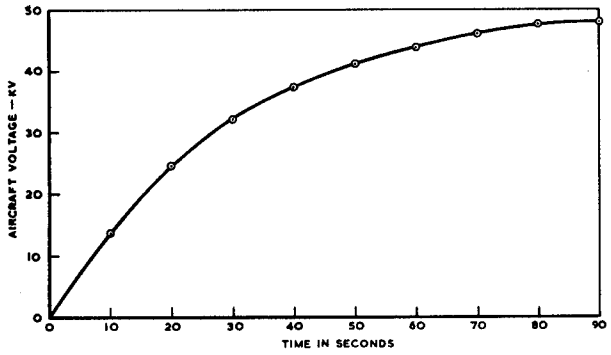

Fig 2 - A Measured Voltage Build-Up for a Whirlwind Mk 10 in Clear Air Conditions

8 Voltage build-ups were not always as regular as shown in Fig 2 but often exhibited abrupt reductions as indicated in Fig 3. (The slow recorder response time has masked the true rate of descent.) These perturbations were found to coincide with aperiodic discharges of carbon particle clouds from the exhaust.

A Suggested Explanation for the Charging Mechanism - This explanation essentially rests on three basic hypotheses.

1 When fuel consumption reaches a critical value (probably 250 lb/hr) thermal equilibrium conditions will exist between the carbon particle and flame temperatures within the reaction zone and ionization will occur. The carbon particles will tend to be positively charged (7).

2 Normal diffusion processes are masked by other factors leading to more positively charged particles reaching the duct walls than negative ones.

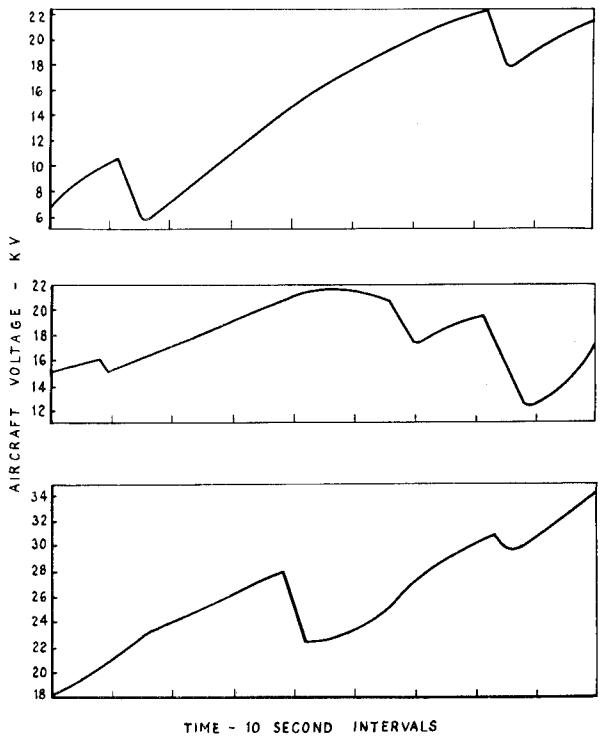

Fig 3 - Aircraft Voltage Build-Ups Showing Effect of Extra Carbon Discharges in the Exhaust

3 Rises in aircraft potential are eventually controlled by the combined actions of neutral carbon particles and ohmic leakages.

The supporting argument for the above hypotheses is as follows.

Within the combustion chamber flame temperatures reach 1800°K. Outside the reaction zone the gases are rapidly cooled by air circulated through the liner walls to temperatures more acceptable to the turbine blades - about 1000°K. The length of the reaction zone increases with fuel flow rate thus allowing more time for the carbon nucleii generated therein to attain thermal equilibrium thereby enhancing their chance of ionization. Beyond a certain point further increases in flow rate will increase both the number of carbon nucleii available and the degree of ionisation (8), thus producing a sharp rise in the number of charged nucleii generated. External evidence demonstrating that such conditions had been reached within the combustion chamber, would take the form of a definite change of slope in the charging current - fuel rate curve. Such a change was a feature of the data shown in Fig 1.

After leaving the combustion chamber the hot gases pass through several turbine stages which considerably reduce their thermal and kinetic energies before final ejection down the short exhaust duct. During this time a decreasing proportion of the thermally dissociated ions will remain separated and thus exposed to processes which preferentially drive the heavier, positively charged particles into contact with the duct walls. The most important of these is the inertia of the heavy particles which causes them to strike the turbine blades rather than deflect through the gaps. Turbulence in the wall region caused by the sudden expansion of the gas stream through the engine bay door section will also encourage contact between the carbon particles and the wall.

Since the soot deposit never exceeds a thin surface layer it follows that a quasistatic equilibrium exists between the number of particles striking and leaving the walls. Of the total number N which hit the side only a fraction n_o will be charged. Thus the maximum charging current will be measured when the aircraft is grounded (through a microammeter) since the neutral particles cannot remove charge when the aircraft is at zero potential.

This current will be given by

$$I_o = n_o q \qquad (1)$$

where q is charge carried/particle.

Consider what happens when the aircraft is isolated from ground. Since it behaves as a capacitor its voltage will rise under the influence of the charging current and this in turn will lead to ohmic leakage and charge removal by carbon particles.

Both processes are proportional to the aircraft voltage V and thus the leakage current can be represented as

$$I_L = K_1V + K_2V$$

where K_1 is a function of the number of particles, contact area, surface charge, K_2 is the effective aircraft conductance to the surrounding air,

or $$I_L = KV \qquad (2)$$

where $K = K_1 + K_2$.

Thus aircraft charging current at any time may be written

$$I_c = I_o - KV \quad . \qquad (3)$$

Knowing the current and capacitance we can write the equation for aircraft voltage change as

$$\frac{dV}{dt} = \frac{I_o - KV}{C_H} \quad . \qquad (4)$$

From Appendix A we see the solution to this equation takes the form

$$V = \frac{A}{B}(1 - e^{-Bt}) \qquad (5)$$

where $A = \frac{I_o}{C_H}$ $B = \frac{K}{C_H}$

I_o and C_H can be measured directly but K cannot. It must therefore be deduced from the experimental data.

Reverting to equation (4) we see that $dV/dt = 0$ when $I_o = KV$ which agrees with experimental observations that final equilibrium voltages are a function of charging current I_o - see Fig 4. The same equation also shows that only an increase in the ratio of neutral to charged particles in the exhaust can decrease the voltage by permitting $KV > I_o$ and dV/dt to become negative. This would explain why the sooty discharges, which result when large lumps of carbon formed near the fuel inlet nozzle in the combustion chamber break off and pass through the flame without attaining ionization temperatures, cause the observed reductions in aircraft voltage noted in Fig 3.

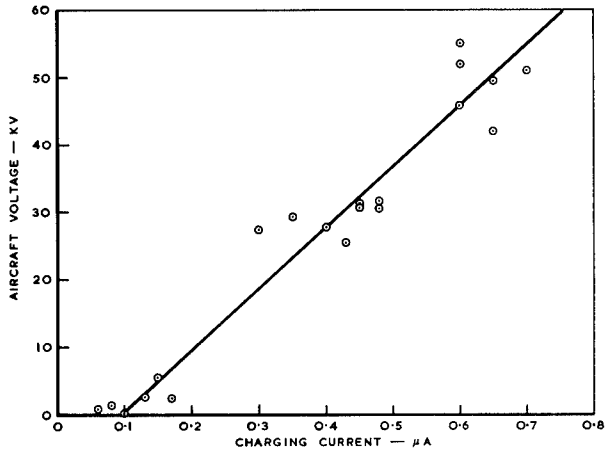

Fig 4 - Variation of Aircraft Voltage with Charging Current for a Whirlwind Mk 10 Helicopter

Finally if the values of A and B (obtained in Appendix A) are substituted into equation (5) it can be seen from Fig 5 that the resulting voltage relationship is of the required general form.

Thus we have an explanation which fits the facts and observed data for this particular engine. However the magnitude of the charging current compared with the number of free ions

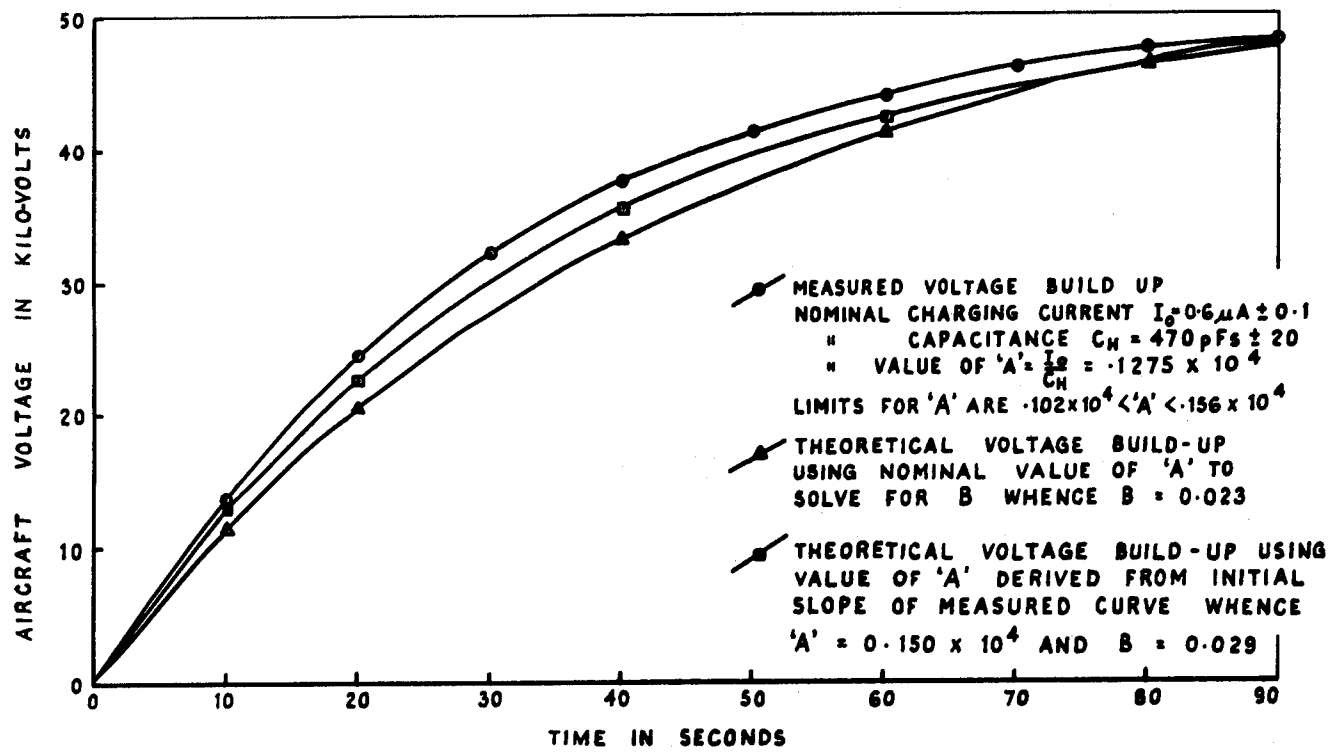

Fig 5 - Comparison of Measured and Predicted Voltage Build-Ups for Whirlwind Mk 10 Helicopter using Equation $V = A/B\ (1 - e^{-Bt})$

produced in the engine suggests that only relatively minor changes in the stated conditions would be needed to significantly change and even reverse the current. Water injection is just such a condition and could lead to negative ions becoming attached to the heavier particles in the form of water droplets and so explain the data found on 707 aircraft. Perhaps some confirmation of the above explained process maybe derived from the small positive charge monitored on another British aircraft (9) - the DH-125 powered by twin Viper turbojet engines.

Our own conclusions on this rather difficult subject are that each engine must be treated on its merits and that differing transport mechanisms and media will be found in many cases.

RAIN PRECIPITATION CHARGING

Preamble - The discovery that charge separation occurs when water drops are shattered is attributed to Lenard (1892), who showed that in general the larger drop fragments acquire a positive charge whilst negative charges are imparted to the air. Elster and Geital used this fact to explain the waterfall charging process, and later Nolan and Enright (1922) demonstrated that the quantity of charge released depended upon the efficiency with which the drop was shattered.

Rain drop charging of aircraft in flight was first studied by Hucke (1939) (10), and later by Gunn et alia (11) as part of the US Army-Navy precipitation static interference programme of (1943-46). Gunn reported that aircraft flying through rain precipitation usually acquired a negative charge. With the aid of a whirling-arm ground rig he was able to show that charging rate increased with impact energy (a fact later confirmed by Adkins (12)), but found the currents generated were small compared with those produced by triboelectrification from ice-particles. In hind-sight it is easy to see why Gunn obtained such low currents but an unfortunate consequence of his results was that rain charging has been largely ignored ever since.

Early Data - At the Royal Aircraft Establishment our interest in this subject originates from the time we attempted to measure "engine charging" currents in rain and found the results bore no resemblance to the currents normally measured. Before long it became obvious that rain precipitation currents could on occasions completely overshadow engine charging. It was also evident that the type of rain was important too because current magnitudes and even polarity would fluctuate wildly in some conditions but were remarkably constant in others. These early measurements led us to define two categories of rain.

i Quiet or Steady Rain - associated with clouds having little vertical development. In such conditions negative charging currents were almost always measured and magnitudes rarely exceeded ±2.0 μA.

ii Shower or Thunderstorm Rain - associated with clouds having marked vertical development. In these conditions current magnitudes and polarity could change rapidly. Although all our data were measured on a Whirlwind Mk 10 (AUW = 8000 lb) recorded currents ranged from -100 μA to +60 μA.

In trying to find an explanation for these data the part played by rain intensity was not immediately obvious, even allowing for the fact that heavier rain intensities are normally associated with shower conditions, since there were occasions when low currents would be measured in very heavy rain. There were other anomalies too. For instance the changes in polarity and magnitude variations not related to rain intensity ruled out the simple shattering process described by Lenard and suggested instead that the drops were pre-charged and simply shared this charge on impact. However it is known (13) that quiet rain brings down predominantly positive charges to earth whilst the aircraft charged negatively. Furthermore an attempt to calculate the charging current measured in stormy conditions using the formula deduced empirically by Simpson (14), ($I_T = 0.04 \times 10^{-5}$ (E-R) esu/cm^2) gave a current of only 0.3 μA (assuming values of a field strength E = 100 V/cm; rainfall intensity R = 100 mm/hr; and fuselage intercept area of 25 m^2) where as values approaching 100 μA were measured in stormy conditions such as these.

In order to resolve this problem, and the more important one of deciding what current output should be specified for an active discharger system which could be fitted to any size helicopter, further trials were conducted in Singapore.

Singapore Data - The trials were conducted during the thunderstorm season of April-May 1967. The location proved to be ideal because of the more predictable weather pattern and the number and variety of aircraft available for tests. In return for the Services' cooperation it was agreed that normal flying routines would be affected as little as possible and that all equipment should be portable and easily removable from the aircraft. The main parameter measured therefore was charging current and this was done by earthing the aircraft through a microammeter with the aid of a weighted drop line. Ground based rain gauges were available but these proved useless because of the wide distribution of the storms and very localized changes of rain intensity within them. All quoted rainfall intensities are estimates made by on-board observers. Despite the crude instrumentation and techniques, the trial did establish the following important points.

i Precipitation charging currents measured on different helicopters hovering in identical conditions are related by the ratio of their respective all up weights.

This result follows a series of experiments in which different helicopters were hovered side by

side and their charging currents measured. To avoid confusion with other possible ratios which might be thought possible, two Whirlwinds at different weights were also monitored. This data is shown in Table 4. This result is significant because it enables data measured on one helicopter to be related to any other helicopter.

Table 4 - Comparison between Ratios of All Up Weight, and Measured Charging Currents for Different Aircraft

Type of Helicopter	Ratio of All Up Weights	Ratio of Measured Charging Current
Belvedere / Whirlwind	2.6/1	2.5/1
Belvedere / Wessex	1.5/1	1.4/1
Wessex / Whirlwind	1.7/1	1.7/1
Whirlwind 1 / Whirlwind 2	1.15/1	1.14/1

NOTE: Whirlwind 1 7700 lb

Whirlwind 2 6700 lb

ii Highest currents occur in heavy rain associated with high ambient electric stresses. This rather brief statement summarizes the analysis of over sixty flights in precipitation covering a wide range of rainfall intensities and electrical activities in clouds. Table 5 shows the measured data grouped according to the observed electrical activity in the cloud, and further broken down into estimated rainfall intensities. The range of currents shown for each reading represents the variations recorded at the given rainfall intensity during a particular flight. Some overlap is inevitable in view of the estimated intensities, nevertheless they do provide a rough guide as to the importance of this parameter. Unfortunately no data were

Table 5 - Charging Currents Measured in Shower Rain Conditions

Measured Charging Current -μA				Weather Conditions	
Whirlwind min	Whirlwind max	Belvedere min	Belvedere max	Rainfall Intensity	Electrical State
+3	+3.5			Nil up to and including medium	Developed Cu - no tendency to lightning activity
+2	+3				
-2					
-0.5	+1.5			Medium to moderate	
-6	-7				
-9	-11				
+22	+25				
-7	-8			Heavy to very heavy	
-2.5	-4.0			Medium and below	Cb prior to any observed lightning activity
		+1.6	-7.0		
				Moderate	
-22	-50			Heavy and above	
-9	-28				
-3	-10			Medium and below	Cb during active electrical stage
-2	+4				
-12	-15				
		-14	-15		
		+10	-32		
-5	-10			Moderate	
	-25				
+10	+48				
-20	-24				
		-20	-32		
-25	-28			Heavy (lower bracket)	
+48	+100				
-24	-52				
+5	+7			Heavy (upper bracket)	
< 0.5				Light	Cb at various stages of its dissipation phase
-0.5	-1.0				
+0.75					
+1.5	+2				
		+2	+3		
		-0.5	-6		
-1	-3				
+2.5	+4				
-3	-8				
-7	-8				
-10					
		+28	+30		
		-32	-40		
-2	-3			Medium	
+2	+4				
-3	-8				
		-5	-8		
		+4	+12		
-5	-6				
+8	+12				
-10					
-10	-15				
		+24	+48		
-7	-14				
		-23	-34		
		+24	+48		
-4	+20				
-20	-40				
		+1	+11	Moderate and above	
+3	-30				
+20	-60				
-26	-50				
-24	-30				
-28	-80				
-60	-68				
		-30	-120		
		-40	-60		
		-64	-80		

available on the magnitude and variations in field intensity and therefore detailed conclusions cannot be drawn from the data as presented. However there is a general pattern which cannot be ignored. Furthermore what is not shown in Table 5 but was quite apparent to observers on the spot was that current variations were typical of the field gradient variations recorded by Gunn (15) and others during thunderstorms. In particular it was noted that lightning flashes often caused a reversal of polarity with a several second delay before the current reached something like its original reading. The proximity of the discharge was observed to affect the magnitude of the current excursion. Thus whilst the documented evidence of a field dependence is perhaps thin, observers were left in no doubt about its importance - and with good reason as will be shown later.

Before leaving these data it is of interest to apply scaling techniques discussed in i above to predict current magnitudes for two of the larger US helicopters. This has been done in Table 6 for some of the higher currents given in Table 5. Scaling factor calculations are based on assumed AUW of 33000 lb and 42000 lb for CH47 and CH53 helicopters respectively.

iii Maximum charging currents recorded on a Whirlwind (AUW 8000 lb) were ±100 μA - equivalent to ±525 μA on a CH53.

iv The conventional high voltage active discharge systems could not be modified to meet these demands (5).

v By taking into account the field dependence of charging current an explanation can be found which accounts for the data.

Table 6 - Predicted Values of Charging Current for CH47 and CH53 Helicopters Scaled from Selected Values of Measured Data shown in Table 5

Measured Data		Predicted Charging Currents -μA	
Aircraft Type	Current μA	CH47	CH53
Belvedere	+ 48	+ 74	+100
Belvedere	-120	-198	-240
Belvedere	- 80	-130	-165
Belvedere	- 32	- 49	- 67
Whirlwind 10	+ 25	+103	+131
Whirlwind 10	- 50	-206	-262
Whirlwind 10	+ 48	+198	+252
Whirlwind 10	+100	+412	+525
Whirlwind 10	- 52	-214	-273
Whirlwind 10	- 60	-240	-320
Whirlwind 10	- 80	-330	-420

Suggested Mechanism for Rain Precipitation Charging of Helicopters - The basic mechanism is seen as an induction process combined with the shattering action of the rotor blade as it impacts with the falling drops. Specifically, induced charges on the tiny water filaments just prior to separation from the main drop would be imparted to the air on tiny drop fragments. Any which avoid subsequent recapture by the air-frame constitute a net charging current of opposite polarity (and thus in sympathy with the field polarity). The obvious advantages of such an explanation are:

a Current polarities and magnitudes would follow those of the ambient electric field.

b The quantity of charge imparted to the air would be a function of the number and size of the fragments produced which avoided recapture. Thus current magnitudes should be proportional to impact energy, and affected by the target material, geometry, and environment.

c Current magnitudes will also be proportional to the number of collisions and thus rainfall intensity, velocity and surface area of the impact structure.

Clearly the final relationship is a complex one which explains the difficulty of deducing the dependence on a single variable from simple observations.

The use of induction charging to explain charges liberated by rain splashing is not a new one but must be attributed to Adkins (12) who demonstrated in the laboratory that such an effect could explain the anomalously high concentration of space charge near the ground in thunderstorm conditions. By separating the variables Adkins was able to demonstrate a linear dependence of charging current on both impact energy and field gradient. He further demonstrated that the hardness of the impacting surface was very important. In considering the application of Adkins work to the helicopter situation, two possible contributions were envisaged.

i Charge released due to drops splashing onto the upper surfaces of the aircraft. Since this so nearly approximates to Adkins own work his empirical formula should be adequate.

Thus

$$I_c = 2.15 \times 10^{-9} \, ER^{1.23} \ \mu A/m^2 \quad (6)$$

Taking values of $E = 100$ V/cm; $R = 100$ mm/hr and Area = 25 m^2.

This gives $I_c = 0.16 \ \mu A$ which is clearly not the major contribution.

ii Charge generated due to impact with the leading edge of the rotor blade. Clearly impact energies will vary with position along the rotor blade and at the outer parts will be very high. Due to the curvature of the blade leading edge and the general helicopter geometry, ambient field gradients will be magnified several times at the impact points. Furthermore the blade cannot sustain a thick film of water and will thus present a very hard target with high local airflow velocities to assist the drop fragmentation. By making some simplifying assumptions an expression for charging current has been obtained in Appendix B which has the form

$$I_c = 2 \times 10^{-15} \, A\phi E' R^{0.88} \ \mu A \quad (7)$$

where the symbols used are as defined in the appendix. Inspection of the equation reveals two constants, A and ϕ. The first relates the quantity of charge released/unit of impact energy/unit of field strength and would have to be determined empirically since it also varies with the nature of the target as explained previously. The second ϕ, represents the blade parameters ($Nw^3 \, t\ell^4$) which in turn are closely related to aircraft all up weight. Thus assuming values of A do not differ widely from blade to blade, different helicopters hovering in identical conditions for E and R should be related by the ratio of their respective ϕ constants. Table 7 compares calculated values of ϕ with the empty all up weights of three helicopters. The empty weights have been taken because no allowance for blade pitch is made in the calculation of ϕ. The agreement is considered reasonable under the circumstances.

Whilst evaluation of charging currents must await the empirical determination of A, and

Table 7 - Data Showing Agreement Between Ratios of Blade Constants ϕ and All Up Weights for Different Helicopters

Type of Helicopter	Ratio of Blade Constants	Ratio of All Up Weights (Empty)
Belvedere / Whirlwind	2.14 / 1	2.45 / 1
Belvedere / Wessex	1.26 / 1	1.42 / 1
Wessex / Whirlwind	1.7 / 1	1.72 / 1

hopefully some measured field data, it is interesting to note that taking the value $A = 6 \times 10^{-8}$ as found by Adkins when he allowed drops to fall on a flat plate in still air conditions, a charging current of $I_c = 57$ μA is obtained. This assumed the usual ambient conditions of $E = 100$ V/cm and $R = 100$ mm/hr. Since true values for A are expected to be anything up to 10 times greater than the Adkins value, there seems little doubt that such an equation can account for the very high charging currents measured in rain precipitation.

SIGNIFICANCE OF CHARGING CURRENT DATA

Two quite different charging mechanisms have been examined in some detail in an attempt to explain the fundamental processes involved, but have they any real practical significance? At first sight it might be thought not in view of the very small engine currents and the quite rare high precipitation currents. Closer examination reveals otherwise however. When assessing the extent of the static hazard it is the aircraft voltage which is of importance not the current. Reference to the Whirlwind data Tables (1-3) show that voltages of 30-50 kV are regularly occurring and since they represent energies in excess of 0.5 Joules at the upper limit, they cannot be ignored.

Conversely, a fact which is also often overlooked is that higher charging currents do not necessarily mean proportionately higher voltages. In any precipitation conditions matter leaving the aircraft will carry off charge in much the same way as the carbon in the engine exhaust. More over above certain voltages, airframe corona discharges would further help to limit charge accumulations. The real significance of very high currents is the difficulties implied in controlling them. As to their frequency of occurrence, even allowing for the normal desire to avoid heavy precipitation where possible, particularly when it is associated with an active thunderstorm, charging currents in excess of 50 μA on a Whirlwind (equivalent to > 250 μA on a CH53) were measured in conditions considered acceptable for normal helicopter operations.

In conclusion it is suggested that this work indicates that more attention should be paid to these two charging mechanisms. In particular rain precipitation charging could be the dominant factor for helicopters operating in tropical and sub tropical areas.

REFERENCES

1. G. J. Born and E. J. Durbin, "An Investigation of Electrical Charging and Discharging of Aircraft in Flight." Princetown University, Report No. 593, December 1961.

2. C. J. Tona, "Study and Investigation of Methods of Dissipation of Static Electricity on Helicopters." Cornell Aeronautical Labs Inc., New York, Report No. BB-1368-H.

3. J. M. Seibert, "Helicopter Static Electricity Measurements." TREC Technical Report 62-72, June 1962.

4. G. Born, E. Sharkoff, E. J. Durbin and R. Creed, "The Electrostatic Charging and Discharging Phenomena of Helicopters in Flight." Technical Report AFAL-TR-68-290, Part II, May 1969.

5. Granger Associates, "Loran D Electrostatic RFI and Null Field Discharger Flight Tests." Part II - Limiting Electrical Energy Transfer from external Helicopter Loads, January 1967.

6. M. E. Rogers and E. B. Minihan, "Evaluation of an Active High Voltage Static Discharge System Installed in a Whirlwind 10." Royal Aircraft Establishment Technical Report TR-68132, May 1968.

7. A. G. Gaydon and H. G. Wolfhard, "Flames - Their Structure, Radiation and Temperature." Chapman and Hall, 2nd Edition.

8. A. Von Engel, "Ionized Gases." The Oxford and Clarendon Press, 2nd Edition.

9. J. E. Nanevicz, "Investigation of Static Noise Problems on the HS-125 Aircraft." Prepared for Granger Associates POS-16724 SRI Project 6746.

10. H. M. Hucke, "Precipitation - Static Interference on Aircraft and at Ground Stations." Proceedings of the IRE, May 1939.

11. R. Gunn, W. C. Hall and G. D. Kinzer, Army-Navy Precipitation Static Project. Part I - "The Precipitation - Static Interference Problem and Methods for its Investigation." Proceedings of the IRE and Waves and Electrons, April 1946.

12. C. J. Adkins, "The Small-ion Concentration and Space Charge Near the Ground." Royal Met. Soc. Quart. Journal., Vol 85, No. 365, July 1959.

13. J. A. Chalmers, "Atmospheric Electricity." Pergamon Press, London.

14. Sir George Simpson, "Atmospheric Electricity during Disturbed Weather." Geophysical Memoirs No. 84 (Fourth Number, Vol Ten), 1949.

15. R. Gunn, "The Electric Field Intensity and its Systematic Changes Under Active Thunderstorms." Journal of Atmospheric Physics, Vol 22, No. 5, September 1965

16. A. C. Best, Quarterly Journal Royal Met. Soc. 76, pp.16-36

Appendix A

DERIVATION OF AIRCRAFT VOLTAGE IN TERMS OF ENGINE CHARGING CURRENT

A capacitance C_H subjected to a charging current I_c will have its voltage change at a rate given by

$$\frac{dV}{dt} = \frac{I_c}{C_H} \quad . \tag{8}$$

If I_c is the net charging current for a particular aircraft voltage V and is given by

$$I_c = I_o - KV \tag{9}$$

where I_o is a constant charging component and the term $-KV$ represents a leakage or discharge current which is proportional to aircraft voltage, then (8) may be rewritten

$$\frac{dV}{dt} = \frac{I_o - KV}{C_H}$$

or

$$\frac{dV}{A - B(V)} = dt$$

where $A = \frac{I_o}{C_H}$ and $B = \frac{K}{C_H}$

whence

$$\frac{dV}{1 - \frac{B}{A}(V)} = A\,dt \quad . \qquad (10)$$

Integrating gives

$$-\frac{A}{B}\log\left(1 - \frac{B}{A}V\right) = At + C_1 \qquad (11)$$

where C_1 is a constant of integration. Solving for C_1 we have that at $t = 0$, $V = 0$ hence $C_1 = 0$,

therefore

$$\log\left[1 - \left(\frac{B}{A}\right)V\right] = -Bt$$

or

$$1 - \frac{B}{A}V = e^{-Bt}$$

which gives

$$V = \frac{A}{B}(1 - e^{-Bt}) \quad . \qquad (12)$$

The constant A is readily determined since $A = I_o/C_H$ but for B we must take a specific value of V against t to solve equation (12) for B.

Theoretically one could deduce K, and hence B, from the relationship

$$\frac{dV}{dt} = 0 \text{ when } I_o = KV$$

but it is difficult in practice to determine the value of V for which $dV/dt = 0$.

Consider the voltage time graph shown in Fig.2:

then $V_E = 48.5$ kV at $t = 90$ sec

and $I_c = 0.60\ \mu A$ with $C_H = 470$ pF .

Putting these values into (12) gives a value for $B = 0.023$. Thus the voltage curve can be expressed as

$$V = 5.55 \times 10^4\,(1 - e^{-0.023t}). \qquad (13)$$

The theoretical plot derived from equation (13) is shown plotted in Fig.5 and is reasonable, but a better fit can be obtained if the value for $A = I_o/C_H$ is taken from the measured slope of the V - t graph at the origin thus reducing the error tolerance on the measured values of I_o and C_H.

In this case A is deduced as 0.150×10^4. Solving equation (13) again but using the new value for A gives $B = 0.029$. Thus

$$V = 5.17 \times 10^4\,(1 - e^{-0.029t}) \quad . \qquad (14)$$

Appendix B

DERIVATION OF CHARGING CURRENT RELATIONSHIP

Consider a rotor of radius ℓ and thickness t rotating with angular velocity ω. Then velocity swept out per sec by small element δr at distance r from the centre is given by

$$r\,\omega\,t\,\delta r \text{ cc/sec}$$

and if mass of water per cc is given by M gm, mass impacting is $M\,r\,\omega\,t\,\delta r$ gm/sec.

Assuming drops acquire velocity of blade after impact, the impact energy is given by

$$\frac{1}{2}r^2\,\omega^2\,M\,r\,\omega\,t\,\delta r \text{ ergs/sec} \quad . \qquad (15)$$

Hence total impact energy over whole rotor is given by

$$\int_0^{\ell} \frac{1}{2} r^2 \omega^2 M r \omega t \, dr = \frac{M}{8} \omega^3 t \ell^4$$

and for N blades

$$\text{Impact energy} = \frac{NM}{8} \omega^3 t \ell^4 \quad . \quad (16)$$

We thus require to find the mass of water M/cc of air. In his analysis of rain drop sizes Best (16) 1950 gives

$F = 1 - \exp\left(-\frac{\delta^n}{a^n}\right)$ as the fraction of the mass occurring in drops of diameter less than δ,

where $a = 1.3 R^{0.232}$

$n = 2.25$

therefore the mass of drops having diameter less than δ is given by

$$M\left[1 - \exp\left(\frac{\delta}{a}\right)^n\right] \quad . \quad (17)$$

In order to evaluate the mass M/cc we must equate the collection rate at the ground with the total vol. swept out by drops of all sizes reaching the ground in unit time. If the measured rainfall rate is R mm/hr this gives collection rate at ground

$$= \frac{R}{3.6 \times 10^4} \text{ gm/sec/cm}^2 \quad . \quad (18)$$

The column of air swept out by the drops will depend upon their terminal velocity which in turn depends upon their size.

According to Adkins, terminal velocity for drops in the 1-100 mg size varies as $m^{1/6}$ or $\delta^{1/2}$ hence

$$V_T = k \delta^{1/2} \quad . \quad (19)$$

Furthermore he states that the terminal energy of a 1 mg drop is 1.13×10^2 ergs therefore

$\frac{1}{2} 10^{-3} k^2 \delta = 1.13 \times 10^2$, and since $\rho = 1$ for water $\frac{\pi}{6} \delta^3 = 10^{-3}$ or $\delta = \left(\frac{6}{\pi} \times 10^{-3}\right)^{1/3}$, hence

$$k = \sqrt{\frac{1.13 \times 10^2 \times 2}{10^{-3}\left(\frac{6}{\pi} \times 10^{-3}\right)^{1/3}}}$$

$$k = 1.68 \times 10^3 \quad . \quad (20)$$

Thus the mass of drops between δ and $d\delta$ per cc $= Mn \frac{\delta^{n-1}}{a^n} \exp\left(-\frac{\delta^n}{a^n}\right)$.

Thus the mass of drops between δ and $d\delta$ reaching the ground

$$= Mn \frac{\delta^{n-1}}{a^n} \exp\left(-\frac{\delta^n}{a^n}\right) k \delta^{1/2} . \quad (21)$$

Thus from (18) and (21) we have

$$\frac{R}{3.6 \times 10^4} = \frac{Mkn}{a^n} \int_0^{\infty} \delta^{n-1/2} \exp\left(-\frac{\delta^n}{a^n}\right) d\delta \quad \ldots . \quad (22)$$

$$= \frac{Mkn}{a^n} \frac{a^{n+1/2}}{n} \Gamma\left(\frac{n + 1/2}{n}\right)$$

$$= Mk \, a^{1/2} \, \Gamma\left(\frac{2.75}{2.25}\right)$$

$$= 0.913 \, Mk \, a^{1/2}$$

therefore

$$M = \frac{R}{3.6 \times 10^4 \times 0.913 \, k \, a^{1/2}} \quad (23)$$

and substituting for a gives

$$M = \frac{R\, R^{-0.12}}{3.6\times10^{4}\times0.913\times(1.3)^{1/2}\ 1.68\times10^{3}} \quad \ldots\ (24)$$

$$M = 1.6 \times 10^{-8}\ R^{0.88}\ \text{gm/cc} \quad . \quad (25)$$

Therefore the equivalent impact energy of all rain striking the blade/sec is given by

Impact energy

$$= \frac{1.6\times10^{-8}}{8}\ R^{0.88}\ N\ \omega^{3}\ t\ \ell^{4}\ \text{ergs/sec} \quad . \quad \ldots\ (26)$$

Now from Adkins work (12) we know that charge liberated/erg of impact energy is directly proportional to the field strength, i.e.

$$q = A\ E'\ \mu\mu\text{C/erg of energy} \quad (27)$$

where E' is the field strength at the impact point, and is assumed = 10 E.

A the constant of proportionality is determined empirically for a given target surface.

Thus charging current generated at rotor blades is given by

$$I_c = A\ E'\ \frac{1.6\times10^{-8}}{8}\ R^{0.88}\ N\ \omega^{3}\ t\ \ell^{4} \times \times\ 10^{-6}\ \mu A \quad (28)$$

$$I_c \simeq 2 \times 10^{-15}\ A\ \phi\ E'\ R^{0.88}\ \mu A \quad (29)$$

where $\phi = N\ \omega^{3}\ t\ \ell^{4}$ and is constant for a given helicopter at given AUW.

700921

STUDIES OF SUPERSONIC VEHICLE ELECTRIFICATION

J. E. NANEVICZ and E. F. VANCE
Stanford Research Institute

ABSTRACT

Theoretical and experimental studies of airborne vehicle electrification processes are described. Laboratory experiments with projectiles fired through an ice-fog cloud were used to study the variation of frictional charging with air speed at supersonic speeds. These experiments demonstrated that the charge imparted by each particle decreases with increasing speed at supersonic speeds, apparently because of ice crystal melting on impact.

Flight instrumentation has been designed and fabricated to measure electrification parameters and effects on a supersonic test aircraft. The instrumentation measures, charging rate, discharging rate, charge per particle, aircraft potential, streamer current and number of streamer pulses, variation of effective frontal area, and noise spectrum. The philosophy of the design and construction of the flight test experiments and equipment are discussed. The flight test instrumentation has been installed on an F-4 aircraft, and test flights are being conducted.

WHEN RADIO COMMUNICATION AND NAVIGATION equipment was first being introduced on aircraft, operators observed that this equipment was completely disabled whenever the aircraft flew into clouds containing ice crystals.[1,2,3]* It was found that the noise was a consequence of frictional charging of the aircraft by the impinging precipitation particles. The charging processes raised the aircraft potential to such high values that noise-producing corona discharges occurred from the aircraft extremities and, sometimes, even from the receiving antennas themselves. Relief from this problem was obtained through the installation of wick dischargers on the extremities and through the use of dielectrically-coated antenna wire to inhibit discharges directly from the antennas.[3]

With the introduction of jet aircraft, the precipitation static problem once again had to be considered. It was found that wick dischargers deteriorated rapidly in the severe aerodynamic environment of a jet aircraft. To overcome this problem, ortho-decoupled dischargers capable of providing the same noise reduction as a new wick, and, at the same time, incorporating a mechanical design such that they would survive the jet environment were developed.[4,5,6,7,8] The high speeds of jet aircraft require careful attention to drag caused by protuberances such as antennas extending beyond the mold lines of the aircraft. Consequently, much work was done to develop flush-mounted antennas for use on jets. Since the antennas must radiate, and must, at the same time, present a smooth aerodynamic surface, the design of flush-mounted antennas often included a dielectric cover flush with the aircraft skin. It was found that these dielectric covers could become sufficiently charged by impinging precipitation that noise-producing streamer discharges would occur across the surface.[9,10] A solution to this problem was found through the use of high-resistance electrically-conducting paint on the outer surface of the antennna to drain away the charge as rapidly as it arrives.

As more aircraft operation was projected for the highly-supersonic speed regime, it became appropriate to reconsider the sorts of natural interference problems that should be expected. It is important that such an investigation be undertaken as early as possible since retrofitting fixes becomes increasily difficult as aircraft speed is increased. Thus it is desirable that the problem be well understood in order that the necessary preventive measures be incorporated into the original design of the aircraft. Furthermore, design restrictions are so severe

*Numbers in parentheses designate References at the end of the paper.

on a highly-supersonic aircraft, that it is essential to avoid unnecessary performance penalties stemming from an overestimation of the severity of the natural interference problem. Conversely, if the aircraft system is to have true all-weather capability, it is important that the magnitude of the problem not be underestimated.

In planning a research program involving the interaction of an aircraft with its in-flight environment, one is tempted to immediately instrument an airplane and start flying. Since we were interested in the speed range to Mach = 10, this obviously was not possible. (Even if an aircraft were available, it is generally perferable to study the problem, as much as possible, in the laboratory and to rely on the flight tests largely to confirm predicted results and to disclose occasional unexpected results.) Thus the present investigation consisted of three distinct phases. First, a laboratory program was undertaken to study the way in which the basic electrification processes are affected by increases in speed.[11] Next, using the results of the laboratory study, a flexible, compact instrumentation system suitable for use on a supersonic aircraft was developed.[12] Finally, the instrumentation system was installed on a supersonic aircraft, and operated in high-altitude clouds to gather flight test data. (Initially, it was anticipated that the tests would be conducted on an F-111 or B-70; however, the tests are actually being conducted on an F-4 aircraft. Unfortunately, since actual flight testing has only recently been initiated, it will not be possible to present flight test results in this paper. Instead we will concentrate on the laboratory work and on the philosophy, development, and installation of the flight test instrumentation.

LABORATORY AND THEORETICAL STUDIES

GENERAL - The same basic vehicle-electrification and noise-generation processes responsible for precipitation static on subsonic aircraft should certainly be expected to occur on highly-supersonic aircraft, but the magnitudes of the various effects may be quite different. The purpose of the laboratory portion of the program was to investigate the way the various processes are affected by a higher speed.

In general the charging current to an aircraft is given by

$$I_{chg} = q_p A_e n V \qquad (1)$$

where:

I_{chg} = aircraft charging current

q_p = particle charge

n = particle concentration

A_e = effective intercepting area

V = aircraft velocity

Subsonic flight-test measurements in ice-crystal clouds demonstrated that for most aircraft, A_e is much less than the projected frontal area, $A_{frontal}$, of the aircraft and that A_e varies with speed and particle character. These same flight test measurements indicate that q_p is independent of V for velocities in the speed range 340 to 600 mph. In general, however, both q_p and A_e may be functions of velocity. In studying triboelectric charging, therefore, it is necessary to design experiments in such a manner that changes in charging due to variations of q_p may be separated from those caused by variations in A_e. NACA studies of water droplet impingement[13-18] are very useful in this regard in that they demonstrate the way in which A_e varies with speed. In particular, the NACA work indicates that if the moving body is made sufficiently small A_e approaches $A_{frontal}$ and is independent of speed. Thus if we are interested in studying variations of q_p with speed, the measurement problem is greatly simplified if we use a small body, since then, any change in I_{chg} can be attributed to a change in q_p.

CHARGING EXPERIMENTS - After considering various possible techniques for simulating in-flight conditions, it was decided that the frictional charging experiments would be made in a refrigerated chamber in which an ice-fog cloud was produced by injecting steam and seeding with dry ice. The experiments consisted essentially of firing a projectile through the cloud and measuring the charge that it acquired.

A schematic drawing of the instrumentation setup is shown in Figure 1. A projectile fired from one of the rifles first passes through the steel sabot-stripper, which stops the aluminum sabot carrying the projectile. The projectile itself (a 5/32-inch-diameter steel ball) then passes through the plates of the gas stripper, which removes most of the accompanying slug of gas. Upon leaving the gas stripper, the projectile breaks an aluminum ribbon which triggers the oscilloscope. Then the projectile enters the refrigerated chamber through an 18-inch-long heavy steel pipe to restrict the dispersion of projectiles which may have struck the gas stripper plates. Finally, the projectile passes through a set of four electrodes spaced 37 cm apart and is caught in a sand-filled steel funnel.

Each probe is simply a metal tube 4 inches long and 1.25 inches in diameter with a grounded

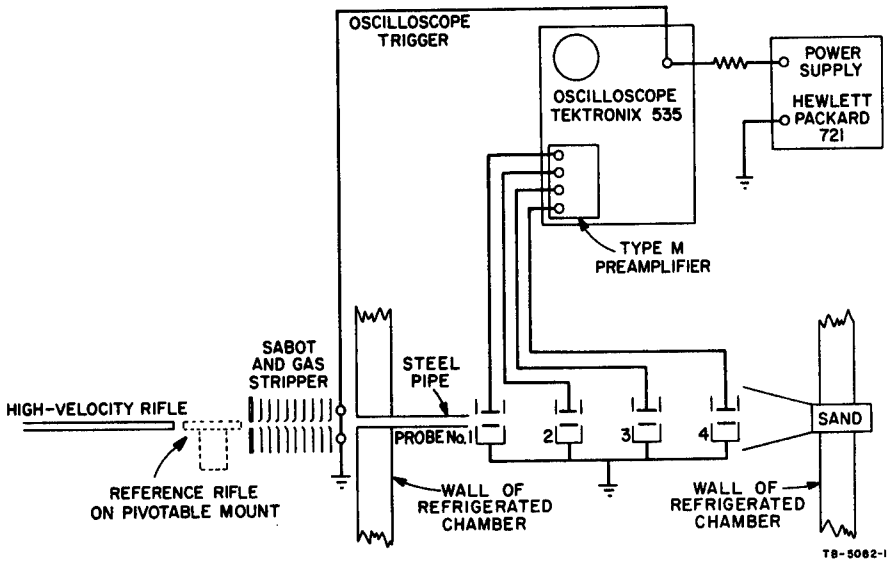

Fig. 1 - Setup for measuring projectile charging

plate positioned adjacent to each end of the cylinder to allow a sharp resolution of the projectile charging pulse. The metal tube is connected to the oscilloscope by 30 feet of RG-58 cable. The dimensions of the projectile and electrode are such that all of the field lines from charge residing on the projectile terminate on the tube. Thus the projectile charge is obtained from the peak induced voltage V measured at the oscilloscope using the relationship

$$q = CV \qquad (2)$$

where q is the projectile charge in coulombs and C is electrode system capacitance in farads (including probe, cable, and instrumentation capacitance to ground--C = 1188 pF for the experimental setup).

A typical set of experimental data is shown in Figure 2. First, two shots were fired from the standard load reference Magnum rifle (always at a velocity of roughly 1600 ft/s). These reference shots were needed to provide information on the fog density within the chamber since it is not possible to reproduce the density accurately. Next, two data shots were fired from the custom-made 36-inch-long cannon having a 22 caliber smooth bore and a 220 Swift breech. Projectile speeds were varied from about 1800 to 4000 ft/s by varying powder loads (1 to 2.5 grams of military 4064 cellulose powder) in the 220 Swift cartridges. Finally, two more reference shots were fired to assure that cloud conditions within the chamber had not changed during the experiment. The increase in projectile charge in passing between successive electrodes is clearly evident in the figure. Also evident is the way in which projectile velocity can be read from the oscillograms simply by measuring the time between successive pulses.

The results of the measurements from probe 4 are shown in Figure 3. In spite of the scatter in the data, it is evident that the total charge acquired by the projectile decreases with increasing speed. In particular, it should be noted that no charging whatsoever was measured on the 16 shots fired at speeds greater than 3000 ft/s. Various experiments were conducted to verify that the absence of charging at speeds above 3000 ft/s was indeed real.

In casting about for explanations for the absence of charging it was argued that the observed effect might be caused by the melting of the ice crystals by the energy of the impact. Flight test experience indicates that clouds composed of water droplets tend to charge an aircraft at a much lower rate than do clouds containing ice crystals. Thus, if an ice crystal is completely melted as the result of an impact, one would expect greatly reduced charging. The maximum possible heat input to the crystal at the time of impact is given by the kinetic energy of motion, $KE = 1/2\ Mv^2$, where M is the ice crystal mass and v is the velocity of the crystal with respect to the projectile. It is shown in Reference 11, that assuming an initial temperature of -55°C, an ice crystal can be completely melted by the kinetic energy of an impact at velocities in excess of 3150 ft/s. At reduced speeds, only part of the ice crystal would be melted. If the charge acquired by an ice crystal is proportional to the mass of the ice it contains, one can argue

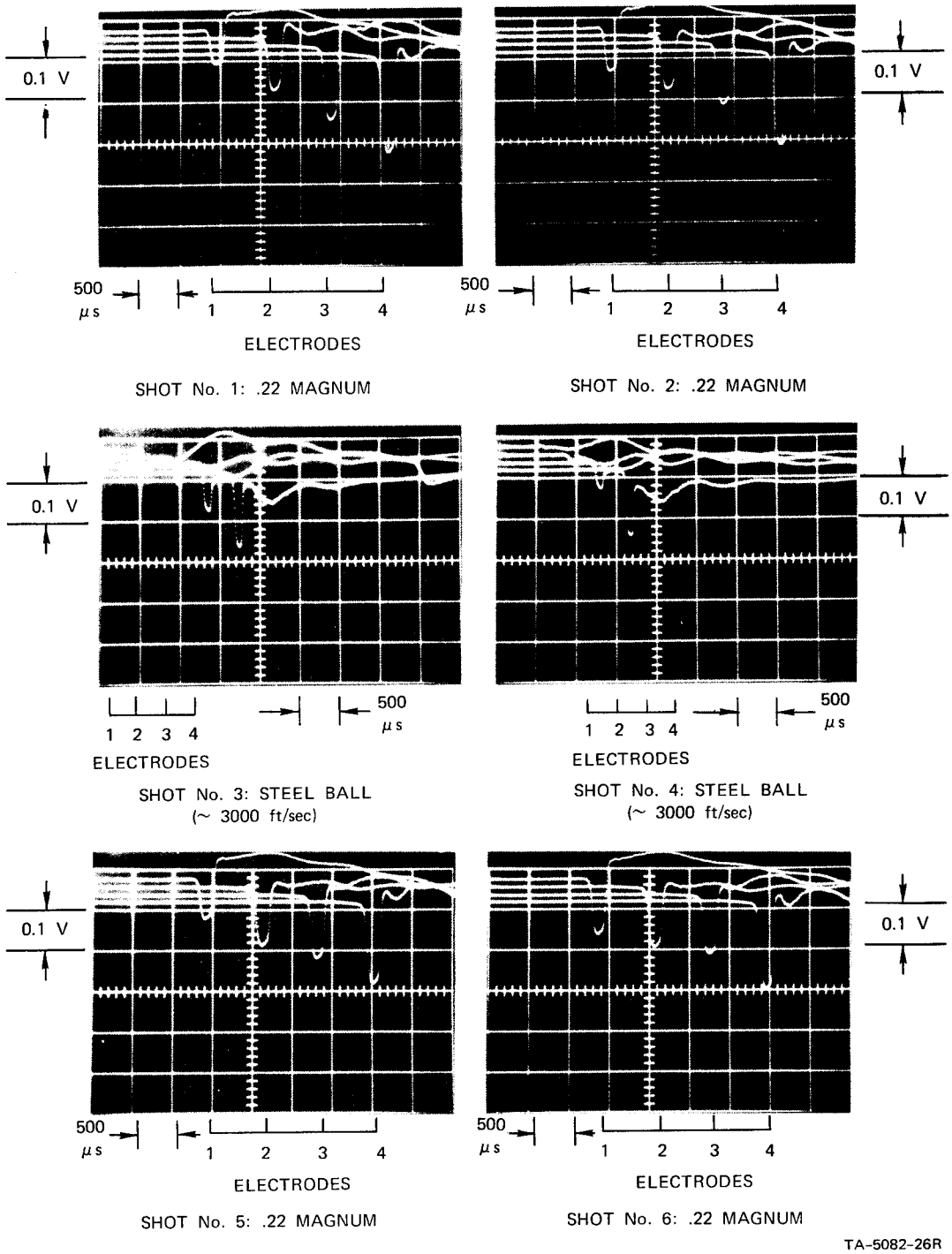

Fig. 2 - Typical projectile charging oscilligrams

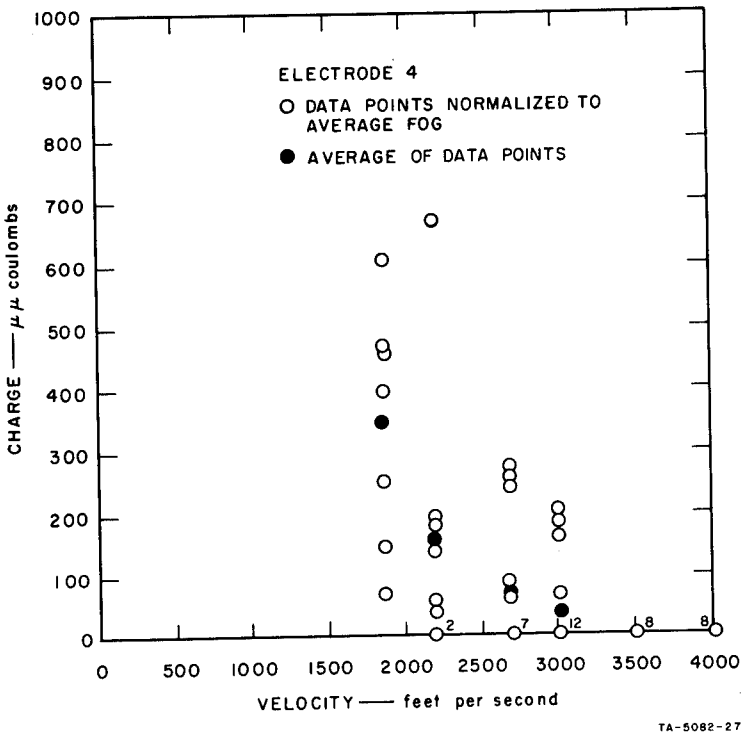

Fig. 3 - Projectile charge 5.5 feet inside chamber

that the particle charge will be proportional to the unmelted ice mass remaining after an impact. A curve of unmelted ice-crystal mass as a function of velocity (assuming that all kinetic energy is transformed to thermal energy) is plotted in Figure 4. Average values of measured charging at the three electrode locations, normalized to fit the curve at 1870 ft/s are also plotted in the figure. The fact that the charging decreases with increasing speed in the same general manner as the unmelted ice mass, and the fact that charging vanishes at roughly the speed required to permit the crystal to melt indicate that melting is very likely responsible for the reduced charging resulting from ice-crystal impacts at supersonic speeds.*

APPLICATION OF ICE FOG EXPERIMENTS TO AIRCRAFT CHARGING - To apply the results of the projectile charging data to aircraft, it is assumed that the ice-crystal sizes and particle concentrations encountered by any vehicle will be similar to those encountered during flight tests on the KC-135 prototype and 707 Aircraft.[5,6] During these tests, maximum charging rates of 5 to 10 ma were observed, but it was found that the charging rate only rarely exceeded 3 ma, so that discharger systems capable of eliminating corona noise under 3-ma charging conditions proved quite effective. During these flight tests it was also determined that the effective area of the KC-135 prototype at 600 mph was only 20 to 25 percent of the projected frontal area of the wings. Using these data and the NACA water-droplet impingement data of Reference 18 for subsonic airfoils, it was determined that this impingement efficiency is obtained if one assumes that the impinging ice crystals are equivalent to water droplets having a diameter of 20 to 30 microns. The data of Reference 19, furthermore, indicate that at subsonic speeds the airfoils are so much more effective in intercepting particles that the contribution of the fuselage can be ignored with little error.

From the speed, altitude, and effective droplet size, the droplet impingement data of NACA for subsonic airfoils can be used to determine

*Dr. E. T. Pierce of SRI has suggested as an alternative explanation the fact that the transfer of charge from an ice crystal requires the migration of ions within the ice crystal. These ions have finite mobilities so that the amount of charge transferred during an impact is proportional to the time duration of contact. No calculations have been carried out yet to test this alternative explanation.

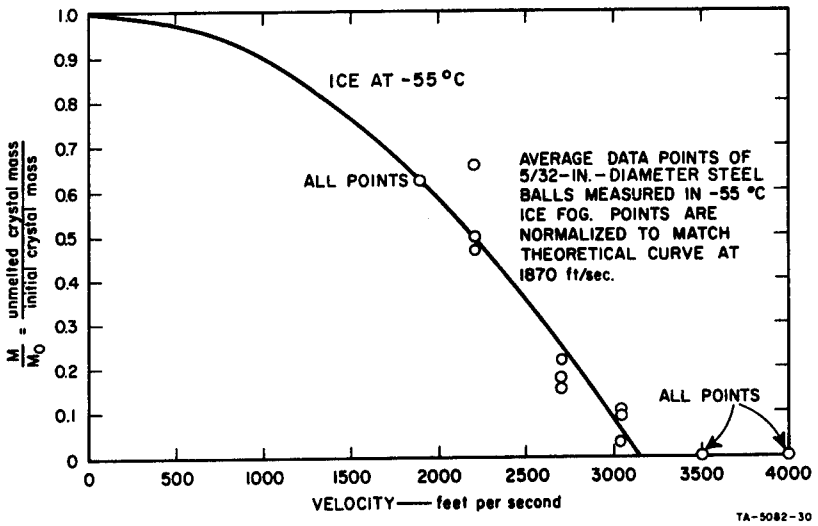

Fig. 4 - Comparing unmelted ice mass to measured charge

the effective area of other vehicles, assuming that the major contribution will continue to be from the airfoils. In addition, impingement data are available for double-wedge airfoils at supersonic speeds in Reference 14. Unfortunately, because both subsonic and supersonic droplet impingement data are not available for a single airfoil, it will be necessary to use an NACA airfoil for subsonic data and a double-wedge of the same thickness-to-chord ratio for the supersonic data.

In the example that follows, the NACA 65_1-208 airfoil was used for intercept area at subsonic speeds, and a double wedge of the same thickness-to-chord ratio, 0.08, was used for supersonic speeds. Figure 5 shows the ratio of the effective area to the frontal area for an effective particle diameter of 20 microns, an altitude of 15,000 ft, and airfoils with a 14-foot chord. The data for the supersonic double-wedge airfoil are available only for the Mach 1.1 to Mach 2 speed range; hence, these data have been extrapolated, as indicated by the dashed portion of the curve, to higher speeds by extending the curve with a straight line with the slope of the curve at Mach 2. The data are discontinuous in the vicinity of Mach 1, but as has been argued earlier, there is no reason to expect that the effective area will undergo drastic changes in this transonic region.

From the variation of effective area and the charge per particle with speed, it is possible to compute the total charging rate that may be expected on a particular aircraft. For the purpose of this computation, it is assumed that the Mach 3 to 10 aircraft will be approximately two-thirds the size of the KC-135 prototype, and that the charging conditions are such that the KC-135 would be charged at the 3-ma rate when flying at 600 mph. The charging current is thus

$$I_{chg} = I_o\left(\frac{A_e}{A_{eo}}\right)\left(\frac{q}{q_o}\right)\left(\frac{U}{U_o}\right) \qquad (3)$$

where subscript zero refers to the value of the quantity at 600 mph. The ratio A_e/A_{eo} is obtained from Figure 5 and the ratio q/q_o is obtained from projectile charging data of Figure 4. The current I_o is the charging current to the aircraft at 600 mph under charging conditions that produce 3 ma of charging current on the KC-135. Because the effective area does not scale directly with the dimensions of the aircraft, however, the droplet impingement data of Reference 18 must be consulted to determine the charging current I_o on the two-thirds-scale aircraft that corresponds to 3 ma on the KC-135. For a unit length of airfoil having a 14-foot chord, the frontal area is 2/3, and the percentage frontal area is 0.825 that of a similar 21-foot chord airfoil. Thus, the ratio of effective areas is 0.55, and

$$I_o = \frac{A_{eo}}{A_{eKC-135}}\,3 \approx 1.65 \text{ ma} \qquad (4)$$

for an aircraft two-thirds the size of the KC-135.

The aircraft charging currents computed by this method are shown in Figure 6 as a function of aircraft speed. It is noted that because of ice-crystal melting, the charging rate decreases rapidly at speeds above 1500 mph. Extrapolation

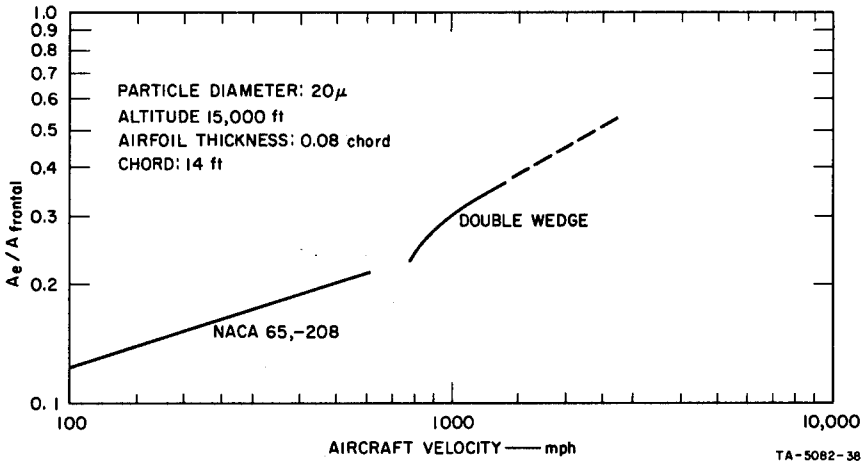

Fig. 5 - Advanced aircraft effective area

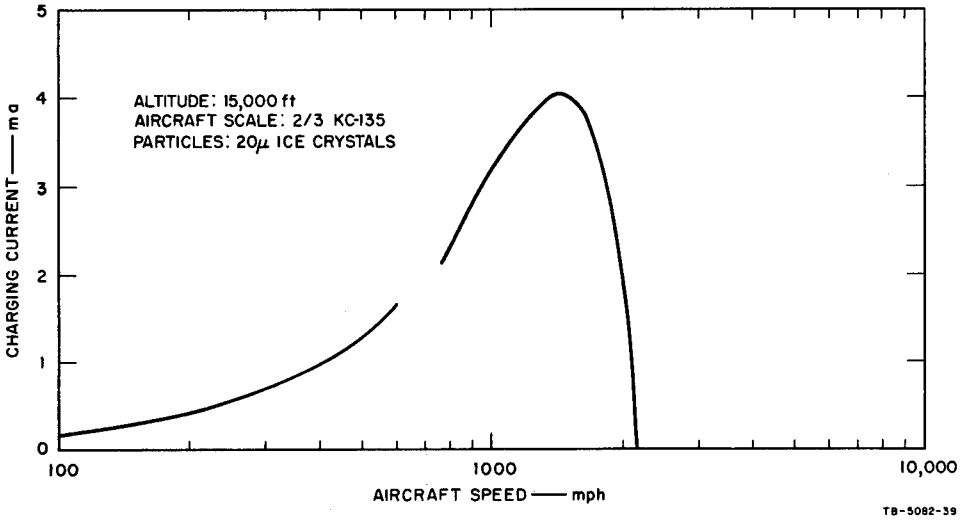

Fig. 6 - Predicted charging current for advanced aircraft

of the effective area data above Mach 2 thus does not affect the critical values of charging current deduced from this analysis. The maximum charging current occurs at about 1400 mph and is only 2.6 times the charging current at 600 mph. It is also noted that the missing transonic data would apparently fall well below the maximum charging rate.

DEVELOPMENT OF FLIGHT TEST INSTRUMENTATION

GENERAL - The results of the laboratory and theoretical study discussed in the previous section served to guide the instrumentation development program. They pointed out areas in which additional flight test data were needed, and they indicated the signal level ranges that should be anticipated at the outputs of the various sensors.

The instrumentation falls into two broad categories: First, the instruments employed to measure various aspects of vehicle electrification, and second, instrumentation associated with noise spectral measurements on the vehicle.

Since the way in which individual particle charge varies with speed on a full-scale vehicle is of great importance, provisions were made to determine the average particle charge as a function of speed. This measurement is required to verify

the results of laboratory charging measurements which were made with both the ice crystals and the moving body being smaller than they would actually be in the case of an aircraft flying through a typical cloud.

Provisions have been included to study the way in which the effective intercepting area of the aircraft varies with speed. This can be done by measuring the current arriving on a series of four isolated conducting patches located at selected points on either an airfoil or on the nose radome of the flight-test vehicle. One patch will be located at the leading edge and succeeding patches will be located farther aft. As speed is increased, patches farther aft on the aircraft should contribute an increasing fraction of the total charging current. This measurement has not been performed on either subsonic or supersonic aircraft.

In connection with studies of subsonic vehicle electrification, laboratory techniques were developed that predicted with considerable accuracy corona threshold voltages, and discharge currents from the extremities of an aircraft.[5,6] It is important to verify the accuracy of these techniques on a supersonic vehicle. The discharge current studies will be accomplished essentially by measuring the current leaving selected dischargers on the airfoil extremities of the test aircraft.

Frictional electrification, resulting from impact with particles in the path of the aircraft, is not the only mechanism by which a vehicle can become charged. Processes occurring within the jet engines can also produce charging currents of hundreds of microamperes.[13,14] As is indicated in Reference 11, at least six possible charging mechanisms have been proposed to explain the observed charging. Furthermore, laboratory experiments with an ethylene-oxygen rocket motor pointed out that relatively trivial details of motor design can have a marked effect upon engine charging current.[11] It is important, therefore, that experimental flight test data on engine charging be obtained from engines of various types and sizes. Such data, in addition to being applicable to the test vehicle in question, will be useful in testing the validity of theoretical predictions.

The instrumentation will include a field meter to measure the potential of the aircraft. By combining the field meter data with either charging patch data or discharger data, it is possible to compute the total charging current to the airplane and to infer the total effective intercepting area for the airplane.

Since the charging of dielectric frontal surfaces on an aircraft results in noise-producing streamer discharges on the surface, provisions are included in the instrumentation system to study this noise mechanism at supersonic speeds.

In the laboratory phase of the present program, calculations were made from which it was possible to postulate the vehicle-induced interference that should be experienced on a vehicle operating in the supersonic speed range.[11] These estimates are based upon predicted charging rates,[11] and upon laboratory studies of noise-generation and coupling mechanisms.[5,6] Noise measurements will be made during the flight tests to verify predicted noise levels, and to determine if any unanticipated sources of vehicle-induced interference exist at supersonic speeds.

DESCRIPTION OF FLIGHT TEST INSTRUMENTATION SYSTEM - A detailed description of the electronic circuitry employed in the instrumentation system will not be attempted here. Instead consideration will be restricted to system design philosophy. A complete description of the system including the sensors and electronic circuitry is given in Reference 12.

In general, all of the equipment was designed and constructed using solid-state circuits to achieve maximum compactness and reliability. The sole exception is the noise source for calibrating the spectrum analyzer receivers, which includes a noise diode vacuum tube. To standardize the instrumentation as much as possible, commercially available operational amplifiers were used wherever practical. Integrated circuits were used to achieve extreme compactness where it was required.

The restrictions imposed by the potential flight-test vehicles dictated many of the characteristics of the instrumentation. For example, it was not possible to carry a flight test observer on any of the vehicles contemplated for the actual flight tests. This means that the instrumentation must be capable of operating virtually without attention. In particular, where instrument sensitivity might change during the flight, the instrumentation must have provision for in-flight calibration. Since it is not possible to adjust gain settings in flight, the dynamic range of the instrumentation must be adequate to cover the anticipated ranges of the variables. (It may be necessary to adjust the overall gain of a particular system to compensate for errors in estimation, but these adjustments will be made on the ground between flights.) The high stagnation point temperatures on a highly supersonic vehicle requires that sensor design be such that its operation is not degraded by high temperatures. Since it was not possible to specify the amount of space that would be available for the flight test instrumentation and since form factor was even

less well-known, all of the instrumentation was designed in the form of modules, which can be assembled and interconnected to suit the available space.

The design philosophy was to make the instrumentation as stable as possible so as to make in-flight calibration unnecessary. In the case of the spectrum analyzer, it was felt that the validity of the data would be enhanced by provisions for in-flight calibration. Dynamic range in the instrumentation is achieved by using more than one output channel per instrument. The sensitivities of the channels differ by a factor of 10. This technique was chosen in preference to automatic gain switching, since experience on previous precipitation static flight tests indicates that the charging and noise vary so rapidly that attempting to adjust gain during a period of charging serves only to confuse and complicate the data-reduction process.

The output from each instrumentation system has been designed to range between 0 and 5 volts dc to make it compatible with standard IRIG subcarrier oscillators. In this way the data can be telemetered or the subcarrier oscillators can be used to enable the data to be recorded on a channel of a wide-band tape recording system. Although a large number of data outputs are indicated, the data rate is sufficiently slow that the outputs could go to a commutator and be recorded on a single tape recorder channel.

A block diagram of the system is shown in Figure 7. Beginning at the top of the figure, we will briefly discuss each of the instrumentation systems in fairly general terms.

The manner in which individual particle charge varies with aircraft speed is studied by means of the particle probe. The probe is an isolated electrode protruding forward of the airplane into a region of undisturbed air. The probe, as shown in the diagram, serves two functions: that of counting the precipitation particles and that of measuring the charge that they impart. A particle striking the probe produces a pulse in the probe; this pulse is amplified by the preamplifier located in the probe housing and is fed to an analog pulse counter. The output of the counter is proportional to the number of particles striking the probe per unit time. Also, each particle striking the probe deposits an increment of charge on the probe equal to the charge acquired by the particle. This charge flows to the input of the dc amplifier through the resistor connected between the probe and the amplifier input. By dividing the probe current by the number of particles striking the probe per second, we obtain the average charge per particle.

The field meter system determines the potential of the aircraft during flight. The field meter consists of a rotating vane detector head (field mill) to be mounted in a hole in the aircraft skin so that the rotating vanes are located on the outside of the airplane. The signal generated in the detector head is proportional to the magnitude of the electric field at its location. This signal is first amplified by the preamplifier in the head, then fed to a system of amplifiers and synchronous detectors to produce a 0 to 5 Vdc output proportional to the magnitude and polarity of the input field.

Provisions are included to measure the charging current to four electrically isolated patches located on a frontal surface of the aircraft (either the leading edge of a wing or the radome). The current arriving on each patch flows to a low-pass filter, eliminating any alternating current signals induced in the line connecting the patch and the amplifier. The output of the low-pass filter is fed to a dc amplifier, producing a 0 to 5 Vdc output that indicates the polarity and magnitude of the current arriving on a patch.

Data from the isolated patches serve two general functions. First, the data provide information regarding the way in which the effective intercepting area of the aircraft varies with aircraft speed. Second, data from the patches are useful in determining the extent to which aerodynamic forces ahead of a blunt body affect the way in which individual particle charge varies with speed. As is indicated in Reference 11, there is some question of the validity of applying data from the bullet-shooting experiments to a full-scale airplane. It was noted that the 5/32-inch diameter steel ball used in the laboratory experiments had a very small shock stand-off distance. Thus, the aerodynamic forces would not appreciably slow the particle before it struck the ball. This is also true to some extent in the case of the particle probe, which is quite small. The electrically isolated patches however, will be located on a large surface typical of normal aircraft frontal surfaces. Thus, by comparing the relative current flowing to the particle probe and to the forward patch, we can infer the extent to which aerodynamic forces slow the particles. This provides an indication of the degree to which the laboratory bullet-shooting data must be corrected before being applied to a full-scale airplane.

The current leaving a set of dischargers mounted on an airfoil tip is measured by passing the current through a low-pass filter and into a dc amplifier. These data will be useful in determining total aircraft charging current, and in verifying laboratory predictions of corona

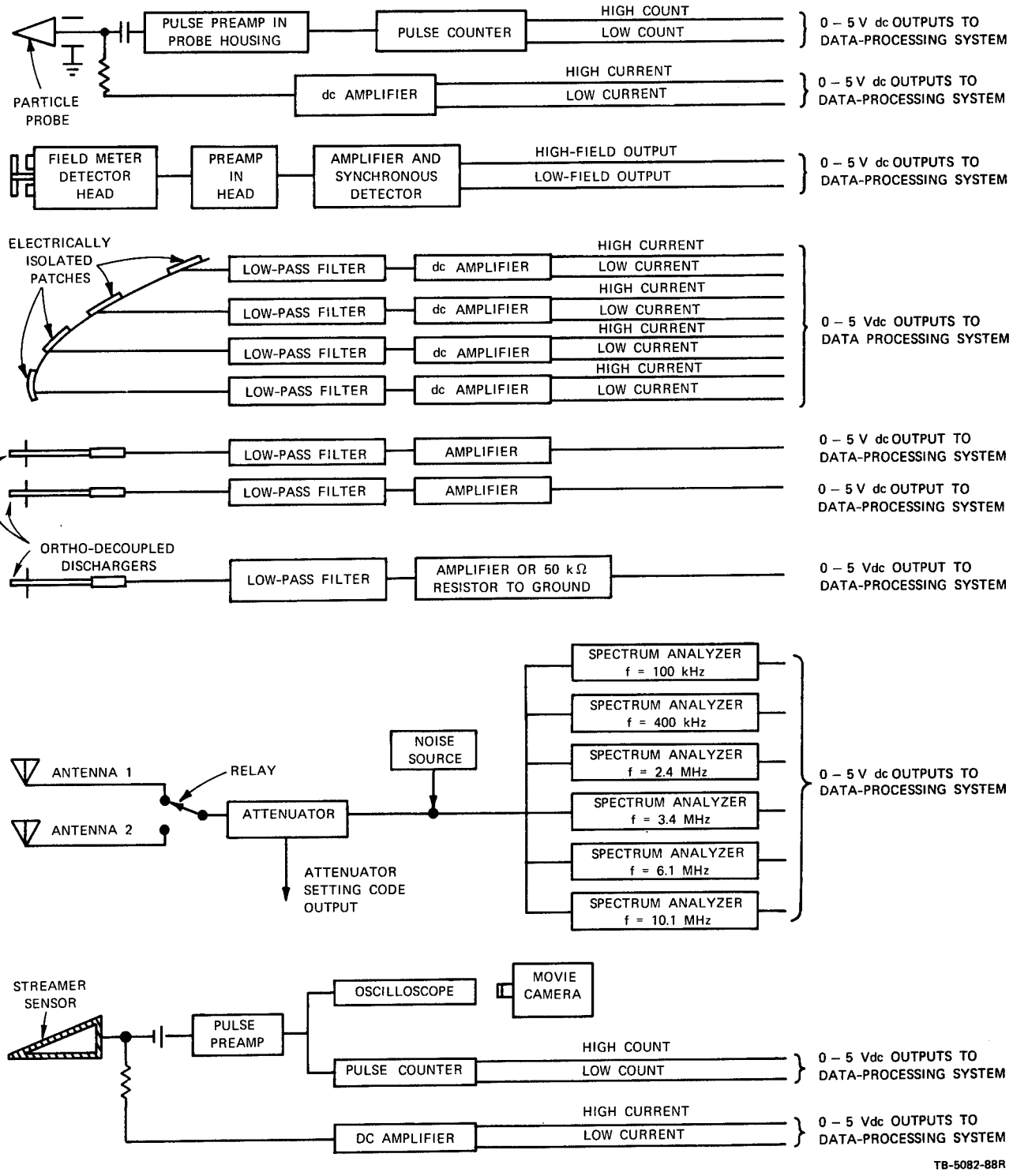

Fig. 7 - Block diagram of instrumentation

threshold. On some flights it is possible to use the same system to study the corona thresholds of external stores mounted on the flight test aircraft.

Included in the instrumentation is a spectrum analyzer to verify the existence of predicted noise levels, to determine whether or not unanticipated noise sources exist, and to test the effectiveness of any noise-reduction schemes that may be incorporated on various flights of the test aircraft.

The spectrum analyzer is designed to measure the noise spectrum existing in two antennas located on the aircraft. The relay ahead of the attenuator periodically switches from one antenna to the other. The attenuator includes a coding system, which permits the setting to be determined from the recorded data. Following the attenuator is a broadband noise source capable of producing noise at three different levels to provide calibration signals at three points on the spectrum analyzer response curve. The noise source will be activated by a calibration order from the pilot prior to beginning the interference study experiment and after it has been concluded. The spectrum analyzer consists of six receivers turned to discrete frequencies between 100 kc/s and 10 Mc/s. Each receiver has provisions to periodically switch its center frequency by up to 20 kc/s to avoid the possibility of a strong signal on the selected channel from completely obliterating the flight test information. (Since the aircraft may operate over a large radius during a flight test, it is usually impossible to set the receivers on unoccupied channels.) The 0 - 5V output from the spectrum analyzer channel will be fed to the data-processing system aboard the aircraft.

The streamer sensor is simply a ring of conducting tape or paint applied around a dielectric region such as a windshield on the front of the aircraft. The system simultaneously records the pulses produced by the individual streamers and measures the total current arriving on the probe. A streamer occuring on the dielectric surface produces a pulse in the probe; this pulse is amplified by a preamplifier located near the probe and is fed to an oscilloscope and to a pulse counter. The waveform displayed on the oscilloscope is recorded by means of a 16 mm movie camera. The pulse counter generates an analog output proportional to the pulse prf. The dc charge flowing to the probe is fed to the input of a dc amplifier through a resistor connected between the probe and the amplifier input.

FLIGHT TESTING

The aircraft used for the supersonic flight tests is an F-4 operated from Eglin Air Force Base, Florida. The general arrangements of the sensors on the test aircraft is shown in Figure 8. Since the test aircraft was already equipped with two receiving antennas, they were used for the noise measurements. One was the standard LORAN antenna located in the plastic vertical fin tip. The second was a special towel-bar-type electric dipole installed on the top of the fuselage ahead of the vertical fin. The charging patches were installed in a row along the top surface of the nose radome. A special housing was built into the chin radome to mount the particle probe protruding forward from the radome. A 1/4-inch-wide band of silver paint just inside the rim on the left side windshield served as the streamer sensor. Three commercial dischargers mounted on the left wing tip region were instrumented to measure discharge current. The major portion of the system electronics was located in an instrumentation pod attached to the belly of the aircraft along the center line. The electric field meter sensor was located in the bottom of the instrumentation pod.

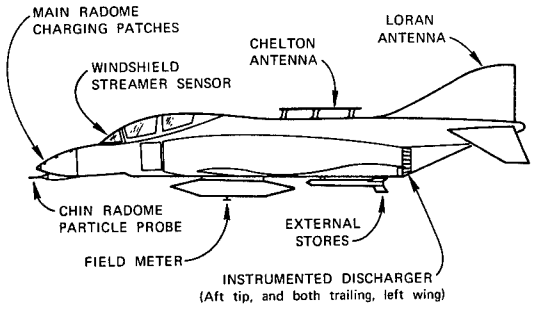

Fig. 8 - Sensor locations on F-4

The Boeing Company was responsible for designing and building all of the special racks and fixtures necessary to integrate the system into the flight test aircraft. Boeing personnel also participated in the actual system installation and checkout.

An idea of the problems one encounters working in a fighter aircraft is evident from Figures 9 and 10 which illustrate the odd forms into which the instrumentation had to be packaged to fit into the available space in the instrumentation pod. (The availability of the pod itself was fortuitous since, otherwise, the packaging would have been even more difficult.) It was possible to place all of the circuit cards in a single

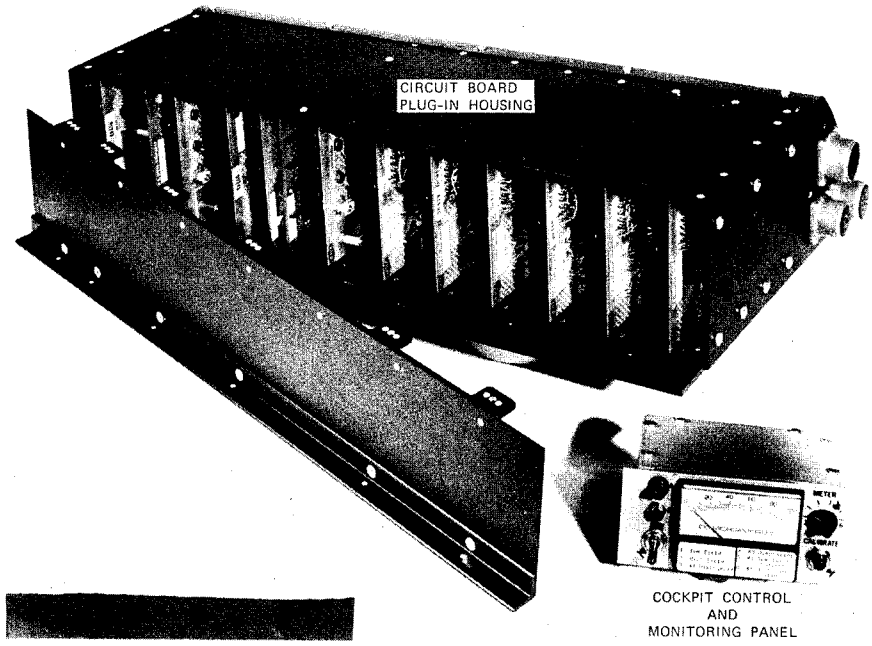

Fig. 9 - Typical instrumentation package for F-4 flight tests

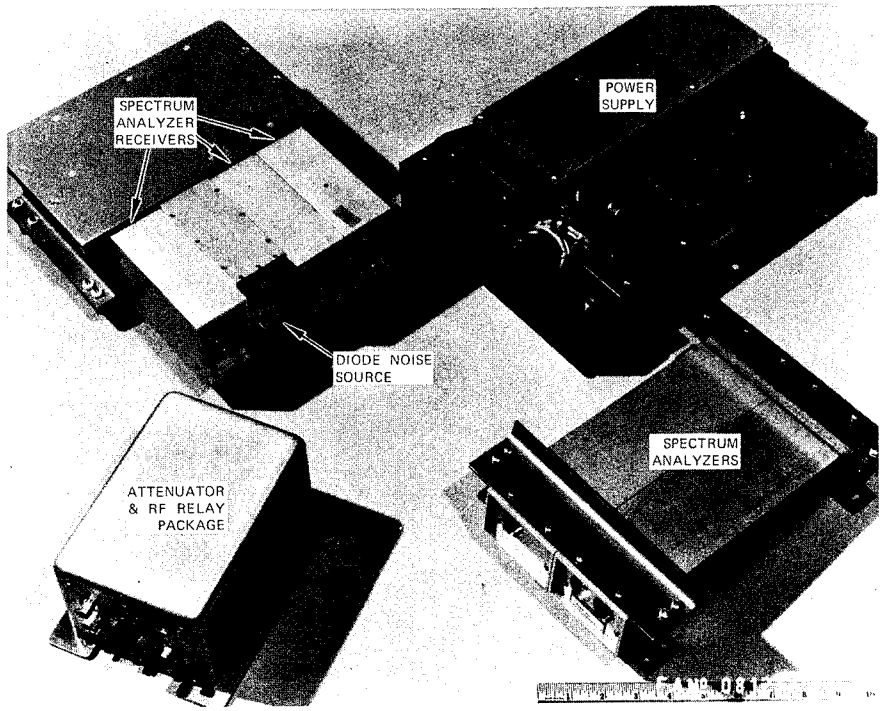

Fig. 10 - Packaging of spectrum analyzer receivers and power supplies

housing as shown in Figure 9. Some of the corners of the box had to be rounded to fit into the pod, but it was possible to get everything in. This same figure shows the control and monitor panel located in the aft cockpit. This panel includes a toggle switch to turn on the entire system, a push button to activate the spectrum analyzer calibration sequence, and a meter which could be switched to monitor any one of six selected system outputs. In the case of the spectrum analyzer, it was necessary to break the system down into smaller pieces as shown in Figure 10.

The sensor installation on the nose of the aircraft is shown in Figure 11. The charging patches were made of thin aluminum strips cemented to the outer surface of the radome. Each patch was connected to the instrumentation system by means of a wire leading to the inside of the radome. A grounded guard ring surrounded each of the patches to intercept any current flowing toward the patch from some other part of the radome. The particle probe was mounted in a position such that it sampled essentially undisturbed precipitation particles.

An illustration of the instrumented discharger installation is shown in Figure 12. Essentially, each discharger was electrically isolated by removing a band of conductive paint in the region where the plastic rod meets the metal shank. The wire to the instrumentation was attached to the discharger aft of this isolation band.

The way in which the instrumentation was made to fit into odd shaped spaces is illustrated in Figures 13 and 14. The recorder used to record the flight test data is also shown in Figure 13.

In general, the design of the instrumentation is satisfactory for the test aircraft being used. As was indicated earlier, if the test aircraft had not been equipped with an instrumentation pod or some other large, empty bay, the problem of installing the instrumentation would have been truly formidable. To insure maximum flexibility in a future flight test measurement program such as this, it would be desirable to keep the system broken down into a large number of small units. If the electronic state-of-the-art permits, the individual subsystems should be made smaller still.

One of the problems encountered in connection with the installation of the present system was that of getting wiring out to inaccessible regions of the aircraft such as the wing trailing edge (where the passive dischargers are mounted. It would be desirable to have some way to get information from these locations to the main instrumentation system without having to run wires. Perhaps a miniature telemetry system could be developed using an RF source or a gallium arsenide laser diode to accomplish this. One might even be able to use the discharge current to power the system.

As this is being written, the shakedown of the system is nearing completion, but insufficient flight test data have been reduced to permit inclusion in this paper.

REFERENCES

1. H. G. Hucke, "Preparation Static Interference," Proc. IRE 27, 5, May 1939.

2. R. C. Ayers and J. O. Jarrard, "Aircraft Precipitation Static Investigation," Contract W 33-106 SC-70, Trans-World Airlines Inc.,August 1944.

3. Ross Gunn et al., "Army-Navy Precipitation Static Project," Proc. IRE 34, 4 and 5, 1946.

4. R. L. Tanner, "Radio Interference from Corona Discharges," Tech. Report 37, Contract AF 19(604)-266, Stanford Research Institute, Menlo Park, California, April 1953.

5. R. L. Tanner and J. E. Nanevicz, "Precipitation Charging and Corona-Generated Interference in Aircraft," AFCRL 336, Tech. Report 73, Contract AF 19(604)-3458, Stanford Research Institute, Menlo Park, California, April 1961.

6. J. E. Nanevicz, E. F. Vance, R. L. Tanner, and G. R. Hilbers, "Development and Testing of Techniques for Precipitation Static Interference Reduction," ASD-TR-62-38, Final Report, Contract AF 33(616)-6561, Stanford Research Institute, Menlo Park, California, January 1962.

7. R. L. Tanner and J. E. Nanevicz, "An Analysis of Corona-Generated Interference In Aircraft," Proc. IEEE, 52, 1, January 1964.

8. J. E. Nanevicz and R. L. Tanner, "Some Techniques for the Elimination of Corona Discharge Noise in Aircraft Antennas," Proc. IEEE, 52, 1, January 1964.

9. R. L. Tanner and J. E. Nanevicz, "Radio Noise Generated on Aircraft Surfaces," Final Report, Contract AF 33(616)-2761, Stanford Research Institute, Menlo Park, California, September 1956.

10. J. E. Nanevicz, "A Study of Precipitation Static Noise Generation in Aircraft Canopy Antennas," Tech. Report 62, Contract AF 19(604)-1296, Stanford Research Institute, Menlo Park, California, December 1957.

11. J. E. Nanevicz, E. F. Vance, W. C. Wadsworth, and J. A. Martin, "Low-Altitude Long-Range All-Weather Vehicle Interference Investigation--Part I Laboratory Investigation," AFAL-TR-65-239, Contract AF 33(615)-1934, Stanford Research Institute, Menlo Park, California, December 1965.

12. J. E. Nanevicz, E. F. Vance, and W. C. Wadsworth, "Low-Altitutde Long-Range All-Weather Vehicle Interference Investigation--Part II

Development of Flight Test Instrumentation," AFAL-TR-65-239, Stanford Research Institute, Menlo Park, California, December 1966.

13. R. G. Dorsch, P. G. Sapar, and C. F. Kadow, "Impingement of Water Droplets on a Sphere," NACA TN 3587, National Advisory Committee of Aeronautics, Washington, D.C., November 1955.

14. J. F. Serafini, "Impingement of Water Droplets of Wedges and Double-Wedge Airfoils at Supersonic Speeds," NACA Report 1159, Lewis Flight Propulsion Laboratory, Cleveland, Ohio, 1954.

15. E. E. Callaghan and J. E. Serafini, "Analytical Investigation of Icing Limit for Diamond Airfoil in Transonic and Supersonic Flow," NADA TN 2861, National Advisory Committee of Aeronautics, Washington, D.C., 1953.

16. M. Tribus and A. Guibert, "Impingement of Spherical Water Droplets on a Wedge at Supersonic Speeds in Air," Jour. Aero. Sci., 19, 6, June 1952.

17. J. E. Nanevicz and W. C. Wadsworth, "Measuring the Electrical Charge and Velocity of a Moving Projectile," First Interim Engineering Report, Contract AF 33(615)-1934, Stanford Research Institute, Menlo Park, California, January 1965.

18. R. J. Brun, H. M. Gallagher, and D. E. Vogt, "Impingement of Water Droplets on NACA 65,-208 and 65,-212 Airfoils at 4° Angle of Attack," NACA TN 2952, Lewis Flight Propulsion Laboratory, Cleveland, Ohio, May 1953.

19. E. F.Vance and J. E. Nanevicz, "Aircraft Propeller Corona Threshold and its Effect on Precipitation Static Noise Reduction," Tech. Report 77, Contract AF 19(628)-325, Stanford Research Institute, Menlo Park, California, November 1963.

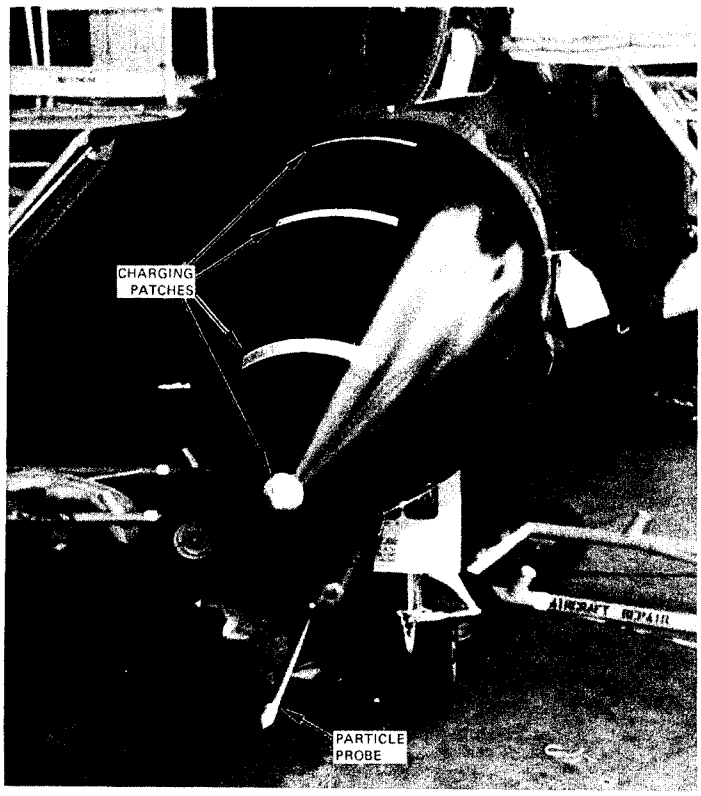

Fig. 11 - Sensor installation on nose of F-4 flight test aircraft

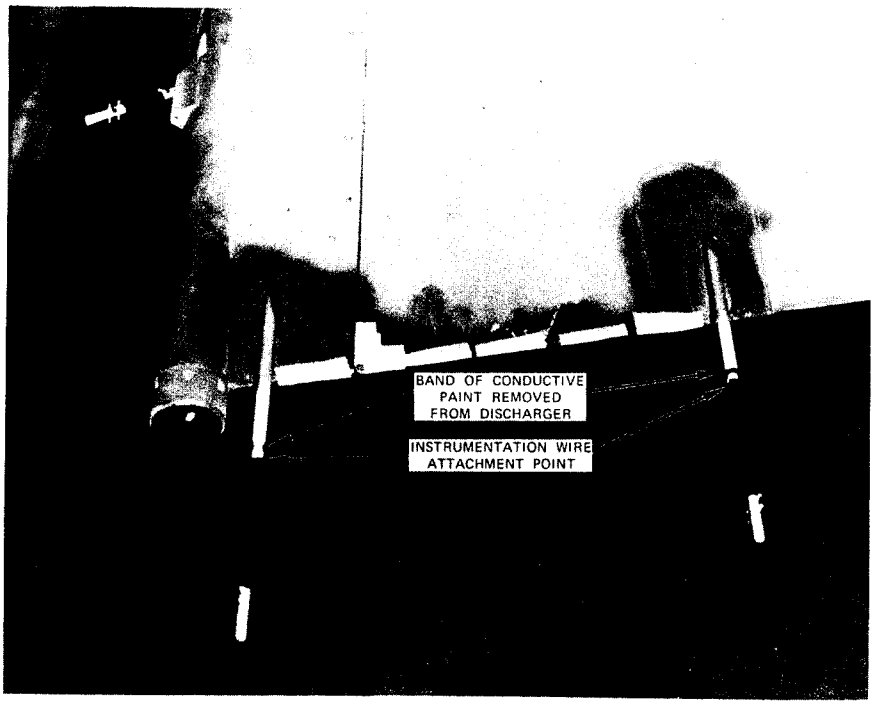

Fig. 12 - Instrumented discharger installation on F-4 test aircraft

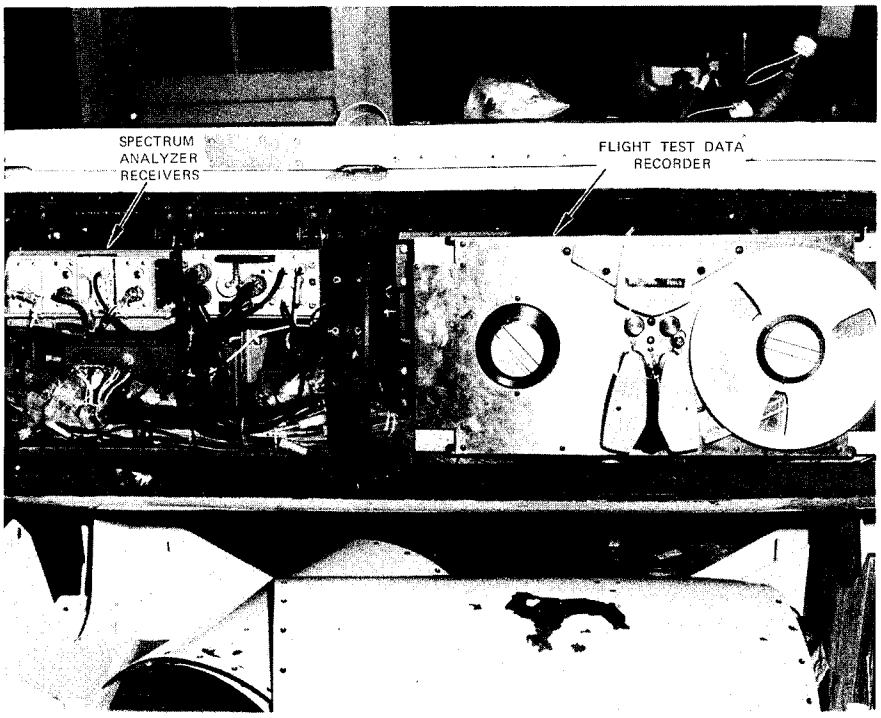

Fig. 13 - Flight test data recorder in instrumentation pod on F-4 test aircraft

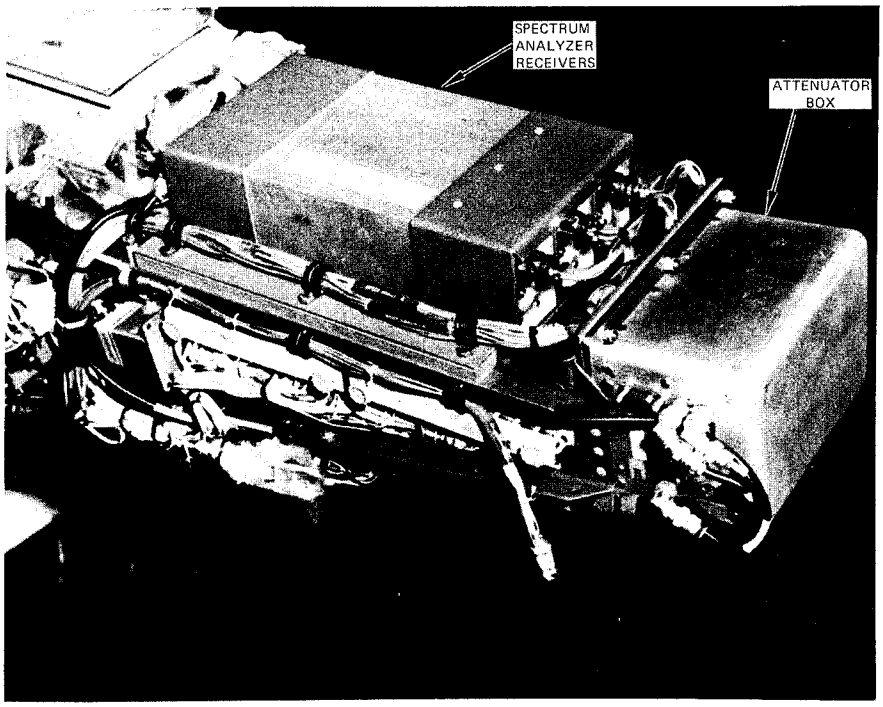

Fig. 14 - Instrumentation installation in pod on F-4 test aircraft

700922

WATERFALLS, BATHROOMS AND--PERHAPS--SUPERTANKER EXPLOSIONS

E. T. PIERCE
Stanford Research Institute

ABSTRACT

The electrical effects developed by Lenard splashing near waterfalls, under laboratory conditions, and within the closed environments of a bathroom and a cargo tank of an oil supertanker during seawater washing operations, show a consistent phenomenology. Both theory and experimental evidence suggest that electrical conditions in the closed container atmospheres are defined by

$$dN/dt \approx Q/e - (10^{-3})N$$

In this equation, N is the number density of large charged carriers (large ions and haze droplets), t is time, and e the electronic charge. The rate of charge production, Q, is approximately -10^{-12} coulomb per gram for the bathroom water and $+10^{-11}$ coulomb per gram for the seawater. These values correspond to number densities of some 10^5 per cm^3 and space-charge densities of $\mp 10^{-8}$ coulomb per m^3. The field within a closed container is approximately proportional to the product of the linear container dimension and the space-charge density.

Conditions within an oil supertanker cargo tank during the washing operations are considered. It is concluded that the electrification is sufficiently intense for a large-scale spark streamer to have a good chance of developing. This chance--and therefore the explosion hazard--becomes larger with an increase in the size of the cargo tank.

BASIC PHYSICAL MECHANISMS ARE OFTEN OPERATIVE in diverse environments. This paper describes how the effects of one such mechanism--the production of static electrification by the splashing of water*--can be identified in the very different circumstances near waterfalls, in a typical bathroom, and within the cargo tanks of large oil tankers during cleaning operations. It is shown, partly by means of simplified theory valid probably to within an order of magnitude, that there is a coherence and consistency of behavior between the electrical effects for all the diverse environments. Consequently, the way in which electrification develops on a large scale in the supertanker can be partially predicted from the experience in the other environments. Since the supertanker electrification has probably been responsible for several disastrous explosions and the loss of one vessel, we have a most interesting example of how the investigation of a basic phenomenon under simple--and in certain instances apparently almost frivolous--circumstances, can contribute quite unexpectedly to the solution of an applied problem of very great magnitude.

WATERFALL ELECTRIFICATION AND THE WORK OF LENARD

The discovery of waterfall electrification is generally ascribed to Lenard, although Lenard's classic paper [1]** starts with the sentence "It has been known for a long time that waterfalls will charge the ambient air with negative electricity." Lenard established by observations in the Alps that splashing at the base of a waterfall introduced negative charge into the atmosphere. This was carried upon fine mist droplets and smaller particles, while the corresponding positive charge flowed away to ground via the large drops and running water. Lenard's experiments were repeated in Yosemite Valley [2,3] and here the results confirmed those of Lenard in every respect where comparisons were possible.

*The process is sometimes known as ballo-electrification.

**Numbers in brackets designate References at end of paper.

Lenard supplemented his waterfall observations by some ingenious laboratory experiments. These indicated that as the violence of the water disruption increased so did the intensity of the electrical effects. However, this tendency did not continue indefinitely; indeed a saturation point appeared to be reached when the velocity of the waterdrops or water-jet, impinging on the disruptive surface, was about 6 m/s. A further increase in this velocity produced--if anything--a decrease in the electrification. It was found that the electrification developed at velocities approaching or exceeding the saturation value was approximately proportional to the mass of water disrupted. There is, however, a considerable spread in Lenard's results, and the values for the quantity of negative electricity produced by the breakup of distilled water range from 10^{-11} to 5×10^{-10} coulomb per gram.

Lenard obtained some most interesting results relating the magnitude of the electrification to the purity of the water. Tap water produced only some 10% of the effect of distilled water. A particularly instructive series of results was obtained with salt (NaCl) solutions. As the solutions increased in strength the size of the effects decreased until for about a 0.01% solution no charge at all was developed when the water disrupted. With a further addition of salt the sign of the electrification reversed, as compared with that for distilled water, and positive charge was introduced into the atmosphere. For a 3.5% solution, which corresponds approximately to surface ocean water, the magnitude of the electrical effects was about 70% of that associated with distilled water but with the reversal in sign.

As first indicated by Lenard the presence of an electrical double layer at the surface is primarily responsible for the electrification produced when water disrupts. For pure water the surface layer contains an excess of OH^- ions, while the H^+ ions tend to reside in the bulk of the liquid. Thus a removal of the surface layer by mechanical disintegration introduces negative charge into the atmosphere on small particles. The addition of salt to the water creates Na^+ and Cl^- ions, and because of the minimum surface energy constraint it is the Na^+ ion that tends to enter the surface layer. Thus the influence of the OH^- ions is reduced and the ballo-electric effect decreased. For sufficiently large salt concentrations the number of Na^+ ions in the surface layer may exceed that of the OH^- ions; there is then a reversal of the sign of the electrification effect [4].

BATHROOM ELECTRIFICATION

Many of Lenard's experimental arrangements are duplicated in the fittings of a modern bathroom; consequently, a bathroom is an extremely convenient environment in which to study the effects of water disruption and to check Lenard's results [5]. Figure 1(a) shows some typical data on the variation of field, E_t, with time within a bathroom of dimensions 3 m × 2 m × 2.5 m. In obtaining Figure 1(a) the shower was operated at a flow rate of 1 liter/s for five minutes, and in this time fields exceeding -500 V/m were developed. After five minutes the shower was shut off, and the field allowed to decay with the bathroom door closed. Figure 1(b) plots field versus time, as measured from the instant of shutting off the shower, on semi-logarithmic paper. The straight line in Figure 1(b) obeys the equation

$$dE_t/dt = -(8 \times 10^{-4})E_t \qquad (1)$$

Obviously the line is an excellent fit to the experimental results.

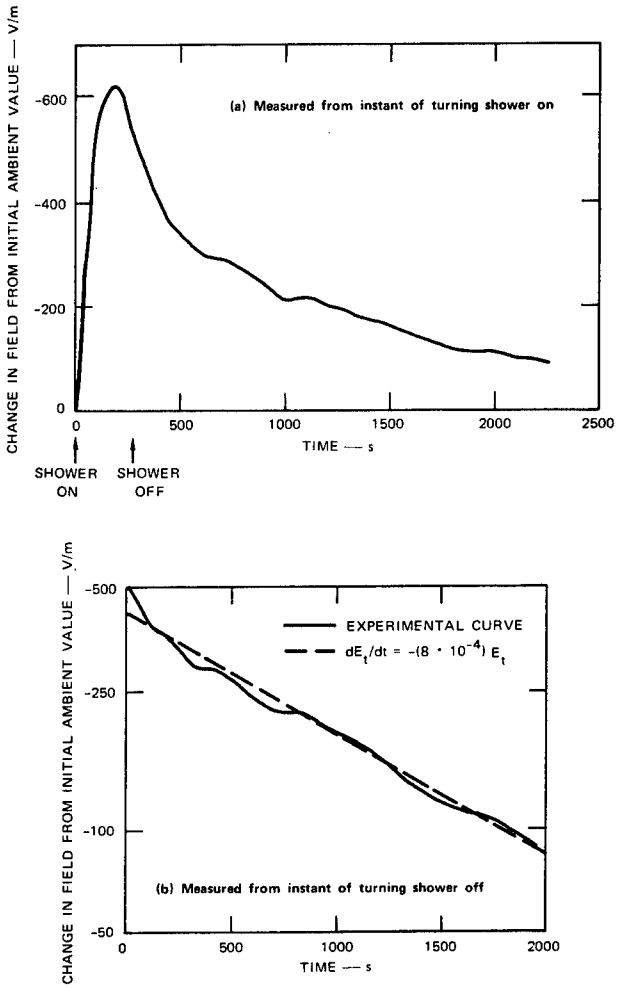

FIGURE 1 FIELD VERSUS TIME IN BATHROOM

SUPERTANKERS. ELECTRIFICATION DURING TANK CLEANING

In December 1969, three disastrous explosions occurred on oil supertankers; one vessel, the Marpessa, sank. All the explosions were associated with the operation of cleaning the cargo tanks. In this procedure strong jets of seawater are used to remove the oil residues. The disruption of the seawater will produce static electrification. It seems quite plausible that the static electrification could become sufficiently intense to generate substantial sparks; these would then ignite an explosive mixture, if such were present within the tank, and thus cause the explosion.

Some pilot measurements have been made of the electrical field produced within a clean cargo tank when the seawater jets are operated.* Typically, in a tank of overall dimensions 46 m × 23 m × 26 m, the measurements indicate that a peak field usually of some +20 kV/m is developed by a water flow of about 100 liters per second. Occasionally, however, fields exceeding 100 kV/m have been measured. The field takes about forty-five minutes to build up to the maximum value; after the operation of the seawater jets has been stopped the decay of the field occupies several hours, and is associated with the disappearance of a bluish haze within the tank.

ELECTRICAL EFFECTS WITHIN A CLOSED CONTAINER

THEORETICAL RELATIONSHIPS BETWEEN ELECTRIC FIELD AND SPACE CHARGE - If we have a conducting spherical container in which the atmosphere carries a uniform space charge of density ρ, the field E_r as a function of distance r from the center of the sphere is defined by Gauss's theorem:

$$\varepsilon_o \iint E_r \cdot dS = \iiint \rho \, dV$$

where the surface and volume integrations apply over a hypothetical sphere of radius r, and ε_o is the permittivity of free space. It follows on evaluating the integrals that

$$E_r = r\rho/3\varepsilon_o \qquad (2)$$

Thus the field is zero at the center of the container (as is obvious from a consideration of symmetry with respect to the space charge) and maximum, $a\rho/3\varepsilon_o$, at the wall (r = a) of the container.

For the more usual case of a symmetrical rectilinear container, such as a room or a cargo tank, the conducting faces--walls, roof and floor--are at the same electrical potential (conventionally taken as zero). In this instance the relationship between the field distribution and the uniform space charge is much more complicated than Eq. (2). An analysis that can be applied is available [6] but the solutions must be numerically evaluated. However, it is again evident from symmetry considerations that the field will be zero at the center of the container; it will also be zero at the meeting line of faces since the electric field cannot be tangential to a conductor. There will be peak values of the electrical field at the mid-points of faces;* for the special case of a cubical container of side b this peak value has been evaluated [7] as being

$$E_b \approx 27 \, \rho b/\pi^4 \varepsilon_o \qquad (3a)$$

or

$$\rho \approx (3.2 \times 10^{-11})(E_b/b) \qquad (3b)$$

APPLICATION OF FIELD/SPACE CHARGE RELATIONSHIP TO BATHROOM AND SUPERTANKER RESULTS - Equation (3) may be applied to derive an approximate value for the space charge developed in a bathroom (Section 3) and in a cargo tank (Section 4). We obtain the effective b by assuming that b^3 is equal to the volume of the container. Hence we have Table 1.

Table 1 - Space Charge Developed within a Container

Container	Volume (m^3)	Effective b (m)	Peak Observed Field (V/m)	Space Charge (C/m^3)
Bathroom (tap water)	3 × 2 × 2.5	~ 2.5	- 600	-7.7×10^{-9}
Cargo Tank (seawater)	46 × 23 × 26	~ 30	+ 20,000	$+2.1 \times 10^{-8}$

*I am very much indebted to Mr. H. O. Valvur and Mr. R. F. Klaver for supplying this information, on the initial results of the tanker experiments, during discussions at Stanford Research Institute on May 20, 1970.

*This field distribution has a practical implication on the best way of measuring the field and space-charge density without the measurement technique distorting the existing conditions. Obviously a field-mill mounted flush at the center of a face is the optimum technique [7].

It is noteworthy that the difference in sign of the space charge for the two conditions confirms the results of Lenard regarding the difference between the break-up of tap water and of seawater. It is most interesting that the order of magnitude of the space charge, 10^{-8} C/m^3, is similar for the two cases of Table 1. This suggests that the limiting charge density is more controlled by processes in the atmosphere of the container than by the container dimensions.

CHARGE CARRIERS AND BALANCE EQUATIONS - If we have a mixture of charge carriers within a closed container then the space charge per unit volume is defined by

$$\rho = \Sigma\, {}_iN_1\, {}_iq_1 + {}_jN_2\, {}_jq_2$$

where ${}_iN_1$ is the concentration of a specific type of positive charge carrier of charge ${}_iq_1$, while ${}_jN_2$ and ${}_jq_2$ are the corresponding symbols referring to the negative carriers. The charges ${}_iq_1$ and ${}_jq_2$ are often taken as equal in magnitude to the electronic charge. It is usual in fair-weather atmospheric electricity to assume that there are only two main types of charged carriers, or--to use the more usual term--ions. We have the small ions, produced by ionizing radiations interacting with the atmosphere, and consisting of a few molecules aggregated to form a particle of radius less than 10^{-3} μ (10^{-7} cm). We also have large ions created by the attachment of a small ion to an Aitken nucleus of radius 10^{-2} to 10^{-1} μ. When the atmosphere contains water droplets as in the case of fog, mist, or cloud, these droplets represent charge carriers of larger dimensions. However, in our closed environments the evidence indicates that the droplets are observed as a bluish haze. It is well known meteorologically that a haze appears blue because of the selective scattering with wavelength of light, provided the haze particles have radii appreciably less than 1 μ. Thus it appears that the dimensions of the haze particles and of the large ions are not greatly different. We will therefore adopt the simplification of assuming only two types of charge carriers--small ions and large carriers; the latter include large ions and charged haze particles.

The concentration of charge carriers of any specific type is controlled by the balance between production and loss processes. These processes include recombination, attachment and coagulation, diffusion and sedimentation (fall-out), and motion under the action of the electric fields. The complete formulation and solution of the balance equations is extremely complicated. However, in our particular examples (bathroom and cargo-tank) some drastic simplifications seem legitimate. Notably if n represents small ions, N denotes large carriers, and the suffices 1, 2, and 0, imply positive charge, negative charge, and no charge, respectively then all indications--both theoretical and experimental--suggest that $\{n_1, n_2\} \ll N_1 < N_o < N_2$ in the bathroom environment, with a reversal of the positions of N_1 and N_2 (sign-change) for the supertanker conditions. This is because within a contaminated atmosphere small ions are very quickly converted to large ions by attachment to nuclei [8,9]; most nuclei and droplets become charged [10,11]; while the production of {negative (distilled-tap water), positive (seawater)} charge by the breaking drops ensures an excess of the large ion carrying the corresponding charge. If we consider the bathroom conditions (negative charge production) we thus have, assuming the ions carry the electronic charge, e,

$$\rho = (n_1 - n_2 + N_1 - N_2)e \approx - N_2 e \ . \qquad (4)$$

Thus the gross electrical conditions are determined primarily by the value of N_2 and it is the balance equation of N_2 that is of most importance.

Consideration of the size of the various terms in the N_2 balance equation leads to the result, when only the apparently more significant terms are included, that

$$dN_2/dt \approx Q/e - \eta_{12} n_1 N_2 - kN_2 \qquad (5)$$

In Eq. (5), Q is the rate of charge production by the Lenard splashing effect, η_{12} the recombination coefficient between small positive ions (n_1) and large negative carriers (N_2), and kN_2 a loss term of the N_2 carriers by fall-out and diffusion to the walls. Physically, Eq. (5) implies that any negative charge produced by splashing resides on the large carriers; even if the splashing originally creates small negative ions it is assumed that these are almost instantaneously attached to large carriers. After production by splashing has stopped (Q = 0) the decay of the negative charge is governed by

$$dN_2/dt = - (\eta_{12} n_1 + k) N_2 \qquad (6)$$

The first term in Eq. (6) represents removal of the N_2 ions by recombination with the small positive ions that are always present at low densities even in very contaminated environments, as a result of the natural cosmic and radioactive ionizing radiations. It should be pointed out that Eq. (6) will be increasingly inaccurate as time increases and N_2 decreases from its abnormally high initial value and approaches more closely to the natural equilibrium condition; such terms as $\eta_{20} n_2 N_o$ should then be included in Eq. (6).

APPLICATION OF BALANCE EQUATIONS TO BATHROOM AND SUPERTANKER RESULTS

Number Density of Charge Carriers - We may apply Eq. (4) to obtain the density of the large charge carriers remembering that the electronic charge $e \approx 1.6 \times 10^{-19}$ C. The results are given in Table 2. The values of Table 2 are large but not unreasonably so.

Table 2 - Number Density of Charge Carriers in Container

Container	Space Charge C/m^3	Number Density of Large Charge Carriers (m^{-3})	Number Density of Large Charge Carriers (cm^{-3})
Bathroom (tap water)	-7.7×10^{-9}	5×10^{10} (negative carriers)	5×10^{4} (negative carriers)
Cargo Tank (seawater)	$+2.1 \times 10^{-8}$	1.3×10^{11} (positive carriers)	1.3×10^{5} (positive carriers)

Obviously the number of charged carriers cannot exceed the total number of nuclei and haze droplets present in the container atmosphere. In an industrial atmosphere the concentration of nuclei can be substantially greater than 10^5 cm^{-3}, while a dense haze may contain over 10^4 particles per cubic centimeter [12,13]. Thus the values of Table 2 although large are not impossible. However, this analysis does suggest that many of the haze droplets in particular could carry multiples of the electronic charge; the number density required to satisfy Eq. (4) is then reduced. Both theory and experiment indicate that when droplets become electrified by the attachment of atmospheric ions most of the droplets are multiply charged [10].

Decay of the Space Charge - Since, approximately, the field E is proportional to the space charge density ρ [Eqs.(2) and (3)] and ρ, in turn, is proportional to the density of large carriers [Eq. (4)] it follows that the relationship experimentally observed in the bathroom for the decay of the field

$$dE_t/dt = -(8 \times 10^{-4})E_t$$

also implies

$$dN_2/dt = -(8 \times 10^{-4})N_2 = -KN_2 \qquad (7)$$

The form of Eq. (7) namely $dN/dt = -KN$ where K is a constant has been identified by Wait and Torreson [11] as controlling the decay of large ion density within a room. Analysis of their results indicates a value of K equal to 8×10^{-5} for some data obtained in a room of 18 cubic meters volume containing tobacco smoke. Another set of data in Ref. [11] gives $K = 4 \times 10^{-3}$ for a room of 62 m^3 capacity after it had been contaminated--presumably with nuclei produced in breath exhalation--by human occupancy. The available supertanker results only provide the rather indefinite information that the field--and therefore the space charge--takes several hours to decay from a peak value of 20,000 V/m. However, if we assume--as seems plausible--a field of about 1,000 V/m after three hours this gives $K = 3 \times 10^{-4}$.

It will be noted immediately that the form of the equation experimentally derived as governing the decay of the large carriers is identical with that--Eq. (6)--predicted by the simple approximate theory. This gratifying agreement can be further checked by comparing the experimentally obtained values for K in Eq. (7) with the most plausible values for $(\eta_{12}n_1 + k)$ in Eq. (6). We should have, of course, the equality

$$K = \eta_{12}n_1 + k \qquad (8)$$

The experimental results for K range from 4×10^{-3} to 8×10^{-5} with the bathroom and supertanker results suggesting that K lies between 10^{-3} and 10^{-4}. Even in a very contaminated atmosphere cosmic and radioactive radiations maintain n_1 and n_2 at the order of a hundred [9]. For the combination coefficients between small and large ions we have [14] $\eta_{12} \approx \eta_{21} \approx 5 \times 10^{-6}$. The η values will be larger for combination between small ions and droplets. If we assume a radius* for the droplets of 2.5×10^{-1} μ, theory [15] indicates $\eta_{12} \approx \eta_{21} \approx 1.5 \times 10^{-5}$. Thus for the products $(\eta_{12}n_2)$ or $(\eta_{21}n_1)$ or $(\eta_{2,}n_1)$ we have values of from 5×10^{-4} to 1.5×10^{-3}; these numbers fall satisfactorily within the range obtained experimentally for K.

The quantity k in Eq. (8) includes contributions due to sedimentation, k_S, and to diffusion, k_D. The sedimentation term k_S will be equal to V_T/b where V_T is the terminal velocity of the charged carriers. Even for particles as large as 1-μ radius V_T is only 10^{-2} cm/s. Since b, the vertical dimension of the rooms and tanks involved always exceeds 10^2 cm, it follows that $V_T/b(< 10^{-4})$ is much less than $\eta_{12}n_2$. The diffusion contribution, k_D, to k may be estimated by considering that the diffusion factor is equally effective in causing the disappearance of nuclei whether they are charged or uncharged. Various experiments [8,9] in sealed rooms with volumes ranging from 0.33 to 216 m^3 all indicate that k_D does not exceed 10^{-5}, and indeed apparently depends little on the volume of the room.

Summarizing, the direct experimental evidence on the charge decay suggests--in terms of an order of magnitude--that

$$dN_2/dt \approx -(10^{-3})N_2 \qquad (9)$$

*This is the radius of smoke particles and haze droplets most effective in producing optical effects such as a bluish appearance [12].

Table 3 - Rate of Charge Production within Container

Container	Time (s)	Number Density of Large Carriers (cm^{-3})	Charge Production ($C/cm^3/s$)	Volume (cm^3)	Total Charge Production in Container (C/s)	Flow of Water (g/s)	Charge Production (C/g)
Bathroom (tap water)	300	5×10^4 (negative carriers)	-3.1×10^{-17}	1.5×10^7	-4.6×10^{-10}	10^3	-5×10^{-13}
Cargo Tank (seawater)	2.7×10^4	1.3×10^5 (positive carriers)	$+2.2 \times 10^{-17}$	2.8×10^{10}	$+6.3 \times 10^{-7}$	8×10^4	$+8 \times 10^{-12}$

An approximate theory also indicates that

$$dN_2/dt \approx -(\eta_{12} n_1) N_2 \approx -(10^{-3}) N_2 \qquad (10)$$

with the dominant process for the loss of the large charge carriers being neutralization by combination with small ions. This, of course, is a property of the atmosphere rather than of the container dimensions.

Rate of Charge Production - Using Eqs. (9) and (10), Eq. (5) can be simplified and rewritten as

$$dN_2/dt \approx Q/e - (10^{-3}) N_2 \qquad (11)$$

This equation has the solution

$$N_2 = 10^3 (Q/e)[1 - \exp(-10^{-3} t)] \qquad (12)$$

on the assumption that $N_2 \approx 0$ at $t = 0$. For the bathroom we have $N_2 \approx 5 \times 10^4$ after a flow of 1000 g/s of water for 300 s; note that at this time Eq. (12) indicates that equilibrium conditions are far from having been attained. For the cargo tank, $N_1 \approx 1.3 \times 10^5$ after 10^5 g/s of seawater has flowed for 2.7×10^3 s; at $t = 2.7 \times 10^3$ Eq. (12) suggests that quasi-equilibrium exists. Using the above information, and some of that previously given, an application of Eq. (12) enables Table 3 to be constructed.

In Section 2 we noted that Lenard's results indicated a production of negative charge of between 10^{-11} and 5×10^{-10} coulomb by splashing of a gram of distilled water. More recent information [16,17] suggests that -3×10^{-11} C/g is an appropriate value for charge production by the Lenard effect. Analysis of the Yosemite results [2,3] suggests a smaller figure than -3×10^{-11} C/g; however, many speculative assumptions must be made in this analysis.

If we adopt -3×10^{-11} C/g as the charge production by the splashing of distilled water, Lenard's result that tap water and oceanic seawater are, respectively, 10% and 70% as electrically effective as distilled water can be used to obtain the appropriate charge productions. For tap water this gives -3×10^{-12} C/g; for seawater $+2 \times 10^{-11}$ C/g. These values may be compared with those of Table 3. We have agreement to well within an order of magnitude with the results of Table 3 being the smaller.

DISCUSSION AND CONCLUSIONS

On the assumption that the production of charge is by splashing water it has been shown that the electrical effects detected near waterfalls; found by Lenard in his laboratory experiments; and observed in the closed environments of a bathroom and a cargo tank on a supertanker, are all self-consistent to well within an order of magnitude. Furthermore, a similar agreement exists between the experimental measurements and the predictions of simple theory. Although this consistency is unexpectedly and gratifyingly substantial its existence should not be taken as implying that conditions within the bathroom and cargo-tank environments are in reality simple, or can be treated--as regards their finer details--by a crude analysis. Many of the approximations introduced into the theory applied in this paper have been specified, while the uncertainties of much of the experimental data have been stressed. Nevertheless, there are several other factors which may be of significance that have not been discussed. For example, as regards the Lenard process itself Adkins [18] finds that space charge quickly built up near the point of splash acts to limit the charge released into the atmosphere by the splashing; however, other work [19] does not confirm the Adkins result. Splashing may not be the only significant charge-producing mechanism within the closed environments; the rupture of water drops while falling--an effect often confused with the true Lenard process--can generate intense electrification if the rupture occurs in the presence of a strong electric field [20].

Conditions inside the bathroom and cargo tank would be better understood if further and more reliable experimental data were available. Most immediately, improved measurements of electric field, E, and its variation with time are needed; in view of

the suggested proportionality of E to ρb [Eq. (3)] simultaneous observations of space-charge density, ρ, would be very desirable. Knowledge of the sizes, concentrations, and charges, of the various particles, would assist in determining how the balance equations can be applied and what simplifications of these equations are legitimate. However, there is a danger that any study of the particle characteristics could easily become very complex and tend to reveal only fine structure details that have little direct relation to the main electrical effects.

The analysis in the present paper suggests the very interesting feature that electrical conditions per unit volume of the closed environments are more controlled by atmospheric processes than by the dimensions of the containers. Such parameters as ρ approach constancy, and scaling equations, for example Eq. (3) indicating the proportionality of E to ρb, are approximately valid. Thus it appears possible to extrapolate results obtained within small containers to the large-scale conditions of the cargo tanks. However, such extrapolation should always be treated with some caution, since all electrical parameters may not extrapolate to the same degree. A notable distinction that may be of much significance, is that corona breakdown occurs at a sharp point provided the point potential differs by more than a few kilovolts from that of the ambient atmosphere. This necessary potential difference is not attained in the bathroom environment but is much exceeded within the cargo tank. Thus the ionization in the cargo tank atmosphere is augmented by corona processes, and, although the space-charge density may be similar to that within the bathroom, the characteristics of the charged carriers in the two environments are not necessarily identical. For these reasons, when considering the supertanker explosion problem small-scale experiments can be useful and informative, but direct measurements within cargo tanks are much to be preferred.

The stimulus for preparing this paper was the possibility that the Lenard effect would create enough electrification during washing processes within the cargo tanks of oil supertankers for substantial sparks to develop. These sparks would have the character of massive streamers, orders of magnitude more intense than corona discharges, and would therefore easily be capable of igniting any explosive mixture within the tank. One result seems to indicate conclusively that conditions within the cargo tanks can be propitious for the development of such streamers. It has been shown [21], from a study of triggered lightning incidents, that the necessary and sufficient conditions for the initiation of large streamers are an ambient field of the order of 10 kV/m and a potential discontinuity approaching 10^6 V between the point from which the streamer starts and the adjacent atmosphere. Within the cargo tanks the fields can certainly exceed 10 kV/m. Any object of length ℓ projecting into the tank will have a voltage difference of approximately $E\ell$ between its tip and the neighboring atmosphere. Measurements within cargo tanks have occasionally indicated fields of some 100 kV/m; with this size of field ℓ need only be 10 m for the potential discontinuity of 10^6 V to be attained. It is beyond the scope of this paper to discuss the protuberances existing within cargo tanks, but in tanks of a 30-m linear dimension, a conducting projection of 10-m length can often be present; a sounding rod or even a water jet itself--especially if it is operated intermittently--are plausible possibilities. Thus the occasional occurrence of large-scale streamers within the tanks seems quite likely.

ACKNOWLEDGMENTS

Mr. H. O. Valvur of Chevron Shipping Company and Mr. R. F. Klaver of Chevron Research Laboratories kindly supplied preliminary quantitative information on the electric fields developed within the cargo tanks. Without this information the order-of-magnitude analysis could not have been applied to tanker conditions.

Some of the experimental work and the preparation of this paper were supported by the United States Office of Naval Research under Contract Nonr-4099(00), Project NR 082 206. Accordingly, reproduction in whole or in part of this paper is permitted for any purpose of the United States Government.

REFERENCES

1. P. Lenard, "Über der Elektrizität der Wasserfälle," Ann. Phys. (Leipzig), Vol. 46, 1892, pp. 584-636.

2. E. T. Pierce and A. L. Whitson, "Atmospheric Electricity and the Waterfalls of Yosemite Valley," J. Atmos. Sciences, Vol. 22, 1965, pp. 314-319.

3. E. T. Pierce and A. L. Whitson, "Rebuttal to Comments on Atmospheric Electricity and the Waterfalls of Yosemite Valley," J. Atmos. Sciences, Vol. 23, 1966, pp. 452-453.

4. W. A. Weyl, "Surface Structure of Water and Some of Its Physical and Chemical Manifestations," J. Colloid Sci., Vol. 6(5), October 1951, pp. 389-405.

5. E. T. Pierce and A. L. Whitson, "Atmospheric Electricity in a Typical American Bathroom," Stanford Research Institute, Sci. Note 8, SRI Proj. 4454, January 1967; Weather, Vol. 21, 1966, pp. 449-455.

6. P. Morse and H. Feshbach, "Methods of Theoretical Physics," New York, N. Y.: McGraw-Hill Book Co., Inc., 1953.

7. R. V. Anderson, "Absolute Measurements of Atmospheric Charge Density," J. Geophys. Res., Vol. 71(24), December 15, 1966, pp. 5809-5814.

8. L. G. Smith and G. F. Schilling, "The Variation of Electrical Conductivity of Air within Sealed Rooms," J. Atmos. Terrest. Phys., Vol. 4 , 1954, pp. 314-321.

9. O. C. Jones, R. S. Maddever, and J. H. Sanders, "Sealed-Room Experiments on the Equilibrium of Ionization in Air," J. Atmos. Terrest. Phys., Vol. 17, 1959, pp. 134-144.

10. R. Gunn, "The Statistical Electrification of Aerosols by Ionic Diffusion," J. Colloid Sci., Vol. 10, 1955, pp. 107-119.

11. G. R. Wait and O. W. Torreson, "Large Ion and Small Ion Content of Air in Occupied Rooms," Heating, Piping, and Air Conditioning, Vol. 7, 1935, pp. 105-110.

12. "Compendium of Meteorology," Am. Meteorol. Soc., 1951.

13. "Handbook of Geophysics and Space Environment," U. S. Air Force, 1965.

14. J. A. Chalmers, "Atmospheric Electricity," New York, N. Y.: Pergamon Press, Inc., 1967.

15. J. Bricard, "L'equilibre Ionique de la Basse Atmosphere," J. Geophys. Res., Vol. 54, 1949, pp. 39-52.

16. H. L. Collin and P. A. Raisbeck, "Errors in Recorded Precipitation Current Caused by Splashing," J. Atmos. Terrest. Phys., Vol. 26, 1964, pp. 1107-1113.

17. L. G. Smith, "The Electric Charge of Raindrops," Quart. J. Roy. Meteorol. Soc., Vol. 81, 1955, pp. 23-47.

18. C. J. Adkins, "The Small-Ion Concentration and Space Charge near the Ground," Quart. J. Roy. Meteorol. Soc., Vol. 85, 1959, pp. 237-252.

19. M. Smiddy and J. A. Chalmers, "Measurements of Space Charge in the Lower Atmosphere using Double Field Mills," Quart. J. Roy. Meteorol. Soc., Vol. 86, 1960, pp. 79-84.

20. J. B. Matthews and B. J. Mason, "Electrification Produced by the Rupture of Large Water Drops in an Electric Field," Quart. J. Roy. Meteorol. Soc., Vol. 90, 1964, pp. 275-286.

21. E. T. Pierce, "Lightning Discharges to Tall Structures," EØS, Vol. 51, 1970, p. 301.

SESSION 2A

COMMERCIAL AIRCRAFT

Organizer - K. A. Moore

Continental Airlines

Chairman, K. A. Moore

700923

Lightning Current Transfer Characteristics of the P-Static Discharger Installations

M. P. Amason
and
J. T. Kung
Douglas Aircraft Company, McDonnell Douglas Corporation, Long Beach, California

ABSTRACT

This paper presents the results of p-static discharger installation lightning tests conducted by the Douglas Aircraft Company at its Long Beach, California facilities and the facilities of the Lightning and Transients Research Institute at Miami Beach, Florida. The paper discusses the lightning current transfer characteristics and lightning protection design considerations for the p-static discharger, the discharger retainer, and the aircraft installation. Laboratory lightning test results are also discussed in relationship with the in-service experience associated with natural lightning stroke incidents.

AIRCRAFT CAN ACCUMULATE static electrical charges by triboelectric charging when operating in a precipitation environment (1)*. The aircraft potential will be increased until it reaches a critical value and corona discharges will take place at aircraft high gradient points. These corona discharges consist of series of short current pulses that, when coupled into aircraft communication and navigation systems, cause radio interference known as precipitation static (1), (2), and (3). An analysis of this corona-generated noise interference and techniques to eliminate it have been discussed in detail in previous publications (4) and (5). These publications show that the precipitation static interference to aircraft communication and navigation systems is completely controllable through the installation of an appropriate number of adequately designed p-static dischargers at proper locations. Such installations are in use on thousands of military and commercial jet aircrafts throughout the world.

A typical configuration of aircraft p-static discharger installations is shown in Figure 1. Here it may be noted that the dischargers are located at the extremities of the aircraft wing and tail assemblies. Lightning attach-point studies indicate that these areas are also closely involved in direct lightning strokes to and from the aircraft, as shown in Figure 2. These direct lightning strokes contain peak currents of several hundred thousand amperes and heavy charge transfers up to the order of 200 to 500 coulombs. These can result in severe damages to aircraft discharger installation components and/or aircraft structures (6)(7), as shown in Figure 3. A properly designed p-static discharger and its aircraft installation can reduce or eliminate these types of damages.

*Numbers in parentheses designate References at end of paper.

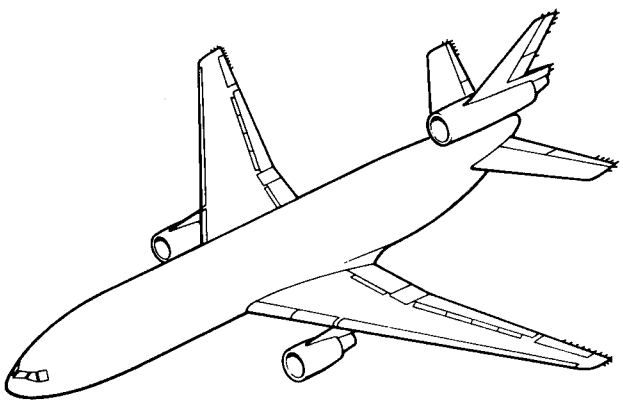

Fig. 1 – Typical configuration of aircraft P-static discharger installation

Laboratory lightning tests were conducted on various types of p-static dischargers and discharger installations using the Douglas lightning simulator (8), as shown in Figure 4, and the Lightning and Transients Research Institute (LTRI) lightning test facilities, as shown in Figure 5. The lightning current transfer characteristics of the p-static discharger, discharger retainer, and aircraft installation are presented in this paper.

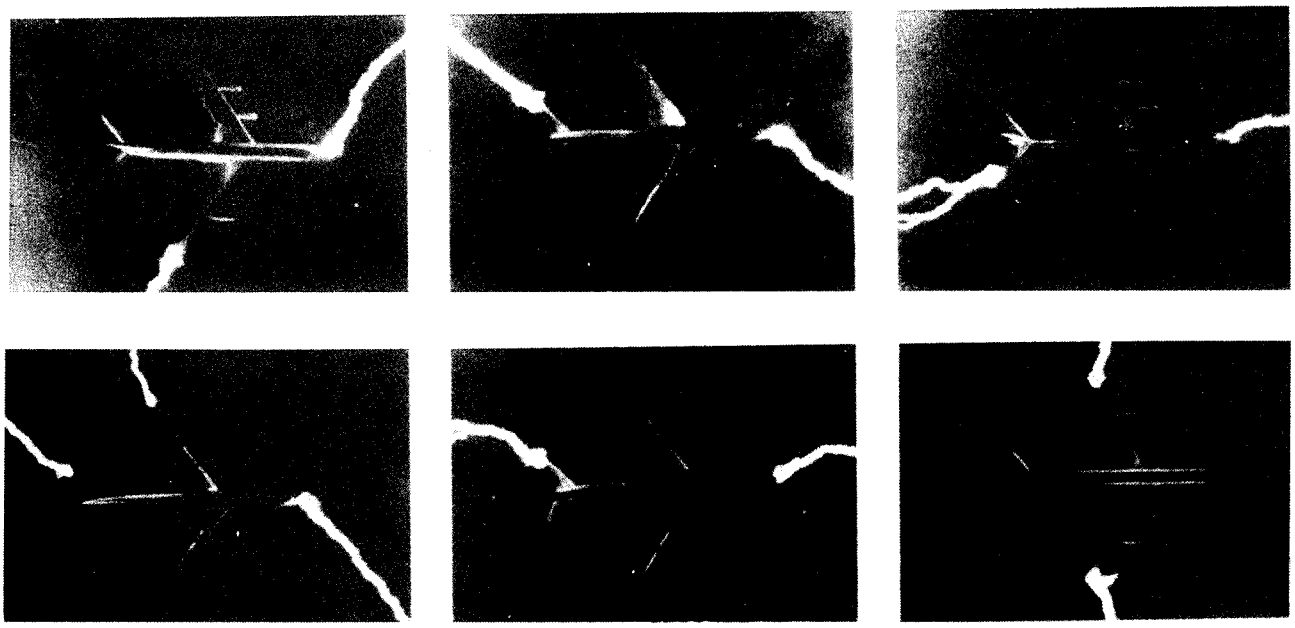

Fig. 2 – Laboratory simulated lightning attach point study of a commercial aircraft model

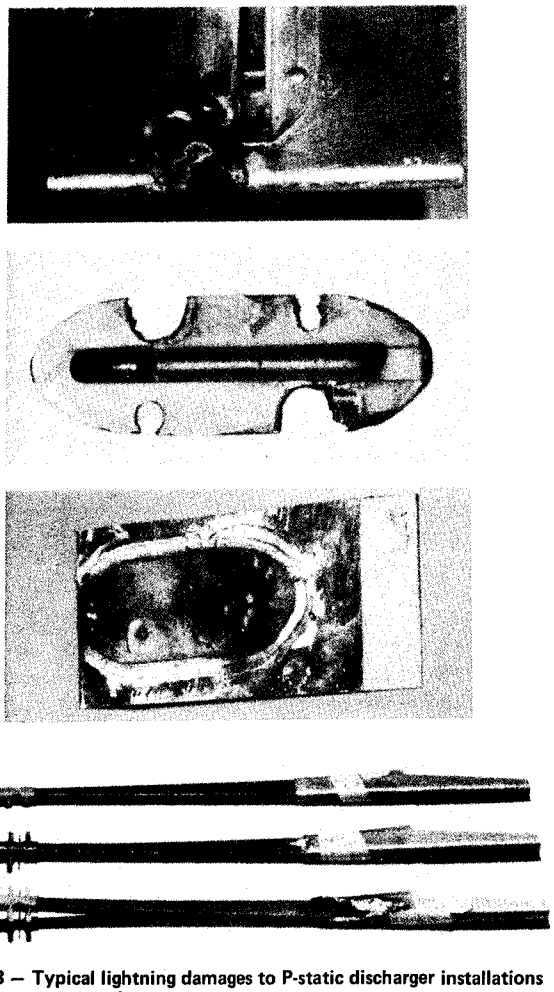

Fig. 3 – Typical lightning damages to P-static discharger installations and aircraft structures

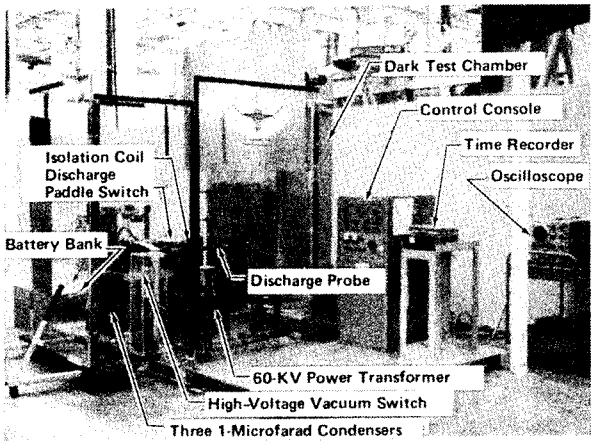

Fig. 4 – Douglas lightning test simulator

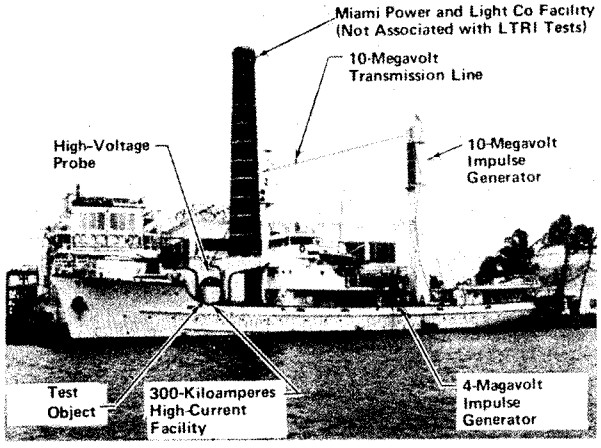

Fig. 5 – LTRI lightning test facility

P-STATIC DISCHARGER

There are two types of p-static dischargers installed on an aircraft, the trailing-edge-type discharger installed on trailing edges and the tip-type discharger installed on tips of the aircraft wing and stabilizer assemblies. Both types of dischargers have two common sections, the discharger tip section and the resistive element section shown in Figure 6. A metal shank section usually incorporated in the trailing-edge-type discharger is also shown in Figure 6. Each section performs somewhat of an independent function during lightning current transfer and, because of differences in physical features, each section is subsequently damaged differently during natural lightning strokes, as evidenced by observation of the discharger shown in Figure 7. Here, the discharger tip section pins are blunted and the protective cap is broken, the resistive element section is burned, and the metal shank section is eroded. The lightning current transfer characteristics of each section of the discharger are discussed in the following paragraphs.

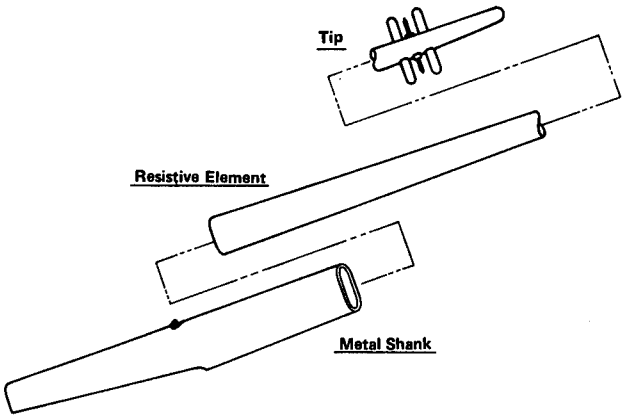

Fig. 6 – Discharger tip, resistive element, and metal shank

Fig. 7 – Typical damages to a discharger resulting from natural lightning stroke

DISCHARGER TIP – The discharger tip is designed to discharge the aircraft's static charges at low threshold potential and thus incorporates sharp metallic points made from small needles or fine wires. As a lightning step leader approaches the regions of the aircraft where dischargers are located, high stress streamers are initiated from the sharp metallic points of the dischargers, as shown in Figure 8. These streamers form ionized channels which provide low-resistive paths that direct the lightning current to these points when or if the particular streamer is selected by the lightning channel step mechanism (9) for the next stage of lightning current transfer. As the initial lightning current flows to the vicinity of the discharger tip, the air is quickly heated and produces gas blast effects which result in physical damages to the discharge sharp points and their associated safety protection caps. These effects have been reproduced in the laboratory.

High-current lightning tests (10) were conducted on various types of discharger tips with the use of the LTRI 100,000-ampere simulated lightning current generator. Figure 9, View A shows discharger tips incorporating fine-wire discharge points before and after lightning test. The fine wires were fused and evaporated by the heat associated with the lightning current. Figure 9, View B shows discharger tips incorporating sharp-needle discharge points and a protective cap assembly before and after lightning test. The needle points were

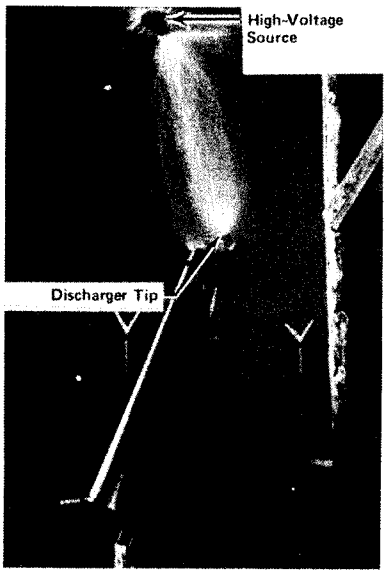

Fig. 8 – LTRI 10-million-volt lightning step leader and streamer current test

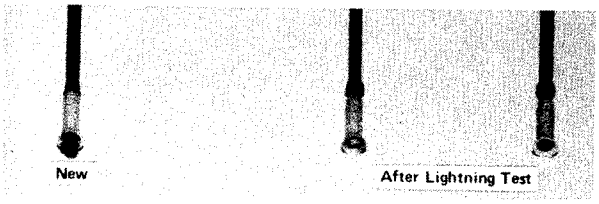

View A – Fine-wire discharger points

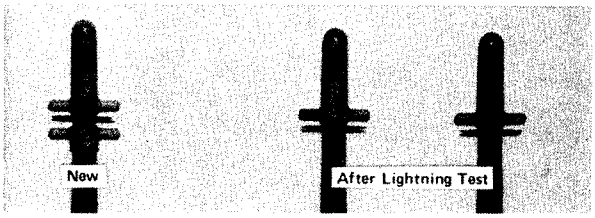

View B – Sharp-needle discharge points with a protective cap

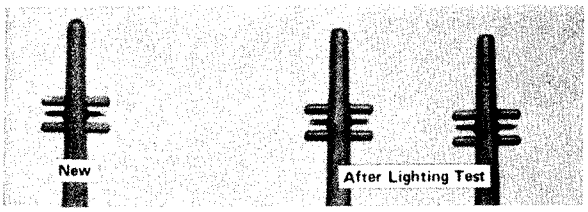

View C – Sharp-needle discharge points with integrated protective guards

Fig. 9 – Discharger tips before and after LTRI 100-ampere lightning tests

blunted but otherwise unharmed; however, the protective cap assembly of each discharger was damaged by the gas blast effect. Figure 9, View C shows discharger tips incorporating sharp-needle points and integrated protective guards before and after lightning test. The needle points were blunted; however, no damage resulted to the protective guards.

These test results indicate that, from the lightning damage point-of-view, the sharp-needle point design is superior to the fine-wire

design, and the integrated safety protection guard is better than a separate protective cap assembly.

DISCHARGER RESISTIVE ELEMENT – The discharger resistive element is a functional part of a p-static discharger. It provides a high-resistive path from the tip of discharger to the metal shank or to the discharger retainer. A resistive value of 8 to 100 megohms is required to make the discharger effective. It is therefore, from a functional viewpoint, important that the resistance value remains within this range after the transfer of lightning current. As lightning step leaders approach a discharger installation, streamer current will flow from the aircraft metal structure to the discharger tip through the resistive element. Because of its high-resistance feature, the potential difference between two ends of the resistive element is high enough to ionize the surrounding air gap, as shown in Figure 10. Once the ionized channel is established, most of the lightning current will transfer through the ionized channel, thus bypassing the resistive element. When the main lightning current dump or charge transfer occurs, the external surface of the resistive elements is exposed to severe heat that can cause physical damage to its exterior surface.

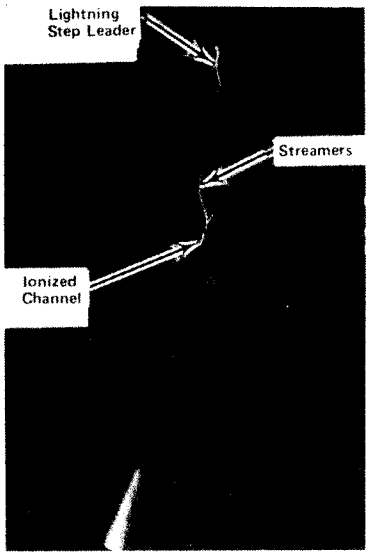

Fig. 10. – Ionized channel established around the discharger resistive element during the lightning step leader and streamer current test

There are two different types of discharger resistive elements; one has an external resistive coating and the other has an internal resistive element, as shown in Figure 11. A rubber sleeve is sometimes used to cover the external resistive coating for rain erosion protection. Figure 12 shows these dischargers during high-current lightning tests, using the LTRI 100,000-ampere simulated lightning current generator. An intense ionized lightning current channel may be observed around the discharger resistive elements. After the lightning tests, visible burning damages were seen on the surfaces of external resistive coatings. The protective rubber sleeve was forced back near the discharger tip end and the resistive coating underneath was burned. However, there was no visible damage on the nylon rod surface of dischargers with internal resistive element. A resistance check after lightning tests indicated that the resistance values of dischargers with external resistive coating all dropped from about 35 megohms to below the 8-megohm minimum resistance limit. It should be noted that, in service, sometimes the external resistive coating is severely burned and becomes open circuited. The resistance values of dischargers with internal resistive element did not change more than 20 percent of their original values and remained well within the 8- to 100-megohm limits after lightning tests.

These test results indicate that the discharger with internal resistive element provides better lightning protection than the discharger with external resistive coating. It is important, when designing the resistive element, to isolate it from the heat generated by the lightning current transfer which can change its resistance value. It is

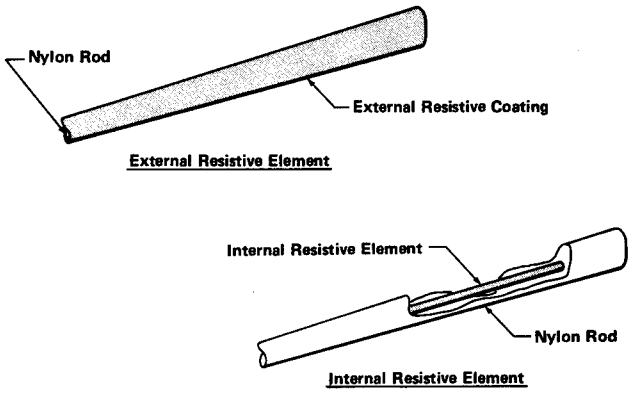

Fig. 11 – Two different types of discharger resistive elements

View A – External resistive element

View B – External resistive coating with protective rubber sleeve

View C – Internal resistive element

Fig. 12 – Ionized lightning current channels around different types of discharger resistive elements during LTRI 100,000-ampere lightning tests

also important, when designing the discharger internal resistive element, to design it in such a manner that an ionization channel will not be established inside the resistive element which would direct the main lightning current inside the discharger nylon rod, thus exploding it.

DISCHARGER METAL SHANK – The discharger metal shank section is not a functional part of the p-static discharger and is designed mainly for aircraft lightning protection. It is designed to confine lightning current "burning and erosion damages" to the discharger itself, thereby protecting the aircraft structure. The burning and erosion damages produced by the heavy coulomb transfer stage of the lightning stroke (10) can be very severe. Figure 13, View A shows an example of severe burning and erosion damages caused by a natural lightning stroke to a well-designed discharger metal shank section. No damage occurred to the aircraft structure during this lightning stroke incident. Figure 13, View B shows the type of damage that would have occurred to the aircraft structure had a discharger with a poorly designed (short) metal shank section been installed at the same location. Laboratory lightning studies and service experience have indicated that only the trailing-edge-type dischargers, not the tip-type dischargers, are installed in areas which are generally susceptible to the burning and erosion phases of the lightning stroke. Therefore, it is necessary for the trailing-edge-type discharger to incorporate a well-designed metal shank section.

View A – Damages to a discharger metal shank section resulting from the natural lightning stroke

View B – Damages to a simulated aircraft structure resulting from the Douglas heavy-charge transfer lightning test of 200 coulombs

Fig. 13 – Burning and erosion damages resulting from the heavy-charge transfer of lightning current

Dischargers with different lengths of metal shank sections were lightning tested. Figure 14 shows the high-current lightning test results using LTRI 100,000-ampere simulated lightning current generator. These test results indicate that, in the case of the discharger with a short metal-shank section, the main ionized lightning current channel terminated at the simulated aircraft trailing edge, while in the case of the discharger with a long metal-shank section, the channel terminated at the metal shank. It should be noted that the heavy charge transfer stage of lightning current, which occurs after the high current transfer stage (10), follows this previously established ionized current channel and can produce burning and erosion damages at components located where the ionized current channel terminates. Therefore, the discharger installation with a long metal-shank section design can prevent lightning damage to the aircraft structure. It is also important to install the trailing-edge-type discharger in such a manner that the AFT edge of the metal-shank section is positioned as far away from the aircraft trailing edge as possible to obtain the maximum lightning protection. Laboratory lightning test results and service experience indicate that a discharger metal-shank section with approximately two inches extended beyond the aircraft trailing edge is sufficient to protect typical aircraft trailing edge structures from direct lightning stroke burning and erosion damages.

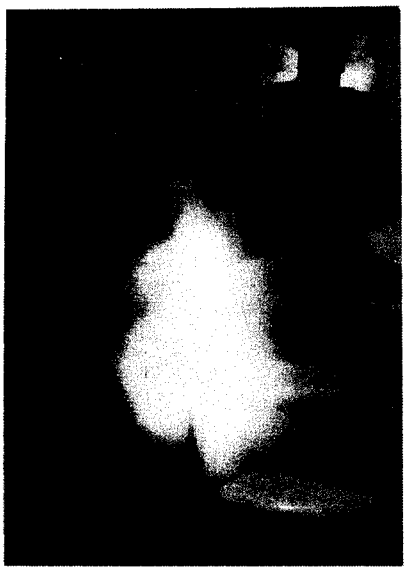

View A – Short metal shank

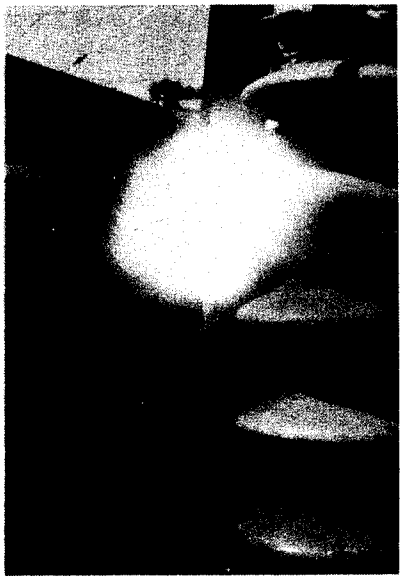

View B – Long metal shank

Fig. 14 – Dischargers with different lengths of metal shank sections under LTRI 100,000-ampere lightning tests

DISCHARGER RETAINER

P-static dischargers are normally installed on aircraft metal structures through standard retainers. Figure 15 shows several typical installations. Each discharger is mounted on a retainer and locked in place by a setscrew. The retainer is riveted to aircraft metal structure. When lightning current attaches to a properly designed discharger, the current will transfer to the aircraft metal structure by way of the discharger retainer. Therefore, the discharger attachment system must be carefully designed to prevent damage when the transfer of lightning current occurs. The lightning current transfer characteristics of the discharger-to-retainer interface and the retainer-to-aircraft interface are different and thus are discussed separately.

INTERFACE WITH DISCHARGER – In-service experience has indicated that the close fitting, single screw lock-type attachment

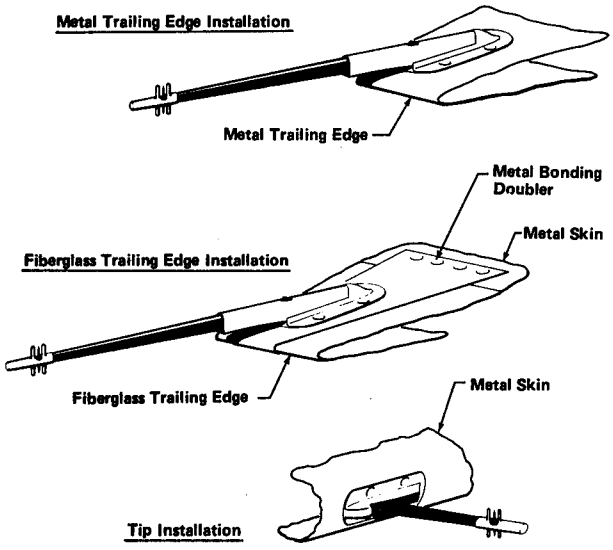

Fig. 15 – Typical aircraft P-static discharger installations

between the discharger and retainer transfers natural lightning current without damage to the faying surfaces of the discharger or retainer. The laboratory high-current lightning test results, however, indicate burning damages of the interfaces. These test results, which can not be supported by the in-service experience, are analyzed with laboratory lightning test setups to determine the true lightning current transfer characteristics of the interface.

Laboratory lightning tests were conducted with the use of two different test setups. Figure 16, View A shows the discharger retainer installation tested inside an isolated test chamber. The lightning current is directed to the discharger retainer installation by a modified discharger with an extended metal shank section through a small hole at the center of a fiberglass panel. The fiberglass panel shields the ionized channel from the discharger retainer installation during the lightning test and, therefore, all the lightning current transfers through the discharger metal shank to the retainer installation. Figure 16, View B shows the discharger retainer installation tested in an open field. In this installation, a portion of the simulated lightning high current will transfer along the surface of the discharger metal shank in an ionized form to the discharger retainer installation shown in Figure 14, View B.

Figure 17 shows a comparison between laboratory lightning test results and natural lightning stroke results. Figure 17, View A shows the severe burning damages inside the holders of two extended discharger metal shanks which were tested in an isolated test chamber as shown in Figure 16, View A. Figure 17, View B shows the holders of two discharger metal shanks with lesser degree of burning damages after lightning tests making use of test setups shown in Figure 16, View B. These test results indicate that the degree of burning damages imposed on the holder of the discharger metal shank is proportional to the amount of lightning current physically transferred through it.

Figure 17, View C shows three discharger metal shanks recovered from service after a natural lightning stroke incident to a commercial aircraft. No evidence of burning damage can be found inside each discharger metal shank holder although the outside surfaces of all three dischargers were severely eroded by the natural lightning stroke, indicating that heavy lightning discharges had occurred.

In the case of a natural lightning stroke, an intense high-stress streamer field exists around the discharger installation as a lightning step leader approaches. After the lightning step leader contacts a particular streamer, the main lightning current channel can transfer through this path, and the high current transfer stage of lightning stroke follows immediately. The lightning high-current phase, with a steep rate of rise at approximately 100,000 amperes per microsecond, transfers in

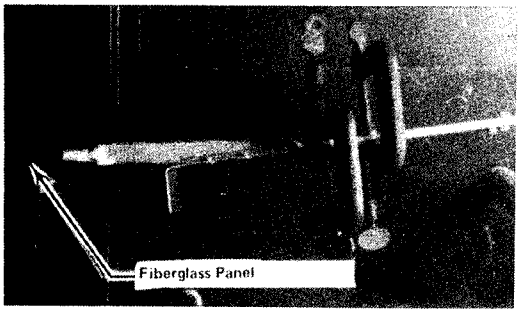

View A – Tested in an isolated chamber

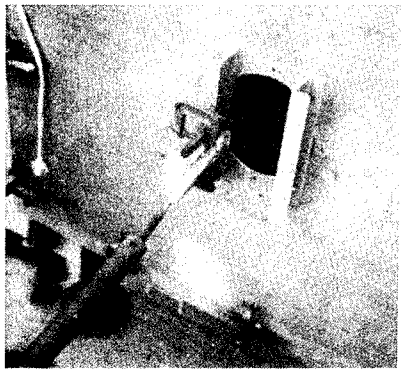

View B – Tested in the open field

Fig. 16 – Laboratory lightning test setups of discharger retainer installations

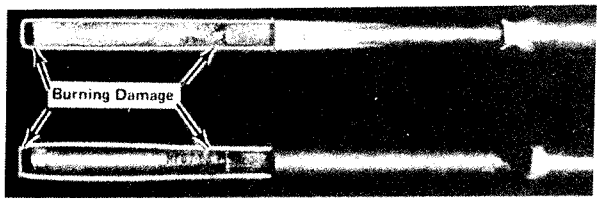

View A – Burning damages resulting from the laboratory isolated chamber lightning test

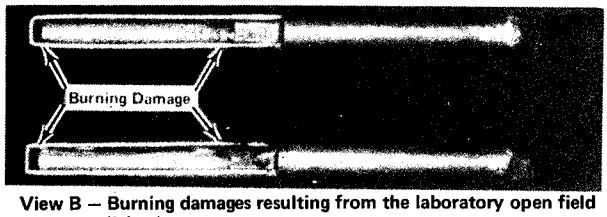

View B – Burning damages resulting from the laboratory open field lightning test

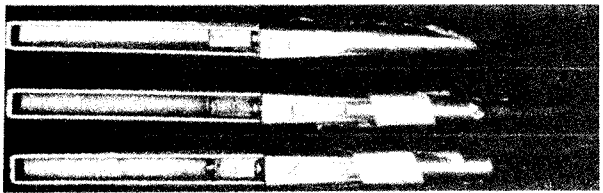

View C – Burning damages resulting from the natural lightning stroke incident

Fig. 17 – Holders of discharger metal shanks after lightning current transfer

the ionized channel that is attached to the discharger metal shank. Because of this steep rate of rise of the lightning current and the skin effect of the discharger metal shank, most of the lightning current flows along the surface of the discharger metal shank and also through the existing streamers around the metal shank to the retainer installation. Therefore, no burning damage results to the interface between the discharger and retainer during the natural lightning stroke. It is difficult in the laboratory to produce a true lightning high-current wave shape with this type of steep rate of rise. It is also difficult to produce the intense high-stress streamer field around the discharger installation during a laboratory high-current discharge because of the relatively large air gap required. The larger than normal high current flowing through the discharger-to-retainer interface in the laboratory high-current lightning tests consequently produced the type of burning damages shown in Figures 17, Views A and B.

INTERFACE WITH AIRCRAFT SKIN – The discharger retainer is normally riveted to the aircraft metal skin or to a bonding doubler when the fiberglass trailing edge is present, see Figure 15. Previously, the use of low-resistance conductive adhesive materials in the interface between the retainer and aircraft skin was considered satisfactory for the prevention of lightning damage. In fact, the use of silver conductive adhesive was established as aircraft industry requirement for these installations. Service experience indicated that the use of silver conductive adhesive resulted in a severe corrosion problem, see Figure 18. Initial investigation indicated the corrosion resulted from the galvanic action between the silver loaded adhesive and the aluminum materials of the aircraft skin and discharger retainer when moisture was present. Numerous efforts were made over the past years to adequately seal the installation, but these efforts were not completely successful in eliminating the corrosion problem.

Fig. 18 – Severe corrosion condition on the aircraft aluminum skin where a discharger retainer was installed

In an effort to resolve this corrosion problem, lightning tests were conducted to determine the lightning current transfer characteristics of the discharger retainer installation to establish the necessity for the use of the costly silver conductive adhesive in discharger retainer installations. Other installation methods, including the use of various types of conductive adhesives, chemical coatings, and a commonly used noncorrosive adhesive, were also investigated.

Conductive Adhesives – The Douglas lightning simulator, shown in Figure 4, was used to initially test the silver conductive adhesive, zinc conductive adhesive, and aluminum conductive adhesive. Standard discharger retainers were attached to 0.020-inch-thick aluminum sheets with different types of conductive adhesive faying surface seals. Rivets were not used in these test samples so that the lightning current transfer characteristics of the conductive adhesives could be studied independently. Test results indicate that all the conductive adhesives tested have explosive characteristics when transferring lightning current. Figure 19, Views A and B show the test results of silver and zinc conductive adhesives, respectively. The aluminum conductive adhesive failed in the same manner. Tests utilizing the more intense LTRI high-current lightning discharges were not conducted on these test samples due to these initial failures.

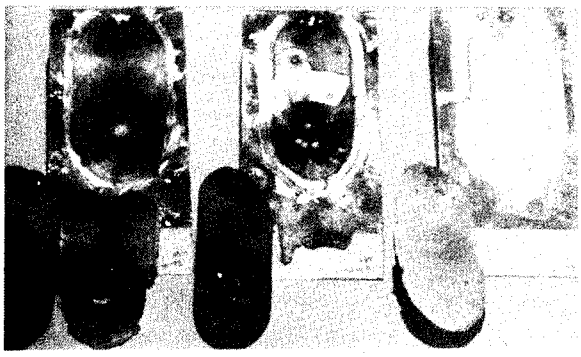

View A – Silver conductive adhesive-bonded interfaces

View B – Zinc conductive adhesive-bonded interfaces

Fig. 19 – Conductive adhesive-bonded interfaces exploded during Douglas 60,000-volt lightning tests

The explosiveness of the silver conductive adhesive, as well as the other conductive adhesives tested, indicates that they do not provide adequate lightning protection for discharger retainer installation when transferring lightning current. Therefore, the requirement for the use of silver conductive adhesive in the discharger retainer installation for lightning protection is not justified.

Conductive Chemical Coatings – Discharger retainer installations, in which the bonding interfaces were treated with conductive chemical coatings, were subjected to lightning tests before and after exposure to corrosive environments. Alodyne 1200 multicolor conductive coating and Alodyne 1500 clear conversion conductive coating were selected for test. Standard discharger retainers with Alodyne 1000 conductive finish coating were attached to the Alodyne 1200 or 1500 coating treated aluminum sheets (0.020 inch thick) with four or six MS20470AD3 rivets. Certain test samples were edge sealed.

The results of exposure of the non-edge-sealed samples to 384 hours of salt-spray corrosion tests indicated that corrosion occurred in the interfaces between the discharger retainer and aluminum sheet, and that the corrosion protection afforded by Alodyne 1200 coating is much better than that provided by the Alodyne 1500 coating, as shown in Figure 20. Tests results of edge-sealed samples indicated the corrosion occurred only around the rivets and that it started at the rivet holes. This shows the necessity for sealing rivet hole areas in addition to the edge seal, in order to prevent corrosion of joint interfaces when conductive chemical coatings are used.

Test samples treated with Alodyne 1200 and 1500 coatings, with and without edge seals and before and after exposure to corrosion tests, were subjected to LTRI 200,000-ampere high-current lightning tests. Figure 21 shows the summary of Alodyne 1500 treated samples after lightning tests. A careful examination of the test samples upon disassembly revealed that no damage occurred in many of the samples. When damage occurred, it was minor and limited to the cases where corrosion was present at the rivet-hole areas, regardless of the corrosion appearing at various other places in the alodyned interfaces. Lightning test results of Alodyne 1200 treated samples were the same.

It is interesting to note that where wet (nonconductive) sealant was used in the installation of the rivet attachments to prevent corrosion from rivet hole areas (Samples 13, 14, and 15 of Figure 21), no damage

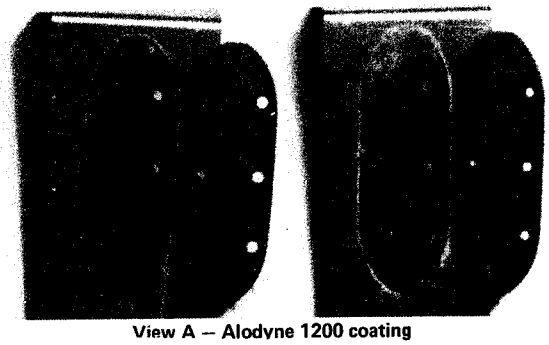

View A – Alodyne 1200 coating

View B – Alodyne 1500 coating

Fig. 20 – Alodyne 1200 and Alodyne 1500 coating treated interfaces after 384 hours of salt spray corrosion tests

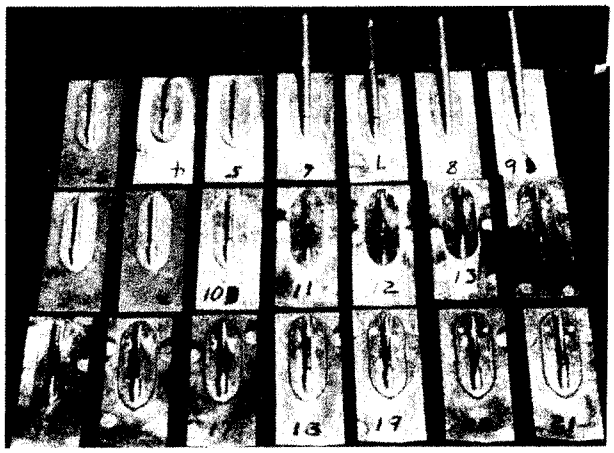

Fig. 21 – High-current lightning test results of riveted samples with Alodyne 1500 coating treated interfaces

occurred to the bonding interfaces during the high-current lightning tests even in the case where other areas of the alodyned interfaces were corroded. Figure 22 shows the bonding interfaces of "wet-rivet" samples after lightning tests.

These test results indicated that the alodyne conductive coating treated discharger retainer installations with four MS20470AD3 rivets can transfer lightning current satisfactorily if the rivet installations remain uncorroded.

Noncorrosive Adhesives – The noncorrosive adhesives selected as feasible candidates for this type of installation are considered to be nonconductive. However, the successful lightning test results of the alodyne coating treated discharger retainers using nonconductive sealant wet-rivet installations indicated that it was possible to use the noncorrosive adhesive on the entire faying surfaces. PR 1422, a noncorrosive adhesive commonly used on aircraft structures, was

Fig. 22 – Bonding interfaces of "wet rivet" samples after LTRI 200,000-ampere lightning tests with no resultant damage

selected, and tests to establish the lightning current transfer characteristics of this type of installation were conducted.

PR 1422 adhesive was applied between discharger retainers and 0.020- or 0.040-inch-thick simulated aircraft aluminum skins, and four MS20470AD3 rivets were installed in each test sample while the adhesive was wet. Tests indicate that in joining thin materials, as the rivet body expands, it squeezes out the adhesive at the edge of rivet holes and makes direct physical contact with the discharger retainer and the aluminum sheet, thereby providing a low-resistive path for lightning current. Resistance checks of all test samples before lightning tests indicated a low-resistance bond was provided for each sample. Samples were subjected to LTRI 200,000-ampere high-current lightning tests. No damage resulted to the bonding interfaces and the low-resistance bond remained good after the lightning tests. Douglas heavy-charge transfer (200 coulombs) test results also indicated no damage.

Complete discharger retainer installations with silver conductive adhesive and PR 1422 adhesive on the faying surfaces were tested under the same test conditions using the LTRI high-current lightning test facilities. Examination of samples after lightning tests indicated that the silver conductive adhesive faying surface seals were damaged as shown in Figure 23, while PR 1422 faying surface seals were intact.

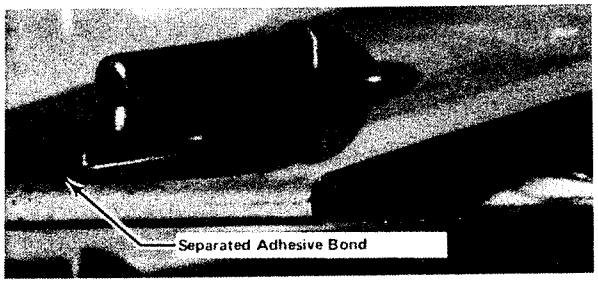

Fig. 23 – Silver conductive adhesive bond damaged after LTRI 100,000-ampere lightning test

These test results indicate the PR 1422 noncorrosive adhesive can be used to replace the silver conductive adhesive in the riveted, aircraft discharger retainer installations to resolve the long-time corrosion problem, while providing better lightning current transfer characteristics. It is interesting to note that, by using the PR 1422 adhesive instead of the silver conductive adhesive in discharger retainer installations, a cost saving of $5.56 per installation ($2.20 for the material and $3.36 for 0.25 manhour labor) has been realized. Based on this figure and assuming 30 discharger retainer installations per aircraft, the total cost savings will amount to $50,000 for 300 new aircrafts and a potential annual maintenance cost of $168,000 will be saved for 1,000 in-service aircraft.

PERIPHERAL TRANSFER – It has been determined in the previous discussion that a portion of the lightning current transfers along the surface of the discharger metal shank to the retainer installation in an ionized form during the high-current transfer stage of a lightning stroke. Special samples were made to determine if the lightning current can also transfer peripherally around the retainer edges to the aircraft metal skin.

Standard discharger retainers were attached to 0.040-inch-thick aluminum sheets with the PR 1422 adhesive faying surface seal and without rivets. Each sample was tested with the LTRI 100,000-ampere simulated lightning current generator. Figure 24 shows a sample during and after the lightning test. It can be seen that, during the lightning test, the main ionized lightning current channel terminated at the discharger metal shank and then transferred peripherally from the retainer edges to the aluminum sheet. The edges of the retainer and the surface of the aluminum sheet received minor burning damages after the lightning test. However, the adhesive bonding was not damaged. This indicated the amount of lightning current transferred through the adhesives was limited and no sparking was generated inside the adhesive-bonded interface.

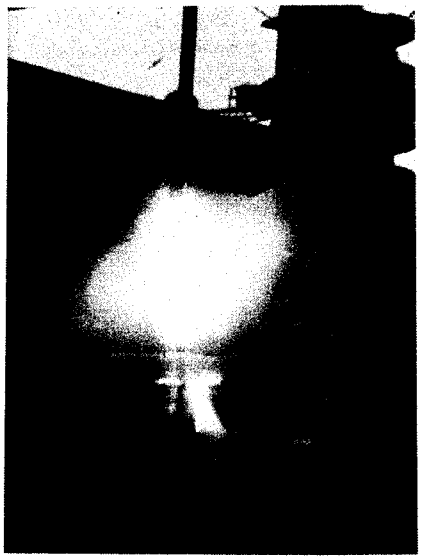

View A – During lightning test

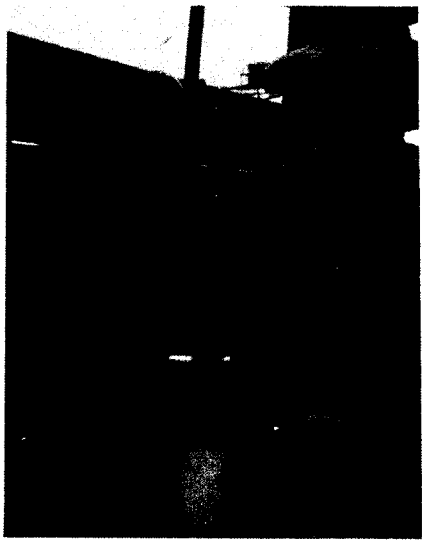

View B – After lightning test

Fig. 24 – Peripheral transfer lightning test

It is interesting to note that this type of peripheral lightning current transfer from the discharger retainer to the aluminium sheet was observed only where the discharger having a long metal shank section was used. When the discharger with a short metal shank section was used, the main lightning current channel terminated directly at the aluminum sheet and there was no evidence of lightning current transfer from the discharger retainer to the aluminum skin as shown in Figure 25.

The above test results indicate that the lightning high current can transfer peripherally around the edges of discharger retainer to aircraft metal skin, and that the PR 1422 adhesive can prevent lightning current from transferring through the interface of the adhesive joint and thereby avoiding the internal sparking and damage. It also shows that a well-designed discharger metal shank section is necessary to guide the lightning current to the aircraft skin through the discharger retainer.

View A – Discharger with a long metal shank section shows evidence of peripheral lightning current transfer from the discharger to the aluminum skin

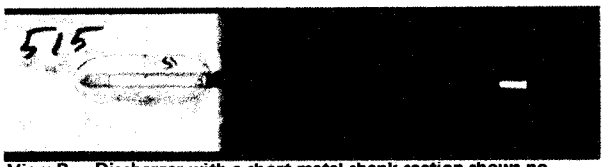

View B – Discharger with a short metal shank section shows no evidence of lightning current transfer from the discharger retainer to the aluminum skin

Fig. 25 – Difference in high-current lightning test results of two different types of dischargers

AIRCRAFT DISCHARGER INSTALLATIONS

IN-SERVICE EXPERIENCE – P-static discharger installations are often involved in aircraft natural lightning stroke incidents. Figure 26 shows a case where 12 dischargers, 9 trailing types and 3 tip types, were damaged in a single natural lightning stroke incident involving both wings of a commercial aircraft. The dischargers were arranged according to their originally installed positions on the left- and right-wing sections of the aircraft. The lightning current channel contacted and damaged the outboard seven dischargers on the left wing, five trailing types and two tip types, and left the aircraft through various other extremities including the right wing tip. It is interesting to note that only the outboard side of each trailing discharger was burned and eroded and that the heat involved in the lightning current transfer caused the discharger nylon rod of each trailing discharger to bend toward the outboard side of the aircraft. Also, there was no damage to the aircraft structure. The 12 dischargers were the only items replaced after this incident.

It has been shown in Figure 8 that intense high-stress streamers are generated around the discharger and aircraft wing tip during laboratory high-voltage test (10 million volts). In the case of natural lightning stroke, the voltage is even higher and it is possible that the whole wing tip is filled with high-stress streamers when the lightning step leaders approach to the wing tip (11),(12). The number and the intensity of the streamers that originate from various points of the wing tip are proportional to its static electric field intensity distribution. The p-static dischargers, which protrude into the air from the uniform aircraft trailing edge or wing tip, are discrete static electric field concentration points. The most outboard trailing discharger generally

has the highest electric field concentration and the strongest streamer. When a lightning step leader approaches the wing tip, it may make contact with streamers coming from several dischargers and form several ionized lightning current channels. As the lightning current transfers through these ionized channels, the current density for each channel is a function of its original streamer intensity. Therefore, the more intense ionized channel (streamer) will transfer a larger percentage of lightning current and cause greater localized damages. Figure 26, Views A and B, show that the most outboard trailing discharger received the severest damage. Figure 27 shows how the discrete ionized lightning current channels could be established at the wing tip of a commercial aircraft. The ionized lightning current channels cover the outboard sides of each trailing discharger and thus the type of burning and erosion damages, as shown in Figure 26, could occur.

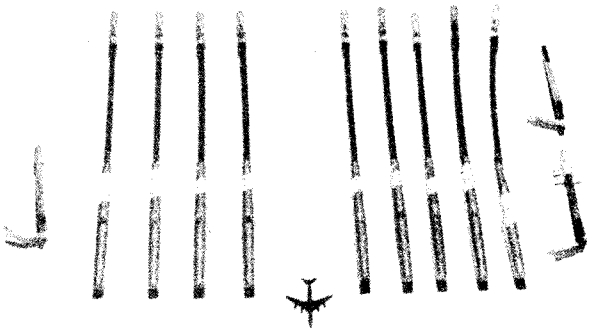

View A — Trailing dischargers bent toward outboard sides of the aircraft

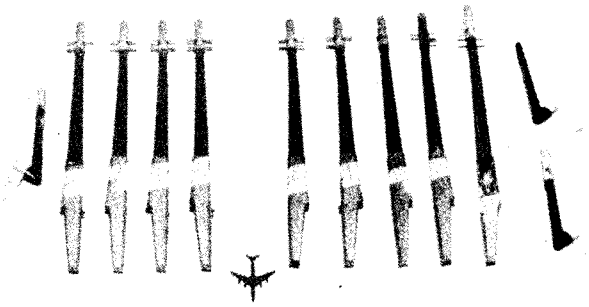

View B — Burning and erosion damages on the outboard side of each discharger

Fig. 26 — Dischargers recovered after a natural lightning stroke incident to a commercial aircraft

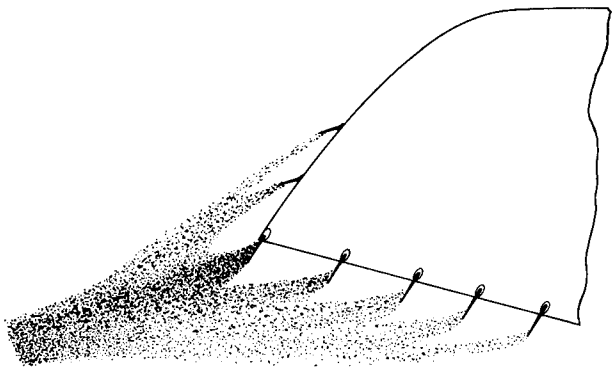

Fig. 27 — Lightning current channels contacting a number of aircraft discharger installations

The in-service experience indicates that all p-static discharger installations should incorporate the lightning protection design and the most outboard trailing discharger installation should be more carefully designed so that all possible lightning damages would be limited to the discharger itself and thus provide lightning protection to aircraft structures.

DIVERTER DISCHARGER — Certain aircraft have navigation lights installed in their aft wing tips. A standard trailing discharger installation cannot always completely protect the light installation from the physical damages caused by direct lightning stroke. A special diverter-discharger with an extended metal shank section can be developed for this purpose. A typical aft wing tip full-scale model with a navigation light installation which could utilize this type of protection was tested with the use of the LTRI 10-million-volt high-voltage generator shown in Figure 5. Figure 28 shows some of the test results. View A shows a long diverter-discharger installation on top of the light assembly that failed to protect the outboard corner. View B shows a regular trailing discharger installation at the outboard wing tip that failed to protect the inboard corner. View C shows an installation of a trailing discharger with extended metal shank section at the outboard wing tip. The lightning current attached to the metal shank ignored the existence of the sharp needle points at the discharger tip. This result indicates that for this type of discharger only the metal shank section should be considered for the diverting function of the lightning stroke. View D shows the diverter-discharger installation having the shortest metal shank section that, in this case, can successfully divert lightning strokes approaching from any possible direction.

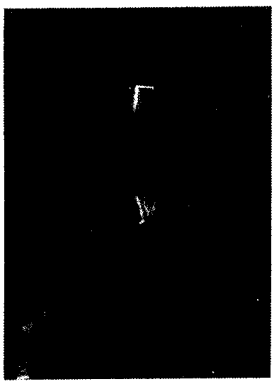

A — Intense streamer current from the outboard corner

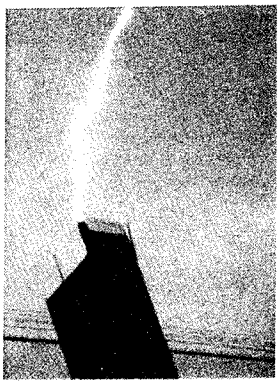

B — Lightning current attached to the inboard corner

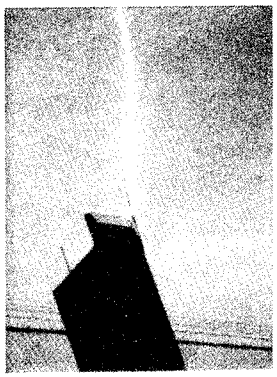

C — Lightning current attached to the diverter-discharger metal shank

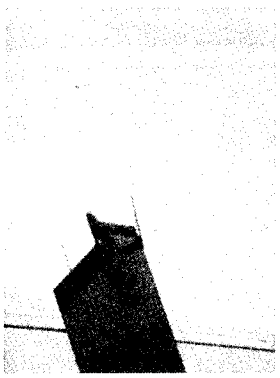

D — Successfully tested diverter-discharger installation

Fig. 28 — High-voltage lightning tests of the diverter-discharger installation on an aircraft wing tip full-scale model

To make the diverter-discharger an interchangeable item with the other trailing dischargers, a diverter-discharger base, as shown in Figure 29, can be made and installed at the outboard wing tip. A regular trailing discharger can be mounted at the end of the base to complete the installation. The length of the diverter-discharger base and its proper location varies for different types of aircraft wing tip installations and can be established by proper high-voltage lightning tests of a full-scale model.

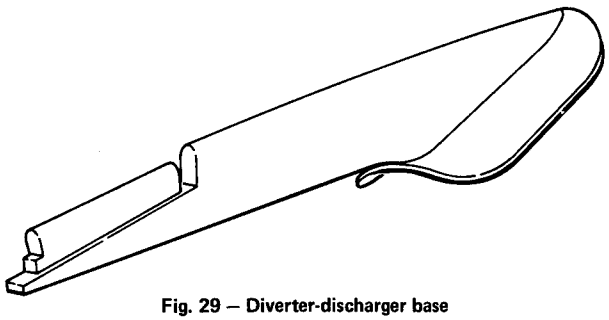

Fig. 29 – Diverter-discharger base

CONCLUSIONS

The lightning current transfer characteristics of the p-static discharger, discharger retainer, and its aircraft installation have been determined through laboratory lightning tests. Significant test results and important design considerations from lightning protection point-of-view are summarized in the following.

P-STATIC DISCHARGER –

(a) Dischargers utilizing needle-type discharge points with integrated safety protective guard can transfer lightning current with the minimum amount of damage.

(b) A properly designed and fabricated internal resistive element is shielded from the adverse thermal effects during lightning current transfer.

(c) Dischargers with a well-designed metal shank section can prevent lightning damage to typical aircraft trailing edge structures.

DISCHARGER RETAINER –

(a) The requirement for the use of silver conductive adhesive in the discharger retainer installation for lightning protection purpose is not justified.

(b) Riveted discharger retainer installations using noncorrosive PR 1422 adhesive as a faying surface seal can transfer lightning current satisfactorily.

(c) A portion of lightning high current transfers peripherally along the surface of the discharger metal shank and around the edge of discharger retainer to aircraft metal structure.

AIRCRAFT DISCHARGER INSTALLATION –

(a) Discharger installations incorporating lightning protection can prevent local physical damage to aircraft structure.

(b) Diverter discharger installations located at aircraft extremities can be developed to protect special components, such as a navigation light assembly, from lightning damages.

ACKNOWLEDGMENT

The information presented in this paper was developed by the Douglas Aircraft Company of the McDonnell Douglas Corporation as part of the company-sponsored Independent Research and Development Program.

REFERENCES

1. R. L. Tanner and J. E. Nanevicz, "Precipitation Charging and Corona-Generated Interference in Aircraft," AFCRL 336, Technical Report 73, Contract AF 19(604)-3458, SRI Project 2494, Stanford Research Institute, Menlo Park, California, April 1961.

2. R. L. Tanner, "Radio Interference from Corona Discharges," Technical Report 37, Contract AF 19(604)-266, SRI Project 591, Stanford Research Institute, Menlo Park, California, April 1953.

3. A. Vassiliadis, "A Study of Corona Discharge Noise in Aircraft Antenna," Technical Report 70, Contract AF 19(604)-3458, SRI Project 2494, Stanford Research Institute, Menlo Park, California, July 1960.

4. R. L. Tanner and J. E. Nanevicz, "An Analysis of Corona-Generated Interference in Aircraft," Proc IEEE, Vol. 52, No. 1, pp 44-52, January 1964.

5. J. E. Nanevicz and R. L. Tanner, "Some Techniques for the Elimination of Corona Discharge Noise in Aircraft Antennas," Proc IEEE, Vol. 52, No. 1, pp 53-64, January 1964.

6. M. P. Amason and J. T. Kung, "P-Static Discharger Evaluation," Report No. DAC 67983, Douglas Aircraft Company, Long Beach, California, June 1969.

7. M. P. Amason and J. T. Kung, "Lightning Protection Study of P-Static Discharger Retainer Installation," Report No. MDC J0654, Douglas Aircraft Company, Long Beach, California, December 1969.

8. M. P. Amason, "Douglas Aircraft Company Lightning Protection Research and Development Capabilities," Douglas Paper 5692, Douglas Aircraft Company, Long Beach, California, November 1969.

9. S. B. Griscom, "The Prestrike Theory and other Effects in the Lightning Stroke," AIEE Trans., Vol. 77, Pt. III, pp 919-931, December 1958.

10. B. J. Peterson and A. R. Wood, "Measurements of Lightning Strikes to Aircraft," Federal Aviation Administration Report No. DS-68-1, Sandia Laboratory Report No. SC-M-67-549, January 1968.

11. M. M. Newman, J. R. Stahmann, and J. D. Robb, "Experimental Study of Triggered Natural Lightning Discharges," Federal Aviation Administration Report No. DS-67-3, Contract No. FA 66 NF-156, Lightning & Transients Research Institute, Minneapolis, Minnesota, March 1967.

12. M. M. Newman, J. D. Robb, and J. R. Stahmann, "Lightning Protection Measures for Aircraft Fuel Systems, Phase I," Federal Aviation Agency Report No. FAA ADS-17, Contract No. FA 64 WA-4955, Lightning & Transients Research Institute, Minneapolis, Minnesota, May 1964.

MEASUREMENTS AND ANALYSIS OF LIGHTNING-INDUCED VOLTAGES IN AIRCRAFT ELECTRICAL CIRCUITS

Paul T. Hacker
Aerospace Safety Research and Data Institute
National Aeronautics and Space Administration
Lewis Research Center
Cleveland, Ohio

and

J. A. Plumer
General Electric Company
High Voltage Laboratory
Pittsfield, Massachusetts

E-5991

ABSTRACT

A series of measurements were made of voltages induced in electrical circuits within a metallic aircraft wing by full-scale simulated lightning currents flowing through its skin and structure. The measured data were mathematically analyzed to enable determination of voltages across load impedances to which the circuits might be connected elsewhere in the aircraft. Relationships between induced voltages and lightning current, wing structural and circuit parameters were determined. Induced voltages of magnitudes likely to cause damage or interference with avionics were measured.

LIGHTNING TO AIRCRAFT has been recognized as a hazard for a long time. The hazards to aircraft due to lightning strikes are manifested in several forms, such as:

(1) Damage to the aircraft structure.
  (a) Pitting and holes in metallic surfaces.
  (b) Delamination and loss of strength of composite nonmetallic materials.
(2) Ignite fuels vapors in tanks through
  (a) Holes burned through or hot spots created on the surfaces of integral fuel tank.
  (b) Arcing across electrical discontinuities such as fuel tank filler caps.
  (c) Ignition of vapors at tank vent exits.
(3) Damage to electrical systems and avionic equipment by
  (a) Direct strikes to external electrical components.
  (b) Indirect or induced electrical voltages in electrical systems.

The mechanical effects, items (1a) and (1b), the thermal effects, items (2a), (2b), and (2c), and the direct electrical effects, item (3a), of lightning strikes have been the subject of many investigations conducted by various government agencies, aircraft industries and research laboratories during the past two or three decades, Refs. 1 to 10.

The indirect or induced effects of lightning on aircraft electrical systems have not received much attention. It has been recognized that voltages could be induced in electrical circuits inside the aircraft by lightning currents passing through the aircraft skin and structure. The magnitude of these induced voltages or the extent to which they interact with and affect aircraft electrical and avionic systems has not been determined. Experience has shown that sensitive avionics, as well as other equipment, have been affected by some characteristic of the flight environment when lightning is present. Communication and navigational equipment have failed and electroexplosive devices have also been actuated (1).* The hazards have been lived with for many years and few if any fatal accidents could be attributed to induced electrical effects. In the past, the induced effects were probably not severe enough to cause extensive damage to electronic equipment because such equipment made extensive use of vacuum tubes and large electronic components which inherently have high voltage breakdown characteristics. Modern aircraft avionics, however, make extensive use of semiconductors and micro-circuitry which are much less tolerant to transient overvoltages and currents.

Some investigations have been conducted to establish the transient voltage and current withstand capability of these new electronic devices. These investigations, however, have been mainly concerned with surges in the power supply. Very little effort, however, has been expended to determine the magnitude of induced voltage arising in aircraft electrical circuits due to lightning strikes or the relationship between the induced voltages and the characteristics of the lightning current that produce them. It is necessary to know the magnitude of these induced voltages before the susceptibility of aircraft electrical systems and components to interference or damage

*Numbers in parentheses designate References at end of paper.

can be assessed.

Thus a program was initiated by the Aerospace Safety Research and Data Institute, NASA, Lewis Research Center, to determine the magnitude of induced voltages and currents which may arise in electrical circuitry within a metallic aircraft structure through which lightning current is flowing. The objectives of the experimental and analytical program were to:

(1) Measure the voltages and currents induced in actual aircraft circuits.

(2) Determine the extent to which these voltages may be coupled to any load (equipment) for which the input impedance is known.

(3) Identify and determine the significance of factors affecting these voltages.

(4) Establish and evaluate techniques for eliminating or reducing the magnitude of the induced effects.

(5) Develop techniques which could be used to evaluate the susceptibility of circuits in any aircraft.

The experimental portion of the investigation was performed with a complete wing of an F89J fighter aircraft and a full scale simulated lightning facility. The program was conducted by the High Voltage Laboratory of the General Electric Company in Pittsfield, Massachusetts. This paper outlines the investigation and presents some of the significant results. Details of the investigation are presented in a General Electric report, HVL 69-161 (11).

THEORETICAL ANALYSIS

INDUCED VOLTAGE MECHANISMS - Voltages can be induced in electrical circuits inside aircraft structures by lightning currents flowing through the structure by:

(1) Magnetic coupling between the current carrying structure and other circuits.

(2) Resistive voltage rises in the structure to which electrical conductors or shields may be connected.

Figure 1 is an electrical circuit representation of an aircraft wing-electrical circuit combination which illustrates how induced voltages are generated. Lightning current, i_L, flowing in the skin and structure generates a magnetic field which links the electrical circuit. This magnetic coupling is indicated by the lumped inductances, L_W and, L, for the structure and circuit respectively. These two inductances possess a mutual inductance, M. Most of the magnetic flux, φ_o, generated will be outside the wing, but a significant amount, φ_i, will be generated inside the wing because of the non-cylindrical geometry and the finite conductivity of the wing. The flux distribution is further complicated by the location of internal structural members, rivetting, skin joints, access openings and openings created by flight control surfaces. The lightning current flowing through the structure also produces a voltage rise along the wing due to the finite resistance, R_W, of the wing. This voltage rise appears in the electrical circuit. In addition to the electrical resistance of the structural material, other sources of resistance are the bondings resistances which appear at junctions; between skin sections, between skin and structural members, or between structural members. The magnetic coupling and resistive voltage rise produce a voltage, e_{oc}, between terminals a and b.

The circuit of Fig. 1 is illustrated in more conventional form in Fig. 2. The open circuit voltage, e_{oc}, appearing across terminals a and b is composed of the magnetically induced voltage, V_M, and the resistive voltage rise, V_R. The magnetically induced voltage is equal to the rate of change of flux coupling the circuit, that is

$$V_M = d\varphi_i/dt \tag{1}$$

The rate-of-change of flux is equal to the product of the mutual inductance, M, and the rate-of-change of current, that is

$$(d\varphi_i/dt) = M(di_L/dt) \tag{2}$$

Thus the magnetically induced voltage is given by

$$V_M = M(di_L/dt) \tag{3}$$

The resistive voltage rise, V_{R_W}, is given by the product of the current and the resistance of the structure along the current path, that is

$$V_{R_W} = i_L R_W \tag{4}$$

The total open circuit induced voltage, e_{oc}, at terminals a and b is the sum of Eqs. (3) and (4).

$$e_{oc} = M(di_L/dt) + i_L R_W \tag{5}$$

The total induced voltage is a function of the rate of change and the absolute value of the lightning current flowing in the wing. Measured characteristics of lightning (12), (13) show that rates of current change of 15 kiloamperes per microsecond and peak current values of 30 kiloamperes are very common. These are fairly large values and would result in large induced voltages if the mutual inductance, M, and the effective resistance, R_W, are significant. The rate-of-change of the magnetic flux linking the circuits or the mutual inductance, M, cannot be readily calculated. The effective wing resistance, R_W, is not the simple direct current resistance of the structure. It is a complex time-varying function of the wing geometry, conductivity and thickness and the time characteristics of the lightning current.

These two factors are thus best determined experimentally. The method used to determine the effective wing resistance and mutual inductance from experimental data by the use of Eq. (5) is presented in the REDUCTION OF DATA SECTION.

The circuit depicted in Figs. 1 and 2 utilized the aircraft structure as a return path. There are circuits present in aircraft which are open ended or "floating" such as antenna and circuits which utilize a separate ground return. In these circuits, the resistive induced voltages will not directly appear across the circuit terminals. There may be, however, an induced voltage due to capacitive coupling between the current carrying structure and the "floating" electrical circuit.

THEVENIN EQUIVALENT CIRCUITS - In the experimental tests of simulated lightning strokes to a full scale F89 wing, which will be described later, the open circuit induced voltages were measured for several circuits at the root end of the wing. The open circuit voltage has little practical significance by itself. What is of importance is the voltage induced across an impedance load (aircraft electrical equipment) to which the circuit is connected, since this voltage determines whether or not damage will occur. The voltage induced across any load in the aircraft to which the wing circuit might be connected can be predicted by determining the Thevenin equivalent circuit for each wing circuit. The Thevenin Equivalent Circuit for the wing electrical circuit of Fig. 2 is illustrated in Fig. 3. The Thevenin Equivalent Circuit consists of a voltage source, e_T, in series with an impedance, Z_T, between the terminals a and b. Comparing the circuits of Figs. 2 and 3, the Thevenin voltage source, e_T, is equivalent to the open circuit voltage, e_{oc}, developed by the mutual inductance and resistive voltage rise across resistance, R_w. Since the open circuit voltage is a function of the lightning current, i_L, Eq. (5), then the Thevenin voltage is also a function of the lightning current or

$$e_T = R_w i_L + M(di_L/dt) \qquad (6)$$

By definition the Thevenin impedance, Z_T, is given by

$$Z_T = e_T/i_{sc} \qquad (7)$$

where i_{sc} is the current flowing in the circuit when the terminals a and b are shorted.

If a load of impedance, Z, is connected across terminals a and b of Fig. 3, the voltage drop across the impedance, V_Z, is given by

$$V_Z = Z/(Z_T + Z)e_T = Z/(Z_T + Z)e_{oc} \qquad (8)$$

Combining Eqs. (7) and (8) gives

$$V_Z = (Zi_{sc}e_{oc})/(Zi_{sc} + e_{oc}) \qquad (9)$$

which indicates that the voltage developed across any impedance, Z, attached to the terminals of the circuit is a function of the open-circuit voltage and the short-circuit current developed in the wing circuit. Thus, in the experimental program both the open-circuit voltage and short-circuit current were measured and recorded oscillographically as a function of time. To use these measured values of open-circuit voltage and short-circuit current in the solution of Eqs. (7), (8), and (9), they have to be transformed into the complex frequency domain since Eqs. (7), (8), and (9) apply in this domain.

The Thevenin impedance, Z_T, may be assumed composed of a combination of resistances and reactances, such as the series connected resistance, R, and inductance, L, shown in Fig. 3. To understand and possibly predict the induced voltage response of a circuit, a knowledge of the magnitude of the components of the circuit impedance is required. A method by which values of effective circuit resistance and inductances can be calculated from measurements of open-circuit voltages and short-circuit currents is presented in the REDUCTION OF DATA SECTION.

EXPERIMENTAL INVESTIGATION

The experimental investigation was performed using a complete right wing of an F89 aircraft and a full scale simulated lightning test facility.

DESCRIPTION OF WING -

Physical Characteristics - A schematic of a plan view of the wing showing approximate size and main components is given in Fig. 4. The wing is of full cantilever, multispar construction using heavy, tapered alclad skin. The principal components are the main wing panel, leading edge, trailing edge and a non-jettisonable wing tip pod.

The main wing panel consists of five heavily constructed spanwise spars, bulkheads, ribs and aluminum honeycomb reinforced heavy tapered alclad skin. The main panel houses a retractable main landing gear and six fuel cells. Access and inspection doors are provided throughout the wing surface.

The leading edge consists of spars, formed ribs, heavy tapered alclad skin and a spanwise anti-icing hot air duct. The leading edge is attached to the forward wing spar with flush-headed screws.

The trailing edge section is divided into a slotted wing flap on the inboard portion and a combination aileron speed brake on the outboard portion. The attachments and actuating devices for these aerodynamics control surfaces required fairly large opening into the interior of the main wing section which could allow externally generated magnetic flux to enter.

The wing is equipped with a 600 gallon wing tip

fuel tank. The tank is mounted on the wing by two bolts and a pin. Flexible fuel hose and electrical cables provide necessary connections between the wing and tip tank.

In general, the alclad wing skin increased in thickness from the wing tip to root. In the main wing panel, the skin thickness ranged from 0.154 to 0.291 in. In the leading edge section, the skin thickness ranged from 0.085 to 0.157 in. In the trailing edge, aerodynamic control surfaces the alclad thickness range from 0.051 to 0.072 in. The thicknesses were required for the mission of the F89 aircraft and are much thicker than some of those found in recent commercial or military aircraft. As a result, the electromagnetic shielding effectiveness of this wing is likely to be greater than that of a wing covered with thinner skins.

The exterior surfaces of the wing skins were chromodized with aladine 1000. The interior wing skins and structural elements were treated with Iridite 14-2, chromic acid anodized and then covered with a green zinc chromate primer. This treatment was given all surfaces, including the mating surfaces between elements. No treatment for improvement of electrical bonding between surfaces was applied. Thus, the resultant electrical bonding between structural elements is mainly accomplished by the fastening rivets and bolts.

Wing Electrical Circuits - The wing contained 29 functional electrical circuits for such functions as: aircraft position light, fuel quantity gages, fuel booster pumps, fuel vent valves, glide slope antenna, and several safety and indicating switches on movable components in the wing. The number of conductors in each circuit ranges from one to more than twenty. There were a large variety of circuits in regards to the type of return path and type of shielding employed. For the investigation only eight circuits were studied. The criteria used for the selection of these eight circuits included:

(1) Function of the circuit.
(2) Location of the circuit.
(3) Type of return path.
(4) Shielding employed.
(5) Applicability to other aircraft.
(6) Characteristics of the circuit.

For this paper, however, only the results for some of the circuits will be presented and discussed. The description of the other circuits along with results of tests are presented in (11). In addition to the regular aircraft circuit, a special multiconductor circuit was installed in the wing to make comparative tests on various types of shielding and length and location of circuit. Results for this circuit will also be presented. A description of each circuit discussed herein is given in the RESULTS AND DISCUSSION SECTION when the test results are presented.

TEST SETUP - The wing was supported on a portable wooden carriage which was positioned adjacent to a high-amplitude simulated lightning current generator in an indoor test bay of the G. E. High Voltage Laboratory. The test setup is shown schematically in Fig. 5. The simulated lightning strike was delivered to the desired location on the wing by the use of a movable electrode. The arc gap from electrode to wing was approximately 8 in. The root end of the wing was joined to a double walled screened instrument enclosure into which the simulated lightning currents passed from the wing. The lightning current return flow path from instrument enclosure to the impulse generator was through a low-inductive aluminum foil along the floor. A current measuring shunt was located in the lightning current circuit at the junction of the instrument enclosure and aluminum foil. A photograph of the wing in the test area is shown in Fig. 6.

TEST CONDITIONS -

Lightning Simulation - The currents which pass through an aircraft when it is struck in flight by natural lightning are believed to be a combination (2, 3) of high-amplitude, short duration "strokes" and low-amplitude, long duration approximately constant value "continuing currents." This combination may be repeated several times in a lightning discharge.

The continuing currents are known to produce thermal and mechanical damage to aircraft skins (3, 4). These currents, however, create very little magnetic flux, and that which is created does not change rapidly. As shown by Eq. (5) in THEORETICAL ANALYSIS, a rapidly changing current or magnetic flux is required to induce voltages in magnetically coupled circuits. Therefore, only the high-amplitude, short-duration strokes were simulated for all of the tests in this program. The current strokes generated were critically damped to obtain a unidirectional wave shape, since natural lightning currents are nearly always unidirectional. Since natural lightning strokes may vary in wave shape, amplitude, polarity and attachment location, it was desirable to evaluate the effects of each of these variables upon the voltages induced in internal circuits.

Two wave shapes were used for most of the test. These shapes are designated as "fast" and "slow." The meaning of these terms and a standard wave shape notation is illustrated in Fig. 7. An impulse current, simulating a high-amplitude, short duration lightning stroke is ideally an aperiodic transient current which rises rapidly to a maximum value and falls less rapidly to zero. The standard notation is based upon the time to crest, T_1, and the time to 50% value, T_2, on the decay. The wave shape is then described by the notation: $(T_1 \times T_2)$. In this notation, the two wave shapes used in most of the tests are $(36 \times 82\ \mu s)$ and $(8.2 \times 14\ \mu s)$ for the "slow" and

"fast" respectively. Oscillograms of these current wave shapes are shown in Fig. 8. For these oscillograms and others presented later, the size of the ordinate and abscissa divisions are shown on the bottom left and bottom right respectively.

To identify those stroke locations creating the most severe induced voltages, a series of preliminary strokes were applied to each of ten locations shown on Fig. 9. An identical 14 kiloampere (12×24 μs) simulated lightning discharge was applied to each location. Open-circuit voltages and short circuit currents were measured at the wing root terminals of two circuits. One circuit was located in the trailing edge and extended the full length of the wing. The other was in the leading edge and extended to about half span. The five position indicated by the large circles in Fig. 9 gave the largest induced effects and were, therefore, used through the remainder of the tests.

It was postulated before any tests were performed, that the induced effects for a given wave shape might be a linear function of the current stroke amplitude. A series of tests early in the experimental program using a (12×24 μs) wave shape and stroke amplitudes from 7 to 70 kiloampere showed a near linear relationship. Thus to minimize the number of tests to be performed most of the remaining tests were made at a stroke amplitude of 40 kiloamperes. This value is near the average amplitude of measured lightning strikes (14). At a maximum current amplitude of 40 kiloamperes the "fast" wave shape (8.2×14 μs) provides an initial rate of change of current (di_L/dt) of 8 kiloamperes per microsecond which is four times as fast as that for the "slow" (36×82 μs) stroke (2KA/μs).

MEASUREMENTS - Measurements made at the wing root end of each circuit for each applied simulated lightning stroke condition included:

(1) Open-circuit voltage, e_{oc}.

(2) Short-circuit current, i_{sc}.

(3) Voltage across a terminating dummy load, e_l.

(4) Current through a terminating dummy load, i_l.

The induced effects were measured for the dummy load to provide a check on the calculated response to the same load impedance using the Thevenin Equivalent Circuit determined from the open and closed circuit tests. The dummy load was a 1 ohm resistance. Measurements were recorded oscillographically using a Tektronix Type 535 oscilloscope with a Type 1A1 preamplifier. Measurements were made at one or more oscilloscope sweep settings as necessary to define the wave shape of the signals being measured. Typical oscillograms of open-circuit voltages and short-circuit currents are shown in Fig. 10. As might be expected from the pulse nature of the applied simulated lightning current and the dependency of the induced open-circuit voltage on the rate of change of the lightning current, Eq. (5), the open-circuit voltage and short-circuit current are both time dependent. They reach a maximum value on the first half cycle and decay rapidly.

For many of the circuits and test conditions, there was a very high frequency damped oscillation at the beginning of the open-circuit voltage trace. This oscillation was not always visible on the oscillograms due to smearing unless fast sweep was used. The amplitude of the first cycle of this high frequency was usually much larger than the amplitude of the slow wave shown in Fig. 10. The amplitude and wave shape of the applied lightning current were monitored and recorded oscillographically for all tests to assure that the desired wave shape was being applied.

The measuring instruments were located inside the double-screened shielded enclosure attached to the root end of the wing. This enclosure provided a magnetic shielding of the oscilloscopes and measurement leads, into which extraneous voltages could otherwise be induced by the strong magnetic field generated by the simulated lightning stroke itself. Checkout tests with the measuring equipment plus measurement of magnetic flux inside the enclosure indicated that the instrument system was not being influenced.

In circuits employing only a single conductor, in which the airframe or a coaxial shield is used as the return path, measurements were always made between the conductor and the airframe or shield. Some circuits, however, have more than one conductor and some do not employ the airframe as a return path. In these cases, measurements of induced voltages and currents were made between pairs of conductors and between individual conductors and airframe when the airframe was used as part of the circuit.

REDUCTION OF DATA

The basic data recorded during the investigation were the open-circuit voltage and short-circuit current for the various circuits, lightning current wave shape and stroke location. These data were reduced and analyzed to determine the following:

(1) Maximum values of induced open-circuit voltages and short-circuit currents.

(2) Values of effective wing resistance and mutual inductance.

(3) Values of effective circuit resistances and inductance.

The maximum values of induced open-circuit voltage and short-circuit current were obtained directly from the respective oscillograms. The other parameters were derived by calculation.

EFFECTIVE WING RESISTANCE, R_W, AND MUTUAL INDUCTANCE, M - The effective wing resistance, R_W, and the mutual inductance, M,

between the wing structure and the electrical circuits were obtained through the use of Eq. (5).

$$e_{oc} = R_w i_L + M(di_L/dt) \quad (5)$$

If it is assumed that the effective wing resistance, R_w, and the mutual inductance, M, are not a function of time or lightning current, then they can be evaluated directly from the oscillogram traces for the open-circuit voltage, e_{oc}, and the lightning current, i_L. The calculation can be illustrated by the use of Fig. 11 which shows a typical lightning current and corresponding induced open-circuit voltage wave form. At time, T_1, the rate of change of lightning current with time, (di_L/dt), equals zero. Equation (5) then becomes

$$e_{oc_1} = R_w i_{L_1}$$

or

$$R_w = e_{oc_1}/i_{L_1} \quad (10)$$

where values of e_{oc_1} and i_{L_1} can be obtained from the respective curves at time, T_1. At time, T_2, the induced voltage is zero and Eq. (5) reduces to

$$M(di_L/dt)_2 = -R_w i_{L_2}$$

or

$$M = -R_w i_{L_2} \Big/ (di_L/dt)_2 \quad (11)$$

The value of the mutual inductance, M, can then be calculated by Eq. (11) by obtaining values of i_L and $(di_L/dt)_2$ from the lightning current trace at time T_2 and the value of the effective wing resistance calculated above by Eq. (10). The above equations illustrate how the effective wing resistances and mutual inductances could be calculated by hand. In the investigation, however, these equations were solved by a computer using approximately mathematical expressions for both the lightning current and the open-circuit voltages as inputs to the computer.

EFFECTIVE CIRCUIT RESISTANCE, R, AND INDUCTANCE, L - The Thevenin impedance, Z_T, as given by Eq. (7) is resolved into an effective resistance, R, and an effective inductance, L, for a wing electrical circuit by the following technique. Using the oscillograms of open-circuit voltage and short-circuit current obtained for a given circuit and test condition, approximately analytical expressions are written for both as a function of time. These analytical expressions are then transformed into the complex frequency domain by the use of the Laplace Transform. After the transformation, the ratio of the open-circuit voltage to short circuit current is calculated as required by Eq. (7). The real part of the resulting complex expression is the resistive portion of the impedance and the imaginary part is the inductive portion.

RESULTS AND DISCUSSION

Typical experimental data and analytical results obtained during the investigation on: (1) induced voltages and currents, (2) effective wing resistance and mutual inductance, and (3) effective circuit resistance and inductance as functions of lightning current amplitude, wave shape and stroke location are presented in Figs. 13, 14, 15, 16, and 19 and Tables I through VII and discussed in the following section. Most of the data presented are for the position light, the E-11 autopilot and the specially installed circuits. Figures 12, 17, and 18 show the location and schematic diagram of these circuits.

CIRCUIT L.050, POSITION LIGHT - The location of this circuit within the wing and wiring schematic is shown in Fig. 12. (Note: On this figure and other places throughout the report, the USAF Code numbers for circuits, conductors, and connectors in the F89J are indicated.) The circuit is routed along the trailing edge of the main span, and is partially exposed in the area of the flap. The circuit passes through the tip fuel tank to the position light. In the fuel tank the circuit is enclosed in a conduit. The airframe is used as a return path. The bulb has a resistance of 2.5 ohms. Perhaps because this circuit extends the longest, is partially exposed, and employs the airframe as a return path, the induced voltage and currents measured were the greatest found in any of the circuits tested. As a result of this, and because this circuit is representative of a type found commonly in many aircraft, the position light circuit was more extensively studied than the others.

Induced Effects - The induced open-circuit voltages and short-circuit currents were measured for various stroke amplitudes, locations, and wave shapes. A preliminary series of tests using a moderately fast (12×24 μs) simulated lightning stroke were made to determine the relationship between the induced effects and the lightning current amplitude. The maximum current amplitude was varied from 7 to 90 kiloamperes. Figure 13 shows the results of these tests. The data points represent the maximum values measured. Both the open-circuit voltage and short-circuit current show an almost linear variation with current amplitude. Based upon these results, most of the subsequent tests were performed at 40 kiloamperes.

Figures 14 and 15 show a complete set of oscillograms for open-circuit voltages and short-circuit currents for five different stroke locations and for both the "slow" (36×82 μs) and "fast" (8.2×14 μs) wave shapes respectively. For the "slow" wave shape the induced voltages ranged between 2 and 20 volts and the induced currents ranged between 0.7 to 9.0 amperes. For the "fast" wave

shape the voltages and currents were greater by about a factor of two in most cases than for the corresponding "slow" wave shape cases. Variations in stroke location resulted in significant changes in induced voltages and currents. In general, delivery of strokes to locations farthest out on the wing and closest to the location of the circuit resulted in the highest voltages. All of the voltage wave shapes shown in Figs. 14 and 15 are composed of both a resistive voltage, in phase with the applied lightning current wave form, and a magnetically induced voltage, proportional to the rate of change of the applied lightning current. The inductive component, as evidenced by high initial rise rate and an undershoot, is greater for the stroke locations closest to the circuit (locations 1 and 5) than for the locations farther away. In the more distant stroke locations, the resistive component seems to be predominant. The voltages induced across and the current through a 1 ohm load resistor placed across the circuit terminals at the wing root end were also measured for the two current wave shapes and 5 stroke locations. The maximum voltage and currents measured are tabulated in Table I along with the corresponding maximum open-circuit voltages and short-circuit currents. As would be expected, the load resistor decreased the induced voltages and currents. In the table, two values of voltages are given for many of the cases. The first value listed is the maximum value of the first half cycle of the high frequency component that occurred in many cases at the beginning of the induced wave. The second value listed is the maximum induced in the slower component of the induced wave.

Wing Resistances and Mutual Inductances - The effective wing resistance, R_W, and mutual inductance, M, were calculated for the position light circuit using the method outlined in the REDUCTION OF DATA SECTION. These calculated values are tabulated in Table II for the two lightning current wave shapes and the five different stroke locations. The data indicate that both the effective wing resistance and mutual inductance are a function of both the applied wave shape and the location of the stroke. As would be expected from the induced effects described above, the largest values of effective wing resistance and mutual inductance occurred for strokes delivered to the wing tip tank. Although the applied wave shapes gave different results, there does not appear to be any consistent trend. For two cases with the "fast" wave shape, negative values of effective resistance were calculated. Negative values of mutual inductances were encountered with other circuits tested. Since a negative element is not possible, the negative values must be due to some other anomaly. Possibly they are the result of the lightning current flowing in a direction with respect to the wing circuit path opposite from that assumed for derivation of the equation which was used as a basis for the calculation. It should be realized that the resistance and mutual inductances calculated are effective values and as such do not describe tangible wing characteristics.

In the derivation of the method for calculating the effective wing resistance and mutual inductance, it was assumed that these two parameters did not vary with time. To verify this assumption, values of effective resistance and mutual inductance were calculated. The values were then used in the Thevenin Equivalent Circuit Equation (Eq. (5)) along with the applied lightning current to calculate the open circuit voltage as a function of time. The results of this calculation are shown in Fig. 16. The agreement with measured induced voltages is very good for the first half cycle.

Circuit Impedances - The effective circuit resistance, R, and inductances, L, were calculated for the position light circuit using the method outlined in REDUCTION OF DATA SECTION. These calculated values are tabulated in Table III. These data show that there is some variation in circuit impedances as a function of stroke location and wave shape. The variations, however, are not as great as was the variation in calculated values of effective wing resistance and mutual inductance for the same test conditions. The values of resistance calculated, 1.23 to 3.09 ohms, compare favorably with the resistance of the light bulb which was 2.5 ohms. The values of inductance calculated for this circuit appear reasonable for a conductor of its length. It appears from all the data obtained in the program that the effective impedances closely approximate the actual wing circuit impedances. A negative inductance was obtained for one test condition.

CIRCUIT F.0511, E-11 AUTOPILOT - The location of this circuit within the wing and a wiring schematic is shown in Fig. 17. This circuit is a part of the autopilot. It extends along the trailing edge to a safety switch located adjacent to the leading edge of the aileron. Its function is to assure that the aileron is in neutral position before firing of rockets which are carried on a pylon below the wing. Both connectors of the circuit are isolated from ground. The circuit is not shielded and is exposed to the outside of the wing for a short distance when the aileron is deflected. The circuit was tested with the safety switch in the closed position and the data presented below were obtained across the two conductors of the circuit.

Induced Effects - The open-circuit voltages, short-circuit currents, the voltages across and current through a 1 ohm load resistor for the same test conditions used on the position light circuit are presented in Table IV. The induced effects are much less than for the position light circuit. The maximum open-circuit voltage (slow component of

wave) was 0.6 volt which was produced by the "fast" lightning wave shape to stroke location number 5. Stroke location number 5 is the closest to the circuit. The short-circuit currents measured were 0.5 amperes or less. The 1-ohm load resistor decreased both the voltages and currents measured but not markedly. The position light circuit is longer than this circuit and in addition, this circuit does not employ the airframe as part of the circuit. The variation of the induced effects due to stroke location and lightning current wave shape is not as great as with the position light circuit.

Wing Resistance and Mutual Inductance - Equation (5), by which the effective wing resistance, R_W, and mutual inductance, M, were calculated for the position light circuit above, was derived on the basis of circuits which use the aircraft structure as part of the electrical circuit. This Autopilot circuit does not use the structure as part of the circuit. Nevertheless, it was found possible to calculate values of effective wing resistance and mutual inductance for circuits which are "floating" or not terminated either directly or indirectly to the aircraft structure.

The calculated effective wing resistance and mutual inductance for the Autopilot circuit are presented in Table V. The largest effective wing resistance was 10.0 microhms for a "fast" wave shape at stroke location number 7. The largest absolute value of effective mutual inductance was 0.187 nanohenry, again for the "fast" wave shape but at stroke location number 4. The calculations show that these parameters for this circuit are also a function of stroke position and applied current wave shape. The values are much less than those for the position light circuit for the same conditions. For this circuit all the mutual inductances were negative.

For "floating" circuits, capacitive coupling between the circuit and the current carrying structure may contribute to the induced voltage. The magnitude would be small compared to that induced magnetically or due to resistive voltage rises.

SPECIAL CIRCUITS - Several additional circuits were assembled and installed in the wing for the purpose of making some comparative measurements, which could not be made satisfactorily with circuits already existing in the wing. The measurements desired were:

(1) Comparison of voltages induced in circuits of different length which lead to the same location.

(2) Comparison of voltages induced in a parallel pair and a twisted pair of conductors.

(3) Comparison of voltages induced in a single unshielded conductor and a coaxial cable.

For these tests, a group of conductors suitable for the above comparisons was assembled and installed in the wing as shown in Fig. 18. The conductors were passed from the instrument enclosure through the leading edge heating duct to the wing tip, thence between the wing tip and tip fuel tank and along the outside of the trailing edge spar to the instrument enclosure. Both ends of each conductor were thus terminated in the enclosure.

The circuits include a conductor bundle containing a single insulated number 16 conductor, a single coaxial cable (RG 58A/U), a twisted pair of number 16 insulated conductors, and a parallel pair of number 16 insulated conductors. In order that the circuits would not be completely exposed anywhere along the path, part of the bundle was shielded by copper braid. This braid was placed over the conductor bundle for its entire path except where the bundle was within the heating duct. The copper braid did not cover the bundle within the heating duct because the duct itself provided shielding for the conductors within it. The braid was solidly connected to the airframe at the point where the bundle leaves the heating duct, and at various points along the trailing edge.

All measurements on these circuits were made with 40-kiloampere "fast" (8.2×14 μs) simulated lightning strokes delivered to location 1 at the forward end of the tip fuel tank.

Two series of measurements were made. The first series consisted of measurements of the voltages induced in the entire length of each conductor. These measurements were obtained by measuring the voltages at each end of each conductor, with the other end connected to the airframe. For the second series of measurements, all conductors, including the coaxial cable shield and the copper braid, were solidly connected to the airframe at a point in the trailing edge between the aileron and flap positions, shown on Fig. 18. This in effect created two sets of circuits terminating at the same point in the wing, but following different paths. The circuits passing through the heating duct and across the wing tip were the longest, at 38 feet. Those running out the trailing edge were only 12 feet long. Identical tests and measurements were made in each set of circuits. Measurements were made from all conductors to the airframe (line to airframe), and between each conductor of the twisted and parallel pairs. The open-circuit induced voltages and short-circuit currents measured in each conductor are listed in Tables VI and VII. The maximum amount of voltage measured in any circuit was 6 volts. This relatively low value is probably due to the overall shielding provided all of the circuits. Placement of these circuits in the leading edge heating duct afforded them greater shielding than they would have if simply routed through the leading edge itself. Similarly, the addition of the copper braid around the rest of the circuit provided greater shielding than was afforded the existing aircraft circuits which followed the same path.

Comparison of voltages induced in the various circuits is of interest. When measured between individual conductors and the airframe, it was found that voltages induced in conductors of the parallel pair were three to six times greater than those induced in the twisted pair (Table VI and VII). Voltages measured between conductors of the parallel pair were between two and ten times greater than those measured in the twisted pair.

A comparison between conductor to airframe voltages measured from the individual number 16 insulated conductor and the center conductor of the RG 58A/U coaxial cable shows little difference in voltage amplitudes (Tables VI and VII). This is probably the result of the substantial attenuation in induced voltages provided both of these circuits by the heating duct and copper braid covering all circuits.

An additional interesting comparison is between the long (leading edge) circuits and the short (trailing edge) circuits, both of which terminate at the same point in the wing. Open-circuit voltages and short-circuit currents measured in the longer circuits were greater in all cases than those associated with the shorter ones. Such a result would be expected, since induced effects are believed to be proportional to circuit length (among other factors).

Similar comparisons were found for short-circuit currents, although the comparison ratios for currents were not the same as corresponding voltage ratios. This would be expected for, while voltages are somewhat proportional to circuit length, currents would be proportional to voltages only to the extent they are not diminished by the additional circuit impedance provided by longer circuits.

These measurements illustrated some important facts, the most significant of which are that a twisted pair of conductors receives substantially less induced voltage than a parallel pair, and that circuits within a shielding braid or conduit are much less susceptible to induced voltages than those relying upon the wing skin itself for shielding.

VOLTAGES ACROSS CIRCUIT LOAD IMPEDANCE - One of the objectives of the investigation was to develop a technique by which the voltage induced across any load impedance attached to the wing root end of a circuit could be predicted from the open-circuit voltage and short-circuit current measured at the same point. Towards this end, a technique, expressed by Eq. (9), was derived based on the Thevenin Equivalent Circuit (see THEORETICAL ANALYSIS). To check the validity of the method, the voltage drop across a 1-ohm resistive load as a function of time was calculated from open-circuit voltage and short-circuit current measurements and compared to actual measurements of voltages developed across a 1-ohm resistor. A sample comparison is shown in Fig. 19. The wave shape and especially the maximum voltage developed show fair agreement indicating that the Thevenin Equivalent Circuit may be useful in determining the approximate level of lightning induced voltages which a wing circuit would impress upon various load impedances.

MISCELLANEOUS RESULTS - Two other observations made during the investigation are worthy of mention. First, a reversal of polarity of lightning current did not produce any significant changes in the induced effects. Second, a radio frequency interference filter was employed in a motor circuit (fuel booster pump). The induced open-circuit voltage wave form was similar to those measured for other circuits but the short-circuit current measurements showed a high-frequency damped oscillation which lasted about five times longer than the open-circuit oscillation. This illustrates the possibility that the addition of a device to an electrical circuit to provide protection against one type of electrical phenomenon may aggravate the lightning induced voltage problem.

CONCLUDING REMARKS

The investigation has shown that lightning strikes to aircraft can induce voltages in electrical circuits inside the metal structure through magnetic coupling and voltage rises in the airframe. The magnitude of the induced voltages is a function of the rate of rise of the lightning current, the amplitude of the lightning current, the location of the lightning stroke with respect to the circuit location, and the physical and electrical characteristics of the electrical circuit. The maximum induced voltage measured in any circuit was 96 volts which was produced by a 40 kiloampere discharge with a rate of current rise of 8 kiloamperes per microsecond. Most of the tests were conducted with current rates of rise between 2 and 8 kiloamperes per microsecond and at a current amplitude of 40 kiloamperes. In natural lightning, 20% of all strokes exceeds a peak amplitude of 70 kiloamperes and rates of current rise of 20 kiloamperes per microsecond. To cover the probable range of natural lightning military specification MIL-B-5087B for electrical bonding and lightning protection testing for aerospace systems requires a peak amplitude of 200 kiloamperes and a current rate of rise of 100 kiloamperes per microsecond. Exposure of the F89 wing to either natural lightning or the military specification could induce voltages in the circuits much greater than those measured in the investigation.

A part of the induced voltage in circuits that utilizes the structure as a return path is due to a resistive voltage rise in the structure due to the flow of the lightning current. This voltage rise

depends upon the electrical conductivity of the structural material and the length of the current path. The F89 wing is relatively short and has relatively thick wing skins compared to modern transport aircraft. The wing material is aluminum which has a low electrical resistivity compared to the metals used or proposed for use on modern aircraft. The modern large aircraft may therefore be susceptible to much higher induced voltages than was found in this investigation. The induced voltage problem may be accentuated by the use of nonmetallic, high electrical resistance materials.

Considerable variation was evident in voltages induced in the various circuits tested. An identical stroke could induce up to 96 volts in some circuits, while only a few millivolts in others. The characteristics of the circuits which received the greatest and the least induced voltages are therefore of interest. In general, these characteristics can be summarized as follows:

Circuit characteristics	Circuit return path	Circuit termination (within wing)	Shielding	Routing	Length
Highest voltages	Use airframe as return	Through low impedance component to airframe	Unshielded and exposed to outside of wing	Exposed to outside and routed across joints to mechanically attached assemblies	Extending through full
Lowest voltages	Use separate conductor as return	Through high impedance element to separate return conductor	Shielded and completely enclosed by wing	Unexposed and entirely within wing enclosure	Extending only short distances in wing

From the above summary, it is apparent that the level of lightning induced voltages is considerably dependent upon the characteristics of the individual circuits. As a result, rearrangement or modification in aircraft electrical circuits where possible in the light of the above findings may be an effective means of minimizing the effects of lightning on aircraft electrical systems.

The method of analysis of data utilized in this program has proven to be effective as a means of determining the amount of open-circuit induced voltage actually impressed upon a load impedance to which the circuit is connected, provided reliable open-circuit and short-circuit measurements can be made. Of equal or greater significance, however, is the ability to analytically relate, in nearly all cases, the measured induced voltages to the lightning current wave shape and amplitude, as well as some effective wing parameters. While the effective wing parameters of resistance and mutual inductance have yet to be expressed in terms of tangible wing characteristics, they do shed light upon the qualitative effects of these electrical characteristics of the wing. These relationships enable greater understanding of the factors permitting lightning to induce significant voltages in aircraft electrical circuits.

One objective mentioned in the INTRODUCTION which has not been discussed is the development of techniques which could be used to evaluate the susceptibility of circuits in any aircraft. The analytical techniques developed during the investigation have significance towards this objective but of greater interest was a preliminary series of tests in which a transient analyzer was used to provide low-amplitude nondestructive current surges to the wing. The transient analyzer is a device developed by the High Voltage Laboratory for similar transient response studies of large power transformers. In this series of tests, the induced voltage response to low-level currents from the transient analyzer was compared with similar measurements of voltages induced by full-acale lightning currents. The comparison was favorable, indicating that the results of low-level tests can be scaled proportionately upward to determine the results obtainable from full-scale lightning currents.

These tests indicated that the transient analyzer has validity as a method of determining induced voltage levels in aircraft circuits. In fact, it has several advantages over the full-scale technique. Aside from being physically portable, it has an electrical versatility lacked by most full-scale impulse generators, and can generate a much wider range of wave shapes. For example, it can generate currents with rise times many times faster than those obtainable with a full-scale impulse generator. This will enable evaluation of induced voltages resulting from a much wider range of lightning current wave shapes than possible with full-scale tests. This practical and nondestructive technique may be applicable to the determination of possible induced voltages in the circuits of operational aircraft. In such a case, the

actual voltages and currents associated with the normal aircraft equipment would be measurable, since this equipment would, of course, already be connected to the circuits.

REFERENCES

1. G. E. Morgan, "Investigation of Inadvertent Firing of Electroexplosive Subsystems on Aerospace Vehicles." Interim Technical Report, AF-33(615)-3853, North American Aviation Inc., August 1966.

2. B. J. Peterson and A. R. Wood, "Measurements of Lightning Strikes to Aircraft." Final Report No. DS-68-1 Federal Aviation Administration, January 1968.

3. J. H. Hagenguth, "Lightning Stroke Damage to Aircraft." AIEE Trans., Vol. 68, Part II, pp. 1036-1044, 1949.

4. F. L. Kester, M. Gerstein, and J. A. Plumer, "A Study of Aircraft Fire Hazards Related to Natural Electrical Phenomena." NASA Publication No. CR-1076, 1967.

5. M. J. Kofoid, "Lightning Discharge Heating of Titanium Aircraft Skins." Boeing Scientific Research Laboratories Document, D1-82-0752, September 1968.

6. J. D. Robb, E. L. Hill, M. M. Newman, and J. R. Stahmann, "Lightning Hazards to Aircraft Fuel Tanks." NACA TN 4326, September 1958.

7. J. D. Robb, J. R. Stahmann, and L. A. Hoehland, "Lightning Electrical Hazards to Flight Vehicles." Lightning and Transients Research Institute, AFAL-TR-69-269, December 1969.

8. M. M. Newmann, J. D. Robb, and J. R. Stahmann, "Lightning Protection Measures for Aircraft Fuel Systems, Phase I." Lightning and Transients Research Institute, FAA Technical Report ADS-17, May 1964.

9. M. M. Newmann, J. D. Robb, and J. R. Stahmann, "Lightning Protection Measures for Aircraft Fuel Systems, Phase II." Lightning and Transients Research Institute, FAA Technical Report ADS-18, May 1964.

10. Anon., "Lightning and Static Electricity Conference." Air Force Avionics Laboratory, Air Force Systems Command, Wright-Patterson Air Force Base, AFAL-TR-68-290, May 1969.

11. K. J. Lloyd, J. A. Plumer, and L. C. Walko, "Measurements and Analysis of Lightning-Induced Voltages in Aircraft Electrical Systems." General Electric Company, High Voltage Laboratory, HVL 69-161, March 1970. Will be published as NASA Contractor Report.

12. J. H. Hagenguth and J. G. Anderson, "Lightning to the Empire State Building - Part III." AIEE Trans., Vol. 71, Part III (Power Apparatus and Systems), pp. 641-649, August 1952.

13. K. B. McEachron, "Lightning to the Empire State Building." AIEE Trans., Vol. 60, pp. 885-890, 1941.

TABLE I. - INDUCED VOLTAGES AND CURRENT

[Circuit L.050, Position Light
Conductor 2L10E18 and Airframe.]

i_L Wave Form:	Slow wave form (36 × 82 μs)				Fast wave form (8.2 × 14 μs)			
Stroke location	Open circuit voltage, e_{oc}, V	Short circuit current, i_{sc}, A	Voltage across 1-ohm load, e_l, V	Current through 1-ohm load, i_l, A	Open circuit voltage, e_{oc}, V	Short circuit current, i_{sc}, A	Voltage across 1-ohm load, e_l, V	Current through 1-ohm load, i_l, A
1 Forward end of tip tank	40/20	9.0	6.0	6.0	96/48	15.0	12.0	11.0
4 Outboard leading edge	6/2.2	0.8	3/0.6	0.6	15/4	1.1	0.7	0.65
5 Trailing edge of aileron	15/3.8	1.3	1.0	1.0	30/12	4.0	3.0	3.0
7 Center of wing surface	10/2.4	0.8	0.8	0.7	20/2	1.5	1.2	1.2
10 Inboard leading edge	10/1.8	0.7	0.8	0.5	17/2.8	1.7	2.8/0.7	0.65

TABLE II. - CALCULATED EFFECTIVE WING RESISTANCES AND MUTUAL INDUCTANCES FOR VARIOUS TEST CONDITIONS

[Circuit L.050, Position Light Conductor 2L10E18 and Airframe.]

i_L Wave form:	Slow wave form (36 × 82 μs)		Fast wave form (8.2 × 14 μs)	
Stroke location	R_W, μΩ	M, nH	R_W, μΩ	M, nH
1 Forward end of tip tank	450.0	16.3	700.0	4.25
4 Outboard leading edge	57.5	0.032	70.0	0.5
5 Trailing edge of aileron	25.0	2.75	-100.0	1.55
7 Center of wing surface	45.0	1.68	-40.0	0.244
10 Inboard leading edge	40.0	0.022	60.0	0.31

TABLE III. - CALCULATED THEVENIN IMPEDANCE SERIES R AND L COMPONENTS FOR VARIOUS TEST CONDITIONS

[Circuit L.050, Position Light Conductor 2L10E18 and Airframe.]

Lightning current wave shape:	8.2 × 14 μs		36 × 82 μs	
Stroke location	R, Ω	L, μH	R, Ω	L, μH
1 Forward end of tip tank	1.98	11.2	----	-----
4 Outboard leading edge	3.33	0.39	2.65	-7.8
5 Trailing edge of aileron	1.23	8.0	2.3	36.2
7 Center of wing surface	----	-----	2.63	8.37
10 Inboard leading edge	3.09	5.7	2.29	9.56

TABLE IV. - INDUCED VOLTAGES AND CURRENTS

[Circuit F.0511, E-11 Autopilot Conductors F572K18 and F755E18.]

i_L Wave form:	Slow wave form (36 × 82 μs)				Fast wave form (8.2 × 14 μs)			
Stroke location	Open circuit voltage, e_{oc}, V	Short circuit current, i_{sc}, A	Voltage across 1-ohm load, e_l, V	Current through 1-ohm load, i_l, A	Open circuit voltage, e_{oc}, V	Short circuit current, i_{sc}, A	Voltage across 1-ohm load, e_l, V	Current through 1-ohm load, i_l, A
1 Forward end of tip tank	0.07	0.3	0.068	0.075	0.4	0.2	0.23/ 0.23	0.2
4 Outboard leading edge	27/0.1	0.25	0.2/ 0.12	0.1	3/0.48	0.5	0.26	0.2
5 Trailing edge of aileron	2/0.2	0.25	0.4/ 0.13	0.1	0.6	0.5	0.3	0.25
7 Center of wing surface	0.1	0.25	0.12	0.1	6/0.5	0.5	0.3	0.25
10 Inboard leading edge	0.1	0.25	0.04	0.04	1.5/ 0.2	0.1	0.1	0.1

TABLE V. - CALCULATED EFFECTIVE WING RESISTANCES AND MUTUAL INDUCTANCES FOR VARIOUS TEST CONDITIONS

[Circuit F.0511, E-11 Autopilot
Conductors F572K18 and F755E18.]

i_L Wave form:	Slow wave form (36 × 82 μs)		Fast wave form (8.2 × 14 μs)	
Stroke location	R_W, μΩ	M, nH	R_W, μΩ	M, nH
1 Forward end of tip tank	0.75	-0.0185	4.5	-0.0698
4 Outboard leading edge	0.50	-0.0684	2.0	-0.187
5 Trailing edge of aileron	1.25	-0.0392	8.25	-0.107
7 Center of wing surface	0.375	-0.0169	10.0	-0.117
10 Inboard leading edge	2.25	-0.043	1.75	-0.0227

TABLE VI. - MAXIMUM INDUCED VOLTAGES AND CURRENTS IN NEW WING CIRCUITS

[Series 1 - Measurements at leading edge on entire length of circuits. Trailing edge terminations connected to airframe.]

Conductor	Open circuit voltage, V		Short circuit current, A	
	Conductor-to-airframe	Conductor-to-conductor	Conductor-to-airframe	Conductor-to-conductor
Unshielded number 16 insulated conductor	1.5	----	0.8	---
RG 58A/U coaxial cable	1.2	----	1.6	---
Twisted pair of number 16 insulated conductors	1.5	0.16	1.0	0.1
Parallel pair of number 16 insulated conductors	5.0	1.6	5.0	0.8

TABLE VII. - MAXIMUM INDUCED VOLTAGES AND CURRENTS IN NEW WING CIRCUITS

[Series 2 - All circuits and shields connected to airframe at location between aileron and flap on trailing edge. Identical measurements on circuits terminating at leading and trailing edges.]

Conductor	Open circuit voltage, V				Short circuit current, A			
	Conductor-to-airframe		Conductor-to-conductor		Conductor-to-airframe		Conductor-to-conductor	
	Leading edge[a]	Trailing edge[b]	Leading edge	Trailing edge	Leading edge	Trailing edge	Leading edge	Trailing edge
Unshielded number 16 insulated conductor	2.0	0.4	----	----	1.6	1.3	---	---
RG 58A/U coaxial cable	2.1	0.4	----	----	2.2	0.4	---	---
Twisted pair of number 16 insulated conductors	1.0	0.5	0.22	0.04	1.4	0.9	0.1	0.1
Parallel pair of number 16 insulated conductors	6.0	1.0	2.3	0.1	6.0	2.0	1.3	0.1

[a]Circuits terminating at leading edge are 38 feet long.
[b]Circuits terminating at trailing edge are 12 feet long.

E-5991

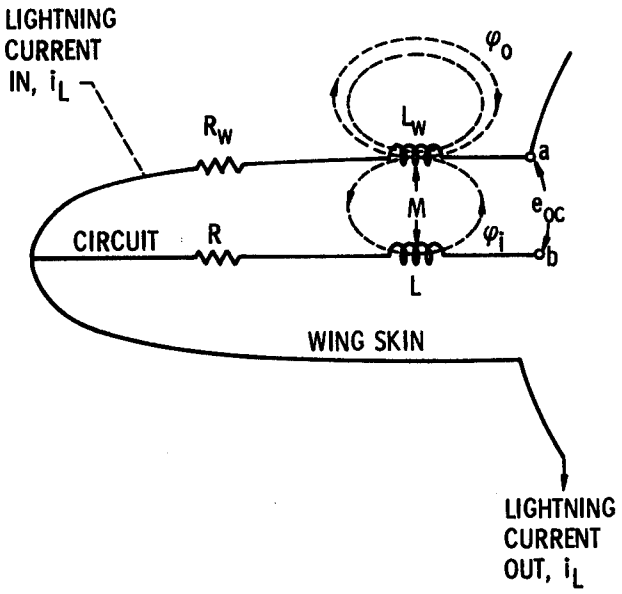

Figure 1. - Circuit representation of aircraft wing-electrical circuit combination.

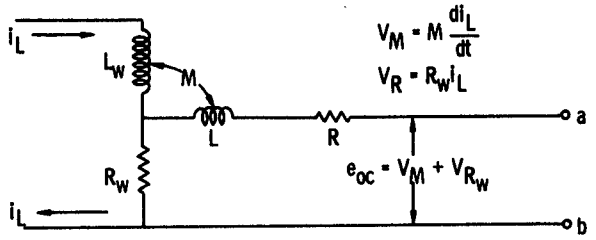

Figure 2. - Circuit representation of wing structure and electrical circuit.

E-5991

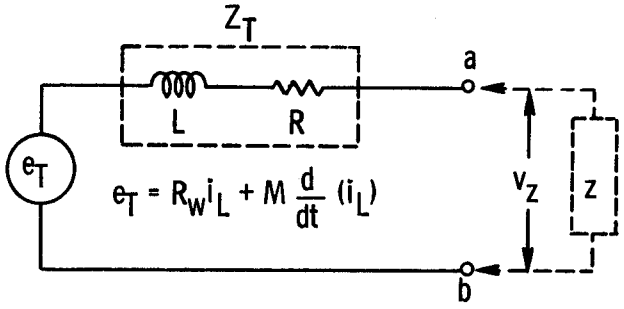

Figure 3. - Thevenin equivalent circuit.

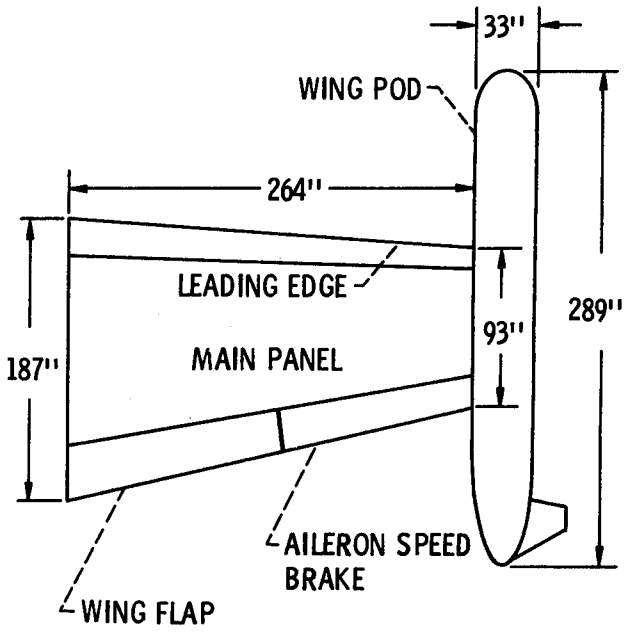

Figure 4. - Schematic plan view of wing.

E-5991

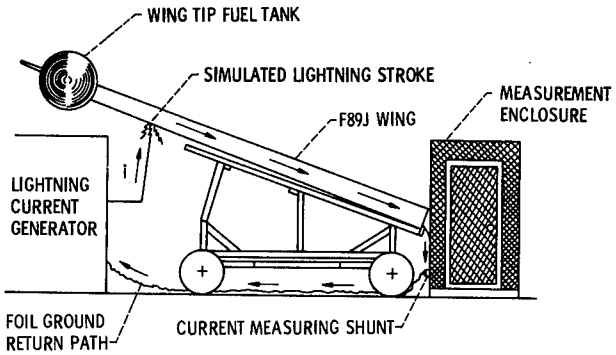

Figure 5. - F89J wing test setup.

Figure 6. - F89J right wing shown positioned for test in high voltage laboratory test bay. Lightning current generator is beneath tip tank.

T_1 - FRONT TIME
T_2 - TIME TO HALF VALUE ON THE TAIL

THE WAVE SHAPE IS DESCRIBED BY THE NOTATION: $(T_1 \times T_2)$

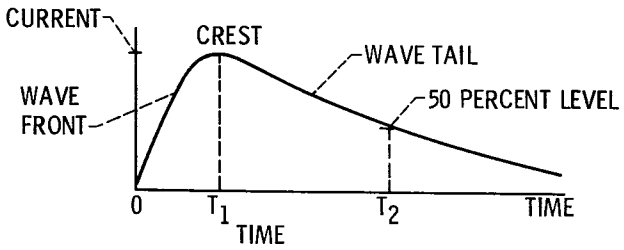

Figure 7. - Simulate lightning wave shape notation.

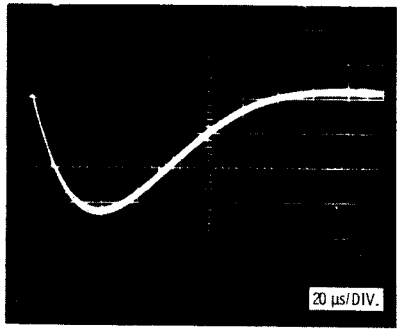

(A) "SLOW WAVE SHAPE" 36 x 82 μs.

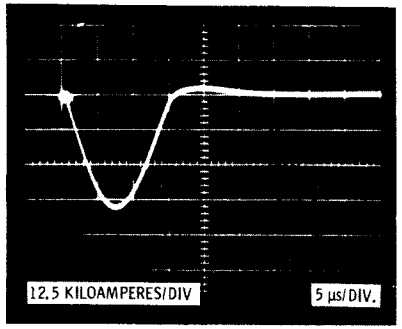

(B) "FAST WAVE SHAPE" 8.2 x 14 μs.

Figure 8. - Simulated lightning current wave shapes (40 kiloampere strokes, applied for induced effects measurements).

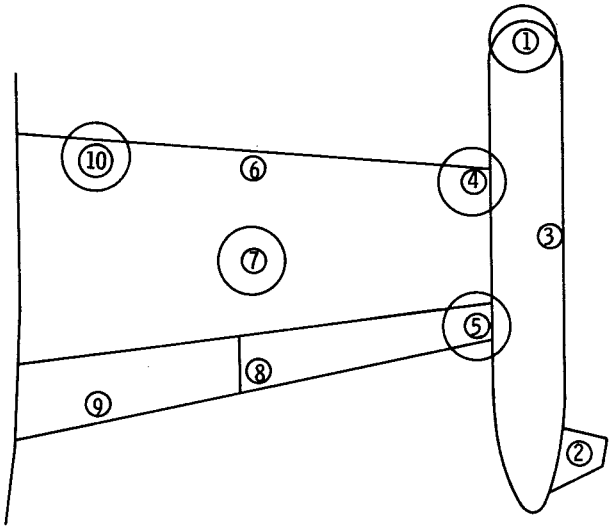

Figure 9. - Simulated lightning stroke locations. Large circled numbers indicate locations selected for extensive testing.

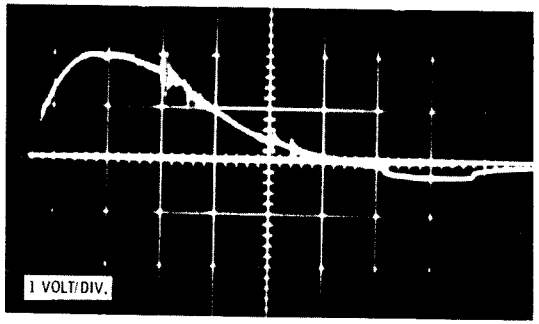

(A) OPEN CIRCUIT INDUCED VOLTAGE.

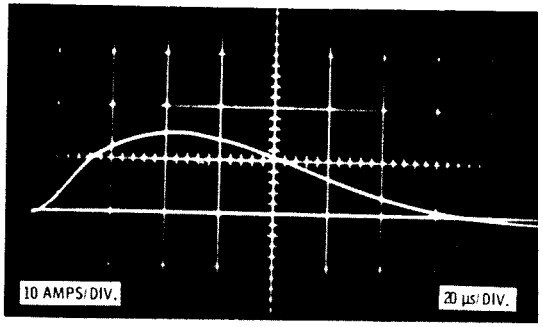

(B) SHORT CIRCUIT CURRENT.

Figure 10. - Open circuit induced voltage and short circuit current. 40 kiloampere 36 x 82 μs lightning stroke to location 1.

E-5991

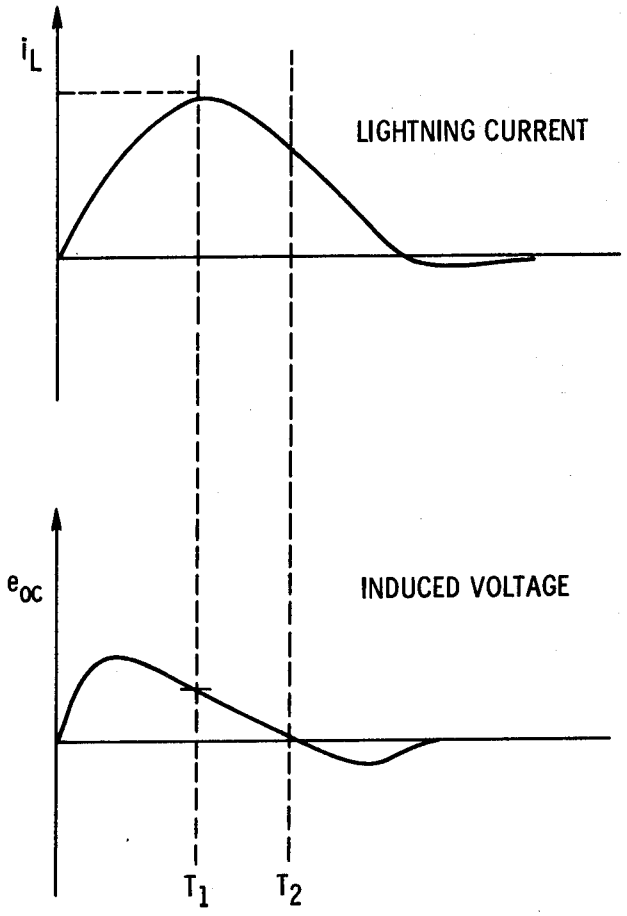

Figure 11. - Typical lightning current and induced voltage wave forms.

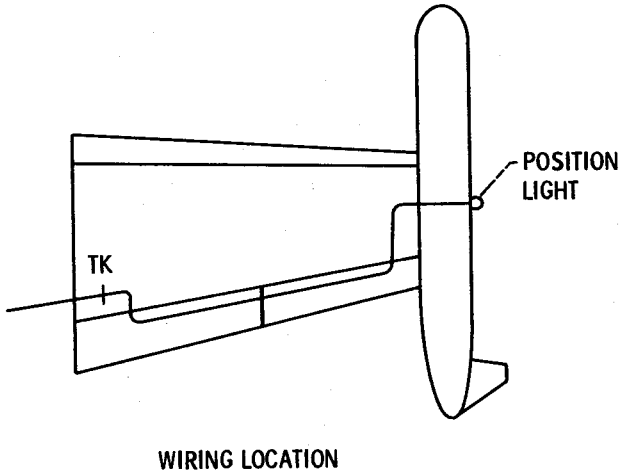

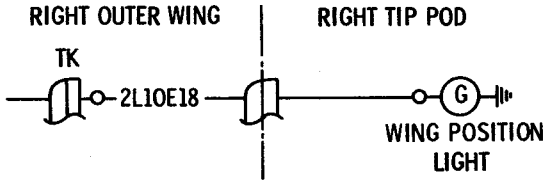

Figure 12. - Circuit 1.050 position lights wiring schematic and location F89J right wing and tip fuel tank.

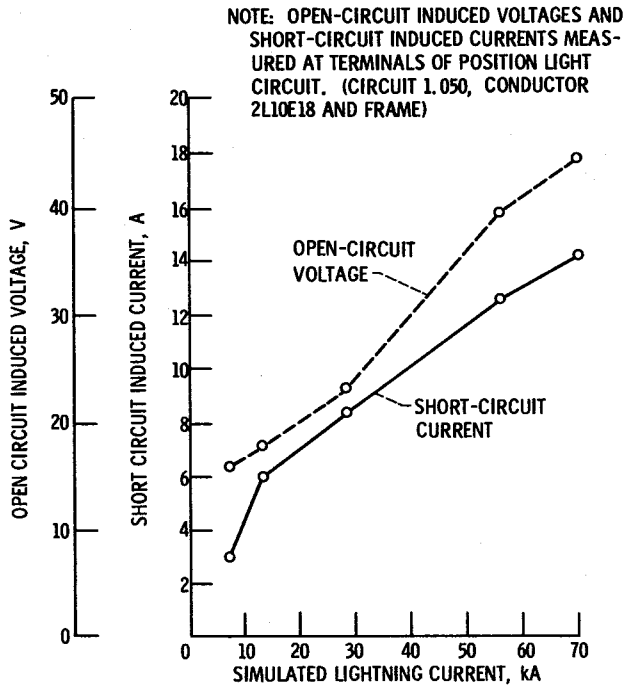

Figure 13. - Amplitude of induced effects versus amplitude of simulated 12 x 24 μs lightning current discharged to location number 1 (forward end of wing tip fuel tank).

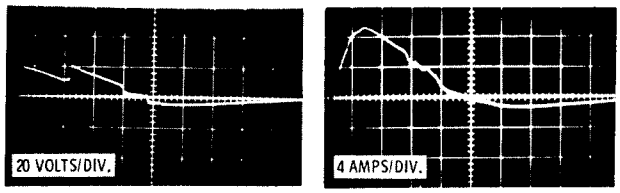

(A) STROKE LOCATION NO. 1, FORWARD END OF WING TIP FUEL TANK.

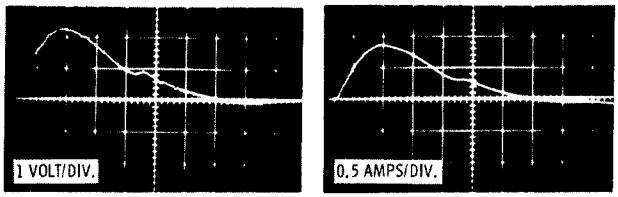

(B) STROKE LOCATION NO. 4, OUTBOARD END OF LEADING EDGE.

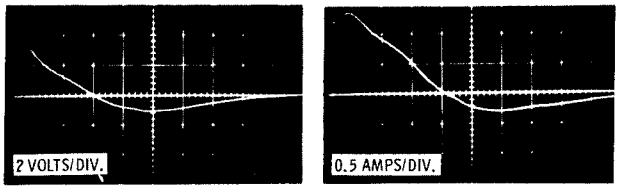

(C) STROKE LOCATION NO. 5, OUTBOARD END OF AILERON.

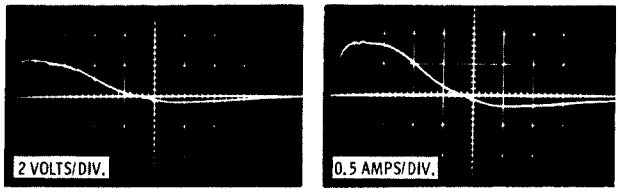

(D) STROKE LOCATION NO. 7, BOTTOM CENTER OF WING.

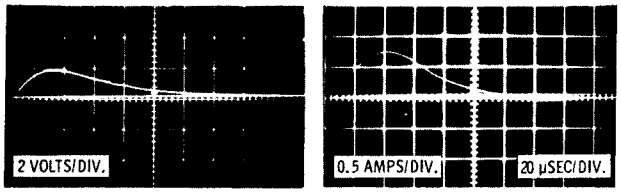

OPEN CIRCUIT VOLTAGE SHORT CIRCUIT CURRENT

(E) STROKE LOCATION NO. 10, INBOARD LEADING EDGE OF WING.

Figure 14. - Open circuit voltages and short circuit currents measured on terminals of circuit L.050 (position light), conductor 2L10E18 to airframe. (36 x 82 μsec, 40 kiloampere simulated lightning current.)

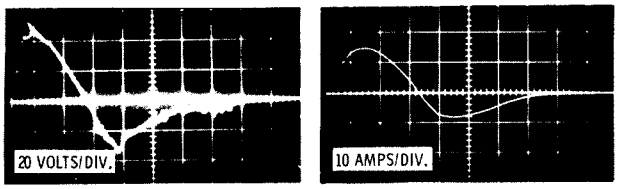

(A) STROKE LOCATION NO. 1, FORWARD END OF WING TIP FUEL TANK.

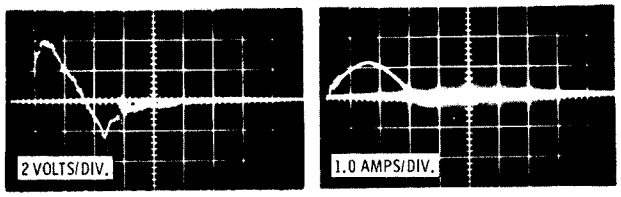

(B) STROKE LOCATION NO. 4, OUTBOARD END OF LEADING EDGE.

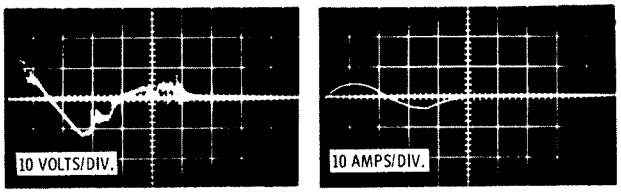

(C) STROKE LOCATION NO. 5, OUTBOARD END OF AILERON.

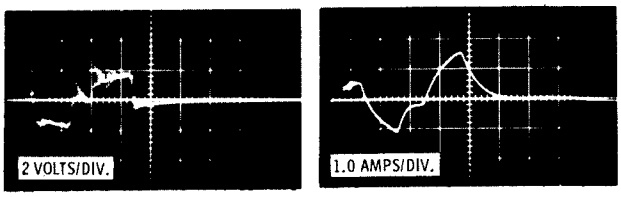

(D) STROKE LOCATION NO. 7, BOTTOM CENTER OF WING.

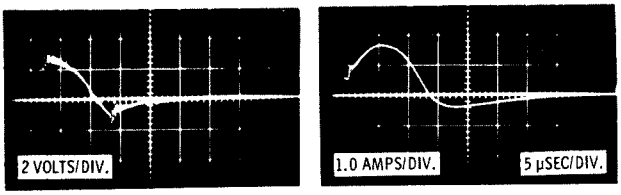

OPEN CIRCUIT VOLTAGE SHORT CIRCUIT CURRENT

(E) STROKE LOCATION NO. 10, INBOARD LEADING EDGE OF WING.

Figure 15. - Open circuit voltages and short circuit current measured on terminals of circuit L.050 (position light), conductor 2L10E18 to airframe. (8.2 x 14 μsec, 40 kiloampere simulated lightning current.)

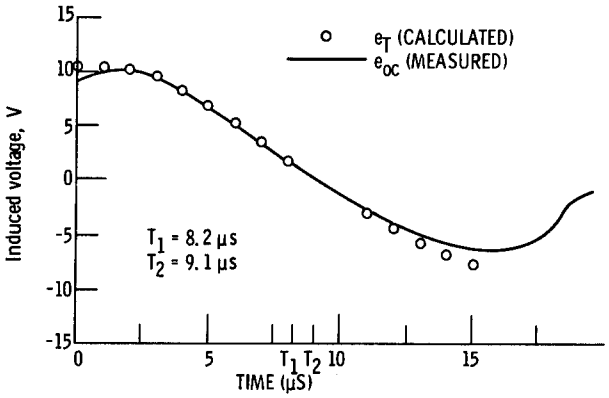

Figure 16. - Comparison of measured e_{oc} and calculated e_T induced voltage wave shapes, resulting from 40 kiloampere 8.2 x 14 μs stroke to location 1.

E-5991

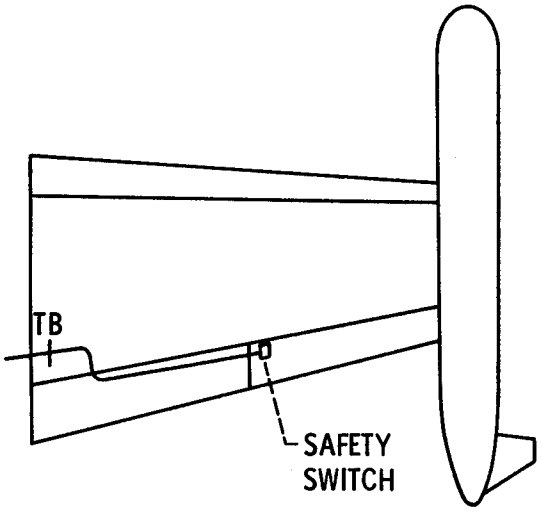

WIRING LOCATION

RIGHT OUTERWING

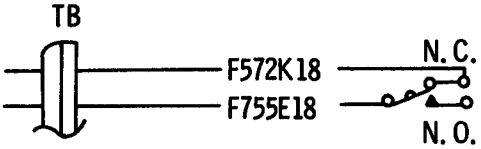

RIGHT ROCKET
SAFETY SWITCH

Figure 17. - Circuit F.0511 E-11 autopilot flap position monitoring switch wiring schematic and location F89J right wing and tip fuel tank.

E-5991

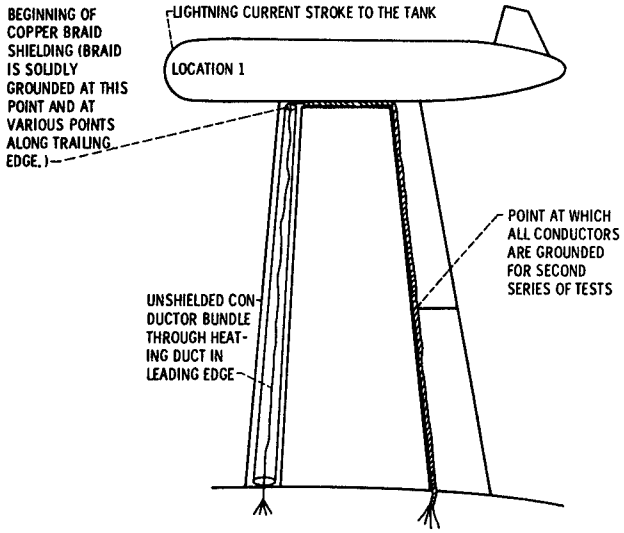

Figure 18. - F-89 Wing showing additional circuits placed in the wing for test.

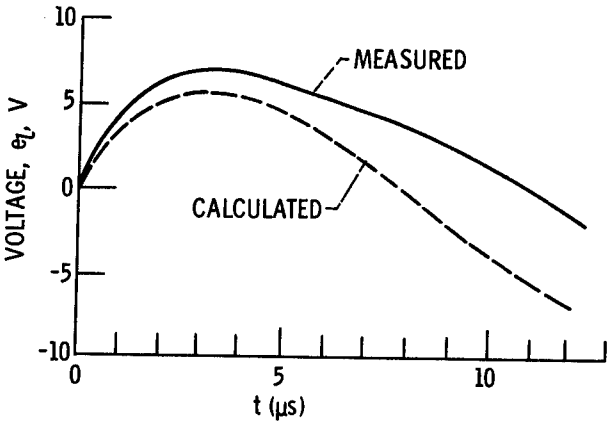

Figure 19. - Verification of Thevenin circuit calculation of voltage across 1-ohm resistive load. 40 Kiloampere, 8.2 x 14 μs lightning current to location 1.

NASA-Lewis

THE EFFECTS OF LIGHTNING ATTACHMENT PHENOMENA ON AIRCRAFT DESIGN

R. O. Brick
L. L. Oh
S. D. Schneider

Electrodynamics Technology
Commercial Airplane Group
The Boeing Company

ABSTRACT

A working knowledge of swept lightning strikes has become a necessity for the aircraft designer involved in lightning protection of aircraft incorporating new structural concepts that depart from the conventional riveted aluminum airframe. Swept strokes have been simulated in the laboratory to determine realistic protection criteria for components. Measurements of the maximum swept stroke dwell time on titanium and aluminum sheet are reported as well as an analysis of various techniques to improve the resistance of fuel tank skin panels to swept stroke effects.

THE MECHANISM OF LIGHTNING STRIKE attachment to aircraft has for many years been a source of interest to the designer concerned with lightning protection. Until recently, however, there has been little need for rigorous investigation of attachment phenomena. In the past, the load requirements of integral wing fuel tanks led to structure that surpassed the established lightning protection criteria. As a result, little had to be known about lightning except the worst type of damage probable, which occurred at the extremities of the airplane. Now, however, advanced structural concepts necessitate a depth of knowledge about lightning not previously required.

This current protection criteria, however, will penalize advanced-technology aircraft structures. Materials such as boron, graphite, and titanium permit innovative structural techniques that are less dense and therefore no longer able to sustain the unrealistic test criteria used previously. To ensure that adequate protection is provided for an optimum structural weight, it has become necessary to understand the exact mechanism by which a lightning strike distributes its energy upon contact with structure. Before discussing our investigations, it is necessary to review several pertinent facts relating to the phenomena of lightning strike attachment:

1. An aircraft forms a part of the discharge path.
   Lightning does not terminate on the aircraft but instead passes through it to another charge center or to ground. Therefore, there is an entrance and exit attachment point on the aircraft for each lightning strike.
2. The lightning strike approach angle is random.
   Lightning can approach an airborne vehicle from almost any angle and is therefore considered random in character. This is due to the wide variance in possible relative positions between an aircraft and the various charge centers as well as to zig-zag excursions of the lightning channel.
3. A discharge can consist of high-current impulses, lower value continuing currents, and restrikes.
   - High-current impulse
     Initially, a lightning discharge consists of a high-current impulse with the time to peak varying from microseconds to milliseconds. Peak currents have been recorded as high as 200,000 A. Laboratory representation of this component is frequently accomplished with a discharge that rises from zero to a crest value of 200,000 A in not more than 15 μsec and decays to 50,000 A in not more than 30 μsec from initiation (1)*.
   - Continuing currents
     The continuing-current component of a natural lightning discharge can consist of tens, hundreds, or thousands of amperes for periods up to 1 sec. This

*Numbers in parentheses designate references at end of paper.

component has been simulated in the laboratory by a discharge having a charge transfer of at least 500 C with a duration of 2 to 5 sec (1).

- Restrikes
  Restrikes are defined as high-current-impulse components that occur after the initial component and are the norm rather than the exception. Lightning discharges have an estimated average of four restrikes per stroke, and as many as 40 have been recorded in a single stroke (2). The maximum peak currents in a restrike are difficult to predict, but currents in excess of 200 kA are believed possible (3).

4. An aircraft lightning environment consists of direct and swept strokes.
   - Direct strokes
     Direct strokes are those that initially attach (or that attach directly) to aircraft surfaces. A discharge may attach to a direct stroke surface of an aircraft and remain attached for the entire discharge, or it may reattach to a swept stroke surface once initial contact has been made to the direct stroke surface.
   - Swept strokes
     Since a discharge can exist, with continuing currents, for periods up to 1 sec, an aircraft can fly a considerable distance once initial stroke contact has been made. The aircraft, in effect, flies through the continuing discharge and, as a result, the lightning appears to sweep back over the aircraft surface.
5. Aircraft can be zoned according to the probability of stroke attachment.
   Zone I is defined as a direct stroke zone, zone II as a swept stroke zone, and zone III covers surfaces not identified in zones I or II. The following definitions are excerpted from reference 1.
   - Zone I
     - All surfaces of the wingtips located within 18 in. of the tip measured parallel to the lateral axis of the aircraft and surfaces within 18 in. of the leading edge on wings having leading-edge-sweep angles of more than 45 deg.
     - Projections such as engine nacelles, external fuel tanks, propeller disk, and fuselage nose.
     - Tail group: within 18 in. of the tips of the horizontal and vertical stabilizers, trailing edge of the horizontal stabilizer, tail cone, and any other protuberances.
     - Any other projecting part that might constitute a point of direct stroke attachment.
   - Zone II–Surfaces for which there is a probability of strokes being swept rearward from a zone I point of direct stroke attachment. This zone includes surfaces that extend 18 in. laterally to each side of fore-and-aft lines passing through the zone I forward projection points of stroke attachment. All fuselage and nacelle surfaces, including 18 in. of adjacent surfaces, not defined as zone I are included in zone II.
   - Zone III–Surfaces other than those covered by zones I and II. Ignition sources in these areas would exist only in the event of streamering.

The zones for individual aircraft types may be ascertained through the use of simulated lightning discharges and a metallized scaled model. The technique that can be used to accomplish this is defined elsewhere (4, 5).

Commercial jet transports normally have portions of their integral wing fuel tanks in a swept stroke zone, thus creating a zone II surface. The engine nacelles are generally direct strike zones (zone I), which create zone II surfaces on the supporting wing as defined above. Leading-edge-slat inboard and outboard tips will sometimes be categorized as being in a zone I and thereby will also create wing zone II areas that are downstream of the zone I attachment point.

Fuel filler caps, drip sticks, sump drains, and access doors that are located in a zone II are proof tested with artificial lightning discharges, as recommended by reference 1, to ensure that they do not arc, spark, or in any way exhibit an ignition hazard when subjected to a test discharge. In addition, zone II fuel tank skins must be able to sustain a swept stroke attachment without puncture or skin heating that could ignite enclosed fuel or fuel vapor.

Although the existence of swept strokes has been acknowledged for years, the mechanism by which lightning sweeps back over an aircraft surface was not known until recently. This presented no difficulty in design of the 700 series of Boeing aircraft, however, because the structural requirements of the wing dictated single-sheet thicknesses of aluminum in excess of the lightning protection requirement. As a result, zone II fuel tank components and fuel tank skins could be proof tested with discharges simulating a zone I environment with no undue design penalty. Due to the ease with which the zone II components could pass the severe zone I test value, there was little economic advantage in effecting a change in the zone II test criteria, and there was no need to ascertain the exact manner in which swept strokes move and distribute energy over an aircraft surface.

CHANGING DESIGN PHILOSOPHIES

New fabrication techniques and structural materials are creating wing skin structures that are stronger and lighter but are no longer amenable to the unrealistic application of zone I test criteria to zone II fuel tank skins. Materials such as titanium, stainless steel, boron/epoxy, and graphite/epoxy are

being used to decrease weight and improve performance of advanced aircraft designs. Additionally, the use of brazing, adhesives, honeycomb core, and wafflelike wing skin panels are permitting optimum-design wing box structures with a minimum of weight. Extension of the lightning protection philosophy used on conventional riveted aluminum aircraft to the new-technology structures would result in an overdesign of wing skin structure due to application of the zone I test criteria to zone II fuel tank skins and would therefore compromise the weight advantages of the newer structural techniques. For example, application of the zone I criteria to a zone II titanium fuel tank skin panel would necessitate a skin thickness of 0.4 in., when in fact a much thinner panel is permitted if the actual protection requirement of a swept stroke zone is acknowledged (5).

In the spring of 1968, The Boeing Company conducted an investigation at the Lightning and Transients Research Institute (LTRI) of Miami in an attempt to develop a technique to simulate swept strokes and thus obtain insight into the mechanism of the phenomenon. In the tests, 3- by 5-ft test panels were mounted in the aperture of an open-throat wind tunnel in the manner illustrated in figure 1. Simulated lightning discharges were initiated at the upstream end of the panel and the arc was allowed to sweep over the panel. The sweeping mechanism of the stroke was recorded with a high-speed camera at frame speeds up to 2,500 frames per second.

The observed phenomena (3) are illustrated in figure 2. The 155-mph wind in the setup is blowing left to right. The sketch illustrates the mechanism as observed from a point normal to the airstream. As shown in the figure, the lightning stroke initially makes contact at X_0 at a time of t_1. At some time, t_2, the wind carries the arc downstream even though its attachment point at X_0 remains intact. At a later time, t_3, the arc is still moving aft, while the X_0 attachment point remains. The arc dwells at X_0 until the impedance drop of the channel between X_0 and X_4 is sufficient to cause a breakdown of the air at X_4 and a new attachment point. Once the X_4 attachment is formed, the X_0 attachment expires. The arc continues to walk or sweep down the panel in this manner until the end of the panel is reached or the arc extinguishes. The effect is considered comparable to the motion of a swept stroke over an airfoil in flight.

Test specimens for the investigation were limited to plain, untreated titanium alloy (Ti-6Al-4V) as well as alclad and anodized aluminum alloy. The panels were completely free of surface irregularities such as joints and splices. Positive and negative discharge polarities were used with airspeeds of 0, 155, and 230 mph.

The primary goal of the early research was the development of a technique to simulate swept strokes; therefore, a rigorous parametric study was not within the scope of the investigation. The trend of the limited data did indicate, however, that the maximum swept stroke dwell time on titanium will not exceed 2 msec; the corresponding dwell time for anodized aluminum was 5 msec.

The investigation is discussed in detail elsewhere (6, 7) and will be clarified below during a discourse on a more recent and more complete investigation of swept stroke effects.

RECENT SWEPT STROKE TESTS

During the spring of 1970, the Miami facilities of LTRI of Minneapolis were again used by The Boeing Company to investigate swept stroke effects. The purpose of this second investigation was to gather sufficient data to establish realistic zone II design requirements and to include development methods for diverting swept strokes from critical zone II areas such as aircraft fuel tank vents and critical tank components located in skin surfaces.

Specifically, the following swept stroke characteristics were evaluated for titanium and aluminum surfaces:

1. Discharge arc dwell times
2. Discharge arc stepping distance between dwells
3. Discharge arc attachment point size and configuration
4. Discharge arc diversion tendencies

In addition, the effect of the following conditions on the swept stroke mechanism was evaluated:

1. Mechanical fastener joints
   - Flush fasteners
   - Protruding fasteners
2. Mechanical joint discontinuities
   - Nonconductive adhesive joints
   - Riveted joints
3. Discrete changes in panel surface conductivity
   - Patches of conductivity higher than the base metal
   - Patches of conductivity lower than the base metal
4. Surface projections
   - Splice plates
   - Vertical fins

The following environmental conditions for the tests were established and were based on the capability of existing test facilities. They are as close as possible to the conditions required for obtaining the desired results:

1. Atmospheric pressure: sea level
2. Windstream velocity: 0, 150, and 250 mph
3. Lightning continuing current: 300 to 500 A
4. Test sample polarity: negative and positive

All the tests were conducted on 3- by 7-ft sample sheets, with the exception of two samples that were 3 by 5 ft. A total of nine titanium and eight aluminum samples were used in the 2-week test. Both sides of each sample were utilized. The test panels are described in table I and illustrated in figure 3. The alphanumeric symbols at the upper left corner of a sample indicate the sample numbers. The letter T stands for titanium,

A for aluminum, and the subscripts a and b for the two sides of the sample sheet–e.g., T3a identifies titanium sample No. 3, side a, and A4b identifies aluminum sample No. 4, side b.

The purpose of the tests on the plain metal surfaces was to gather sufficient data to establish the swept stroke sweeping distances, the dwell time on each of the reattachment points, and the sizes of the burn or pit marks on both titanium and aluminum (including anodized) samples. In the plain titanium samples, three sample thicknesses (0.012, 0.032, and 0.063 in.) were tested, whereas 0.032-in.-thick samples were used for the other surface configurations. In the aluminum samples, including the anodized sheet, the sample thicknesses were all 0.063 in.

The purpose of the Teflon (insulator) tapes adhesively applied to the metal surface was to increase the breakdown voltage in this region. It was expected that the surface area covered by the insulating tapes would be bypassed by the swept stroke. For the surface areas covered by conductive tapes or silver paint, it was expected that, because of the high conductivity of this material, the swept stroke might show an affinity for this region, thus providing a means of diverting the discharge arc from critical areas. Tests on bonded and riveted joints, circular holes, and protruding edges and fins were conducted to observe the affinity of the discharge arc for these surface discontinuities and protrusions and, therefore, the effect of these anomalies on dwell time.

Diagrams of the test setup for the wind tunnel swept stroke studies are shown in figure 1. Aircraft motion was simulated by passing an airstream over the metal surface of the 3- by 7-ft stationary test platform. Two 250-hp electric blowers were used to generate the airstream.

A 1-in.-outside-diameter by 77-in.-long carbon rod was used for the discharge (electrode) probe. The probe was suspended above the test sample and oriented along the centerline of the sample sheet. Initially, the forward (upstream) end of the probe was adjusted for a spacing of 8 in. above the sample surface with the aft end at 10 in. The probe was spatially biased with the forward end closer to the sample to force the discharge to initiate upstream, permitting a maximum sweeping length down the probe and sample. However, for tests on samples with modified surface configurations, it was found convenient to position the probe horizontally 9 in. above the sample while a movable metal collar with a 1-in. protrusion was clamped to it. The collar could be moved to any position along the rod where arc initiation was desired. In some tests, where the horizontal probe could not be used, a 1/2-in.-outside-diameter vertical metal rod was employed as the probe.

The artificial lightning generators consist of a 1.7- to 2.0-MV low-energy Marx generator and a high-current generator comprised of a capacitor bank of approximately 310 μF charged to 20,000 V. The Marx generator was used to initiate the discharge across the 8-in. gap between the sample and the probe, and the high-current generator was used for the sweeping component of the discharge. A resistor in series with the probe was used for shaping the waveform of the discharge current. A high-current shunt and an oscilloscope were used to record the discharge waveform.

A Fastax high-speed motion picture camera operating at 1,300 frames per second was used to photograph the sweeping motion of the discharge across the metal surface of the test samples. Both black and white (B/W) Polaroid and 2-1/4- by 2-1/4-in. colored still photographs of the discharge arc were taken for analysis. The cameras were oriented for a side view of the swept strokes. An additional B/W Polaroid camera was mounted above the test sample to record the lateral paths of the swept strokes.

The maximum sweeping component of the discharge current was approximately 400 A, with a decay time constant of approximately 15 msec. With one wind tunnel blower turned on, the airspeed at the surface of the sample was 155 mph at the upstream end of the test sample and was gradually reduced to 130 mph at the downstream end. The airspeed along the centerline 7 in. above the sample surface was 100 mph. With two of the three blowers turned on, the surface airspeed at the center of the sample was 250 mph.

Test data are given for the titanium panels in table II and for the aluminum panels in table III. The following observations may be drawn from the results of the swept stroke tests on both titanium and aluminum samples.

PLAIN AND ANODIZED SURFACES–The behavior of the swept stroke will not be altered by the sample thickness, except that the discharge arc can burn through thin samples such as 0.012-in.-thick titanium sheet.

The maximum dwell time of reattachment points on both plain titanium and aluminum samples never exceeded 1.6 msec for either sample polarity (positive and negative) or windspeed (150 and 250 mph).

The burn marks on the positive-polarity samples were more pronounced and closer together but smaller in size than those made on samples with negative polarity. The pit marks on the aluminum surface were shallower than those on the titanium and the stepping distances were closer for the titanium samples.

The maximum dwell time observed on anodized aluminum was 4.8 msec. This increase in dwell time over the alclad aluminum case is apparently due to the insulative properties of the anodized layer, which necessitates a higher arc voltage to create a new attachment point. A longer arc is needed to produce the required voltage drop, which results in a comparable increase in the dwell time.

TEFLON-COVERED SURFACES–The surface breakdown voltage of plain metal surfaces may be increased by covering the surface with a thin layer of insulation. Test

results showed that swept strokes never reattached to areas on either titanium or aluminum surfaces that were covered by 0.005-in.-thick Teflon tapes. The discharge arc was observed to jump over a 21-in.-wide area covered with Teflon tapes. The dwell times at the leading edge of the tape were 8.8 and 9.6 msec for the titanium and aluminum samples, respectively. At a windspeed of 150 mph, it takes 8 msec to cross the 21-in. distance. In one test, where the initial attachment was forced to discharge over the tape-covered area, the discharge arc punctured the tape and attached to the surface under the tape. The subsequent reattachments were out of the taped area.

SILVER-PAINTED SURFACES–Test results showed no affinity of the swept stroke for either titanium or aluminum surfaces that were coated with silver paint. Replacing the silver paint strips with conducting copper and aluminum tapes produced similar results. Initially, it was thought that the highly conductive silver paint might provide an easier path for the swept stroke. Apparently, the differences in the surface conductivity of silver, aluminum, copper, and titanium do not significantly change the breakdown voltage of these surfaces.

However, the technique of guiding the swept stroke is still applicable on metal surfaces that are susceptible to oxidation. If an oxidized film is formed on the metal surface, the surface breakdown voltage will be greatly increased. Thus, if a conductive paint that is less vulnerable to oxidation is painted over a metal surface susceptible to oxidation, the breakdown voltage on the painted area will be lower than that for the surrounding surfaces. Consequently, swept strokes will attach to the painted areas.

SAMPLES WITH BONDED AND RIVETED JOINTS–The swept stroke showed no affinity for the joints of either bonded or riveted samples. Tests conducted on the reverse sides of these samples where there are protruding splice plates and rivet heads showed that the arc dwelled longer on the edges of the protruding plate and rivet heads. On the titanium samples, the dwell time on the protruding edges and rivet heads was 1.6 msec. On the aluminum samples, the arc attached to one of the protruding rivet heads for a period of 3.2 msec and on the edge of a splice plate for 4.8 msec. In both instances, the sample polarity was negative.

SAMPLES WITH RECESSED EDGES–Tests on the titanium sample with a 10-in.-diameter circular hole showed a longer dwell time on the edge of the hole. However, this was not observed on similar aluminum samples. The edge dwell time was 2 msec when the titanium sample polarity was negative and 1.6 msec when it was positive. No conclusion can be readily drawn from these results.

SAMPLES WITH PROTRUDING FINS–Tests on the titanium samples showed that the discharge arc in most test runs climbed up to the apex of the triangular fin, but no unusually long dwell times were noted. On the aluminum samples, the arc showed no affinity for these fins. In the case where the fin is on the swept path, the arc climbed up the inclined edge of the fin, but then it either proceeded along the flat surface of the fin or jumped off the fin edge to the plain flat sample surface. In the case where the fins were 6 in. from the swept path, the discharge arc never contacted the fins.

It would be logical to conclude that, because the protruding fins were closer to the carbon electrode, it would be easier for the arc to attach to the fin edges. However, this fails to explain why the behavior of the swept stroke on the titanium differed from that of the aluminum samples. One possible explanation is that, during the tests on aluminum samples, the discharge arc was always closer to the flat metal surfaces than to the fin edges.

From the test results, it appears that swept strokes will reattach to metal surfaces that are closest to the path of the advancing discharge arc rather than to sharp edges farther away. This is due to the lower arc voltage required to break down a shorter air path. This explanation is further supported by the tests conducted on metal surfaces covered with Teflon (insulator) tapes. Although the tapes are in the path of the swept stroke, no reattachment on the tape-covered areas occurred because the breakdown voltage is much higher in these areas than on the adjacent plain metal surfaces.

Typical still photographs showing discharge arc reattachment points are shown in figure 4 for both top and side views. Note how the dwell points on the test panel are manifested by arc intensification in the photo. The stepping distance between dwell points is also illustrated. Similar photographs, as well as high-speed movies, were taken for each test discharge.

HIGH-CURRENT SWEPT STROKE TESTS

In an attempt to determine the effect of the peak discharge current on dwell time, tests were conducted on several panels with discharge currents higher than those used previously. The environment and procedures for the high-current tests were essentially the same as those in the lower current tests, except that the current of the sweeping component of the swept stroke was increased from 400 A to 1,200 A. Tests were conducted on 0.032-in. plain titanium and 0.063-in. plain aluminum samples.

No significant differences in the swept stroke behavior from that of the 400-A tests were noted. The dwell time on both the initial attachment and the reattachment points for titanium and aluminum samples was from 0.8 to 1.6 msec, with the exception of 2 msec for a reattachment point on the titanium sample. This reattachment made a burn track approximately 1/8 in. wide and 1-1/2 in. long on the negative-polarity sample surface.

On the titanium sample, the burn marks were 1/16 in. to 1/8 in. in diameter for positive sample polarity and 1/8 to 1/4 in. wide by 1/4 to 2 in. long for the negative polarity. The sizes of the burn marks were about the same as those made by the 400-A strokes, except that the marks appeared to burn slightly deeper into the sample surface.

On the aluminum sample, the sizes of the burn marks were similar to those made with the 400-A strokes (1/16 to 1/8 in. wide by 1/4 to 3 in. long). The only difference noted was the appearance of clusters of tiny pits ($\simeq$1/64 in. in diameter) on the positive-polarity sample surface.

RESTRIKE SWEPT STROKE TESTS

Restrikes were also evaluated for their effect on the swept stroke mechanism. A simulated lightning restrike was initiated during the sweeping period of the swept stroke 10 msec after the initial attachment. The environment and conditions of the test were identical to those of the earlier swept stroke tests; i.e., sea level, 400 A, 150 mph, and positive and negative sample polarities.

The test setup was similar to that shown in figure 1. The initial discharge of the high-current generator was triggered by burning a thin wire connected across the 8-in. gap between the carbon electrode and the test sample. The restrike was initiated by the 1.7- to 2-MV Marx generator at a peak current of 15 to 20 kA for a pulse width of about 35 μsec. At the time of the restrike, the current amplitude of the sweeping component of the stroke had decayed from a peak of 400 A to 200 A.

Tests on both plain titanium and aluminum samples showed that the behavior of the swept strokes was not altered by the presence of restrikes. No unusually long dwell time was observed at the restrike attachment point. Unfortunately, the burning of the triggered wire caused such a brilliant glow that it was difficult to observe the outline of the discharge in the movie film for the first 2 ft of the swept path.

Tests on titanium samples covered with a 21-in.-wide Teflon tape (fig. 3) illustrate that restrike can puncture the 0.005-in.-thick Teflon insulation and attach to the titanium surface beneath the tape. When the initial swept stroke attachment point was set at 6 in. from the leading edge of the tape, the restrike attachment point occurred on the tape 10 to 14 in. from the leading edge. Figure 5 shows photographs of swept strokes with restrikes on 21-in.-wide Teflon tapes.

When the width of the Teflon tape was reduced from 21 to 13 in. and the restrike was initiated near the center of the taped area, the restrike did not puncture the tape but attached instead to either the leading or trailing edge of the Teflon tape.

SWEPT STROKE DATA AND AIRCRAFT DESIGN

An understanding of swept strokes and maximum dwell times will permit optimum fuel tank lightning protection with minimum weight on the newer technology aircraft. The data should also warrant modification of design specifications that prescribe, or allude to, unrealistic zone I testing for zone II fuel tank surfaces or components.

The fact that swept strokes will dwell on titanium surfaces for less than 2 msec has had a profound influence on the design of lightning-proof zone II titanium fuel tanks (6). Titanium skin as thin as 0.063 in. is permissible in a zone II area without compromising aircraft safety. Application of the previous zone I criteria for a zone II wing skin would have necessitated a 0.4-in.-thick titanium panel, which is both impractical and unnecessary.

It is also noteworthy that the dwell times obtained for plain, uncoated titanium sheets are not appreciably increased by mechanical joints and fasteners and, therefore, for the titanium case, the plain sheet data are adequate for determination of wing skin thickness. That is, each joint design and fastener type used in a zone II fuel tank need not be swept stroke tested for maximum dwell time; the maximum dwell time for the plain, continuous sheet is sufficient for design use. This is true for the alclad aluminum case as well. Whether or not this applies to other materials, such as boron, graphite, and stainless steel, can only be ascertained with swept stroke tests on continuous sheets and on several panels containing worst-case joint discontinuities and maximum fastener projections. It must be emphasized that, although a fastener or joint may increase the swept stroke dwell time for some materials, these discontinuities normally are accompanied by thicker skins, structural pads, or multilayer skins that can sustain a greater dwell time without creating an ignition hazard.

The Teflon patch tests indicate that the use of dielectric layers may be a convenient way to shield critical components that are otherwise difficult to protect. Application of this technique is envisioned as a dielectric patch; e.g., 0.010-in.-thick Teflon over a zone II fuel filter cap (or comparable component) so that the swept stroke cannot attach to the protected fuel tank component but will instead stretch or step over the dielectric patch as the stroke sweeps over the airfoil. Caution must be exercised in using this approach, however, because application of such a patch may increase the stepping distance of the arc and thereby increase its dwell time immediately forward of the patch, which could change the required thickness in that area.

In concept, it appears as though dielectric patches or strips could also be used to protect entire sections of a fuel tank or comparable vulnerable areas. As described in the swept stroke tests, a 21-in. width of 0.005-in.-thick Teflon tape forced an arc to step 21 in., thereby preventing swept

stroke attachment to the taped area. If, for example, a zone II fuel tank area were only 21 in. wide, this technique could be used to protect the tank skin, provided that the increased dwell time created forward of the tape is maintained out of a fuel or fuel vapor cavity and therefore does not create an ignition hazard. A 21-in.-wide patch was the maximum width listed, but other widths should be acceptable. Since the dielectric strength of a sheet is proportional to thickness, and the required breakdown strength is dependent on arc stepping distance, wide dielectric patches may require thicker dielectrics. The dielectric type and thickness required can be determined only with swept stroke tests; the theory should also be verified with an analysis of the attendant potential gradient profile. Restrike effects must also be considered. As shown in the data, restrikes punctured a 21-in.-wide, 0.005-in. tape. A thicker tape, or better dielectric, may prevent this.

The lesser dwell times associated with alclad aluminum, when compared to the nonconductive anodized coating, indicate another promising potential protection technique. If a material's demonstrated dwell time necessitates skin too thick to be practical, a surface can be protected by a conductive layer that will permit small swept stroke steps, lesser dwell times, and, therefore, reduced skin thickness requirements.

An extension of the radome lightning diverter philosophy was attempted as a protective technique for swept stroke zones. Dielectric and conductive strips were applied to aluminum and titanium panels in patterns that appeared to offer the maximum possibility of sideward diversion of a swept stroke. Panels f, h, k, and l of figure 3 were used in the study and, in fact, the data of all panels that utilized projections or surface discontinuities were scrutinized for stroke diversion tendencies.

Although there was a slight tendency for the stroke to be diverted sideways when it initially encountered several test strips, the stroke was diverted for only a brief instant before it continued to sweep aft unaffected by the remainder of the diverter strip. Judging from the limited data available, this technique does not appear promising as a means of diverting a swept stroke around a problem item or an area such as a zone II fuel tank vent aperture.

The protruding fin test panels were used to evaluate the tendency of a stroke to sweep up the leading edge of a vertical stabilizer or some similar projection. The tests were conducted on titanium samples with one and two protruding fins, respectively (fig. 3, q and r). The fins are 6- by 24-in. triangular pieces cut out of titanium sheets. They were bolted onto the titanium sheet and were oriented parallel to the windstream, with the highest point toward the downstream edge. Results showed an affinity of the swept stroke for these fins. In most of the test runs, the discharge arc climbed up the fin edge. When the arc reached the apex of the fin, it detached and sought another reattachment at a lower point on the inclined edge of the fin. The dwell time on the fin edge reattachment points was the same as that on a plain surface. It is believed that the tendency of the stroke to walk up the fin edge is not a function of the angular shape of the surface (except for extreme acute and obtuse angles), and therefore it is prudent to consider the fin edge a swept stroke surface unless tests conducted on a specific fin configuration prove otherwise. Normally, considerations of the fin edge will not introduce weight or design complexities because of the general lack of critical items in the fin edge and the suspected rare occurrence of a swept stroke that passes far enough back on a fuselage to attach to the fin. An awareness must be maintained, however, of the swept stroke implications of the fin edge.

CONCLUSIONS

Swept lightning stroke studies have been conducted on titanium and aluminum test samples using an open-throat wind tunnel and simulated lightning discharges. The following conclusions can be drawn from the data.

1. The swept stroke test technique simulates natural swept strokes adequately for analysis of lightning protection requirements.
2. The arc dwell time on uncoated titanium and aluminum sheets is 2 msec or less.
3. The maximum dwell time for anodized aluminum sheets is 4.8 msec.
4. Teflon or dielectric patches show promise as a protective shield over critical components in a swept stroke zone.
5. The maximum dwell times of titanium and aluminum sheet are not increased appreciably by joints, seams, or protruding mechanical fasteners.
6. Diversion of swept strokes around critical components by means of conductive or dielectric diverter strips located on aluminum or titanium sheet is not a promising protection technique.
7. The leading edges of stabilizer surfaces should be evaluated as possible swept stroke surfaces.
8. The low arc dwell times associated with the swept stroke data indicate that the protection requirements for a swept stroke zone (zone II) are much less stringent than those for a direct stroke zone (zone I).
9. The maximum protection requirement for a swept stroke zone warrants a modification of those design specifications that specify, or imply, that swept stroke fuel tank components shall be protected as though they were in a direct strike zone.

ACKNOWLEDGEMENT

The authors are indebted to a number of people at The Boeing Company and at the Lightning and Transients

Research Institute (LTRI) for their efforts in this investigation.

In particular, we wish to acknowledge the swept stroke test work accomplished by J. R. Stahmann of LTRI and the analytical support of Dr. M. J. Kofoid of The Boeing Scientific Research Laboratories.

The swept stroke studies were funded by the Department of Transportation through the Supersonic Transport Program under Contract FA-SS-67-e.

REFERENCES

1. "Protection of Aircraft Fuel Systems Against Lightning." FAA Advisory Circular AC 20-53, October 6, 1967.

2. E. L. Harder, "Properties of Lightning Strokes." "Electrical World," June 2, 1952.

3. B. J. Solak, "The Influence of Lightning and Static Electricity on Helicopter Design." "Journal of the American Helicopter Society," Vol. II, No. 1, January 1966.

4. R. O. Brick et al., "The Significance of Advanced Structural Fabrication Techniques on Aircraft Lightning Protection." SAE Paper 680290, The Boeing Company, April 1967.

5. R. O. Brick and S. D. Schneider, "Lightning Protection Considerations for the Boeing Supersonic Transport." 1970 IEEE International Symposium, Anaheim, California, July 1970.

6. R. O. Brick, "A Method to Establish Lightning Resistance/Skin Thickness Requirements for Aircraft." AFAL-TR-68-290, Part II, May 1969.

7. "Laboratory Study of Swept Lightning Discharge Current Effects on Titanium and Aluminum," Lightning and Transients Research Institute, Minneapolis, Minnesota, L&T Report 486.

Table I--Test Panels Description

Panel	Description
a,b	Plain, untreated metal sheets.
c, d, e, f	Teflon tape patches.
g, h	Silver paint strips.
i, j	Adhesively bonded joints without fasteners. To take full advantage of these test runs, silver paint strips and conductive tapes were applied to the downstream half of the bonded samples; thus, two tests could be conducted simultaneously.
k, l	Reverse sides of panels i and j.
m, n	Both sides of the sample with riveted joints.
o, p	Both sides of the sample with a circular hole that had a metallic plate backing.
q, r	Samples with two configurations of protruding fins.

NOTE: See figure 3 for test sample configuration.

Table II—Test Results for Titanium Samples (Ti-6Al-4V)

Test	Sample No.	Fig. 3	Sample Polarity	Windspeed, mph	Max Dwell Time, msec: Initial Atch	Max Dwell Time, msec: Reattachment	Max Arc Stepping Dist, in.	Total Swept Dist, in.	Remarks*
1	T0l	b	pos	150	2.4	0.8**	6	36	0.012" x 3' x 5', plain surface
2	T02a	a	pos	150	2.4	0.8	8	27	
3	T02a	a	pos	250	2.4	0.8	10	54	0.032" x 3' x 7',
4	T02b	a	neg	150	2.4	0.8	14	50	plain surface
5	T02b	a	neg	250	2.4	0.8	8	54	
6	T1a	a	pos	150	1.6	0.8	5	42	
7	T1a	a	pos	250	†	†	7	48	0.063" x 3' x 7',
8	T1b	a	neg	150	2.4	1.6	7	34	plain surface
9	T1b	a	neg	250	2.4	0.8	10	65	
10	T2a	c	neg	150	1.6	2.4	7	34	Three 3" Teflon
11	T2a	c	neg	250	1.6	1.6	6	30	tape strips
12	T2a	d	neg	150	1.6	6.4	13	25	12" wide
13	T2a	d	pos	150	1.6	7.2	12	37	Teflon tapes
14	T2a	e	pos	150	1.6	8.8	21	34	21" wide Teflon tapes
15	T2b	f	pos	150	0.8	8.8	††	††	Triangular Teflon tapes (24" x 24")
16	T2b	f	neg	150	1.6	4.0	15	36	Runs 1 and 2: probe tip over plain surface
17	T2b	f	neg	150	7.2	1.6	14	27	Run 3: probe tip over tapes
18	T3a	g	neg	150	†	†	4	25	Four 3" silver paint strips
19	T3a	g	pos	150	2.4	1.6	5	23	
20	T3b	h	pos	150	0.8	1.6	3	20	Silver paint—
21	T3b	h	neg	150	0.8	1.6	3	26	wedge configuration

Table II—Test Results for Titanium Samples (Ti-6Al-4V) (Concluded)

Test	Sample No.	Fig. 3	Sample Polarity	Windspeed, mph	Max Dwell Time, msec: Initial Atch	Max Dwell Time, msec: Reattachment	Max Arc Stepping Dist, in.	Total Swept Dist, in.	Remarks*
22	T4a	i	neg	150	2.4	2.0	4	22	Bonded joint sample
23	T4a	i	pos	150	1.6	1.6	9	50	with horizontal Cu and
24	T4a	i	pos	250	1.6	0.8	3	48	Al tape strips
25	T4b	k	pos	150	1.6	1.6	4	33	Backside of bonded joint
26	T4b	k	pos	150	0.8	1.6	5	42	with diagonal Cu and Al
27	T4b	k	neg	250	1.6	0.8	5	27	tape strips
28	T5a	m	neg	150	1.6	1.6	2	33	Riveted joint sample
29	T5a	m	pos	150	1.6	0.8	4	38	
30	T5b	n	pos	150	0.8	1.6	4	44	Backside of riveted
31	T5b	n	neg	150	1.6	1.6	4	36	joint samples
32	T6a	o	neg	150	0.8	2.0	10	24	Sample with
33	T6a	o	pos	150	0.8	1.6	2	32	10" dia hole
34	T6b	p	pos	150	†	†	4	21	Backside of 10" dia hole sample with 5" x 34" horizontal silver paint strip
35	T6b	p	neg	150	†	†	5	16	
36	T7a	q	pos	150	1.6	0.8	3	33	
37	T7a	q	neg	150	1.6	0.8	4	33	Single fin on sample sheet
38	T7a	q	neg	250	1.6	0.8	4	33	
39	T7b	r	neg	150	1.6	0.8	3	31	
40	T7b	r	pos	150	1.6	0.8	5	31	Double fins on sample sheet
41	T7b	r	pos	250	1.6	0.8	3	31	

* All movies were taken at 1,300 frames per second.
**Duration of each motion picture frame is 0.8 msec; actual dwell time can be less.
† No movies or overexposed movies.
††Arc extinguished before crossing insulated surface.

Table III–Test Results of Aluminum Samples (2024-T0 and 2024-T3)

Test	Sample No.	Fig. 3	Sample Polarity	Windspeed, mph	Max Dwell Time, msec: Initial Atch	Max Dwell Time, msec: Reattachment	Max Arc Stepping Dist, in.	Total Swept Dist, in.	Remarks*
1	A1a	a	neg	150	1.6	1.6	18	49	0.063" x 3' x 7',
2	A1a	a	neg	250	0.8	0.8	12	42	plain surface
3	A8	b	neg	250	1.6	3.2	12	52	0.063" x 3' x 5',
4	A8	b	neg	150	1.6	4.8	8	32	anodized surface
5	A2a	e	neg	150	0.8	9.6	21	45	21" wide Teflon tape
6	A2a	e	pos	150	0.8	9.6	21	51	(21" x 36")
7	A2b	f	neg	150	0.8	3.2	12	34	Triangular Teflon
8	A2b	f	pos	150	0.8	1.6	16	34	tapes (24" x 24")
9	A3a	g	pos	150	0.8	2.0	3	30	Four 3" silver paint strips
10	A3a	g	neg	150	0.8	3.2	5	16	
11	A3b	h	neg	150	0.8	2.4	3	12	Wedge configuration,
12	A3b	h	pos	150	0.8	1.6	2	9	silver paint
13	A3b	h	pos	250	0.8	0.8	5	48	
14	A4a	j	pos	150	0.7	1.4	3	30	Bonded joint sample with 5-1/2" x 38" horizontal silver
15	A4a	j	neg	150	2.4	1.8	12	39	paint strip (movie at 2,900 fps)
16	A4b	l	neg	150	1.75	1.4	4	38	Backside of bonded joint sample
17	A4b	l	pos	150	1.4	1.4	4	40	with 3" diagonal silver paint
18	A4b	l	pos	250	0.35	1.05	6	38	strip (movie at 2,880 fps)
19	A5a	m	pos	150	0.8	0.8	2	38	Riveted joint sample
20	A5a	m	neg	150	0.8	1.6	4	36	
21	A5b	n	neg	150	1.6	4.0	12	34	Backside of riveted
22	A5b	n	pos	150	1.6	0.8	7	34	joint sample

Table III–Test Results of Aluminum Samples (2024-T0 and 2024-T3) Concluded)

Test	Sample No.	Fig. 3	Sample Polarity	Windspeed, mph	Max Dwell Time, msec: Initial Atch	Max Dwell Time, msec: Reattachment	Max Arc Stepping Dist, in.	Total Swept Dist, in.	Remarks*
23	A6a	o	pos	150	1.6	0.8	5	30	Sample with 12" dia hole
24	A6a	o	neg	150	1.6	1.6	15	40	
25	A7a	q	neg	150	0.8	0.8	2	25	Single fin on sample panel (Runs 3 and 4 movies at 3,300 fps)
26	A7a	q	pos	150	0.8	0.8	6	36	
27	A7b	q	neg	150	0.9	0.9	9	30	
28	A7b	q	pos	150	0.9	0.9	2	30	
29	A7b	q	pos	150	0.8	0.8	5	24	Double fins on sample panel
30	A7b	q	neg	150	4.8	**	**	**	

* All movies were taken at 1,300 fps except as noted.
**Did not reattach; produced one long track.

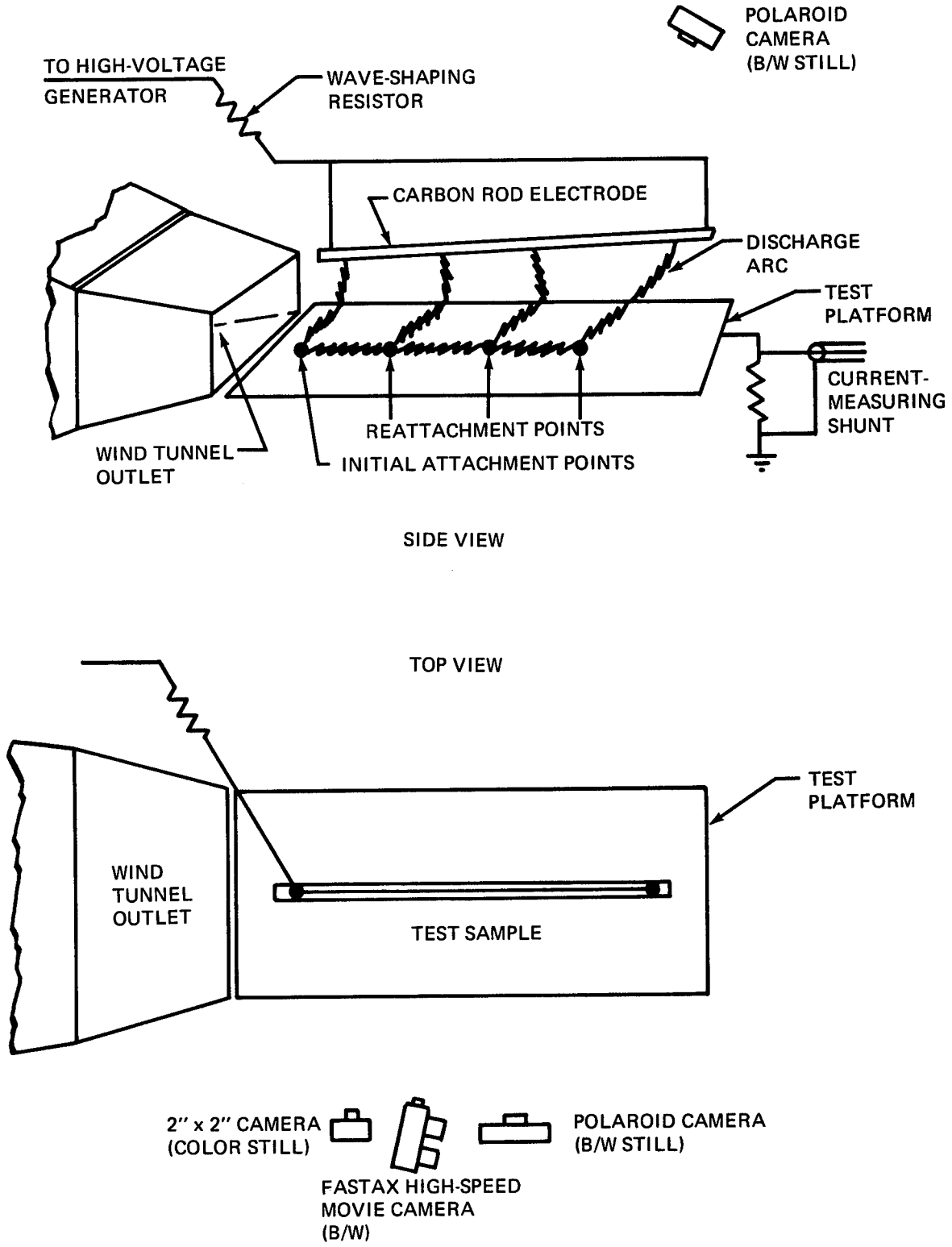

Fig. 1—Sketch of swept stroke test setup

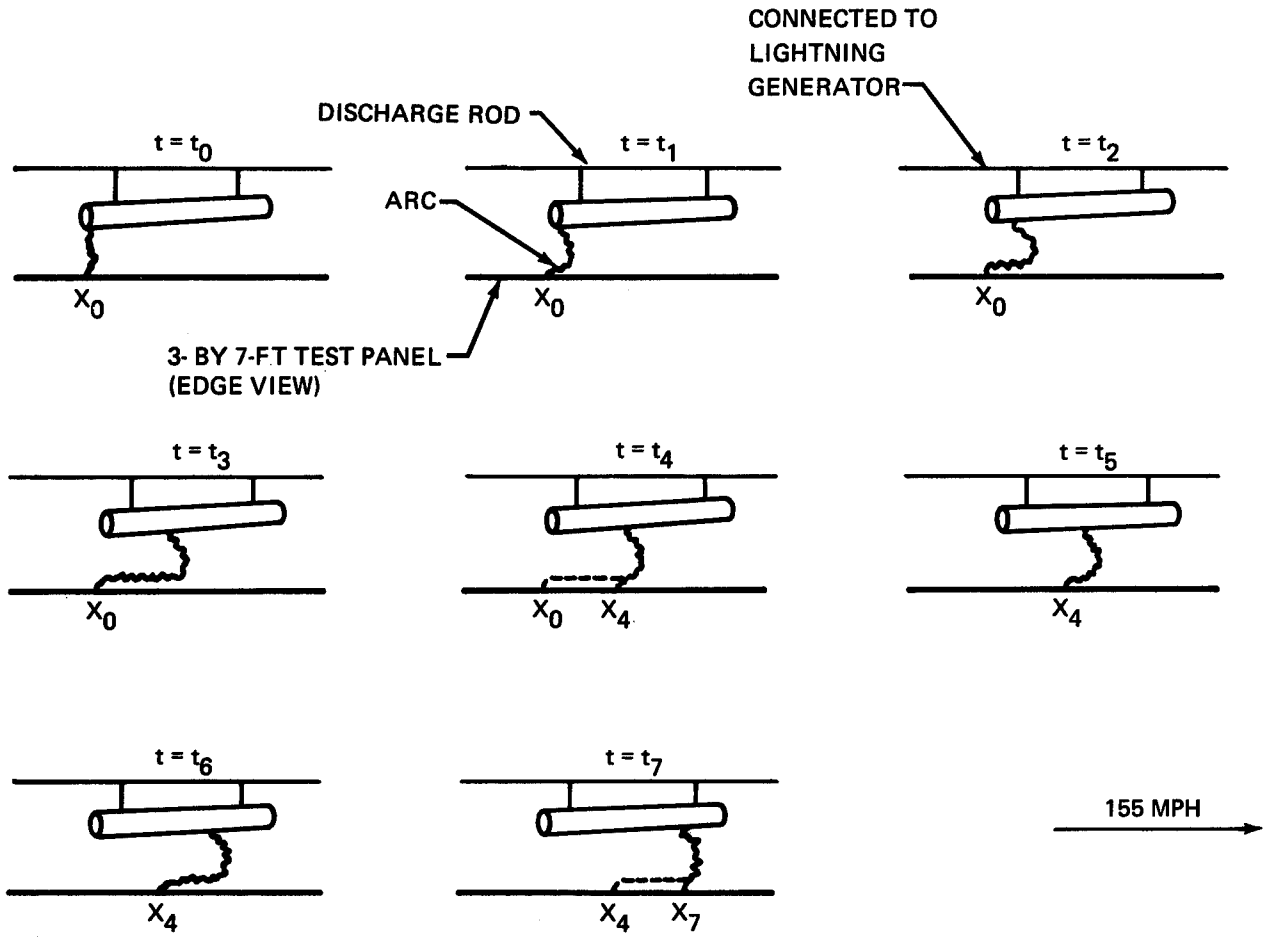

Fig. 2—Sequential sketch illustrating the sweeping action of simulated lightning discharges (not to scale)

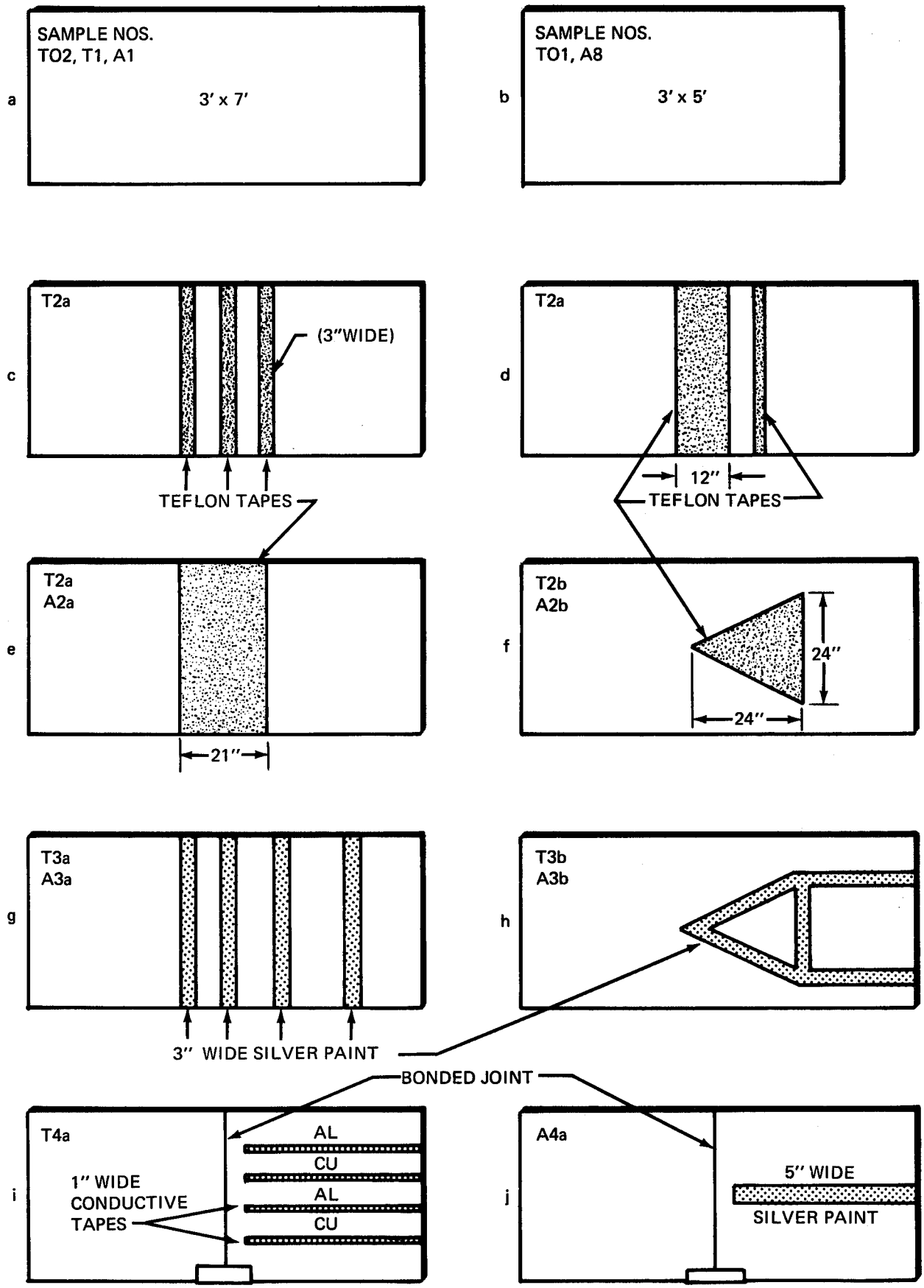

Fig. 3—Test sample surface configurations

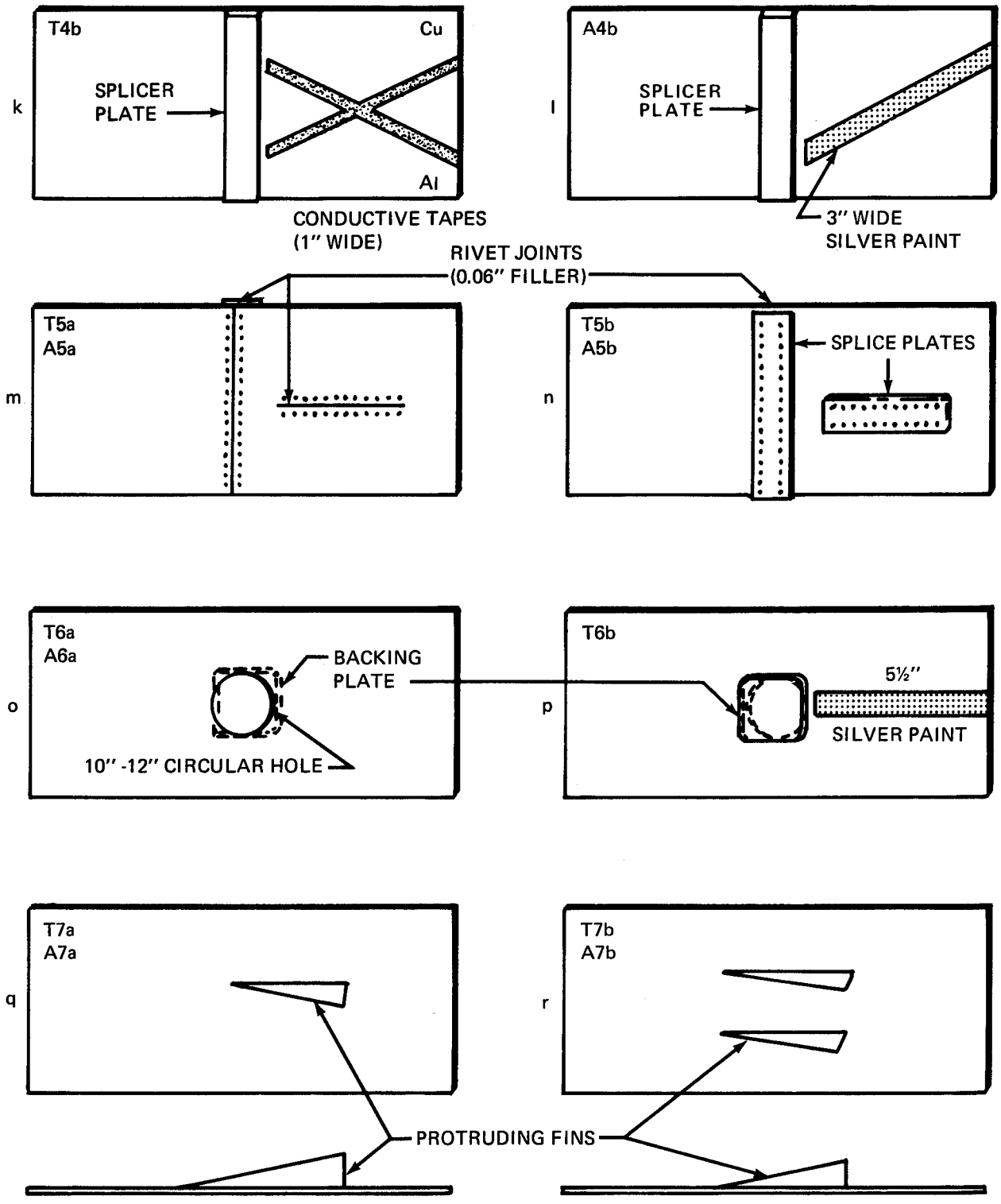

Fig. 3--Test sample surface configurations (Continued)

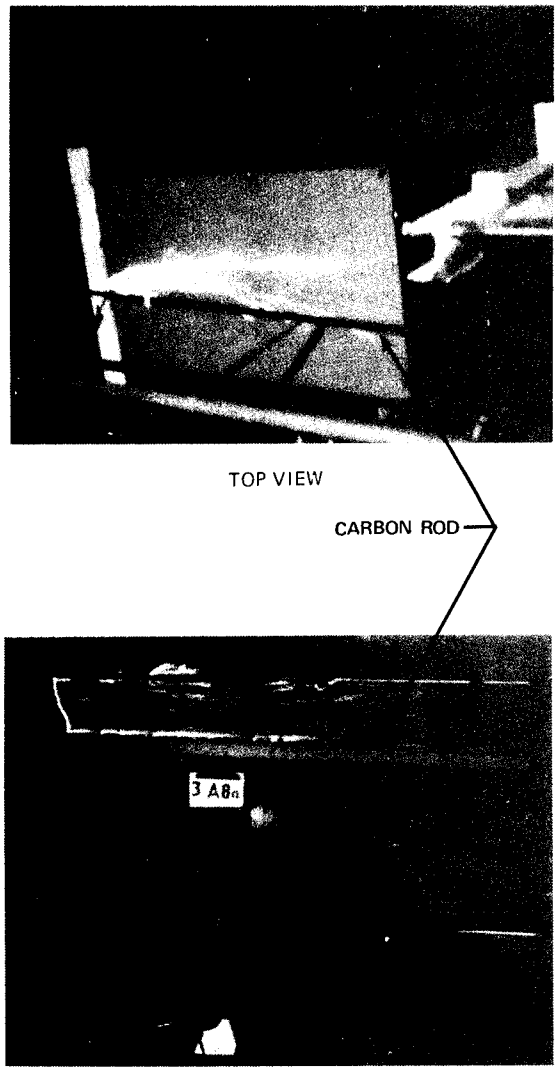

Fig. 4—Swept stroke on anodized aluminum sample

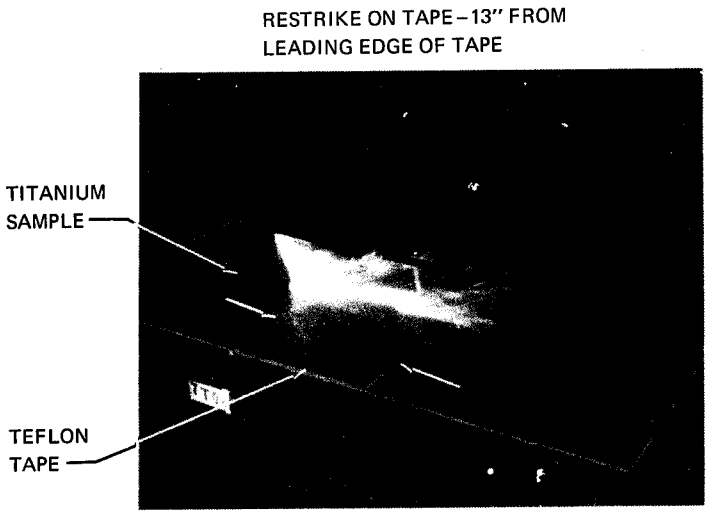

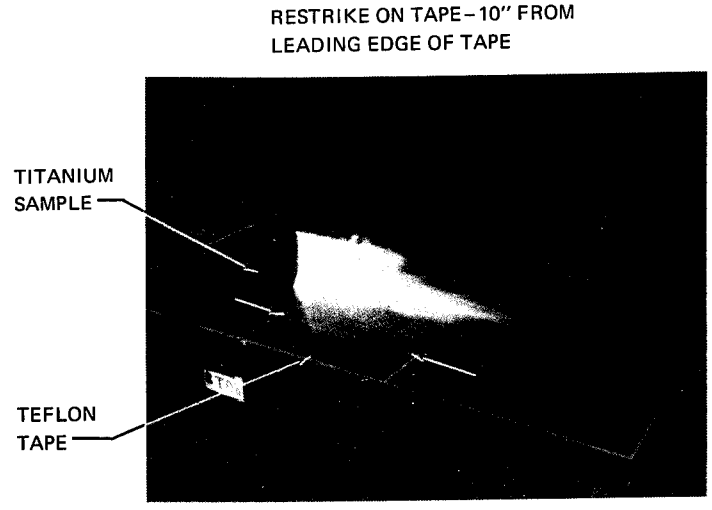

Fig. 5—Restrikes on titanium samples covered with 21-in.-wide Teflon tape

700926

ELECTROSTATIC CHARGING AND NOISE QUIETING

ROBERT L. TRUAX
DAYTON AIRCRAFT PRODUCTS, INC.

ABSTRACT

It's known that aircraft in flight charge electrostatically due to triboelectric contact with precipitation, cross fields and ionization in engines. This charging can create broadband radio frequency noise due to streamer currents across non-conductive surfaces, corona discharge from the aircraft and arcing between structural members.

In the past charging, of an aircraft has been measured, noise sources identified and corrective steps applied. However, such efforts have been principally confined to large commercial and military jet aircraft. Cost had prohibited extensive system treatment of all noise sources preceded and followed by extensive flight test verification of charging phenomena and noise reduction measures.

Smaller, General Aviation aircraft occupy the same flight environment and utilize the same airspace as transport and military aircraft. These aircraft also charge electrically. Noise sources are frequently even more tightly coupled to receiving antennas due to the physically small dimensions of General Aviation airplanes.

A system approach was taken to identifying noise sources due to electrostatic charging, to measurement of charging levels, application of noise reduction techniques and flight test verification.

Streamer currents to 40 microamperes were measured on plastic structural components, cross field stresses exceeding 100 KV/M were recorded and propellor corona currents were observed to exceed 50 microamperes per blade. Precipitation charging rates of 250 microamperes were encountered. One tip type discharger reached a 400 microampere discharge current on one occasion. Discharges of opposing polarities were observed from different aircraft extremities at the same time. A total discharge current of 2.5ma was occasioned.

Steps were taken to reduce noise generation when the aircraft became charged electrically. These included installation of quiet dischargers, conductive coating of plastic frontal surfaces and use of dc sealed antennas.

Actual flight tests demonstrated that with proper application of corrective measures useable navigation and communications could be retained in the most severe conditions encountered. Without the corrective measures, communications and navigation, through the VHF spectrum, were lost for extended periods of time in actual flight.

Electrostatic Charging and Noise Quieting

AS BACKGROUND, electrostatic charging of aircraft in flight, especially during instrument flight conditions, produces radio frequency noise that may be disruptive to necessary received navigation and communication information.

This electrostatic charging may result from flight through precipitation, electric cross-fields, or from engine produced, ionization. The radio frequency noise is generated by streamer currents on plastic prontal areas during precipitation encounters and corona discharge or arcing between airframe structural members, during all charging events.

Laboratory duplication of these phenomena indicates significant broadband radio frequency noise, may be generated in a band extending from essentially dc* through at least 1 GHz.

Aircraft commonly operating in the IFR (Instrument Flight Rules) environment range from General Aviation single engine aircraft, through airline transports and Military supersonic airplanes. Aircraft ground speeds thus extend from 2 to 10 nautical miles per minute or more. Therefore, even brief losses of necessary instructions or navigational position information can be extremely serious, especially in high density terminal areas or during approaches to airports.

Considerable effort has been undertaken, noteably since World War II**, to identify the magnitude of the radio frequency noise interference and to provide means of preventing the interference. Most of this work has been accomplished on large transport or military aircraft. The efforts have also, usually been directed to solution of one specific interference problem on a given aircraft or radio system.

General Aviation accounts for 98% of the civil aircraft in the USA. These aircraft fly approximately 1/2 of the passenger miles accounted for each year. Further, they fly about 1/2 of the instrument flight hours recorded by ATC (Air Traffic Control). Because of their operational envelopes they are more likely to encounter actual instrument conditions during operations controlled by ATC. This is especially true since most General Aviation aircraft are only required to operate IFR when encountering bad weather, while airline and most jet operations must operate under Air Traffic Control regardless of prevailing weather.

A SYSTEM APPROACH to identification of the frequency and magnitude of electrostatic charging, the actual sources of the radio frequency noise, the frequency range of the resulting interference and to methods of reducing the interference to acceptable levels, was undertaken. This involved determination of the noise frequency spectrum, instrumentation of an aircraft, provision for artificially charging the instrumented aircraft in flight, test flights to produce electrostatic charging and observation of the resultant noise, corrective measures to effectively reduce the rf noise produced in flight and, finally, test flights to establish that the corrective measures were effective. Also, instrumentation was installed, and data recorded, to identify when, and by what means, the test aircraft was electrically charging.

Three aircraft were used in this program. They were selected to represent the range of General Aviation aircraft typically flying IFR today. A Beechcraft Bononza represented a typical single engine aircraft. A Cessna 320 was used as a typical twin engine airplane, and a Lear Model 25 completed the series.

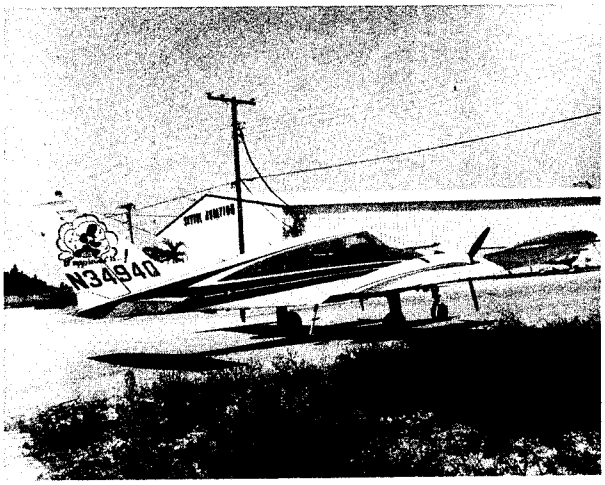

Figure 1 - Beechcraft Bononza

* Abbreviations used identified at the end of paper.
** Bibliography appended at the end of paper.

Figure 2 - Cessna 320

Figure 3 - Lear Model 25

The Cessna 320 was the instrumented airplane. Data acquired, as presented herein, was largely taken on that aircraft. Corrective measures used to reduce identified rf noise sources on the Cessna 320 were then applied to the Beechcraft Bononza and the Lear Model 25.

INITIAL FLIGHT TESTS were conducted with the aircraft as delivered. No changes were made to antennas, plastic frontal areas, nor were dischargers installed. Flights were normal point to point instrument flights, however, an effort was made to obtain altitude assignments that would result in flight through the prevailing clouds.

During the initial flight testing loss of ADF navigational information was frequent and for protracted periods. Loss of HF communications, both AM and SSB, was only a little less frequent.

VHF communication and navigation loss was not uncommon. At other times receiver desensitivation was apparent, as were increased noise levels, and sometimes communications was hard to understand. On one occasion in the Cessna 320 no navigation nor communications was useable for a period of about 9 minutes.

In another instance in the Beechcraft Bonanza, one VOR was unuseable, while the other remained in operation (separate antennas), for nearly 1/2 hour. Noise was severe in all radio receivers. Flight conditions were in clouds and snow, at a temperature of -20° Fahrenheit.

Navigation inadequate signal flags appeared on both VOR's of the Lear Jet anytime there was evidence of St. Elmo's fire on the windscreen, or other parts of the airplane.

Both the Lear Jet and the Cessna 320 were delivered with dischargers installed by the factory.

SPECTRUM CONTENT of streamer pulses, corona discharge and arcing pulses was identified in the laboratory. The actual spectrum was found to be somewhat a function of the energy applied and the physical size of the structures under test. Figure 4 is an averaging of the data obtained.

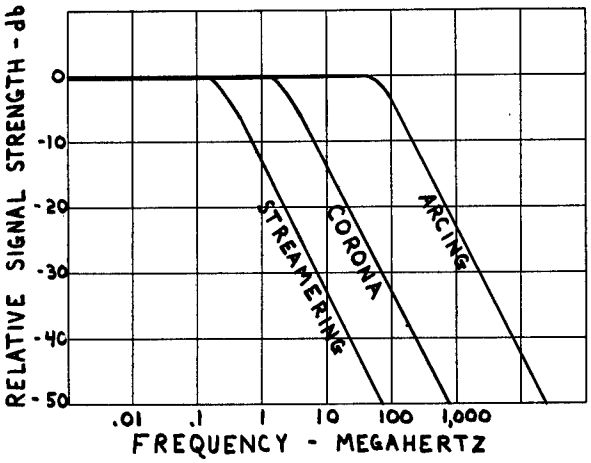

Figure 4 - Noise generated by electrostatic charging

An NF-105 receiver was used to spot check several frequencies in these measurements. An oscilloscope was used to measure noise amplitude.

Electrostatic Charging and Noise Quieting

Streamer currents were generated by blowing non-conductive particles on a sheet of epoxy fiberglas, in a screen room, with a sandblaster. The sheet was bounded by a metallic edge, which was grounded through a microammeter. The sandblaster gun was, also, grounded. An antenna plate, connected to the NF-105, was placed behind the plastic sheet.

A similiar test, where the particles impinged directly on the conductive antenna, also resulted in a measureable current flow. However, only a slight noise increase resulted.

Corona discharge noise spectrum was measured in the MIL-D-9129B rf noise test set. A metal tab was placed on the simulated wing section as the corona current source.

Arcing noise was generated, in a screen room, by impressing high voltage, through a current limiting resistor, on two overlapped metal sheets with a narrow gap of insulating air between them. An antenna wire near the gap received the noise energy.

The frequency signatures thus obtained provided a crude, but effective means, of identifying the causes of noise received during test flights.

No arcing (bonding) noise was detected on any of the aircraft throughout the program.

MICROPOINT DISCHARGERS were installed on three aircraft. The Cessna 320 was equipped with airline type dischargers on the wing tip tanks and General Aviation dischargers elsewhere. The Bononza with General Aviation dischargers and the Lear Jet with airline category dischargers.

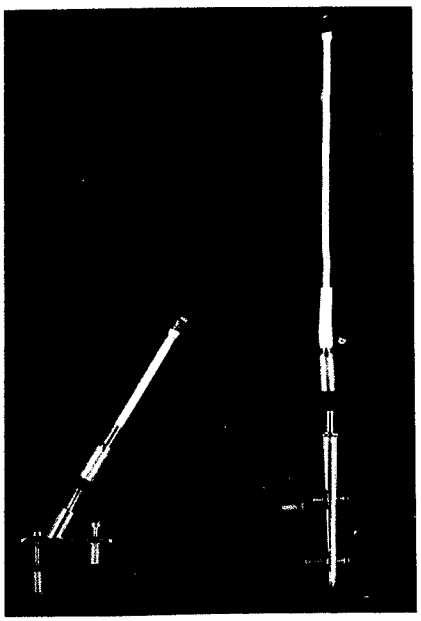

Figure 5 - Airline Micropoint Dischargers

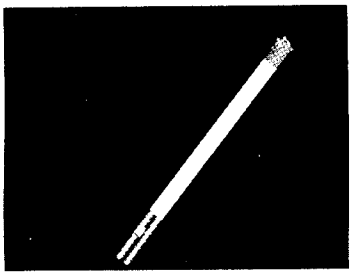

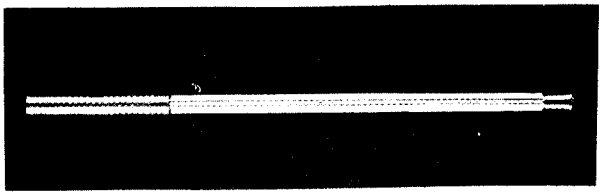

Figure 6 - General Aviation Micropoint Dischargers

Electrostatic Charging and Noise Quieting

The Micropoint Dischargers conform to the operational specifications of MIL-D-9129B. Both categories provide a nominal 50 db of radio frequency noise quieting.

Discharger quantities were based on maximum anticipated charging rates as follows:

Beechcraft Bononza	1 ma
Cessna 320	1.5 ma
Lear Model 25	2 ma

The locations choosen were conventional, in that the dischargers were installed in areas of low pressure vortices and high dc field stress. Figure 7 indicates the quantity and location of the dischargers installed on the Cessna 320.

On the Cessna 320 the dischargers were insulated from their mounts and instrumented so that corona current could be read or recorded. Corona current could be measured from any one, all or any combination of the installed dischargers.

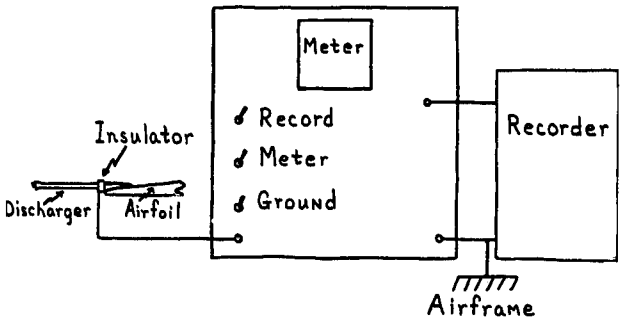

Figure 7 - Discharger Instrumentation

Total corona current measuring capacity initially was 400 microamperes. This was found to be inadequate almost immediately. Figure 8 shows the corona current instrumentation finally provided. This instrumentation has a zero center scale capability so corona of either polarity can be indicated. Low range sensitivity is normally 50 microamperes full scale. And, a total maximum current capacity of 6 ma is provided. The recorders have been replaced by meters providing 0.01 microampere or 15 microampere full scale readings for identifying corona onset and other low current purposes.

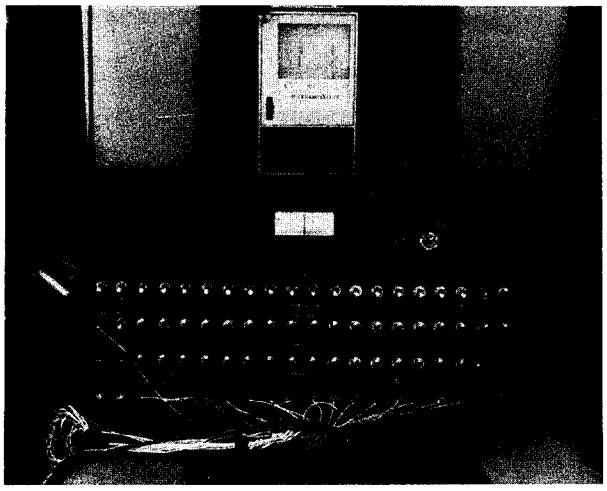

Figure 8 - Corona Current Instrumentation

At the same time, an isolated charge rate probe was installed ahead of the radome. This probe had a known surface frontal area.

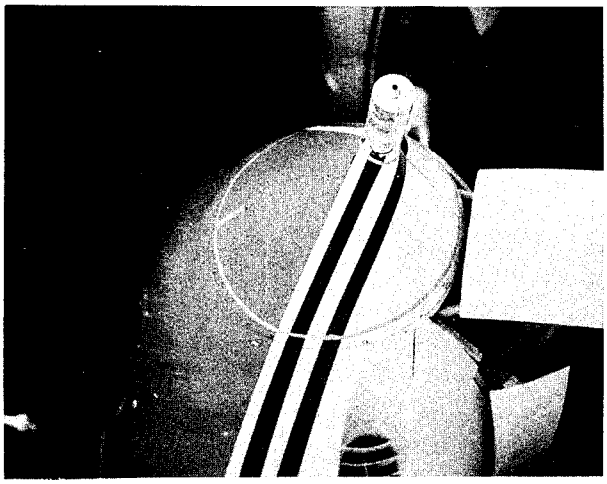

Figure 9 - Charge rate probe and plastic frontal area isolation.

Also, the plastic frontal surfaces were isolated from the metallic airframe by painting a conductive band around the surfaces. This band was then connected to a wire, one end of which was brought into the cabin. This allowed streamer currents to be measured in flight.

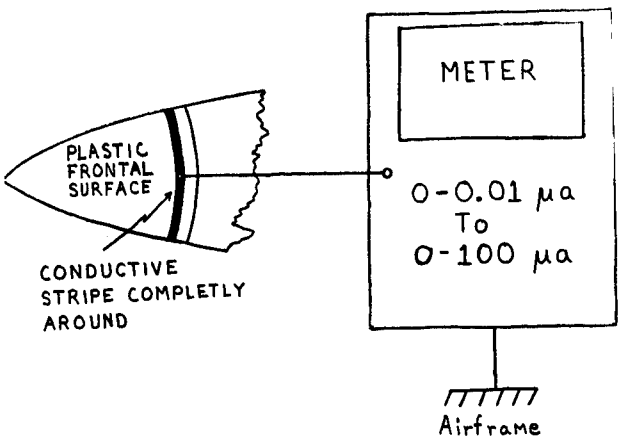

Figure 10 - Streamer Current Instrumentation

Since VHF interference had been observed it was reasonable to assume that corona discharge was occuring directly from at least some antennas. Therefore, all open wire type antennas were replaced by dc sealed antennas on all aircraft. This included ADF sense, HF, VHF communication and VHF navigation antennas.

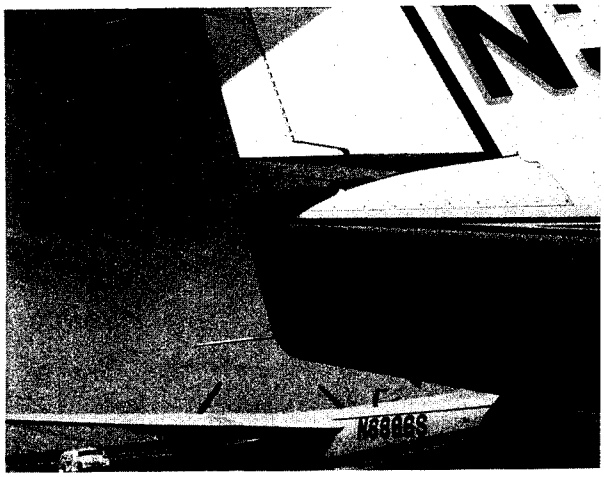

Figure 11 - Lear Model 25 open wire VOR antenna

VHF INTERFERENCE CEASED as a result of installing the dischargers and the use of dc sealed antennas. Though it was demonstrated that both were needed. Without dischargers, the sealed antennas reduced VHF interference, but did not eliminate it. The small dimensions of the aircraft probably resulted in corona rf noise from a nearby area being tightly coupled to the VHF antenna. Installation of dischargers not only controlled the location of corona discharge and lowered the potential stored on the aircraft but also reduced the rf energy content by another 50 db.

Data acquired in flight indicated much higher corona currents, in some flight conditions, than had been anticipated. One instance resulted in a total corona discharge current from the dischargers of 2.5 ma. Corona discharge currents were also observed at times when the aircraft was being flown clear of surrounding clouds and not through precipitation. The radio systems would operate noise-free with discharger currents totaling from 250 to 500 microamperes. At higher currents the ADF was affected, and to a lesser extent the HF.

In precipitation noise did render the ADF equipment inoperative, both aurally and for bearing information. It was observed that at any time streamer currents were measured there was an onset of ADF noise.

Precipitation resulted in measured currents to 0.2 and 0.3 microamperes on the unit area charging probe. The area of the probe is 2.838 square inches. The effective frontal precipitation wetted area of the Cessna 320 was estimated to be 10 square feet. This would indicate a total charging rate of 150 microamperes at a 0.3 microampere unit charging measurement. Actual discharger current measured 270 microamperes during the occurance.

Discharger currents of opposing polarities were frequently observed from different aircraft extremities. This indicated the possibility that the aircraft was in a region of cross fields. Also, discharger current fluxuated too rapidly to accurately collate the current division between dischargers.

MICROPOINT LIGHTNING DIVERTER DISCHARGERS were installed on the Lear Model 25. On two separate occasions lightning did attach to the diverter discharger on the ventral fin of this aircraft. In both cases the base and discharger were blown off the aircraft. Originally the base was attached only be conductive adhesive. The resistance from the base to the airframe was less than 100 milliohms. Still burning occured between the base and the airframe skin in the bond line area. Once severely, Figure 12. The base has since been reinstalled using rivets and non-conductive adhesive. No lightning strikes have attached in the interim.

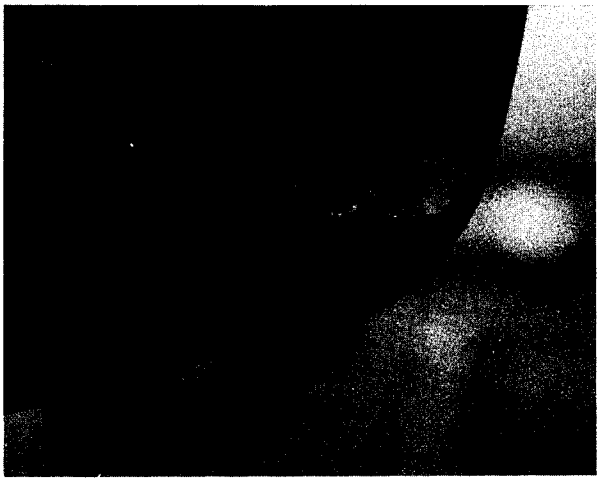

Figure 12 - Lightning damage between discharger base and skin of Lear Model 25

ADDITIONAL INSTRUMENTATION AND CONDUCTIVE COATING OF PLASTIC FRONTAL SURFACES was suggested by the results of the early flight tests. It was felt that on artifical charging system was needed to obtain stable data and to calibrate the instrumentation. A means of identifying corona onset from propellors was needed, for correalation with received noise. A means of recording received noise for later correalation with recorded charging and discharge data was desireable. The evidence that severe cross fields were being frequently encountered made the installation of field mills a requirement. Figure 14 shows the final instrumentation configuration of the Cessna 320.

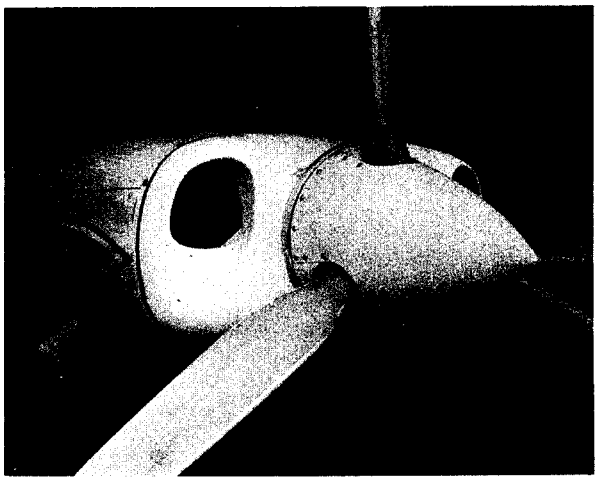

Figure 13 - Plastic frontal area electrical isolation

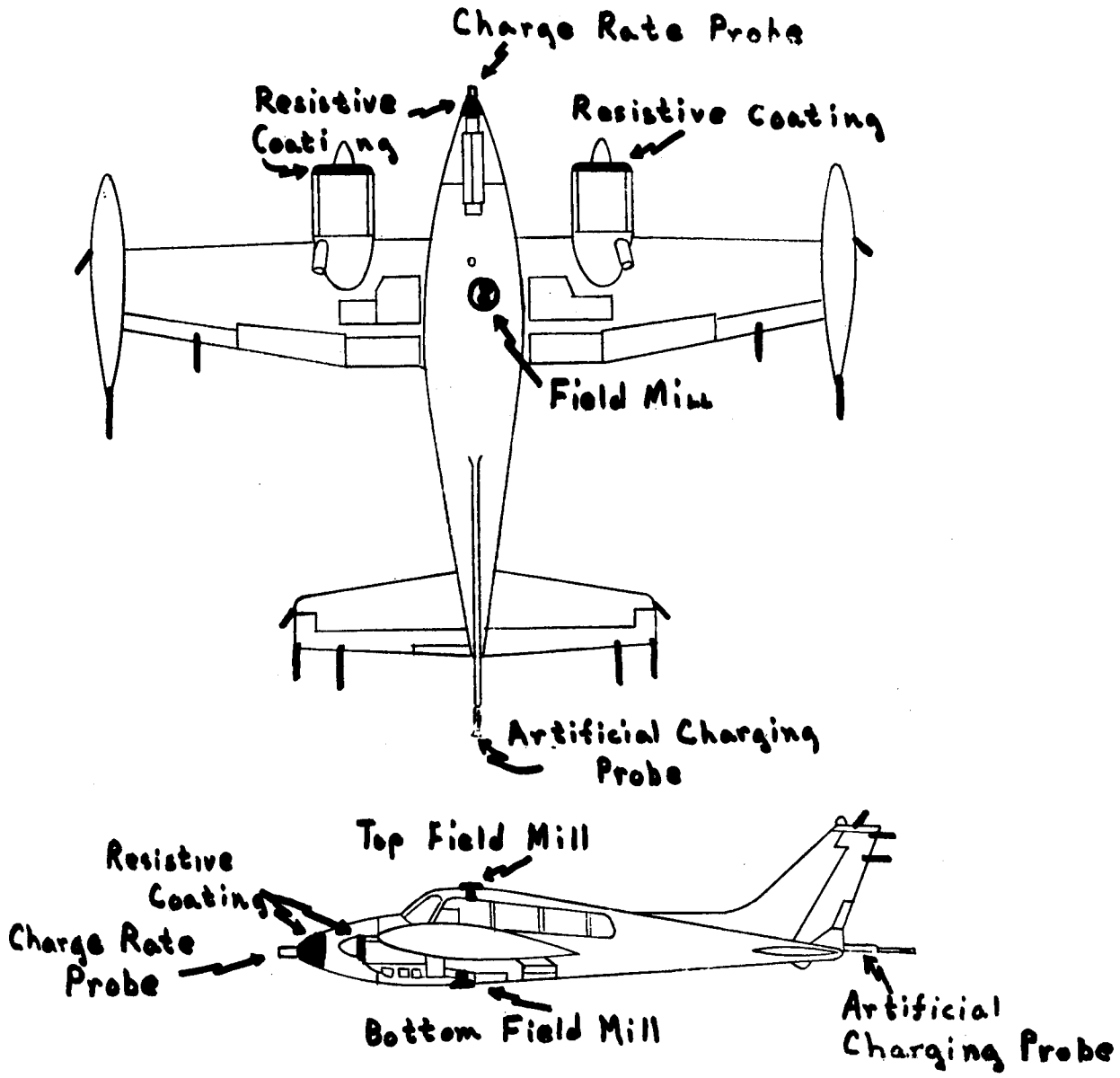

Figure #14 - Final Cessna 320 instrumentation configuration

Plastic frontal surfaces, notably the radome and engine nacelle cowls, were resistively coated with Olin-Mathieson's Anti-static urethane astrocoat. Resistance of the coating measured approximately one megohm per square. The coating was isolated from the airframe so that current could be observed. This coating greatly contributed to noise reduction in the ADF and HF systems. Current from the coatings as high as 20 to 25 microamperes was noted, with no interference evident in the ADF or HF.

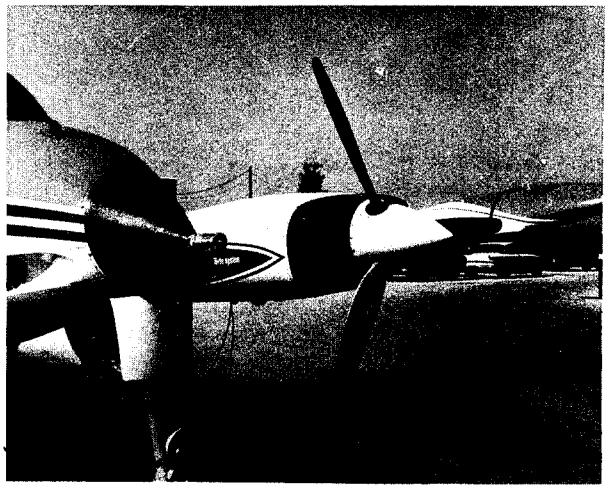

Figure 15 - Conductive coating of plastic frontal surfaces.

A means was developed to indicate current flow from propeller blade tips in flight. Basically this consisted of a battery operated VHF transmitter installed in the propeller spinner. The transmitter was on a frequency that could be received by a conventional aircraft VHF communications receiver.

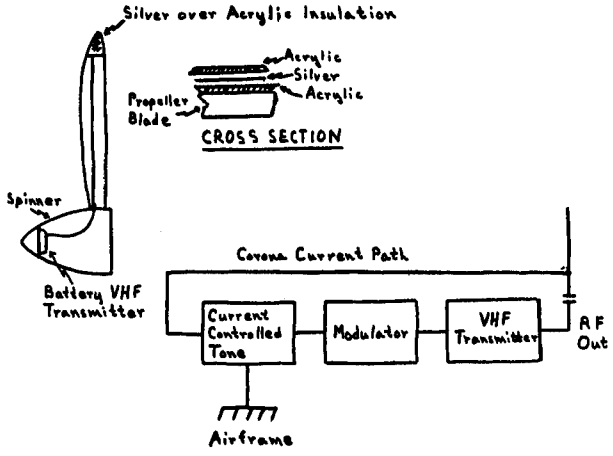

Figure 16. - Propeller current transducer system

The tip of the propeller blade was electrically isolated with an acrylic coating. A stripe of acrylic was continued down the back of the blade to the hub area. The insulated tip and stripe were then coated with a silver loaded conductive paint. To preserve the conductive path the stripe was then overcoated with acrylic. The conductive path served as both a current conductor and an antenna for the transmitter. No particular rotational modulation of the transmitted signal was apparent.

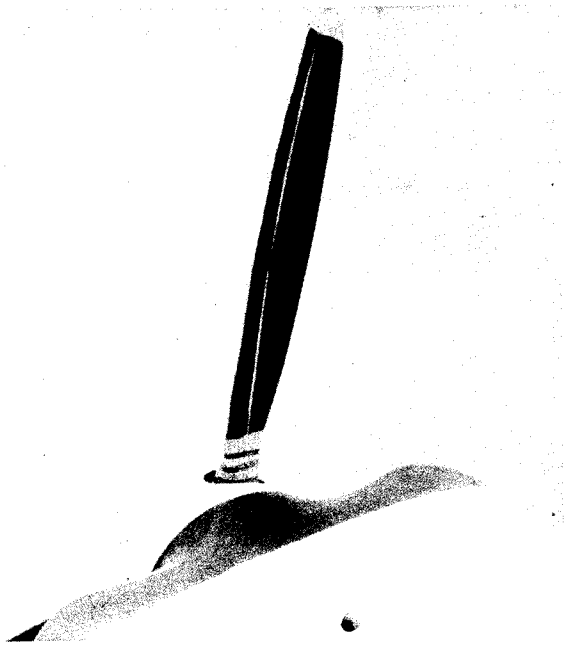

Figure 17 - Propeller blade conductive path

Electrostatic Charging and Noise Quieting

Propeller corona current determined the tone frequency of the modulator for the transmitter. With no current flow the transmitter was modulated with a 1000 Hz tone. Negative current lowered the tone frequency, with a -50 microampere current cutting off the tone multivibrator. Positive current increased the tone frequency. All propeller currents recorded in flight were of a negative polarity. The current swept tone was quite linear, so a current of as little as one microampere was easily identifiable. A demodulator to translate tone to meter current was envisioned, but not constructed as part of this program.

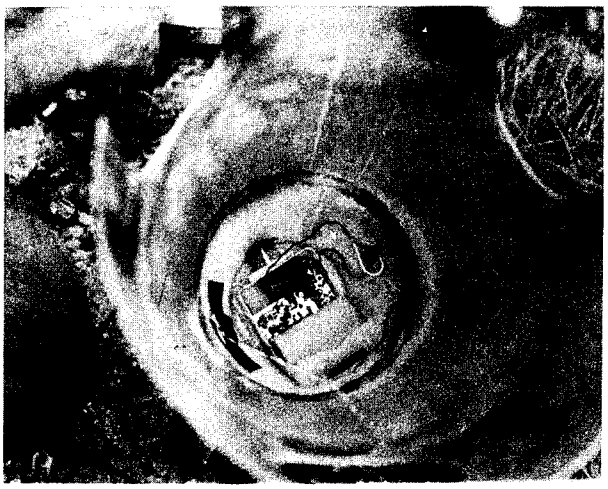

Figure 18 - Propeller current transducer mounted in spinner.

Next an artificial charging system was installed on the Cessna 320. Such a system was found necessary to correalate current division between dischargers. And, to establish repeatable data points.

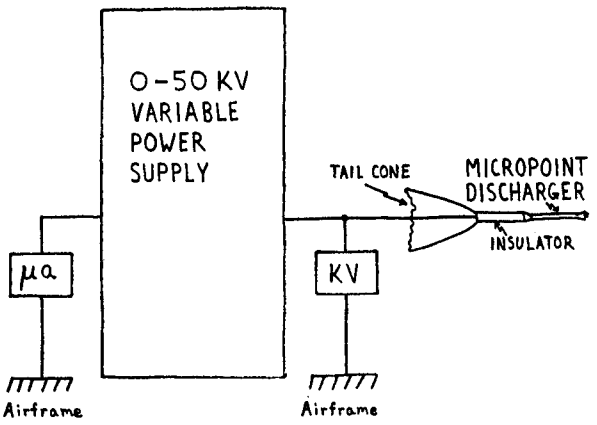

Figure 19 - Artificial Charging System

One of the first measurements made was to determine the point at which the onset of corona occured from the installed dischargers. This was discovered to be a variable related to airspeed, altitude and relative humidity. Typically corona discharge onset ranged from an applied potential of 7.5 to 10KV at a 10,000 foot altitude and a true airspeed of 180 knots.

Current from the artificial charging system itself is presented in Figure 20.

Figure 20 - Artificial charging system current (Microamperes)

Altitude (MSL) Potential KV	TAS 120 kts 1,000	5,000	10,000	TAS 150 kts 1,000	5,000	10,000	TAS 180 kts 1,000	5,000	10,000
	Current			(microamperes)					
	μa	μa	μa	μa	μa	μa	μa	μa	μa
5	1	1	1	1	1	1	1	1	1
10	2.5	2.5	3	3	3	3	3	3	4
15	5	5	6	6	6	6	6	7	8
20	8	7.5	9	9	9	10	10	10	12
25	11	10	11	12	12	14	14	15	16
30	14	14	15	15	16	17	17	18	20
35	16	16	18	19	19	20	21	21	24
40	18	20	21	22	23	24	25	26	29
45	21	23	25	25	26	28	28	30	32
50	24	26	29	29	30	32	32	35	37

The artificial charging equipment consisted of a high voltage power supply, variable from 0-50KV, an insulated lead from the cockpit to the tail cone and an isolated Micropoint discharger installed aft of the tail cone. The high voltage power supply was built for ground use. Therefore, high voltage flashover limited its use to altitudes below 14,000 feet MSL.

Figure 21 - Artificial charging equipment

Corona current distribution between the installed Micropoint dischargers was measured at a true airspeed of 180 knots with an artificial charging system applied potential of 50 KV. These measurements were made a 1,000, 5,000 and 10,000 feet MSL.

Figure 22 - Installed Micropoint discharger current distribution

	Altitude (feet MSL)					
	1,000		5,000		10,000	
	Corona Current					
Discharger Location	μa	%	μa	%	μa	%
Right wing tip	0	0	0	0	0	0
Right wing outboard	2.6	10	2.7	10	3.0	10
Right wing inboard	0.8	3	0.6	2	0.7	2
Right elevator tip	0	0	0	0	0	0
Right elevator outboard	3.0	12	3.1	12	3.4	11
Right elevator inboard	2.3	9	2.6	10	2.9	10
Rudder tip	0.8	3	1.0	4	1.0	3
Rudder outboard	4.3	17	4.4	16	5.0	17
Rudder inboard	2.8	11	3.2	12	3.6	12
Left elevator tip	0.3	1	0.5	2	0.8	3
Left elevator outboard	2.8	11	3.2	12	3.3	11
Left elevakto inboard	1.8	7	2.0	7	2.3	8
Left wing tip	0	0	0	0	0	0
Left wing outboard	2.6	10	3.0	11	3.4	11
Left wing inboard	0.1	0	0.6	2	0.4	1
Total	24.2	94	26.9	100	29.8	99

Though inexact, it was felt that knowing how the current tended to divide amount the installed dischargers would permit later inference of total discharger current. Obviously, the inference applies only when precipitation or engine charging is the operating mechanism.

Some of the current differences can be accounted by realizing that the resistance of the dischargers varies somewhat from unit to unit. Later flights, however, demonstrated that even in apparently clear skies cross field charging of significance can occur.

A stereo tape recorder was also added to the instrumentation. One track was used to record voice notes, observations, etc. The other channel was used to record from the installed aircraft receivers. The intercom muting switches permitted selective recording from these receivers. With a common time base between the tape aural recorder and the strip chart discharger current recorders, and later field mill recorders, data could be gathered much more expediously for subsequent analysis.

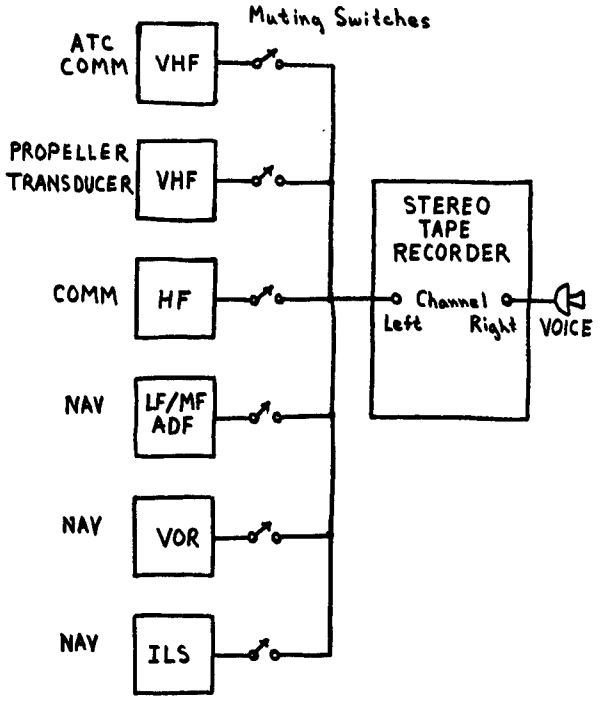

Figure 23 - Aural recording system.

Electrostatic Charging and Noise Quieting

The final instrumentation installation resulted from the fact that discharge currents were often observed when the aircraft was clear of clouds and precipitation. Another influence was the frequently opposing polarity of discharge currents from different extremities of the airplane.

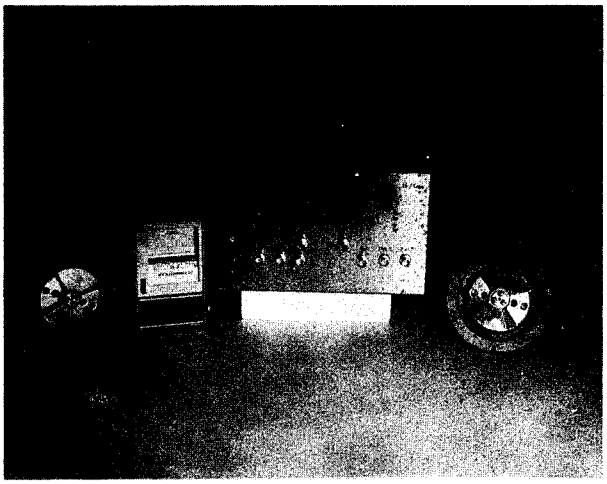

Figure 24 - Field Mill System

Two field mills were installed on the Cessna 320. Both located at the approximate center of the cruciform of the wings and fuselage. One on top of the cabin, the other on the aircraft belly.

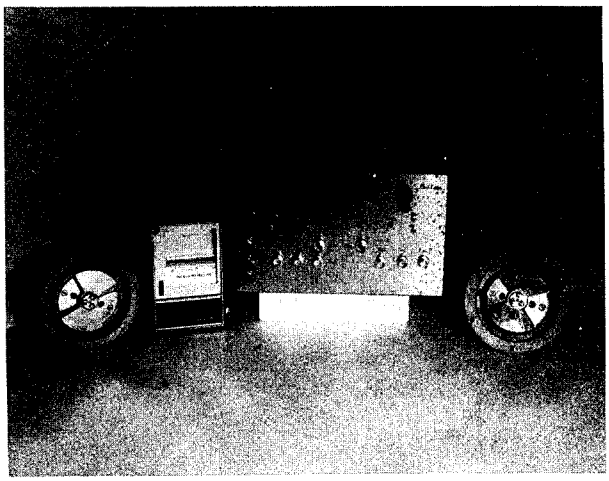

Figure 25 - Field Mill System

- The field mills were designed to sense a wide range of fields. The lowest range being on the order of ± 1 KV/M full scale, and the highest range being more than ± 100 KV/M.

Figure 26 - Field Mill Scales

Scale		Top Mill		Bottom Mill	
	Recorder	5 μa KV/M	50 μa KV/M	5 μa KV/M	50 μa KV/M
1		0.1	1.2	0.06	0.54
2		1.0	3.0	0.15	1.9
3		2.5	5.6	1.4	4.0
4		4.1	11.1	4.0	7.0
5		6.5	19.4	6.0	11.5
6		19.4	50.0	13.0	29.0
7		40.0	114.0	29.0	64.0
8		90.0	243.0	64.0	113.0

Calibration of the field mills was by conventional means. Two metal sheets, large compared to the field mill operature were spaced at a known distance. High voltage was applied to the sheets and metered by a kilovoltsmeter.

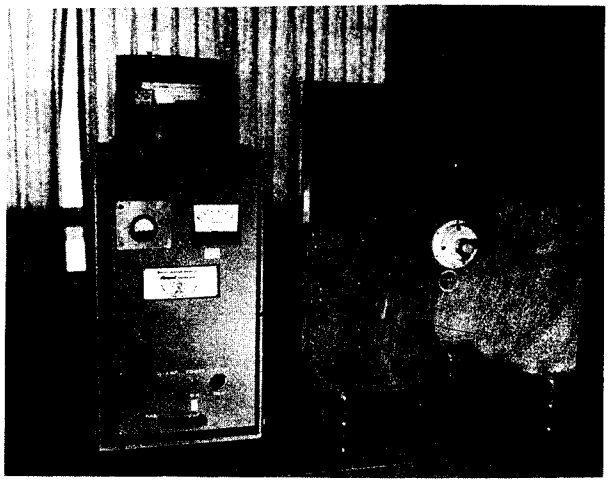

Figure 27 - Field Mill Calibration Equipment

Scales were chosen by a desire to have continuous interpretable data ranging from undisturbed earth's field of about 100 volts per meter, to values approaching the strongest fields expected in the vicinity of thunderstorms. It was also felt to be desirable to have an overlap between scales.

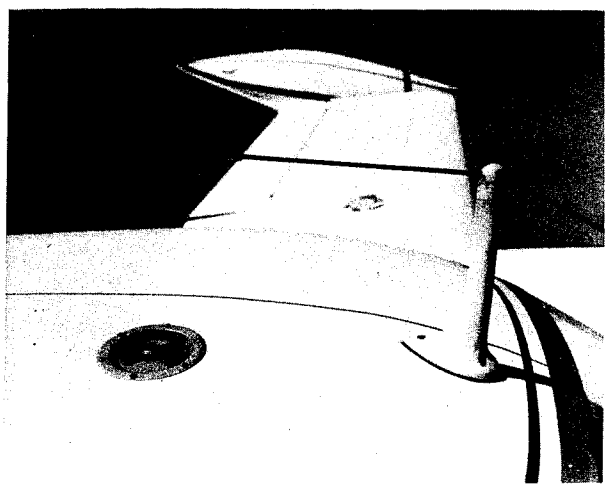

Figure 28 - Top field mill installed on aircraft.

FLIGHT TESTS WITH THE FINAL INSTRUMENTATION confirmed many of the suspicious generated in the early portions of the program. They also proved that aircraft charging is a much more common phenomenon than was previously suspected.

One aspect indicated by the field mills is that aircraft can acquire a charge, albeit small in present experience, even in apparently clear skies. Also, small cross field stresses can occur in apparently good weather. Generally these fields are on the order of a 1 KV/M and discharge currents only a fraction of a microampere.

Used in conjunction with the artificial charging system the field mills confirmed the effectiveness of the Micropoint dischargers in reducing the energy stored on an aircraft. As is apparent in Figure 27 the dischargers

act like field limiting devices through their ability to equalize the charging and discharging currents over a large range without a significant increase in the dc field strength.

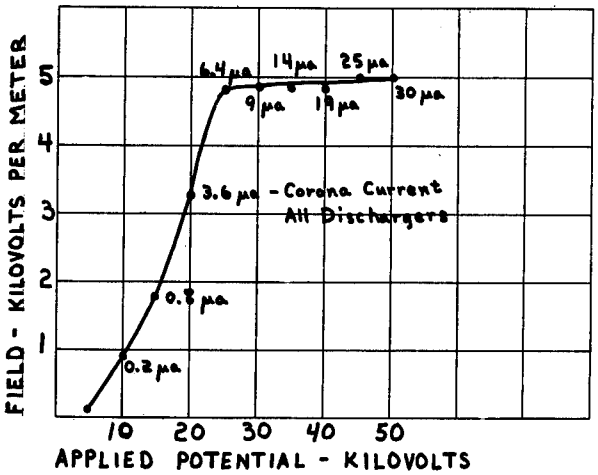

Figure 29 - Fields versus applied potential with dischargers installed.

The field mills also proved that cross field stresses are much more prevalent than suspected. Flights into typical strato-cumulus clouds indicated frequent cross fields of 5 KV/M opposing, between the mills. Such fields were usually brief, and resulted in brief discharge currents approximating those indicated in Figure 27.

The significant feature of these brief, but frequent, fields and currents is that they are of such a magnitude that even though they might not cause objectionable noise, they would cause short term desensitivation of VHF receivers. This of course referring to aircraft not equipped with sealed antennas and dischargers. Early in the flight test program before installing any instrumentation such occurances were encountered, but discounted as meerly annoying signal fades.

Flights through, under and in the vicinity of rain showers, thunderstorms, hurricanes and squall lines showed intense electrical activity. Precipitation in such events resulted in the field mills indicating the same field polarity. Cross fields were of extreme magnitudes and, though variable, frequently protracted. Precipitation in combination with cross fields only resulted in the top and bottom mills showing a difference in magnitude. In this sense precipitation acted much like an artificial charging system which is used to oppose a sensed field. The data certainly raises questions as to the effectiveness of active dischargers in cross field stresses.

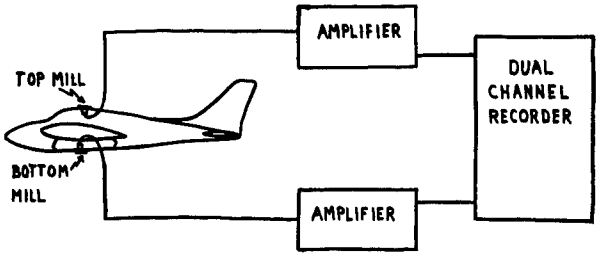

Figure 30 - Field Mill System

Cross field stresses of 5 KV/M to 50 KV/M were common. These resulted in total measured corona discharge currents from the dischargers of 20 to 1000 microamperes.

The propeller current transducer indicated an onset of propeller blade tip corona in field stresses of about 40 KV/M. At somewhere in the vicinity of a 100 KV/M field stress a single blade is discharging 50 microamperes of current, or a total of 300 microamperes for all six propeller blades, if symmetry is maintained.

At the higher levels of propeller corona current, noise prevented reception of an aural ADF signal. Though, surprisingly, a good bearing was maintained at a 50 nautical mile range from the Key West non-directional beacon, with a field stress exceeding 100 KV/M and the instrumented propeller blade exceeding a 50 microampere corona discharge rate. Total discharge current was not recorded, unfortunately, due to a fault in the instrumentation. On the Cessna 320, at least, the propellers do not appear to be as tightly coupled to the ADF and HF antennas as other extremities of the aircraft.

A review of significant data maximums obtained in flight to date is presented in Figure 31.

Figure 31 - Significant data acquired in flight test

Charge rate probe (2.838 square inches)	0.3 μa
Streamer current (left engine cowl)	40 μa
Discharger corona current onset	0.6 KV/M
Single discharger current	400 μa
Total discharger current	2,500 μa
Propeller blade tip current (one blade)	>50 μa
Artificial charging current @ 50 KV, 10,000 feet and 180 KTS TAS	37 μa
Bottom field mill	> + 64 KV/M
Top field mill	>- 50 KV/M
Difference between top and bottom mill	> 114 KV/M

No lightning strikes attached to the Cessna 320. Though there were frequently cloud to ground and cloud to cloud strokes occurring on all sides of the aircraft flight path.

ADDITIONAL TESTS ARE PLANNED prior to the conference in December. Flight tests will continue. A transport category aircraft will be instrumented as was the Cessna 320. Comparative data will be of interest.

A field analysis on a scale model Cessna 320 will be made for the purpose of translating field information to aircraft potential. Figure 32 is a picture of the conductively coated model to be used.

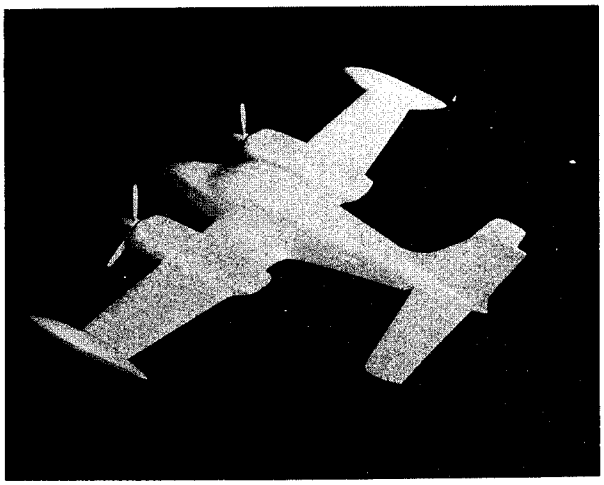

Figure 32 - Conductive scale model Cessna 320

The field analysis will be made in an electrolytic tank. As shown in Figure 33 electric field equipotential lines can be plotted.

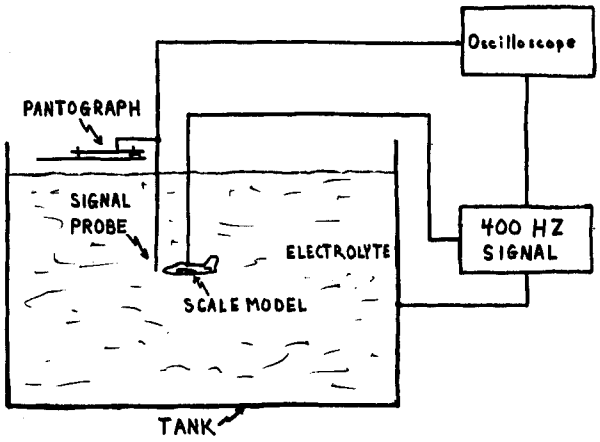

Figure 33 - Electrolytic tank field plotting

Another study was not completed in time for publication, however, the results are expected to be available for the conference.

It is well known that electrostatic noise can overload VHF receivers, causing loss of navigation data. There have been reports of erroneous course data when electrostatic charging occured. There has been a natural tendency to relate the events. An attempt will be made to introduce course errors, not easily identifiable as interference, as indicated in Figure 34.

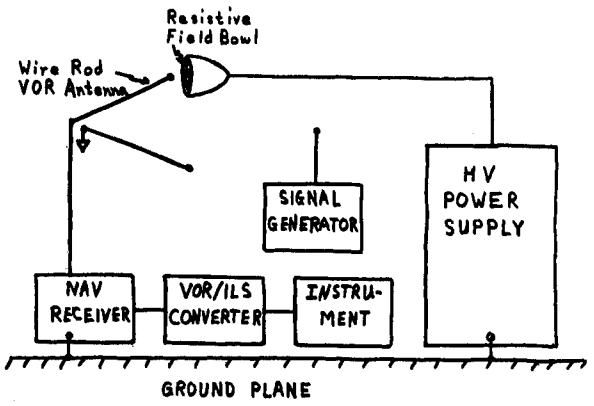

Figure 34 - VOR/ILS interference test

If significant data is obtained between the publication deadline and the conference an addendum handout will be prepared.

IN SUMMARY, proper installation of quiet dischargers and sealed antennas can significantly reduce electrostatic noise interference to General Aviation radio receivers. Electrostatic charging is much more prevalent than previously suspected. Charging and electrostatic noise can occur even though an aircraft is not in clouds or precipitation. And last, additional testing is needed to more accurately collate fields, discharge currents, propeller thresholds and noise levels.

CONCLUSIONS

1. Electrostatic charging during instrument flight conditions is very prevalent.

2. Cross fields are encountered in almost all cumulus type clouds, or in any cloud system containing turbulence.

3. Cross fields frequently reach extreme values in thunderstorms and rain showers for protracted periods.

4. Cross fields may be encountered in apparently clear skies, as well as in the vicinity of cloud buildups.

5. Propeller corona coupling to aircraft receiving antennas needs further investigation.

6. Electrostatic charging, and resultant corona, is sufficiently prevalent that receiver desensitivation is a common problem in instrument conditions.

7. A proper quiet discharger installation and use of sealed antennas can significantly increase General Aviation radio reliability.

8. Standards of electrostatic noise protection should be established for aircraft capable of IFR flight.

CREDITS AND ACKNOWLEDGMENTS

Assistance from the following persons during the conduct of these tests is gratefully acknowledged:

Mr. Harvey Hop - Southeastern Jet Corporation
Mr. Harold Green - Bendix Avionics Div.
Mr. Web W. Moore - Cessna Aircraft Company
Mr. John Robb - LTRI
Mr. James Stahmann - LTRI

Several pilots contributed freely of their time and skill, often under extremely adverse weather conditions when other aircraft were remaining on the ground. Much of the data acquired in this program would have been impossible to obtain without their assistance. Credit is especially due:

Ray Higgins - Burnside - Ott Aviation Training Center, Inc.
Bob Kajawa - USAF, Reserve

BIBLIOGRAPHY:

1. Ross Gunn, et al, "Army-Navy Precipitation Static Project," Proc. IRE 34, 4 & 5, (1946)

2. R. L. Tanner & J. E. Naveviez, "Radio Interference from Corona Dischargers," Tech. Report 37, Contract AF 19(604)-266, (1961)

3. R. L. Tanner & J. E. Naveviez, "Precipitation Charging and Corona-Generated Interference in Aircraft," Tech. Report 73, Contract AF 19 (604)-3458, (1961)

4. Corona Threshold and Its Effect on Precipitation Static Noise Reduction," Tech. Report 77, Contract AF 19(628)-325, (1963)

Electrostatic Charging and Noise Quieting

ADF	Automatic Direction Finder
AM	Amplitude Modulation
ATC	Air Traffic Control
COMM	Communication
db	Decibel
dc	Direct Current
GHz	Gega-Hertz (one billion cycles per second)
HF	High Frequency (3-30 MHz)
HV	High Voltage
Hz	Hertz (cycles per second)
IFR	Instrument Flight Rules
ILS	Instrument Landing System
KHz	Kilo-Hertz (1000 cycles per second)
Kts	Knots
KV	Kilovolts
KV/M	Kilovolts per meter
LF	Low Frequency (30-300 KHz)
Ma	Milliampere
MF	Medium Frequency (300-3000 KHz)
MHz	Mega-Hertz (one million cycles per second)
MSL	Meon Sea Level (altitude in feet above)
NAV	Navigation
rf	Radio Frequency
SSB	Single Sideband
TAS	True Airspeed
VFR	Visual Flight Rules
VHF	Very High Frequency (30-300 MHz)
VOR	Very High Frequency Omnidirectional Range
µa	Microamperes

SESSION 2C

MILITARY AIRCRAFT

Organizer - C. E. Seth

Aeronautical Systems Division (AFSC)

Chairman, C. E. Seth

700927

IMPORTANCE OF LIGHTNING PROTECTION AND STATIC ELECTRICITY DESIGN FOR MILITARY AIRCRAFT

E. R. Rivera

Naval Air Systems Command

(Paper not submitted for publication. For reprints, contact the author or the Society of Automotive Engineers directly.)

700928

Influence of Lightning and Static Electricity as Applied to Helicopter Design

B. John Solak, M.I.E.E.
The Boeing Company, Vertol Division

ABSTRACT

As recently as 1968 there was not a single case on record of lightning striking a helicopter and it was difficult to obtain funds to support a research toward development of lightning protection.

This situation changed in 1969-70. One helicopter was destroyed by a lightning strike, with loss of life; another was hit on the ground with substantial blade damage. So the interest in lightning and static electricity lost somewhat it's "academic only" stamp.

This paper reviews three basic domains of static electricity, affecting helicopter, namely:

1. Protection of the rotor blade against the effects of lightning strike.
2. Cargo hook operation and connected with it the problem of active equalization of potential between the cargo and the cargo handler.
3. Passive static electricity dischargers as a method to radio interference reduction.

All three domains affect the whole blade design with emphasis on the design of the blade tip.

PROTECTION OF THE ROTOR BLADES AGAINST THE EFFECTS OF THE LIGHTNING STRIKE

IF WE CONSIDER that the chances of a lightning hitting the helicopter are basically omnidirectional, due to the known mechanism of breakdown of the air by the streamers, we can conclude by inspection that the greatest potential gradient occurs at the blade tips and the chances for the blade tip being hit are obviously predominant. The two helicopters which were hit, were hit on the blades, which for the moment being constitute a "statistical" chance of 100%. We have therefore to analyze the design of the blade. If the blade spar is metal, e.g. steel, it will provide sufficient conductive path*. It is however seldom, that an equivalent metal path is provided from the metal tip cover to the spar, or that a metal tip cover is provided. Let us hope that the AFCS DH1-4 will enforce such provisions. Thus the problem of the metal spar blade will be solved to a

*In excess of equivalent 40,000 circ mils Cu, required by MIL-B-5087B and the Amendment to AFSC Design Handbook DH1-4 "Electromagnetic Compatibility".

large extent (except for floating metal honeycomb, discussed below). (See Figure 1a)

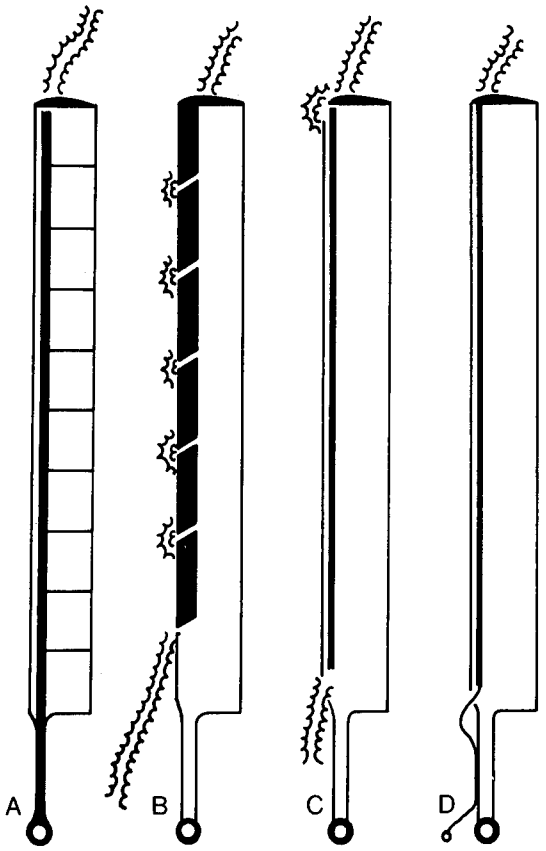

Fig. 1 - Electrical Schematics of Helicopter Blades

If the main spar is plastic, e.g. fiberglass, there are three possibilities:

(a) The abrasion strip on the leading edge is metal (see Figure 1b).

(b) The abrasion strip is metal on the outer portion of the blade and plastic on the inboard portion.

(c) The abrasion strip is plastic in it's entire length (see Figure 1c).

In the first case, the metal is insufficient to provide 40,000 circ mils equivalent copper path due to 50 to 100 times higher specific resistivity of the metals with high abrasion quality. Some experiments conducted by the Helicopter Division of Messerschmitt-Bölkow-Blohm Company in Germany have shown that an average lightning (10 to 30 KA) will damage the abrasion strip insignificantly. A heavier one (100 to 150 KA) may break the chemical bond, but will not constitute a "safety of flight" problem. So the blade designer for the helicopter company is faced with two alternatives:

(a) Prove to the procuring agency by actually conducting 200 KA strikes, that the extent of debonding does not constitute "safety of flight" problem, that the economic loss of a blade is very remote and ask for waiving the 40,000 circ mils Cu path. If he wins, everything is fine - if he loses, he will have

(b) to provide the 40,000 mils Cu path.

It is the opinion of the blade designers that placing a copper path (0.032 square inch cross section) under the abrasion strip would not affect the blade in any way other than costwise and the weight placed so far forward chordwise would be beneficial. If we could provide a copper path, which would match the mechanic and thermal differences of metal and fiberglass the problem could be solved. This is however not an easy matter and probably will require segmenting of the metal. The inboard end connection to the hub would be neglected. The lightning would bridge the gap through the air. The specification requirement to bond the blade to the hub would have to be waived, based on actual tests with a blade and a simulated lightning.

If however, the whole blade is plastic, special attention must be paid to the metal balancing rod inside the blade (see Figure 1c). There is no evidence whether the lightning will seek out such rods and to the knowledge of the writer, no experiments have been conducted. Let us consider the case of the balancing rod, electrically floating inside the fiberglass spar. Let's consider for example a BO-105 blade of original fully plastic design of 180 inches length. Extrapolating standard IEEE Tables for Dielectric Tests the air gap of 180 inches would break down under 2 Megavolts approximately. The dielectric strength of fiberglass is of the order of 1000 Volts per mil. The 2 Megavolt voltage would correspond to 2

inch thickness of fiberglass. This crude comparison which omits electrical stress concentration and streamer mechanism of breakdown is intended to indicate that the possibility of the lightning seeking out the "floating" metal balancing rod should not be dismissed. What are the choices then? The equivalent copper cross section of a balancing rod (lead) is of the order to 10,000 to 30,000 circ mils. An addition of a copper core and assuring good electric contact with the blade end cup could solve the problem. There is however, one more precaution - the lightning should be "let out" from the balancing rod on the inboard end, either by providing a suitable pigtail to the hub or just drilling a hole, through which the lightning current can take to the air without breaking the fiberglass (see Figure 1c & d).

PROTECTION OF TRAILING BOXES OF THE BLADES

SO MUCH FOR THE SPAR and copper path from the blade tip to the hub. Now let us concentrate on the trailing box. Here again we have several alternatives. Let's first consider a fully plastic blade and discuss the problem in general terms.

Years ago it was the accepted thinking that a blade can be "stitched" by the lightning, as it cuts the ionized lightning channel. If one considers the shortest time interval between the lightning strikes (as given by Reference 4) to be equal to 3 milliseconds and the speed of blade tip of 700 ft/sec approximately, the stitching distance could be of the order of few inches. However, for average time intervals of 40 milliseconds the distance between stitches would be of the order of several feet, whereas on metal structures the "stitches" are usually a few inches apart. The experiments conducted by Boeing (Reference 6) seem to indicate that the "stitches" are successive points of reattachment of the arc to the metal surface. If this surface is plastic, it is most unlikely that any arc could attach, let alone reattach itself. It seems therefore that the problem of "stitching" is peculiar to metal surfaces only. So instead of asking ourselves the question: "Can a plastic blade be stitched?" We must ask another question: "Will a fully plastic blade be ever pierced?"

Comparing rough estimates of inductive voltage drop around the half of the blade versus dielectric strength we will find both voltages roughly of the same order of magnitude. If the electrodes are brought to within inches from the blade surface the simulated discharge will go through the blade, rather than around it as has been proven by the Helicopter Division of MBB Company in Germany. Whether a plastic blade will ever be pierced by a discharge of the order of a few yards, we don't know. It would be interesting to conduct an experiment with electrodes yards apart and voltage rises more closely representing the actual conditions in nature. In most experimental arrangements the voltage rise time from zero to full value is of the order of 1 microsecond. In Reference 8 it is pointed out that the rate of voltage rise should be of the order of 24 KV/ microsecond for the studies of lightning stroke, for close approximation of what happens in nature.

So here is one more experiment required and of interest to any plastic blade designer.

On the other extreme of the trailing box design is the plastic skin trailing box with a metal honeycomb. Reference 7 points out, based on the actual experiments, that a metal honeycomb with its sharp edges and electrical stress concentrations presents a very difficult problem indeed. There are two basic alternatives possible:

(a) Honeycomb inside blade with a plastic spar and plastic skin.

(b) Honeycomb in a blade with a metal spar and plastic trailing box skin.

(a) ELECTRICALLY FLOATING HONEYCOMB (See Figure 2) - The peculiar problem was first noticed as the results of tests conducted in 1964 and reported in Reference 7 in 1965. It failed somehow to arouse the concern which it deserved. The problem is restated as follows: The lightning "ignores" the metal path and takes the path through the insulation twice and through the honeycomb (Figures 2b and 2c). An attempt was made to explain this phenomenon by electrostatic induction as

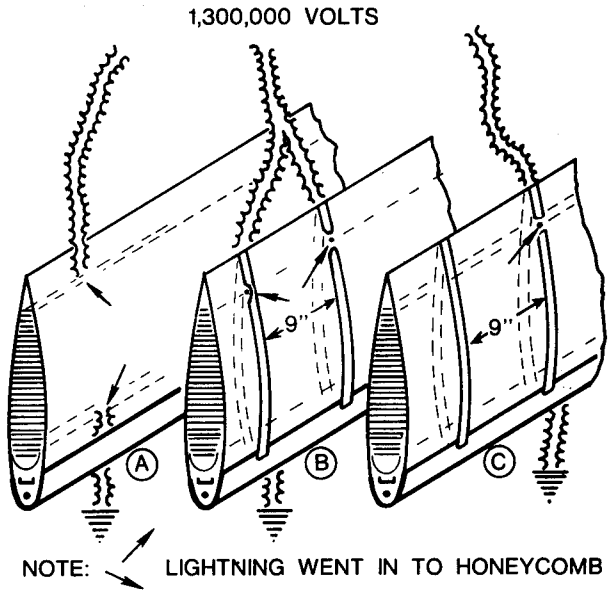

Fig. 2 - Simulated Lightning "Ignores" Metal Strips, Enters Honeycomb

shown in Figure 3 but since 1964 no experiments were conducted to discover what can be done to protect the "floating" honeycomb.

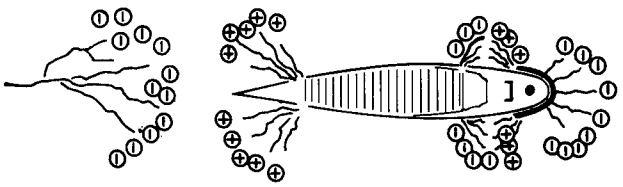

Fig. 3 - Probable Mechanism of Lightning Entering Aluminum Honeycomb

It seems that the voltages induced in the electrically floating honeycomb produce the piercing of the fiberglass skin, so to say "inviting" the strike to take the path through the honeycomb, inspite of the partial Faraday's cage, formed by aluminum strips (see Figure 2). Here a full Faraday's cage, formed by spraying a continuous metal skin on the blade comes to mind. Questions still unanswered are:

(1) Will rounding of honeycomb corners alleviate sufficiently the streamer formation on honeycomb to the extent when a partial Faraday's cage will suffice?

(2) How thick must be the metallization to prevent the lightning from leaving the metal skin and entering the honeycomb? In lightning tests of a blade trailing boxes made of aluminum alloy sheet, the Helicopter Division of MBB Company in Germany obtained a passage of the lightning similar to a bullet passage. Prospects are not encouraging, but experimental data are missing for aluminum spray.

These are the questions which will be equally valid for skins made of boron and carbon filament composites or thin titanium skins on the panels of modern aircraft, containing metallic honeycomb.

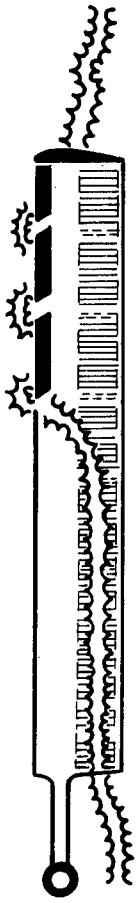

Fig. 4 - Blade Design with Accentuated Lightning Danger

In view of what was said above on honeycomb protection, applies to the rather remote chance of a lightning

striking the blade on the trailing box, rather than on the tip. If however, a hypothetical blade would be contemplated, which would have a plastic spar and a plastic skin, with metal honeycomb, we are really asking for trouble (see Figure 4). The lightning would go through the entire length of honeycomb and split the blade wide open. In view of the fact that we know too little about honeycomb protection a design of such a blade should be approached with extra caution.

(b) METAL HONEYCOMB IN A PLASTIC TRAILING BOX AND A METAL SPAR BLADE (See Figure 5) - If we apply the same

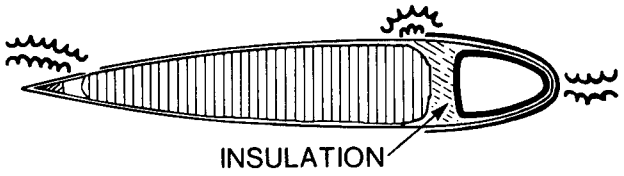

Fig. 5 - Proposed Protection of the Metal Blade Spar

deduction to this type of design, we see the same problem of metal honeycomb plus an additional problem: "will the lightning go through the skin and to the leading edge or will it go into the spar, producing pitting?"

Pitting of the blade spar will not be a "safety of flight" item, but will be a problem of replacing the blade due to pitting of the main spar. Maybe an extension of the abrasion strip over the honeycomb and/or insertion of fiberglass insulation between the spar and honeycomb should be contemplated. Here again no experimental data are available.

If the strike is of the average intensity say 10 KA to 50 KA, the delamination of honeycomb box will be small, few square inches approximately, but if a strike is of the order of 150 KA to 200 KA, a delamination of a square foot area and balling the honeycomb under magnetic forces will occur. This won't destroy the helicopter, but will probably force it down due to severe vibrations.

Flying of unprotected metal honeycomb has another unpleasant aspect. Even when the discharge is very weak, e.g. a severe corona without actual lightning strike, pin holes will appear through which water will accumulate inside honeycomb cells, ultimately debonding them.

CARGO HOOK OPERATION

AS IT IS KNOWN, much confusion exists and much work has been done on this problem and a discussion of the fact, that spark discharges to personnel, fuel and ammo constitute a real danger, would be superfluous. Let's concentrate on the problem of Earth gradient and triboelectric charging separately.

(a) EARTH'S GRADIENT - Let us first consider a helicopter whose blades would not produce triboelectric charging, let us neglect the exhaust charging and concentrate on the Earth's electric field gradient exclusively.

The Earth surface is 300,000 V to 400,000 V negative with respect to ionosphere. Typical potential gradient is 100 V/meter (Reference 2) in the absence of clouds.

Let us assume a simplified situation: Under steady state condition the equilibrium of electrostatic field will

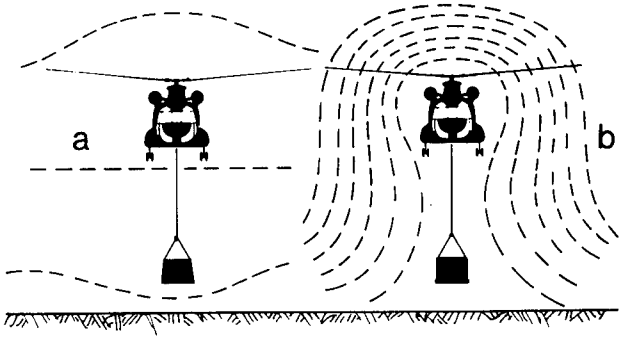

Fig. 6 - Equipotential Surfaces With and Without Active Discharger

be reached in few seconds and the Figure 6a gives a fairly close approximation of the situation on "cargo + helicopter" conductor. The voltage to ground on this conductor will be of the order of 1000 V, capacity of the order of 1000 to 1500 pF, and the person touching the cargo will get approximately 0.5 milli Joule discharge which most probably he won't notice. This is an everyday experience in cargo handling. Under clear sky we have no problem worth speaking of.

If we now assume the presence of a Cu Nimb cloud overhead, the gradient can be positive or negative and its value can reach 20,000 V/meter under large Cu Nimb. The voltage difference between cargo and ground across the 5 ft. gap can be of the order of 100,000 V to 250,000 V with energy levels of 4 to 30 Joules. This is obviously dangerous. The question is, what can we do about it? Again assume an ideal active discharger, which would bring the voltage between the cargo and the ground to zero and keep it that way. The field will look now as shown on Figure 6b. There is quite a voltage gradient on top of this structure and the Figure 7 shows what can happen (Reference 3). So here is a limit, how

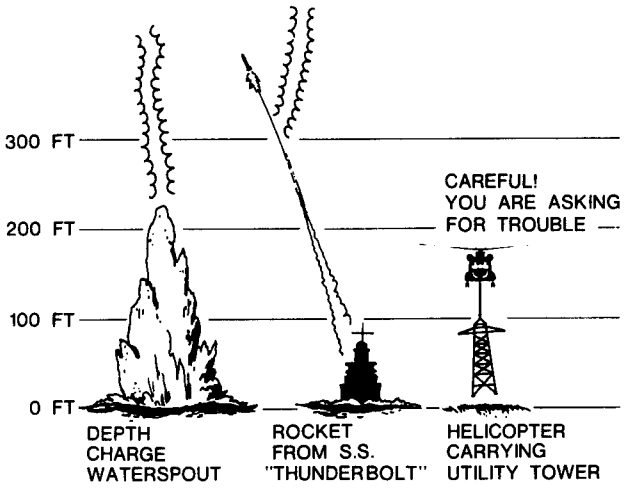

Fig. 7 - Comparison of Triggered Lightning Strikes

far we can go with the business of active discharging even if we finally will get an active discharger, which will work. For the sake of being impartial it must be pointed out that Figure 7 presents too gloomy a picture for the cargo carrying helicopter. The water spout and the rocket have cut through the equipotential surfaces within a second - whereas a helicopter will move in the field gradually. The corona current, leaving both ends of the conducting structure will blunt the potential gradient and ease the danger. Here the experiments conducted by Kaman Company should be mentioned. A long wire was lifted to a few thousand feet without any mishap, but the precautions to guard against any abnormal gradient were strictly observed. On the other hand, Apollo 12 with it's conducting exhaust plume of approximately 1800 ft. (Reference 3) was hit twice when launched through a thermal buildup.

(b) TRIBOELECTRIC CHARGING - Now let us assume completely normal Earth's gradient, say 100 V/meter, no clouds, and concentrate on triboelectric charging. From experience we know that the voltage on cargo under dry snow or dry sand conditions can reach 1,000,000 V approximately with energy levels of the discharge way in the tens of Joules area. We also know that dynamic discharge rate of 100 to 200 microamps would cope with the triboelectric charging. Why then up until now we do not have a completely satisfactory system? The problem reduces itself to two difficulties:

(1) Field Sensing

(2) Recirculation of the discharge current to the helicopter.

Let's consider them one at a time:

(1) FIELD SENSING - The field mill, used to sense the accumulated charge is the known device which measures the field strength: $E = \frac{dV}{dl}$ where E is the electric field, $\frac{dV}{dl}$ is the differential with distance of the potential field. Now let us look at the helicopter with and without the discharger; assuming that the discharger does the job.

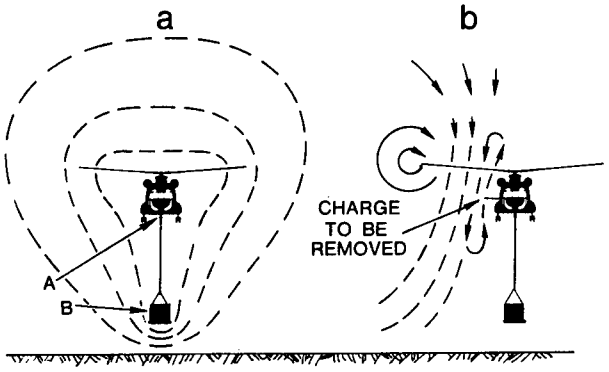

Fig. 8 - Charge Sensing and Active Discharging Schematics

As you can see in Figure 8, by the very nature of things the field mill is situated in the area of a low $\frac{dV}{dl}$, hence

it has a very low sensitivity. To make the problem worse, there is apparently a time lag between the discharge leaving the helicopter and the field mill sensing it, as evidenced by the control loop becoming unstable, oscillating between positive and negative discharge currents. The obvious answer would be to place the field mill on the cargo in the area B, this solution is however logistically impossible. So we are left with the problem of finding the best sensor location taking full precautions when using multiple cargo suspension, which will create a partial Faraday's cage. No successful solution is known. Now let us concentrate on the discharge which is easier to assume than to achieve.

(2) RECIRCULATION OF THE DISCHARGE CURRENT (Figures 8b and 9) - In order to clear the turbulent air flow along the fuselage and avoid recirculation of the

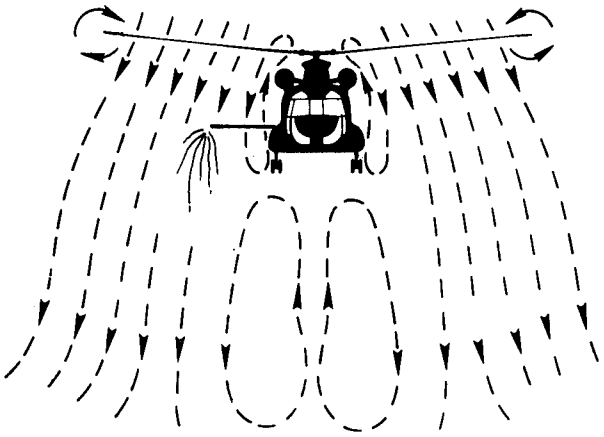

Fig. 9 - Recirculation Problem in Active Discharging

discharge, the discharging probes should reach far out, too far for comfort and logistics. An attempt was made to blow the charges away by placing the discharge probes inside the exhaust plume but the temperature of this gas is too high. The gas is conducting and the idea didn't work.

So we see another tempting alternative location - somewhere near the blade tip and we will come back to this idea after discussing the passive discharging.

Let us however discuss one more point namely - how much good can the active discharger do us for inflight dissipation of charges, to prevent radio interference? Here the situation is radically different than in hover, both in the way of charge sensing and recirculation. The sensor located on the

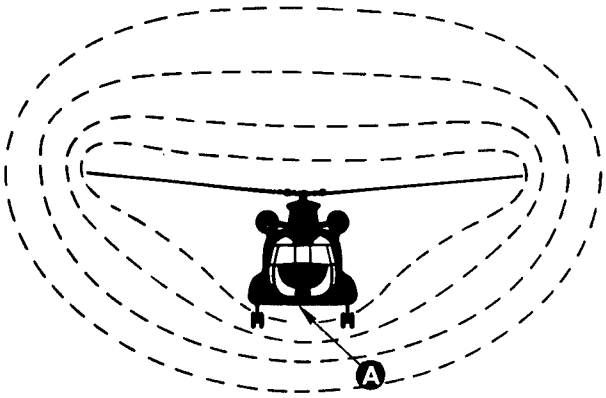

Fig. 10 - Equipotential Surfaces Around Charged Helicopter High Above the Ground

underside of the fuselage will be relatively sensitive (see Figure 10) and the flow of the air along the fuselage in forward speed is sufficiently organized to carry the charges away from even short discharge probes, provided they are located in the aft portion of the fuselage. This seems to be borne out by the experience of the Dynascience dischargers on New York Airways helicopters.

PASSIVE DISCHARGING

THERE ARE TWO CONDITIONS when static electricity will produce brush discharges from any sharp corner of the helicopter:

(a) High gradient under the thunderheads, or

(b) High triboelectric charging.

The second condition is much less severe until we come to hover, and then we can live with the static interference to nagivation equipment. We know where we are. What really brings the static discharger into the limelight is the introduction of low frequency navigational grids. In the Decca operation of the New York Airways the problem of interference was severe enough to dictate the installation of the active and passive dischargers. The actual flying experience has shown that both active and passive dischargers did help, but under severe charging conditions the

active dischargers were more effective. The passive dischargers tested for alleviation of cargo hook operations by another agency, did not produce the desired results, for reasons explained in Figure 11.

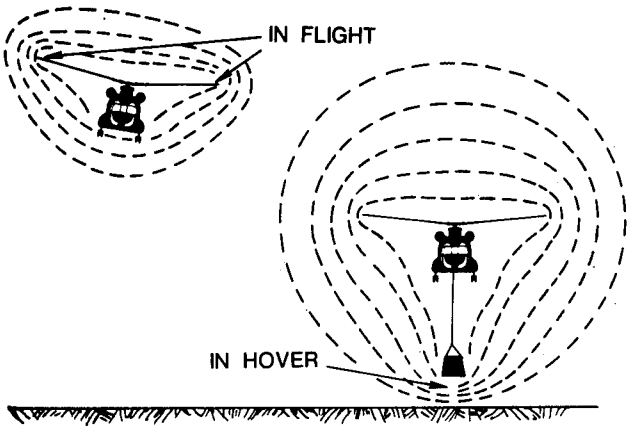

Fig. 11 - Optimum Location of Passive Dischargers High Above the Ground and in Hover

The obvious location would be at the blade tip. In Reference 7 a centrifugally extended passive discharger of the Granger Associates type was suggested to be located on the trailing edge (Reference 7). In discussions with M. Gerstine and D. Hoffstedt at Boeing-Vertol an idea was advanced to have the dischargers on the blade tip and combine them with the active discharging on the either/or basis. The discharger could be "locked-retracted" for the duration of a flag tracking. The high voltage generators would have to be located at the blade tip. So it seems that all attempts to solve the problem converge on the blade tip design which brings us to the concluding portion of this paper. However, before closing the subject, consider what triboelectric charging can do on a plastic skin. Pockets of charge will be created, which ultimately will discharge to the nearest metal if such is available. If not they will seek out the metal honeycomb and produce pin holes. It becomes obvious that if we want to solve the problem of radio interference, the surface of the blade must be conductive. Not much is needed, 1 M ohm per square will do, but it must be there if we want to bring the triboelectric charge to the passive dischargers without flashovers on the blade surface and connected with it radio interference and pin holing the plastic skin. Whether the whole plastic surface must be covered, or the leading edge plastic only, is not quite clear at present.

CONCLUSIONS - It seems obvious that all three discussed domains: lightning protection, active and passive discharging - converge on the blade tip design. A blade tip however, is a very sensitive design area where accelerations of the order of 700 g make every little detail complicated and difficult. So once a blade is designed and tested it is very difficult and very expensive to add any after-thoughts and incorporate ideas - no matter how necessary. The blade tip design should incorporate a metal cap with a bond to the metal path, there should be an active discharger combining the duties of a passive discharger or some purely passive dischargers. Unless we start thinking about such an integrated blade tip design now, and have it ready for any new blade design, the solution of static electricity problem on helicopter will be relegated to yet another generation of blades.

ACKNOWLEDGMENTS

The writer is indebted to:

Mr. John D. Robb, Lightning and Transient Research Institute for critical review and correction of this paper.

Mr. Charles E. Seth, AFSC Wright-Patterson Air Force Base;

Mr. George Hackenburger, Kaman Aircraft Corporation;

Mr. I. A. Brunsch, Messerschmitt-Bölkow-Blohm Company;

for supplying experimental data and technical reports, referenced and used in this paper.

REFERENCES

1. "The Electrostatic Charging and Discharging Phenomena of Helicopters in Flight" by G. Born, R. Creed, E. Sharkoff and E. J. Durbin.

2. RAE Report 67292, November 1967 "Interim Report Reviewing the Present Position on Helicopter Static Electrification Hazards", by M. E. Rogers.

3. Naval Research Reviews, April 1970, "Lightning and Rockets: Some Implications of the Apollo 12 Lightning Event", by M. Brook, C. R. Holmes and C. B. Moore, New Mexico Institute of Mining and Technology.

4. "Lightning" by M. A. Uman (McGraw-Hill), Westinghouse Research Laboratories, Pittsburgh, Pennsylvania.

5. "Tests of Ortho-Decoupled Aircraft Static Dischargers", by R. L. Tanner and J. E. Nanevicz, Stanford Research Institute, Menlo Park, Calif.

6. Boeing Report D6-24398 "Lightning Effects to Non-Metals".

7. "The Influence of Lightning and Static Electricity on Helicopter Design", by B. J. Solak, IAHS, February 1965.

8. Journal of the Franklin Institute, June 1967, Special Issue on Lightning Research.

9. Lightning Susceptibility of HH-43B Helicopter Blades by J. R. Stahmann and J. D. Robb, AFAL-TR-70-76 March 1970.

10. Lightning Vulnerability Measurements on Selected Metal and Non-Metal Helicopter Rotor Blades and Hub Assemblies, by J. R. Stahmann, AFAL Contract F33615-70-C-1256 to Lightning and Transient Research Institute.

11. Investigation of C-54A Electrostatic Charging and of Active Electrostatic Discharge Capabilities by M. C. Becher, Dynasciences Corp., USAAVLABS Technical Report 69-90, Unclassified, U. S. Army Avionics Material Laboratory, Fort Eustis, Virginia.

LIGHTNING PROTECTION FOR NON-METALLIC ROTOR BLADES

J. R. Stahmann
Lightning & Transients
Research Institute

G. I. Hackenberger, Jr.
Kaman Aerospace Corp.

ABSTRACT

This paper discusses general approaches to the design of lightning protection system for non-metallic helicopter rotor blades. Possible effect of stroke currents on conducting parts external and internal to the blade are mentioned, and general recommendations are made for disposition of protective materials. Testing of any such design is considered a necessity. A specific example is described, tracing the development of the protective system for one particular non-metallic rotor blade.

HISTORICALLY, THE HELICOPTER has been much safer from lightning stroke danger than other types of aircraft, but a helicopter pilot being overtaken by an ominous front is less concerned with statistics than with an aircraft which can survive a stroke. The rotor blades, because of their geometry, represent a high-probability target if a helicopter is struck, and blades of all types, metallic and non-metallic alike, have been shown to be vulnerable. This paper will treat some of the basic approaches to lightning protection for non-metallic blades, and will cite a specific example of the application of these techniques.

While the basic spar and skin structure of a nonmetallic blade is nonconducting, the nonmetallic classification does not exclude the use of internal and external metal parts. For example, the blade may have a metal erosion cap on its outboard leading edge and internal metal control linkage with metal mounting brackets. When a lightning discharge contacts the blade, the metal parts may become part of a lightning stroke current path. Their influence on possible discharge paths must be carefully analyzed and investigated. Their size, conductivity, type of material and position in relation to other metal parts must be considered. They do not necessarily increase the lightning hazard to the blade, but may offer some protection. For example, a metal erosion cap, of large enough cross section, provides spanwise lightning protection, as well as reducing erosion.

In general, lightning current paths should be provided on the outside surface of the blade, since arcing inside the blade could permit explosive pressures to build up from vaporization of internal material. To provide a continuous current path to the hub without arcing, the external metal parts should be bonded together. The erosion cap, which is used only on the outboard portion of the blade where the velocities are highest, must be electrically bonded to the hub. It is also generally desirable to bond the internal parts to the external protective system to prevent internal arcing. When the internal parts become a parallel part of the lightning current path, they must be capable of carrying their portion of the discharge current. If feasible, internal current paths can be prevented by the substitution of nonmetallic internal parts for those made of metal.

The lightning protection scheme for a nonmetallic blade should provide a good conducting path for the lightning current from blade tip to hub, incorporating any existing external metal parts and providing additional bonding and shielding conductors. A good external system, taking advantage of the dielectric strength of the skin and internal air insulation, can prevent puncture to internal metal parts. A typical protection scheme might consist of spanwise conducting strips on the leading and trailing edges of the blade, with chordwise strips in between for midchord protection. The distance between the chordwise strips is a

function of the surface "flashover-without-puncture" distance for the skin material used. Closer spacing usually would be required over internal metal part locations. In general, protective schemes must be checked under simulated lightning conditions to reveal any weakness overlooked.

A typical simulated lightning discharge, directed toward midchord on a blade, is shown in Figure 1. Strokes were also directed over the surface of the skin, Figure 2, to simulate attachment of a stroke to the leading edge erosion strips followed by the stroke sweeping over the blade surface due to the motion of the blade. Such strokes reveal possible susceptibility of skin material to puncture. In the study of large, completely nonmetallic blades, with no spanwise metal parts, it is important to direct a stroke spanwise the full length of the blade. For a long blade a very high voltage is required for this purpose.

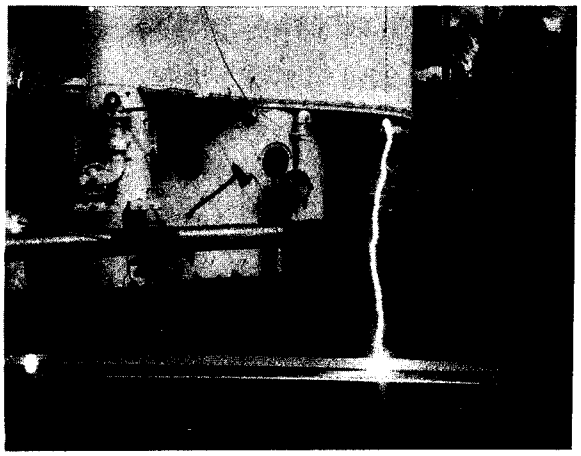

Fig. 1 - Stroke to rotor blade at midchord

Where conducting paint is substituted for conducting metal strips, the strips may continue to function by particle-to-particle arcing, as illustrated in Figure 3, even after the strips are partially vaporized. However, protection schemes using conducting paint must be checked carefully for effectiveness after an initial simulated lightning contact.

Composite blades, using boron or graphite epoxy, may be especially vulnerable to lightning damage due to possible high current flow in the conducting fibers. Thus this type of blade should be carefully checked for both explosive damage and possible deterioration of mechanical strength.

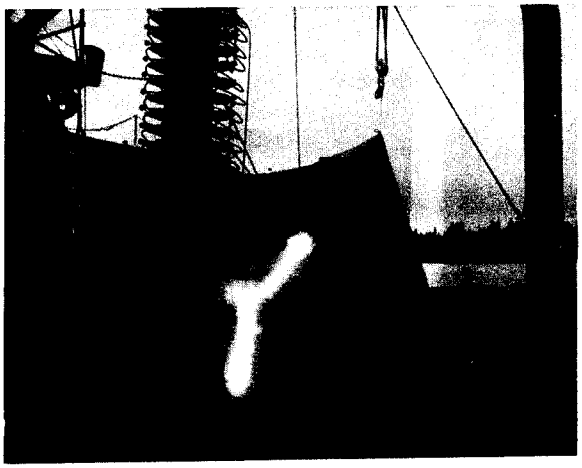

Fig. 2 - Simulated swept stroke

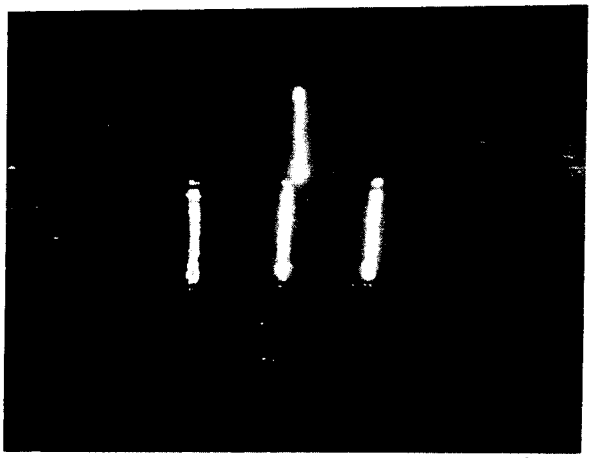

Fig. 3 - Particle-to-particle arcing in conductive paint

A SPECIFIC APPLICATION

Several generalized approaches to lightning protection for non-metallic rotor blades have been discussed. It will be shown here how one of these methods - conductive paint - was applied to provide an improved system of lightning protection for the rotor system of the HH43B/F helicopter.

THE AIRCRAFT - The HH43B helicopter is shown in Figure 4 . It is a turbine powered synchropter having two counter - rotating main rotors, each of which has two blades. Rotor diameter is 47 feet. The pilot's flight controls are mechanically connected to servo flaps, one on each blade trailing edge, which control the aircraft.

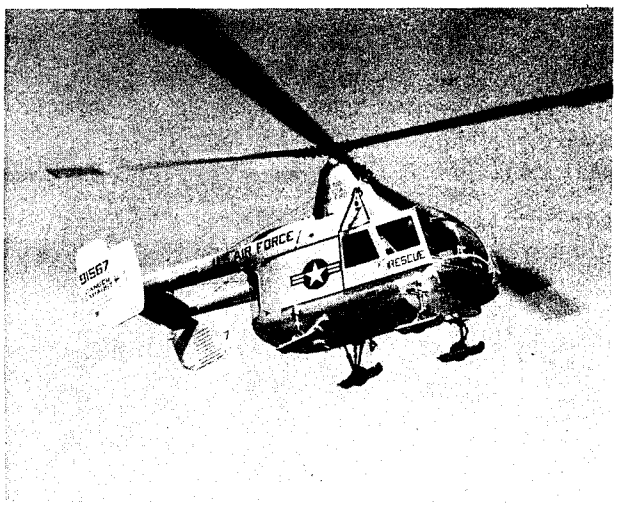

Fig. 4 - HH43B helicopter

The rotor blade is of wood and fiberglass composite construction, as shown in Figure 5. The spar, skins, and ribs are of fiberglass and/or wood. A fiberglass and wood root end is bolted to a metal retention which forms the connection to the hub. The outboard portion of the leading edge is covered by a stainless steel erosion guard, adhesively bonded. A metal control linkage runs within the blade, extending from the rotor hub to the flap, which is of composite fiberglass and wood construction, similar to that of the blade. A metal cable runs within the flap leading edge.

Prior to installation of the protective system to be described, the electrical configuration of the blade was as shown in Figure 6. The outboard steel leading-edge erosion guard was electrically isolated. The metal control rod, with its associated cranks and linkages, provided electrical continuity from the airframe out to, and through, the flap leading edge. The metal retention at the root had continuity via the hub to the airframe. Otherwise, the blade was non-conducting.

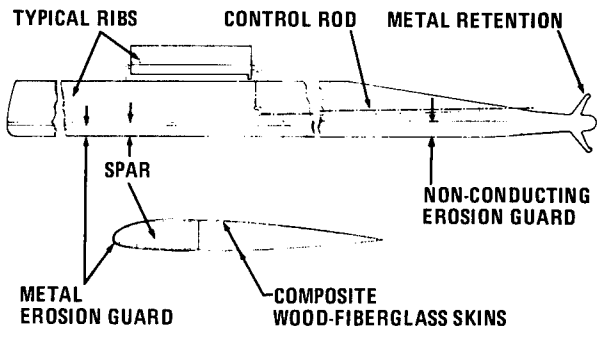

Fig. 5 - Rotor blade construction

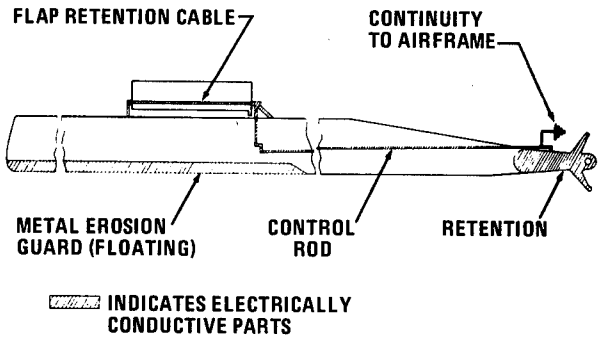

Fig. 6 - Blade electrical configuration

THE PROBLEM - In a previous series of lightning tests on these blades, conducted by Lightning and Transients Research Institute, it had been shown that any penetration of the blade skin by a lightning stroke might produce sufficient internal pressure to cause destructive damage. These tests had also shown that the threshold of breakdown between the blade skin and the internal metal control rod was about 180 KV. Thus the functional requirements for the proposed protective system could be defined as:

(a) Prevent any pentration of the skin by lightning stroke currents, and
(b) Limit the development of a potential (by induction or otherwise) between skin and control rod to values under 180 KV.

A decision was made at the outset that a two-pronged approach would be undertaken:

(1) Develop a protective system which could be installed at field level to provide the greatest possible improvement in lightning protection consistent with field application, and

(2) Simultaneously develop a system which could be incorporated during factory overhaul of blades which could provide protection against a stroke at about the 99th percentile of all natural lightning strokes.

In order for any protection system to be feasible, particularly one intended for in-the-field incorporation, it had to live within certain constraints, including the requirements that blade weight and mass balance not be materially altered, and that the aerodynamics of the blade not be adversely affected. Conductive paint had been shown to be effective protection in other applications, and was attractive in this case from the weight/balance/aerodynamic standpoint, and was tentatively chosen as a basis for the proposed system, subject to test verification.

THE DEVELOPMENT - A series of test panels was prepared and subjected to simulated lightning strokes. The test panels were representative of various parts of the blade, protected with several configurations of conductive paint, and included control samples without conductive paint. The results of this test series indicated that the conductive paint successfully protected certain panels, while similar panels, lacking the paint, were damaged or destroyed. It was also shown that repeated strokes followed the same general path across the protected test panels, although the conductive paint was no longer apparent to either the eye or the ohmmeter. Results were sufficiently encouraging to justify the preparation and test of complete blades.

Two protective systems were designed. One, the prototype of the system for field application, was based upon conductive paint. The other, the functional prototype of the system for factory incorporation, employed conductive paint augmented by metallic conductors secured to the exterior of the blade. One complete blade was prepared in each of these two configurations, for lightning testing. In both cases the conductive paint was applied as an additional step in the normal finish schedule, and a final finish coat of conventional pigmented non-conductive paint was applied on top of the conductive paint.

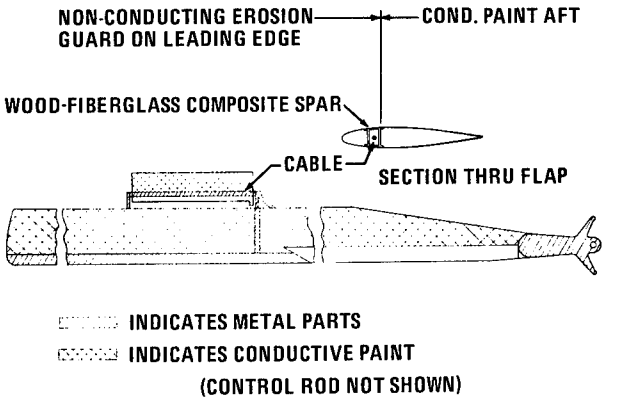

Fig. 7 - Protective system for field application

When the first of these blades was exposed to high-voltage low current (11 to 14 Ka) exploratory strokes to the outboard skins, evidence was noted of small imploded areas, penetrating the skins. This was attributed principally to the confining effect of the outer layer of pigmented paint upon the conductive paint beneath when the latter was vaporized by the lightning current. A secondary cause was felt to be current concentrations caused by the configuration of the conductive paints, which had been applied in a striped pattern. Accordingly, both blades and flap were refinished to assure that the overburden of pigmented non-conductive paint was not excessively thick, and to provide an overall conductive paint covering in those areas which had previously been striped.

The blade incorporating the field application protective system was tested first. Its configuration as finally tested is shown in Figure 7. Streamer patterns were obtained indicating locations of highest lightning strike probability; Figure 8 is typical.

Fig. 8 - Streamer patterns - flap region

These confirmed the supposition that the trailing edges of the blade and the flap, being essentially sharp corners and edges, would show the highest streamer concentration.

During subsequent testing a thorough exploration was made for vulnerability by directing high voltage strokes to all areas of the blade and noting the points of lightning stroke attachment. Deliberate attempts were made to cause stroke penetration to the control rod and to the flap leading edge cable, by positioning the surfaces relative to the electrode for the highest probability of penetration. This series of test strokes included simulation of a swept-stroke, in which a blade might fly into an existing stroke channel. No penetration occurred.

Voltage developed between the blade skin and the control rod was measured. This voltage results from induction in the rod by currents flowing in the skin, and therefore the current rate-of-rise is significant. The inductance of the blade was sufficiently high to prevent the desired 100 Ka per microsecond current rate-of-rise, but the test results were corrected for this factor, and the resulting corrected voltage was found to be less than 40 KV, safely under the 180 KV breakdown threshold previously established.

High-current strokes were directed to the blade in those areas established by previous testing as most probable stroke attachment locations. Currents of 140 to 160 Ka were obtained. The only significant damage produced was several cracks in the flap skin as shown in Fig. 9. Control rods and cranks still operated smoothly, and it was judged that the cracks would not cause loss of flight control; aircraft of this type have been flown and landed safely with complete flaps missing.

This blade swallowed a total of 40 simulated lightning strokes, including 3 high-current strokes in which the currents were 140 to 160 Ka, with only the minor damage previously mentioned, and it was concluded that the first objective, a protective system suitable for field application, for significantly increased lightning protection, had been achieved. The conductive paint system employed weighs approximately 10 grams per square foot. Lighter paints are available, but this one was selected to assure compatibility with the existing blade finish system under field conditions. Field application of this protective system adds approximately 2 lbs to the weight of the blade, which was judged acceptable.

The second of the blades to be tested incorporated a functional prototype of the protective system for installation on factory overhaul. Its configuration is shown in Figure 10.

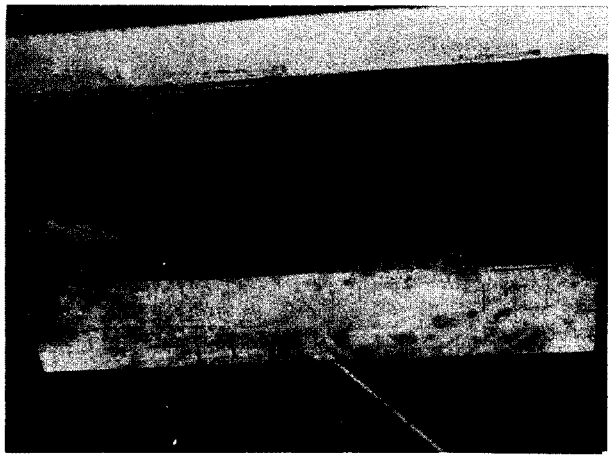

Fig. 9 - Flap after high current stroke

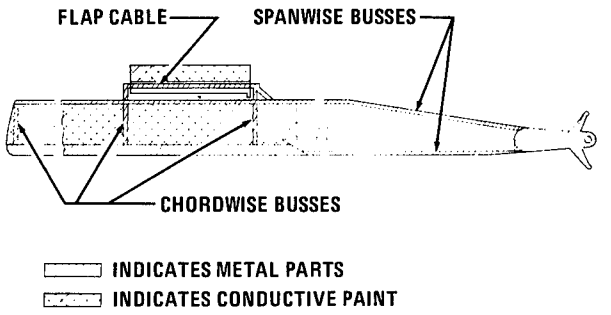

Fig. 10 - Protective system for factory incorporation

In addition to conductive paint, this blade incorporated full-span leading edge and trailing edge busses, and two additional chordwise busses. The spanwise and chordwise metallic busses applied to this test blade were not flightworthy; they were simply .025 annealed aluminum strips adhesively bonded to the blade, with riveted joints as required, for electrical continuity. The intention was to provide an electrical mockup of a protective system which could be refined to a flightworthy design if successful.

The long spanwise control rod which runs from the hub to the flap bellcrank (shown in Figure 6) was not installed in this blade. It had been decided that maximum protection could be achieved by elimination of this rod as a possible stroke path. On the helicopter, this would be accomplished by fabricating the rod from a dielectric material, such as fiberglass; for test purposes such a rod was simulated by simply omitting it.

It was decided to omit exploratory high-voltage strokes to the outer portions of this blade, since results on the previous blade had been acceptable and this blade had to be better. Accordingly, exploratory strokes were directed to the inboard portion, which had no conductive paint on the skin between the leading and trailing edge busses. One simulated swept stroke produced a penetration in this region, and suggested that an overall conductive paint coat was required. This was simulated locally by application of conductive tape, after which another simulated swept stroke to the same region failed to produce further damage. Testing was concluded with a series of high current strokes to various points on the metallic bus system. In no case was structural damage to the blade produced. The mockup bus system, however, was separated from the blade in a number of areas in a manner indicating that the separation was caused by magnetostrictive forces, rather than destruction of the adhesive bond. Riveted joints in the bus system were also destroyed. It was concluded that the metallic bus system concept was effective in protecting the blade and that the cross-sectional areas of the busses were sufficient, but that any final flight-worthy design of the busses would require careful attention to the mechanical strength and rigidity of both the joints and the bus system itself.

SUMMARY

In summary, this paper attempts to show that:

(a) A number of approaches are available to the design of non-metallic rotor blades to provide effective lightning protection.

(b) The conductive paint approach has been successfully applied to provide such a system for HH43B/F rotor blades.

(c) The ultimate conclusion from this work must be that no amount of analysis and speculation should be considered a substitute for a test program.

Lightning Protection on Advanced Fighter Aircraft

G. L. Weinstock
McDonnell Aircraft Company, St. Louis, Missouri

SINCE 1964 LIGHTNING STRIKES have been reported on over 150 fighter aircraft. Lightning strikes are generally reported only if damage occurs; therefore, it is suspected that more than half the lightning strikes on aircraft are never reported. Since no all-weather fighter aircraft can be considered free from the possibility of being struck by lightning, efforts must be made to minimize lightning discharge effects.

To withstand lightning strikes with minimum or no damage, the aircraft skin/structure should be capable of conducting approximately 200,000 A of electrical current with little voltage drop along the structure. Ideally, if an aircraft is constructed of high electrically-conductive material and has no openings or discontinuities in the skin, lightning will strike one point and leave by another without causing damage. For comprehensive protection, lightning discharges must be prevented from entering the aircraft interior and producing damage to electrical and electronic systems inducing fuel system explosions or disabling the crew. Dielectric or unbonded exterior parts are also subject to damage. Thus, discontinuities in the aircraft skin, such as radomes, canopies, camera windows, navigation lights, composites, doors, vents, and atmospheric sensors and probes, reduce the capability of an aircraft to safely withstand lightning strikes.

MCAIR has delivered approximately 4000 F-4 Phantom II aircraft. This all-weather aircraft is widely used throughout the world and therefore has accumulated a significant number of lightning strikes. Several things can be learned by careful analysis of these reports. Attach points and swept stroke zones can be determined from actual experienced strikes rather than the sometimes questionable model tests (particularly in determining swept stroke zones).

Figure 1 shows the strike points on an F-4 and Fig. 2 is a chart which itemizes the strikes by point of entry and damage location. Of particular interest is the effect of the external wing tank. Without the tank, lightning never attached to the leading edge of the wing; but rather attached to either the nose or the wing tip. Thus, attach points on future aircraft with similar wing size, location and angle can be postulated with some degree of confidence.

ABSTRACT

The lightning design challenges and protective measures being used or considered for use on late models of the F-4 Phantom II aircraft, advanced air superiority aircraft and electronic flight control systems are presented in this paper. Ideally, if an aircraft were constructed of high electrically-conductive material and had no electromagnetic openings in the skin, lightning would strike one area and leave by another without damaging the aircraft. For practical aircraft protection, lightning discharges must be prevented from entering the aircraft interior and damaging electrical and electronic systems, causing possible fuel system explosions, and affecting crew capabilities. Openings in the aircraft skin such as radomes, canopies, camera windows, navigation lights, fuel vents, composite materials, atmospheric sensors and unbonded sections all reduce the capability of aircraft to withstand lightning strikes. Unfortunately, advanced fighter aircraft incorporate all these electromagnetic openings. Additional lightning protection requirements have been necessitated by the introduction of electronic flight control systems (a replacement for the mechanical linkage and wire rigging used in present aircraft). Even a temporary loss of electrical power or an induced transient in an electronic flight control system would present a serious flight hazard. Since the system effectiveness of advanced fighter aircraft depends upon increased accuracy and range of their Fire Control Radars, present day methods of radome protection using metallic strips are not usually acceptable. Size, weight, crew visibility, and corrosion prevention are other items critical to high performance fighter aircraft with which lightning protection must be made compatible.

Most of the damage sustained was slight, probably because of the inherent ruggedness of the aircraft and the use of good bonding practices. However, there were a few serious incidents. These resulted in damage to the electrical system and in one case an external fuel tank was dropped and subsequently exploded. The most prevalent point of entry into the electrical system was through the heater wires in the radome pitot boom. The navigation light wiring in the vertical fin cap and wing tips also provided points of entry into the electrical system.

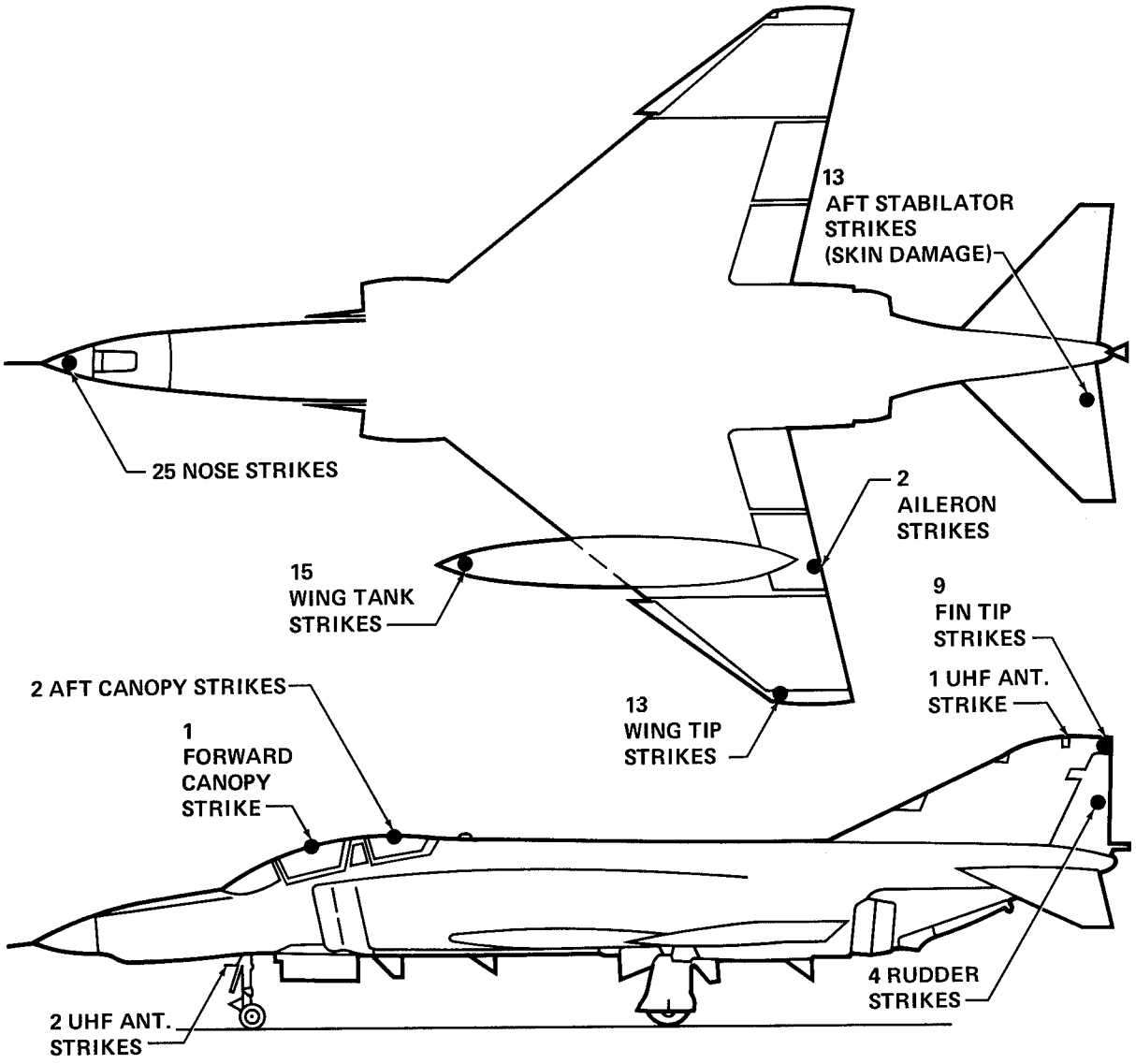

Fig. 1 - F-4 Lightning Strike Points

ATTACH POINT				AFFECTED AREAS															
				NOSE			TAIL			WING					INTERNAL				
NOSE	TAIL	WING	OTHER	RADOME	PITOT	OTHER	V. FIN	STABIL	RUDDER	TANK	LIGHT	OTHER	ENGINE	SKIN	CREW	ELECT	EED	OTHER	
		●								●									
			●				●									●			Upper and Lower UHF Antennas
		●								●									
			●												●				Flash Blindness for 30 sec
●	●			●			●	●											
●	●			●	●				●	●									
		●								●							●		Struck Leading Edge Flap
●				●									●			●			
		●								●				●					
●	●			●	●			●								●			
●		●		●	●						●				●				
	●							●								●			
													●						One Engine Flame-out ①
													●						One Engine Flame-out ①
	●	●						●			●								②
	●							●											②
			●												●				Crew Shock
		●								●	●								
			●												●		●		
		●								●									
●	●	●		●			●				●					●			③
		●									●	●							③
		●										●		●					
●				●									●						
●				●															
●				●	●			●	●										
			●													●			
●	●			●	●			●						●		●			
●	●		●				●												
		●								●									
●	●			●	●		●							●	●	●			
		●								●	●								
		●								●						●			
			●													●			
			●												●	●			
●	●			●				●											
		●														●			④
		●										●			●				④

Fig. 2 - Chart of F-4 Lightning Strikes

ATTACH POINT				AFFECTED AREAS														
				NOSE			TAIL			WING				INTERNAL				
NOSE	TAIL	WING	OTHER	RADOME	PITOT	OTHER	VFIN	STABIL	RUDDER	TANK	LIGHT	OTHER	ENGINE	SKIN	CREW	ELECT	EED	OTHER	
	●							●	●										Scorch on Top of Canopy
	●	●					●				●								⑤
		●									●								⑤
			●											●	●				
		●									●								⑥
		●									●				●				⑥
●				●	●											●			
		●									●								⑦
		●														●	●		⑦
●						●								●					
		●										●	●						
●				●												●			UHF Damaged
●	●			●	●			●								●			
●		●		●	●					●				●	●	●			
			●												●				Shock from Throttle
●		●			●					●	●					●			
	●							●											
		●								●				●					
	●	●						●				●							
			●													●			
			●												●	●			
●				●															
●	●			●			●									●			
		●								●									
●	●			●					●										
		●										●							⑧
		●										●							⑧
		●								●						●			
			●															●	
●	●				●									●		●			
●	●	●			●		●	●				●				●			
			●													●			
●				●	●		●					●	●	●		●			NOTE: Numbers in ◯ indicate lightning stroke jumped from one A/C to other
			●											●					
			●											●					
25	20	32	16	20	13	1	9	13	4	15	13	8	6	12	12	26	3	1	TOTALS

Fig. 2 - Chart of F-4 Lightning Strikes (Cont.)

The RF-4 pictured in Fig. 3 sustained three strikes. The last one was a massive strike that exploded a large hole in the radome. The remaining damage to the radome was done by windloading effects.

There was evidence on several aircraft of swept strokes along the sides of the fuselage. There was no evidence of strokes swept across the sides of the vertical stabilator. The strokes probably swept up the leading edge and finally detached at the trailing edge of the fin cap. The crew in the F-4 is protected from lightning by the dielectic strength of the canopy and by the conductive canopy frame. There has been evidence of lightning burn marks on the canopy but no reports of serious effects on the pilot. The pilots have received mild shocks, probably through the wiring to cockpit switches.

Measures to minimize the effects of lightning discharges on high-performance fighter aircraft, without compromising mission performance, have received serious consideration at MCAIR. Fortunately, many lightning-protective techniques coincide with electromagnetic compatibility protective measures with differences primarily in terms of energy magnitudes. A sample activity flow chart for a fighter aircraft lightning protection program is shown in Fig. 4. This chart illustrates the basic tasks in the overall lightning protection design and test program.

LIGHTNING PROTECTIVE MEASURES

As has been mentioned, the intense electrical currents of lightning discharges must be confined to the exterior surface of the aircraft. Lightning can be conducted into the fuselage through openings and discontinuities in the aircraft skin. Such opening should be minimized, and where their presence is mandatory, they must be carefully analyzed and protected if vulnerable.

Low impedance electrical bonding is necessary between all exterior metallic portions of the aircraft to prevent arcing and provide a low-resistance, high-current path for lightning currents.

RADOME - Of primary concern in aircraft lightning protection programs is the nose radome. This area is particularly vulnerable if a pitot boom is located on the radome. As shown in Fig. 2, the pitot boom was a primary attach point for strikes on F-4's. Even without a pitot boom, the lightning will attach to antennas or wires within the radome.

Structural damage to the radome can be initiated by several mechanisms: (a) The vaporization of materials (metal or otherwise) contained within, comprising or directly attached to the radome wall structure; and (b) The internal pressures caused by the heating of the air contained within the radome (gas blast effect) and the vaporization of components such as wire and small pieces of metal and other materials that can add to the internal pressure within the radome.

The effect of debris resulting from radome structural damage should be investigated; however, this usually is not a problem since present day jet engines can ingest a considerable amount of foreign material. The direct lightning attachment to pitot heater wires must be prevented to protect the aircraft electrical system. This can be accomplished in the following ways, dependent upon allowable radar performance degradation.

A. Solid metallic strips from the pitot mast to the fuselage.

B. A metal tube enclosing the pitot heater wires from the boom to the fuselage.

C. Where radar performance cannot be compromised, a strip of "buttons" cut to minimize radar reflections can be used. This method was developed by the Douglas Aircraft Company[1] and has proved most successful.

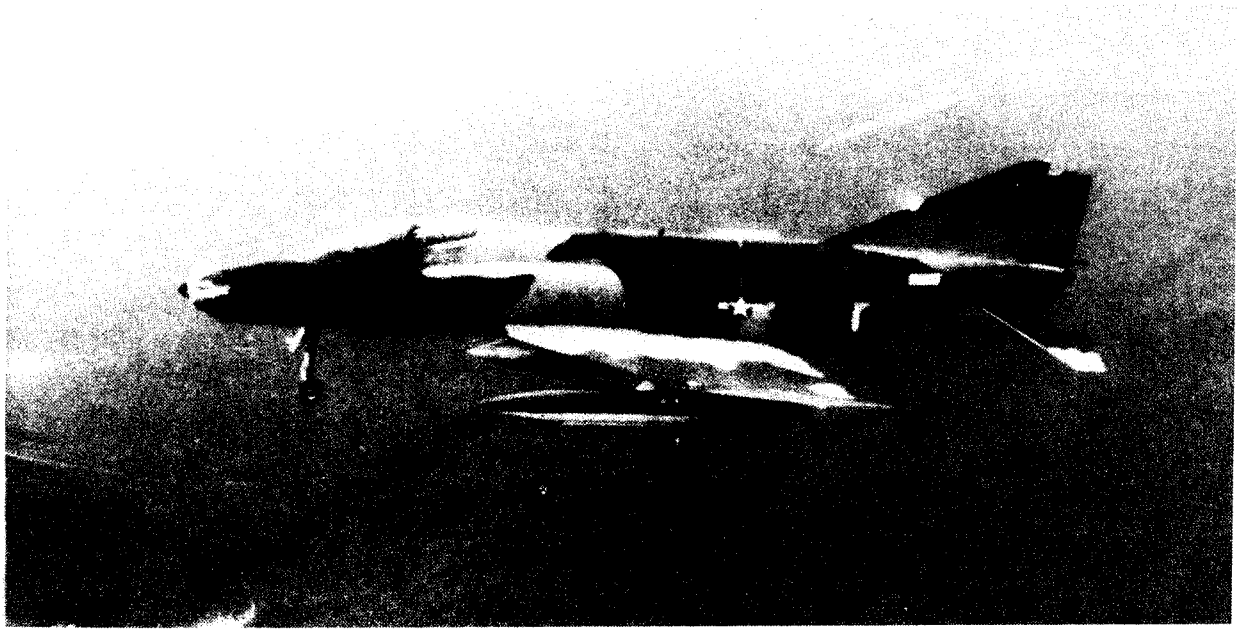

Fig. 3 - Lightning Strike of RF-4C

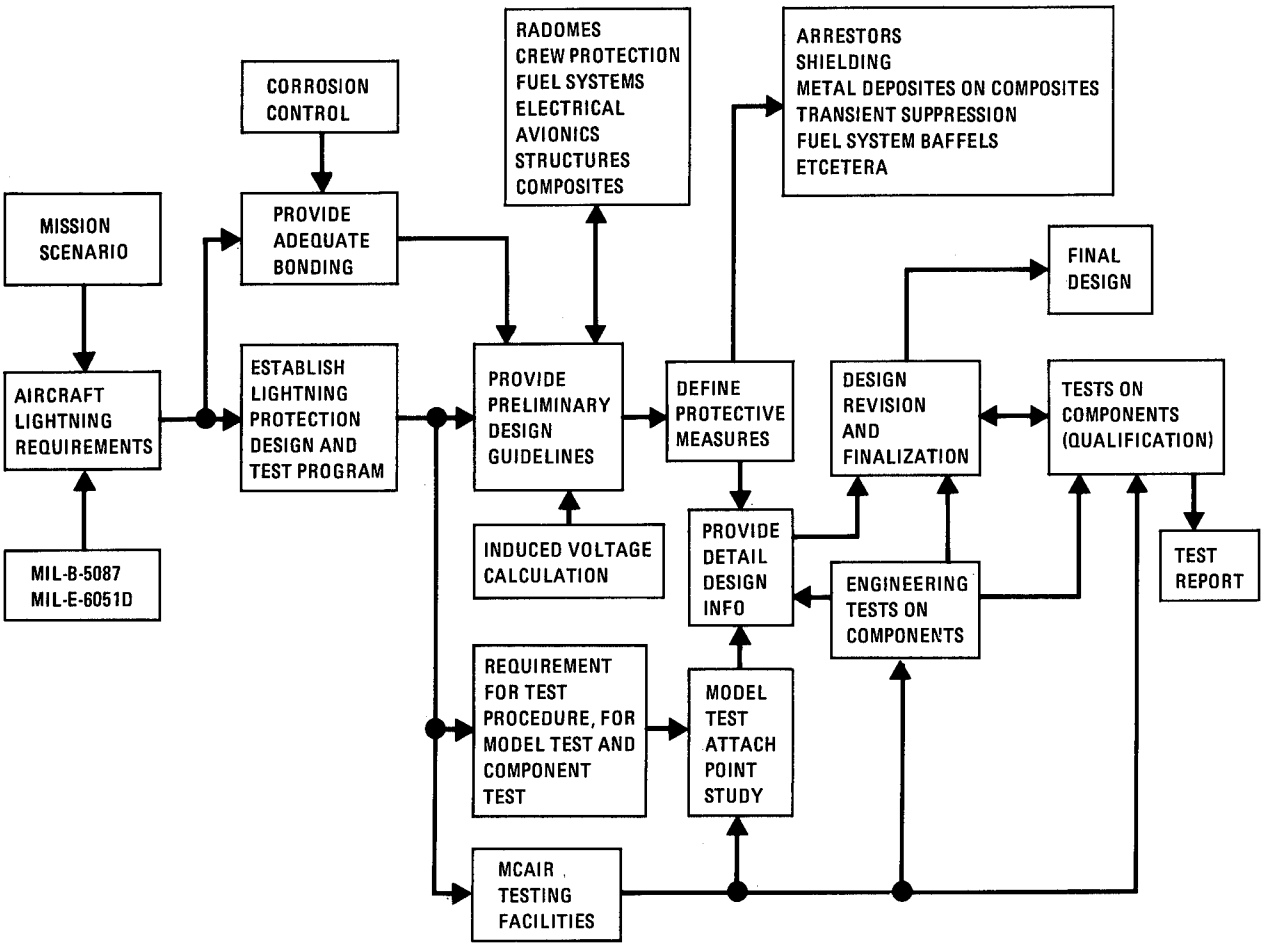

Fig. 4 - Lightning Protection Activity Flow Chart

Another, and less desirable, protection method is to allow radome damage but to protect the electrical system by using lightning arrestors on the pitot heater wires at the point of entry to the fuselage.

A cursory evaluation of the effects of a metal strap on radar performance can be obtained by using a strip of metalized tape. The size, location, and number of tapes can easily be changed while radar antenna patterns are measured.

Both high voltage and high current tests should be performed on the nose radome. The high voltage attach point test should be performed utilizing a full-scale nose mockup and subjecting it to high voltage discharges originating from different directions. This test is of prime importance if there is no pitot boom on the radome, for it will indicate the components to which the lightning strike can directly attach. The high current tests will determine the extent of physical damage and the amount of current directly conducted or coupled into the electrical system. The results of the tests will either demonstrate adequate nose radome protection or indicate where additional protection is required.

ELECTRICAL SYSTEM - The more serious lightning incidents on F-4 have involved the electrical system. Not only must the electrical power system be protected, but other electrical/electronic systems essential to flight must also be protected. An initial step in lightning protection is a mathematical analysis of induced currents in electrical wiring. A typical analysis is presented in a following section of this paper. Protection of electrical/electronic systems can be accomplished in three basic ways.

A. Protect all possible points of entry into the aircraft with lightning diverters or Faraday shields.

B. Protect all possible points of entry into the electrical system (lights, antennas, wiring in radomes, etc.) with lightning arrestors. Also, add surge protectors to the electrical distribution system.

C. Combinations of A and B.

A combination of A and B is more easily optimized for weight and volume, and thus is the preferred method. The over-voltage sensing circuits and other electrical fault circuits should be carefully designed as should fuel gauging, fire warning and flight control system wiring. Since some systems using antennas cannot tolerate the capacitance of lightning arrestors, an alternate method is to separate antenna coaxial wiring from all other wiring. This approach will not, of course, protect the transmitter or receiver but will keep coupled voltages to relatively low values.

From a practical viewpoint, the points of lightning entry into the electrical system must be tested component by component. Pulse coupling tests should be performed with the lights or antennas installed on full-scale sectional mockups. The area of specific interest is whether or not the lightning stroke can sufficiently damage the light assembly or antennas and cause direct current attachment to the associated wiring. This test requires that high current and high charge transfer tests be conducted. The pulse coupling tests utilize the setup shown in Fig. 5.

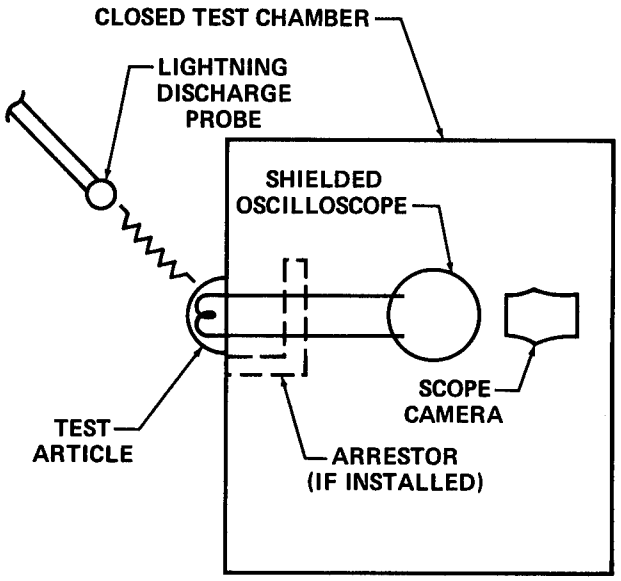

Fig. 5 - Pulse Coupling Set-Up

FUEL SYSTEM - The first step in establishing a lightning safe fuel system is familiarization with the general configuration of the fuel system. As part of the fuel system familiarization, an analysis of the fuel system characteristics pertinent to lightning protection will be made. This includes tank design, intake, vent system, skin thickness, types of fuel covers for filling and gauging, fuel transfer, access doors, and external tanks. This analysis will permit identification of obvious design characteristics which may cause a lightning hazard. Each of the above areas represents a possible source of fuel-air vapor ignition caused by lightning-induced arcing. Although it is possible to design these items so that they are reasonably safe from the effects of lightning, positive verification of the design adequacy can be obtained only by tests on full-scale mockups. The assemblies are subjected to simulated lightning currents and the effects are carefully monitored.

The primary factor in lightning protection design of fuel systems is to provide a good external conductive surface that will prevent sparking in fuel vapor areas. Filler caps are often semi-insulated from the aircraft skin, and a direct lightning strike to a cap will result in internal sparking at the contact surface as shown in Fig. 6A. The explosion which would result can be prevented by designing the cap such that the sparking, if any, occurs outside the 0-ring in a non-fuel vapor area. This can be accomplished by fabricating the internal part of the cap of plastic and providing a good external conductive path with a compressible-contact ring which presses against the mounting flange. This is illustrated in Fig. 6B. Another approach is to locate the cap behind an access door under the aircraft skin, thereby eliminating the possibility of a direct stroke.

Intake or fuel vent openings are external to the aircraft and if struck by lightning could cause an explosion. The best design is to locate these openings in an area that is not subject to a strike or a swept stroke. If this is impracticable, then the vent should be flush mounted, slightly recessed or protected by a Faraday shield. These configurations minimize strike probability without greatly increasing the extent of the flammable mixture region. Also, by maintaining high vent exit velocities circulating air at all times, fuel vapors will be diluted, reducing the probability of combustion. Flame arrestors should also be installed. The manner of installation should not be conducive to flame holding since arrestors are not effective at elevated temperatures.

In internal tank design the location, the skin thickness, type (wet or bladder) and mounting of fuel sensors, must be considered for lightning protection. If the tank is of the wet type and in a strike area, sufficient skin thickness is required to prevent ignition from skin puncture or interior surface heating. The minimum skin thickness recommended for strike areas is 0.08 in. aluminum. The thickness required for other metals is dependent upon resistivity and thermal conductivity. Fuel sensors must be mounted such that no internal sparking can occur. The best method is to locate the mountings under the aircraft skin.

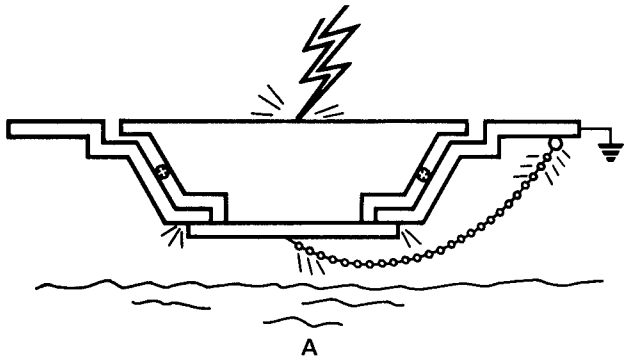

USUALLY SEMI-INSULATED FUEL CAP ARCING INSIDE TANK DUE TO DIRECT STROKE

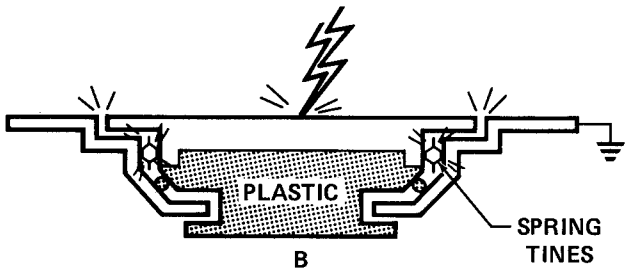

LIGHTNING PROTECTED FUEL CAP ARCING OUTSIDE TANK IN SAFE AREA

Fig. 6 - Fuel System Filler Cap

External fuel tanks and the interconnecting hoses to the fuselage must be designed to prevent sparking internal to the fuel areas. The fuel probes must be well grounded and designed to prevent internal sparking or isolated such that any sparking that takes place will occur on the outside. The external tank must have sufficient skin thickness to carry the high lightning currents and a good electrical ground to the aircraft.

CANOPY - Records of lightning strikes to the F-4 canopy show no evidence of punctures or cracks. Analysis of the dielectric strength of the canopy and the distance to structure also shows that a lightning strike will flash-over rather than punch-through. However, canopies with less framework, greater length between supports or lower dielectric strength can represent definite hazards. There are a number of ways to protect canopies. Some of the more practical methods are:

1. Attach an external metal strap to the top of the canopy. Tests have shown that for mechanical strength (to prevent curl-up resulting from electromagnetic forces) the strip should be approximately 3/8 in. wide by 1/8 in. thick. The attachment of the strap to the canopy is the greatest drawback of this method since conventional bonding will not withstand the wind loading and rivets are probably required. However, some existing canopies are stressed such that rivets could not be tolerated. Drag is also increased since the straps are located in the wind stream.

2. A thin (1 to 3 mil) metalized strip attached externally to the canopy will provide protection. It is easy to install but it has several undesirable features. It will provide protection for one strike only; it will sometimes leave a burn spot on the canopy; and it is subject to erosion caused by rain, dust and other particles.

3. A metal bar inside the canopy will provide protection by inducing a field outside the canopy that provides a discharge path. The bar must have rounded edges since sharp corners would cause high voltage gradients which might result in punch-through. (This is also the reason an inside metalized strip is undesirable.)

Another possibility for canopy protection, as yet unexplored, is the use of a transparent vacuum deposited conductive coating to reduce flash-over voltage. For all canopy lightning protective measures bonding to the structure is important but sometimes mechanically difficult to achieve. The use of expansion joints and requirements for canopy jettison are items that require consideration. Obstruction of field of view is of particular importance for fighter aircraft. Trade-off studies of visibility versus protection should be made before any canopy protection is finalized.

Verification should consist of high voltage tests on an actual canopy. Mockups of the upper portion of the ejection seat and the pilots helmet should be located inside the canopy to test for lightning punch-through.

COMPOSITES - As reported in many published articles, composite materials suffer massive damage when struck by lightning. Since other published data are available, this paper will not discuss lightning effects and protective methods for composites other than to mention that they should be analyzed for vulnerability, strength and effect on safety-of-flight status.

INDUCED CURRENT ANALYSIS

Induced currents resulting from lightning strikes on or near wire loops should be considered in electrical/electronic system lightning protection. Typical tuning loops were used for the analysis presented herein; however, a similar analytic approach can be used for any circuit configuration.

The frequency and current amplitude characteristics of lightning strikes imply that the predominant mode of coupling is mutual induction.

The method of calculation will be to determine the induced loop potential, relate this to the energy absorbed in the wire and, finally, to calculate the temperature rise equivalent to this absorbed energy.

The thermal effect on the wire resistance is accounted for by a piecewise time integration of the integral for the absorbed energy. The closeness of the loop to the strike and the resulting field inhomogeneity required an integration of the magnetic field over the area of the loop. The loop model was assumed to be a square loop.

ANALYSIS METHOD - Lightning pulse form

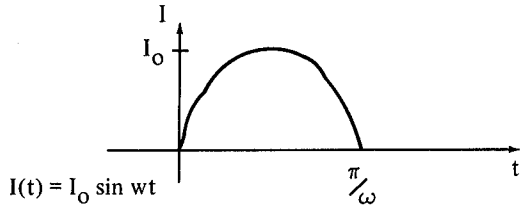

$I(t) = I_o \sin \omega t$

Mutual induction

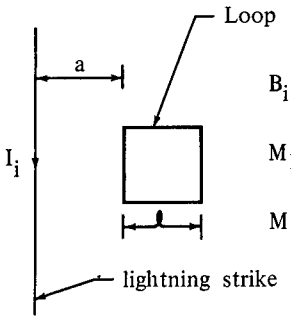

$$B_i = \mu_o \, I_i / 2\pi r \quad (1)$$

$$M_{12} I_1 = \int_{A_2} \vec{B}_1 \cdot d\vec{A}_2 \quad (2)$$

$$M = 2 \times 10^{-7} \ell \ln (1 + \ell/a) \quad (3)$$

where:

loop perimeter = 3 ft

a = distance in meters from strike to nearest side of loop

ℓ = length of each side of the square

Energy absorbed equals

$$\int_0^{\text{pulse duration}} [V(\text{induced})]^2 \, 1/R(\text{temp}) \, d(\text{time}) \quad (4)$$

Mechanical Equivalent of heat

1 cal = 4.19 J

Temperature effect on wire resistance can be represented as:

$$R(T) = R(\text{ambient}) [1 + \alpha (\Delta T)] \quad (5)$$

where:

ΔT = temperature change above ambient

α = coefficient of thermal increase in resistivity

The temperature increase in the wire loop is calculated by converting the energy absorbed by the wire to calories of heat and relating this to temperature increase of the wire by relating the heat to ΔT by:

$$\Delta Q = C_v (\Delta T)$$

where:

C_v = heat capacity of the wire

A basic assumption in this calculation is that the effect of the thermal conductivity of the surrounding medium, i.e., the difference between a wire loop in air compared with the same wire in a dielectric solid is negligible for the time over which the heating occurs. This assumption method is supported by experimental data.

Example calculation:

Initial conditions

$I_o = 2 \times 10^5$ A

$\omega = 1.045 \times 10^5$ rad/sec

Resistivity of copper wire as function of temperature

$$\rho(T) = \rho(100^oC) \left[1 + \frac{a}{\rho(100^oC)} \left(\frac{\Delta T}{100}\right)\right] \quad (7)$$

Resistivity of #38 copper wire per cm is found by multiplying the resistivity by the ratio of the squares of the diameter of 4 mil wire compared with a unit cross section.

4 mil wire diam = 0.004 in. = 1.016×10^{-2}

radius = 5.08×10^{-3}

area = 0.811×10^{-4}

$$R_{\#38\ wire}(T) = 1.12 \times 10^{-6} \left[\rho(100^oC) + 0.8 \times 10^{-6} \left(\frac{\Delta T}{100}\right)\right] (8)$$

$$\rho(100^oC) = 2.28 \times 10^{-6}$$

$$R_{\#38\ wire}(T) = 1.12 \times 10^{-6} \left[2.28 \cdot 10^{-6} + 0.8 \left(\frac{\Delta T}{100}\right) \times 10^{-6}\right] (9)$$

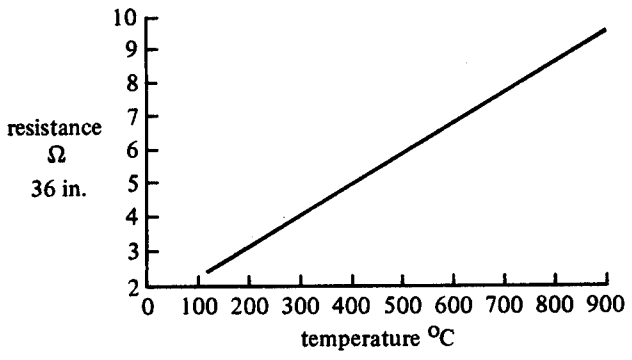

Mutual Inductance Calculation

a = distance from lightning current to loop

ℓ = side of square loop

$$B = \mu_o \frac{I}{2\pi r} \quad (10)$$

$$M = \frac{1}{I} \int_{\text{area of loop}} \vec{B} \cdot d\vec{A} \quad (11)$$

$$= 2 \times 10^{-7} (\ell) \ln (1 + \ell/a)$$

where (ℓ) and (a) are in m

and $\mu_o = 4\pi \times 10^{-7}$

for ℓ = 3/4 ft = .2286 m,

the mutual inductance is a function of (a) only.

$$\text{Energy} = \int_o^{\text{pulse duration}} [V(t)]^2 \frac{1}{R(T)}\, dt \quad (12)$$

where the voltage is a function of time and the resistance is a function of temperature

Example: I ↓ □

$$I_{lightning} = I_o \sin wt \quad (13)$$

$$V_{loop} = M \dot{I}_{lightning} \quad (14)$$

$$I_{loop} = V_{loop}/R_{loop} = w M I_o/R \cos (wt) \quad (15)$$

The integration is carried out in time increment so that the temperature increase of resistance may be taken into account.

Consider square loop = 3 ft perimeter.

Assume the distance (a) = 0.1 m.

$M (a = 0.1) = 5.81 \times 10^{-8}$

Breaking the integration into four equal parts for simplicity:

Pulse duration = 30 μsec

$= 3 \times 10^{-5}$ sec

$$\int_o^{7.5 \times 10^{-6}} (\ ) = 6.137 \times 10^{-6} \quad (16)$$

$$\int_{7.5 \times 10^{-6}}^{15 \times 10^{-6}} (\ ) = 1.37 \times 10^{-6} \quad (17)$$

$$\int_{15 \times 10^{-6}}^{22.5 \times 10^{-6}} (\ ) = 1.37 \times 10^{-6} \quad (18)$$

$$\int_{22.5 \times 10^{-6}}^{30 \times 10^{-6}} (\ ) = 6.137 \times 10^{-6} \quad (19)$$

$$M^2 w^2 I_o^1 = 1.48 \times 10^6 \quad (20)$$

assume cold resistance R(100) = 2.28 Ω

$$\text{Energy} = \frac{1.48 \times 10^6}{2.28} \times 6.137 \times 10^{-6} \quad (21)$$

$$\text{Energy } (\tfrac{1}{4} \text{ pulse}) = 3.984 = 4 \text{ J} \quad (22)$$

1 joule will raise the temperature by 37°C

$$\Delta T \approx 150^\circ C \quad (23)$$

$$R(250^\circ C) = 4\ \Omega \quad (24)$$

For the Second Interval:

$$\text{Energy } (\tfrac{1}{4} - \tfrac{1}{2} \text{ pulse}) = 0.5 \text{ J} \quad (25)$$

$$\Delta T \approx 19^\circ C \quad (26)$$

Using the Same Resistance:

$$\text{Energy } (\tfrac{1}{2} - \tfrac{3}{4} \text{ pulse}) = 0.5 \text{ J} \quad (27)$$

$$\Delta T \approx 19^\circ C \quad (28)$$

$$R(300^\circ C) = 4.4\ \Omega \quad (29)$$

$$\text{Energy } (\tfrac{3}{4} \text{ - whole pulse}) = 2.064 \text{ J} \quad (30)$$

$$\Delta T \approx 77^\circ C \quad (31)$$

Total change in temperature =

$$77 + 2 \times 19 + 150 = 264 \quad (32)$$

$$\text{Final temp.} = 364^\circ C \quad (33)$$

Induced Current Pulse:

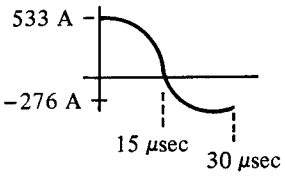

AIRCRAFT LIGHTNING ATTRACTION

That a fighter aircraft can attract lightning is somewhat of a minimal problem. A lightning discharge probably has to be within one or two wing spans of an aircraft before it will strike. Two items frequently discussed as possible attractors of lightning are jet exhaust plumes and high power transmissions. The exhaust plume from a fighter aircraft jet engine is primarily contained within the afterburner and certainly does not extend out of the aircraft more than a few meters. The following observations and calculations indicate why the ionization from an onboard transmitter has negligible effect on lightning attraction.

Several independent sources [2, 3] have led to comparable conclusions which suggest that field strength increases of the order of 7-10 kV/cm can trigger branching corona streamers and consequent draining of charge between cloud formations. Assume for this evaluation, the lower value (7 kV/cm) of field strength as a baseline field strength magnitude required to initiate such corona streamers. Since it is of more interest to make this investigation at 25,000 ft, the corona breakdown field strength will be modified by a factor of 0.4 to account for the associated reduction in atmospheric pressure. This, therefore, will establish a field strength of 0.4 x 7 kV/cm = 2.8 kV/cm as a threshold value for the onset of corona discharge at 25,000 ft for the purpose of this evaluation.

The following calculations are intended to show the insignificant contribution of the radar field strength toward the triggering of a lightning stroke. Therefore, power losses in the calculation are not taken into account and no great precision has been exercised. Consider now, a hypothetical radar that has the following characteristics:

- λ = 1.0 in. (X band)
- Antenna diameter = 36 in.
- Po = Power input into antenna = 5 kW AVE
- Duty Cycle = 100% (CW)
- Antenna efficiency = 65%

The radiation characteristics considered will exhibit a field strength which can be considered gross for most of todays fighter aircraft. CW has been used to simplify the problem. Both of these factors have been selected to assure conservative results.

The field strength in the region from the antenna to the beginning of the Fraunhofer zone in general should not exceed Pn.

$$\text{Pn} = (\text{antenna efficiency}) \times (\text{Po/area of antenna}) \times 4 \quad (34)$$

$$\text{Pn} = (\text{efficiency}) \frac{x\text{Po}}{\pi r^2} = \frac{(.65)\ 5 \times 10^3 \text{ w} \times 4}{\pi\ (0.457 \text{ m})^2} \quad (35)$$

$$\text{Pn} = 19{,}800 \text{ w/m}^2 \quad (36)$$

This power density will exhibit an electric field intensity equivalent to

$$E = (377\ \Omega \times \text{Pn})^{1/2} \text{ or} \quad (37)$$

$$E = (377\ \Omega \times 19.8\text{K w/m}^2)^{1/2} \quad (38)$$

$$E = 2730 \text{ v/m} \quad (39)$$

This field will extend to a range not greater than $2\ D^2/\lambda$ after which the field strength will fall off rapidly as the square of the distance from the antenna.

The calculations show that the field strength never exceeds 2.73K v/m. Thus the 280 k v/m required to trigger a corona discharge is 102 times more than the 2.73K v/m field strength emitted by the radar.

Since the field required to trigger branching corona streamers is more than 2 magnitudes greater than the field strength created by the hypothetical high power radar, there is little reason to consider that rf radiation from fighter aircraft radars could initiate the onset of a lightning strike.

LIGHTNING TEST FACILITY

MCAIR has recently completed construction of a facility for evaluating the effects of lightning strikes on aircraft, structures and components. A sketch of the facility is

shown in Fig. 7 The apparatus fully complies with the simulation requirements of MIL-B-5087B, MIL-A-9094D, and MIL-C-38373. Peak currents to 400,000 A are attainable with waveshapes adjustable over the ranges of interest. The system is designed to produce the primary 200,000 A peak followed by the 2,000 A surge followed in turn by the high Coulomb dump in sequence as defined in MIL-A-9094D. If tests require only one or two of the strike components individually, any combination of the components is available.

The primary current peak is generated by the discharge of a 30 kJ (maximum) high voltage capacitor bank. The secondary peak is generated by a capacitive-inductive circuit whose energy source is a 2,000 J, 1,500 v capacitor bank. The high Coulomb surge is generated by a dc rectifier power supply with a surge capability of 500 A at 200 v (for several seconds).

The high energy strike simulator is supplemented by a full array of laboratory equipment including high-speed cameras with framing rates 10,000 to 7,000,000 frames/sec and streak writing rates from 0.3 to 28 mm/μsec. A number of high voltage power supplies, transient field oscilloscopes with cameras, and other auxiliary high voltage equipment are also available.

The high voltage system employed is a 1,500 kV Marx Surge Generator supplemented by pulse shaping and monitoring systems. Plans call for the voltage capability to be enlarged to 3 million v in the next year with provision for additional future expansion if required. The system is now capable of throwing a 2 m spark and is therefore useful for attach point studies on moderately sized models. Presently, the maximum current of the high voltage system is approximately 20,000 A into a low impedance load.

The testing facilities are located in a building adjacent to an apron at the St. Louis Municipal Airport. This allows complete testing of aircraft, military or commercial, of any size, with relative ease.

CONCLUSION

Efforts are continually being expended by MCAIR Engineering Departments in determining the nature, effects and protective measures for aircraft lightnings strikes. Extensive lightning protective programs are presently being conducted for the F-4 and advanced air superiority aircraft.

ACKNOWLEDGEMENT

Appreciation is expressed to J. L. Bogdanor and R. Aston of McDonnell Aircraft Company for their contributions to this effort.

REFERENCES

1. Amason and Carsell, "Radome Lightning Protection Techniques and their Electromagnetic Compatibility," IEEE EMC Symposium Record 14-16 July 1970 pp 286-304.

2. L. B. Loeb, "Confirmation and Extension of a Proposed Mechanism of the Stepped Leader Lightning Stroke." J. Geophys. Res. 74, 18, 15 Sept 1968.

3. W. N. English, "Corona from a Water Drop," Phys. Rev. 74, 1948

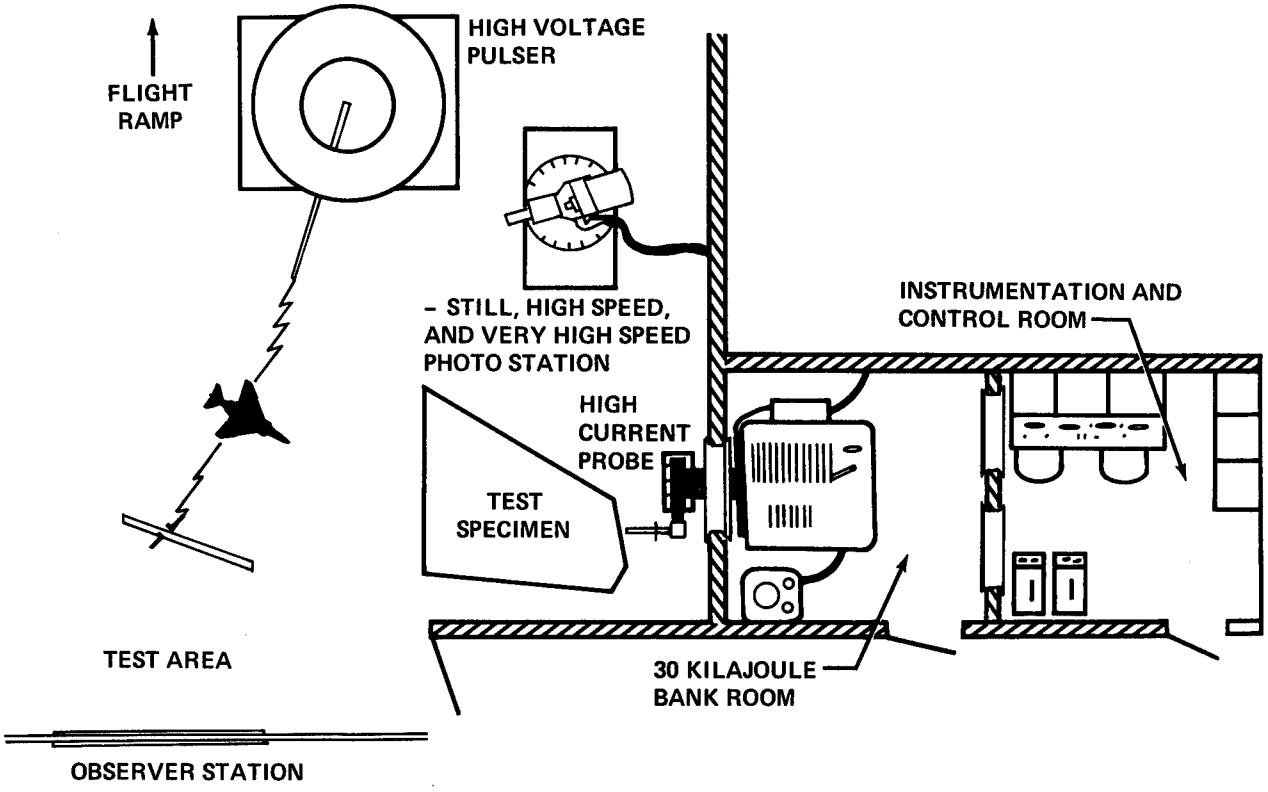

Fig. 7 - McDonnell Aircraft Company Lightning Simulation Facility

LIGHTNING AND SURGE PROTECTIVE DEVICES FOR SURVIVABILITY OF ELECTRICAL SYSTEMS

700931

C. J. Kawiecki, W. H. Kapp, W. T. Pranke,
H. J. Steinhoff, R. E. Thompson
Joslyn Electronic Systems

ABSTRACT

The proper functioning of an aircraft depends upon the reliability of its electrical systems. Circuit pollution by foreign electrical pulses endangers the survival of essential systems. Natural surges such as lightning, and equipment self-generated surges cannot be avoided entirely, but their effects can be minimized using appropriate lightning and surge protective devices.

The surge problem is difficult to cope with; designers often ignore or postpone the problem for lack in knowledge both as to its definition and what to do about it. A cursory treatment of one kind of protector, using sparkgap devices, is presented here for protection against direct and induced lightning strikes, electromagnetic pulses, static charges and equipment self-generated surges.

AIRCRAFT ELECTRICAL SYSTEMS are susceptible to lightning and surge damage. Critical circuits must be protected for successful completion of a mission as well as survival of personnel, the aircraft and its equipment.

Lightning directly striking the aircraft causes a variety of damage such as: direct and induced surge entry to critical electrical and electronic circuits; explosive effects in insulated sections, improperly bonded panels and fuel systems; and minor burns at points of entry and exit.

A nearby lightning stroke, by induction, generates undesired voltages and currents throughout the aircraft and most seriously within the aircrafts' wiring. Flying through electromagnetic pulses creates a similar effect. Other surges in the aircraft are created by the equipments themselves. One piece of equipment may cause surge conditions which are damaging to itself and may transmit these surges throughout associated wiring.

The systems affected are control circuits, communication equipment, AC and DC power buses and branch circuits, etc. Surges are transmitted from one circuit to another by conduction or induction.

Fortunately, protection can be provided when the problems are anticipated or known for a fact to exist and thoroughly studied. The lightning and surge conditions must be characterized and the system checked out on a full fledged scale. A score of protective devices for most situations are available but not necessarily extensively applied. The development of new protective devices await the discovery and further definition of the surge problems.

This paper discusses a variety of protective devices currently used in the suppression of very heavy direct lightning stroke currents and suppression of minor but damaging surges and high voltages. The first line of defense are energy "insensitive", gas filled hermetically sealed spark gaps; in some applications a second line of defense utilizes RLC and semiconductor networks. This paper, although limited to these areas of protection, does recognize that supplementary techniques may be required such as shielding, isolation, grounding, bonding, ground loop avoidance, etc.

ANTENNA LIGHTNING ARRESTERS

Aircraft antenna lightning arresters have been known for over 15 years for the protection of communications' equipment, both transmitting and receiving. When the point of entry of lightning is through the fixed wire, trailing wire, probe, fin cap, wing tip and other isolated antenna systems, the lightning arrester is mounted at the point of the antenna entry into the aircraft. Figure 1 shows the classic circuit of an HF high voltage system. Figure 2 is a photograph of a typical lightning arrester.

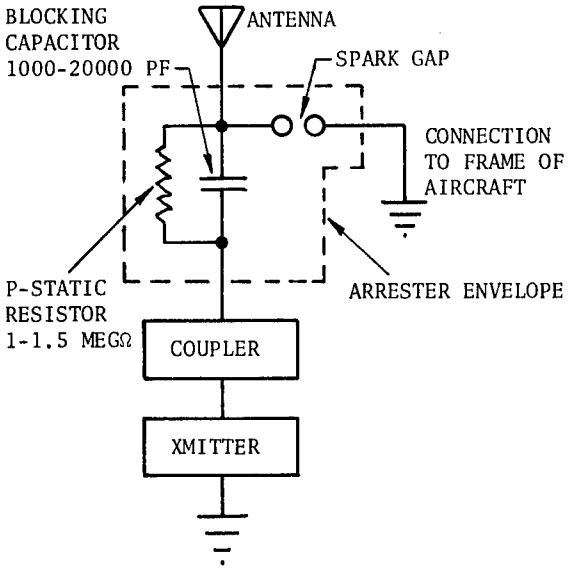

Fig. 1 - Classic circuit for lightning arrester applications on HF equipment

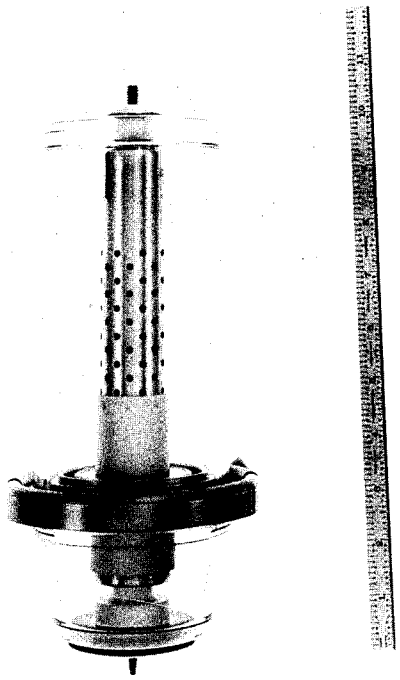

Fig. 2 - Typical lightning arrester. The spark gap is annular in shape located at the grounding flange; the capacitor and resistor are located within the perforated metallic tube; the antenna connects to the top glass bushing and the equipment is connected to the bottom bushing end.

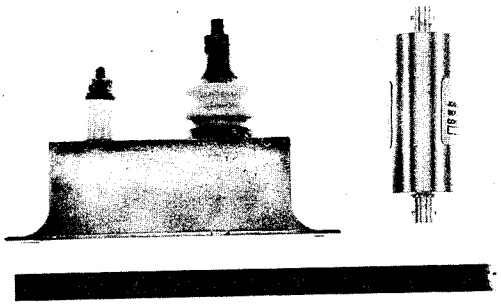

Fig. 3 - Direct stroke receiving antenna arrester (left) with second stage coaxial arrester

For very low voltage transmitting and receiving equipment, the antenna arrester is supplemented with a second stage protector to reduce the voltage spike appearing at the gap of the antenna arrester before it fires. Such secondary protection is mandatory where delicate solid state circuitry is utilized in the receiving equipment. Figure 3 shows a receiving antenna arrester with a secondary coaxial type protector.

Another antenna arrester configuration is depicted in Figure 4 (second unit from the left) which is designed without the series capacitor and shunting P-static resistor. This type has a very low breakdown voltage and the advantage of very low interelectrode capacitance for use on very high frequency systems. Still another configuration (not illustrated) is used for very high voltage transmitting and very low frequency (17KHz) trailing wire systems.

These lightning arresters are designed to the lightning stroke specifications of MIL-A-9094. It appears that this document is serving its purpose quite well. As more data and experience is gathered on lightning strokes to

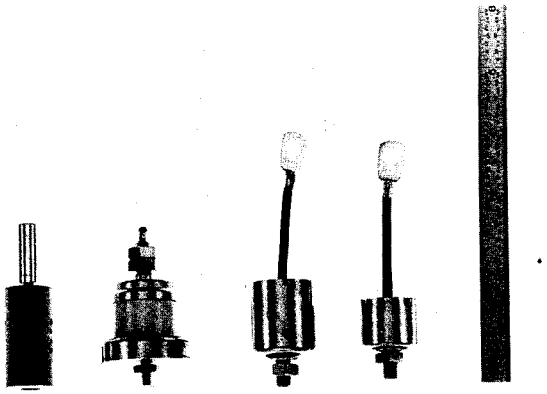

Fig. 4 - Variety of protectors for direct and induced strokes, line surges and component protection

aircraft, and as the state-of-the-art advances in design and materials of aircraft lightning arresters, this specification has been diligently keeping abreast of this knowledge with its revisions. Today's MIL-A-9094D reflects similarities between natural and laboratory made lightning. A study of hundreds of lightning arresters hit by natural lightning shows that some hits are similar to the laboratory stroke described. This specification describes realistic protection criteria; there are no known incidences where radio equipment or aircraft safety were jeopardized by lightning entering through the antenna system, where a MIL-A-9094 arrester was used.

NAVIGATIONAL AND CONTROL PROTECTORS

A direct lightning stroke to any portion of the aircraft, or a stroke nearby an aircraft, or an aircraft exposed to other strong magnetic fields results in induced electrical surges within the aircraft. These surges can be disastrous if allowed to enter control equipment utilizing delicate components such as semiconductor devices, integrated circuits, etc. A surge may be conducted or induced at a wing light for example, and travel along the wiring to the power sources which in turn continue to induce surges to other critical areas; or, the surge can induce secondary surges in adjacent wires which lead to some computer control. It cannot be described just where and how much damage, this kind of "innocent" surge, on a simple insignificant wing light wiring can do; but, imagination can cover alarming possibilities. The best plan is to divert the surge quickly with a protector at the point where the surge is most likely to occur. In addition, a protector must also be used at the vulnerable equipment or component itself. Figure 4 shows some suitable surge protectors consisting of hermetically sealed, high alumina ceramic spark gaps capable of handling repeated surges and over a wide frequency band. These gaps are made in a variety of voltage ranges, and operate with a minimum of delay time. Figure 5 shows the volt-time characteristics of a particular wing tip light protector. Figure 6 shows the circuit location of wing tip light protectors - the plan is not to protect the light itself but to capture and shunt a stroke or induced current from trailing down the light wiring. Other similar applications are: anti-collision lights, tail lights, join up lights, pitot tube heaters, flight control systems, etc.

For very sensitive component part protection, the spark gap is used in conjunction with RLC circuits and semiconductors to effect protection at low levels. The spark gap which can handle enormous energies, in turn protects these RLC semiconductor secondary protectors.

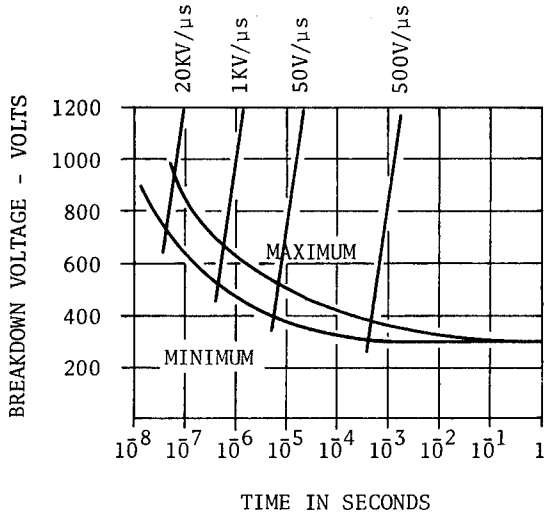

Fig. 5 - Breakdown voltage vs time to breakdown at various voltage ramps

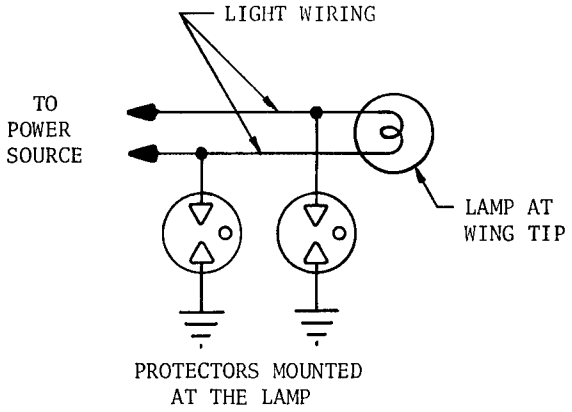

Fig. 6 - Wing tip light protectors used to prevent heavy surges from traveling down the light wiring

The RLC network slows down fast rise time surges to allow minimum voltage overshoot of the spark gap; the semiconductor provides the low voltage level protection.

SPECIFIC COMPONENT PROTECTORS

Aircraft utilizing very high transmitting voltages, for example VLF systems, require the use of protective spark gaps which actually may have to perform as direct stroke lightning arresters. These spark gaps protect the various filter capacitors (vacuum or solid dielectric) at the output stages of a transmitter feeding the antenna. The spark gap at the antenna end must protect the capacitor against transmitter surges and antenna voltage spikes which are too low for the main lightning arrester to pick up. The protector at the transmitter end must protect the capacitor against transmitter surges and power follow until the overload breakers operate. Such protective devices are shown in Figure 7; the fluted ceramic unit is used in HF applications.

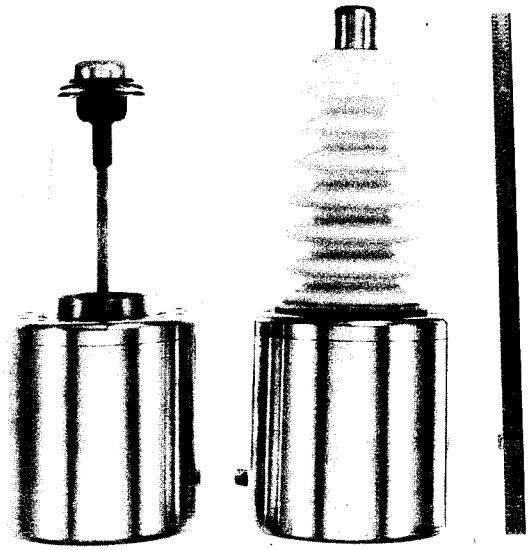

Fig. 7 - Transmitter output capacitor protection for VLF and HF high voltage systems

Another device consisting of a spark gap is used to protect magnetrons in aircraft weather radar equipment. The duty is extremely severe when the gap is performing its function. When the magnetron misfires, the gap clips the overvoltage at a precise moment before the magnetron arcs over internally. Until the overload breakers operate, the energy is diverted through the gap. Figure 4 (extreme left) shows this type of protector.

Figure 8 shows a rate gyroscope with a retrofit in-line protector. The gyro operates off of the 28VDC system on which surges may appear and cause breakdown of components within the gyro. This protector is a composite of a spark gap, resistors, and semiconductors and it mounts in-line using the standard gyro connectors. The protector unit in modified form may be mounted within the gyro case itself.

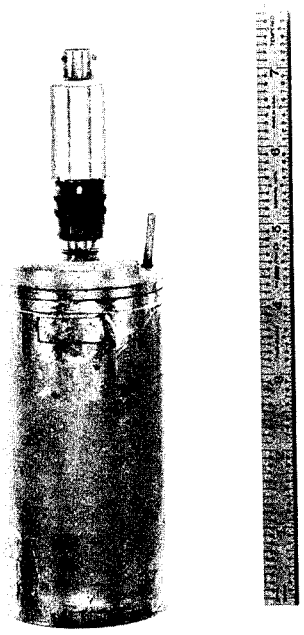

Fig. 8 - Protector (top) connected to a rate gyro (larger bottom part)

POWER SYSTEM PROTECTION

The protection of 400 cycle power equipment is accomplished using protectors such as shown in Figure 9. The large unit is a 3-phase 120/208, 4 wire, wye protector for use directly on a power bus. The smaller units can be used on single phase branch circuits and are usually mounted at the equipment to be protected. Switching and lightning transients can transmit undesirable surge pulses to equipments, the protector senses and rapidly shunts these transients. The resulting follow-on current is automatically extinguished on the first current zero. In many practical installations the resistance of the wiring supplying a certain load will be adequate to limit the follow-on current. When the protector is located directly at the main power bus, a built in impedance is commonly

used to limit the follow-on current.

A second stage of protection may be necessary for more sensitive equipment. This may consist of isolation transformers, series impedances and semiconductor devices.

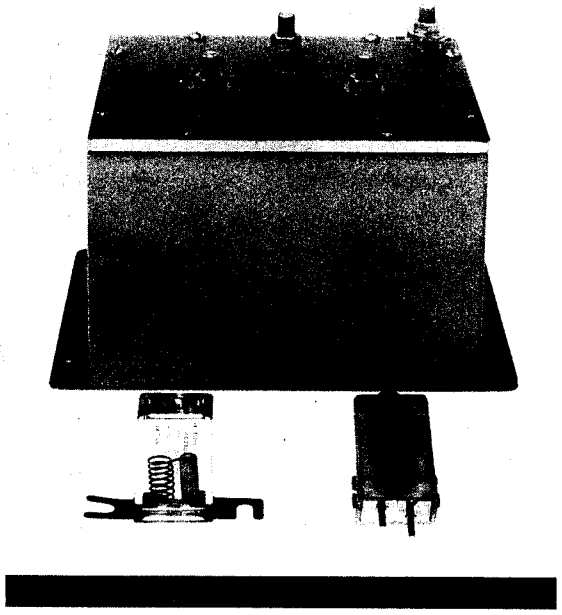

Fig. 9 - Protectors for AC and DC powered equipment

The two smaller units shown in Figure 9 may be used for DC applications as well. DC power protectors are difficult to design because the current does not normally go through a current zero condition. The protector's conducting components must be turned off after the surge occurance by some interrupting means for example, by impedances, fuses, or circuit breakers. If the power current level is low, a simple series resistor is adequate; for high currents, more elaborate means must be used.

CONCLUSIONS

Aircraft electrical systems, which include any and all electrically operated equipment, experience electrical surges. Certain surges are insignificant and produce no ill effects; some significant surges are inconsequential depending on the vulnerability of the apparatus; however, the damaging surges, irrespective of their magnitude, must be rendered harmless. The hermetically sealed spark gap offers a wide range of protection in voltage and current handling capabilities; it is effective and reliable and for a given size and cost it is unsurpassed by any other protective method. For extremely low levels of protection, the spark gap is supplemented with rugged RLC and semiconductor devices. The spark gap acts as a protector to these devices in the event of heavier surges.

The lightning and surge protector shunts destructive currents and voltages. It must be used as the first line and final line of protection. It must be mounted where the lightning and surge are most likely to strike. Additional protectors may be located at the equipment itself, and it may be necessary to mount protectors within the equipment, at the component in potential trouble.

A cross section of a variety of protectors and their areas of application in aircraft systems have been discussed. There are many other variations and applications; each particular application must be evaluated on its own merits and a protector custom designed to the requirements. Designers must recognize the potential hazards of surges created by their own equipment to themselves and to neighboring equipment; also, to surge hazards from without the aircraft such as lightning and electromagnetic pulse. Provision should be made for protective devices at the design stage since retrofitting creates cost and space problems.

SESSION 3A

ADVANCED MATERIALS

Organizer - H. S. Schwartz

Air Force Materials Laboratory (AFSC)

Chairman, H. S. Schwartz

700934

LIGHTNING PROTECTION FOR DIELECTRIC COMPOSITES

J. D. Robb
Lightning & Transients Research Institute

ABSTRACT

Dielectric composites are analyzed in terms of direct damage from shock waves, damage from longer duration slower pressures from vaporization of dielectric or metallic solids, direct magnetic forces and burning from long duration low current continuing components. Studies have included piezo blast gage pressure measurements and Schleiren photography of the shock waves in the laboratory and pressure measurements of triggered natural lightning discharges. Theoretical and experimental analysis of probable maximum shock pressures, magnetic forces and slower pressures indicate that the principal problem is introduced through long arcs developed inside sections and that the best general solution for providing lightning protection is still to keep the lightning discharge currents on the aircraft exterior or provide conductors with sufficient cross sectional area to carry the current where the currents must penetrate the aircraft.

LIGHTNING DAMAGE REPORTS ON DIELECTRIC COMPOSITE MATERIALS such as the fiberglass laminates used on aircraft nose radomes have shown wide differences in the extent of damage produced during their use over a period of approximately 15 years. The variation in effects is attributed to the type of construction, location of the materials and also to the variation in the protection provided. Analysis of this lightning damage has indicated that with proper protection, the damage can be minimized but where proper protection is not provided, major serious structural damage can occur. Thus, a basic understanding of the damage mechanisms and protection principles is most important for aircraft structural designers as lightning protection can be most economically and effectively implemented in early design phases. In this paper, damage mechanisms and typical damage are discussed along with a brief review of the protection approaches used in the past and the problems introduced by new aircraft design techniques.

DAMAGE MECHANISMS

Lightning damage to dielectric composite materials can be produced through several damage mechanisms: (a) direct damage from shock waves to materials close to the lightning channel core, (b) longer duration pressures from lightning arcs contained in closed spaces and generally increased by vaporization of plastic resins or small diameter metallic conductors, (c) direct magnetic forces, and (d) burning through long duration low current continuing components.

An important characteristic of the shock wave issuing from the typical lightning stroke channel is its short time duration. A Schleiren photograph of a shock wave from a half meter long 5000 ampere laboratory discharge is shown in Figure 1 and oscillograms of typical waveforms from laboratory arcs are shown in Figure 2. The maximum stress generation or damage is produced when the time duration of the shock wave (or any impulse) roughly equals the response time of the half cycle period of the natural resonant frequency for the component being shocked. Most often the inertial response times of aircraft components are relatively slow with respect to the ten microsecond rise time and hundred microsecond duration of the fast shock fronts and therefore little damage is produced unless the arc is in direct contact with the material. The short duration of the shock wave and the lack of confinement for external stroke pressures is suggested as an explanation for the lack of extensive external damage on an aircraft. In LTRI lightning damage files there is almost no evidence of severe external pressure effects in the form of skin wrinkling or structural deformities on the outside of aircraft with a few exceptions, one of which is shown in Figure 3. In this

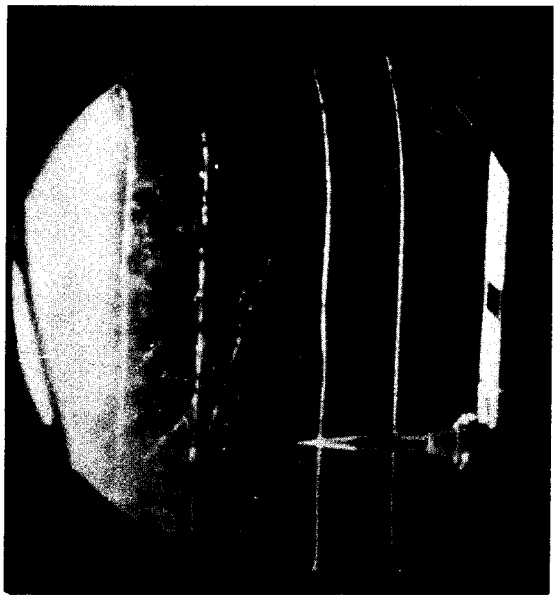

Fig. 1 - Schleiren photograph of shock wave from laboratory high current discharge moving over piezo pressure transducer.

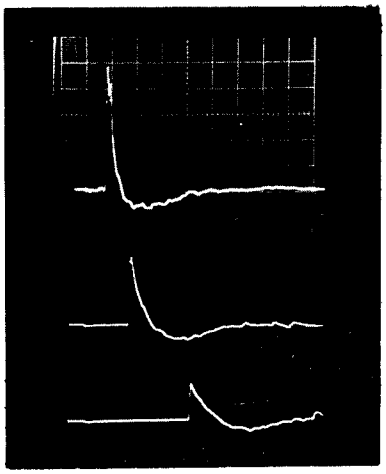

Fig. 2 - Oscillograms of shock pressures at (a) 10 cm, (b) 20 cm and (c) 40 cm from 0.8 meter discharge, 0.008 inch wire initiated 100,000 ampere discharge. All sweeps - 200 μsec/div, vertical sensitivity - 1.9 psi/div.

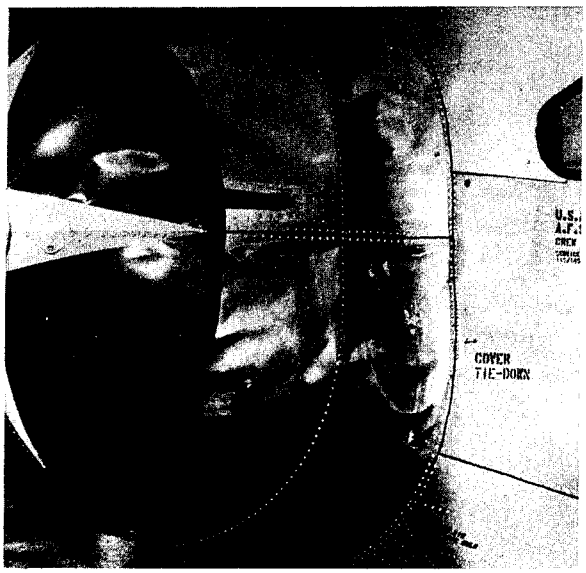

Fig. 3 - Wrinkling of external aircraft skin from lightning strike attributable to shock pressures and/or magnetic forces.

case the skin was thin and flat with low stiffness. Even here it is not clear that the wrinkling could not have been produced by magnetic effects.

The characteristics of the shock wave from the natural lightning return strokes has been the subject for a number of theoretical and experimental investigations and although there remains some areas of disagreement on the exact magnitudes, the differences correspond to probably less than one order of magnitude. The theoretical equations for strong shock waves have been developed for spherical shocks by Taylor (1)* and adapted to cylindrical shock waves by S. C. Lin (2). In this analysis it is assumed that the total energy goes into the acoustic wave to provide an upper bound for the shock pressures and that the energy is released instantaneously along an infinite straight line in the atmosphere, an over-simplification as the channel is never completely straight. Because of the strong shock assumption, the analysis is not valid when the shock pressures become too low nor when the pressure ratio becomes so high that dissociation and ionization become significant.

The pressure peak decays as an inverse square function of the distance in the strong shock region changing to the inverse first power at about 5 atmospheres as an acoustic wave and finally at greater distances reducing to the inverse 3/4 power (3).

*Numbers in parentheses designate References at end of paper.

A graph of the calculated pressure variation with distance based on the theory of Lin for energy inputs of 1000, 10,000 and 100,000 joules per meter of channel length is presented in Figure 4. These are estimated values for moderate to severe strokes based on LTRI studies and theoretical shock profiles are shown in Figure 5.

These calculations indicate lower pressures than indicated by earlier investigators who calculated the pressures from spectroscopic analysis of natural lightning discharges (4). Other experimental and theoretical investigations have been made more recently including investigations of both laboratory long sparks and natural lightning (5, 6). It should be noted that the references are restricted specifically to near zone effects of interest in relation to aircraft damage and do not include studies of thunder and related far zone effects. The studies all roughly indicate values falling near or slightly below the curves shown in Figure 4.

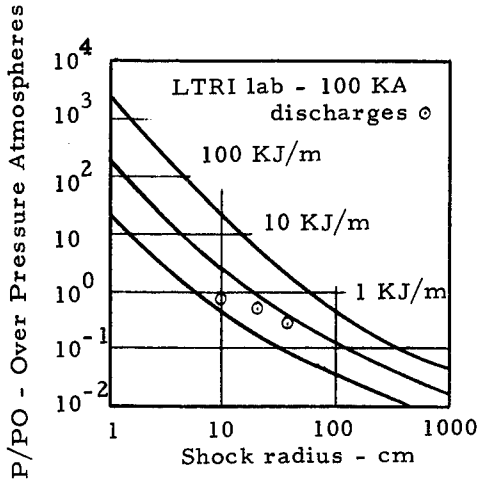

Fig. 4 - Theoretical and experimental variation of shock over pressure with distance.

LTRI has also measured shock waves from triggered natural lightning discharges (7, 8), as illustrated in Figure 6; however, most of the triggered strokes involve upward going step leaders which give lower current rates of rise and probably much lower peak pressures. Thus, the maximum pressures, as indicated by the theoretical and experimental laboratory studies (and the few triggered strokes which LTRI believes to have been downward going step leaders of typical cloud to ground lightning strokes) permit a conservative estimate of the probable maximum shock pressures to be encountered about one foot from the channel core.

The results of these studies indicate overpressures of the order of an atmosphere at a few hundred microseconds. The theoretical studies indicate that the values increased at distances closer to the source as indicated in Figure 4 to peak pressures of the order of 100 atmospheres at the outside of the channel core.

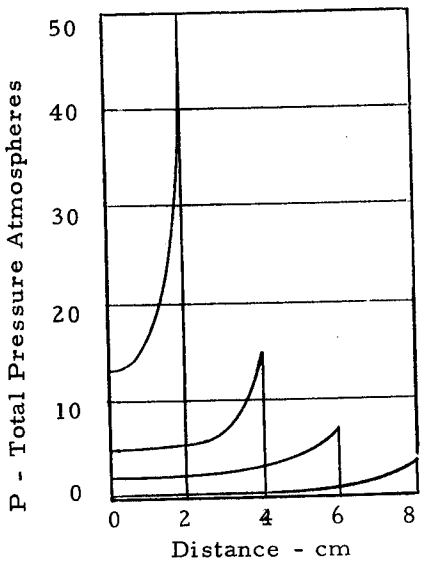

Fig. 5 - Theoretical shock profiles close to channel.

Fig. 6 - Photograph of triggered lightning discharges to LTRI Research Vessel Thunderbolt. One inch pipe railing near channel indicates channel diameters of a few millimeters to a few centimeters.

The peak pressures closer to the core remain to be verified experimentally for both laboratory and natural lightning discharges. The bright core diameter indicated quite clearly in LTRI triggered lightning photographs, Figure 6, vary from a few millimeters for restrikes to a few centimeters for the initial return stroke; however, the initial return stroke in LTRI triggered strokes is affected by metallic ions and probably does not represent the free space diameter.

In regard to aircraft damage, the stroke always terminates on the metal airframe which results in metal ions in the nearby channel. Historically, early investigators reported metal ions in spectrograms of natural discharges to flag poles out to distances of 50 meters. Because of the hugh driving voltages and long path length of a natural discharge, the current waveform will be little affected by the presence or absence of metallic ions. Thus, for study of lightning effects on an aircraft, the metal ions may always be assumed to be present in the channel in the near zone of interest and to have little effect on the current waveform. Measurements of the pressures generated from open air arcs and with 0.008 inch diameter stainless steel wire used in LTRI lightning triggering studies show that the wire does increase the shock pressures about 15% for currents over 50,000 amperes (9). Apparently with energies far beyond the energy required to vaporize the very fine wire, the pressure is not greatly increased.

The question of interest in aircraft lightning protection is - to what extent does the shock wave itself produce aircraft damage? Examination of aircraft damage from lightning provides some clues as to the magnitudes. Where the high current channel is in direct contact with the outside of a plastic section, as for example a radome, and particularly where the channel is confined by exterior heavy paint coatings such as in vaporizable radome protection strips, the damage appears as if the radome external skin had been neatly torn along the arc contact path. The damage is probably due to the lightning channel pressures as the effect seems to be independent of geometry (which primarily determines magnetic force effects as for example, right angle bends). Calculations of the shear pressures required to sever a typical external radome skin indicate pressures of the order of 800 psi or about 50 atmospheres, as illustrated in the following simplified calculation. Assuming a shear strength of the skin of approximately 20,000 psi and a skin thickness of 0.04 inches, a linear force of approximately 800 psi would be required to produce shear failure corresponding to pressures of 50 atmospheres which is a little below the theoretical estimates for pressures close to the lightning channel core shown in Figure 4.

What is much more difficult to resolve is the question of how much damage would be produced at distances of a few inches to a few feet in which the interaction of the shock wave with the material becomes more complex. Viewing the mechanical failure problem as a problem in transient analysis, the impulse time duration, as pointed out earlier, must be approximately matched to the half cycle natural resonant period to produce maximum stress in the material and generally the aircraft components have much slower inertial responses than the hundred microsecond duration of the shock wave. Thus, it is difficult to evaluate the mechanical transient response of components to the shock wave alone without even considering the often inseparable problems of the associated slowly rising pressure waves from vaporized materials and the magnetic forces. Additional complications are also introduced by the fact that the shock front generally does not impact the structure squarely but rather in the form of an oblique traveling wave.

The pressures produced by the more slowly rising confined pressures from vaporized materials can also be calculated approximately on the basis of the pressures required for failure. The time duration of the trapped gas pressure will extend until some type of pressure relief occurs in the form of breakup of confined areas. A typical example is offered in loss of fighter radomes. For one typical fighter, the radome tensile loads were carried by four high strength bolts with a total tensile load capacity of about 20,000 pounds. The radome cross sectional area at the fuselage bulkhead was about 1000 square inches and this would require a pressure of greater than 20 psi to blow the radome off the forward bulkhead of the aircraft as indicated in Figure 7. In this particular radome, a glycol deicer line ran from the fuselage to the forward pitot boom and the high energies in the lightning channel may have vaporized the liquid into glycol steam at the required 20 psi. Similar reports have been received for radomes with #22 pitot heating wires and no glycol lines but with similar results, loss of the radome.

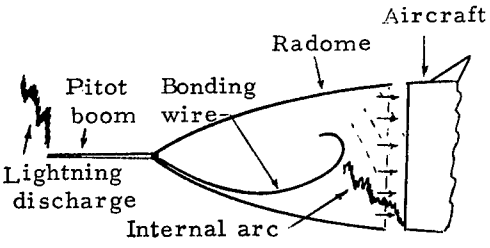

Fig. 7 - Arc from failed bonding wire blows radome off forward bulkhead of aircraft.

These pressures are not too low to have been caused by a shock wave at a distance of one or two feet, but the lack of a uniform wavefront and the short time duration of the impulse makes the shock waves a less plausible reason for failure than the long duration steady pressures.

An example of pressures in a 100,000 ampere laboratory discharge is illustrated in Figure 8. An artificial lightning discharge of 100,000 amperes shattered a tubing of phenolic plastic with 1/8 inch wall. From the tensile strength of the material (about 5000 psi), the pressure which is required to shatter the tube may be calculated and is found to be about 450 psi, about 30 atmospheres ignoring end effects.

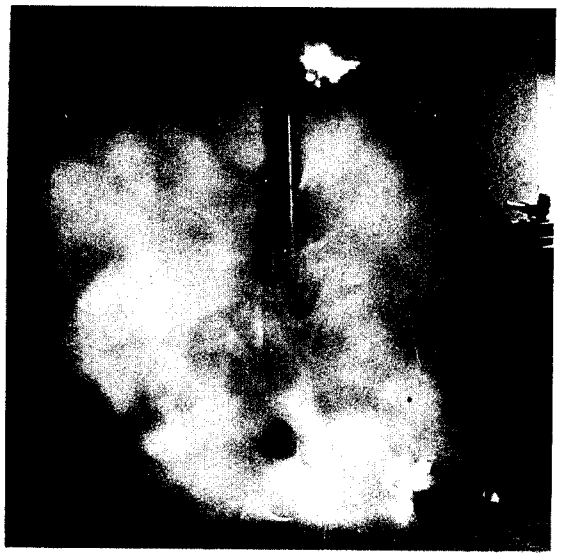

Fig. 8 - Pressure in 100,000 ampere laboratory discharge shatters phenolic tube to indicate pressure.

The magnetic forces produced by current flow through conductors bent at right angles or through the direct force of the arc channel against the plastic surfaces can be calculated and indicate substantial forces of the order of tons. However, because of the very short duration (hundreds of microseconds), the effective force in producing failure (as in the case of the very fast shock front) is greatly reduced and it is estimated that the effective force is probably of the order of one-tenth to one-quarter the peak.

Thus, the major damage produced in aircraft can be explained by anyone of these three effects: the shock wave, the pressures from vaporized materials, and the direct magnetic forces. Burning or ignition of flammable resins usually requires the long duration components. However, consideration of inertial response time for the faster phenomena of the shock waves and magnetic forces greatly complicates any theoretical calculations.

TYPICAL DAMAGE

Typical damage to aircraft parts made of dielectric composites includes damage to radomes, damage to fin cap antenna fiberglass isolation gaps, damage to fiberglass wingtip caps and to miscellaneous fiberglass sections including trailing edges, ventral fins, and plastic antennas. The damage can be further amplified by entrapment of moisture inside the plastic sections through microscopic pin holes produced by lightning streamer punctures which may have been produced in earlier flights. The lightning discharge can produce streamer punctures even though the strike occurred to other parts of the aircraft, by virtue of the intense electrical gradient on the entire aircraft when contacted by a lightning stroke. These pin holes may permit moisture entrapment through breathing and direct raindrop entry with resulting additional vapor production should a stroke puncture occur. The pressure effects, of course, are amplified by the additional vapor no matter what type it may be, steam (water) vapor, polyester or epoxy resin vapor or copper or aluminum metal vapor from vaporized conductors.

The most serious type of damage is produced generally by confined arcs, either inside fiberglass covered sections, between layers or on the outside but confined by heavy external anti-erosion coatings. An example of the latter is shown in Figure 9. A vaporizable foil protection strip was covered to reduce weathering

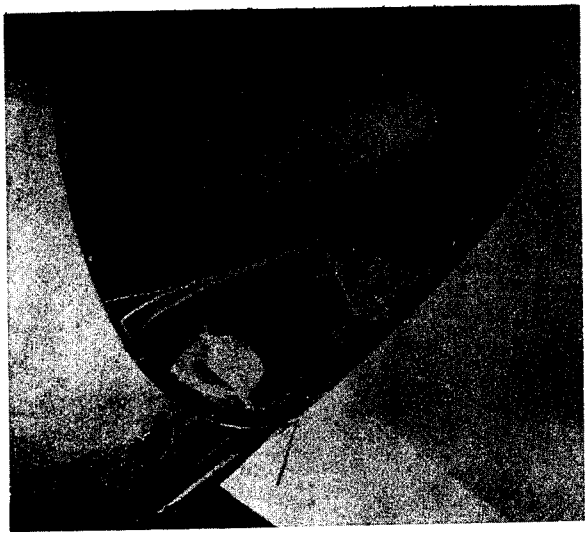

Fig. 9 - Lightning damage to radome with vaporizable foil strip covered with thin coating. Coating confines explosion of strip to produce implosion or shaped charge effect nearly severing radome.

problems. The covering confined the explosion when the strip was vaporized producing an implosion which split the lower skin. Laboratory studies have shown that even thick paint layers over vaporizable strips can produce this effect. Thus, as indicated in the next section, the basic approach to lightning protection for the non-conducting composites is to keep the arc on the outside of the aircraft or if it passes through the interior to provide sufficient conductor cross section and, most important, use tested attachment hardware to prevent internal arcs, as illustrated in the next section.

PROTECTION APPROACHES

The first problem with non-conducting composite materials is to determine whether or not major damage or loss of the fiberglass section would constitute a flight hazard, and if it would not, whether the damage is more acceptable than the cost of installing protection. As an example, for some aircraft, no protection is provided for the trailing edge fiberglass sections on the basis that the loss of extensive sections will have no serious effects on the handling characteristics of the aircraft and that protection would be quite heavy and expensive to provide. Therefore, repair of the fiberglass for infrequent strikes in low probability areas results in the greatest economy.

Where fiberglass sections are located in high strike probability areas, both operational requirements for military aircraft, and economic factors for commercial aircraft, may require protection even if safety of flight is not required.

The earliest protection systems used a solid aluminum bar for radomes and aircraft lightning arresters for fin cap antenna isolation gaps and they successfully demonstrated the effectiveness of these protection approaches. Subsequent to the use of the solid bar system on early military aircraft radomes, a thin foil strip protection was adopted for commercial aircraft nose radomes on the basis that the foil was economical to install, low in weight and could be repaired in the field quite easily after damage. However, it was found that the foil protection systems, even though quite economical to install initially, were quite expensive to maintain and had one serious disadvantage, the generation of radio interference in the VHF-UHF region if these strips became cracked. The strips friction-charged under precipitation charging conditions and sparked over at the frequency corresponding to their natural resonant wave lengths which often falls directly in the VHF-UHF communication-navigation ranges. Thus, the protection strips were replaced with the solid bar conductors, 1/8" x 3/8", which are in current use on most of the commercial jet transport aircraft.

Other approaches have included conducting paint of uniform resistivity which may be used for some geometries, graded resistance paints which are more effective in diverting the discharges over the outside of plastic sections but which are also much more difficult to apply and maintain, as well as the use of aluminum particle paints which are inherently insulating but which provide conducting paths for lightning discharges by breakdown of the aluminum oxide insulation on the outside of the particles.

All of these approaches using conducting coatings are much less effective than the solid metal conductors and are used generally where protection is marginal and the use of these materials will bring the protection effectiveness up to the acceptable level. A simple example is the protection of ECM antennas located under a radome. Any metal strips interfere excessively with the system performance. One solution which proved to be effective was to use acrylic insulation over the shelf which supported the antennas and which was outside the aperture of the antennas, to use aluminum particle paint over the thin forward skin of the radome and protection strips over the aft section of the radome behind the antennas. The aluminum particle paint enhanced surface flashover and prevented puncture providing the acrylic insulator was also used over the shelf area. Surprisingly, eight coats of the aluminum particle paint resulted in a transmission loss of only a few percent.

The use of uniform conducting coatings over all fiberglass areas of large aircraft has been the subject of some debate. Its use does generally reduce lightning damage by enhancement of surface flashover where no metal components are located beneath the surface and also reduces the radio interference associated with atmospheric particle friction charging but it does represent a substantial weight penalty. Therefore, as safety of flight is not generally involved in the use of conducting coatings its use must be justified on an economic or mission importance basis. A probable application would be for aircraft operating in polar regions where snow static could become a serious problem with communications and where low frequency communications particularly susceptible to this type of interference are required for the long range communications necessary because of the sparsity of radio facilities.

A more recent protection approach used for non-conductive composites as well as conducting composites is the development of light weight metallic coatings of various types, including among many, metallic flame spray coating or aluminum foil coating. These can very effectively provide lightning protection as well as provide shielding for EMC (electromagnetic compatibility) purposes and should be evaluated in overall terms of providing these multiple functions. For example, it might be more economical and result in less weight penalty to use a thin metallic coating over a fiberglass section containing unshielded wiring than to provide less lightning protection but then need conduit over the wiring for EMC purposes. The

best approach has proved in the past to be selection of the particular protection technique or combination of techniques for the particular application considering the total problem as demonstrated in final high voltage high current tests.

CONCLUDING COMMENTS

Tests of non-conducting composites have shown that with proper lightning protection, lightning damage can be minimized and that without lightning protection serious structural damage can occur. Where safety of flight is not a factor, protection becomes an option which must be evaluated in terms of economics, and for military aircraft, mission importance.

REFERENCES

1. G.I. Taylor, "The Formation of a Blast Wave by a Very Intense Explosion," Proc. of the Royal Society A, 201, 159, 1950.
2. S.C. Lin, "Cylindrical Shock Waves Produced By an Instantaneous Energy Release," J. Appl. Phys. 25, 54, 1954.
3. D.L. Jones, G.G. Goyer and M.N. Plooster "Shock Wave from a Lightning Discharge," J. Geophys. Res., 73, 10, May 15, 1968.
4. Y.N. Zhivlyuk and S.L. Mendelshtam, "On the Temperature of Lightning and Force of Thunder," JETP, 13, August 2, 1951.
5. W.W. Troutman, "Numerical Calculation of the Pressure Pulse from a Lightning Stroke," J. Geophys. Res., 74, 18, August 20, 1969.
6. M.A. Uman, A.H. Cookson and J.B. Moreland, "Shock Wave from a Four Meter Spark," J. Appl. Phys., 41, 7, June 1970.
7. E.L. Hill and J.D. Robb, "The Pressure Pulse from a Lightning Stroke," J. Geophys.
8. M. M. Newman, J. R. Stahmann and J. D. Robb, "Experimental Study of Triggered Natural Lightning Discharges," Final Report to Federal Aviation Administration under Contract No. 520-002-03X, No. DS-67-3, March, 1967.
9. M. M. Newman, "Use of Triggered Lightning to Study the Discharge Process in the Channel and Application to V.L.F. Propagation Studies" Problems of Atmospheric and Space Electricity, New York, Elsevier Publishing Company, 1965.

700935

LIGHTNING PROTECTION FOR ADVANCED COMPOSITE AIRCRAFT STRUCTURES

by

1st/Lt G.T. Woodrum

AIR FORCE MATERIALS LABORATORY

ADVANCED COMPOSITE DIVISION

WRIGHT-PATTERSON AIR FORCE BASE, OHIO

ADVANCED REINFORCED PLASTICS are invading a number of areas in the aircraft and automotive industry as a direct result of recent development work on composite materials which utilize exotic fibers such as carbon, graphite, boron, or sapphire as reinforcing media in a plastic matrix. Structural designers are attracted to these composites because of the tremendous increase in strength, stiffness, and weight reduction which they offer over conventional production materials such as steel and aluminum. To those of you who are unfamiliar with the significance of this advantage, lets look at the following chart. (Fig. 1) Conventional aerospace materials such as steel, titanium, and aluminum, as we all know, are very strong; and when subjected to a load or force of type they retain their stiffness quite well. Fiberglass, a first-generation composite material that is seeing increased usage in all areas of consumer interest that require structural stability is stronger than the conventional materials and just about as stiff. I am comparing all of these materials now, on an equal weight basis, and what you are seeing is a comparison of the specific strength versus the specific modulus. When we look at composite materials which utilize these exotic fibers, such as boron/epoxy (B/E) and graphite/epoxy (G/E) we see that they are much stronger and stiffer and are therefore better structural materials. The numerical properties of some of these aerospace structural

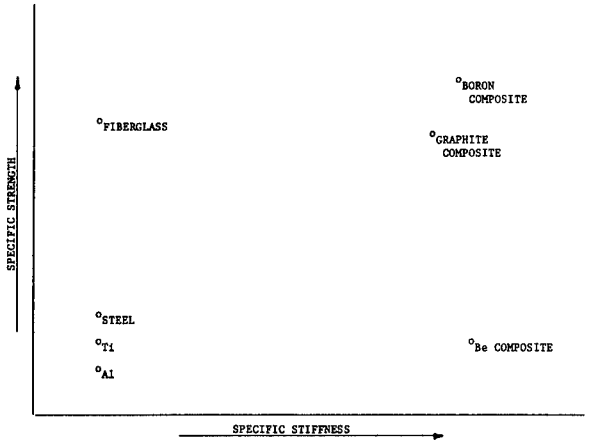

Fig. 1 - Specific properties of aerospace structural materials

materials look something like this. (Fig. 2) As you can see, the combination of specific strength and modulus of composite materials is much higher than any of the other materials on the list. Two of the most promising candidates in this area are boron/epoxy and graphite/epoxy. Both materials offer specific advantages, and it is quite natural to assume that they both will be used in the fabrication of future aircraft systems as well as other commercially oriented products.

Realizing the potential offered by composites, the Air Force Materials Laboratory in 1964, initiated an advanced development program to design, fabricate and flight test prototype structural components such as the fuselage, wings, and empennage from advanced composite materials. A list of hardware components that have been built and tested to date, can be seen in the next figure. (Fig. 3)

MATERIAL	DENSITY lb/cu. in	TENSILE STRENGTH p.s.i.	YOUNG'S MODULUS p.s.i. x 10^6	SPECIFIC TENSILE STRENGTH in x 10^6	SPECIFIC YOUNG'S MODULUS in x 10^3
ALUMINUM	0.100	85,000	10	0.85	100
HIGH TENSILE STEEL	0.283	200,000	30	0.71	110
FIBERGLASS EPOXY	0.076	150,000	5	2.0	90
TITANIUM	0.170	150,000	17	0.9	100
*COMPOSITES	0.06	140,000	36	2.3	600

*VALUES ARE TYPICAL OF ADVANCED COMPOSITES PROPERTIES

Fig. 2 - Basic material properties

F-111 Airflow Director Door	F-104 Fire Access Door
F-111 Wing Trailing Edge Panel	RA-5C Antenna Cover
F-111 Aft Landing Gear Door	F-4 Rudder
A-4 Landing Flap	A-6 Wing Fence
C-141 Wing Tip	C-5 Slat
F-5 Leading Edge Flap	F-111 Horizontal Stabilizer
F-5 Main Landing Gear Door	F-5 Horizontal Stabilizer

Fig. 3 - Composite aircraft flight-test components

Based on the results of these tests several hardware production commitments have been made for future as well as existing aircraft systems. Production emphasis has been placed primarily in the empennage area of the F-4, F-14, and F-15 aircraft systems.

When composites are used as aircraft structural materials, they will be exposed to a wide variety of environmental "hazards". One of the most severe hazards that an in-flight aircraft is exposed to is lightning strike. Metallic aircraft structure provides a natural conductive path for dissipation of electrical current. When lightning does strike it, little structural damage occurs. Non-metallic materials on the other hand do not conduct electrical current and their exposure to lightning produces severe damage, oftentimes destroying the entire mass of material. Advanced composites are hybrid materials as far as electrical conductively goes. The plastic matrix acts as a non-conductive material and the fibers, which are imbedded, but do not touch each other in the matrix, act as conductive materials. Also none of the fibers are exposed on the surface of the laminate. When composites are struck by lightning, damage ranging from slight surface pitting to fiber explosion and even complete specimen destruction can be observed. Many lightning damage studies for composite materials have been made in the last year or so. The studies included both lightning parameter variations as well as variations just mentioned, several lightning protective schemes were also evaluated in these studies. The initial studies were concerned primarily with lightning strike characterization. To determine these effects, a direct comparison of lightning damage to boron/epoxy, graphite/epoxy and fiberglass/epoxy test specimens was made. These three materials were used to study possible effects caused by the fiber reinforcements. It might be noted here that the glass fibers are non-conductive materials. All test specimens were unprotected and two different energy discharge levels were studied: one of a low coulomb and amperage level, the other of a medium to high coulomb and amperage level. The test panels were 6" wide, 12" long, and 0.040" thick. After impact the panels were visually inspected for damage extent. A low level strike (25KA, 0.024 coulomb) produced slight damage in the boron and graphite/epoxy specimens. The fiberglass specimen however showed only limited surface

pitting. When the amperage was raised to the 60 to 100KA and 1.9 coulomb range, extreme laminate damage occurred to the boron and graphite/epoxy specimens. However, the fiberglass specimen remained undamaged, with only minor surface pitting again. The next figure shows the tabulated results of this study. (Fig. 4) Lightning and Transient Research Institute, the contractor who conducted this phase of the study, concluded that plane composite panels must be protected by some mechanism in order to structurally survive a direct lightning strike.

Frequently designers utilize aluminum honeycomb core to transfer sheer forces in composite structures. The possibility of increased lightning damage due to the conductive aluminum core was proposed for additional studies. This study evaluated only sandwich specimens with boron/epoxy (B/E) facesheets. These specimens, which were subjected to varying lightning strike levels as high as 200KA, were unprotected, and contained 6 ply facesheets. Results of this study indicate thateven moderate discharges, in the 50 KA range, produced severe degredation to the specimens. In many of the specimens the honeycomb was literally melted away. Some of the specimens ruptured due to expanding air in the honeycomb cells. All the specimens, no matter what the discharge level, were delaminated at the surface of the aluminum core and the boron facesheet. Again the study concluded that some type of lightning protection must be provided for composite hardware, especially when used in combination with metallic sandwich sub-structure.

PANEL DESCRIPTION	AMPERAGE	COULOMBS	DAMAGE DESCRIPTION
BORON/EPOXY, UNCOATED	25KA	0.024	Localized Laminate Damage
GRAPHITE/EPOXY, UNCOATED	25KA	0.024	Localized Laminate Damage
FIBERGLASS/EPOXY, UNCOATED	25KA	0.024	Surface Markings Only
BORON/EPOXY, UNCOATED	60KA	1.9	Extreme Laminate Damage
GRAPHITE/EPOXY, UNCOATED	85KA	1.9	Extreme Laminate Damage
FIBERGLASS/EPOXY, UNCOATED	100KA	1.9	Surface Markings Only

Fig. 4 - Unprotected lightning study results

The next step in the lightning evaluation studies was to look at techniques which might possibly provide the desired protection for composite structure. Selected protective systems would have to either meet or surpass lightning protection requirments outlined in MIL-B-5087B. Basically this regulation establishes a minimum test waveform for evaluating lightning damage to external sections of the aircraft. Included in this waveform is a 200KA peak value for a width of 5-10 microseconds. Angles of lightning impact are also specified. The three approaches outlined in the table below (Fig. 5) were evaluated in this phase. Heavy emphasis was logically placed on the metallic foil approach since this method was thought to provide the maximum conductive path for current dissipation. The next series of figures (Figs. 6, 7, 8, 9, and 10) shows the various types of metallic protection which were evaluated.

1. METAL FILLED COATINGS
2. PLASMA SPRAYED COATINGS
3. METAL FOIL COVERINGS

Fig. 5 - Lightning protective schemes

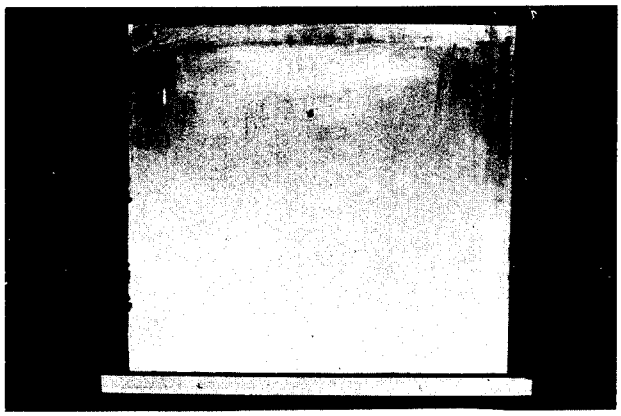

Fig. 6 - B/E sandwich panel with .006" aluminum foil

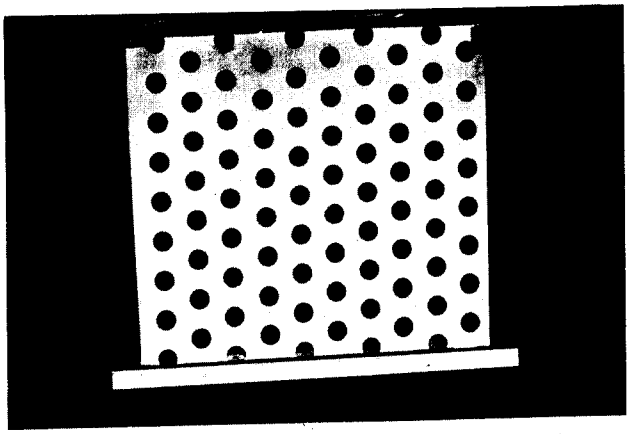

Fig. 7 - B/E sandwich panel with perforated aluminum foil .006" thick

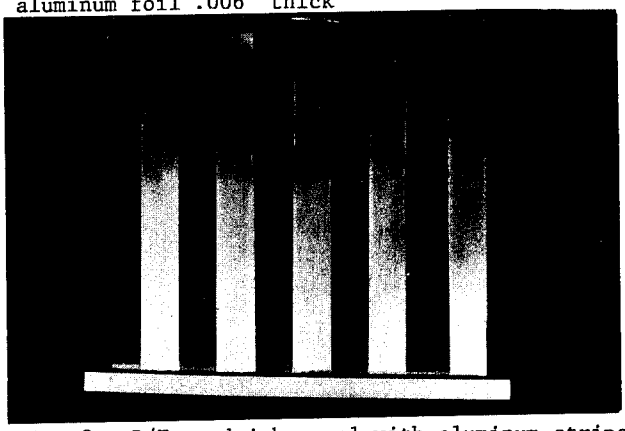

Fig. 8 - B/E sandwich panel with aluminum strips .006" thick, 1" wide, spaced 1" apart

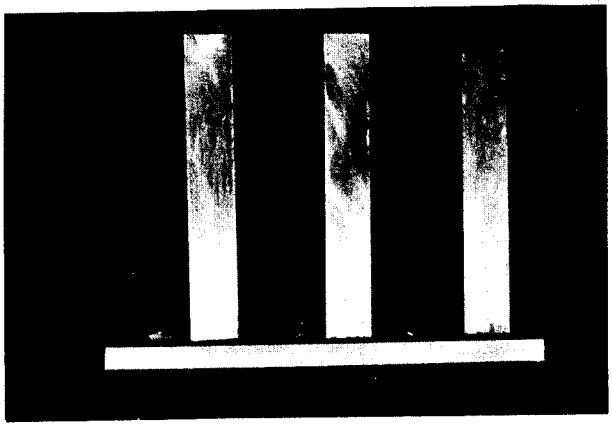

Fig. 9 - B/E sandwich panel with aluminum strips .006" thick, 1" wide, spaced 2" apart

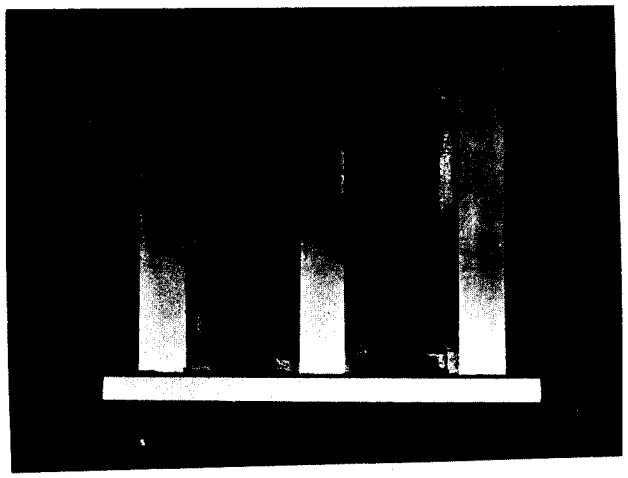

Fig. 10 - B/E sandwich panel with aluminum strips .006" thick, 1" wide, spaced 2 3/4" apart

---

While the composition and thickness of the metallic foil were being held constant, lightning damage to various foil patterns were studied. The idea was to study complete versus partial coverage of the composite test area. Results of this phase of the study are illustrated in the next series of figures (Fig. 11, 12, 13, 14, and 15).

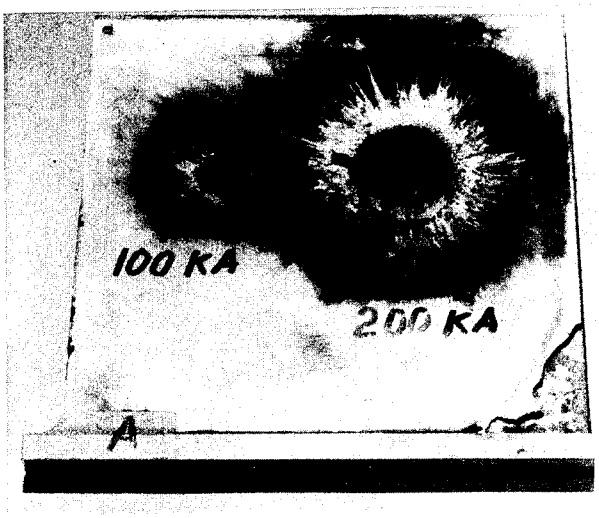

Fig. 11 - B/E sandwich panel with .006" aluminum foil after 100KA and 200KA lightning strikes

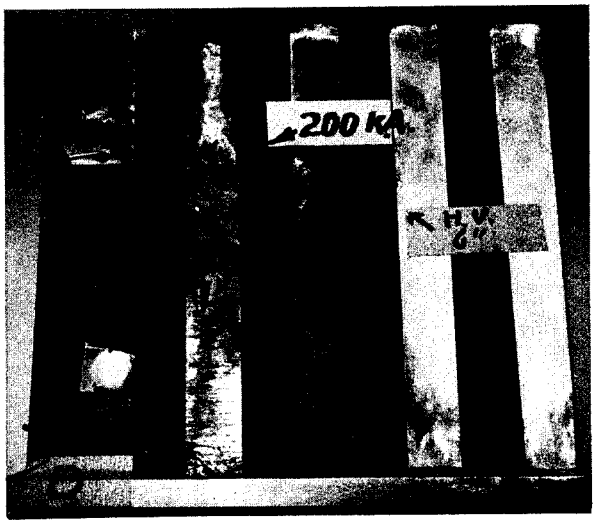

Fig. 12 - B/E sandwich panel with 1" wide aluminum strips, spaced 1" apart after 200KA and high voltage lightning strikes

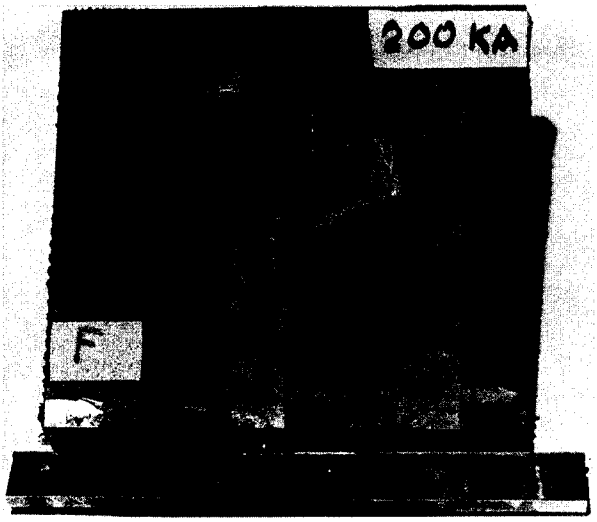

Fig. 14 - B/E sandwich panel with 1" wide aluminum strips, spaced 2" apart, with the aluminum strips removed after a 200KA lightning strike

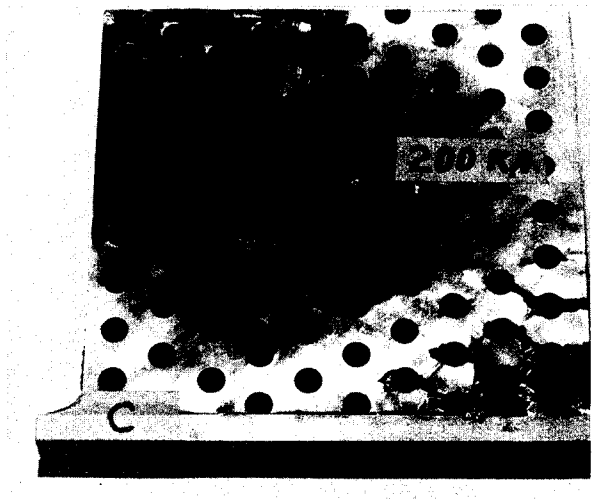

Fig. 13 - B/E sandwich panel with perforated .006" aluminum foil after 200KA lightning strike

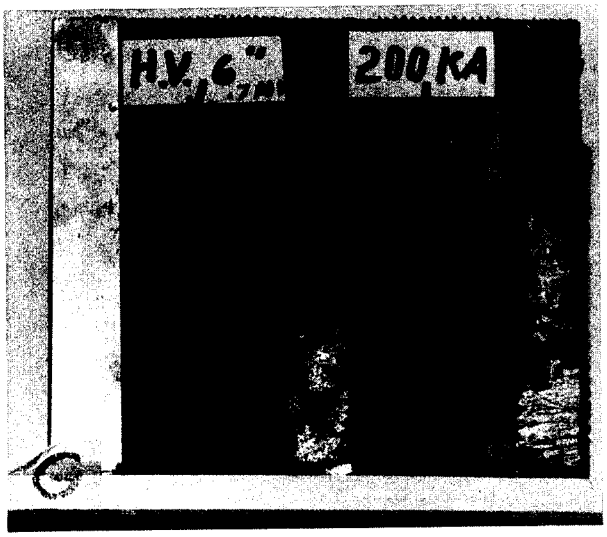

Fig. 15 - B/E sandwich panel with 1" wide aluminum strips, spaced 2 3/4" apart after a 200KA and a high voltage lightning strike

Specimen A which had the aluminum foil covering over the entire test area provided the best protection. Double verification of this fact was obtained when each specimen was cut up and strength and modulus tests run and compared with undamaged control specimen values. This data is shown in Table 1. One of the problems in using this type of protective system is that it is heavy and requires considerable time to install. In the beginning of this paper I stressed the point that one of the major advantages in using composite materials was increased weight savings. However, if heavy foils were used on production composite hardware, a considerable amount of weight would be readded to the part thus reducing the total weight saving. This factor, combined with large application costs would not allow the composite structure to be cost effective. By comparison, the flame sprayed and metal-filled coating techniques offered the same basic protection as the .006" aluminum foil. These methods however, allow a thinner (.003") protective barrier and a faster application time. Metal filled coatings offer one particular advantage over the other two techniques. They can be applied to the composite skin while the skin is being cured in its mold; that is by co-curring techniques. By simply applying the coatings to the inner face of the mold, then laying the uncurred composite skins into the mold and finally the addition of temperature and pressure one can achieve a very economic lightning protection scheme.

Table 1 - Results of Mechanical Tests on Lightning Test Panels at Room Temperature

Specimen No.	Strength	Modulus	
A-1	154 ksi	17.9 ksi	*
A-2	145 "	17.3 "	*
A-3	150 "	17.3 "	
A-4	154 "	18.0 "	
A-5	148 "	17.9 "	
A-6	149 "	17.8 "	
A-7	146 "	18.9 "	
A-10	145 "	17.2 "	*
A-11	147 "	16.8 "	*
A-12	157 "	17.3 "	
A-13	142 "	17.5 "	
A-14	149 "	17.4 "	
A-15	142 "	17.6 "	
B-1	152 "	17.6 "	*
B-2	159 "	17.3 "	*

Table 1 Continued:

Specimen No.	Strength	Modulus	
B-3	124 ksi	16.9 ksi	
B-4	116 "	16.8 "	
B-5	127 "	17.7 "	
B-6	128 "	17.1 "	
B-7	136 "	16.9 "	
C-1	155 "	17.1 "	*
C-2	146 "	16.6 "	*
C-3	146 "	17.3	
C-4	147 "	16.9 "	
C-5	108 "	16.5 "	
C-6	151 "	16.6 "	
C-7	145 "	16.7 "	
G-0	114 "	15.7 "	*
G-1	119 "	15.8 "	*
G-2	115		
G-3	97 "		
G-4	78		
G-5	30 "		
G-6	91 "		
G-7	107 "		
G-9	155 "	17.5 "	*
G-10	141 "	16.8 "	*
G-11	149 "		
G-12	115 "		
G-13	80 "		
G-14	96		
H-1	276 "	33.0 "	*
H-2	274 "	31.2 "	*
H-3	280 "	32.1 "	
H-4	288 "	33.2 "	
H-5	268 "	33.6 "	
H-6	282 "	32.8 "	
H-7	274 "	33.4 "	
H-8	274 "	33.8 "	
H-9	296 "	34.0 "	
H-10	277 "	33.5 "	
H-11	276 "	31.2 "	*
H-12	280 "	33.0 "	*
H-13	284 "	32.4 "	
H-14	291 "	32.8 "	
H-15	272 "	31.6 "	
H-16	271 "	32.8 "	
I-1	158 "	19.7 "	*
I-2	152 "	20.0 "	*
I-3	151 "	19.9 "	
I-4	147 "	20.7 "	
I-5	141 "	19.8 "	

Table 1 Continued:

Specimen No.	Strength	Modulus
I-6	157 ksi	19.8 ksi
I-7	156 "	19.4 "
I-8	155 "	19.2 "
I-9	159 "	19.6 "
I-10	150 "	20.2 "
I-11	155 "	20.0 "
I-12	155 "	19.9 "
I-13	149 "	20.2 "
I-14	136 "	20.4 "
I-15	139 "	19.7 "
I-16	117 "	16.0 "
I-17	60 "	
I-18	88 "	13.0 "
I-19	127 "	18.7 "

* indicates control specimen

Concurrently with the beginning of the lightning strike studies, several composite hardware programs, whose requirments called for the demonstration of the final components via flight testing, were in progress. These programs were building a series of F-111 horizontal stabilizers and a set of F-100 composite wing skins. Both programs attempted to build hardware items that would meet all the design and safety requirments of their aluminum counterparts. Both programs also considered the possibility of lightning strike damage. In the stabilizer program a lightning protective system was suggested by the contractor at the outset of the program. A lightning effects investigation was also proposed by the contractor, but the actual work was done outside the scope of the program. This investigation was based on the design of the stabilizer which contained several detachable edge components. The design consisted of the leading and trailing edge, a center box section, and a tip edge. (Fig. 16) All of these parts were constructed of aluminum honeycomb core and boron/epoxy facesheets. The peripheral components are the detachable articles which were tested for structural and design verification. The design of the trailing edge component was selected for use in building the lightning strike specimens used to evaluate prospective lightning protection systems and also to determine lightning effects on larger test components. Previous investigations on the F-111 aircraft with all aluminum stabilizers, indicated that lightning impact confined itself to these peripheral components in the stabilizer area. This led one to believe that if a conductive path could be provided from the stabilizer into the fuselage area, a large portion of the lightning current could be dissipated without loosing the structural integrity of the stabilizer. Even though these tests indicated that most lightning strikes occur around the edges of the stabilizer, provisions had to be made for sweeping strikes which could jump across the surface of the composite stabilizer and cause additional damage. This is where a protective system would be necessary. Evaluation of the trailing edge specimen tests verified this hypothesis. The results of these tests were reported previously in last years Lightning and Static Conference Report.(1)* The conclusions of this study however, suggested that the flight test stabilizer be protected by both aluminum strip bonded to the perimeter of the stabilizer and a silver filled epoxy paint applied over the entire composite surface. This combination is expected to provide adequate protection against direct lightning strike and secondary streamer effects. It also provides for a conductive path into the fuselage area. This particular system penalizes the composite structure by six pounds thus reducing the weight savings over the aluminum stabilizer to 150 pounds. A schematic view of how this system will work is

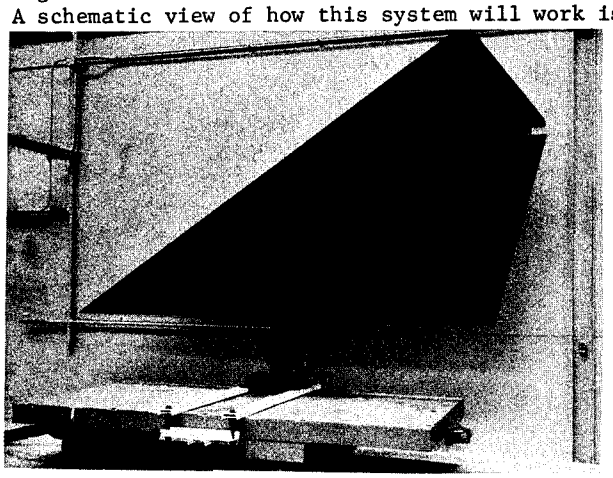

Fig. 16 - F-111 horizontal stabilizer

---

*Numbers in parentheses designate References at end of paper.

shown in (Fig. 17). Attempts are being made to have McDonnell/Douglas test the fatigue stabilizer as part of their F-15 lightning effects investigation. No arrangements have been made as yet but prospects are very promising. When the stabilizer is tested the conclusions obtained in the trailing edge investigation for lightning protection will be strongly recommended.

The objective of the lightning study in the F-100 wing program was to investigate conductive joints. Two series of test panels were evaluated: one series designated "A" panels utilized a silver filled epoxy adhesive to secondary bond .005" aluminum foil to a boron/epoxy surface; and the other series, designated "B" panels used a .002" aluminum foil that was coated with a pressure sensitive conductive adhesive to form the desired overlap joint. High coulomb and high voltage effects were investigated independently of each other. All the specimens were approximately 13" square and .08" thick. The results of these tests and the test conditions are shown in the next table. (Table 2)

The results of the "A" series specimens show that this joint withstood all test conditions without significant damage to the structural elements. It was concluded that this series of panels demonstrate a one strike capability without producing significant damage to an aircraft. Inherent with this protection system is

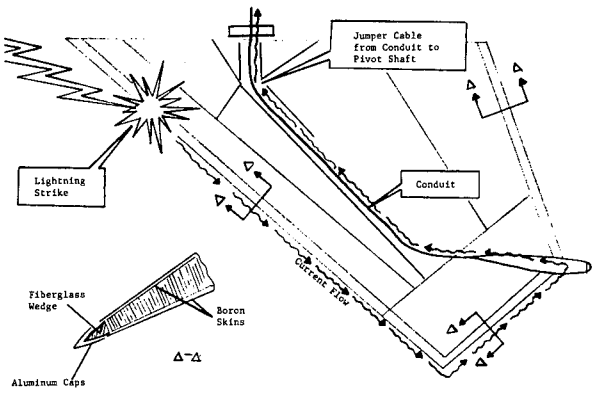

Fig. 17 - F-111 stabilizer lightning protection system

Table 2 - Lightning Strike Data for Boron/Epoxy Laminates with Conductive Joints

Specimen No.	Discharge	Damage
1A	15KA	No Visual Damage
2A	25KA	No Visual Damage
3A	50Ka	100% Adhesive Failure at the B/E-Al Foil Joint
4B	15KA	No Visual Damage
5B	25KA	Blistering of Al Foil
18A	200KA	Removal of Al Foil and Laminate Surface Damage
14A	100 coul.	No Visual Damage
15A	480 coul.	No Visual Damage
16B	100 coul.	No Visual Damage
17B	450 coul.	Adhesive and Foil Arching and Laminate Surface Damage
6A*	4KA/1KA	No Visual Damage
7A*	8KA/2KA	No Visual Damage
8A*	16KA/4Ka	No Visual Damage
9A*	30KA/7KA	Slight Blistering in Foil Lap Joint Area
10B*	4KA/1KA	No Visual Damage
11B*	8KA/2KA	No Visual Damage
12B*	16KA/4KA	No Visual Damage
13B*	30KA/7KA	Slight Blistering and Arching in the Overlapped Al Foil

* indicates that two discharges were made

the capability to repair the lightning protection system of the aircraft.

The "B" series specimen results show that this joint exhibits failure well below the maximum current discharge level. Examination of the specimens indicates that the failure mechanism is associated with the pressure sensitive adhesive rather than the thickness of the aluminum foil. Consequently this method would not be recommended as a good current carrying joint without further investigation and improvement in the conducting adhesive system.

We are just now entering the final development stages of composite empennage technology. Final decisions, by responsible F-14, F-15 personnel, as to what type of lightning protection will be used, have not been made. Production personnel should however, anticipate possible quality control and application problems with the selected protective systems. Chief among these problems are: 1) maintaining uniform coating thickness, especially around critical areas most susceptable to lightning damage; and 2) maintaining a continuity in the protective scheme that is free from conductive path interruptions and breaks. Although many answers have been obtained from the lightning studies which I have just described for you, much more work is and will be required in the future in order to provide an optimum solution to protecting composites from lightning strike damage. At this very moment, major lightning strike studies are continuing at places like the Boeing Company in Seattle, General Electric in Pittsfield, Massachusetts, Lightning Transient Research Institute, the Ohio State University Electrical Engineering Department, the Philco-Ford Corp. and many other contracting facilities. Solutions provided by their work will hopefully give us the optimum lightning protective system.

REFERENCES

1. L.G. Kelly, and H.S. Schwartz, "Investigation of Lightning Strike Damage to Epoxy Laminates Reinforced with Boron and High Modulus Graphite Fibers." AFAL-TR-68-290, Part II, May, 1969.

2. G. Lubin, et al., "Repair Technology for Boron/Epoxy Composites." 2nd Quarterly Progress Report, Contract AF33615-69-C-1498, Grumman Aerospace Corp., Bethpage, L.I., New York, October, 1969.

3. F.F. MacDonald, et al., "Boron/Epoxy Wing Skins." 2nd Quarterly Progress Report, Contract AF33615-69-C-1445, North American Aviation, Los Angeles, California, September, 1969.

4. J.D. Robb, J.R. Stahmann, and L.A. Boehland, "Lightning Electrical Hazards to Flight Vehicles." AFAL-TR-69-269, December, 1969.

5. J.R. Blacklock, "F-111A Boron Horizontal Tail Design and Test." Advanced Composites Status Review Report, AFML/LC, September, 1969.

700936

LIGHTNING PROTECTIVE COATINGS FOR BORON AND GRAPHITE FIBER REINFORCED PLASTICS

Capt. John G. Breland, Jr.
Air Force Materials Laboratory

Dr. John T. Quinlivan
The Boeing Company

and

C. J. Kuo
The Boeing Company

ABSTRACT

Coatings and thin conductive overlays for protecting boron-fiber-reinforced plastics and graphite-fiber-reinforced plastics from structural damage by simulated lightning strikes were investigated. Laboratory tests were made in which test panels, with and without coatings, were exposed to currents as high as 200,000 amperes. The greatest protection of the panels from damage, combined with minimum coating weight, was achieved with aluminum wire fabric and aluminum foil overlays. Other protective coatings which had merit were: plasma-sprayed aluminum; conductive paints used with aluminum foil strips; and conductive coatings applied over high dielectric strength plastic films.

WITH THE INCREASING EMPHASIS on all weather capability of military aircraft, a significant number of hours are spent flying in or near thunderstorms. Therefore, the probability of an aircraft being struck by natural lightning discharges is increasing. It has been estimated, based on data several years old, that each military and commercial aircraft is struck by lightning on the average of once a year, and the current figure is probably higher.

An aluminum aircraft structure is not seriously damaged by such lightning strikes. The aluminum skin and airframe, with their high electrical and thermal conductivity, are capable of sustaining lightning currents of from 100,000 to 200,000 amperes with only minor damage. Usually only localized surface pitting and momentary heating are experienced.

The use of non-electrically conducting structural materials on the surface of aircraft has been limited mainly to glass fiber reinforced plastics (in radomes and small areas of skin) and transparent plastics and glass (windows and canopy area). In contrast to metals such as aluminum, these materials rely on their high dielectric strength to exclude the current in order to protect them from lightning damage. The air near their surface is ionized before the lightning can puncture their surface. Ideally, the resulting plasma then carries the lightning current harmlessly to a nearby metal structure. This phenomenon is known as flashover and will be discussed more later. When additional protection is needed, dielectric structural materials are often coated with metallic coatings or provided with metallic diverter strips. The latter are usually metal bars or rods attached to the structure's surface. The presence of metallic components beneath an unprotected dielectric surface such as a radar antenna under a radome, may increase its susceptibility to puncture by lightning and necessitate such additional surface protection.

Both of these techniques rely upon a high dielectric strength and low electrical conductivity of the dielectric material for their protection and are usually quite adequate for high quality glass fiber reinforced plastic parts such as radomes. However, graphite fiber and boron filament reinforced plastic composites for primary structures of aircraft present an entirely new class of materials to the air-

craft design engineer from an electrical standpoint. These fibers possess an appreciable electrical conductivity and render boron and graphite fiber reinforced plastics electrically inhomogeneous. Due to the electrical inhomogeneity, the response of boron and graphite fiber reinforced plastic to lightning strikes could not be accurately predicted, and therefore the Air Force Materials Laboratory initiated an experimental program to investigate this.

BACKGROUND

In early 1968, the Air Force Materials Laboratory and the Air Force Avionics Laboratory initiated a series of tests to determine the response of these advanced composite materials to simulated lightning discharges. Lightning and Transients Research Institute subjected boron and graphite fiber reinforced epoxy panels, along with control panels of aluminum and glass fiber reinforced epoxy, to a series of simulated lightning discharges.

The results of these tests were presented at the December 1968 Lightning and Static Electricity Conference (1)*. However, in order to establish a frame of reference for subsequent research, a brief summary of this initial work is considered in order.

The thin composite panels which were exposed to simulated lightning strokes consisted of nominally 0.040 inch thick boron, graphite, and glass fiber reinforced plastics made with unidirectional plies laid up in a balanced 0^{o}-90^{o} construction.

During exposure to simulated lightning strikes, bare, "as-fabricated", boron and graphite fiber reinforced panels showed significant damage. Discharge currents of as low as 25,000 amperes caused localized surface damage. A discharge of 60,000 amperes caused extreme damage and loss of structural integrity to the boron fiber reinforced panel and at 85,000 amperes, the graphite fiber reinforced panel was severely damaged. Aluminum pigmented acrylic paints, which enhance surface flashover of glass fiber reinforced plastics, did not provide any protection to either the boron or graphite fiber reinforced plastic.

Damage to the boron panels appeared to be predominantly mechanical, i.e., the boron filaments were fractured. The damage to the graphite fiber reinforced plastics was predominantly pyrolysis of the resin matrix due to high temperatures generated in the graphite fibers by the current.

These initial tests showed that unprotected boron fiber reinforced plastics and high modulus graphite fiber reinforced plastics, in this thin sheet form, suffer considerable damage when struck by simulated lightning strokes. It was apparent that some form of lightning strike protection, such as an electrically conductive coating, was needed for boron and graphite fiber reinforced plastics.

Related investigations (1) showed that 6 mils thickness of flame sprayed aluminum or 3 mils thickness of silver-pigmented paint to be capable of protecting boron fiber reinforced composites from damage by discharges of 200,000 amperes and about 50,000 amperes, respectively. However, the cost and weight of these materials are higher than desired for operational use.

TESTS OF COATED COMPOSITE PANELS

In order to investigate minimum weight, minimum cost concepts of lightning protective coatings for both the graphite and boron fiber reinforced plastics, AFML prepared a second series of coated panels to be tested by L.T.R.I. Information on composition and physical construction of the panels is given in Appendix 1.

TYPES OF COATINGS - The coatings applied to the panels were not necessarily intended to represent practical operational type coatings. They were used to investigate the feasibility of several lightning protection concepts. Each coating system was designed to evaluate a specific potential protection mode. The general classes of coatings were as follows:

Type 1 - A continuous conducting surface represented by an adhesive backed, 3 mil thick aluminum foil tape.

Type 2 - A conductive surface layer (3 mil thick aluminum foil) used in conjunction with an underlayer of high dielectric strength material. The dielectric materials included (separately) polyimide and polyester films, epoxy paints and glass fabric.

Type 3 - Salt-filled paints which were used over a high dielectric underlayer. It was hoped these coatings would vaporize and ionize under the heat of the lightning stroke and form a conducting vapor above the panel.

Each system was crude, but served to provide a prototype for possible future inves-

*Numbers in parentheses designate References at end of paper.

tigation. A description of the coating system applied to each panel is given in Table 1. Test results for high current exposures are given in Table 2.

Table 1 - Description of Coatings Applied to Test Panels

"G" and "L" panels are graphite fiber-epoxy; "B" panels are boron fiber-epoxy

Panel Number	Coating on External Surface	"Underlayer" Coating Between Surface Coating and Panel
L-12B	None	None
L-11A	Aluminum foil, 3 mils thick, pressure sensitive adhesive on one side	None
L-12A	Same as L-11A	None
G-3	Same as L-11A	None
B-3	Same as L-11A	None
G-2	Same as L-11A	1 mil thick polyimide film bonded to panel with 3M pressure sensitive "transfer" adhesive
B-2	Same as L-11A	Same as G-2
G-1	Same as L-11A	3 mil thick polyester film bonded to panel with 3M pressure sensitive adhesive
B-1	Same as L-11A	Same as G-1
G-4	Same as L-11A	One ply No. 112 glass fabric (0.0035" thick) impregnated with epoxy and laminated to panel surface
B-4	Same as L-11A	Same as G-4
G-9	Same as L-11A	Epoxy coating, MIL-P-27316 type, 5 mils thick
B-5	Same as L-11A	Same as G-9
G-10	Potassium oxalate (40% by weight) in MIL-19537 acrylic lacquer; approximately 5 mils thick	MIL-P-27316 epoxy, approximately 5 mils thick
B-6	Same as G-10	Same as G-10

Table 2 - Current Levels and Results of Simulated Lightning Strike Tests on Boron Fiber Reinforced Plastic and Graphite Fiber Reinforced Plastic Panels

Panel Number	Current, Kiloamps	Description of Damage to Reinforced Plastic Panel
L-12B	80	Resin pyrolysis along current flow path resulting in bare fibers in local areas; local delamination of strip of back ply opposite stroke discharge point
L-11A	100	No visible damage
L-12A	100	No visible damage
G-3	200	No visible damage on front surface; small bi-directional crack (1" x 1") on back side opposite stroke discharge point
B-3	100	No visible damage
G-2	100	No visible damage
B-2	100	No visible damage
G-1	100	No visible damage
B-1	100	No visible damage
G-4	200	Similar to G-3
B-4	200	Similar to G-3
G-9	200	Local delamination of narrow strip of front surface ply; backside damage similar to that for G-3 but slightly more severe than for G-3
B-5	200	Similar to G-3
G-10	85	Catastrophic damage to panel; delamination of front surface ply, fiber-matrix debonding, gross buckling of panel
B-6	60	Several cracks across width of panel; panel broken in two across width at point of stroke discharge

HIGH CURRENT TESTS - The protection offered by 3 mil thick aluminum foil to both graphite and boron fiber reinforced plastic panels appeared to be equal to that offered by coatings of flame-sprayed aluminum and superior to silver-filled paints previously tested, from the standpoint of protection per unit weight of coating. Typical results of these tests are shown in Figures 1, 2, and 3. Although an area of the foil near the stroke attachment point has been vaporized, damage to the panel is limited to very minor scorching

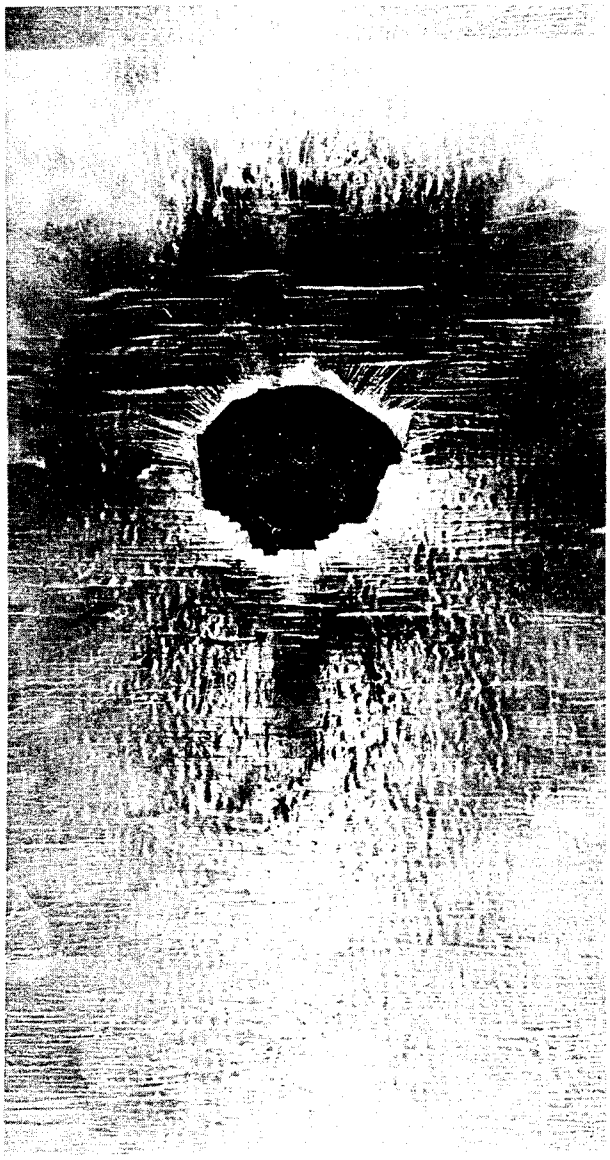

Fig. 1 - Graphite fiber epoxy laminate (Panel L-11A) coated with 3 mil thick aluminum foil after exposure to 100 kiloamps.

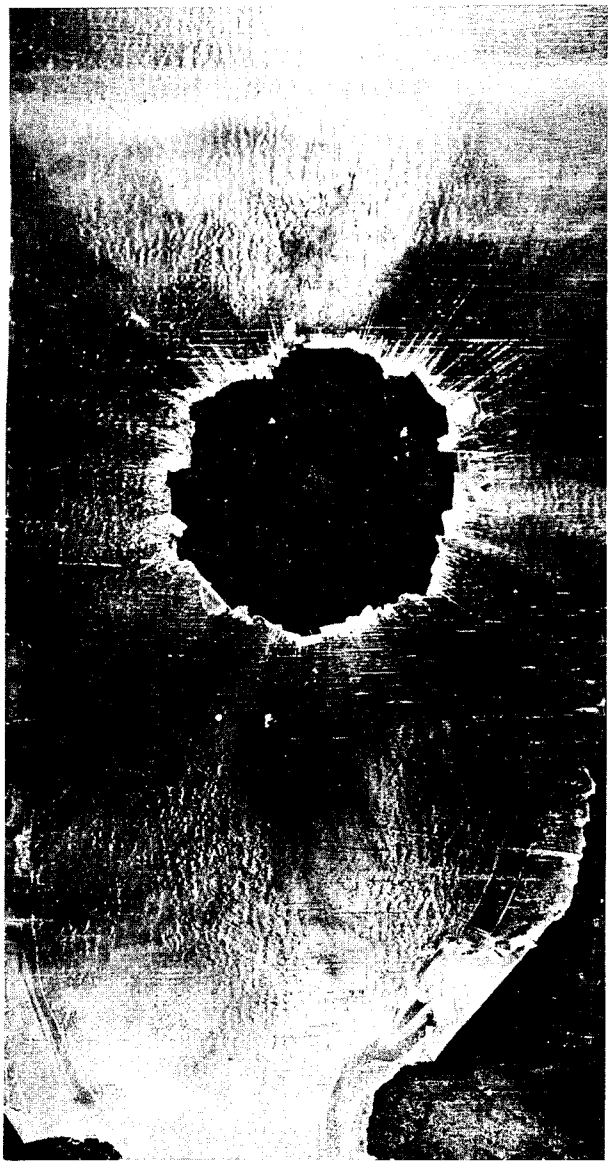

Fig. 2 - Graphite epoxy laminate (Panel G-3) coated with 3 mil thick aluminum foil after exposure to 200 kiloamps.

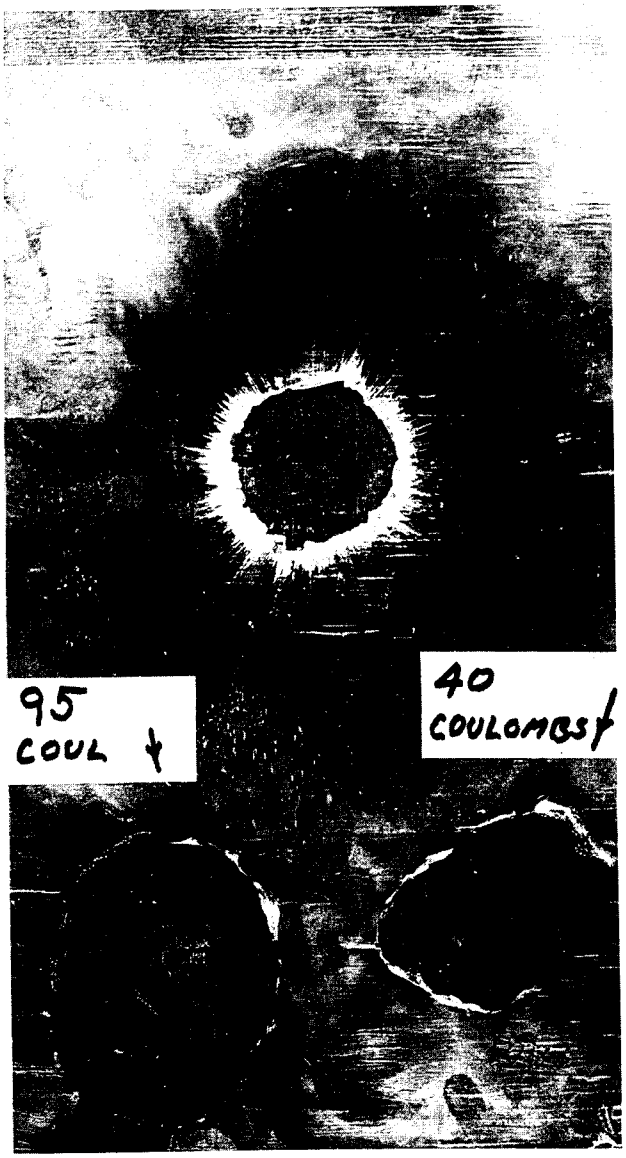

Fig. 3 - Panel B-3 (boron fiber epoxy) after exposure to 100 kiloamps (100 kiloamp discharge at top center - 95 coulomb and 40 coulomb discharges at bottom of panel were done later).

of the surface resin. The use of a high dielectric underlayer increased protection somewhat and protected the panels' surface from resin scorching or vaporization (Figures 4 and 5). At the 100,000 and 200,000 ampere discharge level minor localized backside panel cracking was often observed even when high dielectric strength layers were present (Figure 6). This damage may have resulted from the shock wave effects of the surface vaporization of aluminum.

The salt loaded paint offered no protection (Figure 7).

It has been previously reported that boron fiber reinforced plastics, after exposure to high current flow through the composite, may undergo severe damage to the boron fibers, even though there is no visible damage (2). For this reason, it was decided to perform tensile strength tests on selected boron and graphite fiber reinforced plastics which had been exposed to high current simulated lightning strikes and appeared visually to have no significant damage.

The panels selected for this investigation were as follows:

Boron fiber epoxy laminates -

B-1 - 3 mil thick aluminum foil surface layer with 3 mil thick polyester film underlayer. Exposed to 100,000 amps.

B-5 - 3 mil thick aluminum foil surface layer with 5 mil thick epoxy paint underlayer. Exposed to 200,000 amps.

Graphite fiber epoxy laminates -

G-1 - Same coating system as B-1. Exposed to 100,000 amps.

G-3 - 3 mil thick aluminum foil overlay (coated on one side with pressure sensitive adhesive). Exposed to 200,000 amps.

Each of the exposed panels were cut into nine 0.5 inch wide rectangular strip tensile specimens and the ends of each specimen were tabbed with tapered glass fiber reinforced plastic. For the graphite fiber reinforced plastic, "control" tensile strengths were determined on "as-fabricated" panels L-10 and L-12 which had not been exposed to simulated lightning strikes. No control panels were available for the boron fiber reinforced plastics. However, based on previous tests of boron fiber reinforced plastic of similar layup and thickness, the tensile strength of an as-fabricated laminate was estimated to be 80,000 to 85,000 psi.

The results of the tensile strength tests are shown in Table 3. The specimen suffixes (A through I) are sequential from left to right looking at the coated surface of the panel. Therefore, specimens with suffix "E" represent specimens from the center of the panel, which is where the panels were struck by the simulated lightning discharge. This is the specimen which would be expected to be damaged the most. Specimens with suffixes "A" and "I" were taken from the edges of the panels, farthest from the point of the electrical discharge to the panel. These specimens would be expected to be damaged the least.

The test results for panel B-1 (100,000 amps exposure) show fairly uniform tensile strengths across the width of the panel with

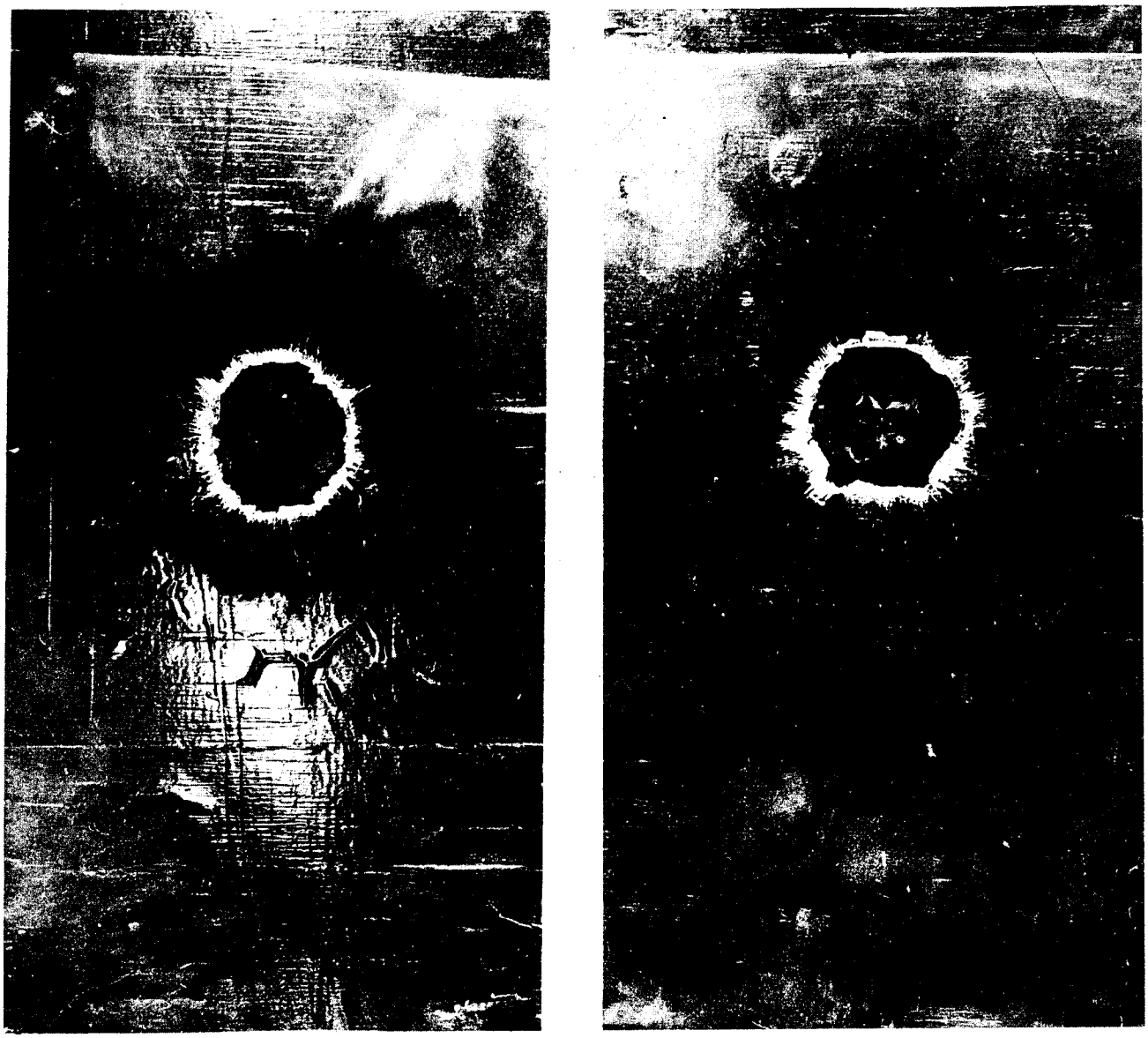

Fig. 4 - Boron fiber epoxy panels B-1 (left) and B-2 (right) after exposure to 100 kiloamps. B-1 had a 3 mil thick polyester film interlayer and B-2 had a 1 mil thick polyimide film interlayer.

absolute strengths close to what one would expect for "as-fabricated" laminates of this type. Test results for panel B-5 (200,000 amps exposure) show that tensile strength of the center third of the panel has decreased by about one-third from the control strength. The outer thirds (left and right sides) of the panel show an average strength loss of about 10%.

For the graphite fiber plastic panels, the center third of panel G-1 (100,000 amps exposure) shows about a 10% reduction in strength from the control strength. The outer-thirds (left and right sides) of the panel do not show any significant loss in strength. For panel G-3, the center third of the panel shows an average of 30% strength reduction from the control strength with specimen "E" showing about 50% reduction in strength. The outer thirds of the panel show an average strength reduction of about 10%.

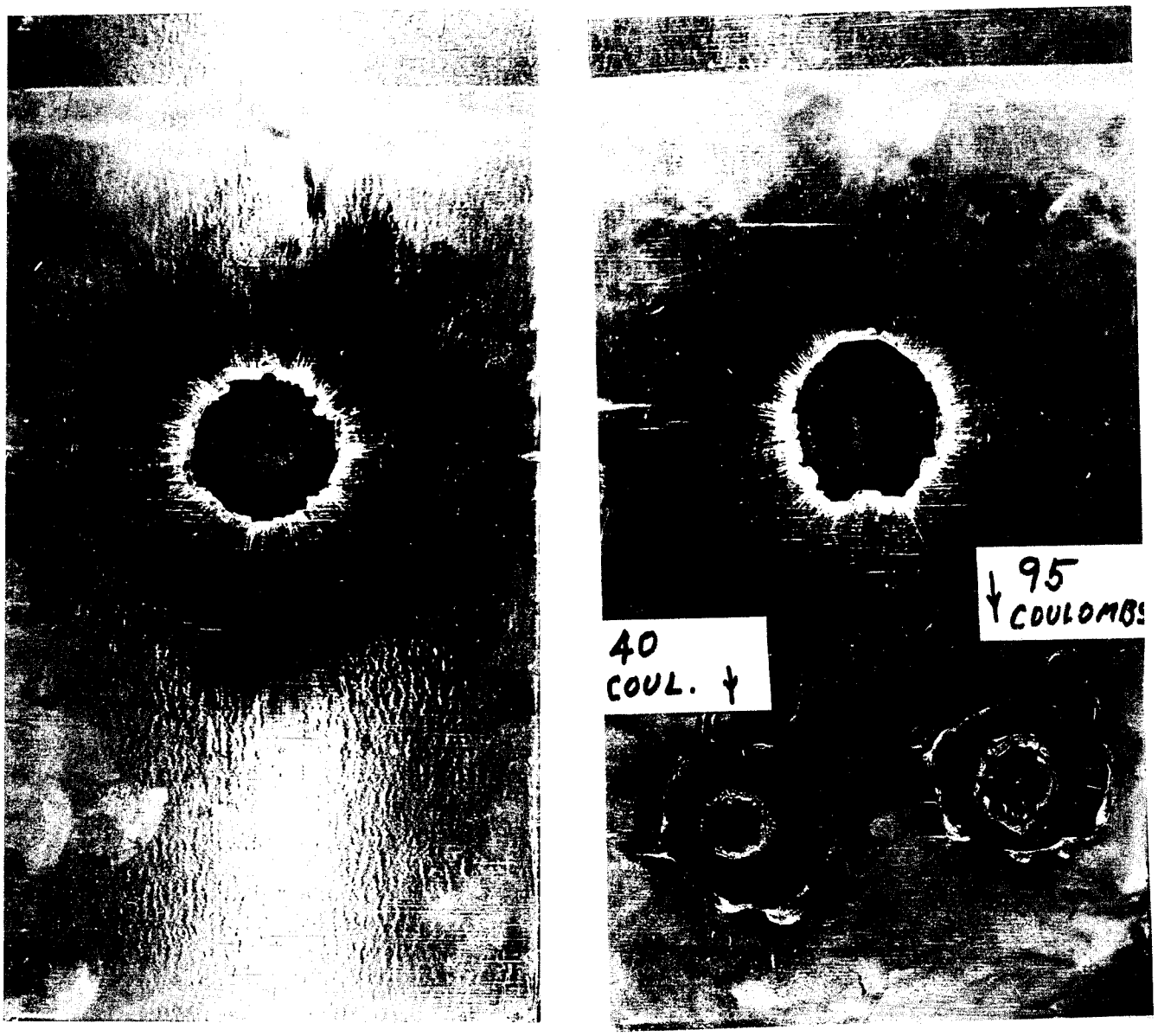

Fig. 5 - Graphite fiber epoxy panels G-1 (left) and G-2 (right) after exposure to 100 kiloamps. G-1 had a 3 mil thick polyester film interlayer and G-2 had a 1 mil thick polyimide interlayer.

The results of these mechanical property tests indicate that 100,000 amps exposure, the reduction in strength was small even at the stroke discharge point, but at 200,000 amps exposure, there was a significant reduction in strength at the discharge point and a small reduction in strength over the outer thirds of the panel.

The strength reduction in these panels, especially that at the discharge point was not necessarily solely due to current flow in the fibers. There was a small biaxial crack visible on the back side of the panels exposed to 200,000 amps. This is believed due to shock wave effects caused by the flash vaporization of aluminum foil on the surface.

HIGH COULOMB TESTS - None of the coatings evaluated protected the panels from damage during exposure to a high coulomb discharge (Figure 8). Such discharges are essentially long duration, high temperature arcs which produce severe, highly localized heating and panel damage. The coatings investigated apparently burned away almost immediately and the arc then established itself to the conductive panel. However, the type of

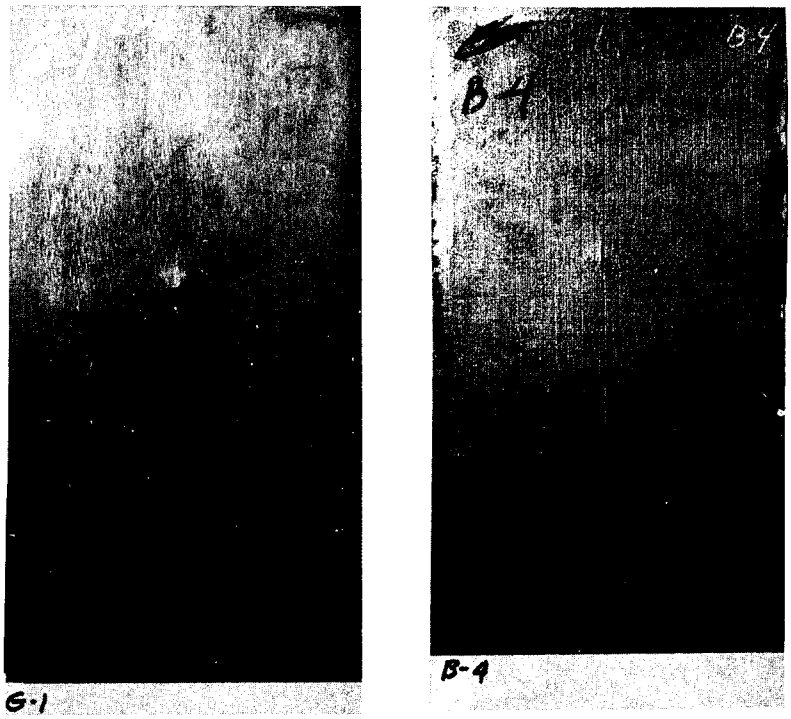

Fig. 6 - At left, back side of panel G-1 after exposure to 100 kiloamps; at right, backside of panel B-4 after exposure to 200 kiloamps.

damage resulting from the high coulomb discharges was very localized, in contrast to the catastrophic damage caused by the high current component of the lightning stroke.

This series of tests showed for the first time that adequate protection from catastrophic lightning damage could be provided both boron and graphite fiber reinforced plastics by relatively inexpensive and light weight materials.

DEVELOPMENT OF LIGHTNING PROTECTIVE COATINGS

Subsequent to the investigations previously discussed, an Air Force sponsored contractual program was undertaken by the Boeing Company to more fully investigate and further develop lightning protective coatings for boron and graphite fiber reinforced plastics. Boeing conducted developmental formulation of coatings suitable for potential lightning protection and performed electrical and lightning strike evaluation in a manner similar to that of L.T.R.I. A test current reaching approximately 100,000 amperes in 10 μ secs and returning to 0 after another 15 μ secs was used in the initial screening. Details on the electrical circuitry and procedures used in conducting the simulated lightning strike tests are given in Appendix 2.

METAL FOILS - The initial part of the Boeing work was concerned with investigating and developing continuous conductive coatings. The intent of this approach was to determine the degree of protection afforded by metal foils of varying thicknesses and metal alloy. The metal foils provided 100 percent coverage of the composite surface nearest the discharge probe. In the simulated lightning test the foils were very successful in preventing puncture of the boron and graphite reinforced laminates. Typical results for aluminum foil are shown in Figure 9. In this case the foil was only 1/2 mil thick. The arc vaporized the foil in a large area at the contact zone, but did not attach to the fibers. Some resin scorching was observed, especially with thicker foils. The size of the vaporized area was roughly inversely proportional to the thickness of the metal. Resin scorching with thicker foils is undoubtedly due to the "hot-spotting" which occurs due to confinement of the energy in a smaller area.

Foils of several other metals were also effective if certain minimum thicknesses were met. In general, the higher the boiling point of the metal, the less the vaporization of the metal coating. Extremely thin foils were nearly completely destroyed by the discharge. While the foil was nearly completely destroyed, no structural damage to the composite was observed.

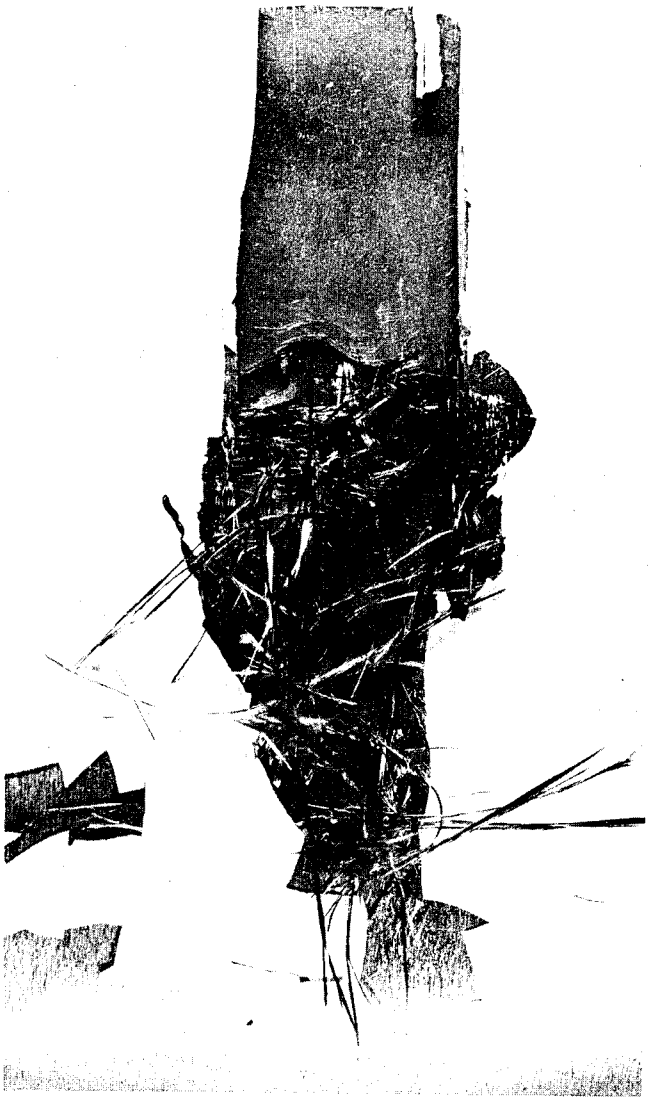

Fig. 7 - Front surface of panel G-10 (coated with potassium oxalate filled acrylic paint) after exposure to 85 kiloamps.

Vaporizable protective strips of aluminum foil spaced about 2 inches between strip edges have also effectively protected boron and graphite fiber composites from a lightning discharge when the discharge was directed to one of the strips. Aluminum foil tapes were bonded to the periphery of the panel and down the center (as shown in Figure 10). The discharge was directed to the center tape. The aluminum tape was severely damaged by the discharge; the center tape being both vaporized and blown from the panel. Damage was not restricted to this center tape, however. Bubbling at tape lap joints and peeling at corners was observed. This indicated that the current was carried to ground by all three of the tapes and not by just the center one. Some arcing from the center to the two edge tapes occurred, as evidenced by the scorching of the resin and vaporization of metal along the inside edges of the two edge tapes opposite the probe. Evidently a continuous path to ground is a preferred protective system.

SPRAYED ALUMINUM - Surface coatings of flame sprayed aluminum were very effective in preventing damage to boron composite panels for 100 KA discharges (Figure 11). The 4 mil thick coating showed discoloration and some cracking in the immediate vicinity of the probe, but no other damage. A 160 kiloampere oscillatory discharge caused extensive damage, however.

Plasma sprayed aluminum displayed quite a different protective behavior. Two and 6 mil thick plasma sprayed coatings were vaporized at the contact zone, much like the metal foils. In addition, the 2 mil thick coating was severely cracked.

Plasma sprayed aluminum provides less effective protection to graphite composites, however, than it provides to boron composites for equivalent coating thickness. In this case, the graphite fiber reinforced plastic panels with two and five mil coatings were severely cracked and evidence of current conduction by the fibers was present.

From these studies it was determined that metal foil, closely spaced expendable metal strips and sprayed metal coatings are very effective lightning protectors. These results were expected as each of these coatings presents a continuous metal pathway (except for initial flashover between metal strips) from the arc contact to electrical ground.

CONDUCTIVE PAINTS - Finely divided silver is frequently employed as a pigment in conductive paints. Optimum silver pigmented coatings are about 300 times more electrically resistant than copper. This level of conduction is sufficient to provide some lightning protection to both boron and graphite composites. The degree of protection depends in large part on the thickness of the coating. To achieve maximum conductivity and composite protection, these coatings must be sufficiently thick to dissipate the immense heat and blast energy from a discharge arc. Coatings which are too thin are effectively "invisible" to the discharge arc, and provide little or no protection. The mechanism for protection appears to be a combination of surface flashover and coating conductance. The former results in

Table 3 - Tensile Strength of Boron Fiber Reinforced Plastic and Graphite Fiber Reinforced Plastic Panels after Exposure to Simulated Lightning Strikes

"G" and "L" panels are graphite fiber-epoxy; "B" panels are boron fiber-epoxy

Panel Number and Specimen Identification	Current Exposed To, Kiloamps	Ultimate Tensile Strength PSI
L-10-A	None-Control	67,700
L-10-B		75,000
L-10-C		65,700
L-10-D		43,500
L-10-E		65,500
Panel Average		63,500
L-12-A	None-Control	72,900
L-12-B		68,400
L-12-C		67,900
L-12-D		70,700
L-12-E		68,000
Panel Average		69,600
G-1-A	100	72,400
G-1-B		74,000
G-1-C		79,400
G-1-D		60,000
G-1-E		64,800
G-1-F		62,900
G-1-G		64,200
G-1-H		63,200
G-1-I		84,100
G-3-A	200	69,200
G-3-B		45,400
G-3-C		67,600
G-3-D		68,000
G-3-E		31,400
G-3-F		36,200
G-3-G		57,000
G-3-H		46,800
G-3-I		61,000
B-1-A	100	71,100
B-1-B		77,400
B-1-C		82,700
B-1-D		72,100
B-1-E		79,400
B-1-F		77,500
B-1-G		70,500
B-1-H		81,400
B-1-I		78,300
B-5-A	200	67,700
B-5-B		79,400
B-5-C		64,300
B-5-D		50,200
B-5-E		58,100
B-5-F		50,400
B-5-G		69,000
B-5-H		79,400
B-5-I		80,800

surface marking; the latter results in coating destruction around the stroke attachment point.

Conductive coatings that employ metal pigments in a sandwich layer have also been tested. These coating systems were prepared by depositing the metal pigment from a solvent slurry. After removal of solvent with consequent compaction of the metal layer, a clear epoxy topcoat was applied. These films were designed to be electrically conductive by particle-to-particle contact. The test results, Figure 12, show that the required conductivity did not develop. Both aluminum and copper sandwich coatings were unsuccessful. The panels were severely damaged by the discharge and the coatings were simultaneously destroyed.

The initial investigations of paint type coatings were on those containing metal pigments. A non-metallic pigment frequently employed in the manufacture of controlled resistance coatings is graphite. Electrically conductive paints were prepared from both moderate and highly conductive graphite pigments. The advantage of the former lies in the large particle size which permits high pigment volumes to be achieved. The latter pigment has a very small particle size. Thus, it is very difficult to obtain high pigment volume concentrations with highly conductive blacks. Paints prepared from these pigments very successfully protect fiberglass composite materials (Figure 13). These same systems provide no protection for boron and graphite fiber plastic composites, however. The typical result is shown in Figure 14. This boron fiber reinforced laminate was punctured by the discharge and significant fiber destruction due to current conduction is visible. Damage to graphite reinforced composites is very comparable except that more extensive resin burn-off occurs. Graphite pigmented paints were very unsuccessful as lightning protective coatings for these composite materials.

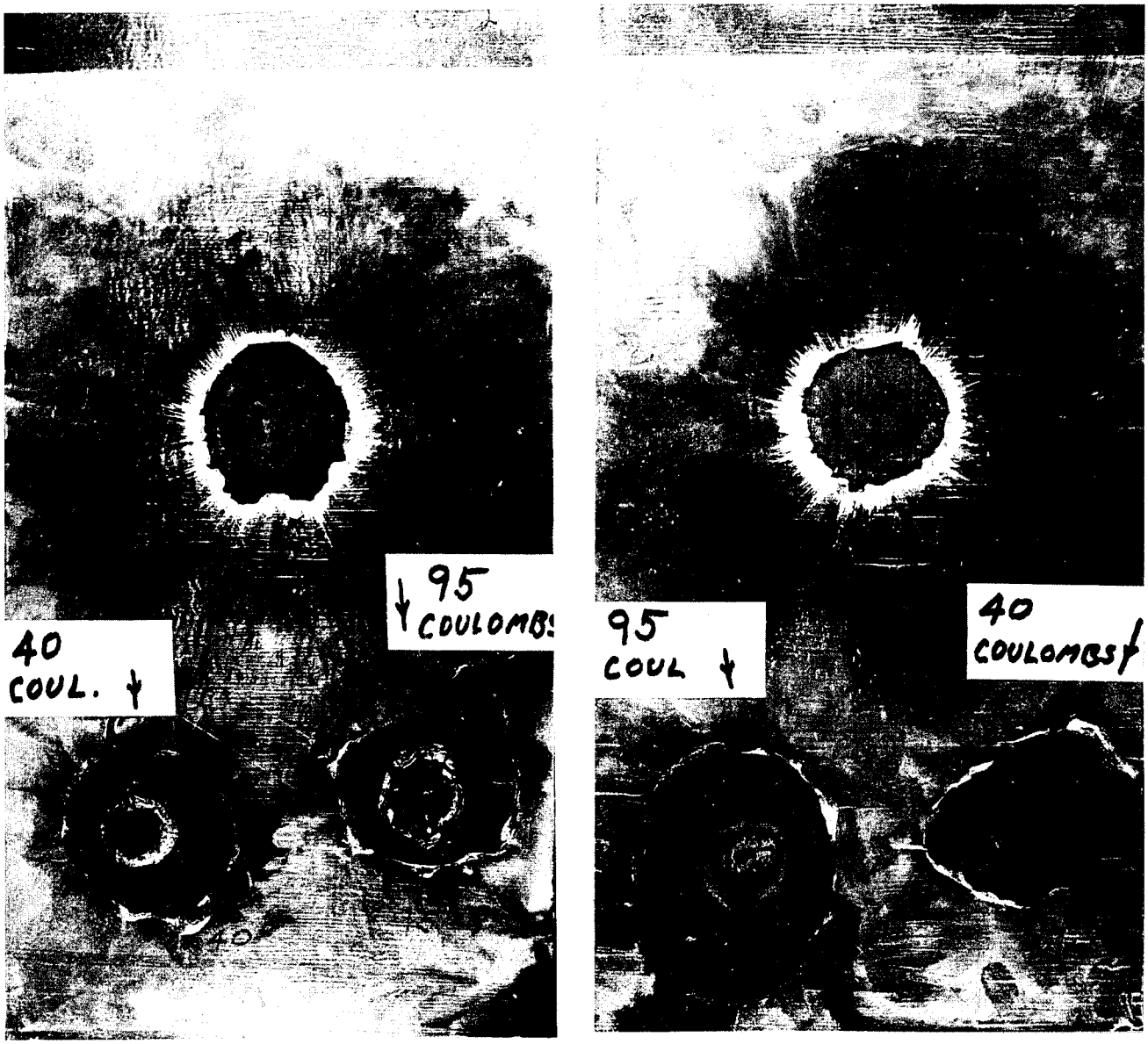

Fig. 8 - Front surface of panel G-2 (left) and B-3 (right) after exposure to 40 coulomb and 95 coulomb discharges.

An alternative coating concept utilizing a carbon pigmented paint was found successful for boron epoxy laminates. In practice, the panel edges were covered with a metal strip to provide a conductive member to carry the lightning currents to electrical ground. Discharge to these panels resulted in very little coating damage, but damage to the expendable metal strip. A typical result is shown in Figure 15 for a boron epoxy laminate exposed to 110,000 amps. Additional work is in progress to define the characteristics of the coatings which lead to these results.

METAL WIRE FABRICS - Metal wires can be fabricated into cloth by the two standard textile processes; weaving and knitting. The former technique yields a closely spaced pattern of wire while the latter process yields a fabric with a large open area. Both systems can yield fabrics with densities less than 2 pounds per 100 square feet. Some of these are highly efficient lightning protective coatings. Metal fabric in these densities possess the hand and drape necessary to use as an overlay on reinforced plastic parts having complex contours. The materials can be easily shaped

Fig. 9 - Front surface of a boron-fiber epoxy laminate coated with a thin metal foil. 100 KA simulated lightning discharge destroyed much of the metal foil but left the composite intact.

Fig. 10 - Front surface of a boron-fiber epoxy laminate coated with an open aluminum network. Damage to the aluminum is due to a 95 KA simulated lightning discharge.

about doubly contoured surfaces and simply utilizes the composite matrix as its bonding agent. These materials could replace the glass scrim cloth utilized as a carrier for pre-impregnated boron filament and used as a surface ply with the wire fabric on the surface.

Aluminum wire fabrics with areal densities of 0.01 to 0.02 pounds per square foot provide lightning protection at 100,000 to 200,000 amperes. For 20 x 40 mesh aluminum wire fabric, 4 mil thick, the fabric is only slightly destroyed at the lightning discharge zone and possesses the capability of sustaining a restrike. In addition very little repair is required. In contrast, a spot several inches in diameter of aluminum foil is destroyed at the lightning discharge zone and must be repaired to possess good restrike protection or to present a smooth aerodynamic surface. The factor most affecting the weight of these fabrics is the wire diameter. The weight of a fabric of a given material and weave construction is proportional to the square of the wire diameter. For minimum weight of protective fabrics, we would prefer to use very small wire diameter. However, cost prohibits the use of aluminum wire with diameters much less than 2 mils. Other metals do not protect composites as well as aluminum for equivalent weight. Those which do possess comparable conductivities are much more dense and destroy the projected weight savings. Consequently, aluminum wire is the chosen material. These aluminum wire fabrics are also capable of withstanding very high coulomb transfer tests, based on a few exploratory tests. Summarizing these data, aluminum wire fabrics possess the best over-all characteristics of the conductive coating systems. They are not only the lightest in weight for a given level of protection but are also the least damaged by simulated lightning discharge currents.

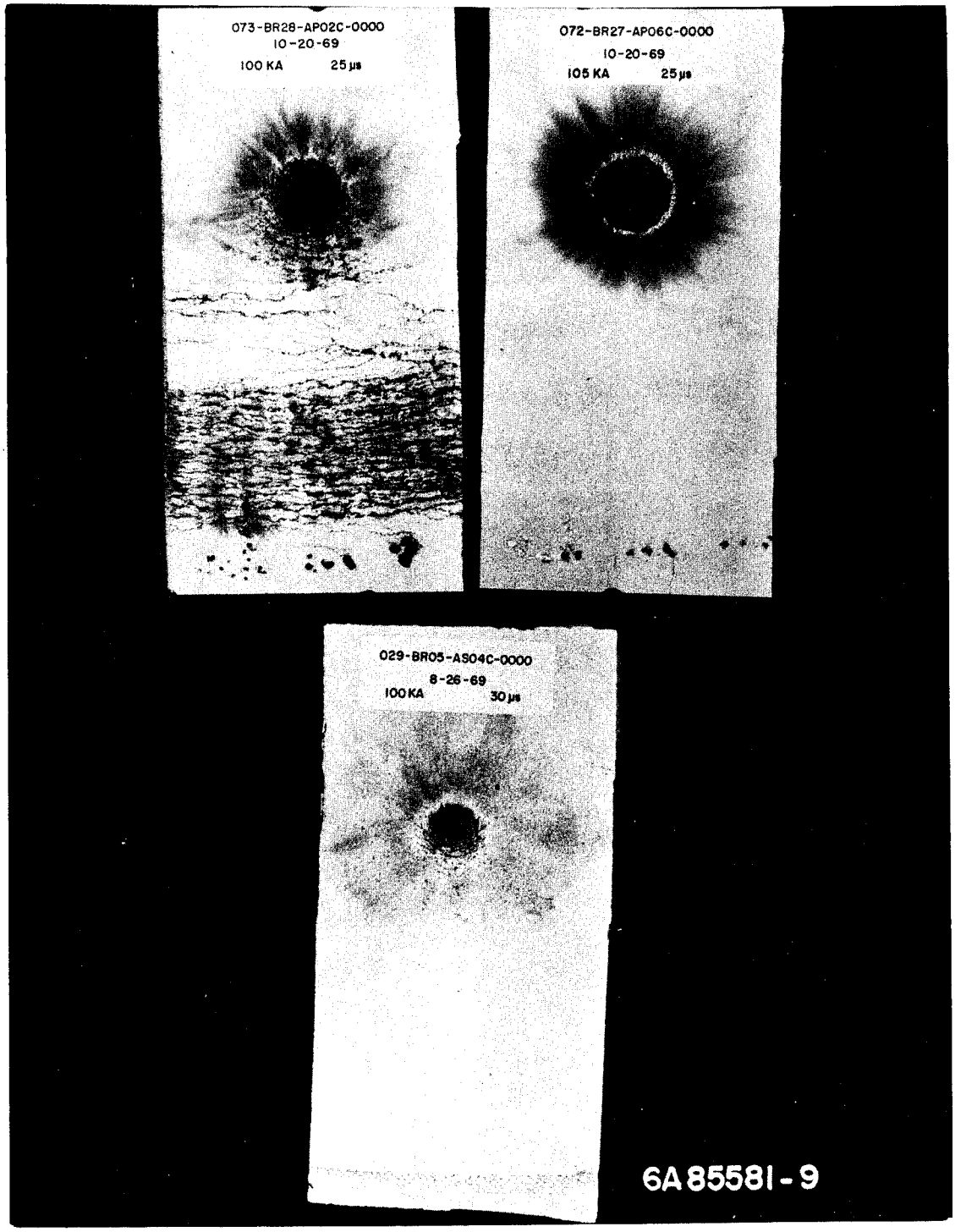

Fig. 11 - Damage to boron-fiber epoxy laminates due to 100 KA simulated lightning discharges. Laminates coated with varying thicknesses of flamesprayed aluminum.

Fig. 12 - Damage to a graphite-fiber epoxy laminate due to 84 KA simulated lightning discharge. Laminate was coated with an aluminum pigmented epoxy slurry.

Fig. 14 - Damage to a boron-fiber epoxy laminate due to 50 KA simulated lightning discharge. Laminate coating was a conductive, carbon black pigmented epoxy.

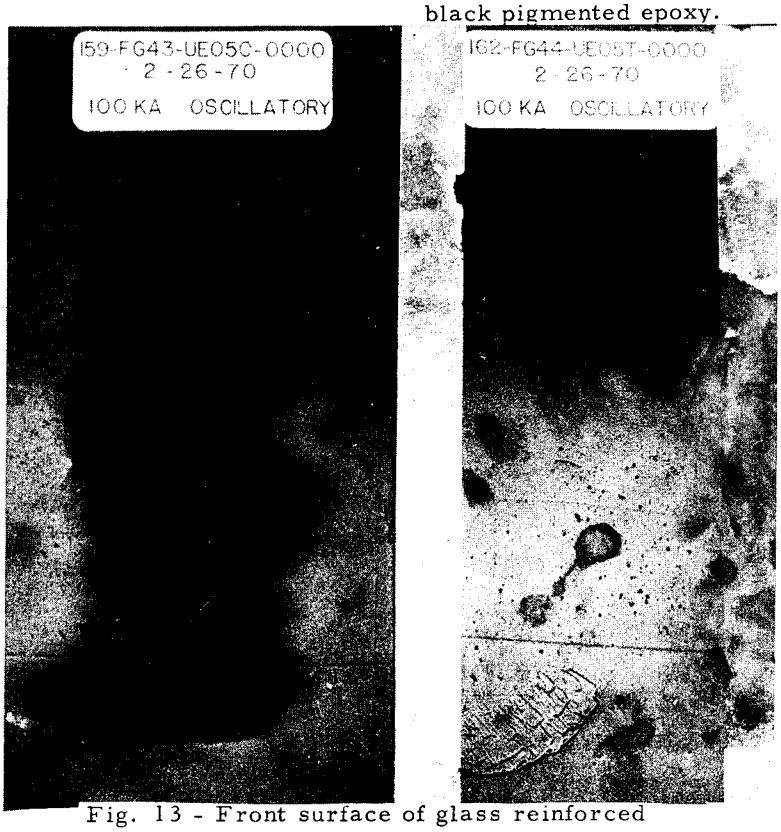

Fig. 13 - Front surface of glass reinforced epoxy laminates coated with a conductive paint. The 100 KA simulated lightning discharges did not damage the panels.

Fig. 15 - Damage to a boron-fiber epoxy laminate due to 110 KA simulated lightning discharge. The laminate was coated with a conductive carbon-black pigmented epoxy and provided with expendable aluminum strips.

SUMMARY

In summary, light weight coatings have been and are being developed to adequately protect boron filament and high modulus graphite fiber reinforced plastic composite materials from lightning discharge damage. The degree of protection offered both types of composites by several classes of coatings have been determined. Additional efforts are currently underway to:

1) Establish minimum coating weight protection at several current levels.

2) Optimize weight, cost, ease of application and repairability of coating systems.

3) Investigate behavior of promising coating systems over a broad range of environmental conditions representing anticipated operational environments.

4) More fully understand the mechanisms of damage caused by lightning and the protective modes of the effective coatings.

REFERENCES

1. L. G. Kelly and H. S. Schwartz, "Investigation of Lightning Strike Damage to Epoxy Laminates Reinforced with Boron and High Modulus Graphite Fibers," AFAL-TR-68-290, Part II, May 1969.

2. W. M. Fassell, A. P. Penton, and J. A. Plumer, "The Susceptibility of Advanced Filament Organic Matrix Composites to Damage by Simulated Lightning Strikes," AFAL-TR-68-290, Part II, May 1969.

ACKNOWLEDGMENT

The authors wish to express their appreciation to personnel of the Air Force Avionics Laboratory, Air Force Materials Laboratory, the Boeing Company, Lightning and Transients Research Institute, the 3M Company, and the University of Dayton Research Institute for their contributions to the work reported in this paper.

APPENDIX 1 - Composition and Physical Construction of Boron Fiber Reinforced Plastic and Graphite Fiber Reinforced Plastic Panels

Property or Characteristic	Boron Fiber - Epoxy Laminate	Graphite Fiber-Epoxy Laminate
Fiber Reinforcement	4 mil diameter boron fiber made using 1/2 mil diameter tungsten wire substrate. No. 104 glass fabric backing for boron plies	Thornel 50 w/PVA size
Resin Matrix	Narmco 5505 epoxy prepreg system. Resin designation 2387	Union Carbide ERLA 2256 Epoxy w/ZZLB 0820 hardener
Layup Pattern	$0\text{-}90^{\circ}\text{-}0^{\circ}\text{-}90^{\circ}\text{-}90^{\circ}\text{-}0^{\circ}\text{-}90^{\circ}\text{-}0^{\circ}$	$0^{\circ}\text{-}90^{\circ}\text{-}90^{\circ}\text{-}0^{\circ}$
Average Fiber Volume %	50.0	50.0 - 55.0
Density, g/cc	----	1.43
Average panel thickness, inches	0.042	0.033 - 0.0040

APPENDIX 2 - Apparatus, Circuitry and Procedures Used in Conducting Simulated Lightning Strike Tests

From the standpoint of simulating the components of a lightning strike that cause damage to materials and structures, two separately generated components are required. One is a high current component which occurs early, timewise in a natural lightning strike, and the other is a high coulomb transfer which occurs later. The maximum value of these two components specified in military specifications are as follows:

A. A high current component rising from zero to a crest value of 200,000 amperes in 10 microseconds and a pulse duration of 20 microseconds with ±50 percent tolerance on time.

B. A high coulomb transfer discharge with total charge transfer equal to or exceeding 200 coulombs in one second or more.

During the initial phase of this investigation a high current component (10 microseconds to 100 kiloampere crest and 20 microseconds to half crest value, ±50% on time) was used. The application of this moderately severe stroke not only screened coating candidates for further study but also served to develop protective coatings for areas requiring only secondary protection. A primary criterion of success for a protective coating is the capability of sustaining the test discharge without structural damage to the composite substrate. That is, the coating must minimize or eliminate the damage at the attachment point and an adequate path must be provided for passage of the lightning currents, thereby preventing the flow of detrimental currents into the structural fibers.

A photograph of the laboratory setup for lightning strike tests is shown in Figure 16. The test panel was clamped to an 18-inch by 18-inch phenolic panel which was bolted to the Faraday Cage. The test panel was electrically isolated from the cage except for the ground strap that was clamped to one end. This configuration assured that the discharge current passed through the maximum available coating surface of a test panel. A positive grounded power supply system was used, i.e., the discharge probe injected electrons toward the test panel and simulates a more severe damage situation than that of a negative grounded power supply. A 1/4 inch diameter tungsten probe was used to direct the discharge to the test

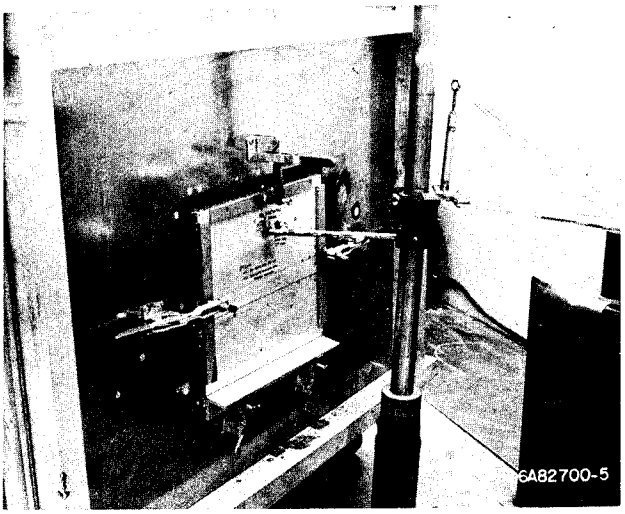

Fig. 16 - Laboratory setup for exposing test panels to simulated lightning strikes.

panel and a 1/4 inch gap was maintained between the probe and the panel.

To simulate a lightning stroke in the laboratory, two different generators were used: the high current component generator shown in Figure 17 and the two component lightning simulator shown in Figure 18. A 42 microfarad capacitor bank rated at 30 KA was used to generate the high current component. The discharge was initiated by closing switch S_1 (Figure 19). The discharging capacitor bank normally produces an underdamped oscillatory discharge. The required single pulse discharge was produced by closing a crowbar switch S_2 to shunt or crowbar the discharge currents parallel to the test panel immediately after the first half cycle oscillatory discharge.

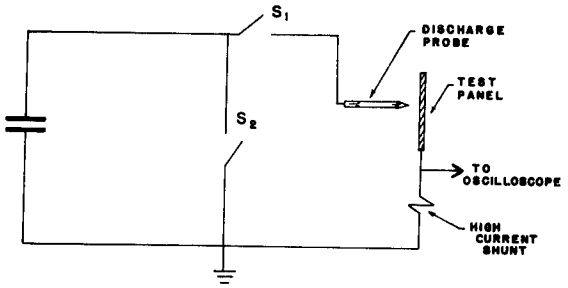

Fig. 17 - Schematic diagram of high current generator.

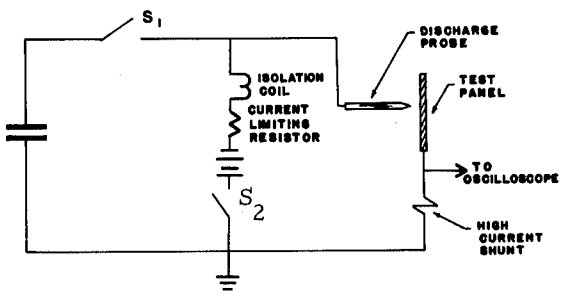

Fig. 18 - Schematic diagram of two component lightning simulator.

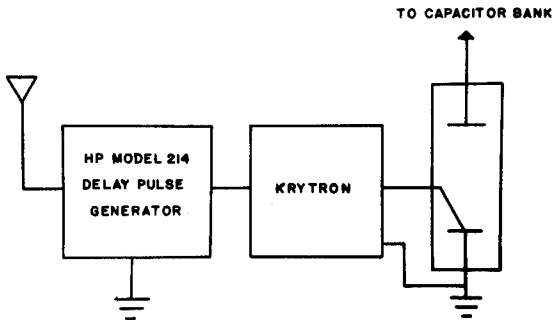

(a) BLOCK DIAGRAM OF CROWBAR SWITCH

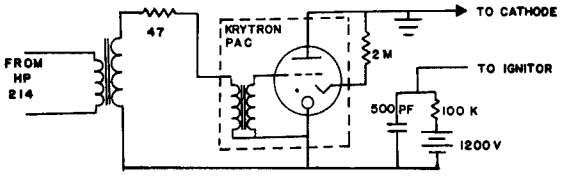

(b) SCHEMATIC DIAGRAM OF KRYTRON CIRCUIT

Fig. 19 - Crowbar switch.

The schematic diagram and the firing of the crowbar switch are shown in Figure 19(a) and 19(b), respectively. As shown, the Hewlett Packard Model 214 Delay Pulse Generator is triggered by the initial voltage induced in the pickup loop by the capacitor discharge. The isolation and step-up transformer then delivers a 200 volt delayed pulse to the triggering terminal of a Krytron (KRP-21, Edgerton, Germeshausen & Grier Co.) The triggered Krytron delivers a 1200 volt pulse to the ignitor of the ignitron tube, thus closing S_2. Theoretically, closing the crowbar switch will shunt the discharge current and will stop all current flow through the test item; however, current continued to flow through the test item after S_2 was activated. This is undoubtedly due to the finite impedance of the discharge path which continued to share current with the lower impedance of the parallel crowbar circuit. Nevertheless, this discharge adequately simulates lightning effects for the screening purposes of the study.

The discharge current was measured by a high current shunt of 60 micro-ohm impedence made by The Boeing Company. The output of this shunt was connected to a Tektronix 549 oscilloscope to record the discharge current.

A schematic diagram of a two component lightning generator is shown in Figure 18. The high current component generator will first establish an arc between the discharge probe and the test item and the high coulomb component generator will then follow-on by discharging a DC component through the established ionized channel to the test panel. The high current component, a high voltage capacitor bank, is electrically isolated from the high coulomb component of a battery bank by the switch S_1 and these two components are transiently isolated by the isolation coil; the total discharge is terminated by opening the switch S_2.

An oscillatory, instead of a previously discussed crowbarring, capacitor bank system is employed with the same 42 microfarad capacitor bank. This is necessary because the high coulomb component currents from the battery bank will flow through both the crowbar switch and the discharge path; the excessive DC current which flows through the crowbar switch will not only degrade the available testing energy but will also greatly reduce the life time of the ignitron tube. The extra coulomb value provided by the additional discharge from the capacitor bank is less than 1 percent as compared to the total amount of a two component stroke.

Two 430 volt battery carts are utilized for the required high coulomb component. Each steel cart has been mounted with 36 12-volt automotive batteries. The system is capable of discharging a DC level up to 3000 amperes and maintaining an arc with a gap of up to a half-inch.

The schematic diagram of the timing switch S_2 is shown in Figure 20. A flash from the initial capacitor bank discharge will turn

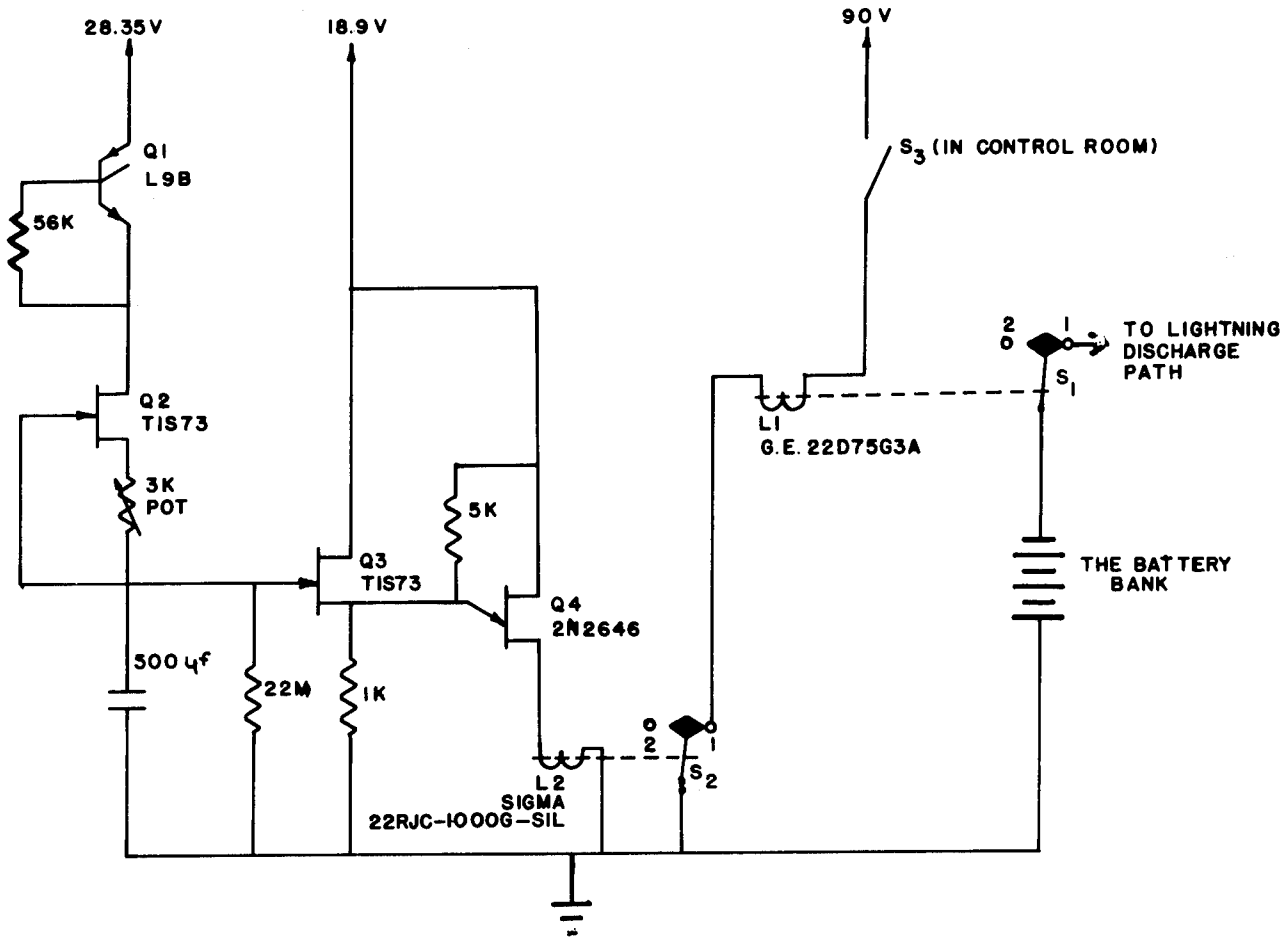

Fig. 20 **SCHEMATIC DIAGRAM OF THE TIMING SWITCH**

on the D_1, a light activated silicon controlled rectifier (LASCR), in less than 6 microseconds. Once the LASCR is on, the 28.35 volt power supply will be latched to the Q_2, a field effect transistor, which works as a constant current source, therefore, the capacitor C will be charged linearly. When the capacitor is charged to 12 volts, the Q_4, an unijunction transistor, will activate L_2 to change S_2 to position 2; then L will be de-activated to change S_1 to position 2. By this procedure the battery cart is disconnected from the lightning discharge path. Q_3 works as a source follower to increase the linearity of the charging rates of the capacitor. The timing of the whole device is controlled by the 3 kilo-ohm pot which limits the amount of current from the current source. Three 9.45 volt mercury cells are used for the 28.35 and 18.9 volts power supply. A 90 volt dry battery is used to power L_1. The GE 1C2800-Y102A-3, normally open circuit breaker is used in the timing switch.

Referring to the schematic diagram of an artificial lightning stroke simulator as shown in Figure 18, the discharge path of the battery bank can be represented by the equivalent circuit of Figure 21.

A circuit analysis yields the following equation for this circuit:

$$I(t) = \frac{V}{R}\left(1 - e^{-\frac{R}{L}t}\right)$$

For a typical operation, i.e., a 250 amp discharge, the rise time will be:

t = 4.1 s for 10% of current rise, or 25 amp

t = 26.9 s for 50% of current rise, or 125 amp

t = 89.3 s for 90% of current rise, or 225 amp

Since the discharge of the battery bank depends on the existence of the conductive channel established by the discharge of the capacitor bank, a time coordination must exist between the capacitor and battery banks. Theoretical calculations show that the central temperature in

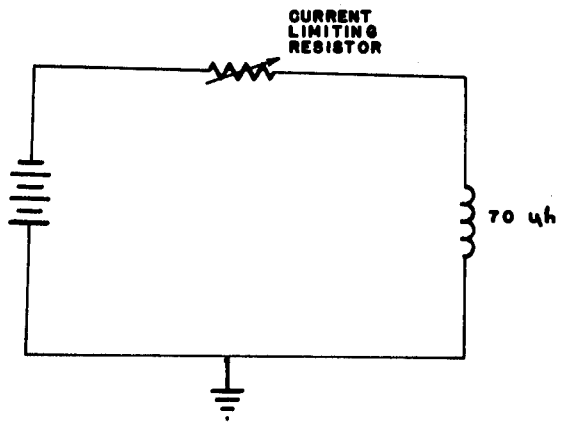

Fig. 21 - Equivalent circuit for discharge path of battery bank.

an ionized channel will drop to 7000°C or 8000°C within 1 millisecond of the cessation of lightning discharge. At these temperatures, the electrical conductivity of air is between 3.90 ohms/cm and 10.4 ohms/cm. These arguments, combined with the rise time calculations of the battery bank, show that the battery bank is able to "follow-on" in the desired fashion.

FUNDAMENTAL INVESTIGATIONS OF HIGH INTENSITY ELECTRIC CURRENT FLOW, PROCESSES AND RESULTANT DAMAGE IN ADVANCED COMPOSITES

700937

Allen P. Penton
and
John L. Perry
Philco-Ford Corporation,
Aeronutronic Division

and

Kenneth J. Lloyd
General Electric Company
High Voltage Laboratory

AS A PART OF THE "1968 LIGHTNING AND STATIC ELECTRICITY CONFERENCE" of the SAE and Air Force Avionics Laboratory, Philco-Ford Corporation and General Electric Company presented their findings relative to damage produced in advanced boron filament epoxy composites as the result of high intensity electric current flow (1)*. In the paper presented, experimental data and initial damage mechanism modeling were presented to show that such composites are significantly degraded when such electric current passes through them. In the paper, this phenomenon was related to the possibility of such damage occurring as the result of electric current flow in the skin of an aircraft as caused by a lightning strike. The original objective of the work reported was initiated because of programs in progress to develop aircraft skin constructions of advanced boron and graphite filament composites.

Since the original work reported in Ref. 1, the Naval Air Systems Command has sponsored a research program to study the damage mechanisms and current flow processes involved in the flow of high intensity electric current in advanced composites (2). The program is being performed by the Philco-Ford Corporation, Aeronutronic Division with the support of the General Electric Company High Voltage Laboratory. In the program, filaments and epoxy resin composites of boron and graphite filaments are being studied. The boron filaments are of the 0.004 inch diameter variety that are manufactured by the chemical vapor deposition of boron onto a 0.0005 inch diameter tungsten wire. Such filaments typically have a 55 x 10^6 psi modulus of elasticity. Two varieties of graphite filaments have been included. One is a 55 x 10^6 psi modulus graphite filament tow as manufactured from a polyacrylonitrile precursor and the other is a 50 x 10^6 psi modulus graphite filament yarn as manufactured from a rayon precursor. The filaments were manufactured by:

United Aircraft Corp.: boron filament
Courtaulds, Ltd.: HM-S 55 x 10^6 psi modulus graphite tow
Hitco: HMG-50 50 x 10^6 psi modulus graphite yarn

In the composites evaluated, the epoxy resin matrices were Whittaker Corp. 2387 for the boron composites and DEN 438/MNA for the graphite composites. Each composite was of 50-55% by volume filament content.

In the investigations performed to date by Philco-Ford Corporation and General Electric Company, the objective has been to perform basic research aimed at establishing a complete relationship between the characteristics of high intensity electric currents and the responses of advanced composite materials to those currents. The approach being used to reach this end is shown in Figure 1. This figure shows that a complete understanding of degradation processes and possible methods for improving composite material response requires the investigation of the following interrelated areas:

1. The resultant degradation mechanisms.
2. The electric current flow process within the filaments and composites.

The approach utilized to date in all filament and composite electric current exposures is to pass the current through a composite. In the case of filaments, the current was passed through a 1/2 inch wide, 0.025 inch thick, by 7 inch length of composite in which all filaments were in the direction of current flow. Available data indicate that high intensity current flow resulting from lightning strikes, rise to their maximum amplitude in a short period of time and decay over a longer period. Typical peaks have front times of one to ten microseconds and decay or tail times of between ten and fifty microseconds (3). The majority of the electric current exposures, to obtain data discussed herein, involved the use of a single unidirectional current pulse with a wave

*Numbers in parentheses designate References at end of paper.

shape front time of three to four microseconds and a tail time of twenty-two to twenty-four microseconds, which was considered to be in the middle of the typical range of current resulting from lightening strikes.

DEFINITION OF THE CURRENT FLOW PROCESSES

As indicated in Figure 1, the investigation into the area of current flow processes has resulted in the construction of initial models of current flow within the composites. The steps which are necessary in developing the equivalent circuit model of the composite materials are:

1. Determination of impedances for boron and graphite filaments.
2. Determination of the impedance of epoxy matrices.
3. Determination of the dielectric strength of all components.

DETERMINATION OF IMPEDANCE - In order to detect any variations in specimen resistance during the period of current flow, the voltage rise across and current through each specimen was measured oscillographically. A point-by-point division of the voltage wave magnitudes by current wave values resulted in a plot of impedance versus time; i.e.,

$$Z(t_1) = \frac{v(t)}{i(t)_{t = t_1}} \qquad (1)$$

In addition to these dynamic impedances, resistance measurements of each specimen were made before and after application of the injected current pulse.

DIELECTRIC STRENGTH - In order to fully determine the current flow pattern within a complete composite, it is necessary to determine the dielectric (breakdown) strengths of those components which are poor conductors. In the graphite composite this is the epoxy matrix, while in the boron composite it is the epoxy matrix as well as the boron itself.

The dielectric strength of the boron surrounding the 0.0005 inch diameter substrate core was determined by applying a voltage stress between the outside of the boron and the substrate, as shown in Figure 2. The significant stress will be across the boron beneath the conducting band (Hg cup) as long as the distance L is maintained much greater than the boron thickness r.

The dielectric strength of epoxy matrices alone was determined using standard test electrodes per ASTM-D149-64. Voltages of varying wave shapes were applied to each epoxy specimen and the voltage breakdown level measured. In this manner, the relationship between breakdown voltage amplitude and duration, known as a "volt-time" (4) curve, is established.

EQUIVALENT MODELS OF FILAMENTS AND MATRICES As a result of these tests, the following models have been generated:

Graphite Tows and Yarns - Both the graphite tows and the graphite yarns may be represented as resistances. These resistances, however, are dynamically nonlinear and vary with the amplitude of the applied current pulse (see Figures 3 and 4).

Boron Filaments - The model for an incremental length of boron filament is delineated in Figure 5. In this case, ΔR_S represents an incremental length of substrate. This resistance is also dynamically nonlinear and varies with current pulse amplitude as shown in Figure 6.

Dielectric strength tests showed the boron surrounding the substrate to behave as a high valued resistor when subjected to very little voltage stress. With a voltage of approximately 20 volts impressed across the boron, the boron experiences a breakdown. These results are modeled by two resistors (ΔR_B) and a double ended Zener diode.

Epoxy Matrix - From the standpoint of a current flow model, the epoxy matrices behave as insulators. Dielectric strength tests discussed earlier show these materials to have a breakdown value of approximately 300 volts per mil. A thickness of epoxy may therefore be represented by the model in Figure 7, where the Zener diode in this model has a voltage breakdown value of 300 volts per mil.

Lightning currents flowing in the epoxy cause voltage rises along (or within) the epoxy, as modeled by resistance until the breakdown strength of the epoxy is reached.

COMPLETE COMPOSITE MODEL - From these simpler models of the components, a model of the complete unidirectional composite material may now be generated. This complete composite model is delineated in Figure 8, and is representative of both boron/epoxy and graphite/epoxy composites. This fact may be justified by realizing that in the model of Figure 5 the effect of the diodes and resistors ΔR_B may be neglected when voltages of 300 volts per mil, associated with epoxy breakdown, are present. It should also be noted that the epoxy matrix model of Figure 7 has also been modified when included here in the general model. Since the filaments, yarns and tows have

much higher conductivities than do the epoxies, they effectively short circuit any resistance in the epoxy adjacent to them. This fact results in two different epoxy models for external and internal layers of epoxy resin as seen in Figure 8.

The model delineated here is that of a finite portion of the whole specimen. Although construction of a model of the entire specimen is possible, it would be extremely complex.

SPECIFIC DISCUSSIONS RELATIVE TO CURRENT FLOW IN UNIDIRECTIONAL COMPOSITES - For this discussion, it will be assumed that current is injected directly into the filaments and that the current is carried uniformly by all filaments within the specimen.

Consider now any two filaments within a laminate (based on the general model presented earlier) as shown in Figure 9. It will be noted that the filament is made up of incremental sections; that is, the total filament resistances are:

$$R_{f_n} = \Sigma \Delta R_{f_n}$$
$$R_{f_m} = \Sigma \Delta R_{f_m} \qquad (2)$$

(The subscripts n and m are used only to facilitate the discussion, by generating a means of differentiating between the two substrates.) Recall also that the Zener diodes represent the breakdown strength of the epoxy resin separating the filaments.

Until now, most composite studies have considered the substrates of boron filaments to be homogeneous, and thus behave as uniformly-distributed resistors as shown in Figure 10. Investigations, however, have shown that the substrates are not pure tungsten, but borides of tungsten. In fact, it has been learned that there is no free tungsten at all within the substrate. The actual make-up of the substrate varies between WB_4 and W_2B_5. It may, therefore, be assumed that the resistance per unit length of each filament will vary, resulting in a nonuniform resistor, and the overall effect will differ from filament to filament. It may also be assumed that a similar nonuniformity exists for the graphite fibers.

Return now to filaments n and m of Figure 9. Since these are two typical filaments, it is entirely possible and probable that their make-ups are different and that neither one is uniform. This situation is shown in Figure 11.

There are two distinct possibilities as to how the specimen initially degrades, the first of which is depicted in Figure 12. Here it can be seen that between points A and B of the curve for filament n, 25% of the total voltage is supported by approximately 7% of the specimen length. This amount of stress could possibly cause a breakdown (flashover) along the filament and thus initiate a "snowball" effect. Just what results after this initial failure is unclear, mainly because of the complexity of the situation. The breakdown would result in a 25% reduction in resistance, with a simultaneous increase in current through the filament and voltage rise across it. At the same time, only 93% of the initial specimen length is supporting the voltage.

It must be pointed out that the failure need not occur at the filament end; the stressed region of other filaments might be internal from the ends. Thus, simultaneously and continuously the current magnitudes and voltage stresses are changing within a laminate, resulting in an extremely complicated situation.

The second possibility for initiation of failure is depicted in Figure 13. Here it is seen that the two filaments under consideration have a difference in potential between them, at one point, which is equal to 45% of the voltage across the entire specimen. Once this potential difference exceeds the breakdown strength of the epoxy resin (approximately 300 volts per mil), the resin will puncture.

Once again, the sequence of events after initial failure is complex and unclear. The two filaments at the point of puncture seek the same potential which is determined by the parallel resistance combinations of their two halves, and again the currents through the filaments and the voltage stresses across them change.

It also becomes evident that combinations of these two mechanisms can occur simultaneously, and to varying degrees, adding further complications after failure initiation. Clearly these initiation factors are of prime importance.

FILAMENT AND COMPOSITE DEGRADATION DUE TO CURRENT FLOW

As previously discussed, electric current exposures of filaments and epoxy matrix composites were performed at various crest current amplitudes using the standard waveform adopted. The results are discussed as follows:

BORON FILAMENT AND COMPOSITE DEGRADATION - The tensile strength of exposed boron filaments was determined subsequent to electric current injection. The results were compared to the tensile strength of non-exposed filaments from the same lot and roll of filament. The results are illustrated in Figure 14. As shown, the tensile strength of the filaments was unaffected until a current crest amplitude of approximately 3.7×10^4 amperes per cm^2 of filament cross-section. The strength degradation then was rapid with total disintegration occurring when crest currents of $7.5 - 8.0 \times 10^4$ amperes per cm^2 were injected. These filaments disintegrated into varying lengths of segments that were often split axially.

Similarly, the boron/epoxy composites degraded as the result of current flow. This is illustrated in Figure 15. The threshold for degradation of the composites appears to be a crest current injection level of approximately 5.7×10^4 amperes per cm^2 of filament cross-section. The current densities were computed by dividing the crest current level by the total cross-sectional area of the filaments within the composite. As noted, the strengths dropped rapidly until a crest current density of 7.85×10^4 amperes per cm^2 was achieved. Attempts to test at current injection levels of greater than 12.3×10^4 amperes per cm^2 (where the composite was degraded to 39% of its original strength) resulted in flash-over across the specimen. It is noted, however, that the composites did not degrade as severely at the same average current densities as was noted in the results of the single filament tests. This can be explained by consideration of two points. First, even though the filaments within the composite may be split and cracked, they still will reinforce the epoxy resin to a degree and the composite will have some (but reduced) structural integrity. Secondly, the current is not distributed equally among each of the boron filaments within the composite. The filaments do carry the current because of the highly non-conductive dielectric nature of the epoxy resin matrix. The boron filaments typically have a resistivity of $4 - 8 \times 10^{-3}$ ohm-cm. As will be noted later, degraded boron/epoxy composites show evidence that only a portion of the filaments were degraded. It is presently thought that the degraded filaments over the 0.025 inch x 0.50 inch cross-section of the composite specimens occurred at random. This occurred even though the composite ends were scarfed, vapor honed to expose all filament ends and over plated with nickel for electrical contact.

Figures 16 and 17 show, respectively, a portion of the cross-section of a non-exposed and an exposed, degraded boron/epoxy composite specimen. The random locations of the degraded filaments are apparent. Figures 18 and 19 show the portion of the surface plies of a non-exposed and an exposed boron composite specimen. As seen in Figure 19, only three of the five filaments shown are degraded. The most typical type of boron filament degradation is magnified in Figure 20. The center 0.0005 inch diameter core is readily distinguishable with the cracks extending radially outward from it. A similar type of degradation is shown in Figure 21. Several other degradation modes have also been noted. For instance, in Figure 22, a 2000X view of the core of a degraded boron filament is shown. The structure of the core indicates that it has melted and resolidified. A similar view of the core of a degraded boron filament is shown in Figure 23, with no evidence of melting. Figure 24 shows the core of a degraded boron filament that apparently has been either vaporized or melted. Figure 25 shows a cracked filament in which the core has melted and resolidified in the crack of the boron. Figure 26 shows a filament in which the core material has diffused outward into the boron to a diameter larger than the original core diameter.

BORON FILAMENT AND COMPOSITE DEGRADATION MODEL - The degradation of the boron filament/epoxy composite is controlled by the response of the boron filaments to current flow. It now appears that the concept involved in the initial boron filament degradation model is correct. That model, as discussed in Reference 1, is based on the fact that the core of the filament (whether it is tungsten or tungsten boride) has a much lower resistivity than does the boron surrounding it. The electric current then flows predominately through the core. Some electric energy then is dissipated within the core as heat. The heat build-up then causes a thermal expansion of the core both radially and circumferentially. The outer boron sheath then acts to restrain the expansion of the core. This then results in an increase in hoop and axial tensile stresses within the boron. These tensile stresses are additive to the residual stresses that are in all probability present as the result of the manufacture of the filament. At such a point when the internal stresses

exceed the strength of the boron, the boron sheath cracks either radially or transversely, whichever the case may be. Efforts are now in progress to improve mathematical interpretation of the degradation model. The evidence of melting vaporization and diffusion in the core region appear to be in support of the probability of intense thermal energy build-up within the core.

DEPENDENCE OF DEGREE OF DEGRADATION ON TOTAL ENERGY INPUT AND WAVEFORM SHAPE - In the majority of the tests performed, a single injected current waveform was utilized and the exposure levels were changed by varying the crest amplitude of the current. This can be a misleading approach. The degree of degradation is not solely dependent on the crest amplitude. Instead, it is dependent on the total energy dissipated within the specimen, which in turn is proportional to the total energy injected. In all current injections made the waveform was continuous, i.e., the filaments did not fail at crest but after the complete waveform. The total energy injected is varied by lengthening or shortening the current waveform shape in addition to varying the crest amplitude. To demonstrate this, current injections of boron filaments were accomplished at the same crest but with different waveshapes. To accomplish this, the front time and tail times of the waveshapes were varied. The results are shown as follows:

	Current Crest, Amperes per cm^2	Front Time/ Tail Time	% Strength Degradation
(1)	8.88×10^4	1.2/13.5	71
(2)	7.40×10^4	4.0/24.0	100
(3)	7.40×10^4	4.0/12.0	13

As can be seen in (1) and (2), a crest current density (8.88×10^4 amperes per cm^2) produced only 71% loss in strength because a shorter waveshape was used, which represented a lower energy input. Also, as can be seen in (3), the same current density of 7.4 amperes per cm^2 produced only a 13% loss in strength with a shorter (lower energy) waveform. Because of these and similar experimental results, it is concluded that the only meaningful relationship between electric current flow and degradation is one which is based on energy input and resulting energy dissipation.

GRAPHITE FILAMENT AND COMPOSITE DEGRADATION - Attempts to produce degradation in high modulus graphite yarn and tow filaments due to current flow per se, were unsuccessful. At advanced current injection levels some degradation was noted, which was accompanied by excitation and movement of the filaments. This has been determined to be the result of the mechanical abrading of one filament by another instead of because of changes within the filaments as the result of electrical energy dissipation. For instance, in the case of the HMG-50 graphite yarns, loss in breaking strength due to this excitation was initiated at crest current injection densities of 19 amperes per cm^2 and higher. In the case of the HM-S graphite tow excitation and movement during current injection was noted at crest current density levels of 29×10^4 amperes per cm^2 and higher; however, degradation in filament breaking strength did not occur until crest current density levels of 86×10^4 amperes per cm^2 were injected. In the case of the tow filaments, it is believed that the excitation did not cause degradation until the movement because very violent because the filaments in the tow bundles are loosely bound. In the case of the HMG-50 yarn the filaments are twisted together and plied so abrasion and degradation begin when the excitation movement is initiated.

In the same manner as for the boron composites, unidirectional HMG-50/epoxy and HM-S/epoxy graphite filament composites were exposed to a series of electric current injection at increasing crest amplitudes, but with the standard waveform. In the case of the HMG-50 composite specimens, no strength degradation was observed at crest current density levels as high as 13×10^4 amperes per cm^2 of filament cross-section. At an injected crest current density level of 20.4×10^4 amperes per cm^2 of filament the specimens burst into flames. The resulting specimens exhibited a 43% reduction in tensile strength. The specimens after exposure are shown in Figure 27. The HMG-50/epoxy unidirectional composite specimens exposed to 24.2×10^4 amperes per cm^2 of filament delaminated in addition to burning, as shown in Figure 28. The HMG-50/epoxy specimen exposed to 55.8×10^4 amperes per cm^2 of filament crest current burned even more violently and delaminated more extensively, as shown in Figure 29.

The Figure 30 photomicrograph shows an HMG-50 specimen after 13×10^4 amperes per cm^2 of filament injection. No damage occurred. Figures 31, 32 and 33 are, respectively, photomicrographs of cross-sections of specimens shown in Figures 27,

28 and 29. The increasing severity of damage for current injection levels of 20.4 x 10^4, 24.2 x 10^4 and 55.8 x 10^4 amperes per cm^2 of filament cross-section is obvious.

Graphite HM-S tow/epoxy unidirectional composite specimens exposed at crest current densities as high as 21 x 10^4 amperes per cm^2 were not degraded. However, identical specimens exposed at 25 x 10^4 amperes per cm^2 burned and charred, as shown in Figure 34. The HM-S/epoxy specimens exposed to 52 x 10^4 amperes per cm^2 burned and exfoliated severely, as shown in Figure 35.

Figure 36 shows a non-damage specimen cross-section of an HM-S/epoxy specimen that has been exposed to 21 x 10^4 amperes per cm^2 of filament crest current. Figures 37 and 38, respectively, show the damaged cross-section of specimens from Figures 34 and 35.

It appears that the crest current density at which flames appear and cause graphite/epoxy composite degradation is approximately 20-25 x 10^4 amperes per cm^2 of filament for both the HMG-50/epoxy and HM-S epoxy. Also, there is no measurable or observable degradation that occurs until flames are observed. Above the current levels where flames initiated, delaminations occur and become more extensive at higher levels. The degradation model for the graphite filament/epoxy composites then is based on the heat generated within the filaments. Graphite filaments are much less resistive than are boron filaments (0.825 x 10^{-3} ohm-cm for HM-S tow and 1.3 x 10^{-3} ohm-cm for HMG-50 yarn as compared to 4-8 x 10^{-3} ohm-cm for boron filaments); therefore, in the case of graphite/epoxy composites the current is also carried by the filaments. Also, the lower resistivities of the graphite filaments results in less dissipation of electrical energy within the filaments as compared to the boron filaments. Heat is generated within the filaments due to the dissipation of the electrical energy. At the higher current densities this heat is sufficient to cause the pyrolysis of the epoxy resin matrix and the smoking evidenced. At the surface of the composite the pyrolysis gases ignite in the presence of oxygen. At still higher levels of current injection the resin pyrolysis is rapid and the build-up of internal pyrolysis gas pressure within the composites cause delamination of the composite. To further clarify this degradation concept, the relationship of filament temperature to current crest was calculated and reported in Figure 37. As can be seen, temperatures of 600-800°F are achieved with crest currents of 150 amperes for the HMG-50 yarn and 1000 amperes for the HM-S tow bundle. These temperatures correspond to where pyrolysis of epoxy resin is initiated. Also, the 150 and 1000 ampere level corresponds to crest current densities of 28 x 10^4 amperes per cm^2 for the HMG-50 and 20 x 10^4 amperes for HM-S tow. As previously noted, flame were initiated in epoxy resin composites of both filaments at crest current densities of 20-21 amperes per cm^2 of filament.

CONCLUSIONS

(1) Electric current flow processes within epoxy resin composites of both boron and graphite filaments is analogous to a complex array of resistors (filaments) with the epoxy resin serving as a dielectric barrier between filaments. The processes, however, that determine the proportions of current flowing in each filament or layers of filaments are very complicated and difficult to mathematically model. Many factors, such as why current flow tends to concentrate at random in a fraction of the total boron filaments in a composite, are not understood at present.

(2) The limiting factor in the degradation of boron/epoxy composites are the boron filaments themselves. The filaments begin to crack and break up at crest current densities of 3.7 - 5.7 x 10^4 amperes per cm^2 for the standard waveform used in the tests reported. Above that point loss in strength is rapid with increasing current levels.

(3) The limiting factor in the degradation of graphite/epoxy filaments is the resin matrix. For the HMG-50/epoxy and HM-S/epoxy composites tested with the standard waveform, degradation by burning of the resin was initiated at crest current densities of 20-25 x 10^4 amperes per cm^2 of filament cross-section. At that point the temperature of the filaments was sufficiently high (600-800°F) to cause pyrolyzation of the epoxy resin.

(4) The controlling factors in the degree of degradation of the filaments and composites tested are the total electric energy input and the fraction thereof dissipated in the form of heat. To demonstrate this crest current amplitude as well as waveform duration was varied.

REFERENCES

1. Lightning and Static Electricity Conference, 3-5 December 1968, AFAL-TR-68-290, Part II, May 1969.

2. A. P. Penton, J. L. Perry, and K. J. Lloyd, "The Effects of High Intensity Electric Current on Advanced Composite Materials." Quarterly Progress Reports #1, #2, and #3, dated 12 December 1969, 15 March 1970, and 15 June 1970, Naval Air Systems Command Contract No. N00019-70-C-0073.

3. USA Standard 062.1, (IEEE Standard No. 28), 1967.

4. "IEEE Guide for Transformer Impulse Tests." No. 93, June 1968.

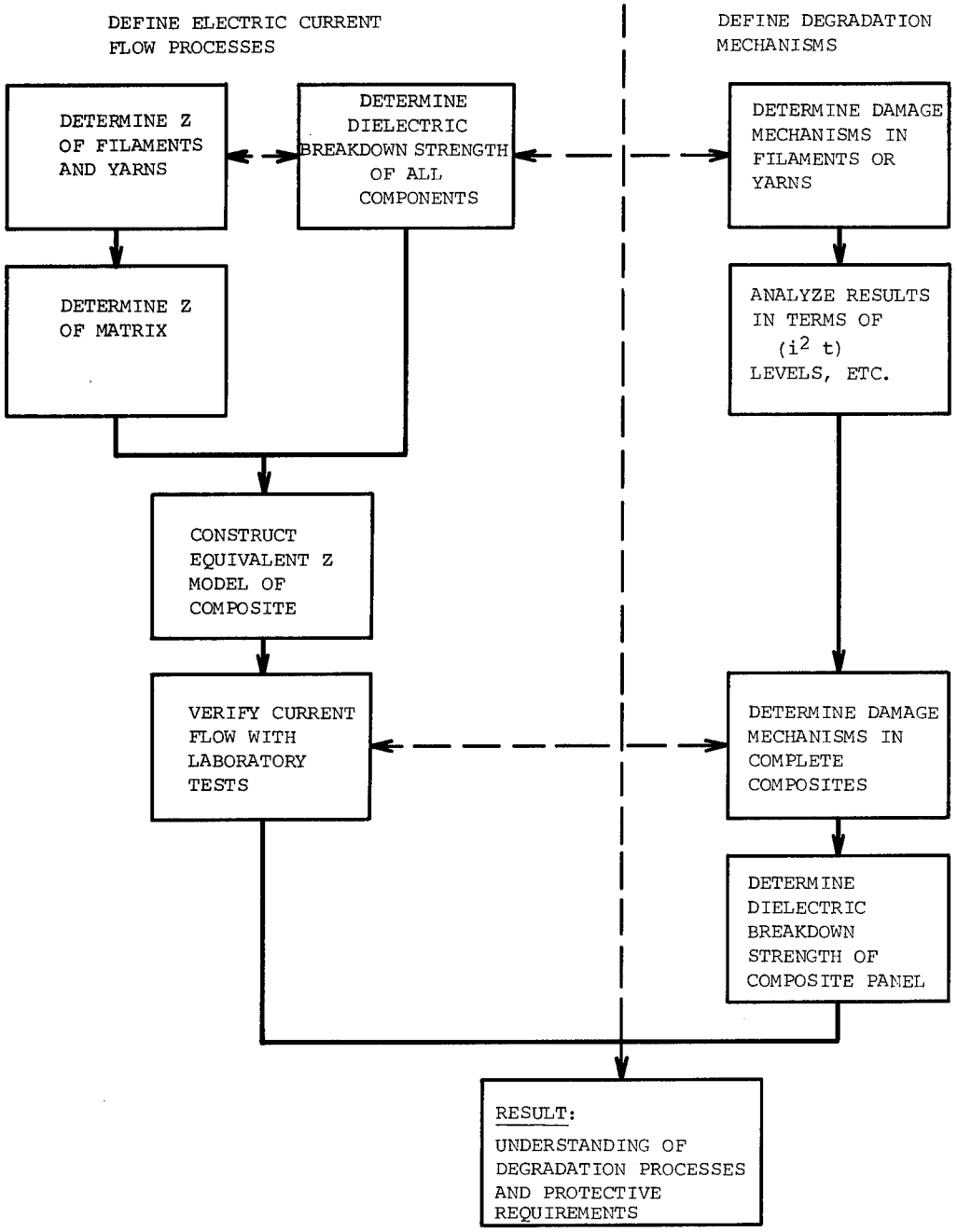

Fig. 1 - Block diagram of program approach

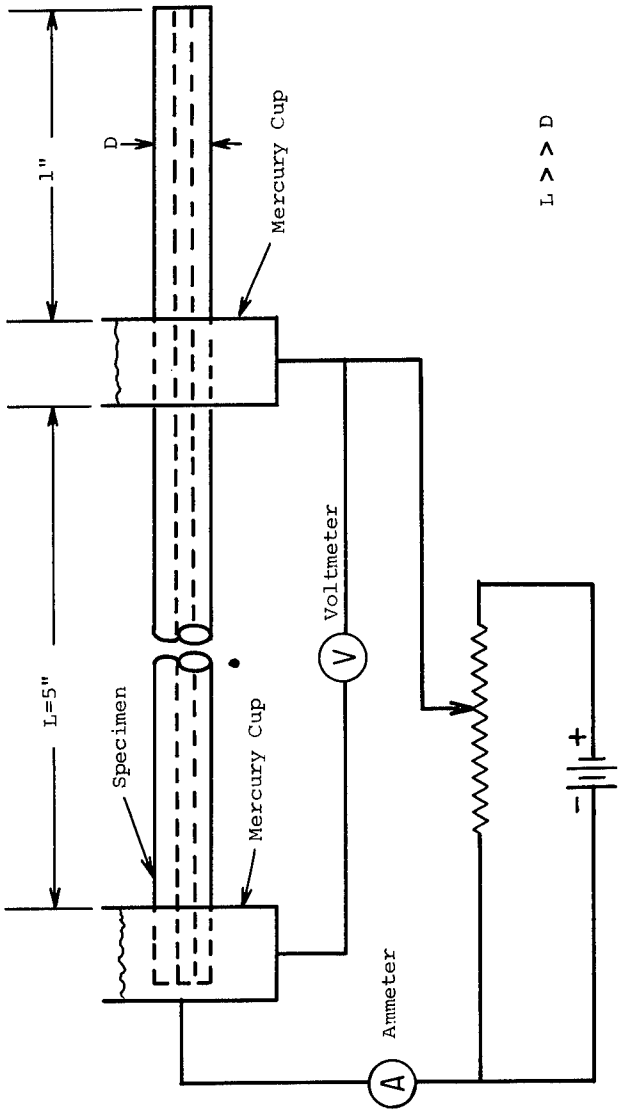

Fig. 2 - Set up to test dielectric strength of boron sheath

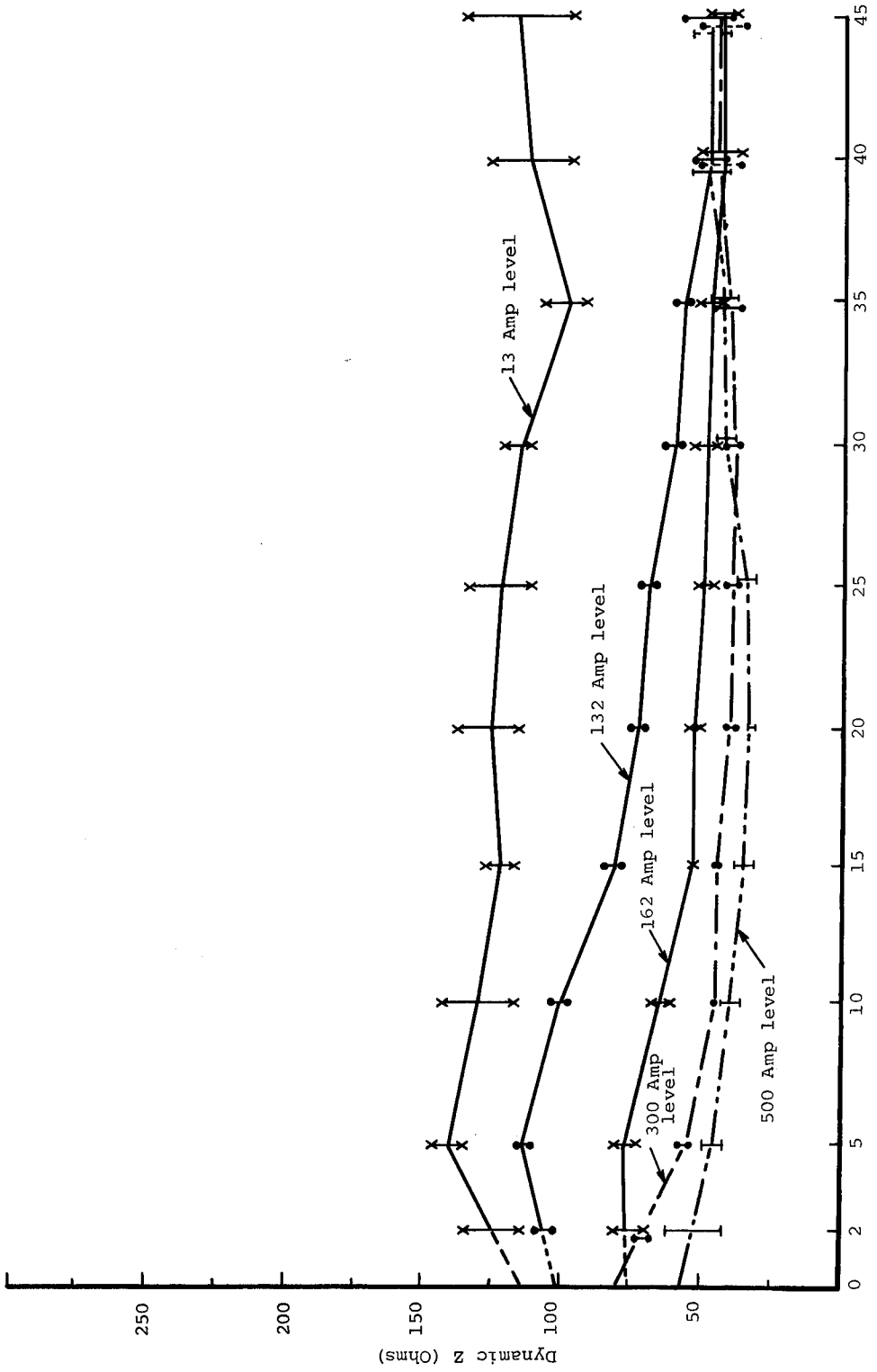

Fig. 3 - Dynamic impedance of HMG-50 graphite yarns

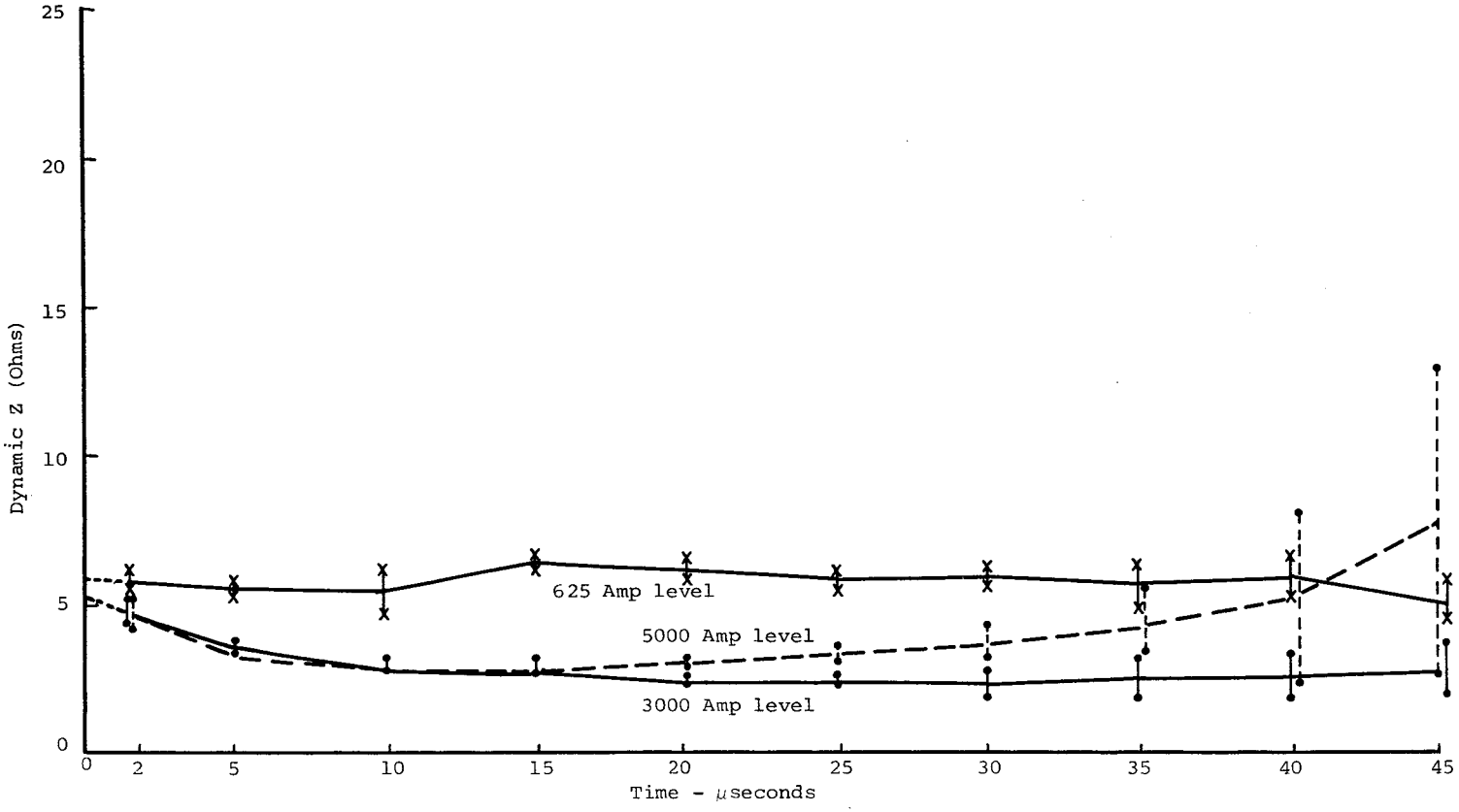

Fig. 4 - Dynamic impedance of HM-S graphite tows

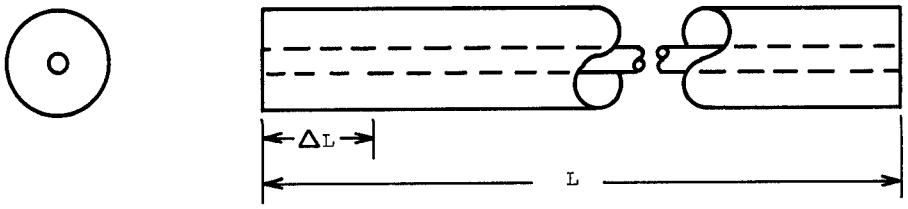

Boron Filament

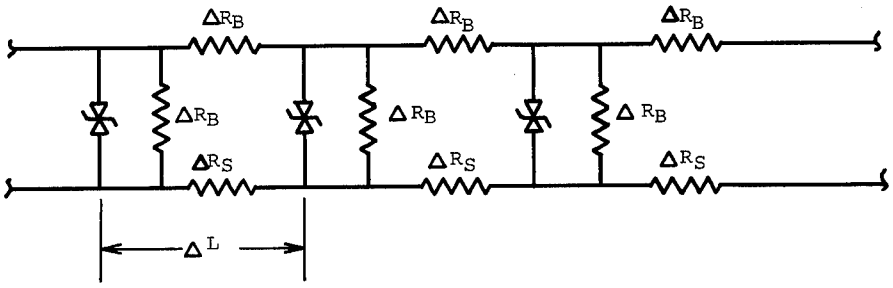

Equivalent Model Of Boron Filament

Fig. 5 - Unit length current flow model for a boron filament

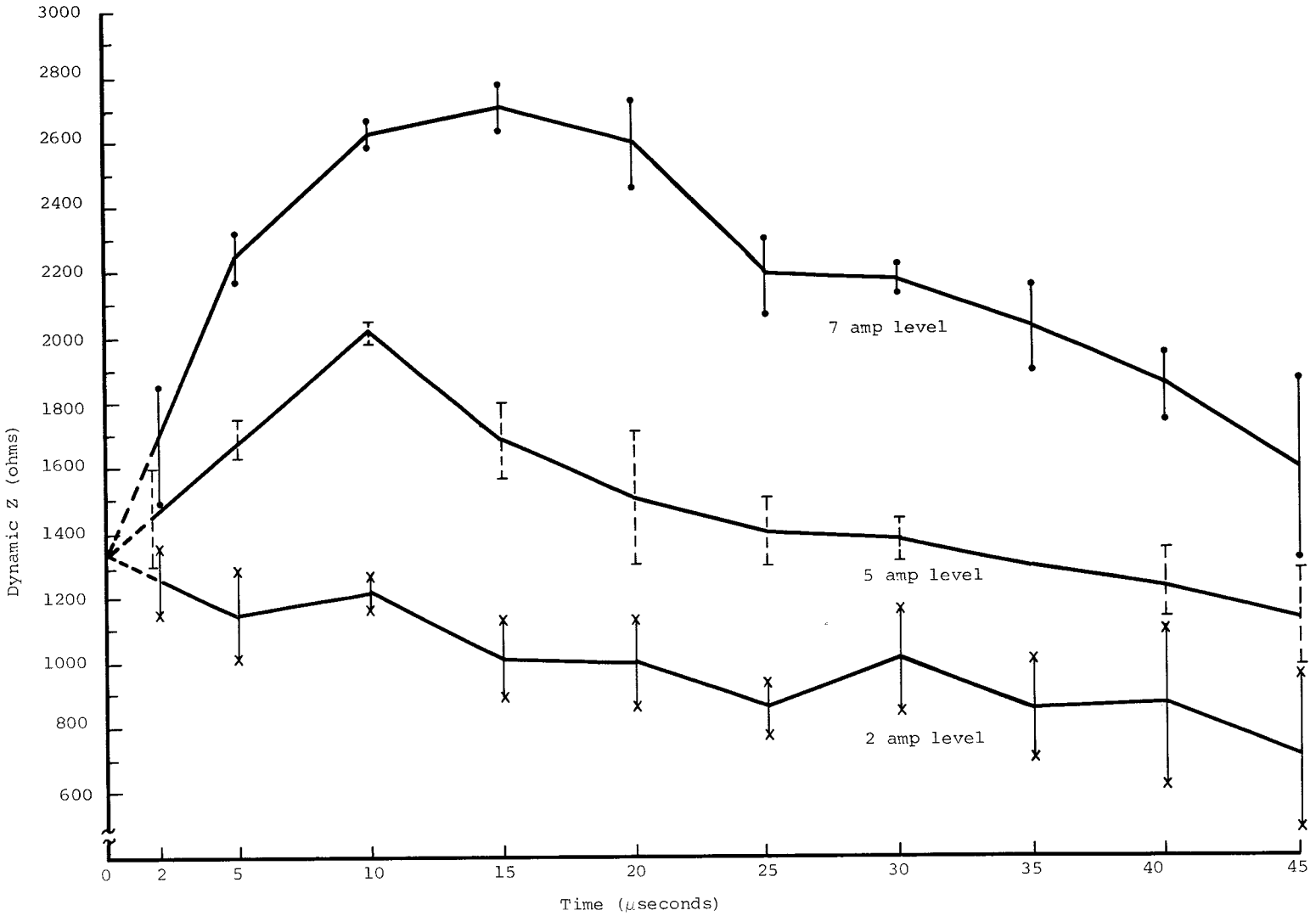

Fig. 6 - Dynamic impedance of boron filament specimens

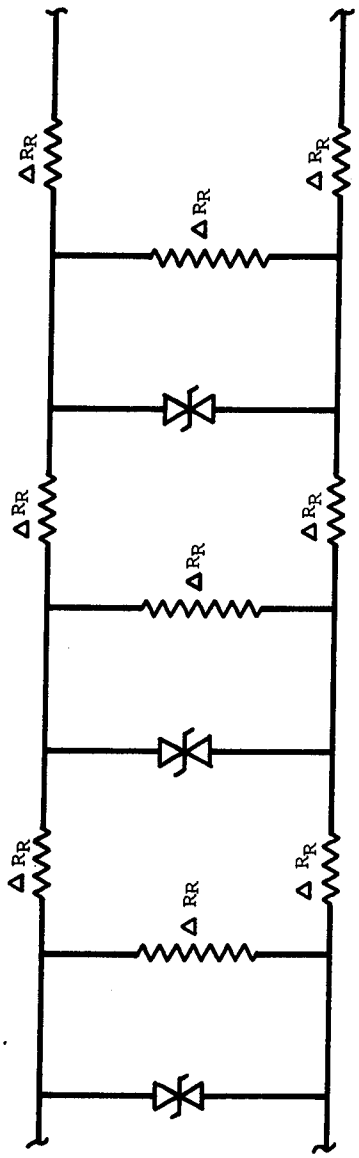

Fig. 7 - Equivalent model of epoxy resin film

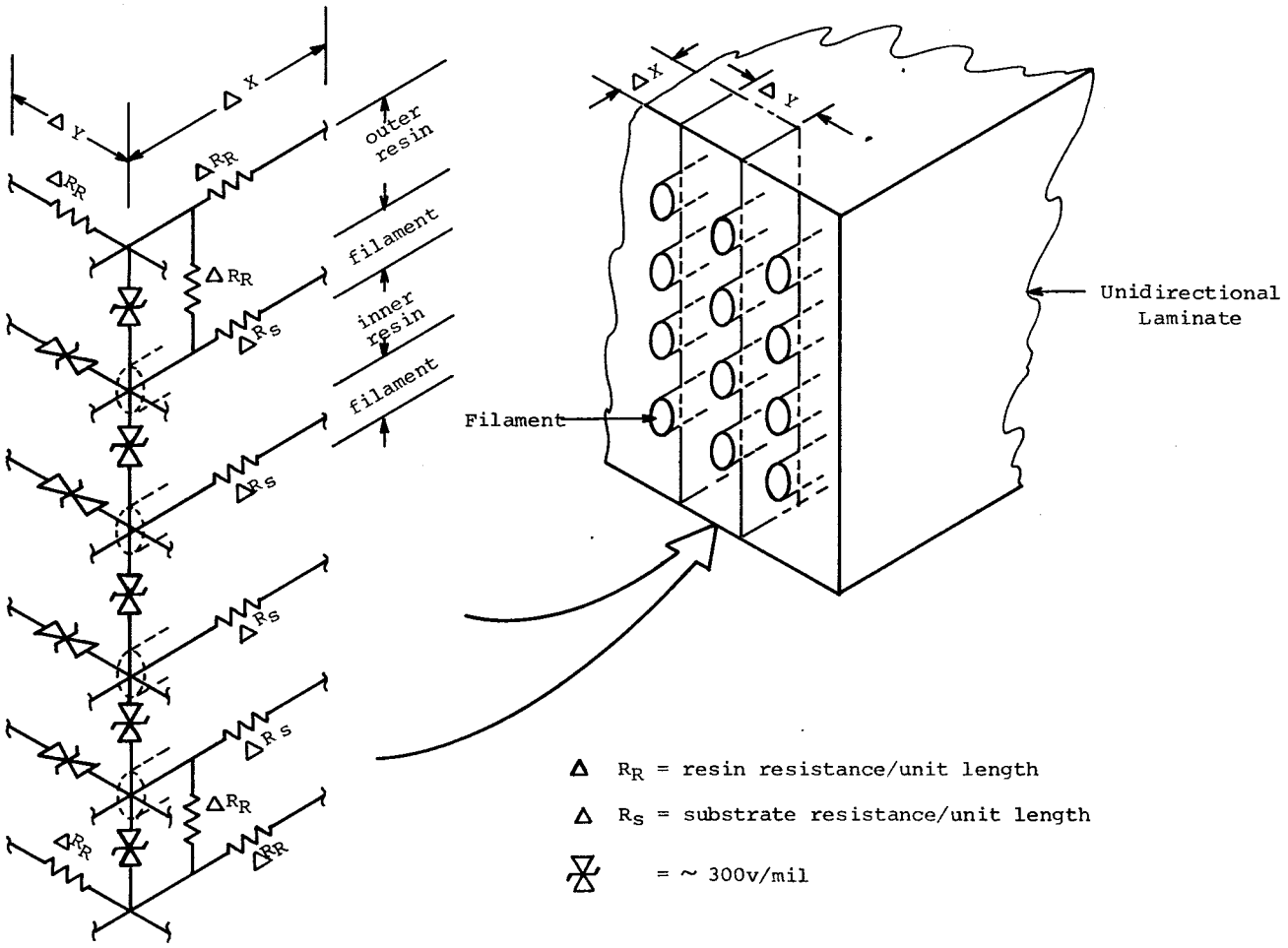

Fig. 8 - Current flow model of boron/epoxy unidirectional laminate

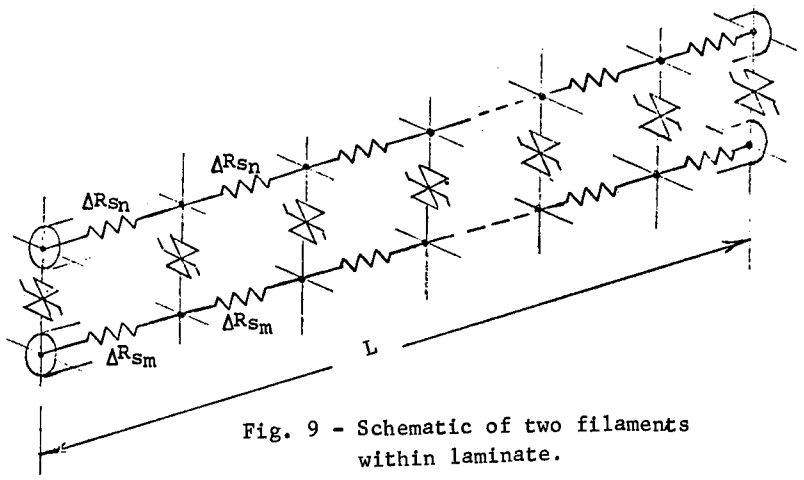

Fig. 9 - Schematic of two filaments within laminate.

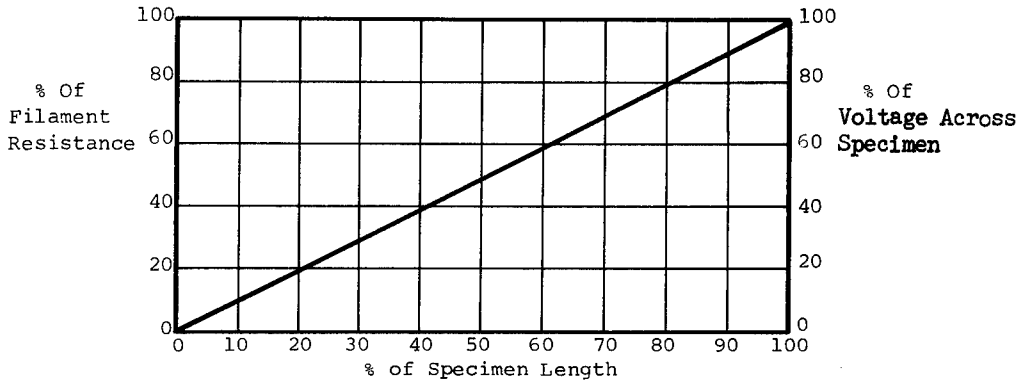

Fig. 10 - Resistance and voltage vs. length of boron composite specimen

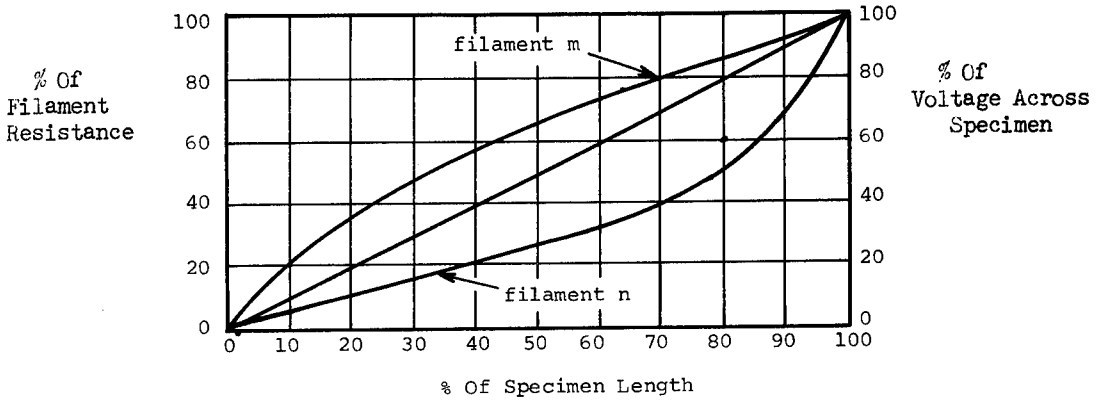

Fig. 11 - Resistance and voltage vs. length of boron composite specimen

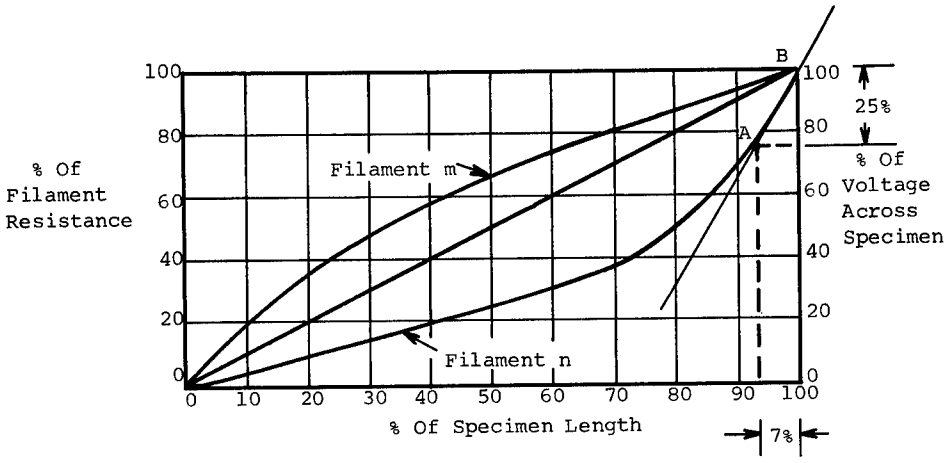

Fig. 12 - Resistance and voltage vs. length of boron composite specimen

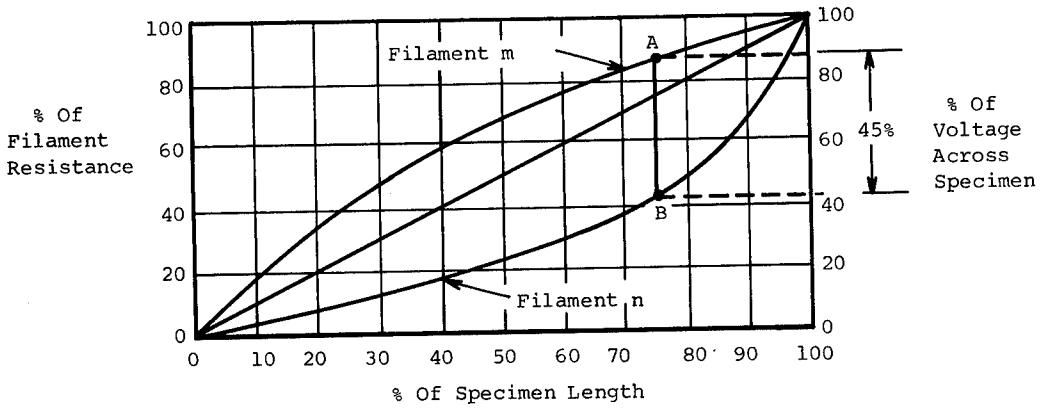

Fig. 13 - Resistance and voltage vs. length of boron composite specimen

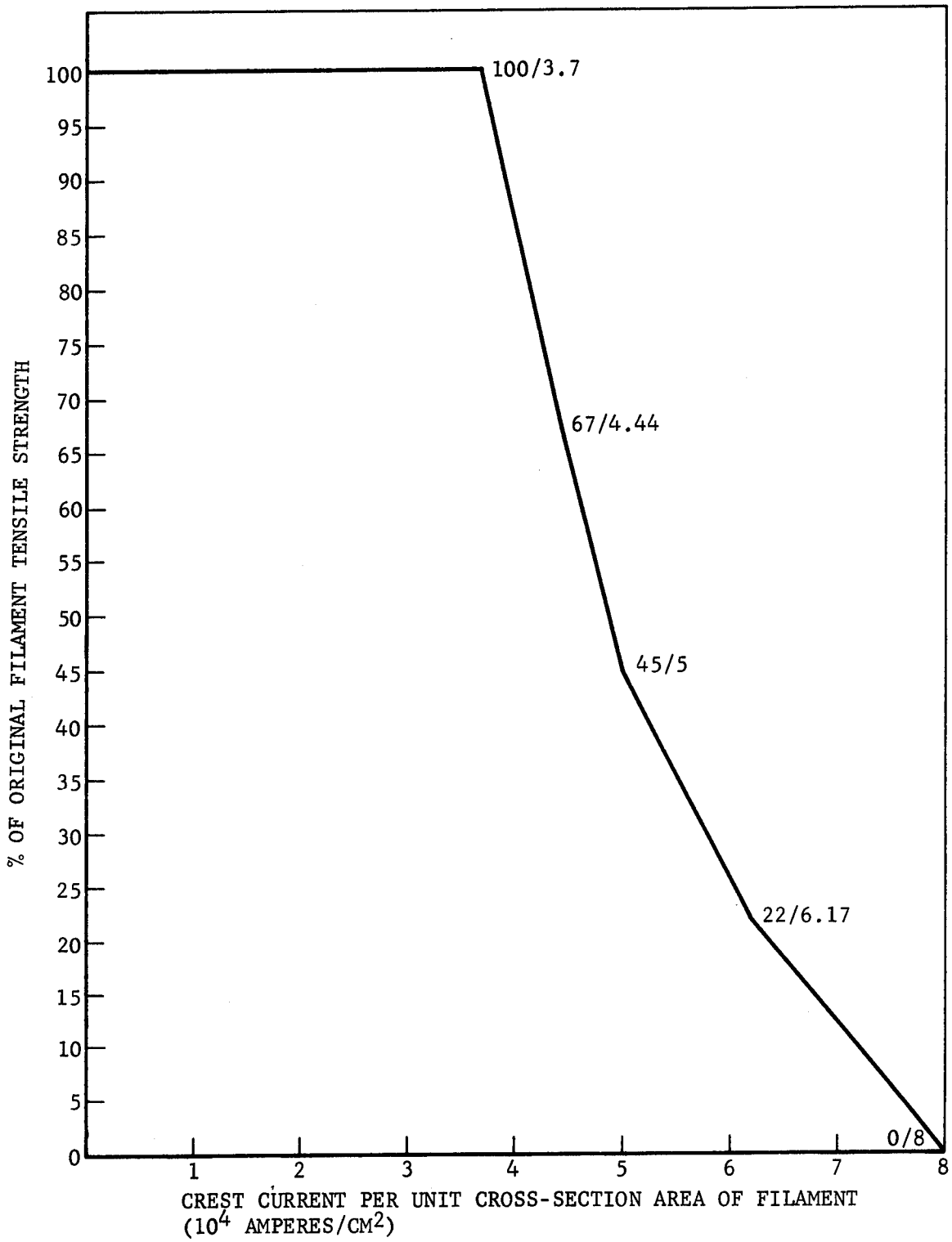

Fig. 14 - Boron filament strength degradation vs. crest current density (for standard waveform)

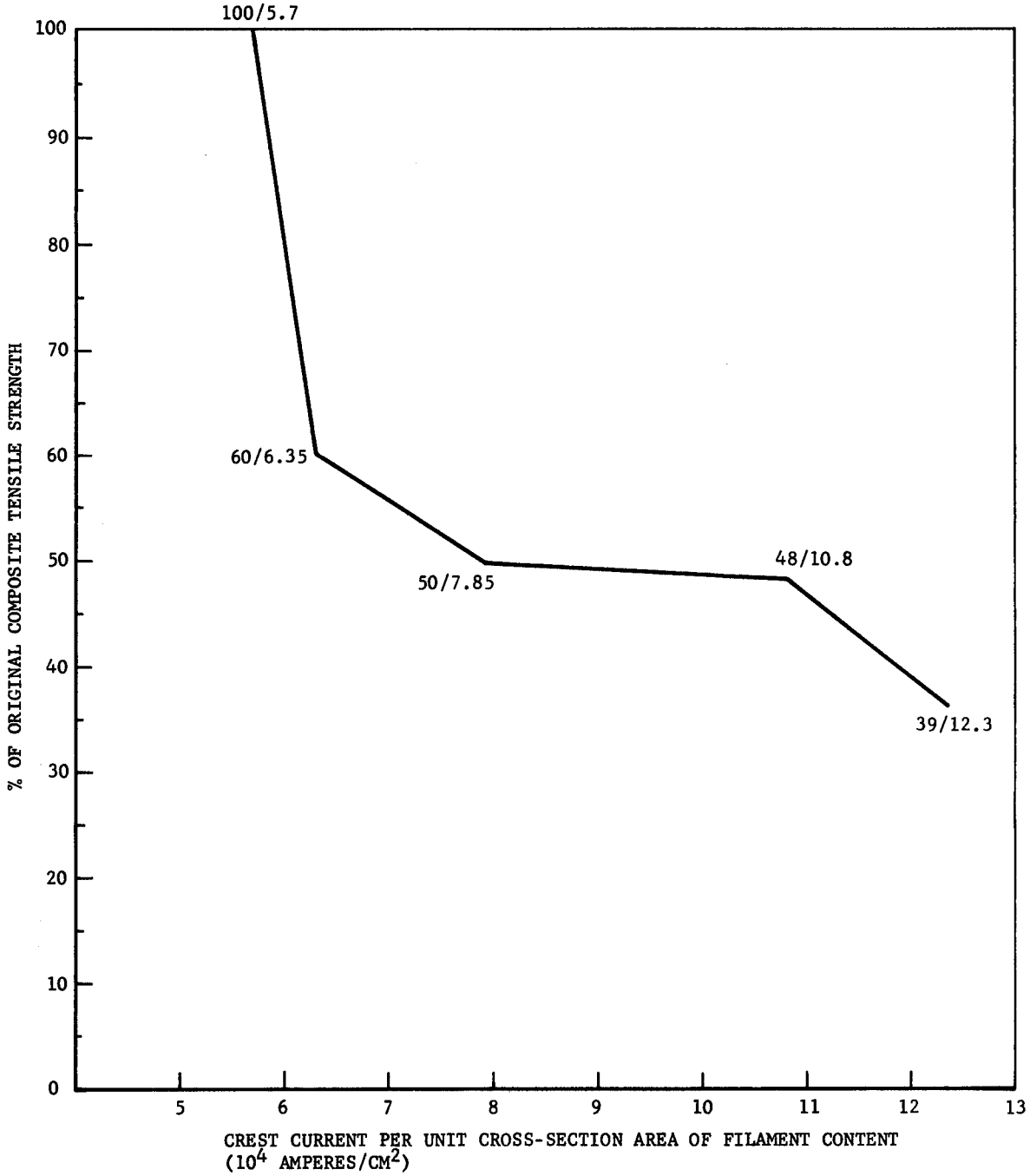

Fig. 15 - Boron/epoxy strength degradation vs. crest current density (for standard waveform)

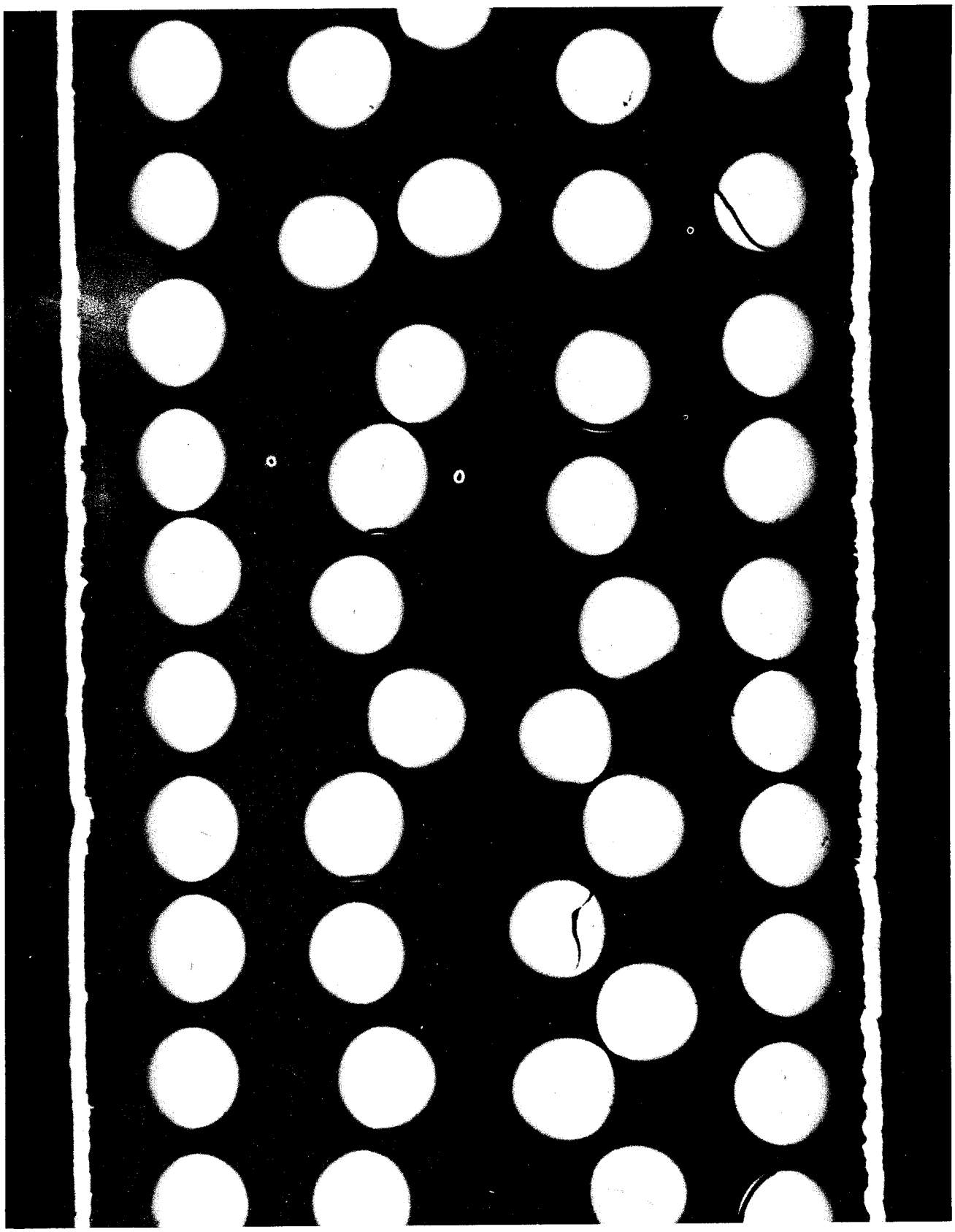

Fig. 16 - (100X) Cross section view of unexposed boron epoxy composite

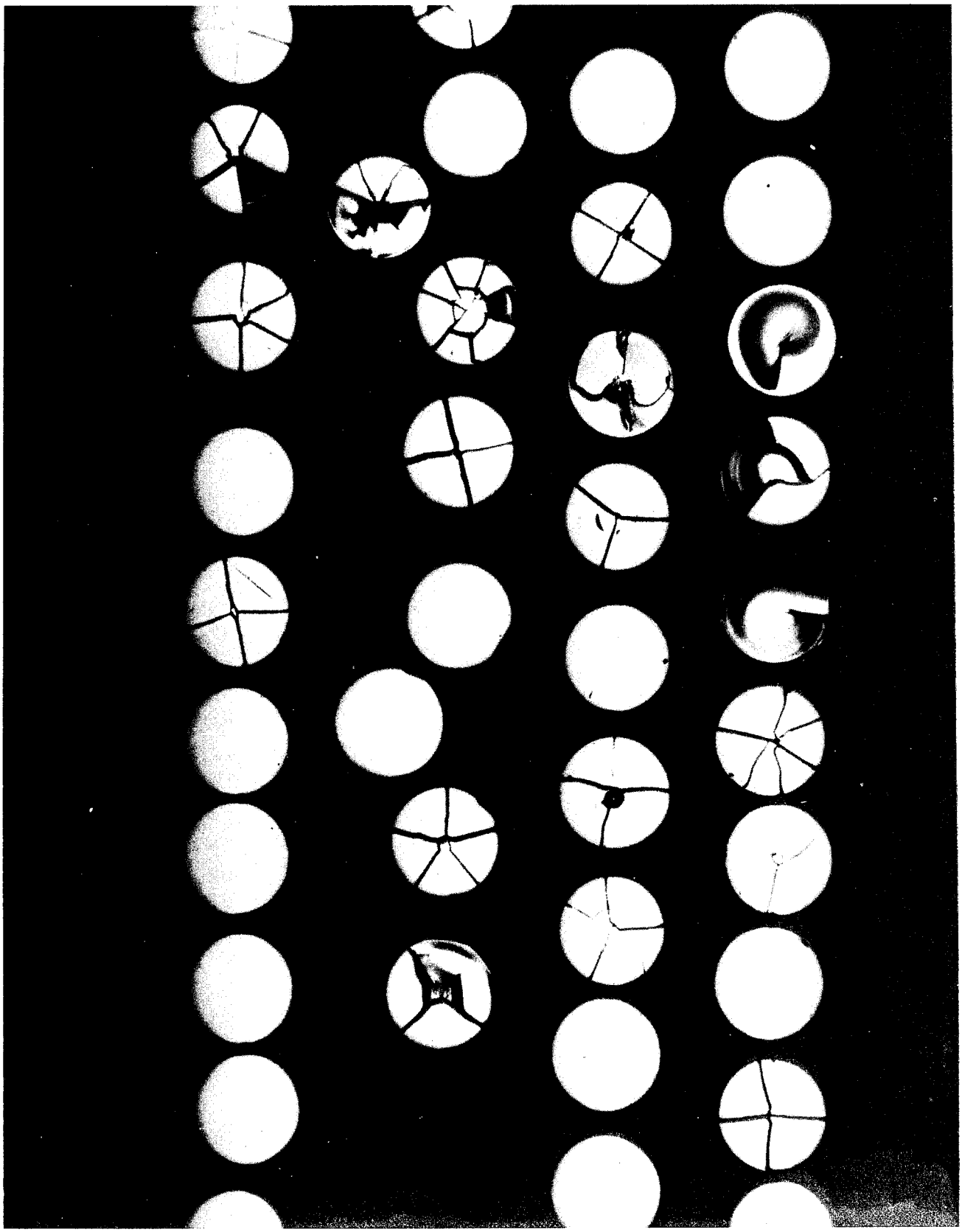

Fig. 17 - (100X) Cross section view of exposed boron epoxy specimen #26 (9.18×10^4 crest amps per cm^2 of filaments)

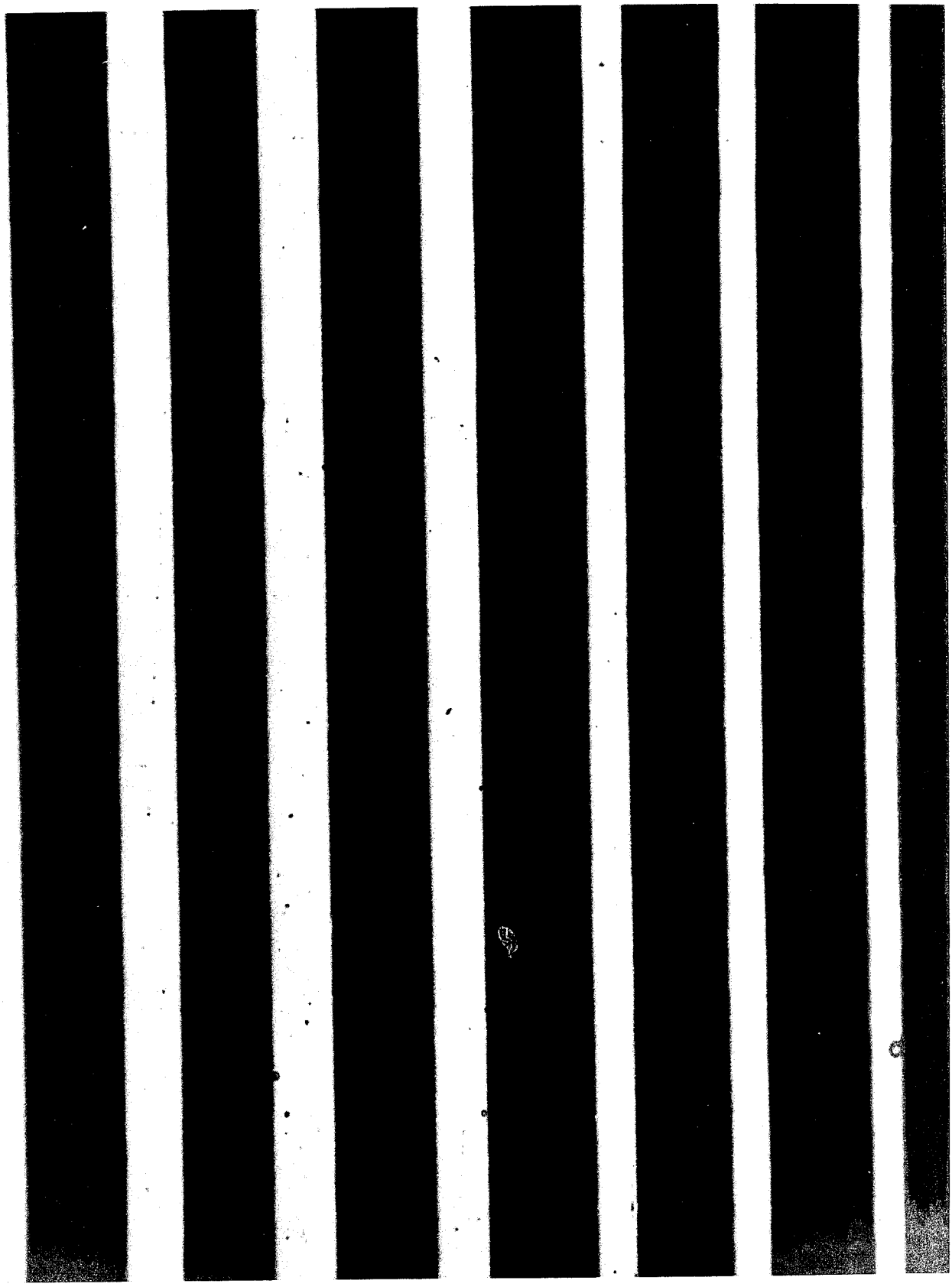

Fig. 18 - (100X) View of unexposed boron epoxy composite surface

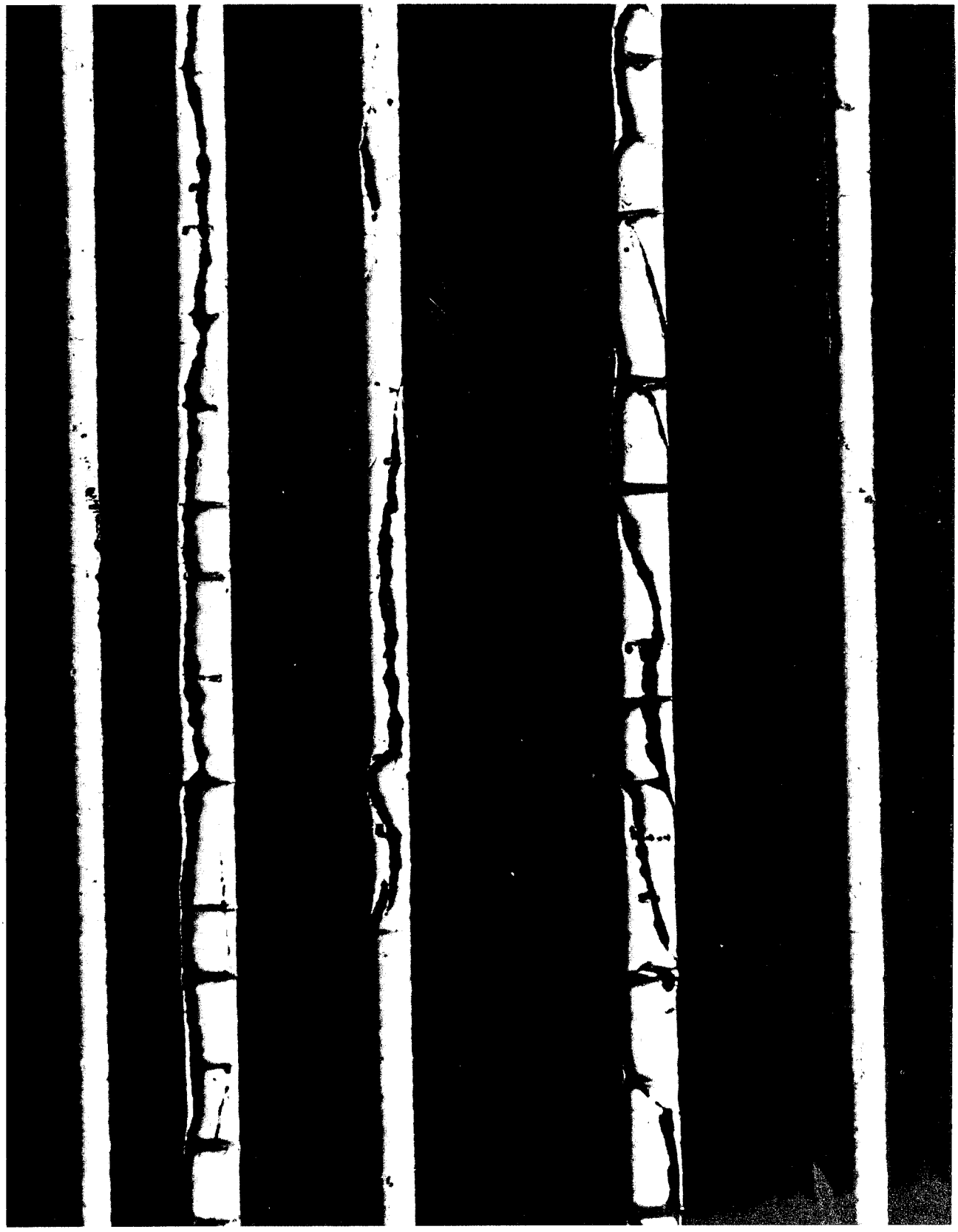

Fig. 19 - (100X) View of exposed boron epoxy composite specimen #13
($\sim$9 x 10^4 crest amps per cm^2 of filaments)

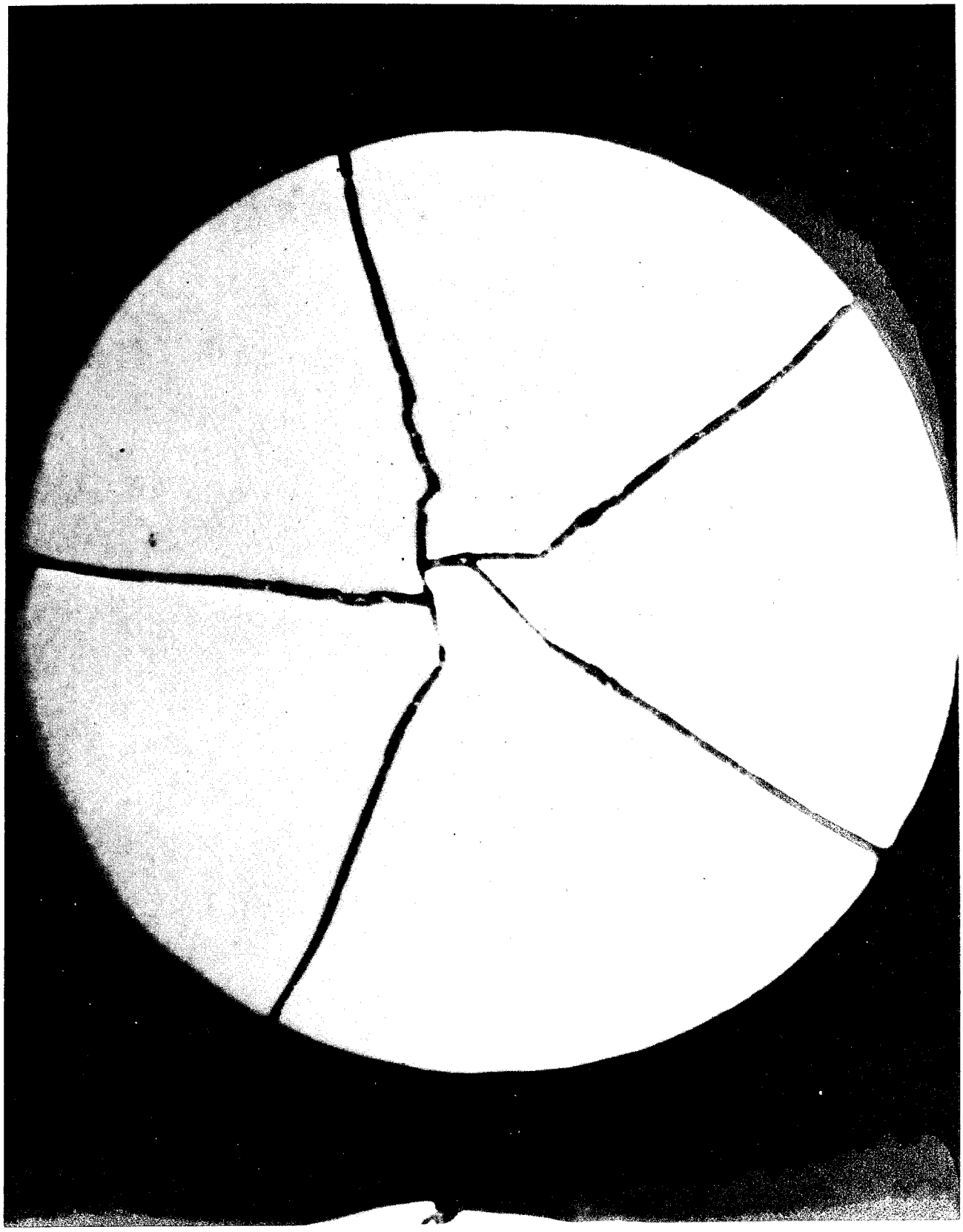

Fig. 20 - (800X) View of electrically damaged boron filament in composite specimen BU #26

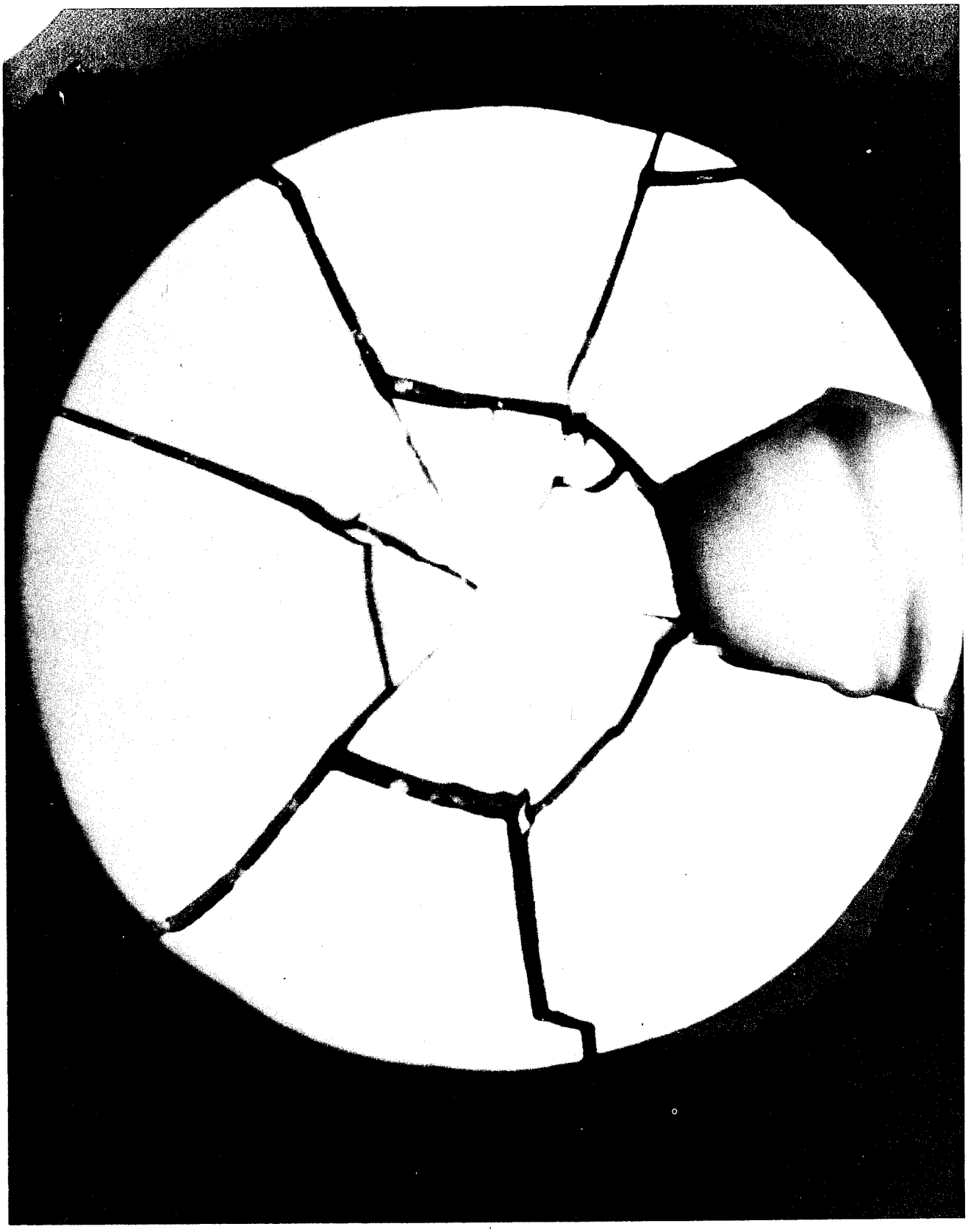

Fig. 21 - (800X) View of electrically damaged boron filament in composite specimen BU #26

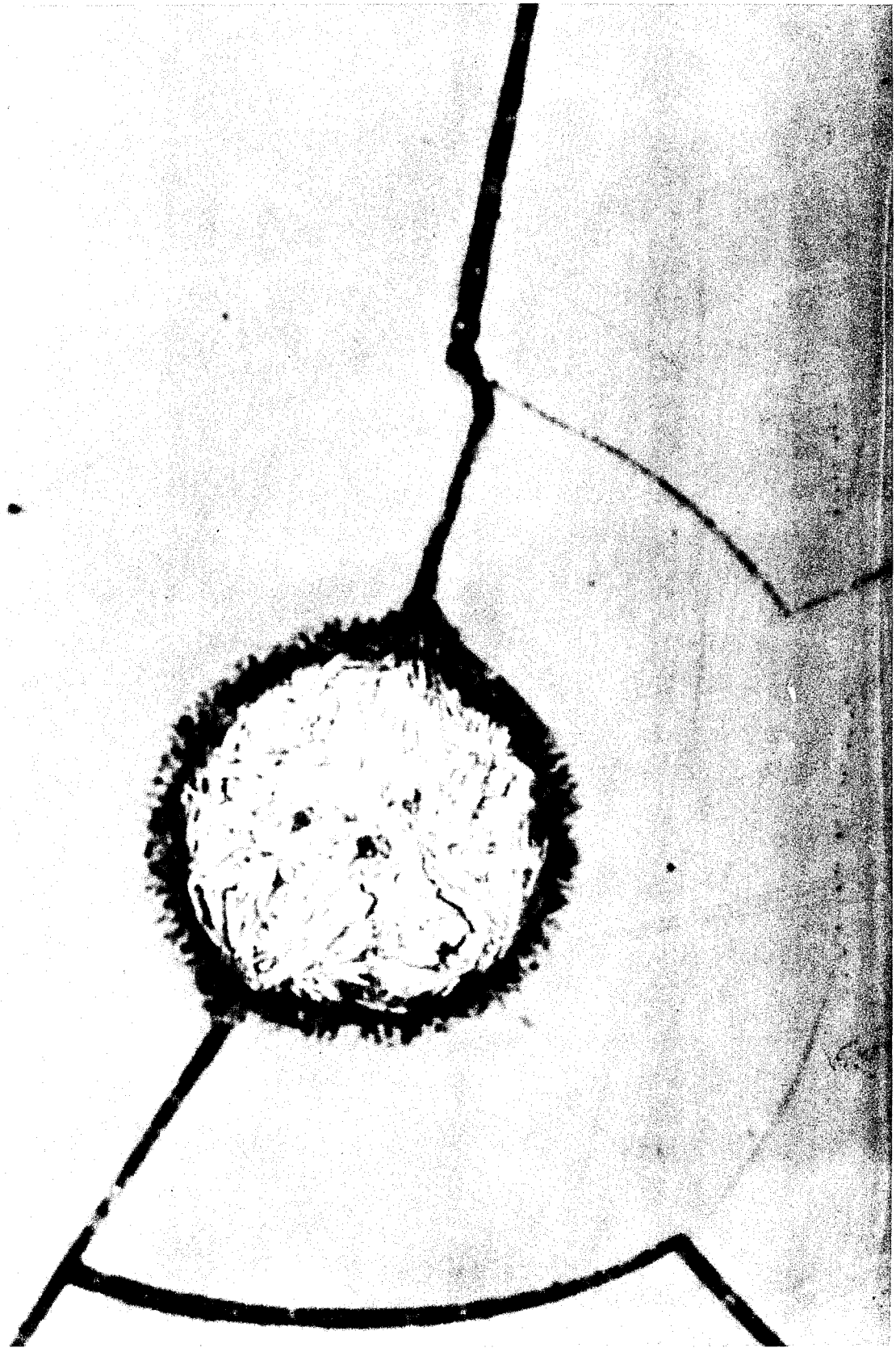

Fig. 22 - (2000X) View of core of damaged boron filament (BU #26) that has been etched to show evidence of melting

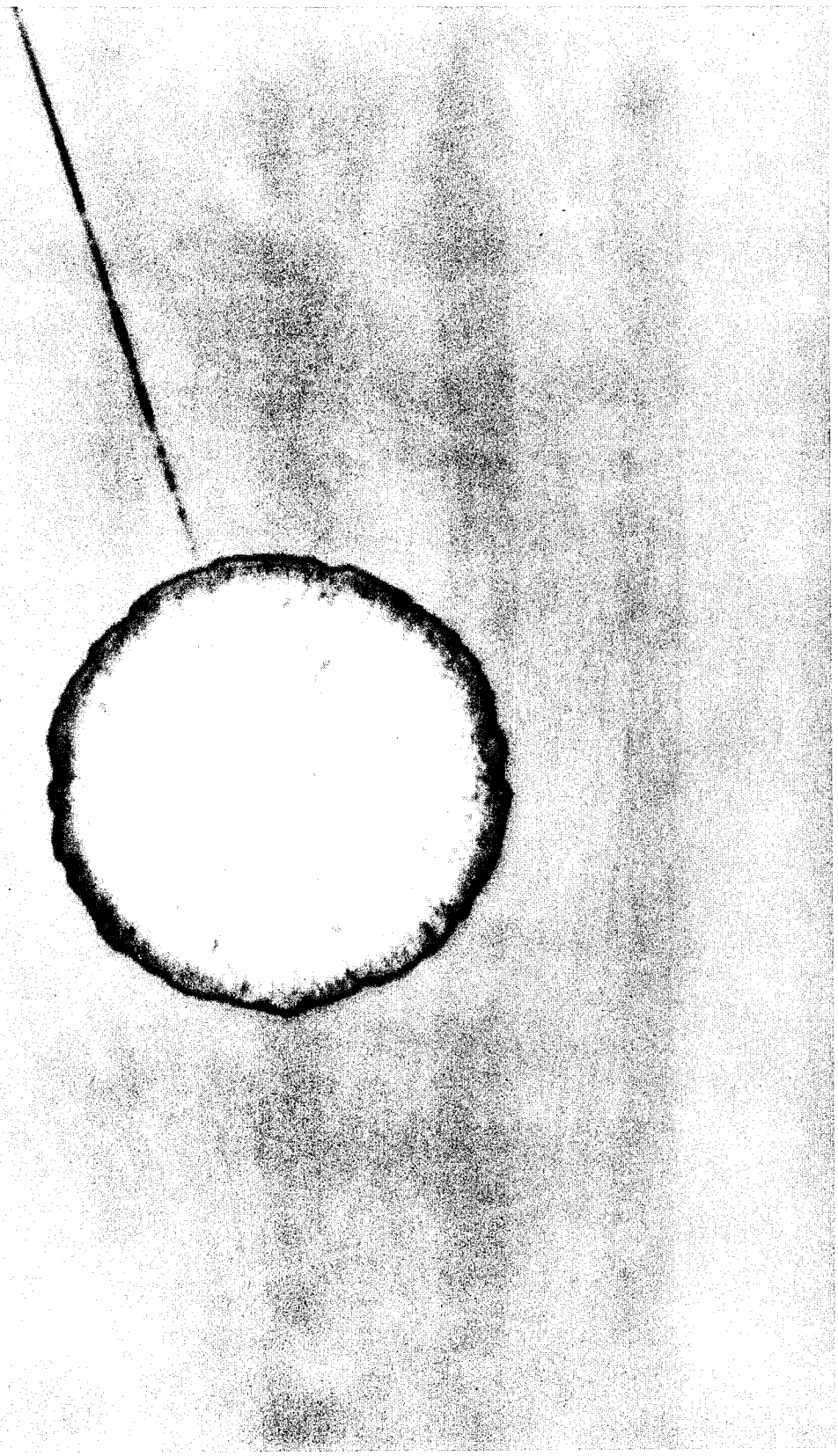

Fig. 23 - (2000X) View of damaged boron filament (BU #26) that has been etched but does not show evidence of melting

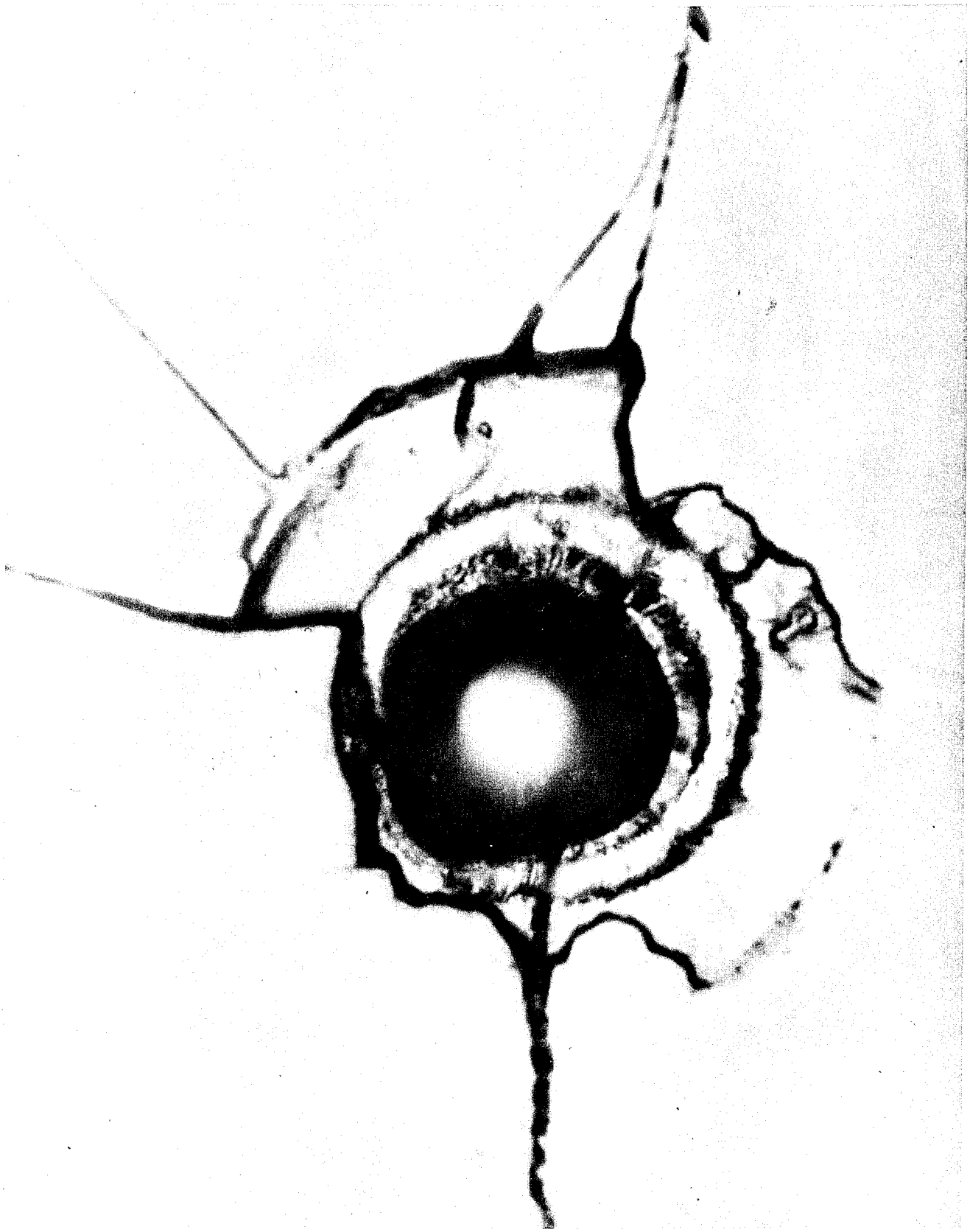

Fig. 24 - (2000X) View of boron filament in BU #26 composite where major portion of the core has been lost due to melting or vaporization

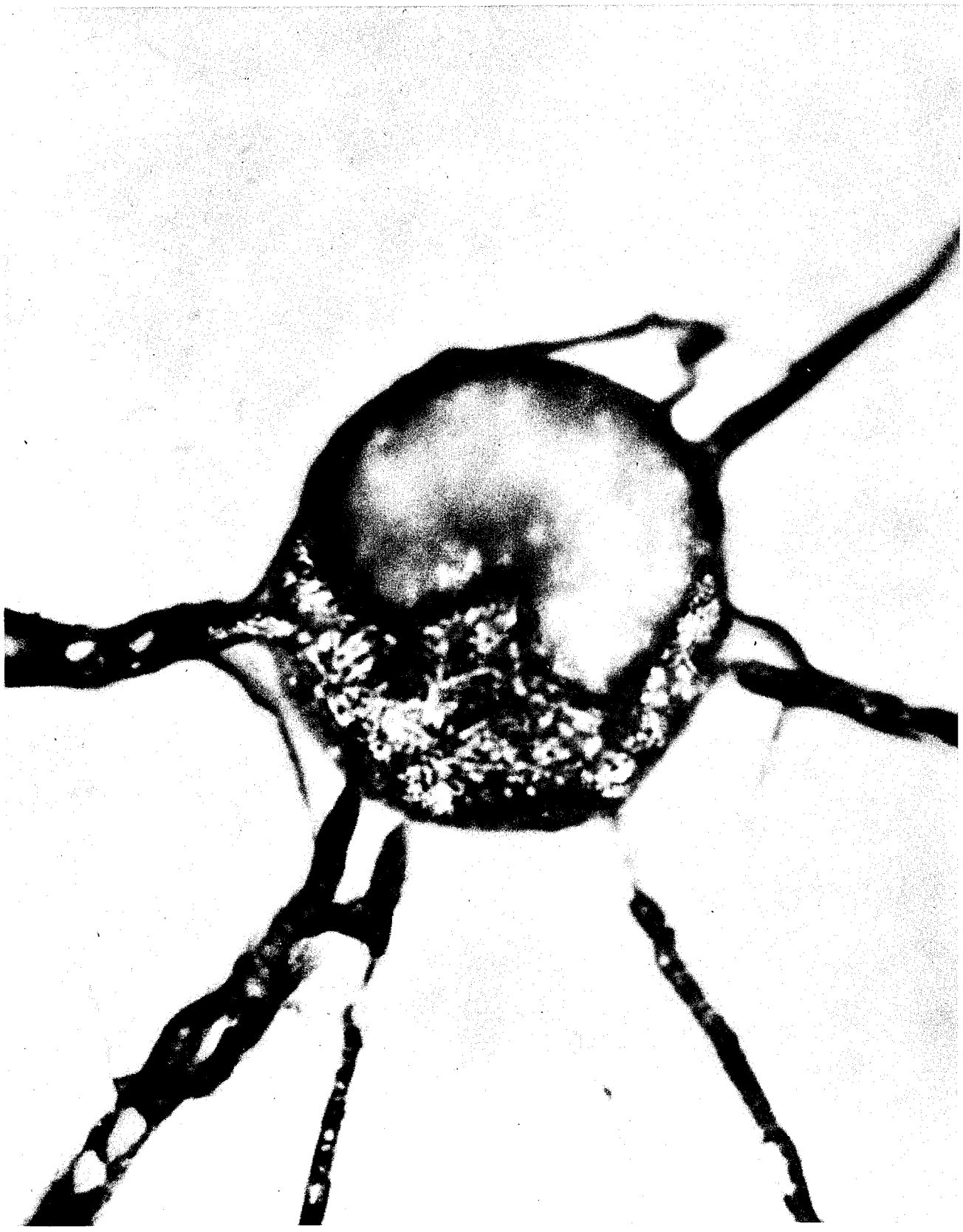

Fig. 25 - (800X) View of electrically damaged boron filament in composite specimen BU #13

Fig. 26 - (800X) View of electrically damaged boron filament in composite specimen BU #13

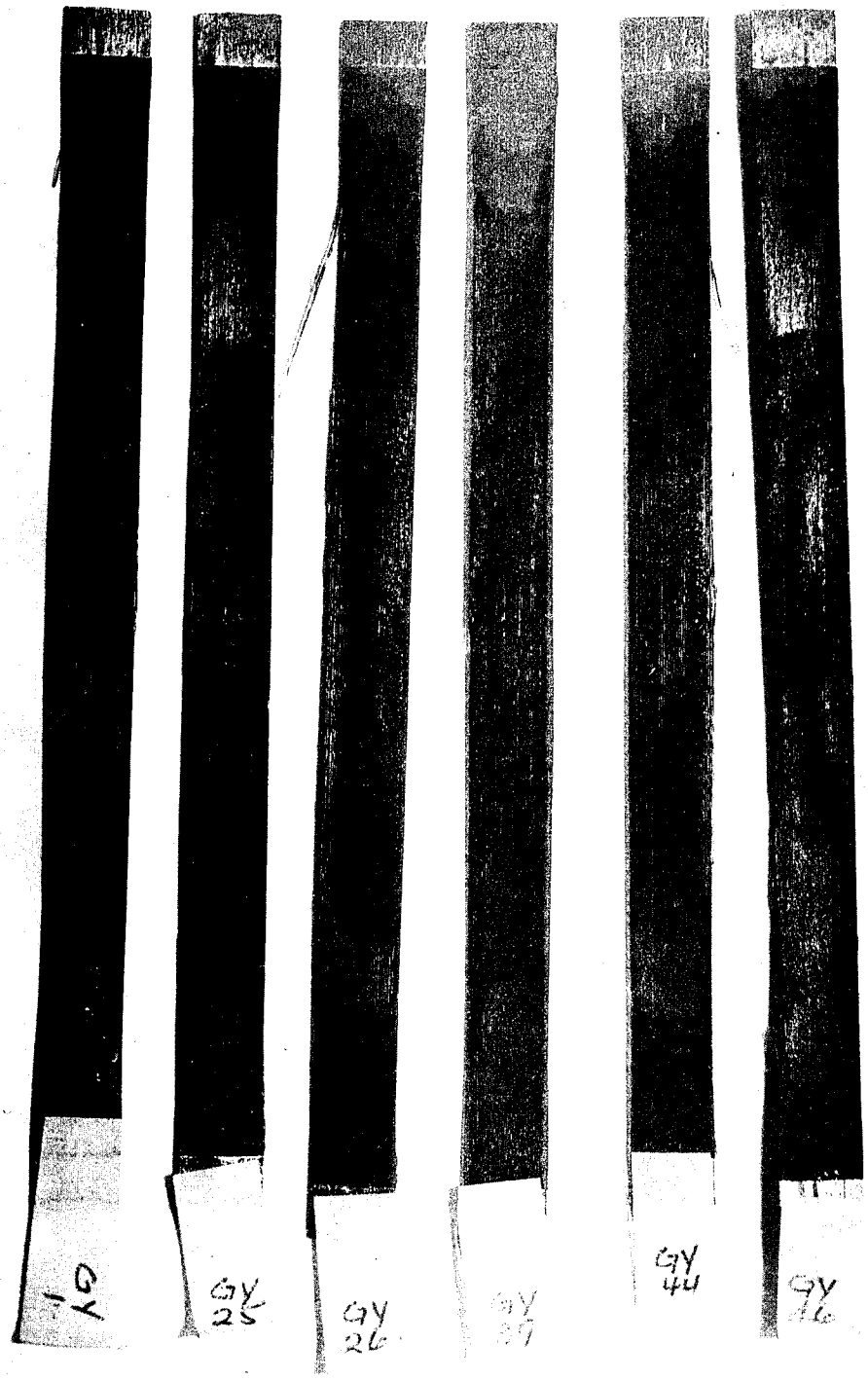

Fig. 27 - HMG-50/epoxy specimens after 20.4 x 10^4 amperes per cm^2 of filament crest current injection--showing charring

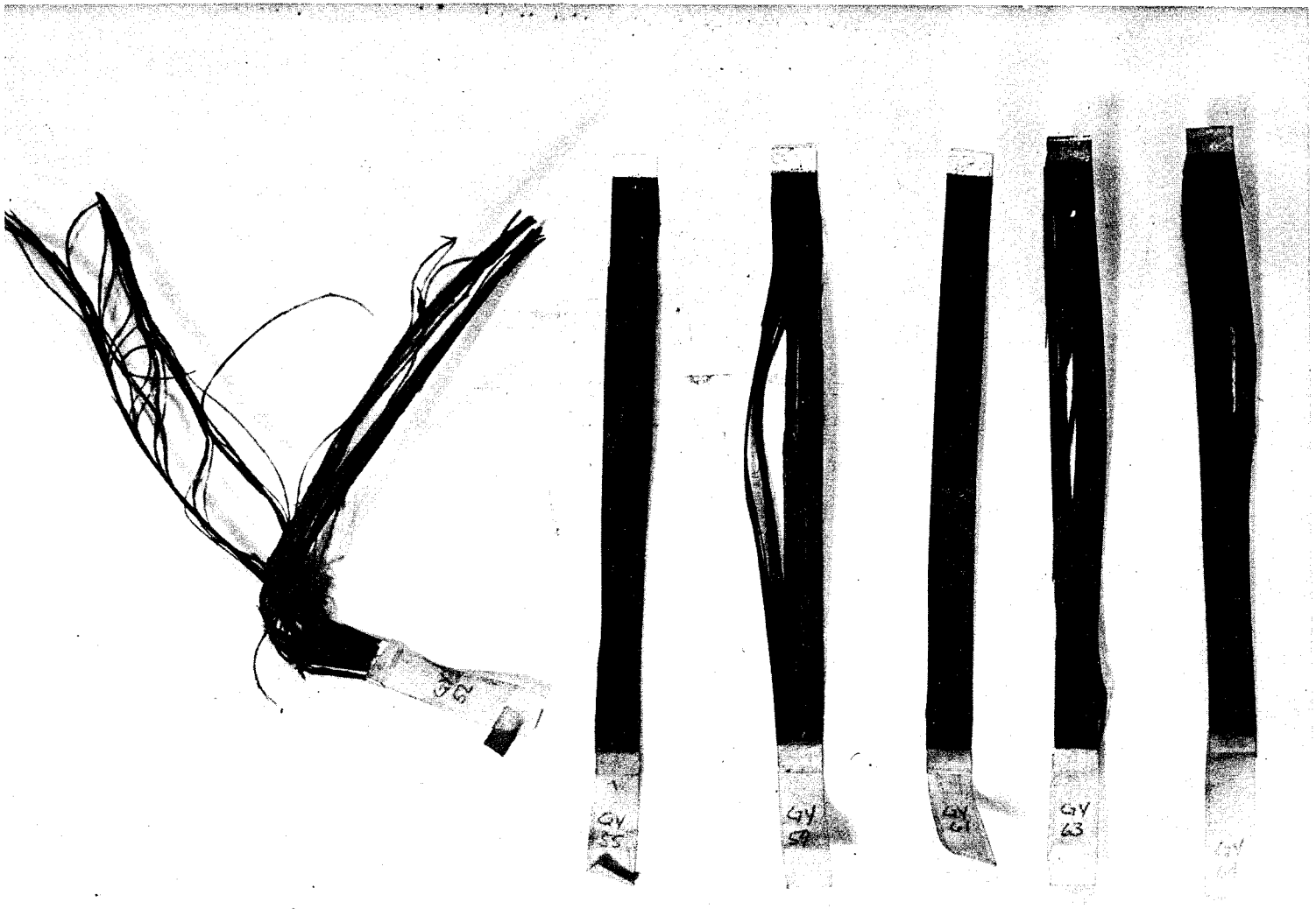

Fig. 28 - HMG-50/epoxy specimens after 24.4 x 10^4 amperes per cm^2 of filament crest current injection--charred and delaminated

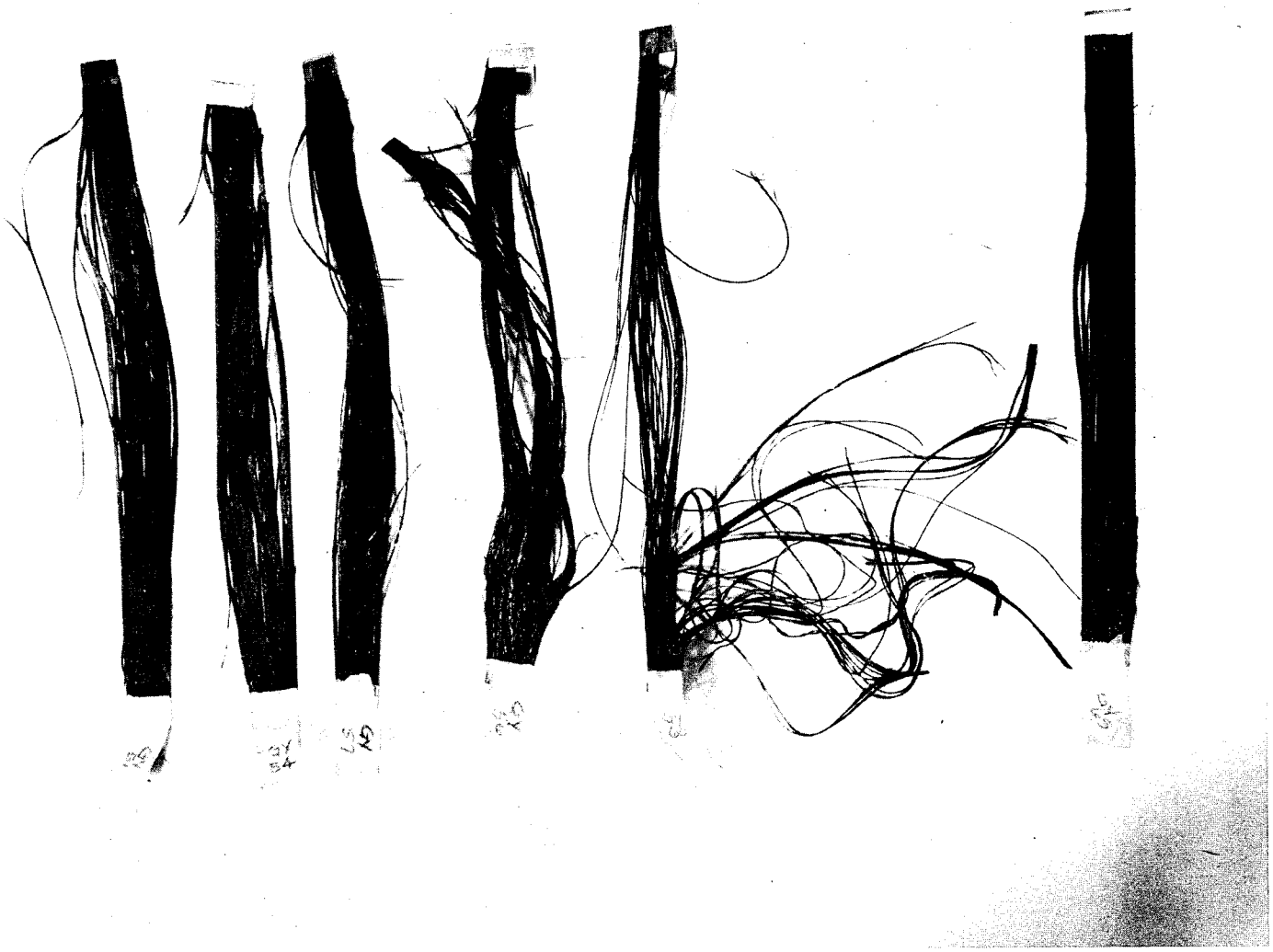

Fig. 29 - HMG-50/epoxy specimens after 55.8 x 10^4 amperes per cm^2 of filament crest current injection--extensively charred and delaminated

Fig. 30 - (100X) HMG-50/epoxy specimen after 13.04×10^4 amperes per cm^2 of filament crest current injection--no damage

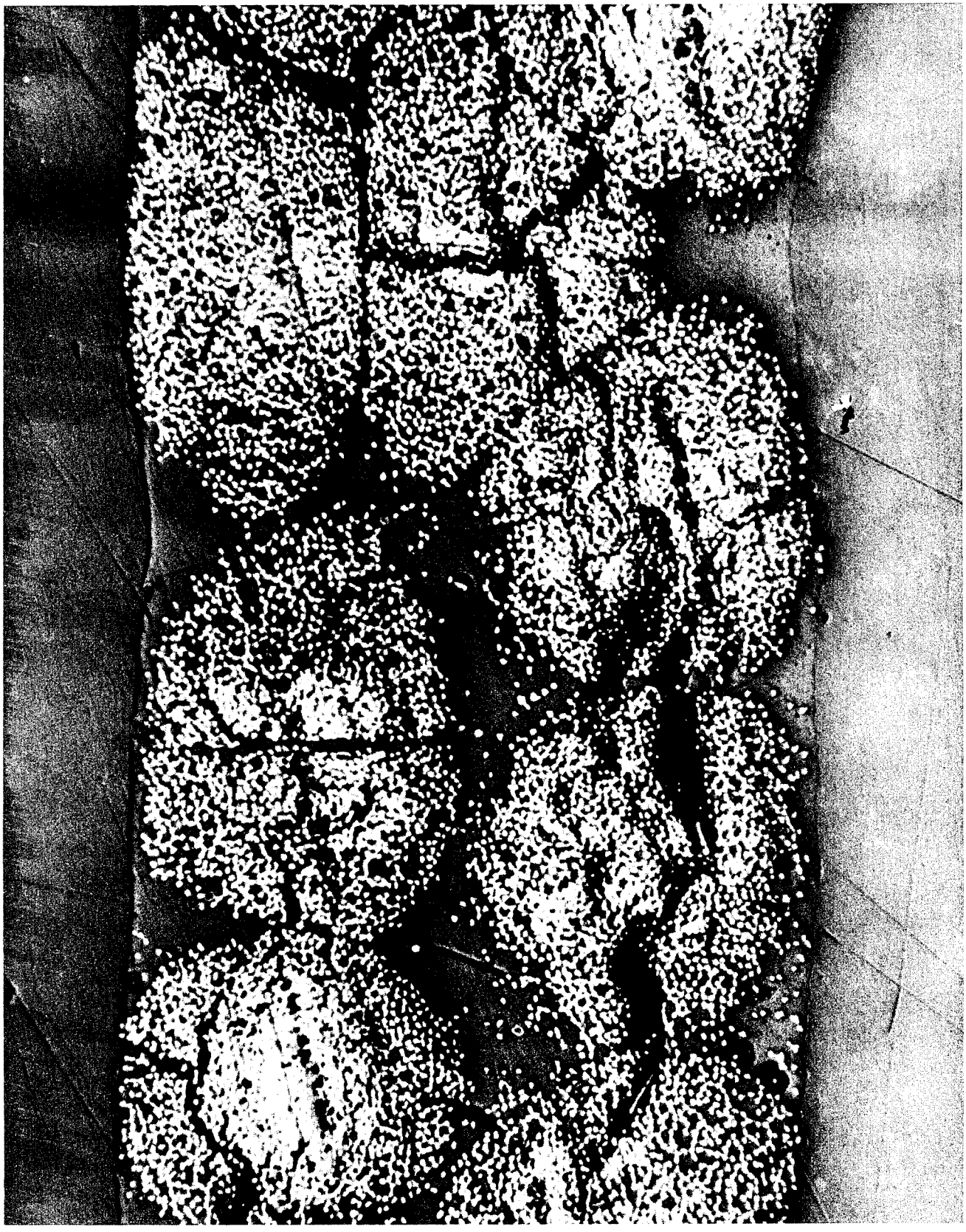

Fig. 31 - (100X) HMG-50/epoxy specimen after 20.4×10^4 amperes per cm^2 of filament crest current injection--burned and delaminated

Fig. 32 - (100X) HMG-50/epoxy specimen after 24.2×10^4 amperes per cm^2 of filament crest current injection--severely burned and delaminated

Fig. 33 - (100X) HMG-50/epoxy specimen after 55.8×10^4 amperes per cm^2 of filament crest current injection--severely burned and delaminated

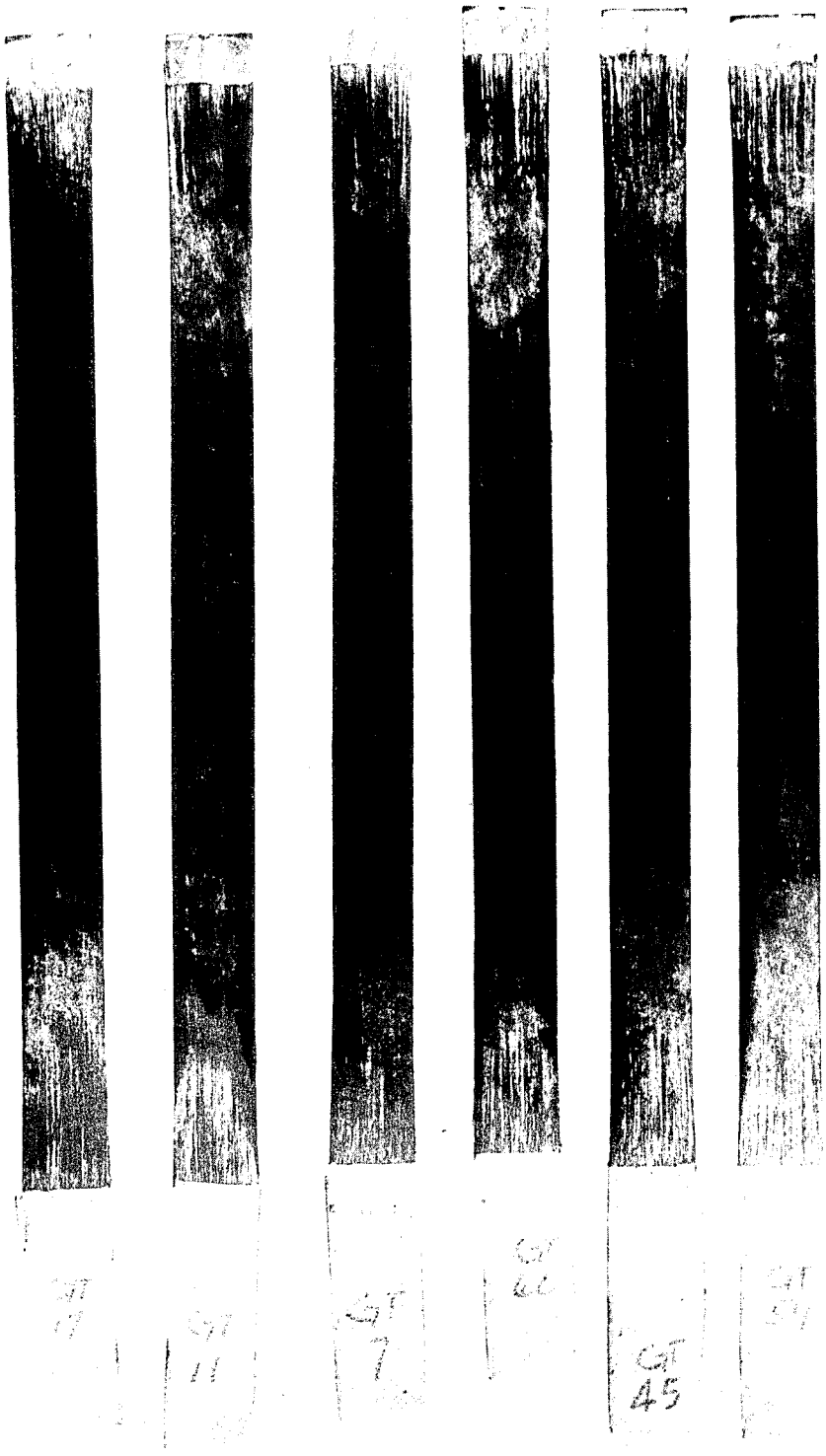

Fig. 34 - HM-S/epoxy specimens after 25 x 10^4 amperes per cm^2 of filament crest current injection--showing charring

Fig. 35 - HM-S/epoxy specimens after 52 x 10^4 amperes per cm^2 of crest current injection--charred and exfoliated

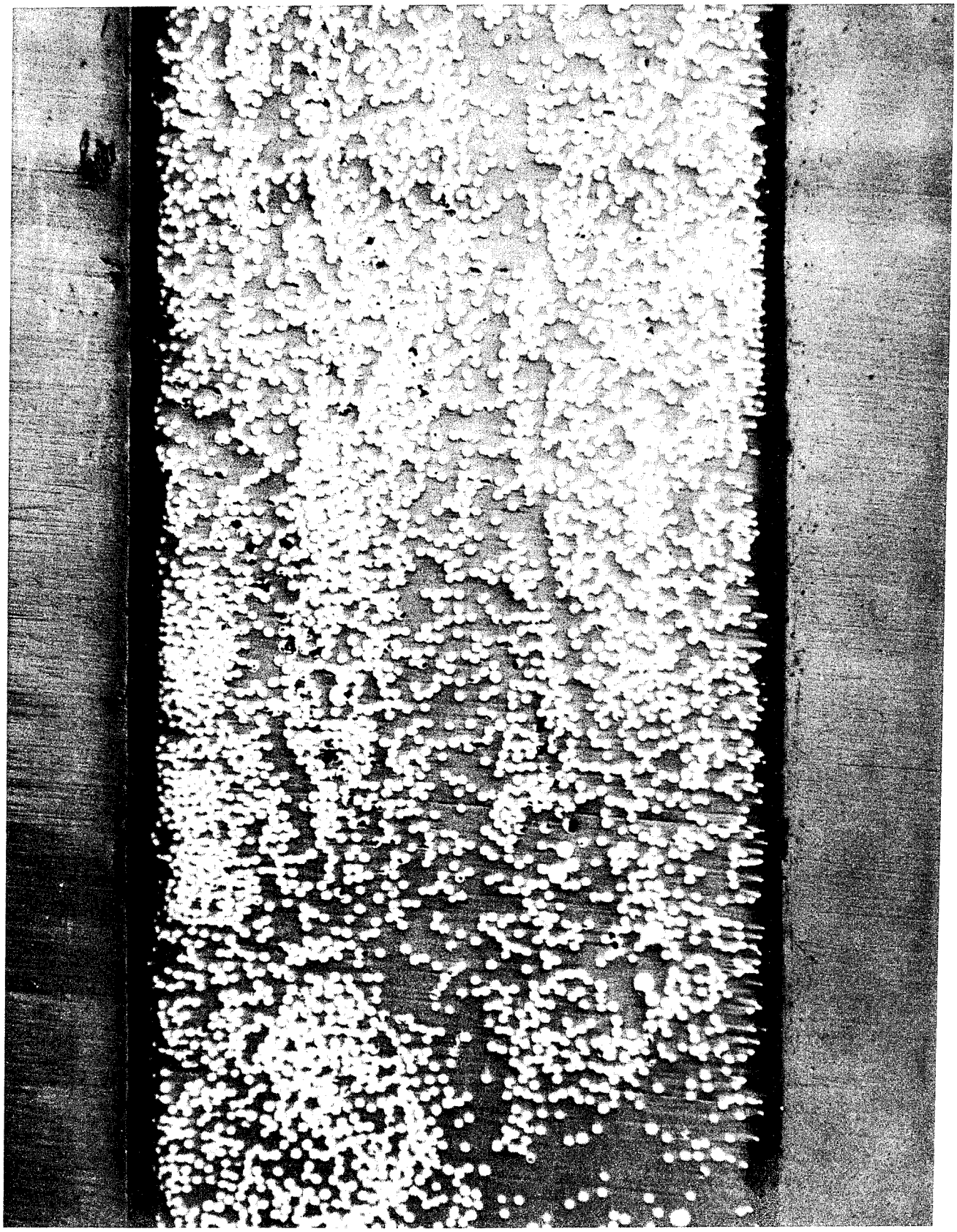

Fig. 36 - (100X) HM-S/epoxy specimen after 21 x 10^4 amperes per cm^2 of filament crest current injection--no damage

Fig. 37 - (100X) HM-S/epoxy specimen after 25 x 10^4 amperes per cm^2 of filament crest current injection--some burning and delamination

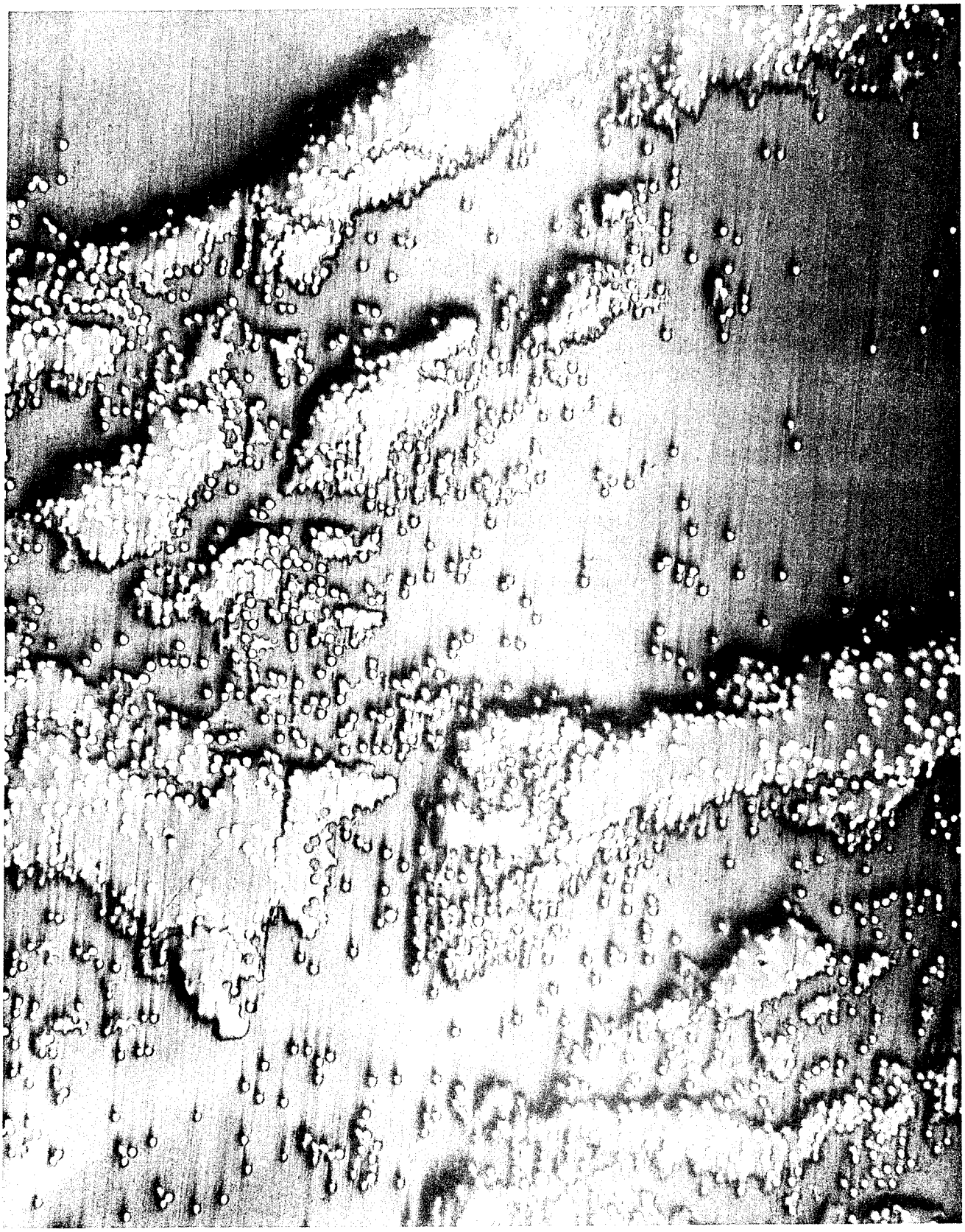

Fig. 38 - (100X) HM-S/epoxy specimen after 52 x 10^4 amperes per cm^2 of filament crest current injection--severely burned and exfoliated

	YARN	TOW
CROSS SECTION	534.2×10^{-6}	5064.5×10^{-6} CM^2
DENSITY	1.68	1.84 GM/CM^3
ℓ	35.6	35.6 CM
RESISTIVITY	1.35×10^{-3}	0.83×10^{-3} OHM-CM
SPECIFIC HEAT	0.3	0.3 CAL/GM/°C

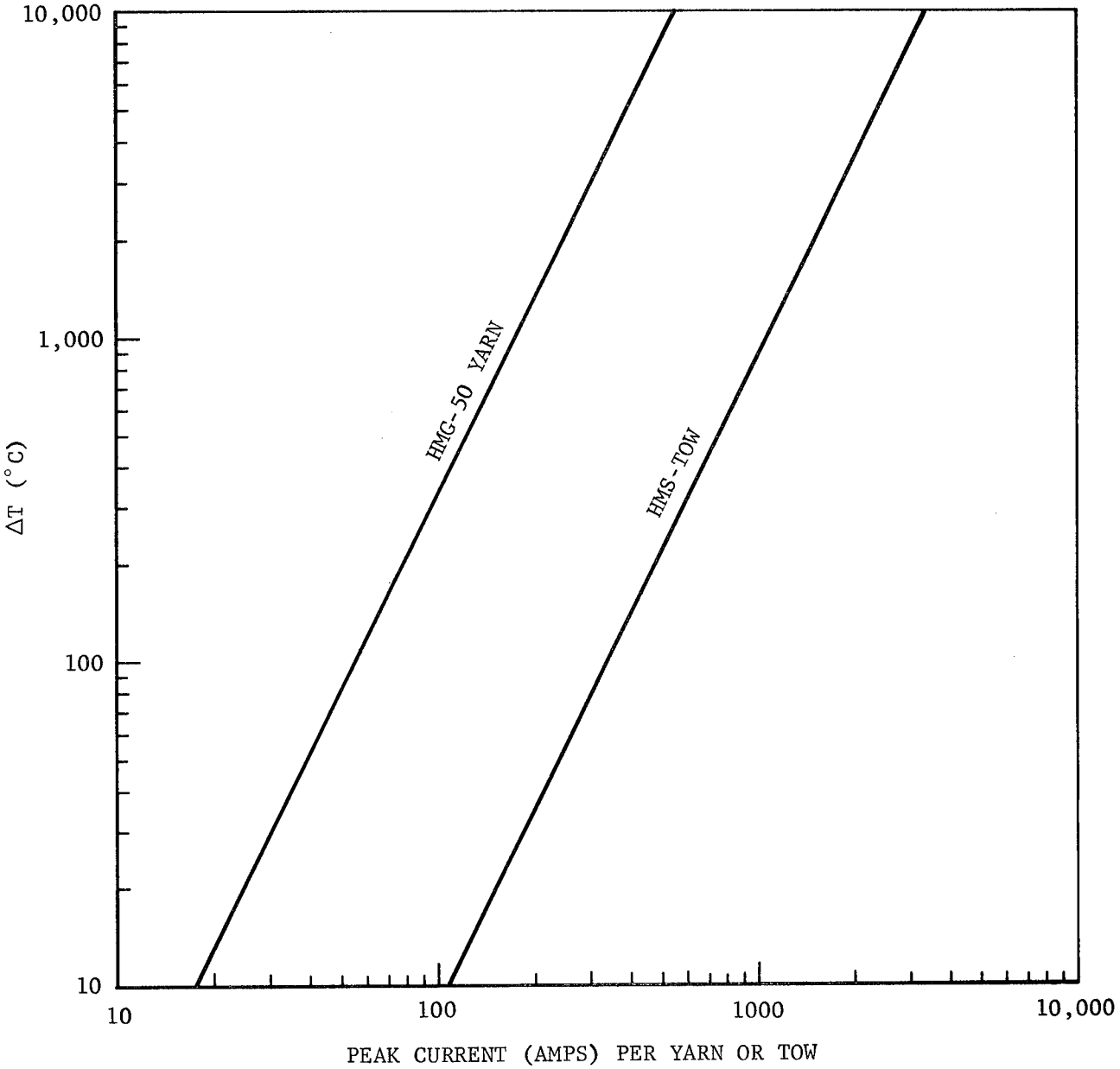

Fig. 39 - Predicted temperature increase in HMG-50 yarn and HMS-tow as a function of peak applied current.

SESSION 3B

GROUND COMPLEXES

Organizer - H. M. Hoffart

General Electric Co

Chairman, H. M. Hoffart

700932

VOLTAGES PRODUCED BY TRANSIENT CURRENTS FLOWING UPON SHIELDS OF CABLES

F. A. FISHER
HIGH VOLTAGE LABORATORY
GENERAL ELECTRIC COMPANY

ABSTRACT

Electromagnetic disturbances to aircraft and to aerospace and industrial ground facilities often produce large circulating currents in the shields of electrical cables. The electromagnetic disturbances may be caused by lightning, switching of high voltage circuits or by other electromagnetic effects. This paper presents experimental data showing how surge voltages are related to the type of construction of the cable, to the material of the cable shield, to magnitude and waveshape of the shield current and the type of termination of the shield. Special attention is given to industrial grade metal conduit since conduit, particularly the rigid steel variety, can have very effective shielding properties.

DURING A LIGHTNING STROKE to an aircraft or to a ground facility, rapidly changing electrical currents are induced on nearby electrical wiring. If the currents flow directly on the active signal or control leads, damage to the electrical circuits is almost certain unless they have been protected with spark gaps or other devices to limit overvoltages to safe levels. However, if the circulating currents are allowed to flow on a shield, the circuits within the shield will tend to be protected against overvoltages. No shield provides perfect protection of course. As in any other shielding problem the effectiveness of a shield over a conductor depends on the material of the shield, its thickness, the way it is manufactured and the way it is used.

Many analyses of the problem of cable shielding have been made. Mostly these analyses have been made in the frequency domain. While in principle the transformation from the frequency domain to the time domain is straightforward, that transformation is generally not made, at least not for the more realistic types of waveforms one encounters in practice.

The purpose of this paper is to present some experimental data showing directly in the time domain how some common types of shielding affect the voltage induced on the signal conductors in a shielded cable.

Two basic types of construction are considered. The first of these is the common flexible conductor shielded with a braided or wrapped shield, usually copper. The second is electrical grade conduit. Conduit can provide very effective shielding, but its shielding properties are not well recognized.

SHIELDING CONFIGURATIONS STUDIED

The basic configuration here considered is that shown in Figure 1a wherein current I is being circulated between two enclosures by a voltage source E. The two enclosures are connected by a shielded cable and there is no other ground connection between the two enclosures. In each enclosure there is an electrical circuit represented by a generalized impedance. These two circuits are connected by a signal circuit within the shielded cable. The total voltage along the signal circuit will divide up in proportion to the impedances Z_1 and Z_2. Two extreme conditions are then seen to be $Z_1 = \infty$ and $Z_1 = 0$, which cases will be referred to in the future as sending end open and sending end shorted. Unless otherwise mentioned, all measurements were made at the receiving end across a load resistance R of either 50 ohms or 75 ohms.

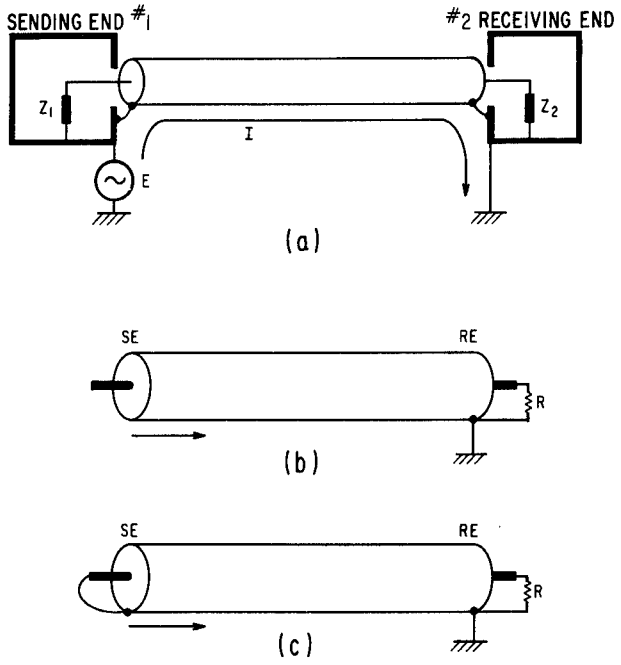

Fig. 1 - Configurations under study

a) Basic configuration
b) Sending end open
c) Sending end shorted

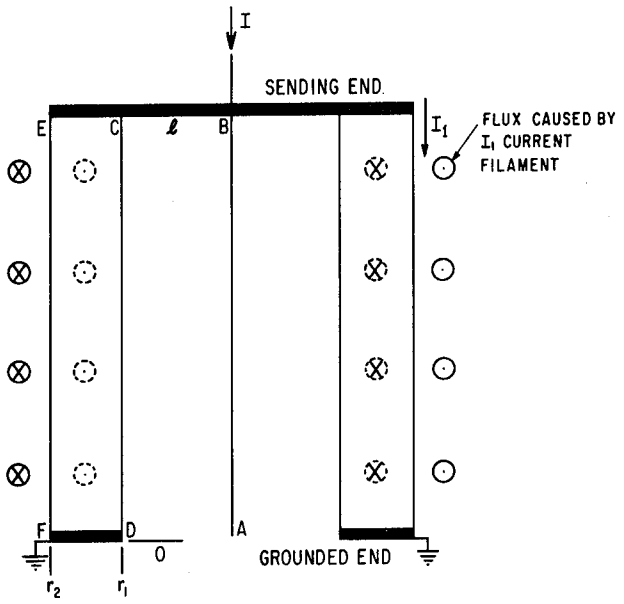

Fig. 2 - Cross section of an idealized conduit and inner conductor

BASIC THEORETICAL CONCEPTS

If a step function of current enters one end of a cylinder conductor whose length is long compared to its diameter, so that end effects can be neglected, the current will initially all be confined to the outer surface. As time goes on the current will diffuse inward and eventually an equilibrium condition will be reached at which time the current density throughout the wall thickness of the cylinder will be uniform.

Likewise the magnetic flux will initially all be external to the cylinder. As the current diffuses through the wall of the cylinder, a magnetic field will also diffuse through the cylinder. When equilibrium conditions have been reached, the magnetic flux density will vary linearly from zero at the inner surface to a maximum at the outer surface.

A conductor running up the center of the tube and connected to the sending end of the cylinder will have a voltage developed between its open end and the ground end of the cylinder. As shown in Figure 2, this voltage may be found by integrating the electric potential along either the path ABCD or ABCEF. If one integrates along the path ABCD, one finds the voltage V_{AD} to be initially zero. This is to be expected since the magnetic fields initially force all the current to flow on the exterior surface of the cylinder. This is the phenomenon of skin effect. The current density at the inner surface is thus initially zero.

As the current diffuses into the cylinder wall, the current density at various times will probably appear about as shown in Figure 3. The current density at the outer surface is initially infinite and confined to an infinitesimally thin shell. For a final condition the current density will be uniform throughout the wall thickness. At any time the area under the current density curve must equal the total input current.

The current density at the inner wall will build up in the manner shown in Figure 4a. Since the current density is assumed uniform over the length of the cylinder (end effects being negligible or ignored), the voltage V_{AD} will be

$$V_{AD} = \int_0^{\ell} J_{r_1} \rho \, d\ell = J_{r_1} \rho \ell \qquad (1)$$

The voltage waveshape will be the same as the waveshape of the build-up of current density at the inner surface.

For a final value

$$J_{r_1} = J_f = I/A \qquad (2)$$

where
I = total current
A = cross-sectional area of the cylinder
also:

$$\rho = \frac{RxA}{\ell} \text{ ohms-meter} \qquad (3)$$

where
R = total resistance of cylinder
ℓ = length of cylinder

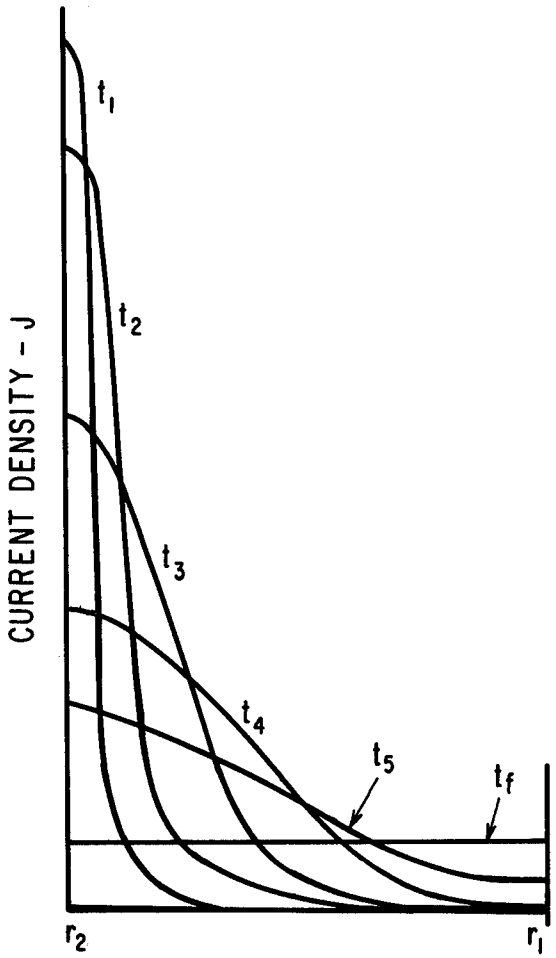

Fig. 3 - Probable current density in cylinder wall at various times

The final value of V_{AD} then becomes

$$V_{AD} = J_f \rho \ell = \frac{I}{A} \cdot \frac{RxA}{\ell} \cdot \ell = IR \qquad (4)$$

which is intuitively the obvious answer.

If one evaluates V_{AD} by following the path ABCEF, the voltage induced by the flux build-up in the cylinder wall must be included. When integrating around path ABCD, there is no inductive term since there is no flux inside the inner wall. V_{ABCEF} is thus

$$V_{AF} = J_{r_2} \rho \ell - \frac{d\phi}{dt} \qquad (5)$$

The flux within the loop ABCEF will have the time history shown in Figure 4b and will reach a final limiting value. The time derivative of the flux will start at infinity and decay to zero. The term $J_{r_2} \rho \ell$ will start at infinity (since J_{r_2} is initially infinite) and decay as the time history shown in Figure 4c to the limiting value

$$J = I/A \qquad (6)$$

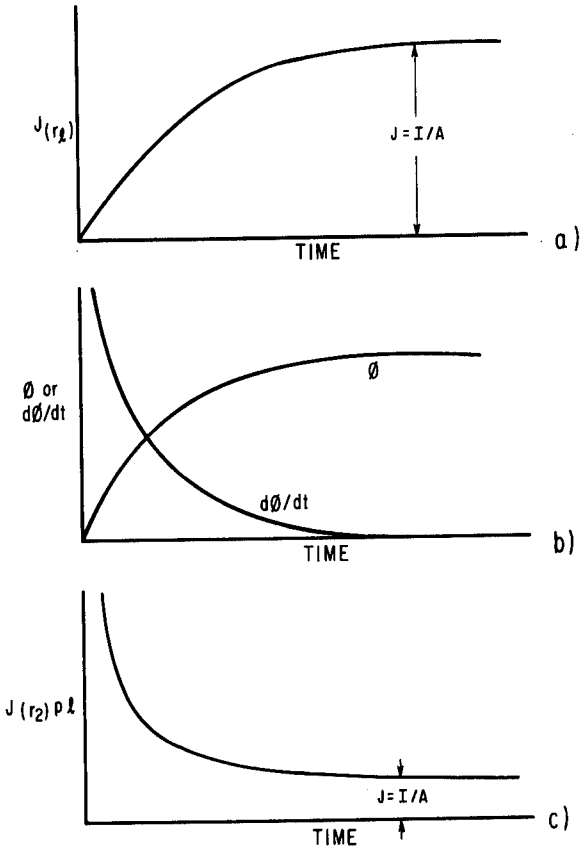

Fig. 4 - Current and flux vs. time

a) Current density at inner wall
b) Flux within the cylinder
c) Current at outer wall

The net voltage is thus initially infinity minus infinity which for this case turns out to be zero. The difference of the $J_{(r_2)} \rho \ell$ and $d\phi/dt$ terms will have the same waveform with respect to time as that of $J_{(r_1)}$ of Figure 4a.

The analytical expressions for this waveform have not yet been evaluated, but certain comments can be made. The waveform of the voltage V_{AD} in response to a step current excitation will be similar to an RC exponential charging curve, or more nearly, to a complementary error function (erfc) waveform.

The standard response time of the build-up of voltage in a solid coaxial shunt as given by Witt(1)* will be approximately

$$T_m \approx \mu o \, \delta^2 / 6\rho \qquad (7)$$

where

δ = wall thickness in meters
ρ = resistivity in ohms-meter
μo = permeability of free space

*Numbers in parentheses designate References at end of paper.

Response time, frequency response and rise time can be related as follows:

$$2\pi f_b T_m = 1 \quad (8)$$

$$f_b T_r = 0.35 \quad (9)$$

f_b = 3dB bandwidth

T_r = 10% - 90% rise time

accordingly the build-up of voltage on a shunt in response to a step function of current would have a rise time

$$T_r = 0.366 \frac{\mu_o \delta^2}{6\rho} \quad (10)$$

The rise time thus varies with the square of the wall thickness of the cylinder, inversely with the resistivity of the material and linearly with the permeability. Witt's derivation was for a nonmagnetic cylinder and thus if the cylinder was of a magnetic material, the equation would be

$$T_r = 0.366 \mu_r \mu_o \delta^2/6\rho \quad (11)$$

where μ_r = relative permeability

(A dimensionless number)

If the center conductor is not connected to the end of the conduit at B but is left open, the voltage appearing around the path will remain the same. This voltage will divide among the two gaps in a direct proportion to the impedance of the two gaps. If in Figure 5 both Z_1 and Z_2 were infinity, the conductor would eventually float half way between V = 0 and V = IR_{DC}. For transient currents it would float at the average voltage along the inner wall of the cylinder or at half the voltage it did when the conductor was connected to the conduit.

If the conductor is grounded at Z_2 (Z_2 = 0) and open at Z_1 (Z_1 = ∞), the same voltage will appear at V_1 as was originally found to appear at V_2.

If Z_1 is open and Z_2 is a resistor, the voltage across Z_2 will be the same as if the high pass filter CZ_2 were excited by the average voltage drop along the inner surface of the cylinder. This average voltage drop is ½ the voltage that would be measured open circuit at V_2 if Z_1 were zero.

LIMITATIONS OF THEORY

All of the above assumes the magnetic fields inside the inner wall of the cylinder to be zero. This can only occur when:

1. The cylinder is round, straight, and long enough so that end effects can be ignored.
2. There are no current carrying members inside the cylinder.
3. There are no joints or holes through which magnetic flux can leak inside.

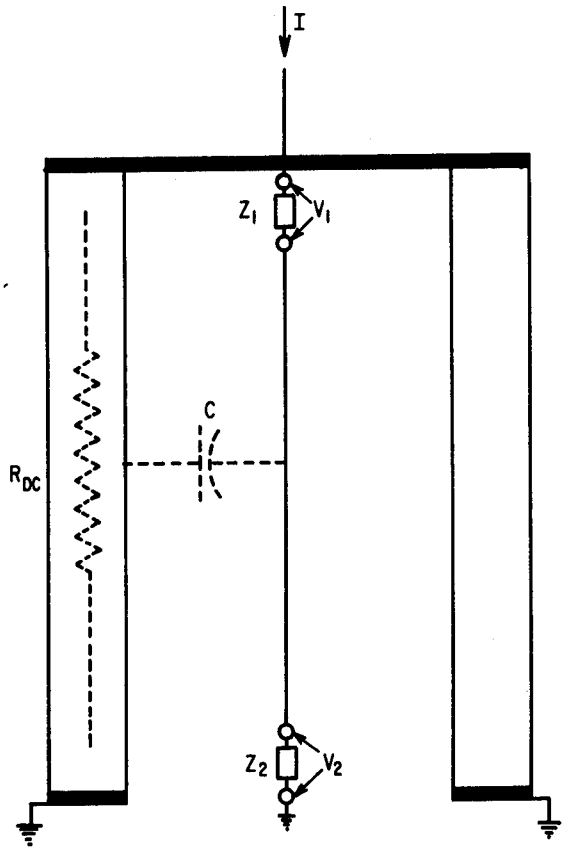

Fig. 5 - Circuit for capacitor voltage on conductors

Corners, ends and wiring fixtures obviously do not fall into this category. In theory, bends should be made as smoothly and with as long a radius as possible.

Likely enough all conduit runs in which current flow might be a problem will be long enough so that end effects can be ignored.

Current flow in conductors inside the conduit can probably be ignored since any practical value of terminal impedance on those conductors would be high enough so that the current flowing in those conductors will be negligible compared to that flowing in the conduit. Only current injected onto the conductors from some source other than the IR (or IZ) drop along the conduit will be important, and that is another problem entirely.

Flux leakage through poorly made joints or through poorly fitting covers is likely to override all bend, end or conduit shape effects. With careful workmanship the induced voltages due to such flux leaks should not exceed the IR_{DC} drop along the circuit.

ELECTRICAL CONDUIT

QUASI-STEP FUNCTION RESPONSE - Some of these

effects are illustrated in Figure 6. Current was suddenly injected into four lengths of 2" rigid steel conduit. Inductance of the circuit controlled the initial rate of build-up of current, and battery resistance controlled the final current. The voltage along the inner surface of the conduit was measured by a conductor tied to the sending end of the conduit. Note that the conductor to ground voltage initially has the same waveform as the applied current, but then slowly rises to a higher voltage and does not reach its final value for nearly 20 milliseconds. The conduit thus acts much like a low-pass filter. The high frequency components of voltage that cause the current to flow on the conduit do not couple through the wall of the conduit onto the inner surface.

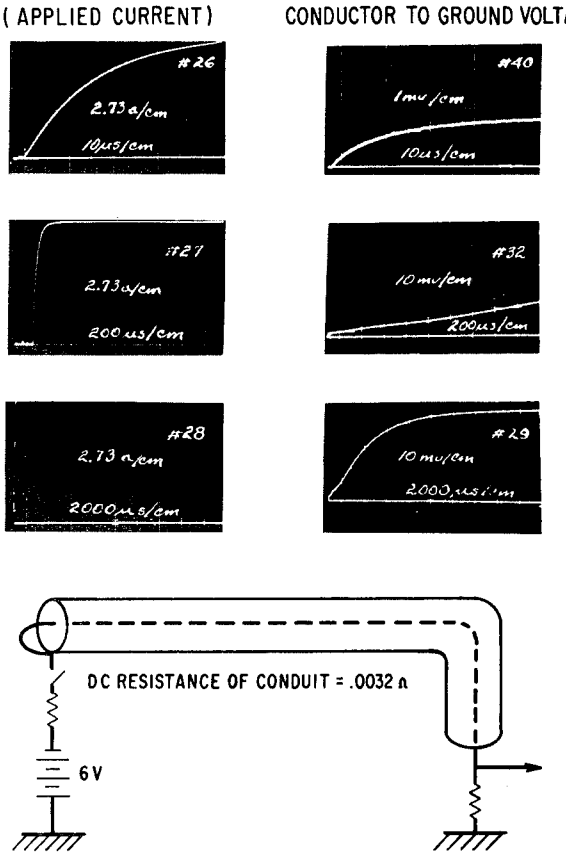

Fig. 6 - DC current injection

If the current through the conduit were of short duration, the current density on the inner surface would never reach its final value and the resulting voltage on the internal conductor would be less. If the conduit current were a square pulse lasting only 1 millisecond, the voltage developed on the inner conductor would be only about 8 millivolts.

HIGH CURRENT RESPONSE - The shielding effectiveness of conduit was also investigated when the driving current was a relatively short current pulse of high amplitude. The basis test configuration is shown on Figure 7. Current was injected into lengths of conduit from a 1000kV Marx circuit impulse generator. The generator circuit constants were adjusted to produce an aperiodic current pulse rising to a peak of 1755 amperes in 0.9 microseconds and decaying to half value in 35 microseconds. This current waveshape is typical of those caused by lightning and other high energy transient sources. It is, however, much shorter than the time required for current on the inner surface of the conduit to build-up to its final value. The current wave was long enough that traveling wave effects on the outer surface of the conduit could be neglected. The current was uniform along the length of the conduit.

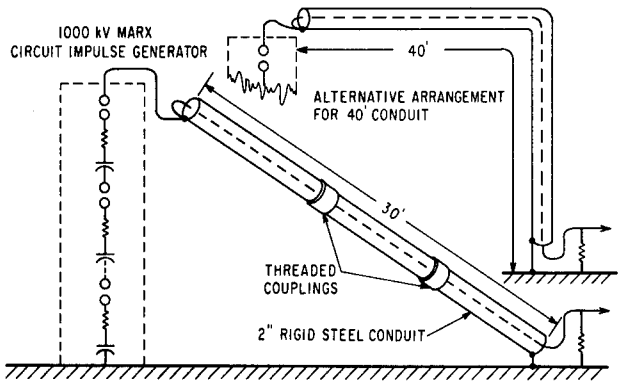

Fig. 7 - Configuration for high current tests on conduit

The current wave is shown on several time scales on Figure 8. This figure also shows the voltage induced on a condutor inside a 40 ft. length of 2" rigid steel conduit. The voltage has three distinct phases. In the first phase the voltage crests at 480mv at about the same time as the current wave and then decays. This voltage is caused by electromagnetic flux leakage at the couplings. Conduit sections were fastened together with threaded connectors. Threaded condulet fittings with removable covers were used at the ends and at the center right angle bend in the conduit. The voltage has a second peak of 40mv at 300 microseconds, this being due to current diffusing through the condulets. The third and final peak of 35 mv is reached at 3000 microseconds, at a time when the driving current has long since decayed to zero. The behavior of the third (and second) peak is similar to the output of a low-pass filter when excited by an input pulse much shorter in duration than the dominant time constant of the filter.

This behavior of the conduits, an output voltage cresting at a short time followed by a second peak at a later time, is typical of the behavior of all the conduits studied. In general it is typical also of the response of flexible shielded cables, a point that will be discussed

in a later section of this paper. The first peak can be described as an induction term as is electromagnetic flux leakage. This term will be proportional to the rate of change of current on the shield. The second term can be described as a diffusion term and is due to the current diffusing through the shield material. It would be proportional to the amplitude of the shield current and perhaps to the duration of the shield current. In most cases of practical concern the induction term will be the larger of the two.

The induction term can be minimized using tightly fitted joints and by avoiding sharp bends in the conduit. At bends the shield current is not uniformly distributed over the surface and the assumption that flux linkages in the interior cancel due to cylindrical symmetry does not hold. Figure 9 illustrates the point. Bends clearly increase the amplitude of the inductive term without affecting the diffusion term.

COMPARISON OF DIFFERENT TYPES OF CONDUIT - This paper can summarize only a few points about the entire series of tests made.

1. Steel conduit has higher shielding effectiveness than aluminum or copper tubing of equal thickness. The higher DC resistance of steel conduit is offset by the longer diffusion times that the permeability of steel provides.

2. Thicker conduit has better shielding properties than thin conduit, hence rigid conduit provides better shielding than does thin-wall or EMT conduit.

3. Tight joints are essential to high shielding effectiveness. Threaded fittings are superior to compression fittings. For critical shielding applications welded joints may be appropriate.

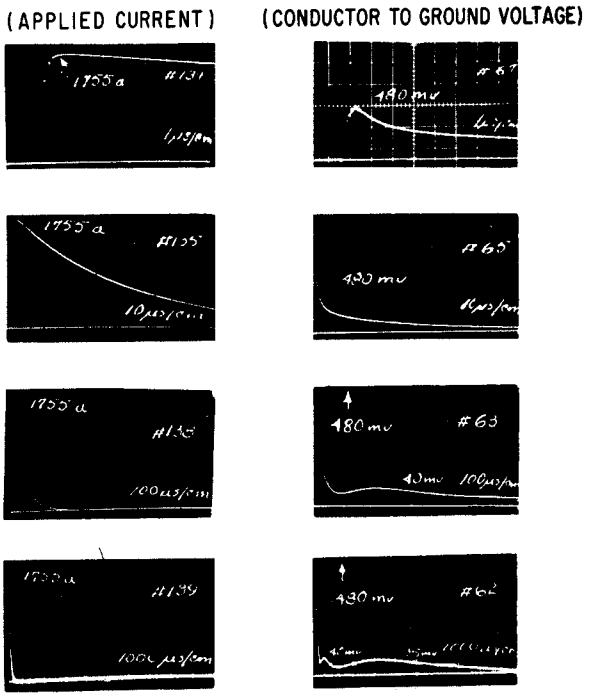

Fig. 8 - Comparison of applied current and conductor voltage to ground

0.9 x 35 μsec applied pulse current (Four lengths 2" conduit with condulet LB's at middle and ends - conductor tied to conduit at line end)

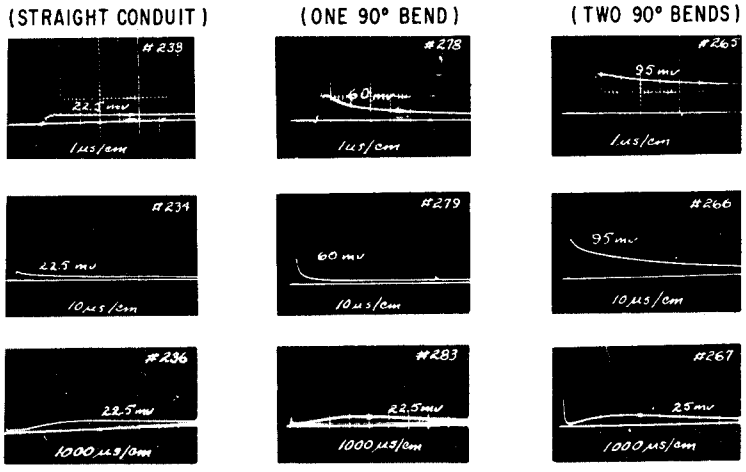

Fig. 9 - Comparison of number of conduit bends upon conductor to ground voltages

0.9 x 35 μsec wave - 1755 amps (Three lengths of 2" conduit-condutor tied to conduit at line end) DC resistance of conduit .0022 ohms

TESTS ON FLEXIBLE CABLES

The shielding effectiveness of several types of flexible cables was also investigated by current injection techniques. The cables were chosen for test on the basis of their wide usage and to illustrate the effects of different types of shield construction. They were not chosen as illustrative of cables having high shielding effectiveness. The cable types are illustrated on Figure 10 with additional information given in Table I.

Current was injected into the cables essentially as shown on Figure 7. The pulse generator used operated at low voltage (<30kV). Both the generator and the current return path were configured to obtain very fast current front times. Two current waveshapes were used during the tests. One rose to 50 amperes in less than 10 nanoseconds and decayed to half value in about 200 nanoseconds. The second rose to 50 amperes in about 200 nanoseconds (in a stepwise manner) and decayed to half value in about 20 microseconds. The current waveshapes are shown on Figure 11.

Typical results are shown on Figure 12. The inductive component of voltage predominates here. Why the voltage on cable #5 initially goes negative is still a mystery, since the injected current was positive. This pattern was typical for all cables having only a single braided shield.

Shielding effectiveness is in broad terms proportional to the thickness of the shield material and to the degree of coverage. These same properties also affect the DC resistance of the shield. The output voltage of the various cables is shown plotted against shield resistance

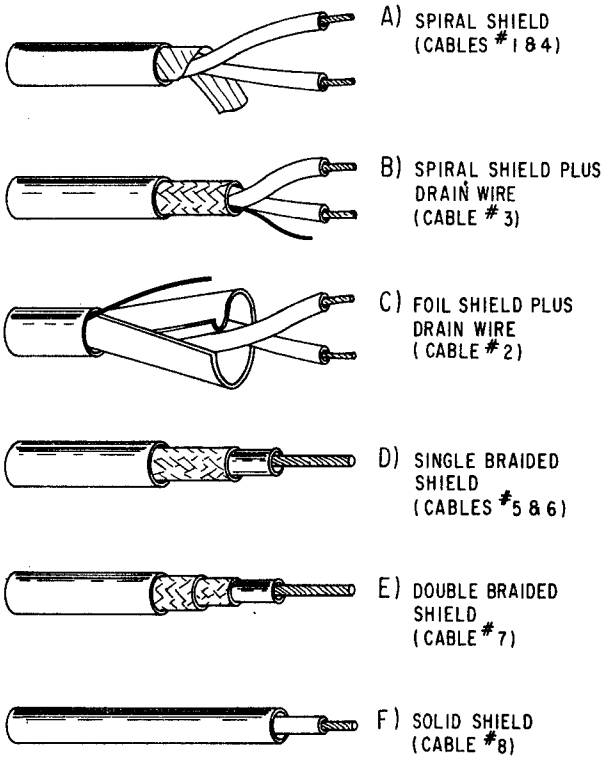

Fig. 10 - Construction of cables tested

TABLE 1 - Cable Parameters

Cable	Cable Type	Manufacturer & Number	Signal Conductors	Shield Construction
1	A	Belden 8737	2-#22 Stranded	Tinned copper - 89.3% coverage
2	C	Belden 8761	2-#22 Stranded	Aluminum backed Mylar with #22AWG drain wire - 100% coverage
3	B	Belden 8437	2-#22 Solid	Tinned copper brass with solid copper drain wire - 88% coverage
4	A	Belden 8790	2-#18 Stranded	Tinned copper - 76.5% coverage
5	D	Belden 8259 (RG58 A/V)	1-#20 Stranded	Single layer braid
6	D	Belden 8214 (RG 8/V Type, foam core)	1-#11 Stranded	Single layer braid
7	E	General Radio 874-A2(50Ω)	1-#14 Stranded	Two concentric tinned copper braids
8	F	-	(1) #20 Stranded	Solid copper tubing - ¼" trade size

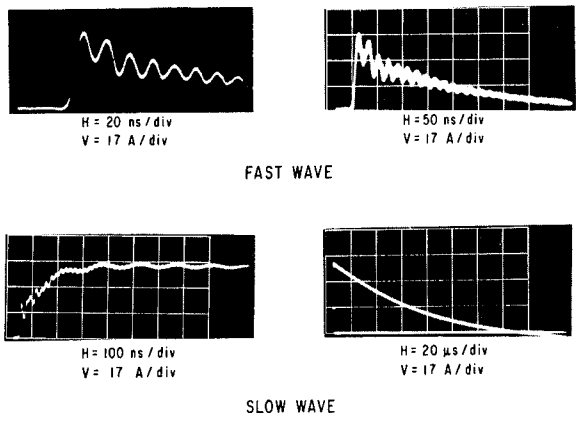

Fig. 11 - Current waveforms used for tests on flexible cables

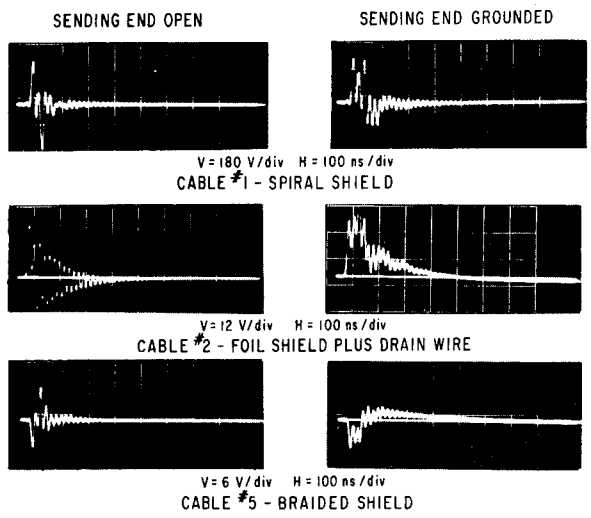

Fig. 12 - Typical results with fast current wave

on Figure 13. For all except cable #7 the voltage per ampere of sheath current is higher than the DC resistance, indicating that the inductive term predominates.

Typical results with the slow current wave are shown on Figure 14. Only the results with the sending end shorted are shown. Here both the induction term and the diffusion term of the cable voltage can be seen, though generally the inductive term is the larger. When studying the conduit, the diffusion term did not reach its crest until long after the current had passed. On the flexible cables, however, the shield is thin, non-magnetic, and not solid, hence the sheath current diffuses through the sheath and reaches its final value very quickly. As a result the diffusion term is essentially the same as the voltage drop across the DC resistance of the cable sheath. This is shown more clearly on

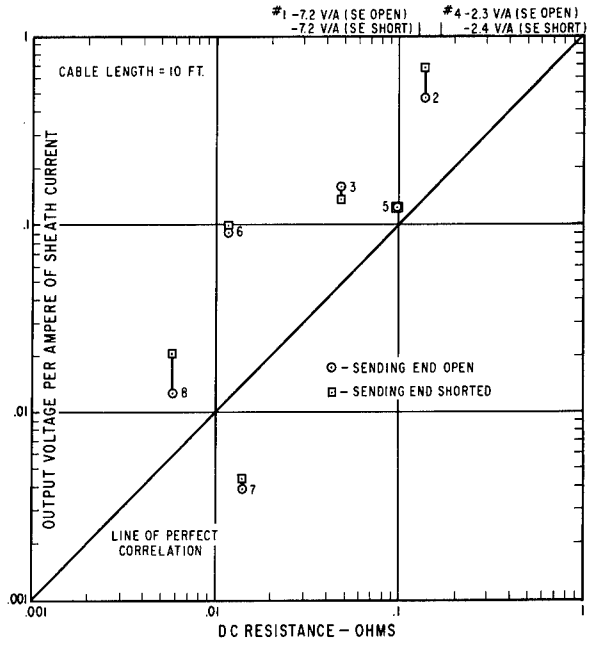

Fig. 13 - Cable output voltage vs. cable resistance

Fast wave

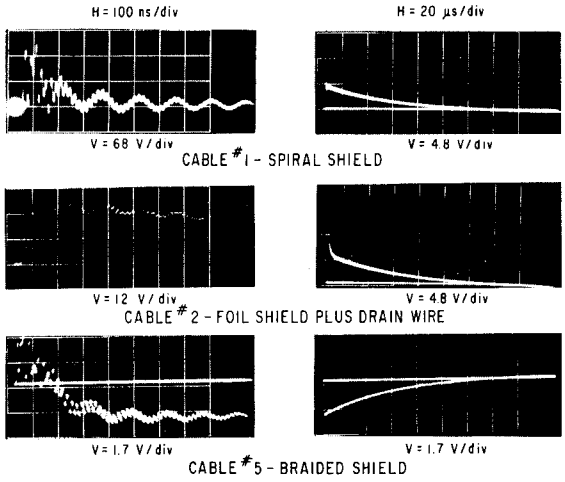

Fig. 14 - Typical results with slow current wave

Sending end shorted

Figure 15 in which the portion of cable voltage due to diffusion is shown plotted against sheath resistance. Only in the case of Cable 5 is the diffusion voltage significantly different from the DC resistance.

Figure 16 shows the total voltage, induction plus diffusion, plotted against cable resistance.

Of the cables tested, Cable #7 had by far the best shielding effectiveness. This was due to the use of two overlapping braided sheaths.

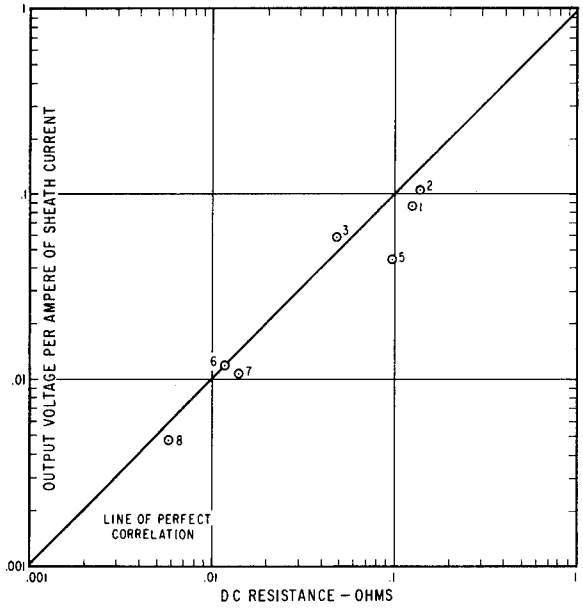

Fig. 15 - Cable output voltage vs. cable resistance

Slow wave - diffusion phase

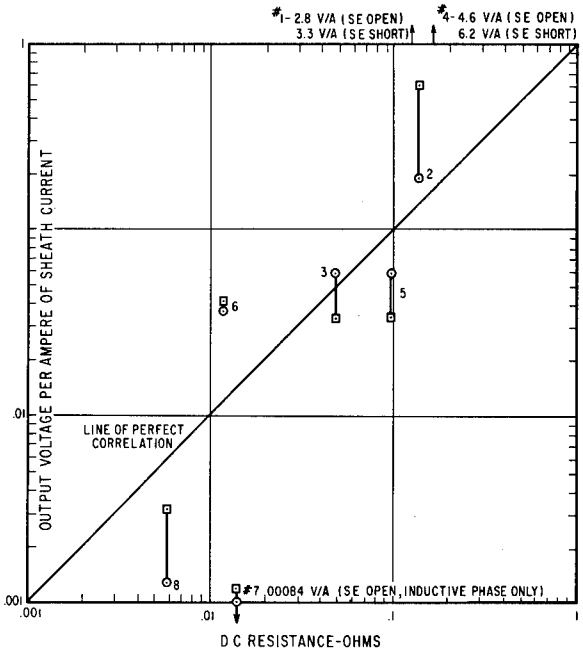

Fig. 16 - Cable output voltage vs. cable resistance

Slow wave

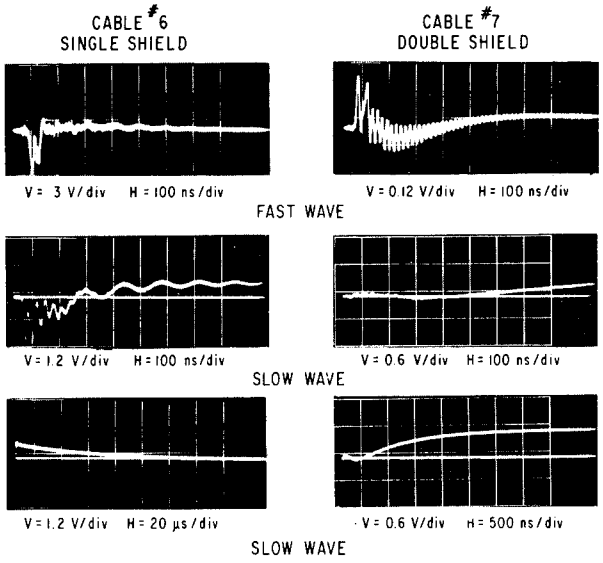

Fig. 17 - A comparison of a single shield and two overlapping shields

Sending end grounded

This sheath was able, on the slow wave at least, to reduce the inductive term of the cable voltage to less than the diffusion term. This was also the only cable that demonstrated a long time for the diffusion term to reach its final value.

Both Cables 6 and 7 are 50 ohm coaxial cables and differ primarily in the construction of the sheath; Cable #6 having only a single braided sheath. The performance of these two cables is shown in Figure 17.

SUMMARY

Current flowing on the shield of a cable produces voltage on the signal conductors. The magnitude of this voltage has been shown to depend on the characteristics of the shield. In general the voltage induced on the signal conductors consists of an inductive term and a diffusion term. The inductive term depends on the amount of magnetic flux that penetrates the shield, this in turn depending on the type of shield construction and the degree to which the shield covers the signal conductors. The inductive term depends to a first approximation, on the time rate of change of shield current.

The diffusion term is proportional to the resistance of the shield. Skin effect is shown to control the rate at which the shield current diffuses through the shield, and thus the time at which the diffusion term reaches its maximum value. In some of the cases shown the diffusion term does not reach its final value until long after the shield current has decayed to zero.

Industrial grade steel conduit has been shown to have excellent shielding properties; these properties in large measure are due to the influence that the steel's permeability has on the rate at which current diffuses into the wall of the conduit. If conduit joints and bends are treated with care, pulse currents of thousands of amperes flowing on the conduit will induce only a few tens of millivolts on conductors within the conduit.

The shielding effectiveness of flexible cables can be related to the DC resistance of the cable shield since most of the properties of shields that contribute to high shielding effectiveness also contribute to low shield resistance. Of the cables tested, the one showing the best shielding effectiveness used two concentric braided shields, the outer shield directly in contact with the inner shield.

REFERENCES

1. Witt, Hans, "Response of Low Resistance Shunts For Impulse Currents." El teknik, 1960, pp. 45-47.

700933

PROTECTION OF GROUND SPACE FACILITIES FROM THE EFFECTS OF LIGHTNING

F. A. FISHER AND T. J. BLALOCK
HIGH VOLTAGE LABORATORY
GENERAL ELECTRIC COMPANY

ABSTRACT

Aerospace and ground facilities are often both extensive in area and located in regions of high lightning activity. While the hazards of fire, explosion, and electrocution caused by direct lightning strokes are generally well recognized, the indirect effects of lightning on electrical and electronic systems are less well recognized. Electronic systems can often be damaged even by lightning strokes that do not hit the buildings or electrical wiring directly. The lightning hazards to electronic systems are often compounded by shielding and grounding practices used for control of lower frequency electromagnetic interference. These shielding and grounding practices are sometimes diametrically opposite to those that should be employed for control of lightning effects. This paper first describes the conflicts, real and apparent, between the grounding and shielding requirements for control of lightning and EMI. It discusses some ways to resolve these conflicts and draws upon a case history to illustrate the points raised.

THE PRINCIPLES OF LIGHTNING PROTECTION of structures have not changed appreciably from those laid down by Benjamin Franklin; intercept the lightning stroke before it can cause physical damage to the structure, carry the stroke currents to ground along a controlled, low-resistance metallic path and allow the energy of the stroke to be dissipated in the resistance of the adjacent ground. In aerospace facilities we have a problem Franklin did not face: protection of large amounts of sensitive electronic equipment. Direct lightning strokes to unprotected structures can certainly cause spectacular damage but in aerospace facilities the indirect electrical effects of lightning are often the most troublesome and expensive problem. Lightning strokes, often even remote ones, can cause such extensive electrical damage that a ground facility may be out of service for long periods of time. Protection of structures against the direct effects of lightning is fairly straightforward; protection against the indirect effects is more complicated.

PROTECTION AGAINST THE DIRECT EFFECTS OF LIGHTNING

This paper will only touch upon the techniques of protection against the direct effects of lightning. For a more comprehensive discussion of lightning protection of structures, the reader is referred to the literature.

Since there is no real evidence that any practical techniques exist for preventing lightning, a balanced protection system provides a means of intercepting a lightning stroke and conducting the current to ground where the stroke energy may be dissipated in a harmless manner. The stroke might be intercepted by some taller object alongside the structure to be protected. A workable rule of thumb, supported by both theory and practical experience, is that a tall object provides shielding against direct strokes for nearby and lower objects. The shielded volume is called a cone of protection. Figure 1 illustrates the concepts. Objects within a 1:1 cone of protection can be called "effectively protected" although an object outside such a cone still has a certain amount of protection against direct strokes. An object within two overlapping 2:1 cones of protection can also be regarded as "effectively protected".

The term "effectively protected" should be regarded in its statistical sense. There is some slight risk of a weak lightning stroke striking an object within a 1:1 cone of protection. The attractive range of an object (that distance within which essentially all strokes will strike the object in preference to other targets) increases with the ultimate stroke current amplitude. The true cones of protection may in fact

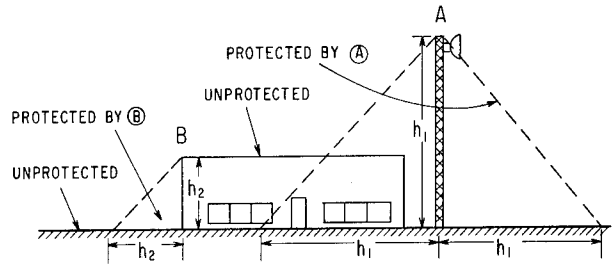

a) 1:1 CONES OF PROTECTION

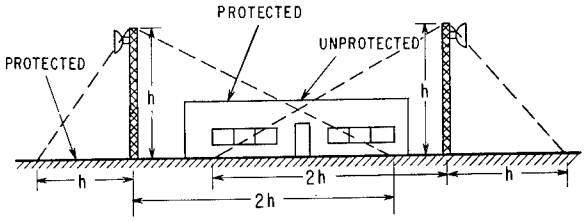

b) 2:1 OVERLAPPING CONES OF PROTECTION

Fig. 1 - Shielding of objects by cone of protection concept

be much greater than 1:1 or 2:1 for the higher energy and more dangerous strokes.

If a structure is not effectively shielded from direct strokes by some tall adjacent structure, it should be equipped with a heavy conductor laid along the exposed edges of the roof and/or with lightning air terminals. If the structure is of metal frame construction, the air terminals may be bolted or connected directly to that frame. If not, the air terminals should be connected to the encircling heavy conductor.

This conductor, and the air terminals should then be connected to ground either by heavy vertical conductors or by the framework of metal frame buildings. Any conductors intended either to intercept the direct lightning stroke or to carry it to ground should, by the terms of the Lightning Protection Code(1)*, weigh not less than 187.5 lbs. per 1000 ft. Copper is the preferred material for lightning conductors, but only because of its resistance to corrosion.

Grounding of a structure is most commonly done by means of driven ground rods or by buried copper conductors encircling the building and connected to the building framework or to the lightning conductors coming from the roof.

GROUNDING

Proper grounding is probably the most important element of any lightning protection system. Since its importance extends equally to protection against the indirect effects of lightning, grounding phenomena will be discussed in some detail.

The most important point to be kept in mind is that lightning currents are quite large (20,000 - 100,000 amperes or more) and that very large voltages will be developed across even small resistances. The Lightning Protection Code recommends that ground resistance be less than 10 ohms.

To define ground resistance, the flow of electric current from ground electrodes must be understood. The simplest electrode to consider is a hemisphere of radius r embedded in the earth. If a current I (in amperes) flows through this electrode, spreading out radially in the ground, the current density at a distance of x meters from the center of the hemisphere is

$$i = \frac{I}{2\pi x^2} \text{ amps/meter}^2 \qquad (1)$$

According to Ohm's Law, such a current density produces an electric-field in the earth of strength

$$e = \rho i = \frac{\rho I}{2\pi x^2} \text{ volts/meter} \qquad (2)$$

where:

ρ = resistivity of the earth in ohms-meter

If this field strength is integrated over a path from the ground electrode to some point x, the voltage difference between the ground electrode and that point is:

$$E = \int_r^x e \cdot dx = \frac{\rho I}{2\pi} \int_r^x \frac{dx}{x^2} = \frac{\rho I}{2\pi} \left(\frac{1}{r} - \frac{1}{x} \right) \qquad (3)$$

where:

r = radius of the hemisphere in meters.

If the field strength is integrated over a path from the ground electrode to some remote point where the current density is negligible, the total voltage drop is

$$E = \frac{\rho I}{2\pi r} \text{ volts} \qquad (4)$$

The total resistance experienced by the stream lines of current diverging from the hemisphere is

$$R = \frac{E}{I} = \frac{\rho}{2\pi r} \qquad (5)$$

The most commonly used ground electrode is the ground rod which has a resistance of approximately

$$R = \frac{\rho}{2\pi \ell} \left(\log_e \frac{4\ell}{r} - 1 \right) \qquad (6)$$

where:

ρ = ground resistivity, in ohms-meter.
ℓ = length of rod, in meters.
r = radius of rod, in meters.

With any type of ground electrode the electric field in the ground depends on the current density and is greatest in the immediate vicinity of the electrode. Thus, there can be high potential gradients in the ground and high voltages between adjacent points in the vicinity of a

*Numbers in parentheses designate References at end of paper.

current carrying ground electrode. Figure 2 shows an example that assumes a hemispherical ground electrode of 1 meter radius in soil of resistivity 100 ohm-meters. From equation 5 this would be seen to have a resistance of 16 ohms. If the ground electrode were carrying a current of 20,000 amperes, between the points a and b, that are respectively 2 meters and 2.5 meters from the center of the electrode, there would be, from equation 3, a voltage difference of 32,000 volts.

It is voltages such as these, existing between points on the surface of the earth, that can be harmful to people and electrical equipment. The same phenomenon, of course, exists for rod electrodes.

The best way to limit these gradients is to use ground electrodes in parallel. This reduces the total ground voltage and simultaneously reduces the current density, particularly inside a cluster of ground electrodes.

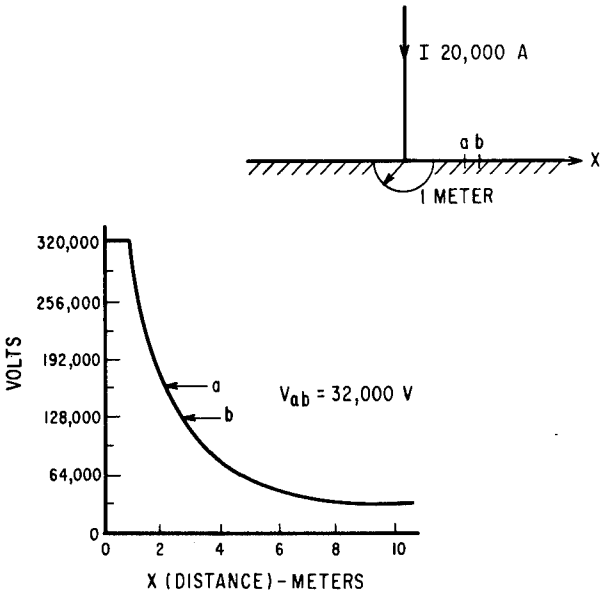

Fig. 2 - Voltage gradients in the vicinity of a buried electrode

PROTECTION AGAINST THE INDIRECT EFFECTS OF LIGHTNING

Even though a system has been protected against the direct blasting and burning effects of lightning, it may still be vulnerable to the indirect effects of lightning. A lightning flash can produce high voltages on electrical circuits, high enough to destroy the insulation of lights, motors and control equipment. The damaging effects of lightning have long been known to users of power equipment and to the electric utility companies supplying power. Techniques for controlling the high voltages and protecting such power equipment from damage are well known and generally are applied as a matter of routine by the designers of such equipment. The techniques of protection for power apparatus consist in essence of jucidious installation of lightning arresters and capacitors.

When it comes to electronic apparatus, the lightning protection problem becomes more involved. Where surge voltages of several thousand volts may be harmless to power equipment, surges of a few hundred volts may be disastrous to electronic equipment. The problem becomes very acute for aerospace ground equipment for four reasons:

1. The equipment spreads over a wide area and so is exposed to surge voltages at many points.

2. The equipment uses semiconductors with their inherent low resistance to surge overvoltages.

3. The equipment is designed, in many cases, by people who are not used to dealing with the problems of lightning.

4. Grounding and shielding techniques employed for control of low-level electrical noise are often completely at variance with the grounding and shielding techniques needed to minimize lightning overvoltages.

Surge voltages can be produced in three main ways: by changing electric fields associated with a lightning stroke, by changing magnetic fields or by the flow of current through ground resistance. These are illustrated in Figure 3.

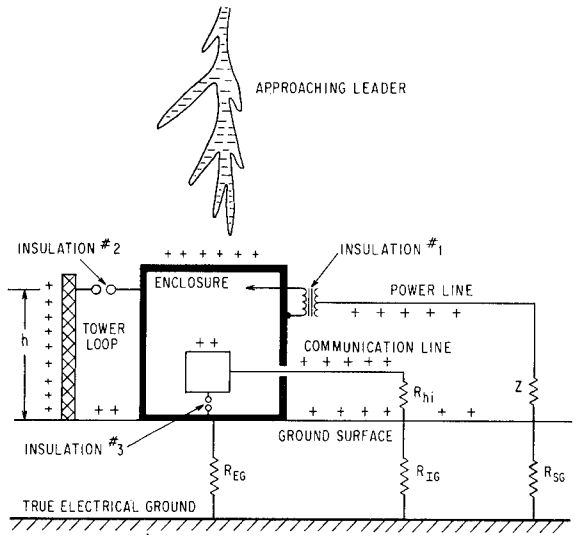

Fig. 3 - Lightning induced voltages (Prior to leader contact)

A lightning stroke consists of two main phases. In the first phase an electrical charge is transferred from a cloud into a column of ion-

ized gas above the ground. This column is called the leader. The leader is charged to a potential of 10^7-10^8 (negative) volts and progresses toward earth slowly enough (about 0.1% of the velocity of Light) that positive charges are induced on objects below the leader, the positive charge being attracted onto conductors through their resistance to ground. The amount of charge will be proportional to the capacitances from each object to the leader and to ground, and will be such that all the grounded objects will assume the same potential. There will be thus no (or in practice very little) voltage difference between these objects as the leader is approaching.

When the leader makes contact with the ground, conditions change abruptly. The positive charge that was collected on the enclosure and the adjacent ground rushes up to neutralize the negative charge within the leader. The charge collected on the loop and on the power line is blocked by insulation from flowing into the leader directly and is released to flow back into the ground from whence it came. The charge on the communication line is trapped there because it cannot flow off through the high resistance fast enough to keep up with the rate at which charge is being neutralized in the leader. The currents that flow as these charges seek new positions set up changing magnetic fields in the regions around the system.

EFFECTS OF THE CHANGING MAGNETIC FIELDS - Voltages are developed between various places in the system in a variety of ways. One is by the changing magnetic fields which are enclosed by a conducting loop, such as that formed between the enclosure and the tower. The voltage V_1 shown in Figure 4 would be proportional to the height of the tower, the effective radius of the enclosure, the distance from the enclosure to the tower, and the rate of change of the stroke current.

Near current carrying conductors the magnetic fields can be very large and surprisingly high voltages can be developed between points where one would not expect any voltage.

If the dimensions of the system are:

r_1 = 0.1 meter

r_2 = 1 meter

h = 10 meters

and if the current is assumed to rise at a linear rate to a value of 20,000 amperes in 2 microseconds, then

$$V_1 = 0.2 \times 10^{-6} \; h \log_e \left(\frac{r_2}{r_1}\right) \frac{dI}{dt} \qquad (7)$$

$$V_1 = 46{,}000 \text{ volts} \qquad (8)$$

The above analysis has disregarded the magnetic fields set up by the redistribution currents, such as I_2 in Figure 4. However, these are often small in comparison to the fields set up by the stroke current.

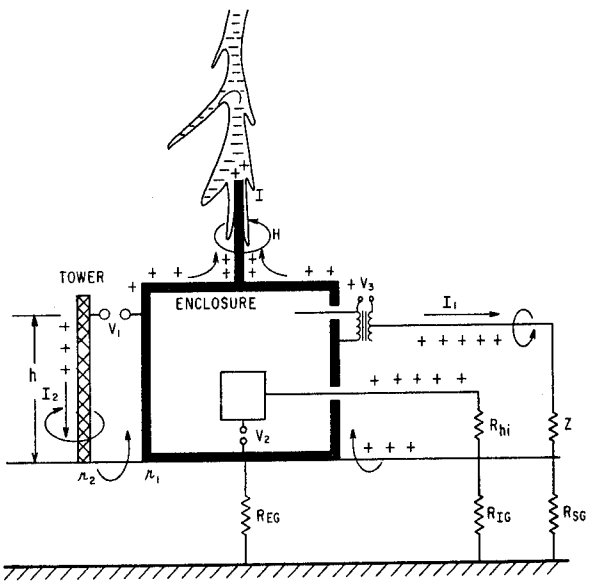

Fig. 4 - Lightning induced voltages (After leader contact)

EFFECTS OF THE CHANGING ELECTRIC FIELDS - The voltage V_2 would be a typical case where voltages are developed by electric induction, or more specifically by capacitive coupling. In this case, charge has leaked onto the communication line through the high resistance R_{hi} while the leader is approaching the ground. When the charge on the leader is neutralized the charge on the conductor is free to move, if it is able. In this case the resistance is so high that the charge cannot leak off as fast as charge is neutralized in the leader. It becomes trapped on the conductor and produces a voltage proportional to the capacitance to ground of the conductor and the charge on the conductor.

$$V_2 = Q/C \qquad (9)$$

Such voltages are the most difficult to estimate since the charge depends on the capacitance between the conductor and the leader and on the voltage of the leader.

These electrically induced voltages would not be present on conductors which are within grounded shields.

EFFECTS OF FOOTING RESISTANCE - Voltage V_3, between the enclosure and the power line in Figure 4 is dependent on the rate of change of the magnetic flux and on the current flowing through the footing resistance R_{EG}. In a practical system the footing resistance voltage is often the most severe and will be considered to the exclusion of the magnetically induced voltage.

As the stroke current flows into the ground through the resistance R_{EG} it raises the enclosure to a voltage:

$$V_3 = IR_{EG} \quad (10)$$

relative to true earth potential while the power and communication lines remain at true earth potential. If the stroke current were 20,000 amperes and the ground resistance were 5 ohms, the voltage generated between the enclosure and the power line would be 100,000 volts, more than sufficient to cause electrical breakdown if protective measures are not taken.

Voltages of similar magnitude can occur any time an electrical system is connected to two isolated ground systems,even if the connection is one that the designer had not intended. The worst instances of electrical damage to electronic equipment usually seem to occur when an extensive electronic system is provided with an instrumentation ground separate from the structural or power system ground of the building in which the equipment is housed.

Consider the voltage V_2 of Figure 4 when the communication line is connected directly to an instrumentation ground R_{IG} instead of being connected through the high resistance shown. As long as the instrumentation ground is located away from the electrical field of the enclosure ground system, the instrumentation ground will remain at "true" earth potential even if the enclosure is raised to a potential far above true earth potential. For the stroke and ground resistance conditions assumed above the enclosure will then be at a potential of 100,000 volts relative to the potential of the instrumentation ground. The electronic equipment in the enclosure is, however, held to the potential of the remote instrumentation ground grid. With no lightning current flowing in this ground grid, the ground bus remains at a low potential, ideally zero, again with reference to "true earth". Thus, if the building goes up 100,000 volts and the electronic equipment stays at "true" earth potential, an operator is exposed to the full 100,000 volt difference.

The hazard to the operator can be removed by connecting the equipment cases to the building ground and connecting the internal circuits to the instrumentation ground bus. The internal circuits are then exposed to the high voltage.

Such a system is inherently vulnerable even if lightning does not hit the buildings directly. Strokes to the ground can inject large currents into the ground cables. As the current flows to ground it will build up high voltages across the inductance of the ground cable, regardless of what the DC resistance of the cable might be.

PROTECTION OF GROUND EQUIPMENT

As can be seen from the foregoing, the voltages that can be developed on large electrical systems are quite high, particularly when considering the operating levels of electronic equipment. Protection of systems from the effects of lightning is perhaps more of an art than a science, but is still founded on certain considerations. Some of them are as follows:

1. Try to divert the stroke away from the system, the farther the better.
2. If the stroke cannot be diverted away completely, it must be carried to ground along a path where it does the least damage. This basically means providing a system of lightning rods and lightning conductors to a low resistance ground.
3. Reduce the resistance along the current-carrying path as much as feasible. This is particularly true of the ground resistance where the lightning conductor is grounded.
4. In buildings housing electronic equipment, establish a uniform potential ground plane over as much of the building as possible. In new buildings all reinforcing steel in concrete and structural steel members should be bonded together and connected to ground rods. These should be located around the periphery of the building. Bonding should be done at many points. All water pipes and utility conduits should be bonded to this ground system where they enter and at frequent intervals within the building.
5. Insofar as feasible, the building should be arranged to form a grounded metal enclosure (Faraday cage). External magnetic and electric fields will not penetrate into a perfect Faraday cage.
6. Power systems should be protected with commercially available lightning arresters.
7. Avoid the use of ground systems for electronic equipment that are isolated from building or power system grounds. This means using a multiple ground system rather than a single-point ground system.
8. Connect the cases of all electronic equipment to the nearest building ground point. This insures that as a minimum the cases will not assume a high potential, under lightning flash conditions, relative to the surrounding structure and so will not present an electrical hazard to people operating the equipment. Ground leads should be as short and direct as possible, possessing a minimum of resistance and (especially) inductance.
9. All wiring between different locations should be carried in shielded cables, with shields grounded at both ends.
10. Electronic equipment should be designed to withstand surge voltages. Surges can be carried into such equipment on input and output leads and on power supply leads and considerations should be given to the use of protective devices on these circuits.

How these principles apply to some of the more common surge voltage problems are illustrated in the following sections.

GROUND RESISTANCE PROBLEMS - In Figure 5 a surge current I is shown entering a piece of electrical equipment and flowing to ground through a ground resistance R_{EG}. A voltage IR_{EG} is developed on the chassis of the apparatus.

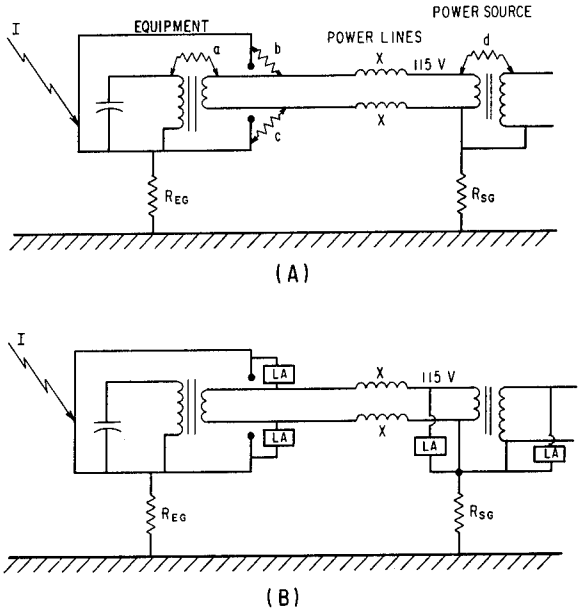

Fig. 5 - Protection of power circuits

This voltage can be high enough to break down the insulation between the equipment and the incoming power line. Such a breakdown could occur within the power supply transformer at (a) or between the 115-V leads and the chassis of the equipment at (b) or (c). Secondary breakdowns could occur in the 115-V power source at (d). Once such a breakdown has occurred, the sixty-cycle power current may follow the path and cause additional damage.

Ascribing personality to the lightning flash, the fundamental problem here is that the lightning current wants to flow to ground through as many paths as possible. If the system designer has not provided a path, the lightning currents can develop enough voltage to break down insulation and find their own paths, regardless of the designer's intentions.

Such failures can be prevented through the use of surge arresters between the power supply leads and the chassis of the equipment. These provide a controlled path for the lightning currents, a path along which the currents can flow without causing damage, Surge current would be carried from the chassis through the lightning arresters into the power lines. This current would flow to ground at the power source. Due to the impedance of the power lines, surge voltages could be developed on the power source equipment even though one side of the power line is grounded. Lightning arresters are thus needed on each side of the power source equipment.

Lightning arresters or circuit protectors can also be used on communication circuits entering an enclosure. Surge voltages would be developed on those circuits just as on the above described power circuits.

INTERCONNECTION OF EQUIPMENT - Figure 6 illustrates how proper interconnection of equipment can minimize surge voltages.

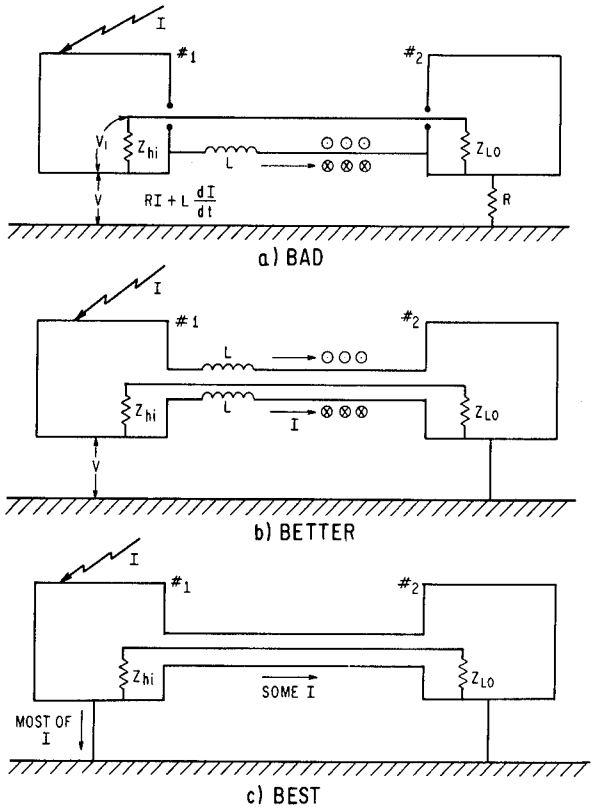

Fig. 6 - Protection of signal circuits

In Figure 6 a surge current I enters a piece of equipment (#1) and is carried to ground via an interconnecting cable running to a second piece of equipment. The current I sets up a magnetic field in the region surrounding the current carrying conductor. This field induces a voltage on neighboring conductors linking the field. The voltage appears across the terminating impedances in proportion to the impedance values. The magnitude of the voltage will depend on the rate of rise of current, on the distance between the two pieces of equipment, and on the spacing between the neighboring conductors and the current carrying conductor. An increase in any of these quantities will increase the induced voltage. It will also depend on the effective diameter of the current-carrying conductor; the larger the conductor, the less the voltage.

In addition to the voltages appearing within the equipment, there will be a voltage developed between the pieces of equipment and ground. At location #1 this voltage will depend on the current and the inductance of the current-carrying conductor.

The first step in improving the situation (Figure 6b) consists of enclosing the conductors

in a metallic sheath. To a first approximation, current flowing in the sheath will not produce a magnetic field inside the sheath and consequently will not induce a voltage on the enclosed conductor. The second step consists of eliminating the ground resistance at location #2. If the equipment at location #2 is grounded solidly (no resistance AND no inductance in the ground lead) there will be no voltage developed between location #2 and ground.

Note that voltages are reduced only if current is allowed to flow along this metallic sheath. If the sheath is connected only at one end (shields grounded only at one end philosophy) the entire purpose of the metallic sheath is eliminated.

These improvements have not yet eliminated the voltage V_2 which is built up across the inductance of the coaxial cable or conduit connecting the two pieces of equipment. When the equipment at location #1 is grounded solidly (Figure 6c) the voltage V_2 will be eliminated.

GROUNDING AND SHIELDING - LIGHTNING VERSUS OTHER REQUIREMENTS

There is some conflict between the shielding and grounding requirements necessary to prevent lightning from causing extensive damage and the shielding and grounding requirements necessary to control normal low-frequency electrical noise and interference. Reduced to simplest terms, good lightning protection requires that all ground systems be thoroughly interconnected and that all wiring between the different centers of an extensive electronic system be carried in shielded cables, with the shields connected to ground at each end. Designers of extensive electronic systems, for many good and legitimate reasons, prefer to have their system grounded at only one point, that one point being separate from any ground provided for a building frame or for an AC power system. Shields of interconnecting cables are often grounded at only one end with the other end insulated from any ground contact.

Superficially, the requirements would appear to be diametrically opposite, In practice, the conflict is more apparent than real and the residue of real conflict is resolvable through compromise or special protective measures.

The important elements of a system which has been used successfully to provide lightning protection of communication systems without compromising the systems steady-state noise performance are as follows:

1. Electrical cables carrying signals between sensitive or critical apparatus in separated locations must have an overall shield. This shield must be continuous and must be grounded at each end to the building ground systems.
2. The individual cables within this bundle should be shielded, but this is not an absolute requirement.
3. The shields on these individual cables should be grounded at each end but may, at the circuit designer's discretion, be grounded at only one end if such a practice is preferable for the control of steady-state noise. As long as the designer leaves the overall shield alone he can do whatever he wishes with any internal shields.
4. The electronic equipment to which the cables connect should have the housings connected to the building ground system.
5. A ground bus within the individual pieces of electronic equipment, but isolated from the equipment case, is often desirable. If such ground busses are provided it is preferable, from the viewpoint of lightning protection, that they be connected to the building ground system at the point of entry of the building ground system.
6. If direct connection of the ground systems cannot be tolerated, a separate electronic ground can be provided. A spark gap or other voltage limiting device should then be provided to limit the surge voltages that can be developed between the two ground systems.
7. If the electronic ground system is very extensive, it may be desirable to provide other voltage limiting elements between the electronic ground system and the building ground system.
8. Electronic cables are generally carried between locations in cable trays. These trays should be connected to the building ground system at each end. The cable trays should be electrically continuous over their entire length. Cable trays, if used,do not eliminate the need for an overall shield on the cables within the tray.
9. If cables are carried between two locations in electrically continuous metallic conduit, such conduit being connected to the building ground system at each end, the overall shield on the cables may be eliminated since the conduit takes the place of the shield. Cables carried in nonmetallic conduit, however, must have the overall shield.

CASE HISTORY

In order to illustrate some of the protection principles discussed above, certain aspects of a protective scheme which has been devised for a telemetry installation will be described. This installation is located in mountainous country with a fairly high level of lightning activity (Isokeraunic Level of 50 thunderstorm days per year). Furthermore, the grounding conditions are very poor due to a high mica content in the deeper soil regions. As a result, the earth resistivity actually increases with depth instead of decreasing which is the more normal situation. This has the effect of forcing the lightning current to spread out near the surface of the ground instead of flowing deeper into the ground. Thus, there is a greater chance of the lightning current coming in contact with buried cables, ground conductors, etc.

As a result of the high lightning activity and poor ground conditions, this telemetry installation had experienced severe equipment damage during lightning storms; in fact, operation

of the equipment during a lightning storm was impossible for reasons of personnel safety. Basically, the protective scheme used for the installation consisted of additional cable shield grounding, bonding between isolated ground systems, and installation of protective devices (Thyrectors®) where bonding or grounding was undesirable due to possible signal noise problems.

This installation was equipped with two systems of buried 500 MCM ground conductors running between structures; one bare and one insulated. The bare ground conductors formed the "Safety" ground system which bonded structural members to ground, and the insulated ground conductors formed the "Signal"ground system which grounded signal cable shields and electronic equipment commons. The Signal ground system was designed as a "low-noise" ground system. Both systems were run to several fields of ground rods which were kept moist for good earth contact. The two systems were supposedly tied together at one point only, that point being one of the ground fields. It was found, however, that unintentional bonds had been made between the two ground systems at several structures, and this apparently had no degrading effect on the noise level in the telemetry equipment.

Most of the lightning related problems at this installation were traced to inconsistencies in the connections to the grounding systems. In order to overcome this, the unintentional bonds which had been discovered were left as they were and additional bonds between the two ground systems were installed where possible. In cases where it was feared that system noise levels would increase as a result of such bonding, Thyrectors were installed between the two systems. These devices provide a high degree of electrical isolation between the systems (at those locations) during normal system operations. However, a high voltage surge travelling on either ground system (lightning related or otherwise) would see a low impedance connection between the two systems at those locations. Figure 7 shows a typical Thyrector installation at the main telemetry system operating center.

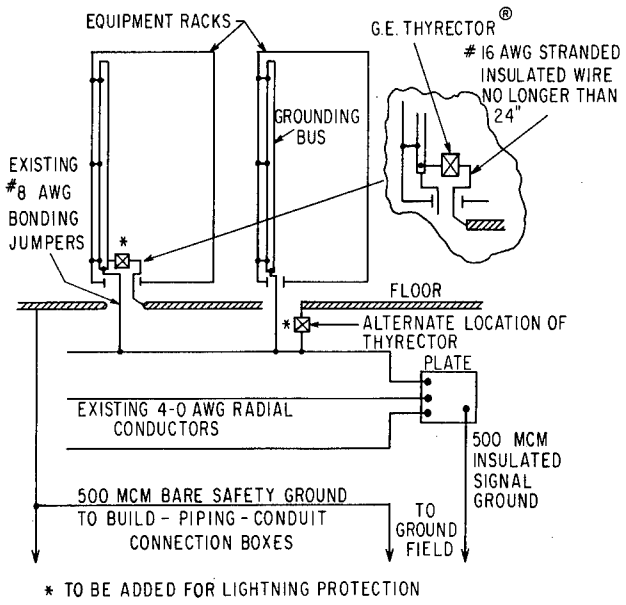

Fig. 7 - Protection of equipment racks

These Thyrectors provide bonding between the equipment cabinets (Signal ground) and the floor of the structure (Safety ground).

As a result of the protective scheme designed and installed on this system, operation of the telemetry equipment during a lightning storm is possible. This has resulted both from a lack of equipment damage during such storms and from a lack of hesitation on the part of the system operators to continue operating the equipment during lightning conditions.

REFERENCES

1. National Fire Protection Association, "Lightning Protection Code NEPA Std. No. 78-1968, p. 14.

SESSION 3C

SPACE BOURNE VEHICLES

Organizer - H. M. Hoffart

General Electric Co

Chairman, H. M. Hoffart

700938

THE ASPECTS OF THE APOLLO 12 LIGHTNING INCIDENT

D. D. Arabian

National Aeronautics and Space Administration

(Paper not submitted for publication. For reprints, contact the author or the Society of Automotive Engineers directly.)

THE PROBLEM OF LIGHTNING AND STATIC ELECTRICITY AT THE KENNEDY SPACE CENTER

by

Ernest A. Amman

National Aeronautics and Space Administration, Kennedy Space Center

ABSTRACT

Lightning and static electricity represent a significant hazard at the Kennedy Space Center to many operations. Aside from the risks to personnel, facilities, and schedules, the financial aspects of failing to minimize the effects of lightning are very significant. Special instrumentation is in continuous use to monitor the lightning threat and facilitate predicting lightning events. The event of triggered lightning which accompanied the launch of Apollo Twelve has been the subject of prolonged investigation and discussion. New Mission Rules were adopted to lessen the risk of a repeat of that incident. Investigations are in progress to assess the possibility of discharging clouds for a significant period of time.

The matter of lightning interference will probably become more critical with the development and operational use of shuttle type spacecraft, since the use of such vehicles will probably require something near an all-weather capability.

METEOROLOGY PLAYS A SIGNIFICANT PART in nearly all activities at the Kennedy Space Center. In most ways, a meteorologist could not ask for a more stimulating assignment. The forecasting problem includes the entire spectrum of types of forecast and types of weather to be predicted; everything, that is, except snow and very cold weather.

However interesting this variety may be, no combination of weather events imposes the same responsibility, or represents an equivalent challenge to the Space Center meteorologist, as does the forecasting of lightning storms. At the launch center, this is a problem that is no respecter of seasons. It never really goes away for any length of time. If, by the first week in October, a forecaster feels that he can draw a measure of relief from the ending of a long summer season of air mass thunderstorms, he is already in the season when cold fronts begin invading Florida, so that he merely has a different kind of challenge from the same type of weather, but resulting from a different cause. Whereas summertime forecasting must emphasize the time of day when the event will occur, and just where it will start, the cold front season features the question: Will it or won't it? Only about one out of three or four cold fronts moving through Central Florida features thunderstorms during the cool season of the year, which means about one or two days per month on which they do occur. But since the thunderstorms are just as likely, or more so, well ahead of the cold front, he is concerned with them on about ten days per month during the predominantly fair weather months.

During the twin peaks of the summer thunderstorm season, which occur around the first of July and the first of August, thunderstorms occur on a little over half the days. During the August peak, especially,

they persist for several hours running, on many occasions often continuing far into the night. Thunderstorm occurrence during the summer months is not a random thing. Synoptic situations conducive to them are usually persistent for several days, at least. It is normal to have thunderstorms for several days in a row alternate with several days having none. This is such a characteristic feature that many objective forecasting schemes include a parameter that makes allowance for whether or not thunderstorms occurred on the preceding date, or perhaps on two or more preceding dates. Such persistence is quite characteristic of tropical areas generally, and for the most part Florida is considered to be tropical-like during the summer months.

Because of the proximity of the Gulf Stream, and its thermal effects on the maritime air mass which is present all summer long, nighttime lightning is visible on many nights irrespective of the occurrence of daytime thunderstorms. On about ten to fifteen days each year, during the summer or early fall months, thunderstorms of this family move westward from the Gulf Stream and either cross the Florida coast line or approach near enough that they may pose a lightning threat during the late night or early morning hours. In the vicinity of the Kennedy Space Center, particularly, and probably to a considerable extent along much of the east coast of Florida, the meteorological conditions most conducive to nighttime or early morning lightning activity are the same conditions that inhibit the afternoon development. Effectively this increases the number of thunderstorm days by several per cent, and tends to keep the night crew on its toes. The sea breeze-land breeze influence upon the prevailing wind is the most significant feature of the summertime thunderstorm regime.

The hurricane season, overlapping as it does the summer thunderstorm season, and frontal thunderstorm season of the cool months, really only introduces an additional bit of variety, since everyone knows that nearly all tropical storms feature imbedded thunderstorms. These, however, command little attention because things are generally pretty well secured when the hurricane flags are flying.

It is not the intent of this paper to elaborate upon the statistics of thunderstorm occurrence at the Kennedy Space Center, except as such statistics relate to the subject of how we attempt to contend with them. Other authors have covered the subject at length, notably Neumann (1).*

Rather, the purpose of the paper is to describe the nature of the lightning and static electricity risk, the consequences of failing to attempt minimization of such risks, special instrumentation used to monitor the atmosphere's electrical characteristics, and programs being pursued with the hope of further minimizing the overall problem.

Considering the frequency of thunderstorm occurrence in the Kennedy Space Center area, and the very high cost of facilities exposed to lightning, one wonders that the incidence of lightning damage is not significantly higher than it is. One seldom hears of a lightning strike on a structure, although a few of them are documented. An estimate (2) of the number of strikes to be anticipated on structures located in the Kennedy launch area shows that on several structures on the Kennedy Space Center, at least four strikes might be expected each year. Yet, by actual count, fewer than this have been detected on all structures since the Space Center was constructed.

*Numbers in parentheses designate References at end of paper.

Undoubtedly many factors enter this consideration, but it is practically impossible to substantiate that any one thing is a true lightning suppressant.

Geography must be a factor. It can be shown that the incidence of thunderstorm development over the Space Center is relatively low as compared to a comparable area of flat brushland on the Florida mainland on the opposite side of the Indian River. Thunderstorms that encroach upon the Space Center are often past the vigorous development stage, and may already be decadent. The large number of tall structures that are spread over the landscape may act as corona points, from which gradual excess lightning charge is bled away without inducing full-scale lightning discharge. Whatever the reason for the apparent low incidence of lightning discharge to structures on the Space Center, it is too obscure to depend upon it for any assurance of safety from the effects of lightning. We must expect that the risk of damage or injury is sufficiently high to require extra precautions. It is necessary to program some means for protection against lightning strikes, or at least provide a means for minimizing their effects.

Personnel, facilities, and schedules are all susceptible to the effects of lightning. If it were not for the latter, it might be a simple matter to minimize the hazard. Just keep people inside and shut down facilities well in advance of the time that conditions become threatening. Most permanent structures are relatively safe from lightning damage because adequate grounding is economically provided during construction, but mobile facilities require extra consideration which will be described later. It is not structures themselves which are susceptible, but instrumentation on or within the structures that is the most cause for concern. Computers and other delicate electronic devices cannot be programmed completely to reject electrical transients that sometimes result from a lightning discharge searching for a route to the ground. Tests, simulations, or real life countdowns are at the least very tricky, if conducted while a thunderstorm is in progress. It is standard practice to shut down electronic equipment that can be spared, while a thunderstorm is in progress.

To the surprise of many of us, at the Space Center it has been determined that personnel involved in work on the large steel structures, unless on the very top of the structure, are relatively safe from electrical effects, and may perform many routine functions, even if the structure takes a direct hit. They might be scared, but should not suffer shock. However, in the course of routine work on the structures, many activities are hazardous, especially those things involving physical contact between facilities or instrumentation not protected by a common channel to the ground; for example, between a swing arm and the space vehicle, from crane blocks to the service structure, elevators, etc. Many activities have to be curtailed, even if it is no longer mandatory that personnel leave the structures during the times when lightning is a hazard, - an old Eastern Test Range rule still applicable most everywhere on Cape Kennedy itself, where the service structures are not nearly so large, and not quite so adequately grounded.

Shutdown of equipment and curtailment of personnel activities impacts on schedules. It is imperative that shutdowns be held to the absolute minimum that may be possible, and it is in this realm that the meteorologist can earn his pay, - sometimes a whole year's pay in a few hours! Idle manpower and facilities are tremendously expensive, even during the most convenient times.

During crucial times, one hour lost might result in missing a launch window. The cost of missed launch windows is not easily evaluated, but it would surely run into millions in some cases.

The Meteorological Prediction Center is charged with responsibility of distributing warnings of all hazardous meteorological conditions. As this responsibility relates to thunderstorms, we have two categories of warning that discriminate on the basis of either the degree of risk, or the expected intensity of the thunderstorm. Purposely, no firm dividing line has been set between severe weather warnings for thunderstorms, and adverse weather warnings for lightning within five miles of a susceptible area. The degree of risk is a variable thing, from day to day, depending upon the configuration of the space vehicle, or the work being accomplished. Identical thunderstorms, if one could imagine such, would present a greater risk to an operation involving fueling, or ordnance installation, than it would during a period of no significant activity on the pad. Intensity of lightning, or its frequency of occurrence, do not lend themselves to easy prediction. So, at best, one might conclude that today's adverse weather alert might result from the same meteorological conditions that brought forth yesterday's warning of severe thunderstorms. In reality, the expected peak wind gust value, which lends itself more easily to prediction, is more likely to establish the warning type that is issued on any particular day.

All operations at the launch pad are under the control of the Test Supervisor. He determines what action, or inaction, will result from any warning. His decision is not taken lightly, and seldom, if ever, without some consultation with the Pad Safety Supervisor, the meteorologist, or both. The Test Supervisor's decision about securing certain operations, or about imposing access restrictions, has to consider the impact upon whatever activity may be in progress. For certain operations he must achieve a different configuration before taking any securing operation. To do otherwise might expose personnel and equipment to unrelated hazards that may be more dangerous than the possible lightning. Because of time needed for safe application of the Test Supervisor's instructions, it is the intent of the Meteorological Prediction Center to distribute the warning no less than twenty minutes prior to occurrence within five miles of the launch pad of any lightning. In fact, that is the time line for which the forecaster strives, to achieve a proper trade-off between the utmost safety and over-warning. Now, such perfection will never be achieved in meteorology, as everyone knows, but nevertheless that is the objective.

Securing from some operations must be initiated more than twenty minutes prior to onset of lightning within five miles. On days when such operations are in progress, close coordination is necessary between the Test Supervisor and the forecaster or the Meteorological Watch. On those days when a high probability for thunderstorms is determined from early morning synoptic conditions and local measurements, the forecaster will nominally request that the Test Supervisor establish time lines at which he wishes to be advised of the atmosphere's progress toward thunderstorm development, and the thunderstorm's relation to operations in progress at the pad. On a given day, the Test Supervisor may wish to be certain within a given range of probability that no lightning will occur during a specified operation. On another day he may require a more precise minute by minute updating on a developing lightning threat. In nearly all cases, he wishes to know immediately when a threat ceases to exist. The Test

Supervisor's special requirements on such days are considered over and above the normal requirements for the distribution of warnings at the twenty-minute line. Similarly, during those times when widespread severe weather which includes thunderstorm conditions threatens an extensive area, a warning will be distributed as far ahead as possible, and updated frequently as conditions warrant.

Scheduling is still important, but things are not like they were before Apollo Eleven, when we were in a race to be first in getting on the moon. Launchings were occurring in Two-month intervals, and every minute counted. Men and machines were swarming on the launch pads and in the pipelines leading up to them. The financial impact of a missed launch window, involving a month's delay, could not even be estimated, but at one time it was reckoned conservatively that an hour's delay might call for $25,000 worth of overtime to catch up with the schedule. Over-warning for a low risk lightning threat could not be tolerated. Hanging on to a warning long after the lightning threat had passed was out of the question. Under today's greatly reduced launch schedule, it is desirable to maintain a comparable standard of support, but there is no longer the same urgency. Preparation and testing leading up to a launch date a month or more away is not accomplished with the same precision of timing. However, some of the operations cannot be stretched out indefinitely without introducing one or another risk to ultimate mission success, and, the economy picture being what it is, no operations testing that runs into the weekend is desirable because of the necessity of overtime or other pay differentials. So there is an obligation to meet a respectable standard in the lightning warning function.

Instrumentation for monitoring local meteorological developments is extensive within the boundaries of the Kennedy Space Center and Cape Kennedy Air Force Station. The Air Force's contractor, Pan American World Airways, is responsible for operation of a standard meteorological program of surface and upper air observations. Supplementary data collection for which they are responsible is accomplished by the automated WIND System. The WIND System includes a network of sixteen meteorological towers erected throughout the Cape Kennedy area and the Kennedy Space Center. Most of the towers are 54 feet in height, two are slightly over two hundred feet, and the NASA special purpose 150-meter meteorological tower is included in the network. Each sensor on every tower is interrogated by computer to report wind conditions and temperature data at various levels. The computer in turn compiles the data and distributes the information via teletype each half hour, or more frequently, to the Cape Forecast Facility of the Air Force, and to the KSC Meteorological Prediction Center on Kennedy Space Center. Data from this micro-meteorological network is indispensable when it comes to the prediction of the time of onset of thunderstorms in the Cape Kennedy area.

An FPS-77 Meteorological Radar at the Range Central Control Facility is operated from the Cape Forecast Facility, and a television picture of the PPI scope is transmitted to the Meteorological Prediction Center.

Special instrumentation for monitoring the atmospheric electric field has been installed at the Kennedy Space Center. A network of potential gradient probes has been established throughout the Space Center, in an array that assures some advance notice of impending lightning storms, either those moving into the area or those that form overhead.

It is recognized that high potential gradient alone is not a sure indication of lightning, but when information from a network of sensors is interpreted together with other visual or instrumental indications, the system has proven to be quite reliable as a forecasting tool, especially for moving storms. A sferics lightning detection system consisting of two ground receivers and a semi-automatic plotter has not proven to be of much assistance to the forecaster, since the information available from it is usually known by either visual or other instrumental means. But, as with a network of corona current detectors sited in conjunction with the potential gradient probes, it is useful backup information, for those times when some other system is not in operation or quite conclusive.

For the purposes to which the Meteorological Prediction Center is dedicated, there is no substitute for a good visual watch on developing situations. The Meteorological Prediction Center is not the best facility for observing from all directions, but for observing in the direction from which at least ninety per cent of all lightning storms arrive, or for observing strictly local thunderstorms over the area of most concern, a good meteorological watch can be maintained from the same room in which all instrumental indications are depicted. The same individual can both monitor the instruments, and visually observe development of weather events that may be of concern. By integrating all of the information that individual can come reasonably close to the twenty-minute time line which is the standard for warning interested parties.

For those who were not a party to the investigation, or have not read the report thereof, the incident of lightning striking Apollo Twelve must seem like a contradiction of the preceding paragraphs pertaining to the diligence with which the lightning threat is monitored. The facts brought out in the investigation do not substantiate such reasoning. It was not the purpose of that investigation, nor is it the purpose of this paper, to absolve anyone of responsibility for having paid insufficient heed to a threatening condition. The facts revealed that the cold front which arrived over the launch pad almost precisely with termination of the countdown of Apollo Twelve was not a lightning producer. No official observations from the Central Florida area, nor the lightning detection systems in use at the Kennedy Space Center, showed more than the two electrical events which coincided with transients that affected several systems on the Apollo Space Vehicle. There seems to be no disagreement among the investigators, which include many of the outstanding scientists in the field of atmospheric electricity, that the lightning which struck Apollo Twelve was triggered by the vehicle itself, and would not have occurred had the vehicle remained on the launch pad. It is now recognized that the application of the same techniques for predicting lightning events for normal ground operations are inadequate for a launching during marginal weather conditions. High potential gradient, even when also extremely variable, is not of itself a sure indicator of impending lightning. Other considerations are almost equally important. On November 14, the other criteria were not being satisfied, and no lightning was anticipated. Mission rules in effect at the time made no provision for delay in the launch because of the weather conditions, such as those being observed at the time. Although a delay in launching was discussed during the last two hours of the countdown, the Launch Director had no firm basis for such a decision. To hold up a launch unnecessarily poses hazards that may be even more undesirable.

The report (3) of the incident represents concensus opinion of many scientists and emphasizes the discharge as being one of very few well documented cases of triggered lightning.

Since the event, new Mission Rules have been adapted to prevent a recurrence of such an incident. The rules are subjective and undoubtedly over conservative. The decision to make the rules relate to type and dimension of clouds, rather than to specific "red-line" values of some instrumental readings stemmed from experience with the network of potential gradient indicators. There has been a history of uncertainty about the exactness of electric field measurement with the sensors being used at Kennedy Space Center. Unreasonably high fair weather fields have been observed from time to time, and exposure of the sensors, as well as contamination, is known to produce quite different readings from two sensors observing essentially identical electrical fields. In application of the new Mission Rules, the electric field measurements will be taken into consideration when marginal conditions prevail, or if changeable cloud conditions make the assessment of risk difficult or impossible. It is hoped that an improvement in the sensors and their exposure, which is underway, may lead to confidence in measurement of the electric field, such that it will be possible to establish constraints on the launch that are based upon reliable measurements of some atmospheric parameter.

Kennedy Space Center has awarded a study contract for attempting to discharge electrically active clouds by firing into them rockets with or without trailing wires. Obviously to be worthwhile, even if demonstrated to be feasible, such discharging would have to continue to be effective for an appreciable time interval, such as a minute or two as a minimum. It seems quiteunlikely that the large cumulonimbus associated with Florida's summer thunderstorms can be successfully subjected to such treatment. For other types of clouds, particularly those associated with the mild cold fronts of the cool season, the method may hold some promise. It seems within the realm of possibility that one substantial lightning stroke, initiated by a rocket firing, could render a cloud impotent for further discharging through a space vehicle climbing through the cloud in the next few seconds. At least, it is worth trying to find out if the possibility exists. The project will in all probability be drawn out over an extended time period, since application in the foreseeable future is related to advanced programs, rather than to the Apollo Program.

REFERENCES

1. Charles J. Neumann, "Frequency and Duration of Thunderstorms at Cape Kennedy: Parts I and II." Weather Bureau Technical Memorandums SOS-2, June 1968, and SOS-6, May 1970.

2. Glenn E. Daniels, "Terrestrial Environment (Climatic) Criteria Guidelines for Use in Space Vehicle Development, 1969 Revision." NASA Technical Memorandum 53872, September 8, 1969.

3. National Aeronautics and Space Administration, "Analysis of the Apollo Twelve Lightning Incident." MSC-01540, prepared by Marshall Space Flight Center, Kennedy Space Center, and Manned Spacecraft Center, February 1970.